Integrated Assessment of the Impacts of Climate Change on the Hydrology of Narmada Basin through Hydrological Modelling Approaches (SP-28/2017-18/PDS-17)

National Hydrology Project
Department of Water Resources, River Development and Ganga Rejuvenation, Ministry of Jal Shakti, New Delhi

Water Resources Department
Govt. of Madhya Pradesh

National Institute of Hydrology
Central India Hydrology Regional Centre, Bhopal

March, 2024

Dr. T. Thomas
Scientist 'F'

National Institute of Hydrology, Central India Hydrology Regional Centre, WALMI Campus, Kolar Road, Bhopal – 462016, M.P

PREFACE

The ever-increasing water demands of a growing population and their associated demands from various competing water users, make the water resources management, a very complex task. The appropriate water resources management is crucial for the development of any region. Even though the country receives sufficient rainfall, but the spatial and temporal variability of the rainfall is a matter of great concern. Moreover, the overall water resources management should take into consideration the supply side management along with the demand side management. As a result, while many parts of the country are reeling under floods, many other regions are facing drought and water scarcity. Many of the major river systems which used to be perennial are no more so, and flows only during the monsoon season.

Climate change, which has now become a reality is one of the biggest challenges facing the world today and almost all sectors are ought to be impacted. The water resources sector is one of the key sectors that may be impacted through which other water dependent sectors like forest, health, urban, and agriculture sectors are likely to be impacted. Climate change has resulted in the increase in frequency of extreme events like droughts and floods. The variability of rainfall has increased and many new areas are coming under drought and water stress. This situation may lead to a scenario of uncertain water availability scenario in the future. Narmada river basin in Central India is facing the impacts of climate change and human-induced activities, and its implication can be observed in increased variability in the water resources availability and frequent occurrence of extreme events.

The rainfall is highest in the Upper Narmada basin, which is also responsible for maintaining the perennial nature of the river. As such, investigation of the impacts of climate change in Upper Narmada basin is of greatest importance, in order to ascertain the future prospects of surface and groundwater availability along with the future projected extreme events that may lead to floods and droughts. Hydrological modelling approaches are one of the sophisticated tools available for assessment of the impacts of climate change on surface and groundwater availability, and changes in frequency and magnitude of extreme events. This will help decision makers to fine tune the policies according to these anticipated changes, so that the water availability continues to remain as much in future too.

This report focuses on the application of suite of hydrological and hydrodynamic models to simulate the various facets of the water resources and assessment of the climate change impacts on the water availability and extreme events. The study has been carried out by Dr. T. Thomas, Scientist-F & PI; Dr. B. Venkatesh, Scientist-G; Dr. P. C. Nayak, Scientist-F; Dr. Surjeet Singh, Scientist-G; Dr. Archana Sarkar, Scientist-F; Dr. Manish Nema, Scientist-E; Dr. P. K. Mishra, Sc-E and Ms. Shashi P. Indwar, Scientist-D as Co-PIs and Dr. Rishi Pathak, Research Scientist, Er. Lokesh Patel, JRF, Er. Suryansh Mandloi, Scientist 'B' and Ms. Deepshikha Negi, JRF under an able guidance of Dr. A. K. Lohani, Scientist-G & Coordinator, RC Bhopal.

Roorkee **(M. K. Goel)**
25.03.2024 Director

Project Team	
National Institute of Hydrology, Central India Hydrology Regional Centre, Bhopal	Dr. T. Thomas, Scientist 'F' (PI) Dr. N. C. Ghosh, Ex-Scientist 'G' (Co-PI) upto March 2019 Dr. B. Venkatesh, Scientist 'G' (Co-PI) Dr. Surjeet Singh, Scientist 'G' (Co-PI) Dr. P. C. Nayak, Scientist 'F' (Co-PI) Dr. Archana Sarkar, Scientist 'F' (Co-PI) Dr. Manish Nema, Scientist 'E' (Co-PI) Dr. P. K. Mishra, Scientist 'D' (Co-PI) Ms. S. P. Indwar, Scientist 'D' (Co-PI) Dr. Rishi Pathak, Research Scientist Er. Lokesh Patel, JRF Er. Suryansh Mandloi, Scientist 'B' Ms. Deepshikha Negi, JRF National Institute of Hydrology, Central India Hydrology Regional Centre, WALMI Campus, Kolar Road, Bhopal.
Water Resources Department, Govt. of Madhya Pradesh	Director Hydrometeorology (PI) Dr. Brijendra Baghel, Dy. Director & Database Administrator (Co-PI) Sh. M. K. Paliwal, Dy. Director (Co-PI) Sh. Sanjiv Das, Ex-Dy. Director & DBA (Co-PI upto 30.09.2020) Water Resources Department, Govt. of Madhya Pradesh, Jal Sansadhan Bhawan, Tulsi Nagar, Bhopal.
Consultant/s, if any (enter each consultant in a separate row)	None

Document control sheet

Title	Integrated Assessment of the Impacts of Climate Change on the Hydrology of Narmada Basin through Hydrological Modelling Approaches
PDS number	SP-28/2017-18/PDS-17
Date of approval	16.02.2018
Budget in time of original approval (For Partner and for Lead)	Rs. 250.0 lakhs (NIH - Rs. 250.0 lakhs, WRD-MP - Nil)
Revised Budget (For Partner and for Lead)	No revision
Date of commencement	16.02.2018
Date of completion	31.03.2024
Number of pages	415
Number of figures and tables	Figures: 250 & Tables: 54

Abstract

The present study is a large-scale hydrological simulation in the Upper Narmada basin up to Hoshangabad in Madhya Pradesh, carried out extensively for assessing the impacts of climate change on the water availability in a spatially heterogeneous area under projected future climate scenarios. A comprehensive literature review was carried out wherein the application of various models and their performance under different climate and topographic settings were studied based on the various case studies done worldwide. The ensemble modelling approach has been adopted in this study wherein ensemble of hydrologic models and ensemble of Global Climate Models (GCMs) have been considered for modelling the hydrologic processes related to surface and groundwater systems. The report highlights the key findings from hydrologic and hydrodynamic modelling exercise and assessments of the impact of climate change on the future surface water availability, high and low flows, groundwater recharge, groundwater levels and drought, desertification and climate change perspective for Upper Narmada basin in Central India.

In order to assess the impacts of the climate change in the Upper Narmada basin various hydrological models pertaining to both surface water as well as groundwater hydrology have been applied to simulate daily/monthly surface runoff, groundwater recharge, and groundwater flow. SWAT, HEC-HMS, MIKE11-NAM, WEAP and VIC models have been used for simulating the daily

surface runoff in the Upper Narmada basin, whereas WetSpass has been used to estimate the groundwater recharge in the problematic Narsinghpur district, and MODFLOW has been used to simulate the groundwater flow the in Narsinghpur district. These hydrological models have diversity in the conceptualization, parameter calibration as well as the model's applicability assessed of model performance evaluation statistics. SWAT and VIC are semi-distributed process-based complex models but SWAT requires lesser/easier calibration while it provides good results and can be applied equally well in small watersheds to very large river basins, whereas VIC is comparatively a more complex model, as data preparation is tedious requires programming skills and is designed for large river basins. However, WEAP is conceptual model, lesser complex to calibrate with few parameters, but requires more manual procedures for data preparation and to operate the model. WEAP, MIKE11-NAM, and HEC-HMS are not that complex with fewer parameters. HEC-HMS has the advantage that it can be used for both event-based and continuous flow simulation and the model outputs can be used for hydrodynamic modelling with HEC-RAS. However, it is always argued that complex modelling does not always guarantee better results. Most of the model performances for daily runoff simulation vary between satisfactory and good.

The comparison of the maximum temperature during the baseline period (1961-1990) and present period (1991-2019) indicated the warming is taking place at unprecedented rates in the Upper Narmada basin with the average annual maximum temperature increasing at the rate of 0.75^{o}C/100 years. The annual average rainfall has seen a steady decrease from 1102.3 mm during baseline period (1961-90) to 1060.2 during the present period (1991-2015). The 1-day maximum rainfall varied between 131.4 mm to 716.1 mm, but no significant trends have been detected.

The assessment of the impacts of climate change on the future water availability, high flows, low flows, and droughts have been assessed using the CMIP6 high resolution bias-corrected future climate data at 0.25^{o} x 0.25^{o} resolution of 13 Global Climate Models (GCMs) for two future climate scenarios, SSP245 and SSP585. The study period has been divided into five time-horizons viz., baseline

period (1961-1990), present period (1991-2019), near-term (2020-2040); mid-term (2041-2070) and end-term (2071-2100).

The analysis pertaining to climate change based on the future climate datasets, indicated that the average maximum temperature and the average minimum temperature are projected to increase continuously during all future time periods. the average maximum temperature is projected increase at the rate of 1.58^{o}C/100 year under SSP245 scenario and 2.61^{o}C/100 year under SSP585 scenario. Similarly, the average minimum temperature is projected increase at the rate of 2.14^{o}C/100 year under SSP245 scenario and 3.62^{o}C/100 year under SSP585 scenario. The extreme heat events represented by the 1-day maximum temperature is projected to increase in future also, and may lead to more frequent occurrences of heat waves. The 1-day minimum temperature is also projected to increase in future which may have significant implications on the crop growth as well as crop yields. The frequency of very hot days (MaxT > 40^{o}C), hot days (MaxT > 35^{o}C), very hot nights (MinT > 25^{o}C) and tropical nights (MinT > 20^{o}C) are all projected to increase substantially in future whereas the number of cold nights is projected to decrease significantly in the basin. This clearly indicates the warming of the basin in future as a consequence of the climate change.

The average annual rainfall is projected to increase considerably during all future time periods under both future climate scenarios. The 1-day maximum rainfall and the 3-day consecutive rainfall is also projected to increase considerably during all future time periods under both future climate scenarios. Also, the number of days with heavy rainfall (> 50 mm/day), very heavy rainfall (> 100mm/day) and extreme rainfall (> 200 mm/day) are all projected to increase in all future time periods under both scenarios, the highest being under SSP585 scenario.

The future streamflow has been simulated using the hydrological modeling approach using SWAT, VIC, WEAP, MIKE11-NAM which have been calibrated and validated with the streamflow available at various gauging sites on various tributaries and main river during the historical time period. The average daily stream flow is projected to increase substantially under all future time periods for

all the major tributaries (headwater catchments) and the Narmada River (main river catchments) The high flows represented by the 1-day maximum runoff and Q5 & Q10 are also projected to increase substantially in all tributaries and the main river. The marginal projected increase in the low flows (Q90 & Q95) for the future in the tributaries and main river, augurs well for the Narmada River system as it will help to sustain the perennial nature of the river in future also.

Higher groundwater recharge is projected in future in the Narsinghpur district as evaluated using WetSpass model mainly due to the increase in rainfall in the district. The higher groundwater recharge is responsible for getting translated into higher groundwater levels in future as evaluated by distributed. The groundwater recharge and the groundwater levels are projected to be marginally higher under SSP245 scenario as compared to SSP585 scenario.

The droughts are expected to increase in future. The drought duration as well as the drought magnitude is expected to increase considerably in all future time periods, the highest increase being projected during the end-term. The supply demand analysis has highlighted the fact that due to the anticipated changes in the future cropping pattern, there will be some areas like Gadarwara catchment where all demands cannot be fully satisfied with the available resources. The potential of lift irrigation and pressurized irrigation systems needs to be explored along with artificial recharge of groundwater in potential recharge zones.

The hydrodynamic modelling has been carried out and flood plain mapping has been carried out for Hoshangabad city using the HEC-RAS model. The worst floods that occurred at Hoshangabad were simulated based on the actual flood water releases from various dams along with the flood hydrographs from the major tributaries. The model was calibrated based on the field information on the extent and depth of water spread. Few hypothetical scenarios were also modelling to study the impact of possible worst-case scenarios on the flooding at Hoshangabad.

Originating unit	National Institute of Hydrology
Key words	climate change, modelling, groundwater, floods, drought, Narmada
Security classification	Restricted
Distribution	Restricted

Contents

List of Figures

List of Tables

1.0 INTRODUCTION

Water is the most essential resource for sustenance of all forms of life and is the key resource linked to the societal development, improvement in livelihood and prosperity of any region. The regions facing water scarcity are deprived of the basic facilities of life and often subject to hardships due to the harsh living conditions in such areas. At present, a significant proportion of the world's population is currently suffering from water stress (Oki and Kanae 2006). India possesses a great variety and diversity of climate, varying from extremely hot to extremely cold, from extremely arid regions to extremely humid regions, and from drought-prone areas to flood-prone areas.

Climate change has emerged as one of the most-significant global environmental issue and has attracted the attention of scientists, policy planners, governments and politicians worldwide. The Sixth Assessment Report (AR6) of Intergovernmental Panel on Climate Change (IPCC) indicates certain consequential concerns about the changing climate. The projected climatic changes are likely to affect adversely the key economic sectors and therefore, the sustainable development. Human-induced global warming has already caused multiple observed changes in the climate system (high confidence).

The increasing concentrations of the GHGs have been the most important drivers for increase in global temperatures. Climate change also shows its impact on the biodiversity, which is the very basis of existence for mankind. The warming is projected to increase for the next few decades and more the climate is disrupted, more are the chances of extreme risks and irreversible impacts. IPCC (2014) suggests that the human influence on the climate system is clear and it is extremely likely that the anthropogenic influences are the dominant cause of warming since the mid-20th century.

Empirical evidence continues to show that climate change remains a threat to the stability of the hydrologic system. As the climate system interacts with the hydrologic cycle, one significant repercussion of global warming includes changes in water availability at both regional and local scales. Changes of hydrological parameters arise from the combined effects of climate, land use, and anthropogenic activities in the basin. Due to increasing concentrations of greenhouse gases and

therefore global warming, the impact of climate change on water resources is expected to increase. Due to climate change, developing countries are facing several challenges in water resource management (Batchelor et al. 2003; Mujumdar 2008; Aggarwal et al. 2009). Climate change also affects the water resources diversity and availability in the future (Beniston and Stoffel 2014; Emami and Koch 2019).

Climate related changes can cause increase in the frequency, intensity, duration and magnitude of disasters. The extreme events are expected to increase under this warming scenario of the climate system, leading to intensification in the amount of precipitation as well as increase in the frequency and intensity of droughts. Some of the changes in the extreme weather and climate events observed since 1950s have been linked to human influence. The extreme events such as floods and droughts are expected to increase causing serious implications for the water sector.

The rainfall intensity is expected to increase manifold leading to flash floods in cities and river systems. It is also expected that both floods and droughts may occur in the same water year. The erratic pattern of the rainfall and its distribution will enhance the occurrence of dry spells. The drought affected areas are expected to likely increase in its extent. It is also very likely that hot extremes, heat waves and heavy precipitation events will continue to become more frequent. The extreme events will have a direct bearing on the water availability scenario. There may be sharp decline in the water availability in some regions whereas other regions may get more water. The groundwater recharge and availability shall also be affected due to the climate change.

River water management on basin scale is important as there may be a series of small, medium and large projects on almost every river basin in the Indian subcontinent. Extreme weather events in combination with poor basin management approaches could result in extreme disaster leading to flash floods and submergence in flood plains. The frequency and the magnitude of the floods have increased considerably in many coastal states of India. Also, urban flooding is now a common phenomenon in big urban centres causing hardships and loss of life and property. Similarly, the drought characteristics are also directly influenced by the impacts of climate change and therefore it is of prime importance to evaluate the drought

characteristics under a changing climate. In the Indian context, it is most relevant to understand the climate change impact from drought perspective, due to large dependency of Indian agriculture on the monsoon season which may see substantial changes and variabilities due to climate change.

There exists an intricate relationship between hydrological processes such as streamflow and climatic variables like temperature and rainfall across many river basins. As such, to examine the effects of climate change on streamflow, a mix of hydrological models and climatic projections from GCM / RCMs are commonly utilized. Hydrological models are applied to simulate the impact of a changing climate on the water cycle as well as to project future hydrological regimes. Large scale hydrological modelling involves many challenges such as uncertainties in scenario-based driving by climate models and their projections, spatial variability across large watersheds (topography, soil characteristics and land use / land cover changes) and selection of suitable hydrological models (Rickards et al., 2020). The hydrological modelling approach has been adopted to assess the impacts of changing climate on the highly regulated and complex Narmada River system. This modelling approach with application of different models including WEAP, SWAT, MIKE11-NAM, HEC-HMS, VIC, MODFLOW, and HEC-RAS will be helpful in the assessment of future water availability and extreme events in the Upper Narmada basin. It is under this background, the comprehensive analysis has been taken up for the assessment of the impacts of climate change on the future water availability, supply-demand scenario, droughts and floods, with the following objectives.

i) Application and performance evaluation of select hydrological models for simulation of surface water, and groundwater processes.
ii) Assessment of present and future water availability under alternate scenarios of climate change.
iii) Integrated water allocation planning and management based on future scenario of water availability.
iv) Flood plain mapping in flood prone areas.
v) Formulation of adaptation measures in the context of climate change.

2.0 REVIEW OF LITERATURE

2.1 Climate change

Climate change refers to the process in which a significant deviation from the mean climatic state is observed, for a significantly long period of time due to both natural and/or anthropogenic influences (Solomon, 2007). Over the past century, a noticeable shift in the climate has been observed, as global temperatures have continued to rise steadily, which has been more pronounced over the last few decades. The rapid warming of the Earth's climate system has taken place since the 1950s, and these changes are unlike any, that have occurred in the past (Pachauri et al., 2014). Furthermore, each of the past three decades has been successively warmer at the Earth's surface than all the previous decades.

The human activities, particularly the burning of the fossil fuels have resulted in the drastic increase in the greenhouse gas (GHGs) emissions. According to the Fifth Assessment Report of the Intergovernmental Panel on Climate Change (IPCC AR5), the rate of the global average surface temperature increased by 0.197°C ± 0.031°C per decade over 1951-2012 (IPCC, 2014). Generally, the smaller climatic shifts are due to the results of the natural climatic variability but the unprecedented warming can largely be attributed to anthropogenic activities resulting in the large-scale emission of greenhouse gases (GHG's). The human activities, particularly the burning of the fossil fuels have resulted in the drastic increase in the greenhouse gas (GHGs) emissions. These drastic climate shifts will have a wide array of impacts, including increased temperatures, shifting precipitation amounts, rising sea levels, and higher variability in cyclonic events.

Trend analysis of precipitation and temperature have been carried out extensively in India vis-a-vis climate change (Thapliyal and Kulshrestha, 1991; Mehrotra and Mehrotra, 1995; Kothyari and Singh, 1996; Naidu et al., 1999; Stephenson et al., 2001; Lal and Singh, 2001; De, 2001; Wilk and Hughes, 2002; Kumar et al., 2006, 2010; Dash and Hunt, 2007; Dash et al., 2007; Krishnamurthy et al., 2009; Pal and Al-Tabbaa, 2009, 2010; Krishnakumar et al., 2009; Bhan, 2010; Guhathakurta et al., 2011; Aufhammer et al., 2012, Ghosh et al., 2012; Patra, 2012; Rai et al., 2014; Mondal et al., 2015; Thomas et al., 2015; Radhakrishnan et al., 2017). An increase in frequency and intensity of extreme rainfall events have been

observed in several sub-divisions in India while the trend is decreasing in a few (Guhathakurta and Rajeevan, 2008). The increase in the number and intensity of extreme point rainfall events are reported for India (Khaladkar et al. 2009), notably for peninsular, east, and north east India (Guhathakurta et al., 2011).

Jain and Kumar, (2012) performed the trend analysis of rainfall and temperature for India using the MK test and SS estimator. The basin-wise trend analysis indicated that 15 basins depicted decreasing trend in annual rainfall but only one basin showed significant decreasing trend at 95% confidence level. Among the six basins showing increasing trend only one basin showed significant decreasing trend at 95% confidence level. All the basins had the same trend in rainfall and rainy days at the annual and seasonal scale. The analyses of 100-year data (1901–2000) for rainfall for 236 districts in Ganga basin revealed that 39 districts displayed a significant negative trend, attributable to climate change (Bera 2017). Another study with 111-year rainfall data (1901–2011) for Madhya Pradesh reported decreasing rainfall trends for all seasons, particularly monsoon (Kundu et al. 2017).

Mahmood et. al., (2019) used the non-parametric Mann-Kendall test (MK Test) and Sen's Slope (SS) to identify statistically significant trends in temperature and precipitation after application of pre-whitening for Lake Chad basin. The precipitation in the study area depicted strong decreasing trend (38%) and very strong decreasing trend (9%) whereas the remaining 53% showed no signals or weak decreasing signals and suggested that if the present situation continues to prevail, then the basin will receive approximately 20-25% less rainfall in future. About 84% of the time series related to temperature show an extremely strong increasing trend and the average rate of increase in temperature was estimated to be 0.022^{o}C/year.

Panda and Sahu, (2019) examined the long-term changes and short-term fluctuations in monsoonal rainfall and temperature over Kalahandi, Bolangir and Koraput (KBK) districts in the state of Odisha using Mann–Kendall test and Sen's slope estimator and concluded that the annual maximum temperature and annual minimum temperature have shown an increasing trend, whereas the monsoon's maximum and minimum temperatures have shown a decreasing trend. The annual

rainfall depicted a quite strong increasing trend. Khan et. al. (2022) used the MK test and other statistical tests to assess the changes in temperature and precipitation over Pakistan from 1962-1990. The MK test demonstrated increasing precipitation (DJF) and decreasing maximum and minimum temperatures (JJA) at the meteorological stations located in the Karakoram region. These changes are highly significant at 5% level of significance at most of the stations.

The adverse effects of climate change on agriculture in India have been highlighted (Bhardwaj et al. 2022; Baig et al. 2022; Kulanthaivelu et al. 2022). The effects of climate change on groundwater hydrology have been investigated (Swain et al. 2022). The negative impact of deforestation and climate change on the biodiversity in North-Eastern India has been identified and remedial measures have been suggested (Gogoi and Lahon 2022).

2.1.1 Climate Change Scenarios

Climate change scenarios or socioeconomic scenarios are projections of future greenhouse gas (GHG) emissions used by analysts to assess future vulnerability to climate change. Future greenhouse gas (GHG) emissions are the product of very complex dynamic systems, determined by driving forces such as demographic development, socio-economic development, and technological change. However, the future evolution of GHGs is highly uncertain. Scenarios are alternative images of how the future might unfold and are an appropriate tool with which to analyze how driving forces may influence future emission outcomes and to assess the associated uncertainties.

IPCC-AR6 constitutes a new range of scenarios viz., Shared Socio-economic Pathways (SSPs) which have been used in the Coupled Model Intercomparison Project Phase 6 (CMIP6). Five SSP scenarios have been suggested which includes SSP1-1.9, SSP1-2.6, SSP2-4.5, SSP3-7.0, and SSP5-8.5. In the SSP labels, the first number refers to the assumed shared socio-economic pathway, and the second refers to the approximate global effective radiative forcing (ERF) in 2100 (IPCC 2021). Compared to the previously used RCPs, the new SSP scenarios have been improved in many ways.

Five narratives describing different development paths of society were designed and form the basis of the so-called SSP scenarios viz. SSP1 (sustainable

and green pathway), SSP2 (middle of the road or medium pathway), SSP3 (regional rivalry), SSP (inequality) and SSP5 (fossil-fueled development). The classes of climate effects (radiative forcings) employed roughly correspond to RCP scenarios RCP2.6, RCP4.5, RCP6.0 and RCP8.5, complemented by a few additional classes. The four RCPs are named after a possible range of radiative forcing values in the year 2100 relative to pre-industrial values (i.e., +2.6, +4.5, +6.0, and +8.5 W/m^2) viz., i) RCP 2.6 (Rising radiative forcing pathway leading to 2.6 W/m² in 2100), ii) RCP 4.5 (Stabilization without overshoot pathway to 4.5 W/m² at stabilization after 2100), iii) RCP 6 (Stabilization without overshoot pathway to 6 W/m² at stabilization after 2100) and iv) RCP 8.5 (Peak in radiative forcing at 8.5 W/m² before 2100 and decline. RCP2.6 assumes that global annual GHG emissions peak during 2010-2020 with emissions declining substantially thereafter whereas the emissions in RCP4.5 are assumed to peak around 2040 and then decline. However, RCP6 assumes the emissions to peak around 2080 and then decline thereafter whereas the emissions in RCP8.5 are assumed to continue to rise throughout the 21st century (Figure 2.1).

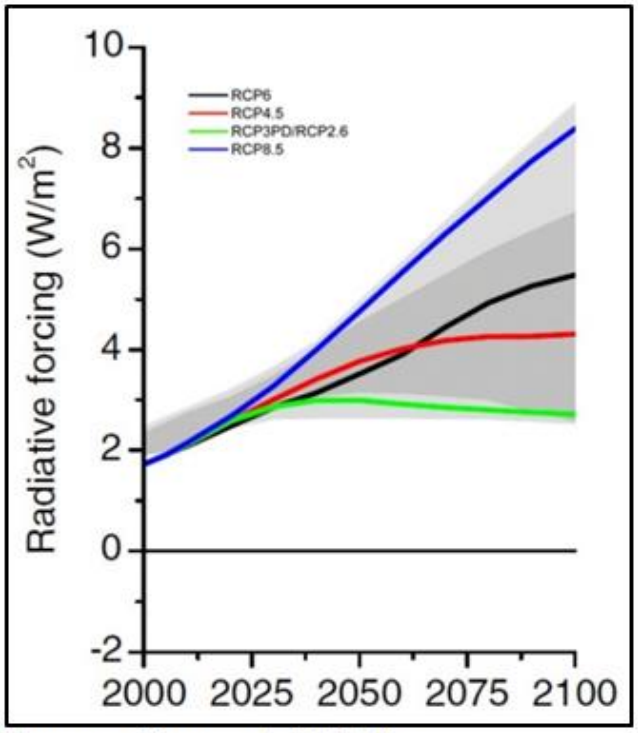

From van Vuuren et al (2011)

Figure 2.1: Representative Concentration Pathways (RCPs)

Combining the five pathways with the different climate forcings yields a scenario matrix (Figure 2.2).

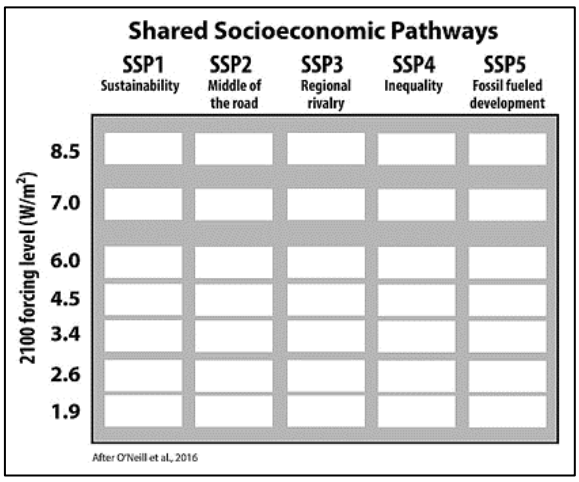

Figure 2.2: Shared Socio-economic Pathways (SSPs)

The four standard SSP scenarios based on the global agreement include i) SSP126 (scenario with 2.6 W/m² by the year 2100 is a remake of the optimistic scenario RCP2.6 and was designed with the aim of simulating a development that is compatible with the 2°C target), ii) SSP245 (radiative forcing of 4.5 W/m² by the year 2100 represents the medium pathway of future greenhouse gas emissions), iii) SSP370 (radiative forcing of 7 W/m² by the year 2100, this scenario is in the upper-middle part of the full range of scenarios), and iv) SSP585 (radiative forcing of 8.5 W/m² by the year 2100, this scenario represents the upper boundary of the range of scenarios). The standard SSP scenarios are given in Figure 2.3.

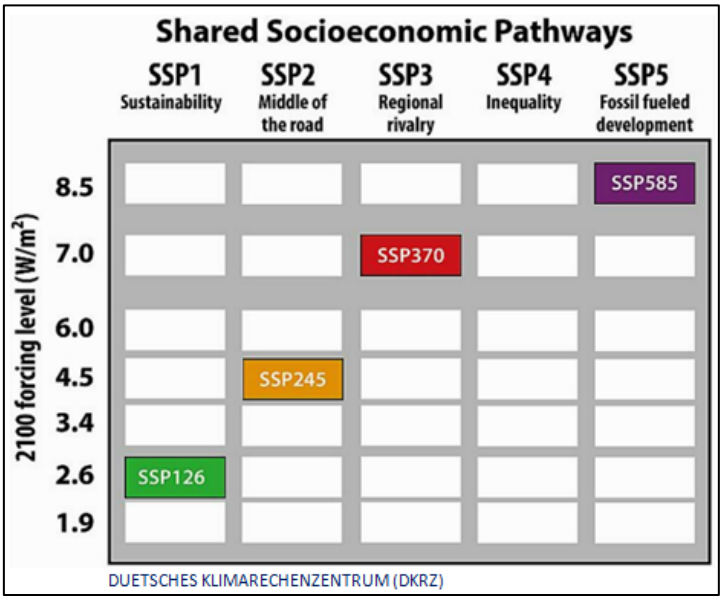

Figure 2.3: Four standard Shared Socio-economic Pathway Scenarios

2.2 Soil and Water Assessment Tool (SWAT)

Muttiah and Wurbs, (2002) studied the changes in mean and variance of water balance components for six different watersheds in Texas using SWAT, due

to variability in soils and climate. The available water capacity, moist soil albedo and bulk density were selected as soil parameters. They concluded that changes to mean and variance of water balance components as a function of geographic scale, suggest the presence of scale-dependent water balance 'uncertainty'. Kaur et al., (2003) estimated the water and sediment yields for Damodar-Barakar basin wherein SWAT based SDSS was used to predict the average water and sediment yields and concluded that the proposed SDSS could be used to identify areas having high water and soil losses.

Tripathi et al., (2003) applied SWAT model to model runoff and sediment yield of a small agricultural watershed in eastern India using generated rainfall. The model capability for generating rainfall was evaluated for a period of 18 years and concluded that SWAT model can generate monthly average rainfall satisfactorily and can be used for developing multiple year plans for critical prone areas.Singh and Bengtsson, (2004) investigated the sensitivity of water availability to climate change using hypothetical scenarios viz., (T+1^{o}C, T+2^{o}C, T+3^{o}C) as temperature scenarios and (P-10%, P-5%, P+5% and P+10%) as precipitation scenarios, for Satluj basin which receives runoff from rain, snow and glacier melt.

Jha, (2005) used (SWAT) model to assess the climate change impacts on the hydrological variables using GCM downscaled future climate inputs and concluded 43% increase in groundwater recharge, 51% increase in annual stream flow and 50% increase in total water yield for Upper Mississippi river basin. Chaubey et al., (2005) studied the effects of DEM data resolution on SWAT simulations for Moores Creek watershed, USA. Seven scenarios at increasing DEM grid sizes (30 m^2, 100 m^2, 150 m^2, 200 m^2, 300 m^2, 500 m^2, 1000 m^2) were used to study the impacts. The results indicated that DEM resolutions affect the watershed delineation, sub-basin classification and stream network generation and concluded that the minimum DEM data resolution ranged from 100 to 200 m^2 to achieve less than 10% error in SWAT model outputs for stream flow, nitrate and total phosphorous predictions.

Gosain et al., (2006) quantified the impact of climate change on the water resources of Indian river systems for simulating 12 Indian river basins. HadRM2 (daily weather data) is used along with SWAT hydrological model. The analysis revealed increase in severity of droughts and intensity of floods in various parts of

the country under greenhouse gas (GHG) scenarios. A. Mishra et al., (2007) used SWAT model for assessment of sediment transport in Banha watershed in India with on-stream sediment control structures. The sediment loss could be reduced up to 64% by adopting structures like check dams. Zhang et al., (2008) used a single objective optimization method (GA) and a multi-objective optimization algorithm (SPEA2) to optimize the parameters of SWAT model at three monitoring sites in Reynolds Creek Experimental Watershed, Idaho. They observed that the parameters estimated by optimizing the objective function at three monitoring sites consistently produced better results than those obtained by optimization at a single monitoring site.

Jeong et al., (2010) tested a sub-hourly rainfall-runoff model using SWAT wherein, the surface runoff, infiltration, impoundments, flow routing and lagging of surface runoff algorithms were modified to allow simulation with a sub-hourly time interval of one minute and tested on a 1.9 km^2 watershed near Lost Creek in Austin Texas, USA. They concluded that the sub-hourly version of SWAT is a promising tool. Jain et al., (2010) used SWAT model to estimate the runoff and sediment yield in Satluj river basin in western Himalayas and concluded that model is capable of simulating the runoff and sediment yield satisfactorily from the study area. Setegn et al., (2010) used SWAT model to predict monthly sediment yield and assess the impacts of subbasin delineation and effect of slope discretization in Anjeni watershed, Ethiopia. The annual average sediment yield was found to be 27.8 and 29.5 t/ha for calibration and validation respectively which showed good relation with observed values.

Lee et al., (2011) used SWAT model to simulate runoff in two watersheds viz., a) rural watershed draining into Matagorda Bay and b) urbanized watershed draining into Galveston Bay. The daily streamflow calibration at each USGS gage station showed a decent coefficient of determination (r^2) ranging from 0.496 to 0.736 with Nash Sutcliffe coefficient (NS) ranging from 0.372 to 0.643. Oeurng et al., (2011) used SWAT model to estimate discharge, sediment transport and associated particulate organic carbon yield in a catchment in southwest France wherein the management practices like planting date, crop rotation, irrigation and fertilizer quantity were also incorporated. The model was calibrated and validated with observed data and gave satisfactory results. An empirical correlation between

water and sediment yield and organic carbon content were developed on an annual basis along with the identification of potential erosion areas.

Betrie et al., (2011) applied SWAT model in eastern Nile River basin flowing in Egypt, Sudan and Ethiopia to estimate soil erosion, identification of area prone to soil erosion and assess the impact of different Best Management Practice (BMP) scenarios on sediment reduction. The tested scenarios included maintaining existing conditions, introducing filter strips, applying stone bunds (parallel terraces), and reforestation. The model result was satisfactory with NSE value greater than 0.83. Reduced sediment yield was estimated in the three scenarios at subbasin and outlet as compared to the existing conditions. Garg et al., (2012) applied SWAT model in Upper Bhima River Basin to characterize the hydrologic process and assess the crop water needs. Several scenarios of different cropping patterns were tested to increase the economic water productivity in the Ujjani Irrigation Scheme. The results suggested that maximization of the crop area by provision of supplemental irrigation to rainfed areas, as well as better on-farm water management practices can provide opportunities for improving water productivity.

Perrin et al., (2012) demonstrated the applicability of SWAT model for the assessment of water resources at watershed scale and the impact of management measures in a semi-arid crystalline watershed of southern India with nonperennial surface water source. The results showed that evapotranspiration is the largest water flux and the role of percolation tanks is significant as it provides about 23% of the annual aquifer recharge. They concluded that SWAT can be an adequate modelling framework for simulation of water resource in semi-arid hard-rock region, where groundwater vertical fluxes largely prevail over regional lateral flows at km scale. Singh et al., (2012) estimated the monthly sediment yield in the Nagwa watershed in Jharkhand, India using SWAT model and multilayer perceptron (MLP) artificial neural network model. Both the models was calibrated and validated during period 1993–2004 and 2005-2007 respectively. The annual average sediment yield was found to be 5.0 and 3.1 t/ha for SWAT and MLP model respectively and the measured sediment yield was 3.7 t/ha. NSE and r^2 values for SWAT and MLP model were found to be within satisfactory limits and MLP artificial neural network model was found to be more suitable for simulating sediment yield.

Wagner et al., (2013) applied SWAT model for the assessment of the impact of land use changes on water resources of Mula and Mutha river catchments upstream of Pune, India. Two model runs were performed, one with LULC of 1989-90 and other with LULC of 2009-10. At the catchment scale, the impacts of the land use change on the water balance cancel each other out. However, due to urbanization, the changes in water yield increased upto +7.6% at sub-basin scale along with decrease in evapotranspiration, while due to increase in cropland area, evapotranspiration increased upto 5.9%. Narsimlu et al., (2013) applied SWAT model in the Upper Sind River Basin to determine the future climate change impacts on water resources wherein the Sequential uncertainty fitting (SUFI-2) was used for model calibration and uncertainty analysis. It was found that the average annual streamflow could increase by 16.4% for the mid-century and a significant increase of 93.5% by the end- century.

Chandra et al., (2014) used SWAT model for sediment yield estimation in Burhanpur subbasin in Upper Tapi for simulation of run-off and sediment yield. The RSR and NSE was found to be within satisfactory limits with the values of 0.36 and 0.85 for respectively. Fukunaga et al., (2015) evaluated the ability of SWAT model in simulation of daily streamflow of the Upper Itapemirim River basin, Brazil. The model was found to be highly sensitive to baseflow. Validation results with NSE of 0.67; logNSE of 0.68; PBIAS of 22% and RSR of 0.57 indicated that the performance of SWAT model was satisfactory. Jain, (2015) applied SWAT and VIC models to estimate the snowmelt runoff in Ganga basin. For larger basins, Ganga Basin at Farakka Barrage, SWAT model gave better results in simulating melt runoff as 15% as compared to the 17% obtained from VIC model. But for the smaller sub-basin SWAT is not consistent when compared to energy balance for the snowmelt as well as other hydrological parameters.

Prabhanjan et al., (2015) applied SWAT model for modelling runoff and sediment yield in Khadakohol and Harsul watersheds, India. Due to non-availability of observed data regionalization of parameters was attempted. The calibrated parameters at Khadakohol watershed were used for Harsul watershed and its applicability was assessed. The simulations result with parameter regionalization were better as compared that with default parameters. The coefficients of

determination for sediment yield were found to be less than those for runoff. This study demonstrated the capability of SWAT model in ungauged river basins.

Uniyal et al., (2015) modelled the impacts of climate change in Baitarni basin using SWAT model. The SWAT model was calibrated using the daily stream flow during 1998-03 and validated during 2004-05. The NSE during calibration was 0.88 and 0.95 for daily and monthly time-steps. The study reported a reduction in runoff to the extent of 4% to 40% for the temperature increase of 1^{o}C to 5^{o}C, whereas an increase of rainfall by 5% to 10% resulted in increase in surface runoff by 13.2% to 26.3%. Priyanka and Patil, (2016) carried out the runoff modelling in Mala Prabha basin, Karnataka, India using SWAT model and reported satisfactory results during calibration (1982-85) and validation (1986-89). Himanshu et al., (2016) applied SWAT model for simulating runoff, sediment and water balance for the Ken River basin in Central India. The water balance indicated that evapotranspiration accounted for more than 44% of the average annual precipitation and the average annual sediment yield was very high at 15.41 t/ha/yr. Many other studies on application of SWAT model have also been reported (Ghosh and Dutta, 2012; Diwakar, et al., 2014; Jain and Sharma, 2014; Shivhare et al., 2014; Khare et al., 2014; Swain et al., 2016; Sahu et al., 2016).

Kumar et al., 2017 used SWAT model to simulate the runoff in Tons River basin, India. The calibration was performed for 1979-2000 and validation for 2001-2011. In calibration and validation, the p-factor and the r-factor was obtained as 0.54, 0.76 and 0.68, 0.56 respectively. The R^2, PBIAS, NSE, and RSR (RMSE-observations standard deviation ratio) were 0.74, -3.55, 0.73, and 0.54 respectively during the calibration whereas during validation the values were 0.75, 18.55, 0.69, and 0.56 respectively. They concluded that SWAT model can be effectively applied for the study area for simulation of runoff. Zhao et al., 2018 used SWAT model Jingchuan River Basin (JCRB) on the Loess Plateau, China for simulation of runoff. Three methods were used to quantify the parameter uncertainty of SWAT model, i.e. Sequential Uncertainty Fitting (SUFI2), Parameter Solution (ParaSol), and Generalized Likelihood Uncertainty Estimation (GLUE). SOL_K, CN2, and ALPHA_BF were the most sensitive parameters for the simulation of average flow, peak flow, and low flow, respectively. ParaSol method showed limited ability in uncertainty analysis due to the narrower 95CI and poor P-factor and R-factor. In

contrast, the 95CIs in SUFI2 and GLUE were wider than that in ParaSol. SUFI2 was found to be more superior to GLUE for model prediction uncertainty, within the same parameter range and therefore SUFI2 can be a potentially efficient tool for the parameter optimization and uncertainty analysis.

Pandey et al., (2021) proposed a complete integrated approach for simulating hydrological responses in the Upper Narmada Basin, India, under dynamic land use land cover (LULC) and climate change scenarios. To simulate the hydrological responses, five CMIP5 GCMs climate data were combined with SWAT model. Because of the large basin's heterogeneity, the Sequential Uncertainty Fitting (SUFI-2) algorithm was used for multi-site calibration and parameter sensitivity analysis. The calibrated model was combined with historical and projected land use scenarios (1990, 2000, 2010 and 2030) to estimate the hydrological sensitivity of the model to land use change. Their findings suggested increase in precipitation in the late twenty-first century, while annual mean temperature could rise by 1.79°C and 3.57°C by the end of the century under mid and high emission scenarios, respectively. During the 2050s (2041–2070) and 2080s (2071–2100) also, the annual and monsoon flow in the basin is expected to increase.

Mengistu (2021) applied SWAT model in the Upper Blue Nile (Abay) River Basin to assess the impact of climate change on water resources using a regional climate model (RCM), and COSMO Climate Limited-area Model (CCLM). The SWAT model was calibrated and validated using observed streamflow data from four gauging stations. In most regions of the basin, climate change estimates predicted an increase in mean annual temperature and a decrease in precipitation. The SWAT model was run with previous (1981-2010) and future (2010-2039, 2040-2069, and 2070-2099) climatic scenarios. In comparison to the baseline period, RCP8.5 data suggested a 27% rise in potential evapotranspiration (PET) and increase in surface runoff by14% by the end of the twenty-first century. RCP4.5 and RCP8.5 scenario-based model runs indicated that the basin's total water output is expected to decrease by 1.7 to 6.5% and 10.7 to 22.7% respectively. The contribution of baseflow to the overall water supply of the basin is expected to fall from 41.3% during the baseline period to 11.4% by the end of the twenty-first century. The reduction in the overall water production in the basin is partly

explained by the decrease in baseflow and the changes in the hydrologic equilibrium will have a substantial impact on the basin's water management.

Oliveira et al., (2021) used SWAT model to study the impact of changes in land use and land cover (LULC) on the local hydrology and sediment production in the Brazilian Amazon with three main objectives viz., a) to diagnose flow and sediment yield, b) to assess the effects of LULC changes on hydro-sedimentological variables over the previous 40 years, and c) to investigate the impacts of the possible trends or breaking points in the flow, surface runoff, and sediment yield series. The study looked at the effects of 40 years of LULC changes in an Amazonian basin on hydro-sedimentological variables, which can as well change the hydrological cycle. The SWAT model has been found to be a good estimator of hydro-sedimentological processes in Amazonian basins and can be used by decision-makers in water and environmental resource management

2.3 Water Evaluation and Planning System (WEAP)

Arranz, (2006) used Water Evaluation and Planning (WEAP) model to evaluate impact of future water demands for Olifants catchment, which is one of the 19 Catchment Management Areas (CMA) in South Africa. For each scenario, the unmet water demands for the different water sectors, stream flows at the outlet of the Olifants catchment and the water stored in the reservoirs were analyzed. WEAP21 was applied to manage the water resources of Guadiana River basin, Portugal through stakeholder participation for vulnerability and adaptation (Ortega et al., 2006).

Haddad et al., (2007) studied the applicability of Decision Support System (DSS) tool of WEAP21, on the water resources system of Tulkarem district, Palestine. The plan for future yield, reliability, risks and water allocation prices along with constraints, competitive uses, and priorities have been taken into account for the sustainable development of water resources in Tulkarem district. Arranz and McCartney, (2007) applied WEAP model for the complete Olifants catchment to evaluate the impacts of three water demand growth scenarios up to year 2025, implementation of environmental reserve (ER), international agreements (IA's) and water conservation and demand management (WC & DM) strategies on the

catchment water resources. The hydrology of the basin was simulated using rainfall and naturalized stream flows at five gauging stations on the Olifants River. The impacts of climate, changes in water demand, water resource development and land use were considered to be inherently integrated in the observed stream flow data, i.e. these impacts would manifest themselves in either increased or reduced stream flows.

McCartney and Arranz, (2007) carried out another study using WEAP model to assess the historic scenario of water resource development in the Olifants catchment from 1920 to 1989, giving a picture on how the water infrastructure developed in context of increasing water demand. This was followed by evaluation of the impacts of previously developed plausible future scenarios for water demand (Arranz et al., 2007). WEAP21 was also used in the Perkerra catchment of Kenya as a Decision Supportive System (DSS) to evaluate the current water management scenario and the effect of proposed water development projects in future (Mugatsia, 2010). Hoff et al., (2011) applied WEAP model to analyse the management of transboundary water resources in the Jordan River basin, which is very complex due to political conflicts in the region. Various unilateral and multilateral adaptation options were tested using WEAP model, considering climate and socioeconomic changes.

WEAP model was used to analyse water and agricultural policies to conserve groundwater resources and maintain rural livelihoods in the basin (Ortega et al., 2011). The overexploitation of the large aquifer in central arid region of Spain and the degradation of wetlands caused by exhaustive groundwater mining for irrigation gave rise to notable social conflicts in recent years. Ospina et al., (2011) used WEAP model to develop few baseline and adaptation scenarios for water supply and demand in the Sinú-Caribe river basin in Colombia and projected the potential impacts of climate change in the basin.

Mounir et al., (2011) studied the water resources management in Niger River basin with the main objective to propose a significant method to assist reduction of extreme poverty and the famine in Niger by 50% upto year 2015. WEAP model was used for providing a seamless integration of the physical hydrology and water management infrastructure of the region, that governs the

allocation of available water resources to meet various water demands. The result suggested for construction of a hydro-electric dam on Niger River, which will helpful to control the flows of low water levels on the river. The dam will also make it possible to find adequate drinking water for the two main growing cities Niamey and Tillabéry.

Azadani, (2012) studied the effects of climate change using WEAP on the water resources and water demands in the Arkansas River Basin in Colorado, which is one of the major rivers in Colorado that provides water for 650,000 people and irrigates 280600 acres of agriculture land. Based on the results from the two climate scenarios, a warmer and drier climate is anticipated for the region which indicated that global warming is a serious issue for water management in the basin. Gutierrez et al., (2013) studied the integrated assessment of policy interventions for promoting sustainable irrigation in a semi-arid Guadiana basin using a hydro-economic modelling framework. Guadiana basin, Portugal is a vulnerable drought-prone agro-ecological area. Modelling includes a risk-based economic optimization model and a hydrologic water management simulation model using WEAP21, including various policy initiatives and climate variability. The results indicated that the current patterns of excessive irrigation water use may put environment flow demand at risk. That study illustrates the need for considering the social, economic, institutional and technological factors in addition to bio-physical conditions for designing and developing water management. The research initiative demonstrated that hydro-economical model can explicitly integrate all these issues, constituting a valuable tool that could assist policy makers for implementing sustainable irrigation policies.

Bhave et al., (2013) used an integrated approach by considering the hydrological modelling to assess the impact of stakeholder prioritized adaptation options for the Kangsabati River basin, India. A series of multi-level stakeholder consultations were used to ascertain locally relevant, 'no-regret adaptation options' using Multi-Criteria Analysis (MCA) and scenario analysis methods. Subsequently, the validated WEAP model was used to project the effect of three options a) check dams (CD), b) increasing forest cover (IFC) and c) combined CD and IFC, on future stream flow during 2021–2050. The results indicated that although all three

adaptation options reduce stream flow as compared to the scenario without adaptation, but their magnitude, temporal pattern and effect on high and low stream flows are different. IFC option and combined CD and IFC option reduce stream flow percentage by higher magnitude greater as compared to CD option.

Singh et. al., (2014) highlighted the application of Integrated Water Resources Management (IWRM), using WEAP model for the hydrologic simulation of Mahanadi River basin, India. A monthly time step hydrologic model was developed using rainfall-runoff method incorporated in WEAP, with the main objective to address the challenge of water resources estimation in Mahanadi River basin. Hydrological processes occurring in the catchment were modelled and the stream flow was simulated on a monthly time-step and compared with the measured flow for six sub-catchments. The variation between measured and simulated stream flow during calibration was less than 10% and as such, the calibrated and validated WEAP model was applied for runoff simulations in other basins with similar hydro-meteorological conditions. WEAP21 was used to carry out the economic valuation of water resources in Masouleh River in Guilan province, Iran (Rahimi et al., 2014)

Nayak et al., (2015) evaluated the impact of climate change on groundwater storage for Joga distributary of Sirhind command area falling under Satluj River basin, India. In this analysis, observed gridded data and Regional Climate Model (RCM) data for mid-century and end-century period have been used. Seasonal variation of different climate parameters showed that rainfall may increase nearly 30% during the monsoon period, by the end of the century as compared to the current climatological baseline. The whole basin is projected to warm significantly, with minimum temperatures rising most pronouncedly. WEAP model has been used to estimate the groundwater storage and different scenarios were developed using WEAP model. The analysis shows that a shift to direct seeded rice, along with improvement in irrigation efficiencies, would improve the sustainability of groundwater use.

Tsoukalas et al., (2015) investigated the potential of Efficient Global Optimization (EGO) algorithm and explored the capabilities of WEAP21 water resources management model within PSO framework. They further validated and compared the results of WEAP21-PSO using the well-known hydro-system

management model, Hydronomeas, coupled with Evolutionary Annealing Simplex (EAS) optimization algorithm. The results confirmed that EGO has the potential and capability to handle computationally demanding problems and is capable of locating the optimal solution within few simulations.

Hao et al., (2015) observed that water resource management is becoming increasingly challenging in northern China because of the rapid increase in water demand and decline in water supply due to climate change and provided a case study based on integrated watershed management in Chifeng City, China. They examined the impacts of various climate change scenarios and the adaptive management options on water supply, by integrating the SWAT and WEAP models. Their study concluded that constructing more reservoirs can alleviate the current water shortage and groundwater depletion problems, although it may not necessarily be the most effective measure to solve water supply problems. Instead, improving irrigation efficiency and changing cropping pattern may be more effective and as such advocated the need for combined measures of reducing water demand and also increasing supply to deal with the water shortage problems in the study area.

Bhatti and Patel, (2015) used WEAP model for irrigation scheduling from Sardar Sarovar Project (SSP), India for the cotton crop in the semi-arid climate of Vadodara district. WEAP model was used to determine the crop water requirements and effects of irrigation strategies on Water Use Efficiency (WUE), Irrigation Water Use Efficiency (IWUE) and crop yield, for five different scenarios of irrigation water stress. Scenarios of conventional irrigation, deficit irrigation (water stress during flowering and ball formation stages), no irrigation stress during vegetative phase and no stress allowance for the whole growth were generated. The results showed that the amount of irrigation given in the case of no stress allowance is highest (307 mm) and thus there is a significant increase in yield of cotton crop while there is not much deviation in WUE. The reduction of transpiration is also noticed in other scenarios as compared to no-stress allowance case.

Yilmaz, (2015) applied WEAP to assess the impacts of climate change in an agriculture dominant Gediz basin, Turkey. The simulations of ECHAM5 and RegCM3 GCMs have been used in WEAP to estimate supply/demand ratios, unmet

demands and the decrease in the crop yields. The model was calibrated for the stream flow and storage volume of the Demirkopru dam of the region. The NSE and Pearson correlation coefficient indicated the model performance as very good. The results showed that the basin is under water stress and under the climate change scenarios, the situation can become worse, indicating the need of alternate supply sources and demand management strategies. Maharaj and Cashman, (2016) studied the supply demand scenario in the area located on Barbados' West Coast, Speights town which encompasses a well-developed tourist spot, residential and agricultural area. Here, groundwater is the main water source that may be adversely affected by the projected changes in climate. In order to investigate the potential impacts on the Speights town area WEAP model was applied. The projected estimations can assist water managers to better evaluate and identify trends in water use and formulate adaptation measures to offset future deficits.

Shahraki et al., (2016) used WEAP model to study water resources management under environmental scenarios in Hirmand catchment, Iran. The dust stabilization and animal-plant sustainable ecosystem scenarios were applied and further economic assessment of these scenarios was carried out. WEAP model was formulated with three scenarios viz., reference scenario (SC1), dust stabilization (SC2) and animal plant sustainable ecosystem (SC3) scenarios. The results have shown that the amount of unmet demand has increased greatly under SC2, SC3 scenarios. WEAP was also modelled to assess the economic benefits from the application of SC2 and SC3 in the agricultural sectors. The results indicated that the economic benefits decreased in the SC2 and SC3 scenarios as compared to the reference scenario. It was therefore suggested to give special priority to environmental scenarios to protect wetland ecosystems.

Alexander Psomasa et al., (2016) have studied designing water efficiency measures in Ali Efenti catchment, in Upper Pinios basin, Greece using WEAP and SWAT models. WEAP and SWAT follow two different modelling approaches and differ greatly in concept, structure, methodology and operational orientation. WEAP follows a balanced approach between being an integrated water resources planning and management tool and a hydrological model. SWAT follows a more sophisticated approach in modeling hydrology and crop growth and its scope is focused on agricultural catchments, processes and practices. Deficit irrigation and

upgradation of the irrigation network in the area could save up to 23% and 7% respectively of the baseline water use.

Alslevavni et al., (2017) developed a model by integrating WEAP and MODFLOW for Nineveh Province, Iraq to analyze the reliability of the supply system. A conceptual model was converted into numerical model using Groundwater Modelling System (GMS) by mapping the aquifer. The aquifer boundary was delineated and elevation data of reservoir and rainfall recharge to groundwater was used. MODFLOW was calibrated using conductivity and storage coefficients obtained from pumping test data in the selected wells in study area. The 'Link Kitchen tool' was used to link WEAP and MODFLOW to predict the change in the groundwater levels under various scenarios of pumping. The results of reliability of supply showed that continuous pumping has substantially reduced the groundwater level and therefore it was suggested to use an integrated approach for conjunctive use.

Kanani et al., (2017) applied WEAP model to evaluate the drinking water supply scenario for Vapi, Gujarat in 2014. WEAP model was used to simulate the future water demand with the forecasted population using the geometrical increase method. The model was calibrated with observed and simulated demand with an error of 3.73% in 2014. The calibrated model was then used to predict demand with increased population scenario for 2041 which is less than the inflow in Madhuban dam for the dependable flow of 75%. The results showed that the model can perform well to assess future demand. Mansouri et al., (2017) developed WEAP model for inter-regional planning of water resources in Seybouse's Wadi basin under five different scenarios namely, a) current situation, b) high population growth rate (1.8% to 5%), c) water reuse and recycling of wastewater, d) industrial water reuse and e) effects of desalination plant, to reflect the best and worst conditions of demand and supply so as to evaluate the water demand deficit and help planners for alternative management options. Berredjem and Azzedine, () applied WEAP model in the northern region of Seybouse Valley, to simulate the current and future water balance so as to analyze the situation of water supply-demand scenario for different sectors. Also, a scenario for extended dry climate was generated and simulations showed that the demands will increase drastically.

Arsiso et al., (2017) applied WEAP model to investigate water demand and supply under the impact of climate change and urbanization in 2039 for the city of Addis Ababa, Ethiopia. The hydrological data of reference scenario, 2012 was taken as input to WEAP and climate model outputs of NIMR- HadGM2-AO model for RCP4.5 and RCP8.5 scenarios were used to make assessments on reservoir storage volume in WEAP. The key assumptions such as population growth rate, water pricing and GDP growth rate etc. were defined. WEAP was tested with the observed and simulated demand data for baseline period 2012. Scenarios of low population growth (2.5%) and high population growth (3.3%) were generated under each of the RCPs. The results showed that during most of the years, the unmet water demand under RCP4.5 is higher than that under RCP8.5 scenario. However, with the population growth rate, there will be substantial shortage of supply in the city under both RCP scenarios. Among all the demand management policies explored, updating water tariffs is suggested as the better option with seasonal price adjustments, as the unmet demand in this case turns out to be the least.

Pankaj Kumar, (2018) used WEAP model to model river water quality using two scenarios viz. a) business as usual (BAU) and b) scenario with mitigation measures for Gomti River in Lucknow City, India under the main drivers of global changes namely climate change and population growth. Water quality simulation was done along 24 km stretch of the Gomti River from downstream of near Moosa Bird Sanctuary to near Bharwara. The results indicated that the water quality will rapidly deteriorate and will be not suitable for many aquatic lives by 2030. The results based on the 'scenario with mitigation measures' suggests that the current planned wastewater treatment plants and policies are not sufficient enough to achieve desirable river water quality within class B and hence call for immediate and inclusive action.

Metobwa et al., (2018) used WEAP model to simulate the water resources and demand in Mara River basin (MRB), Kenya considering 2010 as reference year for the simulation scenarios up to 2045, in order to mitigate the overuse practices in the basin. WEAP was calibrated with Parameter Estimation (PEST) tool for discharge and the performance of the model was evaluated with NSE, RMSE and other indicators. The linear population growth rate of 3% was assumed. The water demand projections at all nodes show a remarkable increase in the abstraction levels

from 0.3 BCM in 2013 to 2.65 BCM in 2045. The results indicated that the basin is projected to experience stress on its water resources in the coming years but the proposed scenarios showed that enhanced policy implementation will sustain water resources for the future in Mara basin.

Agarwal et al., (2018) used WEAP-MABIA method for analysis and simulation of agricultural water demands in the Ur River watershed, Tikamgarh, Madhya Pradesh. WEAP- MABIA method uses dual crop coefficient approach, which helps to compute separate soil evaporation and transpiration under various water availability situations. The year 2012-13 was used as reference year for customizing WEAP model for 8 sub-watersheds. The model was calibrated using PEST tool, available in WEAP. The calibrated model was used for estimating future water demands and unmet demands by using future climate data. The results of the study demonstrate the potential of using WEAP model for water resource management and assessment of future resource development in the basin.

Jonathan Opoku Oti et al., (2020) studied the hydrologic response to climate change in Densu River basin, Ghana using WEAP model during 2051-80. The basin is projected to be warmer in the future with expected mean temperature increase of 8.23% over the study period. The projected rainfall at the end of the study period is anticipated to see a drastic decline of -17%. The overall results showed a decrease in stream flow due to climate change by approximately 58% by the end of the study period primarily due to reduction in rainfall as predicted by the future climate scenarios. The study therefore recommended future research on climate change adaptation for better water management in the Densu River basin.

Bazzi et al., (2021) carried out a study on climate change for the Sistan Plain, Iran which receives little precipitation. It was critical to examine past evaporation fluctuations as well as projected trends in evaporation for water resource planning and management. The study was carried out to forecast the variation in the rate of evaporation from the surface of Chahnimeh reservoirs for future decades in order to manage water resources in the region. To simulate evaporation in the coming decades, the SDSM model was used in the 2050-2030 and 2080-2000 time periods. The evaporation rates are projected to increase by more than 300 mm as a result of climate change. Based on the WEAP model application, the Zahedan and Zabol

urban sectors absorb a large portion of the water from the Chahnimeh reservoir as compared to the Sistan Plain's agricultural sector, which receives a smaller amount of water. In the coming years, the withdrawal rates from these reservoirs will increase with the population growth rate, and the rate of evaporation will also rise in tandem. As a result, even if the water inflows into the Chahnimeh reservoirs continue to remain same in future as of now, significant water stress will still occur in the Sistan Plain and Zahedan and Zabol urban sectors.

Fard and Sarjoughain (2021) suggested that looking into the need for integrating water system models with other types of models, it was recommended to create a Componentized-WEAP (C-WEAP) by embedding the WEAP system in a RESTful framework. With the ECORE modelling methodology, the water system entities are linked to meta-components. In the WEAP system, every meta-component has a tangible equivalent. The C-WEAP RESTful framework is used to develop an existing water system model. The computational cost of the proposed framework is demonstrated via simulation of this water system. The C-WEAP RESTful framework that was created encourages integration with other software systems.

2.4 Hydrologic Engineering Centre–Hydrologic Modelling System (HEC-HMS)

Knebl et al., (2005) developed a framework for regional scale flood modelling integrating HEC-HMS/RAS with NEXRAD Level III rainfall in San Antonio River Basin, Central Texas, USA. HEC-HMS was run on a 4×4 km grid and the watershed parameters were calibrated manually for simulation of discharge in 12 sub-basins. Bournaski et al., (2006) applied HEC-HMS model for the promotion of common water management issue of the Mesta/Nestos River, a transboundary river between Republic of Bulgaria and Republic of Greece. HEC-HMS model was applied and found to have the capability to simulate precipitation-runoff and routing processes for both natural and controlled flows. The model was used for continuous flow simulation after its calibration using daily precipitation and daily streamflow.

Yusop et al., (2007) examined the rainfall-runoff process in a small oil palm catchment in Malaysia using HEC-HMS model. The hydrographs were satisfactorily modelled using HEC-HMS model. Despite low initial losses in catchment, the base flow was in quite high proportion. The model efficiency during calibration and validation were 0.81 and 0.82, respectively. The results suggested that the oil palm plantation would be able to serve perfectly in regulation of the basic hydrological functions. Kalita, 2008 compared the response of a storm using HEC-HMS model and CWC reports of North Brahmaputra and South Brahmaputra subzones. Considering a 50-year return period storm, flood hydrographs were developed for each of the 35 catchments in both zones. Snyder and SCS unit hydrograph transform methods were considered in HEC-HMS model. The resulting flood hydrographs were compared to understand whether HEC-HMS model can be used with the same degree of reliability as the CWC report-based flood hydrographs. The results indicated that HEC-HMS model can be reliably used for design flood estimates in both North Brahmaputra and South Brahmaputra subzones. The SCS unit hydrograph transform method has been found to give better results in North Brahmaputra, while the Snyder unit hydrograph method performs better in South Brahmaputra.

Chu and Steinman, (2009) used HEC-HMS model for both event-based and continuous hydrological modelling in Monalack watershed in West Michigan, USA. The model simulations provided hydrologic details about quantity, variability, and sources of runoff in the watershed and the model-outputs suggest that fine-scale (5-min time step) event hydrologic modelling, supported by intensive field data, is useful for improving the coarse-scale (hourly time-step) continuous modelling by providing more accurate and well-calibrated parameters. Verma et al., (2010) carried out rainfall-runoff modelling in Upper Baitarani River basin in Eastern India using HEC-HMS and WEPP models. The results show that both models over predict the stream flow during 2001 and 2003 and under predicts during 1999, 2002, 2004, and 2005. The percent deviation of total runoff volume simulated by WEPP model ranges between −13.96 and 13.05% while it varies from −2.55 to 31% by HEC-HMS model. Even though WEPP model simulates annual flow more accurately than HEC-HMS for most years, but overall, it can be concluded that the

HEC-HMS model is superior to the WEPP model for simulating daily streamflow in the Upper Baitarani River basin.

Sardoii et al., (2012) compared the results of different methods of runoff loss evaluation Initial and constant, Green &Ampt, SCS curve number available in HEC-HMS model for Amirkabir Dam watershed, Salt Lake basin, Iran. The results indicated that Green & Ampt and SCS-CN and Initial and constant method are placed in first to third preferences, respectively. Halwatura and Najim, (2013) employed the HEC-HMS model to generate long-term flow for Oya River and its tributaries using three different approaches to calibrate and validate the model. The calibration was performed separately for using three selected methods viz., deficit constant loss method, Snyder unit hydrograph method, Clark unit hydrograph method and SCS-CN loss method. The calibrated model was validated with a new set of flow and rainfall data (2008 - 2010). It was found that the Snyder unit hydrograph method simulates flows more reliably than the Clark unit hydrograph method whereas the loss method and the SCS-CN method does not perform well.

Roy et al., (2013) carried out hydrologic modelling of streamflow for Subarnarekha River basin in Eastern India using the SMA algorithm. The sensitivity analysis showed that the soil storage, tension storage and groundwater storage coefficient are the most sensitive parameters. The NSE, PEV, PEP have been used for performance evaluation and the ranges of these performance indicators range between 0.72 to 0.84, 4.39 to 19.47%, and 1.9 to 19%, which can be considered as good. Meenu et al., 2013 applied HEC-HMS model to evaluates the impacts of possible future climate change scenarios on the hydrology of the Tunga–Bhadra River catchment located upstream of Tungabhadra dam. The calibrated model was run for three future periods viz., 2011-2040, 2041-2070 and 2071-2099 and the climate change impacts on the basin hydrology were assessed by studying the changes in future streamflow and future evapotranspiration. The results of the water balance suggested increasing precipitation and runoff and decreasing actual evapotranspiration over the various sub-basins in the study area.

Abushandi and Merkel, (2013) applied the IHACRES and HEC-HMS rainfall runoff models to simulate a streamflow event of 31/01/2008in Wadi Dhuliel arid catchment. The models were simulated at an hourly time scale and were were

calibrated and validated using the observed streamflow data set collected at Al-Zaatari discharge station. The results indicated that the performance of IHACRES was weak but good performance was observed in the stream flow simulated by HEC-HMS with Nash-Sutcliffe efficiency (NSE) of 0.51 and 0.88 for IHACRES and HEC-HMS models, respectively. Zope et al., (2015) studied the impact of urbanization on flooding of Mithi River catchment in Mumbai city, India which is a coastal urban catchment using HEC-HMS model. The flood hydrographs for different land use conditions were derived using SCS-CN and kinematic wave method available within the HEC-HMS was used for routing. The flood plain maps, along with the flood hazard maps for different land use scenarios were developed by integrating HEC-HMS and HEC-RAS with HEC-GeoHMS and HEC-GeoRAS as well as with ArcGIS and remote sensing datasets. The results revealed a marginal increase in the runoff peaks and volumes within the catchment. However, this combined with tidal influence, may cause a major flooding issue in the city.

Laouacheria and Mansouri, 2015 applied HEC-HMS and WBNM models to evaluate the impact of land use / land cover change on runoff process in Azzaba City, Algeria. The results indicated that HEC-HMS model gave satisfactory results in simulating the flood events as compared to the simulations with WBNM model. Singh et al., (2015) used HEC-HMS model with SMA algorithm for Vamsadhara River basin, India. The model has been calibrated during 1984 to 1989 and validated during 1990 to 1993. The model performance was found to be varying from good to very good based on the NSE, R^2, Percentage Error in Peak (PEP), Index of agreement (d), and Percentage Error in Volume (PEV). The results during calibration included NSE of 0.70, R^2 of 0.71, PEV of 2.64% and PEP of 0.21% whereas during validation the results included NSE as 0.762, R^2 as 0.78, d as 0.93 and PEP and PEV as -15.2% and 12.33% respectively.

Zema et al., (2016) carried out a study in Mésima Torrent, Southern Italy for comparison of different infiltration methods in HEC-HMS model. The study focused on high magnitude flash flood and corrosive events that frequently took place in the semi-arid torrents. SCS-CN, Green-Ampt and Initial and Constant methods were evaluated and the results showed that SCS-CN method was satisfactory. Initial and constant method proved to be more suitable and effective and reliable for estimating peak flow and satisfactory for runoff volume. However,

Green Ampt equations showed low performance and was thus found not suitable. The performance analysis was based upon the mean, standard deviation, R^2, Min and Max values, RMSE and CRM of observed and simulated flows using different methods.

Ibrahim-Bathis and Ahmed, (2016) used HEC-HMS model in Doddahalla watershed, Krishna basin, India. The TRMM 3-hourly and IMD daily rainfall datasets were used and the SCS unit hydrograph and SCS-CN loss model was applied to simulate direct runoff in the watershed. Muskingum-Cunge model was used for routing. The study concluded that the stimulated flows can be useful for the water and land resource planning and devising management practices in the area. The models can be best utilized in ungauged watershed and water scarce region limited gauged data. Gao et al., (2017) applied HEC-HMS model in Qinhuai River basin, China for simulating basin runoff and examining the impact of urban agglomeration polders (UAP) on flood events and other hydrological process due to urbanization. The results show that UAP could increase the peak flow and flood volume. The closer the polder is to basin output, the smaller the influence it has on peak flows. The potential change in flood volume and peak flow with increasing impervious rate shows a linear relationship.

Gumindoga et al., (2017) applied HEC-HMS model in ten ungauged and gauged micro-catchments to simulate runoff in Upper Manyame basin, Zimbabwe. Based on parameter transfer from gauged subbasins, the Snyder Unit Hydrograph method was used for ungauged sub basins. The usefulness of model parameter transferability was tested by proxy catchment approach and NSE and (RVE) Relative Volume Error criterion was used to study the performance. The model outputs suggest that model predicted gauged catchment peak flows and runoff satisfactorily with optimum parameters. The ungauged micro-catchments contribute to 88 % of Upper Manyame catchment's runoff. The results suggest the HEC-HMS simulation is suitable for continuous runoff in watershed with numerous micro-watersheds.

Thakur et al., (2017) applied HEC-HMS for Copper Slough Watershed (CSW) in Champaign, Illinois, which has undergone major land use changes, with resulting increase in flooding issues. HEC-HMS (rainfall-runoff) and HEC RAS (to

estimate flood plain inundation area) models were applied to evaluate the flood plain and its extent, utilizing the known precipitation and land use. HEC-HMS was calibrated by altering the Manning's n and Curve Number. The results suggest that model is highly sensitive to CN as compared to Manning's n. The output of HEC-HMS is further used as input for HEC-RAS and flood inundation maps for 2015 were generated.

Chea et al., (2017) used HEC-HMS model for simulation of daily rainfall-runoff in Stung Pursat catchment of Tonle Sap Lake basin, Cambodia. The NSE was 0.45 for daily simulation and 0.61 for monthly simulation. The mean annual flow volumes were also successfully generated in this study on continuous time scales. The study demonstrated that HEC-HMS can be considered as useful tool for estimation of flows in lakes for the assessment of water availability. Further, planning strategies can be developed based on these outcomes. The sensitivity analysis of this study also suggested that groundwater storage, groundwater coefficient and groundwater percolation are some of the prime factors affecting runoff volume.

Ouédraogo et al., (2018) used HEC-HMS model for Mkurumudzi River catchment, Kenya for continuous simulation of runoff. The soil moisture accounting (SMA) method was used for generation of runoff from daily precipitation. The sensitivity analysis showed that the groundwater storage (mm), groundwater coefficient (hr) and groundwater percolation rates (mm/hr) for different layers along with percentage imperviousness are the most sensitive parameters. Tassew et al., (2019) simulated the surface runoff using HEC-HMS model for Gilgel Abay catchment, Upper Blue Nile Basin, Ethiopia. The meteorological model was developed within HEC-HMS from rainfall data and model calibration and sensitivity analysis was performed. The result of the sensitivity analysis showed that the CN is the sensitive parameter. The model validation indicated the HEC-HMS model is appropriate for stream flow simulations in the Gilgel Abay catchment.

Abdessamed et al., (2019) used HEC-HMS and HEC-RAS models for rainfall-runoff modeling and development of flood inundation maps for AinSefra City, Ksour Mountain, Algeria. HEC-HMS and HEC-RAS were used for flood

event simulations of 10-year, 100-year and 1000-year return periods. The study showed the HEC-HMS simulations can be useful in such flash flood scenarios. The study suggested use of retaining wall and significant reduction in flood area. This use of HEC-HMS along with HEC-RAS can be a good option for countering extreme events, which are more feasible in future due to climate change and scenarios can be developed for such conditions.

Kabeja et al., (2020) investigated the effect of land use / land cover change on flood peak discharge in two mountain catchments in China. Landsat 5 Thematic Mapper (TM) and Landsat 8 Operational Land Imager (OLI) dataset of 30 m spatial resolution has been used for the years 1990, 2000, 2002, 2008, 2010, 2016 and 2017. The study showed increase in forest cover by about 18% in Yanhe and by 16% in Guangyuan. A decreasing trend in flash flood peak discharge by 14% has been simulated in Yanhe and 6% decrease has been simulated for Guangyuan. The findings provide vital information for decision makers to establish proper flood control measures.

Ismail et al., (2020) HEC-HMS model with the most widely applied SWAT model to assess the impacts of climate change on streamflow at Bernam Basin, Malaysia. The analysis was performed during 2010-2039, 2040-2069 and 2070-2099 and compared with the baseline period (1976-2005) using an ensemble of ten CMIP5 GCMs under three future RCP scenarios viz., RCP4.5, RCP6.0 and RCP8.5). HEC-HMS model performed better as compared to SWAT with R^2, NSE, PBIAS and RSR of 0.74, 0.71, 4.21 and 0.37 and RSR of 0.71, 0.69, 5.32 and 0.31 during the calibration and validation periods. A decreasing pattern in streamflow has been projected for future periods, with a higher percentage (-5.94%) expected for the RCP8.5 scenario in the late century (2080s) during the dry-season period. In the wet-season, streamflow decreases have been projected in all future time periods except for RCP4.5 where it is expected to increase by 0.36%.

Sahraei et al., (2020) performed signature based multi-modeling and multi-objective calibration of HBV-EC and HEC-HMS models in Upper Assiniboine River Basin, Canada. A segmentation-based weighted average combination technique was built to let each model have a different contribution to the simulation of high-, mid-, and low-flow ranges. The HBV-EC and HEC-HMS models join the

multi-model combination helping to enhance the model-wrapper simulation in comparison with its individual hydrologic model components. The model-wrapper is expected to perform better than its individual model components regardless of region of study and type of hydrologic modelling. Dukic et al., (2021) studied different configurations of Système Hydrologique Européen TRANsport (SHETRAN) and HEC-HMS for simulating flash flood runoff for Jicinka River catchment in the Czech Republic. The satellite data for soil moisture from the European Space Agency (ESA) Climate Change Initiative (CCI) Soil Moisture (SM) project was used. Both models were compared for runoff simulations at outlet and soil moisture simulations. The results of this study indicate better performance of HEC-HMS model in case of soil moisture and better performance of SHETRAN in case of runoff simulations due to its higher complexity.

2.5 Variable Infiltration Capacity model (VIC)

Abdulla et al., (1996) estimated the parameters of a macroscale land surface hydrology model for Arkansas-Red River basin wherein the macroscale land surface hydrology model parameters were estimated for 44 catchments. The model-generated long-term mean stream flows were compared with the observations. The model underestimates the seasonal peak streamflow in late spring and overestimates for the early fall and is minimum during late summer. Lohmann et al., (1998) ccoupled the two-layer VIC-2L macroscale hydrological model to a linear routing scheme which is optimized with measured precipitation and streamflow data. The results indicated that the linear routing scheme was sufficient for the transformation of runoff to streamflow and the VIC-2L model contains parameterizations which are physically based and/or have been justified by field measurements. The base flow curve in the model can be seen as a simple parameterization of the base flow processes.

Matheussen et al., (2000) analysed the hydrological effects of changes in vegetation for the Columbia River basin over the last century using two landcover scenarios, viz., a) historical and b) current. The simulations were performed using the VIC model, applied at one-quarter degree spatial resolution during 1979 to 1990. The mean monthly simulated flows based the current vegetation were in good agreement with the corresponding observed discharge. The annual average increase

in runoff in the sub-basins ranged from 4.2 to 10.7% and decreases in evapotranspiration ranged from 3.1% to 12.1%. The removal of forest cover increased the streamflow as a result of reduced evapotranspiration and increased peak flows due to higher groundwater table.

Maurer et al., (2001) carried out the detailed diagnosis of VIC model results over the central U.S. as part of the Land Data Assimilation System (LDAS) project, which included retrospective simulations (eventually for 50 years) for long-term validation against basin discharge and to test model parameterizations. Good agreement was observed between the spatially averaged station soil moisture and simulations of the same from VIC model. They found an excellent model agreement with the observed moisture flux (change in soil moisture) over an annual cycle and concluded that VIC land surface model can provide fields of surface hydrologic states (soil moisture, surface temperature and snow extent and water equivalent) of sufficient accuracy to allow simulations of synthetic satellite observations.

Lettenmaier, (2001) described the development of VIC model and its application, for a) effects of climate change on the hydrology of major continental rivers and b) effects of vegetation change on the hydrology for the Columbia Rivers system (U.S. and Canada). Warrach et al., (2002) used two hydrological models namely, VIC and modified TOPMODEL to incorporate the sub-grid variability in soil moisture and runoff production into the soil vegetation atmosphere transfer (SVAT). Both the models represent computationally efficient ways to represent hydrologic processes within the context of regional and global modelling. Results shows that runoff simulation is superior during low flow period in TOPMODEL. The drawback of VIC model is it requires more calibration due to its freer parameters, which is not needed in TOPMODEL. However, TOPMODEL requires extensive pre-processing of topographic data.

Liang et al., (2003) used three-layer VIC-3L model over two watersheds in Pennsylvania to represent groundwater and surface water interaction dynamics for land surface model. The results revealed that VIC-ground can properly simulate the movement of groundwater table over multiple years in daily time step. Initial evaluation of VIC simulations, with and without considering groundwater and surface water interaction dynamics, showed its impact on the various water budget

components. VIC-ground gives lower surface runoff, higher base flow and less ET compared to VIC-3L results at the two sites. Yuan et al., (2004) applied the three-layer VIC-3L land surface model to simulate streamflow for Hanjiang River basin, China. The daily runoff was simulated by VIC-3L and the output routed to the outlets at six stations and compared with observed streamflow both at daily and monthly basis. The results show that the model can simulate the streamflow well with reasonable accuracy.

Sheffield and Wood, (2007) analysed the drought occurrence over global land areas during 1950-2000 using soil moisture data from simulation of water cycle through VIC land surface model. Meteorological data sets from observation stations were used as forcing for the model. Based on percentile soil moisture values, a monthly drought index was analysed at global and regional scale. Droughts of duration less than 6 months (short-term) are more common in Tropics and mid-latitudes; medium-term droughts (7-12 months) are more frequent in mid- to high-latitudes. Long-term (more than 12 months) droughts are generally restricted to sub-Saharan Africa and higher northern latitudes. The drought index also identifies certain well-known events, including the 1965/66 Indian, 1983/4 Sahel, 1982/83 Australian and 1988 US droughts which are generally ranked as the most severe and most spatially extensive in records.

Hurkmans et al., (2008) investigated and compared the accuracy of runoff simulations for Rhine River basin from two different approaches viz., a) water balance approach - Spatial Tools for River basins and Environment and Analysis of Management (STREAM), and b) land surface model VIC. The outputs were validated using observed streamflow and lysimeter data. They found that VIC is a robust model and less dependent on calibration. Nash-Sutcliffe efficiency for STREAM model was 0.47 whereas for VIC model is 0.29. VIC more accurately simulates discharge during the validation, including peak flows. Also, the annual evaporation cycle at the lysimeters is more realistically simulated by VIC.

Guo et al., (2009) applied VIC model with grid resolution of 9 km^2 in Hanjiang basin in order to predict future hydrological scenario. The output from GCM is downscaled and used for forcing the VIC model. After validation, the results show that Smooth support vector machine (SSVM) can predict temperature

and precipitation reasonably well. The simulation of runoff can be performed by VIC model with high efficiency and low relative error. SSVM model shows a decreasing trend of precipitation in the 2020s, mixed trend in 2050s and increasing trend in 2080s. The impact analysis on runoff from VIC model shows similar trends. Dadhwal et al., (2010), modelled the hydrology of Mahanadi River basin using physically based, distributed VIC model to assess the impacts of land cover change on streamflow at various locations along the river. The model performance was found better for monthly simulations with NSE of 0.89. They also concluded that a decrease in forest cover by 5.71% in the Mahanadi River basin has caused the river flow to increase by 4.53%.

Wu et al., (2011) applied the VIC land surface macroscale hydrology model to generate the daily soil moisture to reconstruct the 1951-2009 drought history of China. Grids of 30 km x 30 km was generated and driven by daily maximum and minimum temperature and precipitation. The modelled soil moisture was used to calculate the Soil Moisture Anomaly Percentage Index (SMAPI), which further can be used as a measure of the severity of agricultural drought on a global basis. The result showed that the severe drought events of 1978, 2000 and 2006 are well reconstructed and on an average, up to 30% of the total area of China is prone to drought. The study demonstrates the applicability and the value of using modelled soil moisture for reconstructing drought histories, and SMAPI is useful for analysing drought at different spatial and temporal scales.

Wang et al., (2012) established VIC model is with a resolution of 50 km x 50 km to assess the implications of climate change on water resources in China. Due to similar climatic, soil and other conditions, model parameters were transferred to other areas not covered by the calibrated catchments. The impact of climate change on runoff was studied under three emissions scenarios, A2, B2 and A1B. The results shows that the annual runoff over China as a whole may increase by 3-10% by 2050 with uneven temporal and spatial variation. Aggarwal et al., (2013) studied the ability of VIC model to assess the run-off potential and other hydrological components for entire India. Time period was 15 years at daily time step over 25 km x 25 km grid size. They found that VIC model is an idealistic model as it incorporates large number of parameters influencing the hydrologic processes.

VIC model can also process enormous amount of data which makes it suitable for large river basins.

Shiradhonkar, (2015) performed VIC model in Narmada basin to assess the change of hydrological parameters due to change in land use / land cover and concluded that VIC model is a model with the highest precision. Main advantages of VIC model was that it simulates on the sub-grid basis, it considers the non-linear baseflow, and it takes into account the LULC at a sub-grid level. Also, VIC calculates water balance at the sub-grid level and estimates the water balance of the grid as a sum of all sub-grids. The lake/wetland parameter is optional but if provided as one of the inputs to the model, it finely computes the water budget components.

Pan et al., (2016) compared the soil moisture retrievals from the Soil Moisture Active Passive (SMAP) mission to simulations from a land surface VIC model with meteorological forcing downscaled from observations and in-situ observations from sparse monitoring networks within continental United States (CONUS). To closely match the spatial resolution of the finest SMAP product resolution (3 km radar retrievals), the VIC simulation was performed on a 1/24° (~4 km) grid at an hourly time step over the CONUS. On comparing the soil moisture product with in-situ and model output data they found that on average, SMAP Passive has a better correlation with in-situ measurements at the point scale than the VIC model. Simulations with the VIC model has similar and additional challenges related to input and model parameter uncertainty.

Xue et al., (2016) used a novel multisite cascading calibration (MSCC) method using shuffled complex evolution optimization method to calibrate the VIC model, for the Red River basin. The model was simulated at 35 nested gauging stations. VIC model performance can be improved at specific single-site calibration but with limitations in upstream locations. To overcome these limitations, MSCC utilizes all available stream flow and gives better spatial heterogeneity representation in the model parameters. Results indicate that by eliminating number of stations having negative NSE values from 69% for a priori parameters to 37% for single site calibration to 3% for MSCC and increase the number of stations with positive NSE from 9% to 23% to 34% across all sites.

Narendra and Eldho, (2016) used the VIC model in the Ashti catchment, a sub-catchment of the Godavari River basin, India for the assessment of LULC and climate change on its hydrology. The model was calibrated for 20 years (1971-1990) and validated for the next 20 years (1991-2010). From the results obtained, a fairly good agreement between the observed and simulated runoff was seen and hence it was concluded that VIC can evaluate the hydrological changes satisfactorily for the basin. Also, no such significant changes were observed in the case of climate change. Stewart et al., (2017) applied five different erosion and sediment load algorithm within a common land surface common framework, to estimate the uncertainties and evaluate its prediction ability in a forested catchment in Front Range of the Colorado Rocky Mountains. The algorithms chosen are empirical based Modified Universal Soil Loss Equation (MUSLE) and mono-variate rating curve (MRC), conceptual Hydrologic Simulation Program Fortran (HSPF), physically based Distributed Hydrology Soil Vegetation Model (DHSVM) and the stochastically based Load Estimator (LOADEST). All the algorithms were used by the meteorological inputs and hydrologic fluxes generated from LSM based VIC model. Each algorithm was calibrated and validated after optimizing parameters. Performance was found to be in decreasing order when parameter sets were applied to periods with greatly differing suspended sediment load variability relative to the calibration period. The results show that the performance of extra complex and process-based algorithm, the DHSVM and HSPF were good specially in the transfer to a different catchment scenario.

Narendra et al., (2017) applied VIC-2L over the Tekra catchment, Godavari River basin, India. They divided the whole catchment into uniform grids of 25 km x 25 km cell size. The model showed satisfactory results with NSE greater than 0.6. However, the relative error was 30.03% thereby suggesting overestimation of simulated streamflow. Srivastava et al., (2018) used the VIC-3L model in the Kangsabati River basin, West Bengal with the primary aim of comparing the evaporation estimated by the Hargreaves method and the VIC model. It was found that the evapotranspiration estimated by Hargreaves method was highly overestimated. Therefore, to improve its applicability it was coupled with a genetic bias correction approach resulting in the improvement of NSE values. Das et al. (2018) used VIC model to study the impact of LULC change on the runoff, base

flow and evaporation dynamics in Eastern Indian River basins. Decadal LULC maps of 1985, 1995 and 2005 were used. It was observed that the LULC is responsible for increasing the ET and decreasing the base flow contribution. Also, there was an increase in a trend seen in the runoff.

Hengade et al., (2018) used VIC-2L model to assess climate change impacts on the hydrology of the Godavari River basin in peninsular India. The model calibration and validation showed reasonable agreement between observed and simulated flows at Polavaram, demonstrating the suitability of the VIC model to simulate the Godavari River basin hydrology. They concluded that the VIC model accounts for a large number of data, such as topography, land cover, soil, precipitation and wind speed, and minimum and maximum temperature, to represent the physical, meteorological and hydrological characteristics of the river basin. The over-prediction or under-prediction of extreme flows is an inherent problem in hydrological modelling of a basin due to the lack of model capability to simulate extreme events.

Wang et al., (2019) simulated the outflow and storage variations for multiyear and multipurpose reservoir at a daily time step for Xinfengjiang Reservoir in South China. In order to represent the weights of the outflow for different operation purposes like water supply, flood control and hydropower generation, the new parametric functions were used. Further this scheme was integrated with VIC model. The result showed that the time-varying operation-based parameters can reflect the changes of reservoir storage but not in the reservoir outflow. Further, results reveal that the proposed reservoir scheme has a wide applicability for reservoir storage and outflow simulation, especially for the reservoirs with limited reservoir management data.

Dash et al., (2020) compared the performance of the SWAT and VIC model in simulating the water balance components. From the statistical evaluation, it was seen that both the models gave satisfactory NSE values with better NSE values for SWAT model. It was also observed that SWAT gave higher runoff values for the low and medium flows as compared to VIC-3L. Schaperow et al., (2021) applied the VIC model to the Upper Colorado Basin along with other 12 basins ranging from 1500-25000 sq. km. The primary aim of the study was to prepare a fine-

resolution input dataset. Here, the dataset was prepared at a spatial resolution of 1/16°. The model was run taking the years from 1990-92 as spin-up years, 1993 as the calibration period and 1994-2011 as the validation period.

2.6 MIKE11-NAM

Supiah and Hashim, (2002) carried out a study on Layang River using MIKE 11-NAM mode and satisfactory and reliable results were obtained. The peak flow observed in the year 1992 was 20.94 m^3/s. The model was calibrated and validated which provide NSE of 0.75 and Root Mean Square Error of 0.08. Célleri et al., (2003) set up the NAM module of the MIKE-11 for four Belgian catchments to find the relationships between model parameters and physical catchment descriptors. Ten out of maximum 15 set of parameters were used. Model was calibrated using hydrological time series of 7 to 12 years. 9 out of 10 parameters were found to be statistically independent. The relationships between the retained 9 parameters and 12 physical catchment descriptors (PCD) were studied, and high correlation were found between them. Only three relationships (U_{max}, $CK_{1,2}$ and C_{area}) were found statistically significant, and the drainage density was found to be the most important physical catchment descriptor.

Khu et al., (2004) proposed the use of meta-models to replace the numerical simulation models for the calibration of MIKE 11-NAM model applied to the Treggevaede catchment in Denmark. The proposed meta-model reduces the number of simulations runs required in the numerical model making the automatic calibration of computationally intensive simulation models viable. The results indicated that the proposed model was able to reduce the required simulation runs to 40% of Genetic algorithm while achieving comparable calibration and validation results.

Ilias et al., (2006) simulated the single rainfall-runoff events in Ali-Efenti basin, a subbasin of Pinios river catchment in Greece. Three winter storm events were selected for simulations using MIKE 11-NAM model. The NAM model is based on semi-empirical equations, which describe the physical structures and procedures as lumped, and it treats each catchment as a single unit. A different choice of the initial condition drives the calibration process to different results,

considering the model parameters. Two of the events were used for the calibration phase, while one was used for the verification giving results with good accuracy. Keskin et al., (2007) calibrated and validated MIKE 11-NAM model to simulate the runoff from snowmelt in a semi-distributed manner. To simulate the rainfall and snow melt runoff, the model was setup for Yuvacık basin during 2001 and 2006. The whole basin is divided into three sub-basins and each sub-basin are subdivided into elevation zones and model was calibrated with snowmelt and rain on snow events. The modelling studies give promising results for the computation of runoff mainly due to snow during different seasons of the year.

Lan Anh et al., (2008) compared three lumped conceptual rainfall-runoff models viz., NAM (DHI), TVM and FEH (UK). TVM and NAM models are representative for continuous modelling while the FEH model is event-based type. These models were applied to the Bradford catchment in UK on a seasonal basis with a time step of hourly or quarter hourly. Results suggest that the selection of the models is highly dependent on the purpose of studies. The FEH model is good for single storm or flood analysis but not for long-term analysis. NAM model has an advantage over FEH model by being able to simulate data continuously. Tran and Nguyen, () carried out a study using MIKE 11-NAM for Ben Hai River basin, with the idea of combining auto calibration with the trial and error approach in model. They concluded that the good agreement of hydrograph's shape and total flow volume between simulation and observation indicates the model parameters are consistent.

Doulgeris et al., (2011) carried out a study in the Strymonas River catchment using MIKE 11-NAM model. The model's parameters were calibrated using auto calibration and thereafter, the trial-and-error approach was used and concluded that it satisfactorily predicted the river discharge. Odiyo et al., (2012) conducted a study on Latonyanda River Quaternary (LRQ) catchment using MIKE 11 NAM model. They concluded that the observed and the simulated runoff flow for LRQ catchment correlated well except for under-prediction of peak events and a few low flows. In addition to this, a few over predictions occured due to illegal irrigation abstractions as they reduce the observed flow values.

Hafezparast et al., (2013) carried out a study at the Sarsoo River basin using MIKE 11-NAM model using auto calibration. The calibration of the model was done using streamflow data and then validated for three years. They concluded that the runoff values have a significantly good relation between the observed and simulated flow values with the value of the coefficient of determination of 0.74. Amir et al., 2013 used MIKE 11-NAM model with auto calibration approach at Fitzroy basin, Australia. The calibration and validation of the model were done and it was found good and represented in the form of hydrographs. The reliability of the model is given by the efficiency index (EI) lies between 0.849-0.961 and index of agreement (IA) lies between 0.821-0.951.

Galkate et al., (2014) used MIKE 11-NAM model for Bina River, Madhya Pradesh. The model was developed, calibrated and validated using streamflow data at the Rahatgarh site. The coefficient of determination during calibration and validation were 0.796 and 0.609 respectively, which shows a good relationship between observed and simulated flow in respect of rate, timing and volume and shape of the hydrograph. The model performance measured in terms of NSE and the Sum of Square of Error (SSE) resulted in NSE of 0.81 and was therefore found suitable for the extended time period in Bina basin. Singh et al., (2015) performed rainfall-runoff modelling using MIKE 11-NAM model for Vinayakpur intercepted catchment in Chhattisgarh state, India. The model was calibrated using measured runoff data for the period 2001 to 2004 and then validated from period 2005 to 2007. A water resources management model MIKE BASIN was used with output of calibrated NAM model data. The R^2 value of model calibration and validation were observed to be 0.79 and 0.75, respectively.

Loliyana and Patel, (2015) applied MIKE 11-NAM model in Yerli catchment in Upper Tapi basin Maharashtra in Western India. The sensitivity analysis of runoff volume and peak-runoff has been undertaken with reference to 9 NAM parameters using the data of calibration period. The calibrated model has been validated for independent stream flow data of Yerli gauging site and Gopalkheda gauging site. The results show that calibrated model is able to simulate hydrographs satisfactorily for Yerli as well as Gopalkheda sub-catchments at monthly time scale. Tiwari and Chouhan, (2016) applied MIKE 11-NAM model in

Shipra basin, Madhya Pradesh, India to understand its execution, proficiency and appropriateness. The weighted precipitation, potential evapotranspiration and observed runoff were used as input data for the model execution for the period of 11 years (1996 to 2006). The model was calibrated for the first 6 years and validated for the next 5 years. The coefficient of determination R^2 for calibration and validation period was observed 0.720 and 0.502 respectively. The NSE for calibration and validation is 0.76 and 0.85 respectively. The NAM model was found appropriate for simulation and prediction of daily runoff with good degree of accuracy.

Abdul Razad et al., (2018) used MIKE 11-NAM rainfall runoff model for long-term and short-term inflow prediction. Four main rivers namely Telom, Habu, Ringlet and Betam contribute their water to Ringlet Reservoir in Cameron Highlands. Results shows that the peak flow is sensitive towards any change in CQOF, TG, Umax, CKIF CK1,2 and CKBF. At two streamflow locations, the bnbv model was calibrated for the period of 1999 to 2016 and validated for the period from 2010 to 2012. Results suggest that the model is reliable to simulate flow satisfactorily especially during flood events. Good calibration results were achieved for all scenarios, with NSE > 0.66, RSR < 0.6, R2 > 0.74 and PBIAS (%) <15%.

2.7 WetSpass

Batelaan et al., (1996) estimated the spatial groundwater recharge at seasonal and annual scales using WetSpass model. They suggested that the regional groundwater models used for analysing recharge-discharge relations are often quasi-steady and need long-term average recharge input that accounts for the spatial variability of the recharge. The recharge output from WetSpass can be used for groundwater flow modelling. WetSpass is especially suited for studying long-term effects of land-use changes on the water regime in a watershed and was founded on the time-dependent spatially distributed water balance model. Inputs for this model include grids maps of land use, groundwater depth, precipitation, potential evapotranspiration, wind-speed, temperature, soil, and slope and parameter tables such as land-use and soil types are connected to the model as attribute tables of their respective grids. The model makes use of grid GIS technology and digital data to

partition the precipitation into surface runoff, evapotranspiration and groundwater recharge.

Batelaan and De Smedt, (2001) used WetSpass model, a flexible, GIS based, distributed recharge methodology for regional groundwater modelling for analysing groundwater recharge in Grote Nete basin, Belgium. In this study, the effects of land-use changes on the groundwater discharge areas were analysed. The values range from -384 to 461 mm/year, with an average of 282 mm/year. Negative and low recharge values, due to high evapotranspiration, are found in the river valleys and especially at locations of groundwater discharge. The highest values are found under bare soil on the interfluves. Scanlon et al., (2002) explained in brief about the groundwater recharge estimation methods. Groundwater recharge methods have been classified based on hydrological zones from which the recharge data is obtained as surface water, unsaturated zone and saturated zone. The groundwater recharge estimation methods are further classified into physical techniques, tracers and numerical modeling within each of the hydrologic zones. Groundwater recharge cannot be measured directly and is difficult to accurately estimate it. Groundwater recharge estimation is very significant for effective and sustainable management of groundwater systems.

Arefaine and Nedaw, (2004) estimated the distributed groundwater recharge, surface runoff and evapotranspiration in Ilala subbasin using WetSpass model. Long-term mean hydro-meteorological data and physical characteristics of the catchment including land use/land cover, soil type, topography, groundwater level and slope were used as model inputs. The mean annual groundwater recharge, evapotranspiration and runoff were found to be 66, 440 and 40 mm respectively. Accordingly, the recharge accounts for 12% of the precipitation while the rest 81% and 7% becomes evapotranspiration and surface runoff respectively. The study area is characterized by low groundwater recharge due to high evapotranspiration rate associated with high temperature, dry wind, low rainfall and relative humidity, though it marginally large as compared to some parts of the northern Ethiopia They concluded that 25% of the annual groundwater recharge can safely be abstracted, which is about 17.2 mm of the recharged water, that can be abstracted annually in a sustainable manner without having an adverse effect on the groundwater resource.

Kuisi and El-Naqa, (2007) estimated the spatial groundwater recharge based on and application of WetSpass model for arid regions. WetSpass was integrated in the GIS ArcView as a raster model, coded in Avenue. Parameters pertaining to land use and soil texture were connected to the model as attribute tables of the land use and soil raster maps. This facilitates the definition of new land use or soil types, as well as changes to parameter values (Batelaan and De Smedt, 2007). The soil texture classification used for the WetSpass model is obtained from soil maps in addition to measurements, which were performed on 50 soil samples collected from the basin. The WetSpass model requires five categories of input data viz., climatic, catchment configuration, vegetation, soil properties and boundary conditions. The climatic data includes precipitation, potential evapotranspiration, wind speed and Penman coefficient, while catchment configuration considers land use types, slope and groundwater depth. The soil parameter data consists of hydraulic properties and empirical coefficients for modelling evapotranspiration and surface runoff. Boundary conditions take into consideration the extension of the area to be modelled. Similarly, the output from the WetSpass model includes the actual evapotranspiration, surface runoff and groundwater recharge distribution over a region. The results from different scenarios of land management practices can then be used by decision-makers to prepare land management plans. The results of the modelling are constituted by digital images of the spatial distribution of annual average values of actual evapotranspiration, surface runoff and groundwater recharge in the 30-year period from 1976 to 2005. These maps are raster-shaped, in which every pixel represents the magnitude of the respective component of the water balance, expressed as layer thickness (in mm).

Batelaan et al., (2010) used the WetSpass model or estimation of the long-term average spatial patterns of surface runoff, actual evapotranspiration and groundwater recharge in Gaza Strip, Palestine. The model is especially suitable for studying long-term effects of land-use changes on the water regime in a basin. The groundwater level is input to the WetSpass simulation. Therefore, the groundwater and WetSpass models have to be performed one after the other, while exchanging recharge and groundwater depth. This will lead to a stable solution for the groundwater level and discharge areas after a few iterations.

Asefa et al., (2013) explained the application of WetSpass model for analysis of the effect of land use changes on the groundwater discharge areas for a basin, of the area WetSpass recharge outputs for the river basins were used as an input for the groundwater model. Total discharge and surface runoff and base-flow were used for the calibration of the WetSpass water balance components. The associated groundwater model was also calibrated along with the WetSpass model calibration. Lastly, the resulting groundwater discharge areas were verified by mapped areas. It is also used in the analysis of hydrological characteristics of the sub-basin.

Salem and Mustafa, (2019) carried out the assessment of groundwater recharge, evaporation, and runoff in the Drava Basin, Hungary using WetSpass model. WetSpass-M, a GIS-based spatially-distributed water balance model, was implemented to assess monthly, seasonal, and the annual averages of groundwater recharge, surface runoff and actual evapotranspiration during 2000 to 2018. The basic input-data for the WetSpass-M model was prepared as grid-maps using the ARCGIS tool. It comprises monthly climatological data (rainfall, temperature, wind speed), distributed land cover, soil map, groundwater depth, topography, and slope. The findings of the WetSpass-M model are intended to support integrated groundwater modelling. The analysis of simulation results shows that WetSpass-M model works properly to simulate hydrological water budget components in Drava basin. Moreover, a better understanding of the simulated long-term average spatial distribution about water balance components is useful for managing and planning the available water resources in the Drava basin. The outputs of the WetSpass-M model revealed a favourable structure of water balance in the Drava flood plain, with the dominance of groundwater recharge. Thus, using this estimated groundwater recharge assessment is recommended for developing groundwater flow.

Mathenge and Gathuru, (2020) evaluated the spatial-temporal variation of groundwater recharge from precipitation in the semi-arid Stony Athi sub-catchment. The study demonstrated the importance of physically-based spatially-distributed hydrological models in estimating water balance. The study provides a theoretical basis for scientific, rational resource allocation and utilization as well as creating awareness of the need to enhance groundwater governance. Results from this study

can be used as an input for building an integrated groundwater model and also for evaluation of potential sites for managed artificial recharge through harvesting runoff to improve groundwater storage.

2.8 Modular Finite Difference Groundwater Flow Model (MODFLOW)

Among the most used approaches in groundwater modelling considering physical parameters, numerical techniques namely, Finite Element Method (Zienkiewicz, 1971; Pinder and Gray, 1977; Yeh and Huff, 1983; Voss, 1984; Istok, 1989 and Kazda, 1990) and Analytical Element Method (Freeze and Witherspoon, 1966) and Finite Difference Method (Pinder and Bredehoeft, 1968; and McDonald and Harbaugh, 1988). All techniques have their own advantages and limitations with respect to availability, costs, user friendliness, applicability, and required knowledge of the user. However, the application of the three-dimensional groundwater models has been limited in developing countries due to the lack of adequate and good-quality data. Although a lot of studies are available in the area of groundwater flow simulation modelling, most of them deal with the simulation of groundwater flow in single-layered aquifer systems. Very limited studies exist in the literature concerning the simulation of groundwater flow in multi-aquifer systems.

There is no unique criterion that defines a good calibration. Out of many advisable calibration aids graphical comparisons are extremely useful (Hann et al., 1982). Continuous time series plot of the recorded and simulated series and a scatter plot of observed heads plotted against simulated heads are used. These graphical techniques simulate very important man-machine interaction in model calibration. Louie et al., (1984) developed linear programming software to solve multi-objective optimization problems with linear constraints. Their study simultaneously considered three different objectives namely, a) the location of the water supply, b) water quality control, and c) the prevention of groundwater overdraft. The response matrix then links the optimization and simulation models.

Willis and Liu, (1984) developed a bi-objective optimization model for the Yunlin area of southwest Taiwan, in which the response matrix was used to predict an inhomogeneous and isotropic aquifer system. Parametric linear programming

was used to generate optimal planning policies (the set of non- inferior solutions), and determine the relationship of the total water deficit with the maximum pumping rate and minimum permissible head values in the aquifer system. The groundwater resources management problems have been solved by using a large number of simulation (Freyberg 1988; Sorooshian and Gupta 1995; Hunt et al. 1998; D'Urso et al. 1999; Kite and Droogers 2000; Pint et al. 2003; Poeter 2007; Michael and Voss 2008; Budge and Sharp 2009; Harou et al. 2009; Wondzell et al. 2009; Yang et al. 2009; Sanford and Pope 2010; Sherif et al. 2012; Singh 2013a) and optimization (Andricevic and Kitanidis 1990; Misirli and Yazicigil 1997; Mantoglou 2003; Ayvaz 2009; Gaur et al. 2011; Tan et al. 2011; Singh 2012c, 2013b, 2014a) models. However, during the recent past, researchers have actively sought to combine simulation models with optimization techniques to address the groundwater management problems.

MODFLOW a modular three-dimensional groundwater flow model assumes that aquifers consist of porous media only [McDonald and Harbaugh, 1988]. Because of its ability to simulate a wide variety of systems, its extensive publicity, available documentation, and its rigorous USGS peer review, MODFLOW has become the worldwide standard groundwater flow model. MODFLOW is used to simulate systems for water supply, contaminant remediation and mine dewatering. When properly applied, MODFLOW is the recognized standard ground Water model (Kumar, 1992; Pollock, 1994; Anderman and Hill, 1997; Restrepo et al., 1998; Hill et al., 2000; Konikow, 2001, Jyrkama et al., 2002).

Sophocleous et al., 1995 used MODFLOW to assess the predictive accuracy of stream-aquifer solutions; the three most important factors tested, which relate to the multidimensional nature of the aquifer flow conditions, were namely, a) streambed clogging as quantified by streambed-aquifer hydraulic conductivity contrast, b) degree of stream partial penetration and c) aquifer heterogeneity. Numerical modelling of groundwater flow in a multi-aquifer system is quite recent advancement. Studies on groundwater flow in multi-layered aquifer systems have been carried out by several researchers using analytical techniques. Some recent studies dealing with the numerical simulation of groundwater flow in a two or more-layer aquifer system are discussed here. A four-layered groundwater flow model was developed by Amar et al., (1997) using MODFLOW. Modelling indicated that

the groundwater recharge was required to prevent soil desaturation, to minimize the recontamination of groundwater due to rebounding water levels and to provide continuous flushing of soils. Model results were used successfully to modify the existing record of decision design.

Modelling of an aquifer in basin wise scale is quite a difficult task because of high heterogeneity (Singhal and Gupta 1999; Bridget et al. 2003; Nico and David 2007). This basic fact inherently renders the discretization of the medium and interpolation of the hydrogeological parameters, which is relatively difficult and at times unrealistic. Inspite, of these difficulties, many researchers (Rani and Chen 2010; Bridget et al. 2003) have successfully utilized numerical models in estimating the regional groundwater budget in hard rocks as well as in karst aquifer groundwater systems.

Thangarajan et al., (2000) simulated a multi-leaky aquifer system in Shashe river valley (Okavango delta), Botswana to study the aquifer response and thereby evolve the optimum pumping schemes. In order to quantify the upward flow from the saline unit, a multi-layer model was constructed and calibrated for both steady state and transient state condition. The calibration showed that vertical conductivity (K) of the confining layers has a considerable influence on the hydrodynamics of multi-aquifer system. The upper reaches of the middle semi-confined aquifer are likely to become concentration of total dissolved solids. The study suggested that the situation may be improved by reconfiguration of well fields.

Three-dimensional groundwater modelling experiments have been developed by Reeve et al., (2001) to simulate the groundwater flow in the Glacial Lake Agassiz Peatlands of northern Minnesota, USA. The steady-state MODFLOW model encompassing an area of 10,160 km^2 was constructed for groundwater simulation. The calibration of the model was done by adjusting hydraulic conductivity values and was based on comparison of measured hydraulic heads with simulated heads, creation of flowing artesian conditions in areas where flowing wells are known, and comparison of stream gauging data with simulated runoff. The sensitivity of the model parameters was determined by calculating a mean absolute error (MAE) within the layer of the model. Numerical solutions indicated that the Itasca Moraine, located to the south of the peatland, acted as a recharge area for regional groundwater flow. Groundwater flow within the peatlands consisted of

local-flow systems with streamlines less than 10 km long and the groundwater from distant recharge areas did not play a prominent role in the hydrology of these peatlands.

In order to determine the groundwater interface movement in unconfined aquifer of Punjab, Pakistan, MODFLOW and MT3D model was developed by Asghar et al., (2002). The hydraulic conductivity (horizontal and vertical) and specific yield of the aquifer were used as parameters during calibration of MODFLOW, whereas the longitudinal, horizontal transverse and vertical transverse dispersity were used as parameters during calibration of MT3D model. The sensitivity of the depth to water table, discharge rate, thickness of the fresh groundwater lens, well penetration ratio, and daily operating hours on salinity of pumped groundwater was studied. The model results indicated that the skimming wells of 10-18 m can be installed and operated successfully with 60-70% well penetration ratio for an operating time of 8-24 h/day from an unconfined aquifer having 15-18 m thick relatively fresh groundwater lens. However, the extraction of water using skimming wells from inappropriate depths and rates will cause upcoming of the interface between the relatively fresh groundwater Jens and salty groundwater.

Stream-aquifer interaction from seasonal groundwater pumping was studied by Chen and Shu, (2002) in China using MODFLOW. The river package in MODFLOW was used to simulate the flow between the stream and aquifer, where groundwater is pumped for 90 days followed by a 275-day non-pumping period. Depletion rates and volumes of reduced base flow and induced stream infiltration during pumping and post-pumping periods were analysed. The model results suggested that for a shallow penetrating stream with a low streambed conductance, base flow reduction accounts for a significant percentage of the total stream depletion with longer residual effects during post pumping. In contrast, the contribution of the induced stream infiltration to the total stream depletion was much smaller, and its effect became negligible shortly after pumping was stopped. Similarly, to investigate the effects of stream aquifer fluctuations, aquifer properties, and the hydraulic conductivity of streambed sediments, regional hydraulic gradient and recharge and evapotranspiration rates on stream aquifer interaction are necessary.

A mathematical model was developed by Anandha and Sinha, (2003) using MODFLOW to generate alternative management scenario to evolve optimal conjunctive use strategy. The model was calibrated using field hydrographs and observed and computed water table contours. It was then used to develop different water use scenarios and their effect on the groundwater regime. The studies showed that the water logging condition prevailing in part of the Hirakund command area can be controlled by development of groundwater in conjunction with surface water without any deterioration to the groundwater regime.

Chen and Chen, (2003) conducted a numerical modelling study using MODFLOW and MODPATH. They concluded that bank storage solely caused by stage fluctuations differs slightly between losing and gaining streams. Lin and Medina, (2003) incorporated transient storage concept in modelling solute transport in the conjunctive stream-aquifer model. Three well- documented and widely-used USGS models were coupled to form the core of this conjunctive model viz., a) MODFLOW for simulating groundwater flow in the aquifer, b) DAFLOW for computing unsteady streamflow and for simulating stream-aquifer interaction, and c) MOC3D for simulating solute transport in the groundwater zone. In addition, an explicit finite difference package was developed to incorporate one-dimensional transient storage equations for solute transport in streams. The quadratic upstream interpolation algorithm was employed to improve the accuracy of spatial differencing and an adaptive step-size control algorithm for the Runge-Kutta method was used to increase overall model efficiency. The modelling results indicated that the conjunctive stream-aquifer model with a transient storage can effectively handle the bank storage effect during flooding event.

A conjunctive management model developed by Barlow et al., (2003) by coupling a numerical simulation model MODFLOW with a linear optimization model to evaluate trades off between groundwater withdrawals and streamflow depletions for the Hunt- Annaquatucket -Pettaquamscutt stream- aquifer system of Central Rhode Island, USA. The objective of the optimization model was to maximize total annual groundwater withdrawal from the aquifer, subject to streamflow depletion constraint and pumping capacity constraint. The developed optimization model was solved using LINGO software. The results of the

simulation-optimization model indicated that it is possible to increase the amount of current withdrawal from the aquifer by as much as 50% by modifying current withdrawal schedules, modifying the number and configuration of wells in the supply well network, or allowing increased streamflow depletion in the Annaquatucket and Pettaquamacutt rivers.

Similarly, Chen and Chen, (2003) conducted a numerical modelling study using MODFLOW and MODPATH to investigate the effects of stream aquifer fluctuations, aquifer properties, hydraulic conductivity of streambed sediments, regional hydraulic gradient and recharge and evapotranspiration rates on stream aquifer interaction. They concluded that bank storage solely caused by stage fluctuations differs slightly between losing and gaining streams.

Palma, (2003) conducted a study in the Leon-Chinandega aquifer located northwest of Nicaragua. This shallow unconfined aquifer of 1300 km^2 is one of the most important groundwater reservoirs in the country. A sub-basin of 330 km^2 was selected to study the groundwater flow system using a numerical groundwater flow model using Visual MODFLOW. Transient and steady state models were constructed based on a comprehensive conceptual model. Two flow systems were identified viz., a) a deep regional system recharged in the Cordillera and discharged in the central and lower plain and b) a shallow local system, recharging in the central plain and discharging at lower elevations. Rivers are responsible for the relative stability of hydraulic heads in the system, but base flow is very sensitive to any stress change. Decrease in river discharge induced by pumping becomes very critical during dry periods. It was found that the response time of the aquifer is about one hydrologic year, which allows developing management strategies within short time horizons. Simulations can be used to establish a balance between desirable groundwater development and reasonable levels of surface water depletion.

Vijaya Lakshmi, (2004) used MODFLOW in Munneru river basin and concluded that groundwater levels are progressively lowering and recommended for groundwater recharge in the basin. Mahesh Kumar, (2004) developed a steady state ground water flow for north-east Musi basin using Finite Difference method with MODFLOW by assuming 8 to 10% of annual recharge. The recharge was

estimated as 2.4 MCM based on the water balance computation in steady-state, out of which 1.1 MCM was contributed by lakes. The outflow and groundwater draft were estimated as 0.4 MCM and 2.1 MCM respectively. It has been found that the total input and output to catchments of Ownansagar and Himayathsagar reservoirs are 33.69 MCM, 36.99 MCM and 83.62 MCM, 82.68 MCM respectively under 8-10% of recharge conditions (EPTRI and NGRI, 2005). Under steady-state groundwater flow model using Visual MODFLOW the draft is found to be 35 MCM and 77 MCM for catchments of Osmansagar and Himayathsagar reservoirs respectively.

Neville and Tonkin, (2004) proposed numerical analysis of flow through wells in multi-aquifer system using both conventional (WEL package) and advanced (MNW package) approaches. They described a method in which the contributions of the aquifers are assigned in proportion to their transmissivities using MODFLOW. They examined the performance of the above two methods in the context of a benchmarking study against the analytical solutions of Papadopulos, (1966). It was found that the results obtained by the MNW package closely matches with the exact solutions for pumping and non-pumping conditions using both coarse and fine grids.

Abdulla and Assad, (2005) have studied modelling of groundwater flow for Mujib aquifer, Jordan. The results of the calibrated model showed that the horizontal hydraulic conductivity of the B2/A7 aquifer ranges between 0.001 and 40 m/d. The calibrated specific yield ranged from 0.0001 to 0.15. The water balance for the steady state condition indicated that the total annual direct recharge is 20.4 $\times 10^6$ m^3, the total annual inflow is 13.0 $\times 10^6$ m^3, springs discharge is 15.3 $\times 10^6$ m^3, and total annual outflow is 18.7 $\times 10^6$ m^3. Different scenarios were considered to predict aquifer system response under different conditions. The results of the sensitivity analysis showed that the model is highly sensitive to horizontal hydraulic conductivity and anisotropy and with lower groundwater level to the recharge rates. The model is also sensitive to specific yield.

An integrated groundwater modelling approach done by Sekhar, (2005) for better assessment of water balance components. The study showed the impact of pumping resulted in regional groundwater flows influencing the hydro geological

regime in the recharge zone of the sub basin. MODFLOW was calibrated assuming specified transmissivities for each of the zone, obtained from several pump tests in the region. The calibrated model was used to simulate the behaviour of the groundwater system using variable draft systems. The simulated responses for the water levels were in good agreement with the observed data.

Gurwin and Lubczynski, (2005) developed a numerical groundwater model for a multi-aquifer system of the Swidnica area. In this study, groundwater modelling system (GMS) was used to develop a conceptual model on the basis of borehole-log data and for calibration of the multi-aquifer flow model. The conceptual model revealed that the upper aquifer is unconfined and the two deeper aquifers are confined in nature bounded by two aquitards consisting of clay formations. A steady state calibration was performed using groundwater level (quasi-natural simulation) data and transmissivity data from pumping test data analysis. In the calibration process, a total of 386 uniformly distributed piezometers were used, 219 points in Aquifer I, 172 in Aquifer II and 95 in Aquifer III. A good calibration match between observed and calculated groundwater levels was achieved for all the three aquifers. The calibration results indicated a substantially lower horizontal hydraulic gradient in the third aquifer as compared to the other two aquifers because of the higher transmissivity values. The three aquifers were found to receive recharge from the groundwater inflow from the Sudety mountains along the fault zone boundary, from rainfall, recharge from river and from lake infiltration. The regional groundwater flow direction as obtained from simulation is from the SW to the NE boundary of the model. It is recommended that systematic monitoring of the groundwater level and river discharges is needed to simulate dynamic hydrogeological processes in a more reliable transient manner.

An artificial groundwater recharge model was developed using MODFLOW in the Xanthi plain, Greece by Pliakas et al., (2005). During calibration, the model sensitivity to the transmissivity of the aquifer system was the main focus as the storage coefficient had a negligible effect on the simulated groundwater levels. The validation of the model was found to be good for the first 7 years (1995 to 2001), while for the remaining 2 years (2002 and 2003), the results of groundwater level simulation were unacceptable because of the presence of low dam across the stream course.

A groundwater/surface-water interaction model using MODFLOW and its stream package was developed by Rodriguez et al., (2006) for the shallow alluvial aquifer of Choele Island, Patagonia, Argentina. The model was successfully calibrated by trial-and-error procedure by matching simulated heads with observed heads and simulated stream stages, during July 1998 to April 1999. The results indicated that drainage through streams was significantly higher than drainage through artificial drains. The stream-aquifer interaction was found very approachable to water-table rises due to irrigation and it was considered as variation in gaining/losing character of stream reaches. The model presented a better perceptive of the coupled system to explicate some of the causes of a rising water table on the island.

Venkateswara Rao, (2006) developed a steady state groundwater flow model of Upper Musi basin using MODFLOW. The groundwater draft (output) has been estimated to be about 177.5 MCM and river leakage was estimated as 120 MCM with outflow of 0.4 MCM under the assumed groundwater recharge of 8-10% of the annual rainfall. A combined distributed hydrological model using WetSpass and MODFLOW models was designed by Idrysy and Smedt, (2006) for modelling in the Trifa aquifer, Morocco. The study yielded information on relevant parameters including groundwater recharge and the estimated amount of pumped groundwater needed to meet the irrigation demands. The basin-scale modelling provided an insight into the status and evolution of the groundwater reserves. The results of this study were useful to predict the sustainability of groundwater resources in the Trifa plain for evaluation of possible management actions. The model indicated that a reduction in groundwater abstraction by at least 25% was necessary to achieve sustainable conditions.

Madabhushi et al., (2006) had attempted to solve the problem of groundwater flow in porous media using MODFLOW. While MODFLOW performs satisfactorily in solving simple two- or three-dimensional problems, it takes a large computational effort when used to solve flow through layered soil strata with varying hydraulic conductivities. The modular structure of the code renders itself for the development of a parallelized code. Barth et al., (2006) carried out the application and investigation of a loosely coupled modelling approach,

combining two well-known models the Precipitation Runoff Modelling System (PRMS) and MODFLOW in order to simulate complex hydrological processes in Esperstedter Ried basin, an ungauged, mesoscale groundwater-dominated catchment in central Germany. The results of the case study demonstrated the potential of coupling of surface water model and groundwater model to obtain more complex and accurate analyses and simulations of hydrologic systems.

Abu-El-Sha'r and Hatamleh, (2007) used MODFLOW and MT3D groundwater flow and transport models as a management tool for Azraq groundwater system, Jordan. Five scenarios of pumping with different abstraction rates during years 2005 through 2020 have been explored using MODFLOW PM5. The solute transport model, MT3D was used to predict the transport of total dissolved solids given in terms of electric conductivity (EC). Different parameters including EC, groundwater recharge, model boundary conditions and advection parameters were adjusted for model runs and simulations. The simulation results indicated that the effect of the different scenarios on EC are less profound as compared to their effects on drawdown values.

MODFLOW was employed by Yaouti et al., (2008) in Groundwater Modeling System (GMS) to simulate the behaviour of flow system, under different stresses in the unconfined aquifer of Bou-Areg, Morocco. The two-layer model was calibrated in two steps viz., a) a steady-state calibration using observed groundwater levels of l990, and b) a transient calibration and verification, using observed groundwater levels from 1990 to 2006. The mean error (ME) and root mean squared error (RMSE) were used as evaluation criteria during calibration in which the hydraulic conductivity distribution was optimized using a combination of trial-and-error and automated inverse methods. The results of the model validation showed a reasonable agreement between observed and simulated groundwater levels. The model was found more sensitive to recharge than to hydraulic conductivities and storativity. Simulation of the hydraulic heads the results indicated that in order to raise the groundwater level by 1 m, there must be 50% increase of recharge and 50% reduction of groundwater withdrawal.

The semi-distributed SWAT model was integrated with the fully distributed groundwater-flow model, MODFLOW by Kim et al., (2008) and applied this

combined model to Musimcheon basin, Korea. The calibration and validation of SWAT were carried out using daily streamflow data of 2000- 2002 and 2003-2005, respectively. The SWAT-MODFLOW model reproduced the streamflow dynamics of the basin better than the sole SWAT model. It was demonstrated that an integrated SWAT-MODFLOW model is capable of simulating spatio-temporal distribution of groundwater recharge rates, aquifer evapotranspiration and groundwater levels. The advanced water transfer method in the SWAT-MODFLOW was successfully tested, and reproduced the distributed drawdown and reduced streamflow by pumping with multiple wells. It was concluded that the developed model would be beneficial in planning for the sustainable development of groundwater resources.

Visual MODFLOW was used by Zume and Tarhule, (2008) to evaluate the impacts of groundwater exploitation on streamflow depletion in the Alluvium and Terrace aquifer at Beaver-North Canadian River (BNCR) in north western Oklahoma, USA. Using MODFLOW's streamflow routing package, the pumping-induced changes in base flow and stream leakage were analysed to estimate streamflow depletion in the BNCR system. The simulation results indicated that groundwater pumping reduced the base flow to streams by approximately 29% and also increased stream leakage into the aquifer by 18% for a net streamflow loss of 47%. The magnitude and intensity of streamflow depletion, however, varied in different stream segments. The method provided a framework for isolating and quantifying impacts of aquifer pumping on stream function in semi-arid alluvial environments.

Aquifer response to various pumping strategies were analysed by Rejani et al., (2008) using the two-dimensional groundwater flow and transport model MODFLOW for the Balasore coastal groundwater basin. The transient model calibration was done for 1997-2000 and validation was done for 2000-2001 periods. The mean error (ME) and root mean squared error (RMSE) were used as evaluation criteria. Using the calibrated and validated model, the groundwater response to five pumping scenarios under existing cropping conditions was simulated. The results of the sensitivity analysis indicated that the Balasore aquifer system is more susceptible to the river seepage, recharge from rainfall and interflow than the horizontal and vertical hydraulic conductivities and specific storage. Based on the modelling results, salient management strategies were suggested for the long-term

sustainability of groundwater resources of the basin. The most promising management strategy for the basin was found to be a reduction in the pumpage from the second aquifer by 50% in the downstream region and an increase in the pumpage to 150% from the first and second aquifers at potential locations.

Rao et. al., (2009) studied groundwater flow modeling in the upper Anga River watershed, Yaounde, Cameroon. The simulation converged after 170 iterations with a convergence criterion of 0.01 m. The computed groundwater level are resembled with the observed groundwater levels. The results indicated that the topography controls the groundwater flow in the watershed and that base flow to river is an important factor that moderates the groundwater movement. Kushwaha et. al., (2009) used MODFLOW based groundwater resource evaluation and prediction in Mendha subbasin, Rajasthan. The model was run to generate groundwater scenario for a 15-year period from 2006 to 2020 considering the existing rate of groundwater draft and groundwater recharge. The water budget indicated a decrease from 349.50 to 222.90 MCM in the groundwater storage, whereas groundwater abstraction showed an increase from 258.69 to 358.74 MCM per year.

Mondal and Singh, (2009) used mass transport modelling of an industrial belt using Visual MODFLOW and MODPATH. The study indicated that even if the pollutant sources were reduced to 50% of the present levels, the TDS concentration level in the groundwater, would not be reduced below 50%, even after 20 years. The study suggested immediate measures for arresting the deterioration in groundwater quality and augmentation for restoration of the aquifer in some parts of the study area.

Studies on groundwater flow modelling of Yamuna-Krishna interfluve, a part of Central Ganga Plains, Uttar Pradesh was carried out using MODFLOW by Ahmed and Umar, (2009). The horizontal flows, seepage losses from unlined channels recharge from rainfall and irrigation return flows were simulated using different boundary packages available in the Visual MODFLOW. Transient calibration of the model was done using the groundwater level data during 1999 to 2007. The sensitivity of the model to input parameters was tested and it was found that the model is most sensitive to hydraulic conductivity and recharge parameters.

Three scenarios were considered to predict aquifer responses under varied conditions of groundwater abstraction. The simulation results for different scenarios indicated that artificial recharge of groundwater and conjunctive use of surface and groundwater is required in order to mitigate the water table decline.

AI-Salamah et al., (2011) used MODFLOW for groundwater modelling at Saq aquifer, Buraydah Al Qassim, Saudi Arabia. Transient calibration of the model was carried out using the observed groundwater level data during 1999 to 2008. Model predictions were done for very long future period of 27 years (2008-2035) for different scenarios of pumping rates. It was concluded that a decrease in pumping rate by 10% for 10 years can result in the prolonging of aquifer life by about 50%. The prediction results indicated that pumping from the Saq Aquifer in Buraydah area would result in significant drawdown by 2035, if the existing excessive pumping rates prevail in the study area.

Mondal et al., (2011) estimated the average groundwater recharge in hard rock area in southern India as about 80-250 mm/year, which is equivalent to 12-37% of annual rainfall. The total groundwater abstraction is about 80.43% of annual groundwater recharge. Hernandez et. al., (2012) worked on modelling groundwater levels on the Calera aquifer region in Central Mexico using MODFLOW. The results of the model evaluation were good with coefficients of determination of 0.81 and 0.67 and root mean square error value lower than 25.1 and 25.9 m during calibration and validation respectively. These results are indicative of a good agreement between predicted and observed groundwater levels. However, further improvements in the conceptual model may be needed to improve prediction for evaluating alternative groundwater management strategies.

Xu et al., (2012) used the SWAP package with MODFLOW-2000 for proper estimation of groundwater recharge and evapotranspiration in Upper Yellow River basin of North China. The entire aquifer system was vertically divided into four different layers and drainage ditches were considered as drain boundaries. The model performance was evaluated by using root mean squared error and model efficiency for the groundwater level data of ten observation wells. The calibration and validation results indicated a good correlation between observed and simulated groundwater levels, thereby implying reasonably well simulation of groundwater

levels and vadose zone dynamics. It was concluded from the results that the coupled SWAP and MODFLOW provides greater insights into spatial and temporal variation of groundwater and evapotranspiration in the study area.

Shri Kant et al., (2013) studied the groundwater flow in Sonar subbasin, Madhya Pradesh using Visual MODFLOW. The simulated results obtained from the calibrated and validated model were found to be in good agreement with the observed data. A comparative evaluation of Visual MODFLOW and artificial neural network (ANN) for simulating groundwater levels was carried out by Mohanty et al., (2013) in a river island within Mahanadi deltaic system, India. The transient calibration of the model was performed using weekly groundwater level data of 19 observation wells for the period 01 February 2004 to 04 June 2006 and validation was carried out for June 2006 to May 2007 period. The performance of the model was evaluated by using statistical as well as graphical indicators. In case of ANN, feedforward neural network architecture was used, which has one hidden layer, 40 nodes in the input layer and 18 nodes in the output layer. Out of the available 174 weeks dataset, 122 datasets were used for training ANN models and 52 datasets were used for testing them. The comparative study revealed that ANN provides better prediction of groundwater levels as compared to MODFLOW for short-term predictions, whereas MODFLOW is more appropriate for long-term predictions.

Complex drainage problems in an irrigated date palm orchard of Argaman, Jordan Valley, Israel was studied and resolved by Mirlas (2013) based on the drainage model developed using MODFLOW. The hydrogeological conditions of the study area including groundwater status, dynamics, and other required parameters to perform the modelling were calculated by survey of the study area. The study area was conceptualized as a three-layered aquifer system. The developed model was calibrated by using the water level from 11 observation wells during July 2010 to July 2011 and the comparison of observed and simulated groundwater levels was found to be reasonable. The sensitivity analysis showed that the developed model is insensitive to changes in specific storage and hydraulic conductivity of the study area. The groundwater depth after one year was predicted, in different drainage conditions using the developed model. It was suggested that a drainage system comprising of 4.5 m deep primary drains combined with 3 m deep

drains installed with different spacing and of different lengths would be helpful in overcoming the salinity related issues in the Argaman orchard.

Nassim et al., (2013) used MODFLOW for evaluation of groundwater resources in the alluvial aquifer in Evan sub basin, Iran. The model was calibrated and validated using historical and observed groundwater level data during 2005 - 2006 and 2006 - 2007, respectively. The model was run to generate groundwater scenario for a 10-year period from 2005 to 2015 considering the existing rate of groundwater draft and recharge. The water budget predictions indicated a decrease in groundwater storage from 8.34 to 4.43 MCM. The study indicated that over exploitation of groundwater will lead to extreme reduction of water resources.

The groundwater resource modelling was done by Tiwari V., (2014) in Narsinghpur district of Madhya Pradesh, using Visual MODFLOW based multi-layer ground water model. The ground water predictions were made considering 12% increase of annual groundwater abstraction till year 2025. The results indicated decline of water level up to 2-7 m from existing level, similarly the recharge scenario was also predicted for annual increment of recharge by 9%. The study concluded there will be a need in future to use groundwater cautiously to arrest the groundwater depletion. The study emphasized on reducing irrigation stress, increasing recharge and change in cropping pattern in future for sustainable crop production.

An assessment of groundwater resources and analysis of future groundwater exploitation scenarios was studied by El Alfy, (2014) using a three-dimensional numerical model using MODFLOW in the east part of Owienat, Western Egypt. The transient calibration of the model was performed for 1984-2010, whereas model validation was carried out for 2011. The groundwater response to three scenarios for different management scenarios were evaluated for the future, 2011-2041. The results of sensitivity analyses revealed that hydraulic conductivity and boundary conditions are highly sensitive for groundwater level simulations, whereas specific storage of the aquifer was found to be least sensitive. Based on the modelling results, a pumping scenario comprising of a gradual increase in pumping over the next 30 years, with 150% from the current conditions at the end of 30 years, was found to be appropriate for sustaining long-term groundwater availability. Looking into the ever-increasing demand for water for irrigation, it was

recommended to use modern irrigation techniques to reduce major wastages in agricultural sector.

Lathashri and Mahesha, (2015) used SEAWAT-2000 to simulate groundwater flow and transport for a coastal stretch in Karnataka, India. SEAWAT is a coupled version of MODFLOW and MT3DMS designed to simulate three-dimensional, variable density groundwater flow and multi-species transport. The variable density flow process uses the familiar and well established MODFLOW methodology to solve the variable density groundwater flow equation. The aquifer considered for the present study is bounded by Arabian sea on the west, the ridge line along the east and Shambhavi and Pavanje rivers along the northern and southern sides respectively. The aquifer parameters were estimated by calibrating the model for two-year period at a daily time step. The aquifer can be categorized as unconfined having good groundwater potential with aquifer transmissivity and specific yield ranging from 10 to 810 m^2/day and 0.0008 to 0.0122 respectively.

Putthividhya and Laonamsai, (2017) carried a study for in Sukhothai province of Thailand. The SWAT model was used for the spatio-temporal simulation of surface water and for estimation of groundwater recharge. The sensitivity analysis, calibration, validation, and uncertainty analysis were performed using SWAT-CUP. Due to the semi-distributed features of SWAT and the difficulty of calculating groundwater distributed parameters, recharge values estimated by SWAT were used as input to MODFLOW, for steady and unsteady state simulation of groundwater levels. SWAT and MODFLOW models were successfully tested and the results of the combination of the two models were found acceptable for effective water management and conjunctive use of surface water and groundwater in the study area.

Moharir et. al., (2017) used MODFLOW to study the shallow aquifer in the Deccan Basalts. The inverse modelling of aquifer parameters in basaltic rock have been carried out with the help of pumping test. The shallow aquifer within the Deccan Basalts rock to understand the groundwater system and management including quantification of the groundwater recharge and assessment of the effect of pumped irrigation wells on the local water level table was studied in this shallow aquifer. It was advocated that there is a clear need for such research involving the results of pumping test and inverse modelling.

Saleem et al., (2019) assessed the behavior of the flow system and water balance for a part of Yamuna-Hindon River by groundwater flow modeling. MODFLOW was used to quantify groundwater flow, using steady-state finite difference model with groundwater data from 26 tube wells in the Greater Noida region. In this study, hydraulic conductivity and recharge parameters are analyzed using MODFLOW. Sanginabadi et. al., (2019) studied groundwater drought, water scarcity, and their compound impact in over-drafted aquifers based on a new evaluation index. Groundwater drought analysis was performed using the standardized groundwater index (SGI) on the naturalized groundwater level time series. The MODFLOW groundwater simulation tool and a surrogate ANN model were adopted to obtain the time series of the naturalized groundwater level in Qazvin plain, Iran, during 1966 to 2016. Moreover, a water scarcity index, namely the deficit rate (DR), and a drought water scarcity (DWS) index were introduced. The results indicated that the abstraction could cause a severe negative trend in the groundwater level in comparison with natural causes (drought). Furthermore, the use of the DWS index revealed that the safe yield of the Qazvin aquifer was about 44% of the existing abstraction volume. It was concluded that the DWS index represents a comprehensive criterion in water resource assessment and groundwater safe yield computations.

Bailey et al., (2020) suggested an updated version of SWAT-MODFLOW that allows its application to large river basins in semi-arid region. SWAT-MODFLOW performance was demonstrated for the 470 km^2 Middle Bosque River watershed, Texas, USA. The model captured the dominant baseflow patterns throughout the watershed and the key patterns of water table dynamics and its relation to nearby streams. MODFLOW provides spatial values of groundwater head, groundwater flow rate, and exchange rates of groundwater and surface water that are provided to SWAT stream channels for stream flow simulation whereas SWAT provides the groundwater recharge as input to MODFLOW. Lamichhane and Shakya, (2020) studied the rapid urbanization in Kathmandu Valley and quantified the spatial distribution of recharge and changes in drawdown under pumping rate as well as land use / cover change scenarios. Both scenarios were incorporated in MODFLOW. The results of this study quantified the spatial distribution of recharge rate and depth, impact of recharge area encroachment and

increase in pumping rate and its effect on the groundwater level and drawdown which may be useful in planning groundwater management, groundwater allocation, and design of interventions for sustainable management of groundwater resources in the Kathmandu Valley.

Patil et al., (2020) studied the impact of climate change and its effect on groundwater levels in the Hiranyakeshi watershed using Visual MODFLOW Flex. The model calibration was achieved by Parameter Estimation (PEST), and the model performance was evaluated using R^2, RMSE and NRMSE. It is observed that R^2, RMSE and NRMSE obtained are 0.98, 1.68 and 3.41% respectively. The results from the model simulation gave an increase in head of 1.8 m during the five years of simulation period. The model was again simulated for the A1B climate change scenarios for the period 2021-2050 using Hadley Regional Model 3 (HadRM3) to measure the effects of climate change on the groundwater recharge. Based on the long-term output analysis, it is expected that there may be an increase in the average annual temperature by 2.59^{o}C, precipitation by 81.50% and groundwater recharge by 24.91%.

2.9 Model MUSE

Model Muse, developed by the U.S. Geological Survey (USGS), is a widely used groundwater modeling software known for its user-friendly interface, robust numerical algorithms, and flexibility in model construction (Niswonger et al., 2011). It incorporates various modeling components, including MODFLOW for flow simulations, MT3DMS for transport modeling, and PEST for parameter estimation (Hill et al., 2000). Model Muse has been applied in diverse hydrogeological settings, such as aquifer characterization (Abd-Elhamid et al., 2010), and analysis of managed aquifer recharge (Niswonger et al., 2013). Its versatility allows for the simulation of complex hydrogeological processes, including groundwater-surface water interactions (Morway et al., 2016) and multi-phase flow (Thorne et al., 2015).

Nyende et. al., (2018) studied numerical simulations of a conceptual hydrogeological model to demonstrate that flow to highly transmissive fractured zones is primarily regulated by their transmissivity or structural properties. While

recharge remains a significant factor, predominantly via leakage through the regolith unit, especially near the outcrop of the fractured zone where the overlying rock is thinner, which ensures groundwater availability. This scenario is demonstrated in the Pallisa aquifer in eastern Uganda, situated within a crystalline rock geological setting, where shallow fractured zones serve as the primary water source for rural communities. The hypothesis of a continuous porous medium unit was sustainable as a first approximation to construct a numerical Model MUSE model covering the full extent of the aquifer. Simulation results underscore the potential of weathered and fractured zones as aquifers across diverse hydrogeological contexts, emphasizing the significance of regolith leakage in enhancing water availability in the basement complex fractured rock unit.

Mescher, L., (2018) used MODFLOW 2005 with MT3D to build a model for simulating contaminant transport in Borden, Ontario. At the Borden site, in 1982, a solution of eight solutes were injected to test the transport of contaminants over three years. Initial simulations showed similar transport characteristics for chloride and carbon tetrachloride as compared to observed results. However, the concentration distributions varied significantly between observed and simulated results. MODFLOW with MT3D-USGS proved effective in modeling transport characteristics for the Borden site.

Tsela et. al., (2021) recommended numerical modeling is an effective tool for managing groundwater resources and predicting future responses. MODFLOW 6 and Model MUSE was used to assess the groundwater flow in Pointe-Noire coastal aquifers. Different model parameters including evapotranspiration, recharge, model boundary, etc. were adjusted to run and fine-tune the model. The results showed that the scenario with the highest pumping rate has the biggest effect on the drawdown and seawater intrusion extent.

2.10 Hydrologic Engineering Centre – River Analysis System (HEC-RAS)

Flood inundation modelling comprises hydrologic modelling, hydraulic modelling, and terrain analysis (Jung, 2011). Hydrologic modelling involves estimating flow discharges, either by employing regression equations to compute peak-flow data (Bisese, 1995; Austin et al., 2011) or by conducting detailed rainfall

simulations across the watershed drainage area to generate runoff hydrographs (Bravo et al., 2012; Kingston, 2012). Hydraulic modelling utilizes the discharge data to calculate water surface elevations and the spatial extent of flood inundation. It offers an accurate depiction of flow routing through the modelled river network, taking into account the backwater effects of floodplains in moderating and delaying peak flows (Bravo et al., 2012). Terrain analysis involves outlining the inundated floodplain areas in conjunction with Digital Terrain Models (DTM).

Hodges, (2009) defines hydrodynamic modelling as the application of conservation equations for momentum, continuity, and transport to represent the evolving fields of velocity, density, and scalar variables. This modelling approach provides valuable insights into spatial and temporal changes in physical processes that may be less evident from direct field observations (Hodges, 2014). The mathematical models, which try to reproduce fluid movement, are hydrodynamic models and they characterize the movement of water through the resolution of formulas generated by the rules of physics. The simulations can be categorized as 1D, 2D and 3D versions based on their spatial representation of flood plain stream (Teng et al., 2017).

Numerous researchers worldwide have effectively utilized the 1D HEC-RAS model for various rivers, such as the Al-Kahla River (Awad, 2015b) in Iraq, the Kalu River in Sri Lanka (Nandalal, 2009) and the Lighvan Chai River in Iran (Khaleghi et al., 2015). Additionally, Indian rivers like the Mahanadi (Parhi, 2013), Godavari (Kute et al. 2015), Tapi (Timbadiya et al., 2011a) (Timbadiya et al. 2014) (Mehta & Joshi, 2014), Jhelum (Ahmad et al. 2016), Waingangā (Ingale & Shetkar, 2017), Yamuna (Kumar et al. 2017), and Purna River (Azazkhan et al. 2017) have been successfully simulated using the 1D HEC-RAS model in recent years.

Similarly, the 2D HEC-RAS model has been applied globally for river basins and urban areas, such as the Kosi River basin (Kafle & Shakya, 2018), Bolivian Amazon (Quirogaa et al. 2016b), Cambodia (Thol et al., 2016), Kirsehir city area (Yalcin, 2019), the Greater Toronto area (Rincón et al., 2018), and the Lower Indus River basin (Rind et al., 2018). Additionally, researchers like Nandurkar et al. (2017) and Rangari et al., (2019) have effectively utilized HEC-RAS for developing 2D hydrodynamic models for Pune and Hyderabad cities, respectively, in India. The

combined use of 1D and 2D hydrodynamic models has been effectively applied for the development of coupled 1D/2D models for the Dharla River basin (Navera, 2018) and Jamuna River Basin (Ali et al. 2016) in Bangladesh, as well as the Lower Tapi River and Surat city (Patel et al., 2017) to generate flood inundation maps as part of flood management activities.

2.10.1 One-Dimensional hydrodynamic modelling case studies

Nandalal (2009) created an HEC-RAS model for a 79 km segment of Sri Lanka's Kalu River, from Ratanpura to Kalutara, to evaluate water levels. Using field surveys, the model incorporated 86 cross-sections from 1:10,000 toposheets. Calibration involved five steady-flow profiles, and comparing the computed water levels at three gauging stations with observed ones. The model simulated an unsteady flood event from May 17 to 20, 2003, with Manning's n calibrated from steady flow, showing good agreement. It simulated fifty flood events to establish upstream-downstream flood levels and depicted inundation extents with three-dimensional views. The author concluded that the developed model can predict downstream water levels based on upstream levels, allowing for informing downstream communities about water flow based on the experiences of upstream communities.

Yarrakula et al., (2010) created a flood forecasting model for the Subernarekha River spanning 154 km, integrating HEC-RAS and GIS to predict flood levels and inundation maps and damage areas. They generated 239 river cross-sections using a 10 m grid DEM obtained from CARTOSET 1 stereo data from NRSC. The CARTOSET 1 DEM's 10 m resolution elevation data was compared and verified with toposheets, showing a sensible fit. The upstream and downstream boundary conditions were set using stage hydrographs at Jamshedpur and near Bhosraghat, respectively. The model was calibrated using stage hydrographs from 1985 and 1988, Manning's roughness coefficients as 0.11 for banks and 0.047 for the channel. The validation involved discharge and water level data from June 16 to September 22, 1997, using statistical performance indices. The study concludes that the hydrodynamic model, developed using a 10 m grid CARTOSET 1 DEM for the Subarnarekha River, can effectively forecast floods for various return periods.

Masood and Takeuchi, (2012) developed a 1D hydrodynamic model for a 37 km^2 area in mid-eastern Dhaka using SRTM DEM with a 90 m grid and flood records spanning 32 years (1972-2004). The study found limitations in simulating the Balu River due to the DEM's resolution constraints. To address this, the authors resampled the 90 m DEM to 30 m using bilinear interpolation, modifying it to match the actual river cross-section. Using the Gumbel distribution, maximum water levels for a 100-year return period were calculated and applied as boundary conditions. RAS simulation results were used to delineate risk zones based on inundation depth and exposure of people and property to flooding. The study demonstrates the effective integration of HEC-RAS with DEM data for flood risk management.

Timbadiya et al., (2014) constructed a 1D unsteady HEC-RAS model utilizing physically surveyed geometric and flood data from 1998, 2003, and 2006 for the Lower Tapi River. They delineated river geometry with 135 cross sections along a 103.5 km stretch, assigning a single Manning's roughness coefficient of 0.035 for the entire river reach. Upstream and downstream boundaries were defined using flow hydrographs at Ukai dam and stage hydrographs at Hope Bridge, Surat city, respectively. The model simulated extreme flood years with a 10-minute computation time step, examining stage hydrographs at Kakrapar weir and Ghala station. Comparison of observed and simulated stage hydrographs at two gauging stations involved statistical parameters such as percentage error, root mean square error, mean absolute difference, and mean difference. The authors concluded that the HEC-RAS simulated stage hydrographs closely matched the observed ones.

Azouagh et al., (2018) utilized HEC-RAS and HEC GeoRAS tools along with ArcGIS to develop floodplain maps for a 30 km segment of the Martil River in Morocco, known for its torrential nature. Due to the need for precision, aerial photographs with 2 m resolutions were combined with DEMs (30 m, 12 m, and 10 m) to create geometry data comprising 146 cross sections using the HEC-GeoRAS tool. Discharge data from three stations (1970-2013) were analysed, considering maximum discharge for each station for model simulation. The 1D HEC-RAS model simulated flood zones for return periods of 10, 20, and 50 years. Results identified flood zones and hydraulic parameters like water levels and velocity,

consistent with the area's morphology. The study concludes that integrating HEC-RAS software with aerial photographs effectively delineates flood risk areas and aids in flood management and mapping efforts.

2.10.2 Two-Dimensional hydrodynamic modelling case studies

Ali et al., (2016) created a combined 1D and 2D hydrodynamic model using HEC-RAS and GIS for the Jamuna River Basin to generate flood inundation maps. They utilized a 10 m grid re-sampled DEM in HEC-GeoRAS to construct a 1D HEC-RAS model for the river, excluding nearby floodplains. Subsequently, they converted the adjacent floodplain areas into a 2D mesh with 300 m x 300 m cell size. The model calibration yielded Manning's values of 0.032 for the main channel and 0.035 for the floodplain. The validation was conducted for various flow conditions over a 5-year period from 2004 to 2008. Flood inundation maps were created using GIS, and it closely corresponded to MODIS data maps. The study showcased a methodical approach to developing flood inundation maps through a combined 1D and 2D model, integrating HEC-RAS and GIS tools. The authors affirmed the compatibility of HEC-RAS, ArcGIS, and HEC-GeoRAS for building coupled 1D/2D models.

Quirogaa et al., (2016) constructed a 2D HEC-RAS model for Bolivian Amazonia using geometric data derived from a 90 m grid SRTM DEM and flood data spanning from February 02, 2014, to March 02, 2014. They designated the flow hydrograph and normal depth as upstream and downstream boundaries, respectively, at the extremities of the Mamore River. To ensure model stability, the authors employed a 15-second time step determined by the Corant-Friedriches-Lewy condition. The study demonstrated that the model effectively predicted flood levels and closely matched satellite-derived data. Additionally, the simulated model provided supplementary information such as water depth, velocity, duration, and inundation boundaries, facilitating the analysis of potential flood management strategies.

Siqueira et al., (2016) suggested real time updating of HEC-RAS model for streamflow forecasting using an optimization algorithm. The study discussed the complex nature and expertise required for operational use of HEC-RAS model and developed a real time updating procedure for streamflow forecasting in HEC-RAS

using the Shuffled Complex Evolution - University of Arizona (SCE-UA) optimization algorithm. The study used corrections in boundary conditions and the algorithm works in an optimization window in order to minimize an objective function, given by weighted sum of squares of errors between simulated and observed flows, wherein, the differences in later intervals i.e. at the start of forecast are more penalized.

Patel et al., (2017) developed a combined 1D/2D hydrodynamic model for the Tapi River and Surat city, integrating GIS with HEC-RAS software. They conducted 1D modelling of the Tapi River using 299 cross sections spaced at intervals of 150-200 m, and 2D modelling using geometric data from SRTM DEM at 30 m and 90 m resolutions. The study replicated the 2006 flood scenario, analysing flood depth, water surface level, flow velocity, arrival time, distance, and flooding at seven locations. The model was simulated with and without bank protection to assess future flood risks. The validation was performed against regional flood level maps and observed flood depths.

Nandurkar et al., (2017) created a model for urban flash flood prediction by integrating remote sensing data with the HEC-RAS hydrodynamic model. Rainfall data of Pune district since 1998 was analysed for heavy rainfall and average daily rainfall over the past 20 years. Cross-sectional data for the Mula and Mutha Rivers were derived from a 1-meter contour map, with missing sections of the Mutha River in the city area estimated using a regular 1-meter interval triangular shape assumption. Pune city's geometric data was extracted from SRTM DEM at 30-m resolution. Recent LANDSAT data was utilized to determine impervious surface coverage, and urban areas were classified into various vegetation, impervious surface, and soil classes for assigning Manning's roughness values. HEC-RAS simulation was conducted to calculate flood flow depths at different city locations. The study concluded that HEC-RAS effectively predicts water depths during heavy urban rainfall, requiring detailed terrain models for accurate geometry. The authors suggested extending the work to include vulnerability assessment and mitigation plans by incorporating more information through physical surveys or remote sensing and GIS.

Rind et al., (2018) established a 2D hydrodynamic model for the Lower Indus River, spanning from Kotri Barrage to the Arabian Sea, specifically for the flood year 2010. They employed HEC-RAS 2D in conjunction with ArcGIS and HEC-GeoRAS tools to prepare the necessary data. Their primary objective was to create flood inundation maps and identify areas susceptible to future flooding. The researchers utilized the freely available ALOS World 3D digital surface model with a resolution of 30 m to generate detailed bathymetry of river sections, integrating GIS in the process. They also utilized LANDSAT 8 Archive for land use / land cover data, validated against FAO and SUPARCO Atlas. Different Manning's n values were assigned to various land use categories based on their characteristics. The model was calibrated for 2010 based on Manning's roughness, and validated for the 2015 flood event. Comparison of simulated flood inundation results were done with the MODIS data using various spatial metrics. The study aims to develop an adaptive flood management plan applicable at both local and regional scales. The authors propose that utilizing higher-resolution topographical data could enhance the proposed framework, potentially aiding in hazard assessment, flood insurance, future flood forecasting, and land use planning.

Adams et al., (2018) carried out analysis of hydrological forecast based on US NOAA, NWS and HEC RAS model for an approximate 12 month hindcast model validation period using observed precipitation and an independent five-month operational, real time forecast period using quantitative precipitation forecast (QPF). Operational complications such as problems related to handling real time gate operations on the Ohio River mainstream are discussed in the study. The results of the study showed that verification statistics of model hindcast during the validation period are comparable to goodness of fit statistics obtained from the model calibration period from 2013. The study also discussed the operational complications such as inaccurate cross section data for Ohio river, problems in low flow simulations, insufficient discharge measuring stations etc.

Ranagari et al, (2019) assessed inundation risk in urban floods using HEC-RAS for Hyderabad city, India. The study used 2D flow computations along with 10 m mesh in HEC-RAS for simulation. The result of study show that the model produces relative flooding based on underlying terrain quality and input parameters. The critical events are generated using 2D flood models for various critical storm

conditions. The flood inundation maps so developed can be used for developing flood risk maps, and setup of flood early warning system to alert population before extreme events. Wara et al, (2019) developed river rating curves for simple and complex hydraulic structures based on calibrated HEC-RAS model in Kwale, Coastal Kenya. Results shows the establishment of stage discharge relationships, developing a good understanding of the flow conditions within the section and reach and increased reliability of river flow data. The study concluded that HEC-RAS approach should be used to develop rating curves for total range of flows but should not be considered for low flow analysis.

Liu et al., (2019) conducted a comparative analysis of HEC-RAS 1D, HEC-RAS 2D, LISFLOOD-FP sub-grid, and LISFLOOD-FP diffusive models. They evaluated their performance and sensitivity to surface roughness categorization using identical input data and boundary conditions for four historical flood events in USA. The study found that the sinuosity, length, and wavelength of the river were not significantly affected by the geometry of the 1D or 2D models when the same roughness set was applied. The quality of 1D model was comparable to that of 2D models, albeit with slightly better results for the latter. Additionally, the study observed that the quality of 2D models improved with increasing channel roughness, allowing more water to enter the floodplain, while higher roughness in the floodplain positively influenced the quality of 1D model. Furthermore, the researchers compared uniform and distributed roughness classification in the floodplain, concluding that uniform categorization yielded better results than distributed roughness categorization.

3.0 STUDY AREA AND DATA USED

3.1 Hydrology, Land use and Soils

The Narmada River, rises in the Amarkantak Plateau of Maikal range in Shahdol district of Madhya Pradesh at an elevation of 1057 m above mean sea level and at a latitude $22^{o}04'$N and longitude of $81^{o}45'$E. The Narmada basin extends over an area of 98,796 sq. km falling between $72^{o}38'$ to $81^{o}43'$ E longitudes and $21^{o}27'$ to $23^{o}37'$ N latitudes. The basin covers large areas in the states of Madhya Pradesh and Gujarat and comparatively smaller areas in Chhattisgarh and Maharashtra. It is bounded on the on the east by the Maikala range, on the west by the Arabian Sea, on the north by the Vindhyans, and on the south by the Satpuras. The river travels for a distance of 1312 km before it falls into Gulf of Cambay in the Arabian Sea near Bharuch in Gujarat. The first 1079 km of its run is in Madhya Pradesh. In the next length of 35 km, the river traverses along the boundary between the states of Madhya Pradesh and Maharashtra. It forms the boundary between Maharashtra and Gujarat for the next length of 39 km and the last length of 159 km lies in Gujarat. The Narmada River has 41 tributaries, and of these, 22 are on the left bank and 19 on the right bank. The important tributaries of Narmada are Barna, Hiran, Tendoni, Kolar, Man, Burhner, Banjar, Sher, Shakkar, Dudhi, Tawa, Orsang, Uri, Hatni, Ganjal, Chhota Tawa, Kundi, Goi and Karjan. Banjar River is the longest tributary (266.70 km) followed by Hiran (205.0 km) and Burhner (182.20 km).

The five physiographic zones of the basin include, i) The Upper hilly areas, ii) The Upper Plains, iii) The Middle Plains (iv) The Lower hilly areas and (v) The Lower Plains. The hilly regions are in the upper part of the basin, and lower middle reaches are broad and fertile areas well suited for cultivation. The climate of the basin is humid and tropical, although at places extremes of heat and cold are encountered sometimes. The hot dry season starts in March and extends up to the second week of June with May being the hottest month. The remaining three seasons include cold weather, south-west monsoon and post-monsoon. The south-west monsoon sets in by the middle of June and withdraws by the first week of October.

Heavy rainfall occurs in the Upper hilly and Upper Plains regions of the basin and gradually decreases towards the Lower Plains and the Lower Hilly areas

but increases again towards the coastal regions. The average rainfall in the Upper Hilly regions is about 1400 mm whereas it decreases to 1000 mm in the Upper Plains regions. It decreases further to about 650 mm at Barwani but increases to about 750 mm in the Lower hills region. About 90% of the annual precipitation occurs in the south-west monsoon season. The maximum temperature occurs during May whereas the minimum temperature occurs in January. The temperature in the upper reaches of the basin is lower as compared to other regions. As the sea influence is predominant in the lower regions, the temperature is lower than the middle regions but higher than the upper reaches of the basin.

Agriculture, forest, wasteland, water bodies and built-up area are the major land use / land cover classes in the basin. Three types of crops seasons include kharif crop, rabi crop and summer/zaid crop. Paddy is grown in the upper reaches of the basin where rainfall id high whereas wheat is grown abundantly in the middle and lower reaches of the basin. Tropical, moist, deciduous type forests are found in the upper reaches whereas in the middle and lower reaches the forests are of tropical dry and deciduous type. Southern dry, deciduous type forests are found along Maharashtra and Gujarat. Waste land (6%) and scrub lands are located in the lower reaches. Few large water bodies in the basin include Bargi, Tawa, Barna, Kolar, Indira Sagar Project, Omkareshwar Project and Saradar Sarovar Project among many others. Few more medium projects have been planned in the basin.

The soils in the Upper hilly regions of the basin are mostly shallow red and yellow having low fertility. The Upper Narmada plains have deep black soils and are quite broad and fertile areas well suited for cultivation extending up to East Nimar district. These soils are highly water retentive in nature. Thereafter medium black soils are found in West Nimar, Dewas and Barwani districts mixed with skeletal red and yellow soils. The Lower hilly portions in Madhya Pradesh Maharashtra and Gujarat have mostly shallow red and yellow and skeletal soils of low fertility. There are alluvial deposits on the banks of most of the major tributaries of the Narmada River. The coastal plains in Gujarat are composed of alluvial clays with good drainage and are extremely fertile and support good crops. About 50% of the basin area is covered with fine texture soils followed by the medium textured soil of about 45%. About 20% soils are highly productive whereas about 28% soils are moderately productive. Severe soil erosion is experienced in the Upper hilly and

Upper Plains regions whereas erosion is less in the Middle Plains and Lower Plains region of the Narmada basin. (Source: Water Year Book, CWC, 2002-03).

The study area is limited to the Upper Narmada basin (UNB) up to Hoshangabad (now Narmadapuram). Major districts falling in the UNB include Dindori, Mandla, Jabalpur, Narsinghpur, Anuppur, Shahdol, Balaghat, Seoni, Chhindwara, Betul, Sehore, Raisen, Sagar and Hoshangabad. The index map of UNB is given in Figure 3.1.

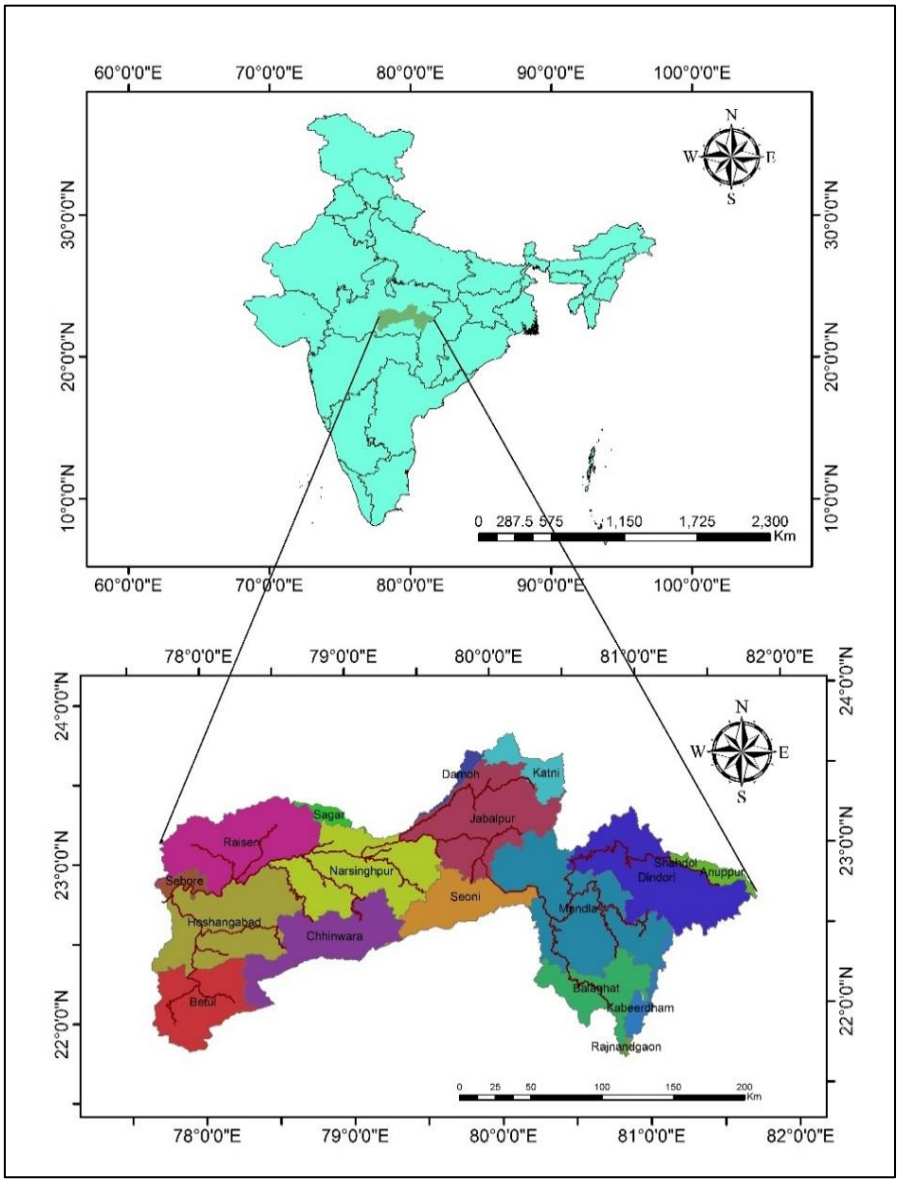

Figure 3.1: Base map of Upper Narmada basin up to Hoshangabad

3.2 Data used

The meteorological data of the India Meteorological Department (IMD) Pune for the period 1961-2015 including precipitation, maximum and minimum

temperature, wind speed, sunshine hour, relative humidity and rainfall has been used for the study. The high-resolution gridded rainfall data at 0.25^o x 0.25^o resolution and the gridded temperature data at 1.0^o x 1.0^o resolution has been used for the analysis of detecting climate change signals and for model setups and runs for the baseline (1961-1990) and present (1991-2019) time periods. The daily time series of observed discharge data at the various gauging sites located on the main Narmada River and its various tributaries obtained from Narmada Basin Organization, Central Water Commission has been used for the calibration and validation of the surface water models setup for UNB. The hydraulic particulars of the existing and proposed projects in the UNB have been collected from Narmada Valley Development Agency (NVDA) and reservoir related information including salient features, gate operation and water demands for multiple users were obtained from the Project Authorities at dam sites of Water Resources Department, Govt. of Madhya Pradesh (MP-WRD) and NVDA.

The Digital Elevation Model (DEM) with a spatial resolution of 30 m have been downloaded from SRTM (https://cgiarcsi.community/data/srtm-30m-digital-elevation-database) and DEM for Upper Narmada basin have been extracted in ArcGIS 10.4 after the processing and analysis to remove the inherent errors. The DEM of the study area is given in Figure 3.2. The LANDSAT8 remote sensing data at 30 m resolution have been used in the study and the details are given in Table 3.1. The land use / land cover classification has been carried out in GIS environment using ArcGIS 10.4 and few field visits were carried out during kharif and rabi cropping seasons for ground truth verification of the generated land use map. A considerable portion of the study area is under agriculture whereas forests are located along the ridge lines all throughout the study area. The land use / land cover map of the study area is given in Figure 3.3. The soil map of Madhya Pradesh at 1:2,50,000 scale have been obtained from NBSSLUP (National Bureau of Soil Survey and Land Use Planning), Nagpur. Thereafter it was scanned, georeferenced and digitized for preparation of soil map for the study area which is presented in Figure 3.4. The soil texture and properties of the various types of soils are given in Table 3.2.

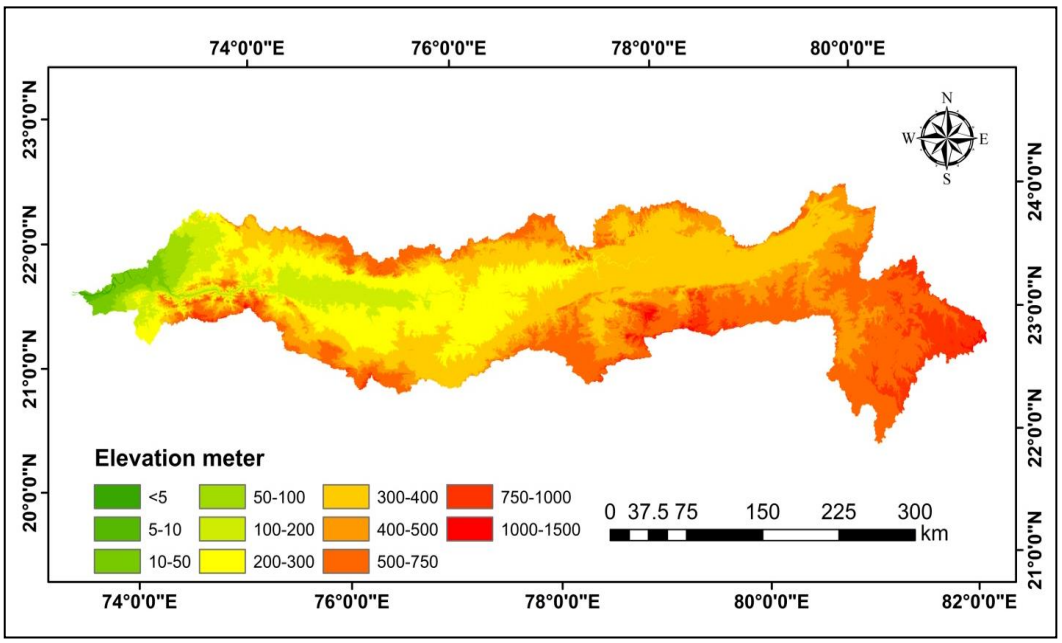

Figure 3.2: DEM of the Upper Narmada basin

Table 3.1: Satellite images used in Narmada basin

S. No.	Satellite	Spatial resolution	Source
1.	LANDSAT8	30 m	http://www.landcover.org

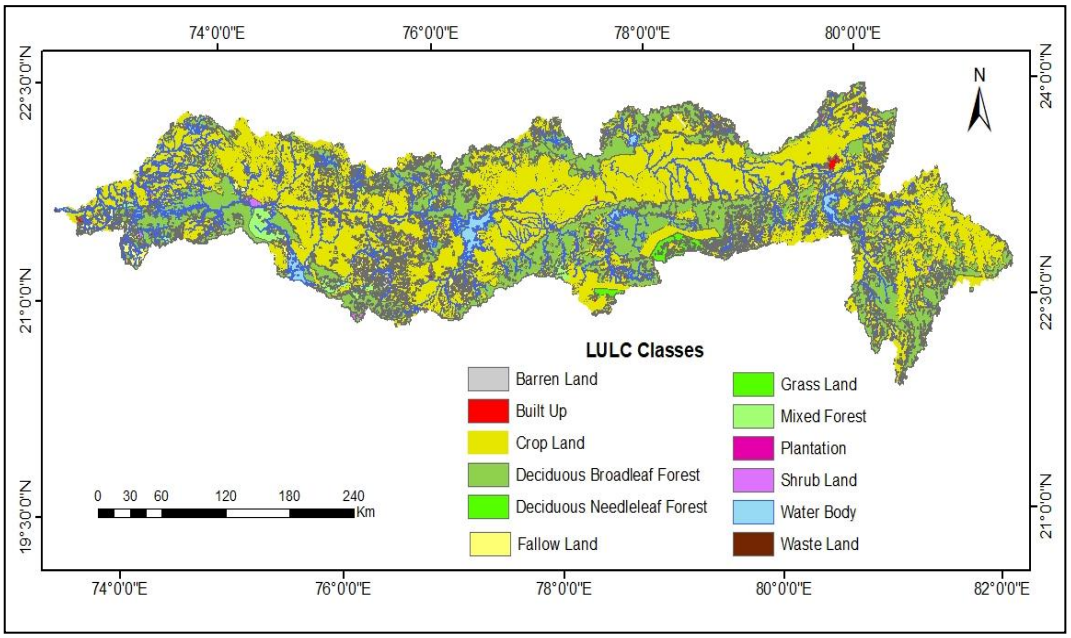

Figure 3.3: Land use / land cover map of Upper Narmada basin

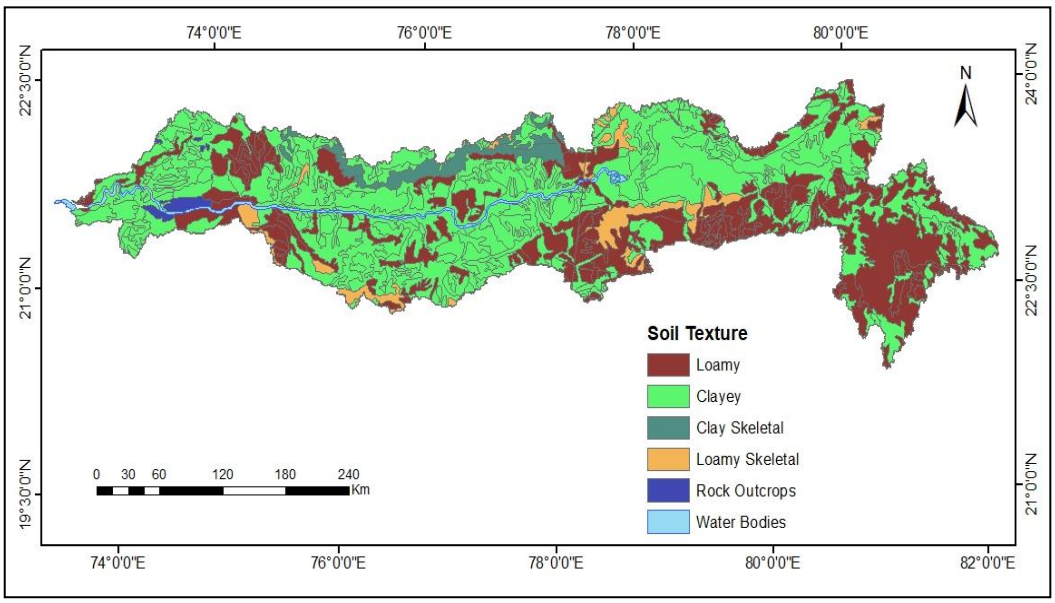

Figure 3.4: Soil map of Upper Narmada basin

Table 3.2: Soil texture and properties

Soil texture	Porosity, (cm^3 /cm^3)	Saturated hydraulic conductivity (cm/hr)
Sandy	0.437	21.0
Loamy sand	0.437	6.11
Sandy loam	0.453	2.59
Loam	0.463	1.32
Silt loam	0.501	0.68
Sandy clay loam	0.398	0.43
Clay loam	0.464	0.23
Silty clay loam	0.471	0.15
Sandy clay	0.43	0.12
Silty clay	0.479	0.09
Clay	0.475	0.06

The Narmada Valley is a rift valley situated between the Narmada North fault and the Narmada South fault. These are part of the longer Narmada-Son lineament, which is an active fault zone. Deccan Traps which are extensive basaltic flows have originated from these faults and underlie most of the basin. Also, there are some granites, Gondwana shale and sedimentary rocks in some parts of the hills and plains and alluvial deposits near the river courses. The geological map of the study area is given in Figure 3.5. Similarly, the hydrogeological map of the study area is given in Figure 3.6.

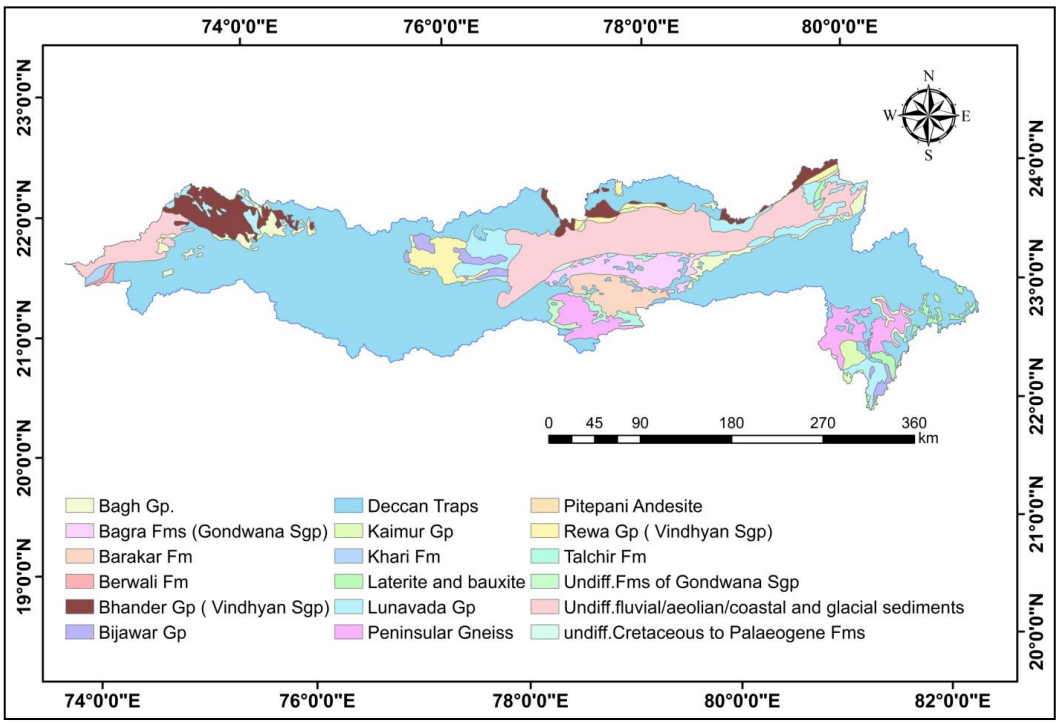

Figure 3.5: Geology map of Upper Narmada basin

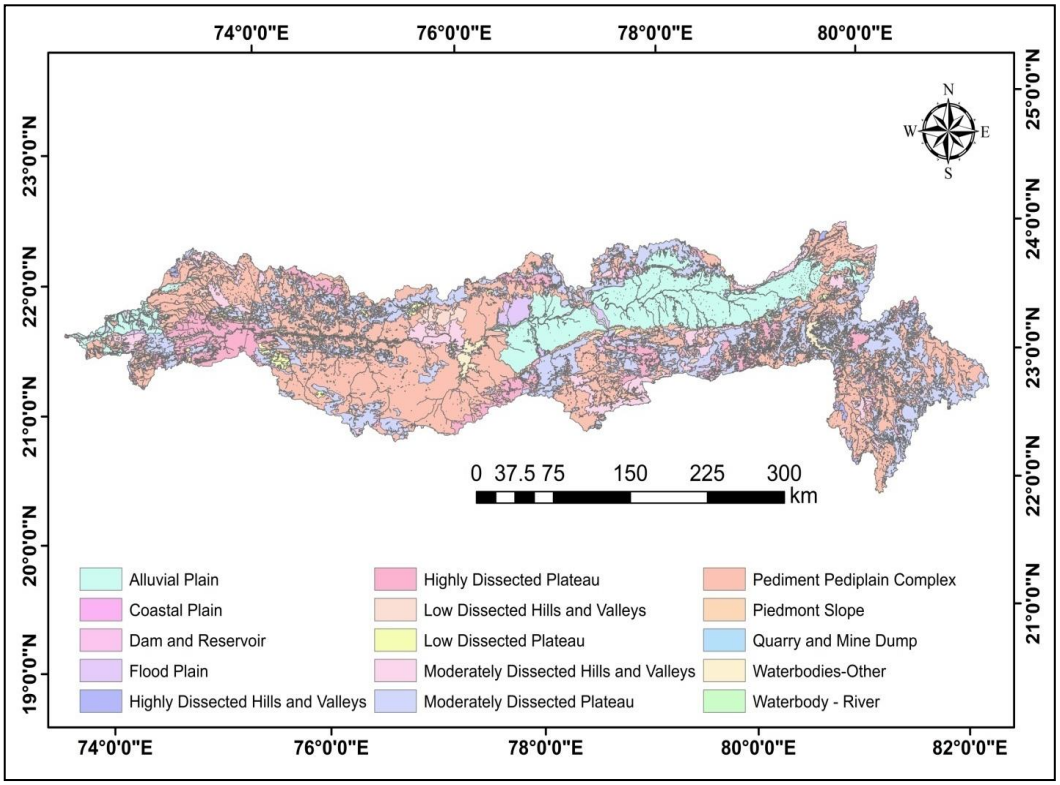

Figure 3.6: Geomorphology of Upper Narmada basin

The detailed information on land use pattern and crop grown has been extracted from the District Statistical Handbook of State Planning Commission and Krishi Vigyan Kendra (KVK) of concerned districts. The crop map was prepared

in GIS environment and ground truth verification was done for both kharif and rabi crops through random sampling of fields in various districts falling in the study area. The canopy interception is given in Table 3.3.

Table 3.3: Canopy interception (Holberg, J ,2014)

Type of Vegetation	Canopy interception (mm)
General vegetation	1.270
Grasses and Deciduous trees	2.032
Trees and Coniferous trees	2.540

To assess the future climate, hydrology, drought and desertification scenario over the study area, the bias-corrected daily precipitation, maximum and minimum temperature from 13 CMIP6 GCMs under two future emission scenarios SSP245 and SSP585 at 0.25˚ x 0.25˚ resolution was downloaded from CMIP sites (https://esgf-node.llnl.gov/projects/cmip6/). The projections used consisted of two time periods viz., historical period (1951–2014) and future period (2015–2100). The Empirical Quantile Mapping (EQM) approach was used for bias correction of the CMIP6 GCM outputs at a daily time scale against the historical reference period (1988–2014) period for Asian region (Mishra et al., 2020). The selection of scenario mainly encompasses the moderate scenario case (SSP245) and worst scenario case (SSP585). Table 3.4 gives the details of the 13 CMIP6 GCMs used in the study with all necessary details.

Table 3.4: CMIP6 GCMs models utilized in the study

General Circulation Models (GCMs)	Abbreviation	Reference
AccessCM2	Australian Com. Clim. and Earth Syss Simulator Clim. Mod. Version 2	Bi et al., (2013)
Access-ESM1-5	Australian Com. Clim. and Earth Sys. Simulator Earth Sys. Model Ver 1.5	Ziehn et al., (2017), Bi et al. (2013)
EC-Earth3	European community Earth-System Model 3	N/A
EC-Earth-Veg	European community Earth-System Model 3 (Vegetation)	N/A
BCC_CSM2-MR	Beijing Climate Center climate	Wu et al., (2019)

	system model version 2	
CanESM5	The Canadian Earth System Model version 5	Swart et al., (2019)
INM-CM4-8	Institute for Numerical Mathematics	Song et al., (2020)
INM-CM5-0	Institute for Numerical Mathematics	Song et al., (2020)
MPI-ESM1-2-HR	Max Planck Institute for Meteorology Earth System Model version 1.2 (higher resolution version)	Müller et al., (2018)
MPI-ESM1-2-LR	Max Planck Institute for Meteorology Earth System Model version 1.2 (lower resolution version)	Mauritsen et al., (2019), Gutjahr et al. (2019)
MRI-ESM2-0	Meteorological Research Institute Earth System Model Version 2.0	Yukimoto et al., (2019)
NorESM2-LM	Norwegian Earth System Model version 2 Low Resolution	Seland et al., (2020)
NorESM2-MM	Norwegian Earth System Model version 2 Medium Resolution	Seland et al., (2020)

4.0 METHODOLOGY

4.1 Investigation of the Climate Change Signals

The Expert Team on Climate Change Detection Indices (ETCCDI) formed by World Meteorological Organization (WMO) finalized 27 core indices for climate change detection based on daily precipitation and temperature. These indices provide data on change in the frequency or severity of extreme climate events. As per the suitability of the parameters to the study area, few important indices were considered and the changes observed in daily, monthly, seasonal and annual patterns of the selected indices have been studied. The selected indices are although similar to the indices suggested by ETCCDI, but the thresholds may vary slightly according to the climatic conditions prevailing in the study area. The various indices evaluated for the study area are given below,

1. Very hot days: Annual count of days when daily maximum temperature is greater than 40^{o}C.
2. Hot days: Annual count of days when daily maximum temperature is greater than 35^{o}C.
3. Cold days: Annual count of days when daily maximum temperature is less than 15^{o}C.
4. Very cold days: Annual count of days when daily maximum temperature is less than 10^{o}C.
5. Highest maximum temperature: Highest value of 1-day maximum temperature observed in a year.
6. Very hot nights: Annual count of days when daily minimum temperature is greater than 25^{o}C.
7. Hot nights: Annual count of days when daily minimum temperature is greater than 20^{o}C.
8. Cold nights: Annual count of days when daily minimum temperature is less than 10^{o}C.
9. Very cold nights: Annual count of days when daily minimum temperature is less than 5^{o}C.
10. Highest minimum temperature: Highest 1-day minimum temperature observed in a year.
11. Lowest maximum temperature: Lowest value of minimum temperature observed in a year.

12. Rainy days: Annual count of days when daily precipitation is greater than 2.5 mm.
13. Heavy precipitation: Annual count of days when daily precipitation is greater than 50 mm.
14. Very heavy precipitation: Annual count of days when daily precipitation is greater than 100 mm.
15. Extreme precipitation: Annual count of days when daily precipitation is greater than 200 mm.
16. One-day maximum precipitation observed in a year.
17. Five-day maximum precipitation (AMC) observed in a year.
18. Annual total wet day precipitation: Annual precipitation observed on rainy days.

The above indicators have been computed and changes that have taken place during the present time horizon (1991-2019) vis-à-vis baseline period (1961-1990) have been evaluated.

4.2 Evaluation of Hydrological Soil Properties

Infiltration and hydraulic conductivity are the important hydrological soil properties in any study area. The double ring infiltrometer has been used to estimate the infiltration capacity of the various soil types in the study area. The procedure of conducting the infiltration tests using double ring infiltrometer can be obtained from standard text. The details of the double ring infiltrometer is given in Figure 4.1.

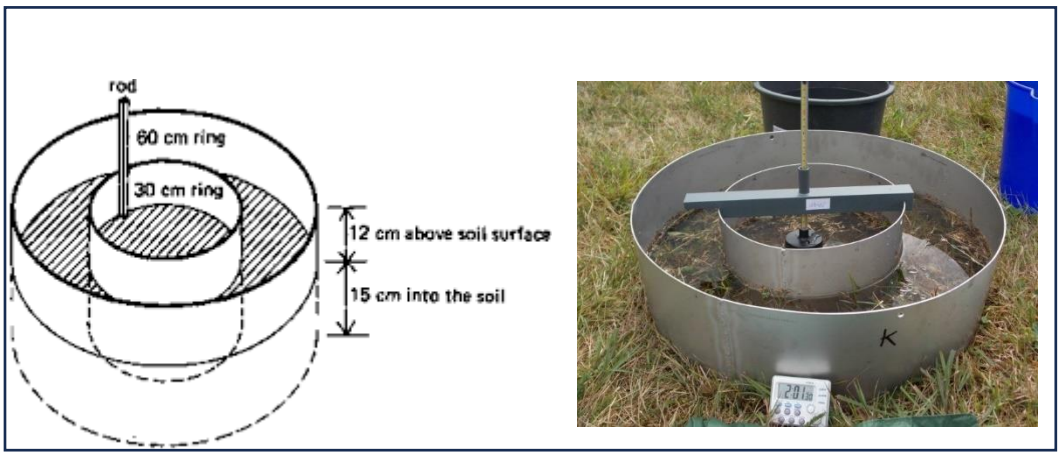

Figure 4.1: Double Ring Infiltrometer

The Guelph Permeameter has been used to quickly and accurately measure in-situ hydraulic conductivity. The Guelph Permeameter comes as a complete Kit

consisting of the permeameter, field tripod, borehole auger, borehole preparation and cleanup tools, collapsible water container, and vacuum test hand pump, all in a durable carrying case. Accessory attachments are available to extend the measurement capability of the permeameter. The Guelph Permeameter is an in-hole constant-head Permeameter, employing the Marriott Principle. The method involves measuring the steady-state rate of water recharge into unsaturated soil from a cylindrical well hole, in which a constant depth (head) of water is maintained. A constant head level in the well hole is established and maintained at the level of the bottom of the air tube by regulating the position of the bottom of the Air Tube, which is located in the centre of the Permeameter. As the water level in the reservoir falls, a vacuum is created in the air space above the water. The vacuum can only be relieved when air of ambient atmosphere pressure, which enters at the top of the Air Tube, bubbles out of the Air Inlet Tip and rises to the top of the reservoir. Whenever the water level in the well begins to drop below the Air Inlet Tip, air bubbles emerge from the tip and rise into the reservoir air space. The vacuum is then partially relieved and water from the reservoir replenishes water in the well. The details of the Guelph permeameter is given in Figure 4.2.

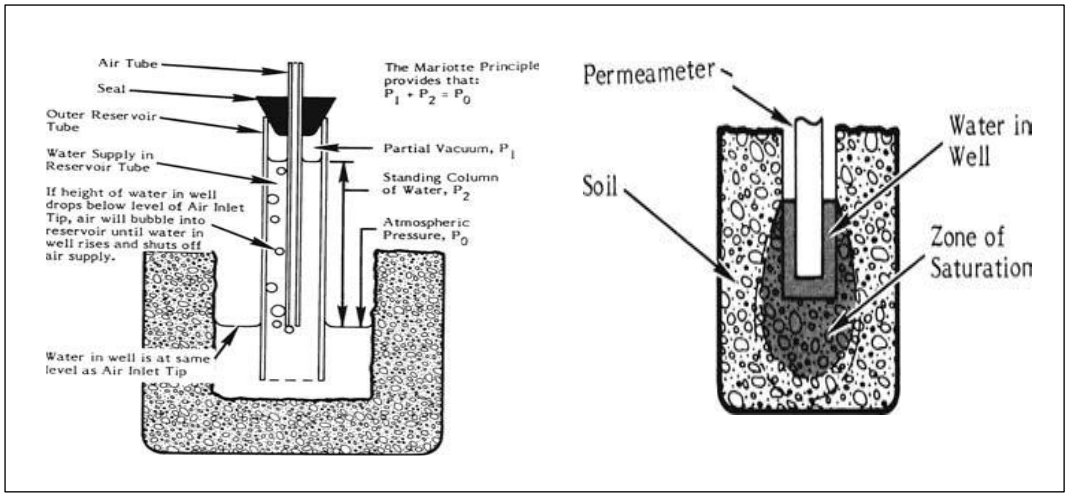

Figure 4.2: Guelph Permeameter

4.3 Hydrological Modelling using SWAT

The Soil and Water Assessment Tool (SWAT) is a semi-distributed watershed model capable of performing simulations on a daily time scale for very long continuous periods (Arnold et al., 1999) and can be used to assess the impacts

of alternate management practices, land use change and climate change on the water resources, sediment, and non-point pollution in large river basins. The model was developed with an objective to assess the impacts of alternate management practices on the water resources and non-point pollution in large river basins, by the United States Department of Agriculture (USDA) in the early 1990's and has been updated regularly. SWAT can be used in ungauged watersheds also to predict the effect of land use changes and water resources management on the water, sediment, and agricultural chemical yields. The input database for the setup of SWAT model comprised of the following,

For system characterization

i) Base map of watershed
ii) Drainage network map
iii) Topographic map
iv) DEM
v) Slope map
vi) Soil Map
vii) Land use and Land cover map

Input forcing data

i) Daily rainfall data
ii) Daily weather data including minimum and maximum temperature, relative humidity, wind speed and solar radiation
iii) Crop data and cropping pattern
iv) River flow data
v) Reservoir properties

The spatial variability in the watershed is represented in SWAT by dividing the basin into multiple subbasins which are further sub-divided into hydrologic response units (HRUs), which comprise of homogeneous land use, topography, soil characteristics, and management practice (Neitsch et al., 2002). The water balance is the basic principle behind all the processes in SWAT and as it impacts the plant growth, movement of sediments, nutrients, pesticides and pathogens. The forcing

variables used to run SWAT include daily precipitation, maximum and minimum temperature, solar radiation, relative humidity, and wind speed all which directly control the water balance, which is simulated separately for each HRU including canopy interception of precipitation, partitioning of precipitation, snowmelt water, and irrigation water, redistribution of water within the soil profile, evapotranspiration (ET), lateral subsurface flow from the soil profile, and return flow from shallow aquifers. These weather variables or the missing weather variables can also be generated using the weather generator available within the model.

The watershed simulation is separated into a land phase, which controls the amount of water, sediments, pesticide loadings and nutrients coming into the main channel in each sub-basin, and b) the in-stream or routing phase which is the movement of water, sediments, nutrients and pesticides through the channel network of the watershed to the outlet. SWAT takes into account a range of hydrologic processes such as canopy storage, surface runoff, infiltration, evapotranspiration, lateral flow, snow accumulation and melt, consumptive use through pumping, return flow, recharge by seepage from surface water bodies, pond and tributaries. The surface runoff from daily rainfall is estimated using the modified Soil Conservation Service Curve Number (SCS-CN) model, whereas the land cover is simulated using plant growth models. The Manning's roughness coefficient is used for the overland and channel flow analysis and sediment yield is simulated using the Modified Universal Soil Loss Equation (MUSLE). The potential evapotranspiration (PET) is computed by any one of the three methods viz., (Penman, 1948; Monteith, 1965; Priestly Taylor, 1972; or Hargreaves, 1982). The Richard's equation is used in flow calculations in the unsaturated zone, whereas the Darcy's law and the mass conservation of 2D laminar flow are used for the groundwater flow through saturated zone.

The SWAT operates on a daily time scale and mathematically, the water balance equation as conceived in SWAT is given by,

$$\sum Input - \sum Output = Change\ in\ storage$$

……..... (4.2)

The detailed components representing the major hydrologic processes in SWAT is given by,

$$\sum_{i=1}^{t}(P + W_{ia}) - \sum_{i=1}^{t}(Q_{surf} + E_t + Q_{lf} + W_{seep} + Q_{rf.sh}) = (SW_t - SW_o)$$

…….…….... (4.3)

where, SW_t is the final soil water content on any day *i* (mm); SW_o is the initial soil water content on day i (mm); P is the precipitation amount on day i (mm); Q_{surf} is the surface runoff consequent to the precipitation in mm; E_t is the evapotranspiration on day i (mm), Q_{lf} is the lateral flow or interflow component (mm); W_{seep} is the amount of water entering the vadose zone from the soil profile on day i (mm); W_{ia} is the irrigation application amount on day i (mm); and $Q_{rf.sh}$ is the return flow or base flow component (mm). The representation of the various flow processes and their interactions in SWAT model is illustrated in Figure 4.3. The surface runoff Q_{surf} has been estimated using the SCS Curve Number (SCS-CN) (SCS, 1972) procedure and is given by,

$$Q_{surf} = \frac{(P - I_a)^2}{(P - I_a + S)} \quad \text{for} \quad P > I_a$$

$$\text{else} \quad Q_{surf} = 0.0$$

..……..…… (4.4)

where, I_a is the initial abstraction, which includes the surface storage, interception and infiltration prior to runoff (mm); S is the soil moisture retention parameter (mm), which generally varies spatially due to changes in the soil type, land use pattern and management practices and temporally due to changes in water content. The parameter S is related to the curve number (CN) by the SCS equation (USDA, 1972) given by,

$$\frac{25400}{CN} - 254$$

..……..…… (4.5)

The CN here represents the curve number used for Antecedent Moisture Condition-II (AMC-II). The CN suitable for the different soil-crop combinations have been used for Indian conditions for the AMC-II condition. The retention parameter varies according to the variation in the soil water content in the soil profile. The retention parameter S can also be assumed to vary with the accumulated plant evapotranspiration. The irrigation application component W_{ia} can be computed externally using the expression given by,

$$W_{ia} = \{(Q_{si} + F_1 Q_{w,sh} + F_2 Q_{w,dp})/A_{ia}\}$$

..... (4.6)

where, F_1 and F_2 are the fractions of the shallow and deep groundwater withdrawals used for irrigation; $A_{ia}$is the area of irrigation water application. The water seep component W_{seep} is computed implicitly from the analysis of vadose zone soil water profile and shallow aquifer water profile.

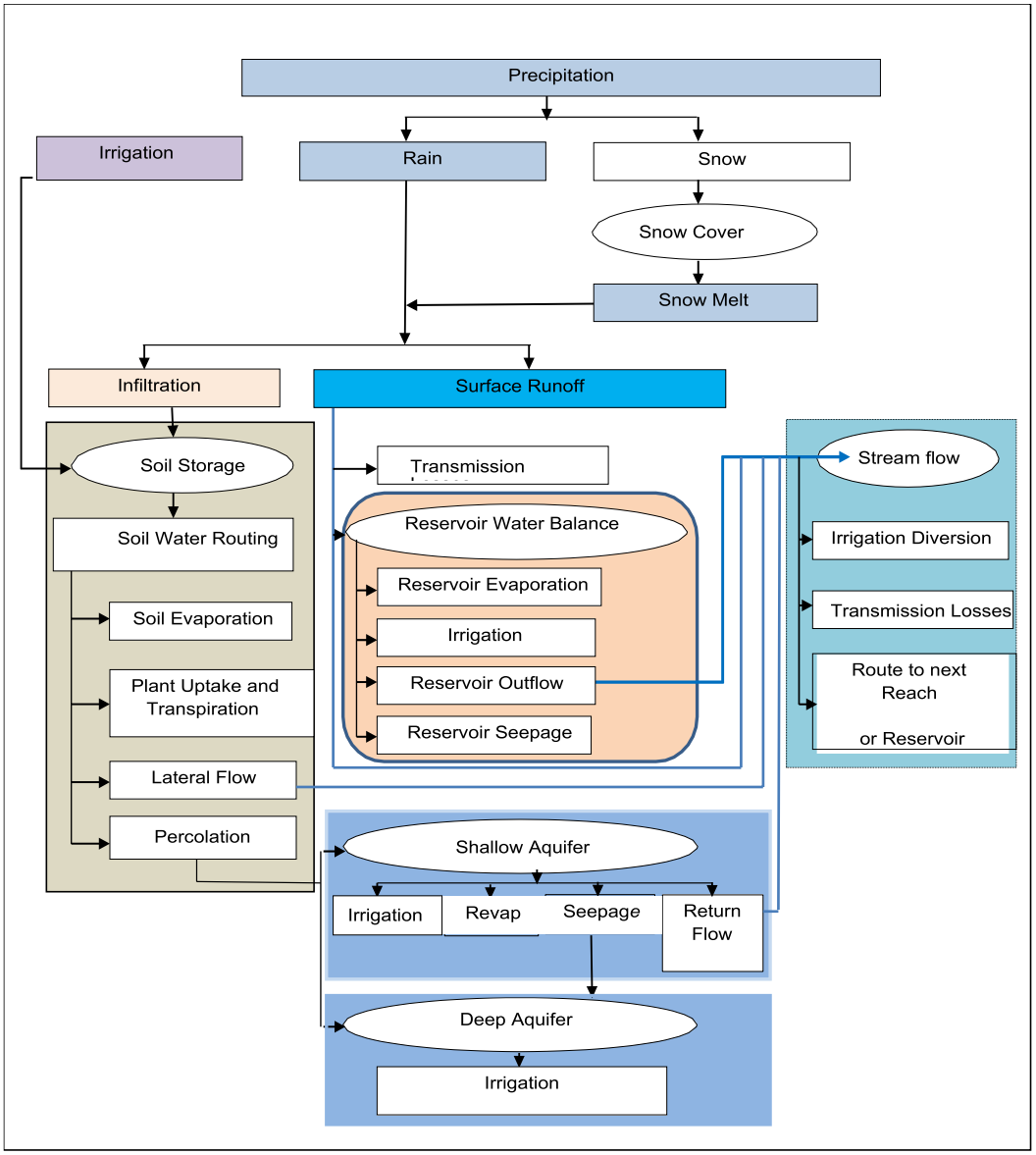

Figure 4.3: Computational workflow of SWAT (Source: Uhlenbrook, 2008)

The potential evapotranspiration (PET) can be computed by any of the three available methods including Penman Monteith method, Priestly Taylor method or the Hargreaves method depending on the availability of data in the basin. The Penman-Monteith method has been used to estimate the potential

evapotranspiration (PET) in the study area. The lateral flow in the soil profile takes place for soils with high hydraulic conductivities in the surface layers and an impermeable or semi-impermeable layer at a shallow depth. The lateral flow taking place in each soil layer once the soil in that zone becomes saturated is given by,

$$Q_{lat} = 0.024.\left(\frac{2.SW_{ly,excess}.K_{sat}.slp}{\emptyset_d.L_{hill}}\right) \quad \text{..... (4.7)}$$

In the above equation, K_{sat} is the saturated hydraulic conductivity (mm/hour); $SW_{ly,excess}$ is the drainable water stored (mm) in the saturated layer when the water content exceeds the layer's field capacity and is the difference between the soil water content on a given day minus the soil layer field capacity; L_{hill} is the hill slope length (m); $\emptyset_d$ is the drainable porosity of the soil layer (mm/mm); slp is the slope.SWAT simulates two aquifers in each sub-basin viz., the shallow aquifer (unconfined aquifer) $Q_{rf.sh}$which contributes to the main channel or reach, based on the Darcy's equation. However, the deep aquifer (confined aquifer) is assumed to contribute to the stream flow outside the watershed (Arnold et al., 1993). The water balance of the shallow aquifer is given by,

$$aq_{sh,j} = aq_{sh,j-1} + w_{rchr,sh} - Q_{rf.sh} - w_{revap} - w_{pump,sh} \quad \text{..... (4.8)}$$

where, $aq_{sh,j}$is the amount of water stored in shallow aquifer on day i (mm); $aq_{sh,j-1}$ is the amount of water stored in shallow aquifer on day i-1 (mm); $w_{rchr,sh}$ is the amount of recharge entering the shallow aquifer on day i (mm); $Q_{rf.sh}$ is the groundwater flow or base flow into the main channel on day i (mm); w_{revap} is the amount of water moving into soil zone in response to water deficiencies on day i (mm); $w_{pump,sh}$ is the amount of water removed from the shallow aquifer by pumping on day i (mm).

The amount of recharge entering the shallow aquifer is given by,

$$w_{rchrg,sh} = w_{rchrg} - w_{deep} \quad \text{..... (4.9)}$$

where, w_{rchrg} is the total daily recharge in both aquifers in mm and w_{deep} is the amount of recharge entering the deep aquifer on day i (mm)and is given by,

$$w_{rchrg,sh} = w_{rchrg} - w_{deep} \quad \text{..... (4.10)}$$

where, β_{deep} is the aquifer percolation coefficient.

4.3.1 SWAT multisite calibration, validation and uncertainty assessment

The model calibration is one of the most important procedures in any hydrologic modelling study, the basic aim of which is to reduce the model simulation uncertainty (Engel et al., 2007). It typically involves the sensitivity analysis followed by manual or automatic calibration. There are several parameters which affect a complex hydrological modelling and values of these parameters are not exactly known due to their spatial variability, measurement error, incompleteness in description of both the elements and processes present in the system (Holvoet et al., 2004). Sensitivity analysis is the process of determining the rate of change in model output with respect to rate of change of model parameters (Arnold et al., 2012). The sensitivity analysis helps to determine the most sensitive parameters for the given basin and sub-basins and the parameter precision required for calibration. For SWAT modelling generally, two types of sensitivity analysis are available viz., i) local sensitivity analysis or one at a time (OAT) sensitivity analysis in which only one parameter is allowed to change while keeping all other parameters at the fixed values, and ii) global sensitivity analysis in which all parameter values are allowed to change simultaneously, but this technique requires very large number of simulations.

During the calibration process, the model is parameterized based on the given set of data and local conditions so as to reduce the simulation uncertainty. Care should be taken to select the model parameter values within their respective uncertainty ranges by comparing the simulated flows with the observed flows at the gauging site of interest. The calibration can be accomplished manually or by using the calibration tools in SWAT (van Griensven and Bauwens, 2003; Van Liew et al., 2005) or SWAT Calibration and Uncertainty Programs (SWAT-CUP) (Abbaspour et al., 2007). The water balance components should be checked during the calibration process to make sure that the simulations are reasonable for the basin.

After the calibration process has been completed, the model needs to be validated by running calibrated model using the independent dataset that was not used for calibration and then comparing the simulated and observed flows during the validation period, so as to develop confidence in the model developed for the

basin. SWAT-CUP has been used for the calibration and uncertainty analysis and validation of the SWAT model setup for the study area. SWAT sensitivity analysis at the outlet of the watershed. Some of the important parameters that mainly affect the surface runoff include CN2, SURLAG, ESCO, SURLAG, EPCO, CANMAX and SOL_AWC, the and the important parameters that affect base flow generation include GW_REVAP, GWQMN and ALPHA_BF. The details of the sensitive parameters and their range is given in Table 4.1.

Table 4.1: List of sensitive parameters and their ranges

S. No.	Sensitive parameters	Parameter code	Range
1.	Surface runoff lag time	SURLAG	0.05-24
2.	Soil evaporation compensation factor	ESCO	0-1
3.	Plant uptake compensation factor	EPCO	0-1
4.	Ground water delay	GW_DELAY	30-450
5.	Groundwater revap coefficient	GW_REVAP	0.02-.0.20
6.	Base flow alpha factor	ALPHA_BF	0-1
7.	Maximum canopy storage	CANMX	0-100
8.	Manning's "n" value for the main channel	GWQMN	0-2
9.	Available water capacity of the soil layer	SOL_AWC	0-1
10.	SCS runoff curve number for moisture	CN2	25-98

4.4 Hydrological Modelling using WEAP

The catchment modelling has been carried out for the various sub-basins using the Rainfall Runoff - Soil Moisture method in WEAP. In this method the catchments are represented with two bucket layers. In the upper bucket layer, it simulates evapotranspiration by considering rainfall, irrigation on agricultural land, runoff and shallow interflow, and changes in soil moisture. This method allows for the characterization of land use and/or soil type impacts to the processes. Baseflow routing to the river and soil moisture changes are simulated in the lower bucket layer. The method is based on empirical functions which illustrate surface runoff, sub-surface runoff, percolation and evapotranspiration for catchment units. This method also incorporates the impacts of land use and /or soil types to the processes.

The percolation within a catchment unit can be transmitted to groundwater storage through a link between catchment node and groundwater node, if link is not made available, the transfer can contribute to a water body as baseflow.

A catchment unit can be divided up into N fractional areas, having shares of the total area of the catchment unit, to represent different land use/ land cover types. The water balance is then computed for each fractional area, j of N, considering the climate uniform for each fraction of the catchment unit, and the water balance is given as:

$$Rd_j \frac{dz_{1,j}}{dt} = P_e(t) - PET(t)k_{c,j}(t)\left(\frac{5z_{1,j} - 2z_{1,j}^2}{3}\right) - P_e(t)z_{1,j}^{RRF_j} - f_j k_{s,j} z_{1,j}^2 - (1 - f_j)k_{s,j} z_{1,j}^2 \quad \text{..... (4.11)}$$

where, $z_{1,j} = [1, 0]$ is the relative storage given as a fraction of the total effective storage of the root zone, (mm) for land cover fraction, j. The effective precipitation, P_e, includes snowmelt from accumulated snowpack in the sub-catchment, where mc is the melt coefficient given as,

$$m_c = \begin{cases} 0 \\ 1 \\ \dfrac{T_i - T_s}{T_1 - T_s} \end{cases} \quad if \quad \begin{cases} T_i < T_s \\ T_i > T_1 \\ T_s \le T_i \le T_1 \end{cases} \quad \text{..... (4.12)}$$

where, T_i is the observed temperature for month *i*, and T_l and T_s are the melting and freezing temperature thresholds. Snow accumulation, Ac_i, is a function of m_c and the observed monthly total precipitation, P_i, by the following relation,

$$Ac_i = Ac_{i-1} + (1 - m_c)P_i \quad \text{..... (4.13)}$$

with the melt rate, m_r, defined as,

$$m_r = Ac_i m_c \quad \text{..... (4.14)}$$

The effective precipitation, P_e, is then computed as

$$P_e = P_i m_c + m_r \quad \text{..... (4.15)}$$

If the timestep length is less than one month (General, Years and Time Steps), then the snow accumulation and melt model is modified to restrict the snow melt rate by the total heat available to transform ice to water. The total heat available

is calculated as the sum of the net solar radiation and the heat introduced to the snow pack by rainfall. Albedo for the net solar radiation calculation is computed as a function of snow accumulation and ranges from a value of 0.15 to 0.25 with increasing snow pack depth.

In Equation 4.11, the calculation for the potential evapotranspiration, PET is done using the reference crop calculation described in the Handbook of Hydrology (1993) in section 4.2.5 using the Penman-Monteith equation modified for a standardized crop of grass, 0.12 m in height and with a surface resistance of 69 s/m. In this implementation two modifications to the equation have been made viz., the albedo varies over a range of 0.15 to 0.25 as a function of snow cover, and the soil heat flux term, G, has been ignored.

Continuing with Equation 4.11, $k_{c,j}$ is the crop coefficient for each fractional land cover. The third term represents surface runoff, where RRF_j is the Runoff Resistance Factor of the land cover. Higher values of RRF_j lead to less surface runoff. The fourth and fifth terms are the interflow and deep percolation terms, respectively, where the parameter $k_{s,j}$ is an estimate of the root zone saturated conductivity (mm/time) and f_j is a partitioning coefficient related to soil, land cover type, and topography that fractionally partitions water both horizontally and vertically. Thus, total surface and interflow runoff, RT, from fraction of catchment at time t is given by,

$$RT(t) = \sum_{j=1}^{N} A_j \left(P_e(t) z_{1,j}^{RRF_j} + f_j k_{s,j} z_{1,j}^2\right) \quad \text{..... (4.16)}$$

For applications where no return flow link is created from a catchment to a groundwater node, baseflow emanating from the second bucket will be computed as,

$$S_{max} \frac{dz_2}{dt} = \left(\sum_{j=1}^{N} (1 - f_j) k_{s,j} z_1^2\right) - k_{s2} z_2^2 \quad \text{..... (4.17)}$$

where the inflow to this storage, S_{max} is the percolation from the upper storage given in Equation 4.11, and K_{s2} is the saturated conductivity of the lower storage (mm/time), which is given as a single value for the catchment and therefore does

not include a subscript, j. Equations 4.11 and 4.17 are solved using a predictor-corrector algorithm.

When an alluvial aquifer is introduced into the model and a runoff/infiltration link is established between the catchment unit and the groundwater node, and the second storage term in Eq. 4.17 is ignored, and recharge R (volume/time) to the aquifer is given by,

$$R = \sum_{j=1}^{N} A_j \, (1 - f_j) k_{s,j} z_{1,j}^2$$

..…….…… (4.18)

where, A is the catchment unit's contributing area. The stylized aquifer characterizes the height of the water table relative to the stream, where individual river segments can either gain or lose water to the aquifer. The conceptual diagram and equations incorporated in the Soil Moisture model is described in Figure 4.4.

The irrigation runoff can be included in total runoff emanating from a catchment. WEAP calculates this irrigation runoff by first assuming no irrigation exists and calculating flows accordingly. WEAP then performs the calculations incorporating irrigation, assuming all requested irrigation is supplied. Knowing how much more runoff would flow due solely to irrigation; WEAP calculates an "average" irrigation runoff fraction (that goes to a river and/or groundwater). This fraction is then applied to the quantity of irrigation that was actually supplied, and essentially becomes the runoff fraction. This irrigation runoff fraction is specified

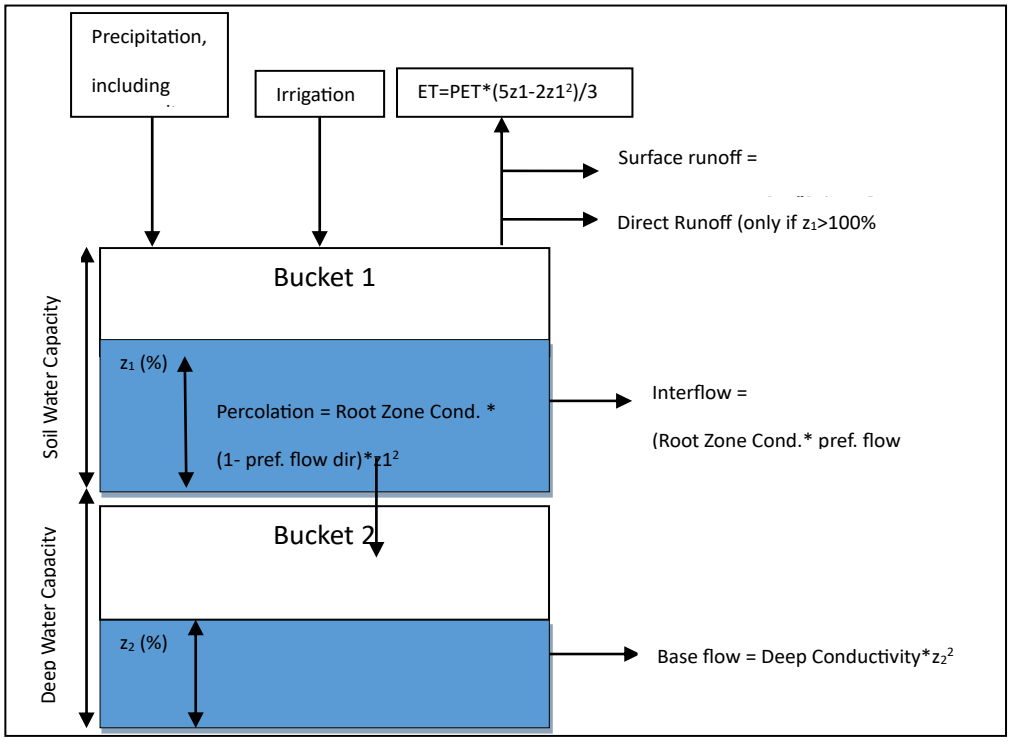

Figure 4.4: Conceptual diagram and equations of the Soil Moisture model

as data by the user when simulating a catchment with the Simplified Coefficient method.

Standing water on the land surface, also known as "flooding" or "ponding", can occur due to rice cultivation, managed or unmanaged wetlands, or river flooding onto a floodplain. In the case of rice cultivation, irrigation is applied if the level falls below the minimum depth to bring it to the target depth, and can be released and replenished in order to maintain the desired water temperature for the rice. The water can be held in place either by artificial structures (e.g., a dike, for rice cultivation) or by the natural topography of the land. Once the water depth reaches the level of the confinement, it will overflow and runoff to the river along the runoff link.

The ponding can exist only when the root zone is saturated ($z_1 = 1$). The Soil Moisture Method calculates fluxes out of the root zone due to evapotranspiration, interflow and deep percolation, which will occur at their maximum rates when $z_1 = 1$. As water leaves the top bucket, ponded water will enter the soil to take its place, causing the depth of water above ground to decrease. In addition, any water released because of the release requirement will also decrease the depth above ground. If the root zone is saturated, water can pond on the surface if there is a confinement in

place to hold it (Maximum Depth) and/or hydraulic restrictions on the outflow (Flood Return Fraction). A mass balance equation of inflows and outflows, tracks the amount of water stored on the surface from one timestep to the next as given below,

$$Surface\_Storage_t = Surface\_Storage_{t-1} - PET_t - Infiltration\_To\_Top\_Bucket_t - Release\_Requirement_t - Overflow_t + Precipitation_t + Irrigation_t + River\_Flood\_Inflow_{t-1} \quad \text{..... (4.19)}$$

where,

$$\text{Infiltration\_To\_Top\_Bucket} = \text{Amount of water needed to saturate top bucket} \quad \text{..... (4.20)}$$

$$Release_{Requirement} = \text{Flow through requirement, to bring in fresh water for rice} \quad \text{..... (4.21)}$$

$$\text{Irrigation} = \begin{cases} \text{Amount of water needed to get to Target\_Depth} & \text{Surface\_Storage} < \text{Min.\_Depth} \\ 0 & \text{Surface\_Storage} >= \text{Min.\_Depth} \end{cases} ; \quad \text{..... (4.22)}$$

$$\text{River\_Flood\_Inflow} = \text{River flood inflow to sub catchment from previous timestep} \quad \text{..... (4.23)}$$

The Minimum_Depth, Maximum_Depth, Target_Depth, and Release_Requirement are data variables.

4.5 Hydrological Modelling using MIKE11-NAM

The flood forecasting system developed in the MIKE11 environment is composed of the following modules i) Rainfall-Runoff module (RR), ii) Hydrodynamic module (HD), and iii) Updating Procedure module (FF). The Nedbør-Afstrømnings-Model (NAM) forms part of the rainfall-runoff (RR) module of the MIKE11 river modelling system. It is a lumped, conceptual rainfall-runoff model, simulating the overland flow, interflow and base flow components. The RR

module can either be applied independently or used to represent one or more contributing catchments that generate lateral inflows to a river network. In this manner, a single catchment or a large basin is schematized as an ensemble of many catchments connected with a complex network of rivers and channels. Furthermore, NAM can be used either for continuous hydrological modelling over a range of flows or for simulating single events.

The NAM model describes the behaviour of each individual component in the hydrological cycle, at catchment level, by using a group of interconnected conceptual elements. In particular, it simulates the precipitation-runoff process by continuously accounting the moisture content in four storages, which represent physical elements of the catchment viz., snow storage, surface storage, root zone storage, and groundwater storage. Based on the meteorological input data, NAM produces catchment runoff as well as other components of the hydrological cycle, such as evapotranspiration, soil moisture content, and groundwater level. The resulting catchment runoff is split conceptually into overland flow, interflow and baseflow components. In addition, NAM allows man-made interventions in the hydrological cycle, such as irrigation and groundwater pumping, to be included.

NAM can be used as event type or continuous type model and for different hydrological regimes. This implies that the number of model parameters can be different depending on the requirements. As default, nine parameters representing the surface zone, the root zone and the groundwater storages are considered in the automatic calibration routine and their ranges are given in Table 4.2. The time resolution depends on the objective of the study and time scale of the catchment response. In many cases, daily rainfall values are sufficient, but in rapidly responding catchments where an accurate representation of the peak is required, rainfall input must have a finer resolution. The spatial resolution is linked to the schematization of the basin, which can be considered as a single element or an ensemble of subbasins. The basic input requirements for the NAM model consist of a) model-parameters, b) initial conditions, c) meteorological data and d) stream flow data. The basic meteorological data are rainfall and potential evapotranspiration. If snow melt has to be represented, temperature and radiation (optional) data are required. The observed discharge data at the catchment outlet are needed for comparison with the simulated runoff and also for model

Table 4.2: Parameters considered for auto-calibration

Parameter	Unit	Description	Parameter ranges	
			Lower	Upper
U_{max}	mm	Maximum water content in the surface storage. This storage can be interpreted as including the water content in the interception storage, in surface depression storage, and in the uppermost few cm's of the soil	5	35
L_{max}	mm	Maximum water content in the lower zone storage. I_{max} can be interpreted as the maximum soil water content in the root zone available for the vegetative transpiration	50	350
CQOF		Overland flow coefficient. CQOF determines the distribution of excess rainfall into overland flow and infiltration	0	1
TOF		Threshold value for overland flow. Overland flow is only generated if the relative moisture content is large than TOF	0	0.9
TIF		Threshold value for interflow. Interflow is only generated if the relative moisture content in the lower zone storage is larger than TIF	0	0.9
TG		Threshold value for recharge. Recharge to the groundwater storage is only generated if the relative soil moisture content in the lower zone storage is larger than TG	0	0.9
CK_{if}	hour	Time constant for interflow from the surface storage. It is the dominant routing parameter of the interflow because $CK_{IF} >> CK_{1,2}$	500	1000
$CK_{1,2}$	hour	Time constant for overland flow and interflow routing. Overland flow and interflow are routed through two linear reservoirs in series with the same time constant $CK_{1,2}$	3	72
CK_{BF}	hour	Base flow time constant. Base flow from the groundwater storage is	500	5000

		generated using linear reservoir model with time constant CK_{BF}		

calibration and validation. The rainfall-runoff module can either be applied independently or used to represent one or more contributing catchments that generate lateral inflows to a river network. The model provides catchment runoff hydrographs at the outlet of the basin or at the outlet of the subbasins which furnish the input to the hydrodynamic model (HD).

4.6 Hydrologic Modelling using VIC

The Variable Infiltration Capacity (VIC) model developed by Gao et al., 2009 at the University of Washington, Department of Civil and Environmental Engineering is a semi-distributed, macro-scale hydrological model that works on both water and surface energy model within a grid cell and captures the sub-grid variation effectively. Primary characteristics of the model include sub-grid variability in land surface vegetation classes, soil moisture storage capacity and drainage from the lower soil moisture zone known as base flow as a non-linear flow. The model accepts multiple soil layers with variable infiltration and nonlinear base flow.

In VIC, the whole basin is divided into n number of grids and each grid is simulated independently of the other. The model generates the surface runoff and the base flow for each grid known as fluxes. The soil column can be divided either into two layers or three soil layers. Evaporation is calculated through the Penman-Monteith equation. Based on the variable infiltration curve, surface runoff is calculated in the upper layer whereas the nonlinear Arno recession curve is used to simulate the base flow release from the lowest soil layer. Moreover, deep underground water is not considered in the model. The fluxes generated for each grid are routed separately using Lohmann et al (1996 & 1998) routing model. This model transports the fluxes generated by VIC to the outlet and then to the river system. The input datasets required to run the VIC model include,

1. Soil parameter file
2. Vegetation library file
3. Vegetation parameter file

4. Meteorological forcing file

Similarly, the main input files for the routing model include,

1. Flow direction file
2. Fraction file
3. Station location file
4. UH file

VIC calculates the flux by using either of the two methods which are the Water balance or the Energy balance method. In the water balance method, the continuity equation is the basic equation. The only inflow considered here is precipitation. This mode assumes that the soil surface temperature is equal to the air temperature for the current time step. By eliminating the ground heat flux solution and the iterative processes required to close the surface energy balance, the water balance mode requires significantly less computational time when compared with the other mode. The Energy balance mode solves not only the complete water balance but also minimizes the surface energy balance error. The surface energy balance is closed through an iterative process which tries to find a surface temperature which adjusts surface energy fluxes (sensible heat, ground heat, ground heat storage, outgoing longwave and indirectly latent heat) so that they compensate for incoming solar and long wave radiation fluxes. This mode requires more computational time compared to the water balance mode as this requires a sub-daily simulation time step in contrast to the water balance mode which requires daily time step data. The main features of the VIC model include,

a) The land surface is modelled as a grid of large (>> 1km), flat uniform cells and sub-grid heterogeneity (elevation, land cover) is handled via statistical distributions.
b) Inputs are time series of sub-daily meteorological drivers (precipitation, air temperature, wind speed, radiation, etc.).
c) Land-atmosphere fluxes, and water and energy balances at the land surface, are simulated at a daily or sub-daily time step depending upon the mode chosen for the model to run.
d) Water can only enter a grid cell via the atmosphere,

» Non-channel flow between grid cells is ignored because it is assumed that the surface and sub-surface runoff portions crossing the grid cell boundaries are way less than the portions reaching the local channel network

» Once the water reaches the channel network, it is assumed to stay in the channel i.e. it cannot flow back into the soil.

Figure 4.5 shows the schematic of the VIC model with a mosaic representation of vegetation coverage and three soil layers.

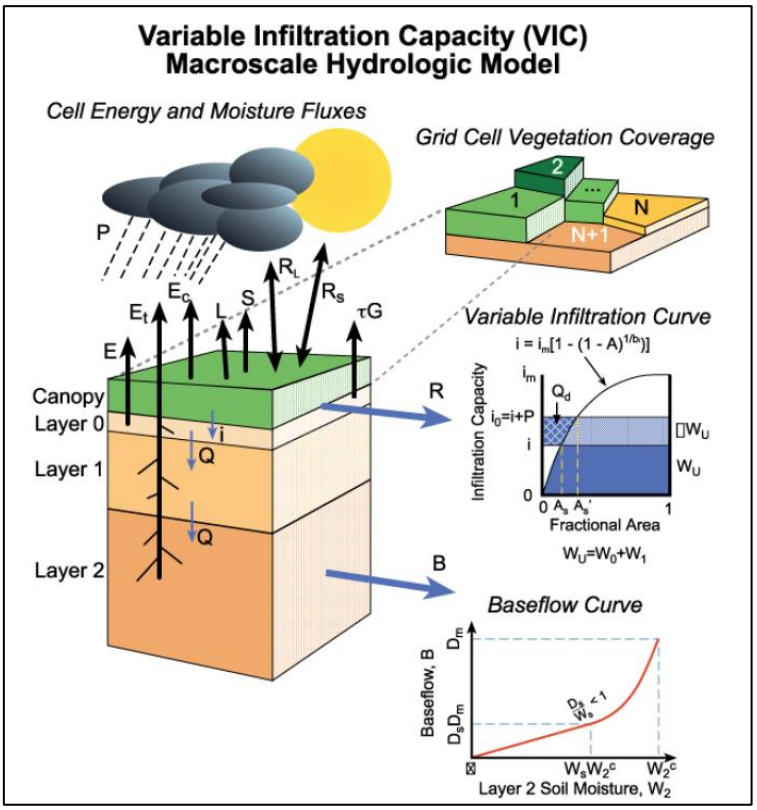

Figure 4.5: Concept of VIC model (Source: VIC-website University of Washington)

The continuity equation is the basic equation for water balance and is given by,

$$\frac{\partial S}{\partial t} = P - R - ET \qquad \text{..... (4.24)}$$

where, dS/dt = change of water storage; P = precipitation (mm); R = runoff (mm); ET = evapotranspiration (mm).

For over-vegetated areas, where the canopy interception takes place, the water balance equation can now be is given by,

$$\frac{dW_i}{dt} = P - E_c - P_t$$

..... (4.25)

where, W = canopy intercepted water (mm); E_c = evaporation from canopy layer (mm); P_t = throughfall (mm)

There are three types of evapotranspiration that are considered by the VIC model which include,

a) Evaporation from the canopy layer (E_c^*, mm)
b) Transpiration (E_t, mm) from each of the vegetation tiles
c) Evaporation from the bare soil (E_1, mm)

The total evapotranspiration over a grid cell is computed as the sum of the above components, weighted by the respective surface cover fractions (Liang et al., 1994). The total evapotranspiration is given by,

$$E = \sum_{n=1}^{N} C_n . \left(E_{c,n} + E_{t,n}\right) + C_{N+1} . E_1$$

..... (4.26)

where, $E_{c,n}$ = evaporation from the canopy layer of each vegetation tile (mm); $E_{t,n}$ = transpiration from each of the vegetation tiles (mm); E_1 = Evaporation from the bare soil (mm); C_n = vegetation fractional coverage for the n^{th} vegetation tile; C_{N+1} = bare soil fraction.

$$\sum_{n=1}^{N+1} C_n = 1$$

..... (4.27)

For the 'canopy evaporation', the canopy evaporates at the maximum value when there is intercepted water on the canopy. The maximum canopy evaporation (E_c^*, mm) from each vegetation tile is calculated as given by,

$$E_c^* = \left(\frac{W_i}{W_{im}}\right)^{2/3} E_p \frac{r_w}{r_w + r_0}$$

..... (4.28)

where, W_{im} = maximum amount of water the canopy can intercept (mm), which is 0.2 times LAI (Dickinson, 1984); the power 2/3 is as described by Deardorff (1978); r_o = architectural resistance caused by the variation of the humidity gradient between the canopy and the overlying air (s m^{-1}). In the model, r_0 is assigned for each land cover type according to the vegetation library.

r_w = aerodynamic resistance. It represents the transfer of heat and water vapour from the evaporating surface into the air above the canopy (s m^{-1}).

The aerodynamic resistance (r_w, s m^{-1}) is described after Monteith and Unsworth (1990) as given by,

$$r_w = \frac{1}{C_w u_z} \quad \text{..... (4.29)}$$

where, u_z = wind speed (ms^{-1}) at level z; C_w = transfer coefficient for water which is estimated taking into account the atmospheric stability. The algorithm for calculating C_w is based on Louis (1979); Ep = potential evapotranspiration (mm) that is calculated from the Penman-Monteith equation (Shuttleworth, 1993) with the canopy resistance set to zero, as given by,

$$\lambda_v E_p = \frac{\triangle (R_n - G) + \rho_a c_p (e_s - e_a)/r_a}{\triangle + \gamma} \quad \text{..... (4.30)}$$

where, $\boldsymbol{\lambda}_v$ = latent heat of vaporation (J kg^{-1}); R_n = net radiation (W m^{-2}); G = soil heat flux (W m^{-2}); (e_s-e_a) = vapour pressure deficit of the air (Pa); $\boldsymbol{\rho}_a$ = density of air at constant pressure (kg m^{-3}), c_p = specific heat of the air (J kg^{-1} K^{-1}); $\triangle$ = slope of the saturation vapour pressure-temperature relationship (Pa K^{-1}); $\boldsymbol{\gamma}$ = psychrometric constant (66 Pa K^{-1}).

The Penman-Monteith equation as formulated above includes all parameters that govern the energy exchange and corresponding latent heat flux (evapotranspiration) from uniform expanses of vegetation. When the continuous rainfall rate is lower than the canopy evaporation, the intercepted water is not sufficient for meeting the atmospheric demand within the one-time step. In such a case, the canopy evaporation (Ec, mm) is given by,

$$E_c = f . E_c^* \quad \text{..... (4.31)}$$

where, f = fraction of the time step for canopy evaporation to exhaust the intercepted water and is given by,

$$f = \min\left(1, \frac{W_i + P.\triangle t}{E_c^* . \triangle t}\right) \quad \text{..... (4.32)}$$

The 'vegetation transpiration' (E_t) is estimated using the equation given below (Blondin, 1991; Ducoudre et al., 1993),

$$E_t = (1 - \left(\frac{W_i}{W_{im}}\right)^{2/3}) E_p \frac{r_w}{r_w + r_0 + r_c} \quad \text{..... (4.33)}$$

where r_c is the canopy resistance (s m^{-1}) given by

$$r_c = \frac{r_{0c} g_T g_{vpd} g_{PAR} g_{sm}}{LAI} \quad \text{..... (4.34)}$$

where, r_{oc} = minimum canopy resistance (s m-1) according to the vegetation library; g_T = temperature factor; g_{vpd} = vapour pressure deficit factor; g_{PAR} = photosynthetically active radiation flux (PAR) factor; g_{sm} = soil moisture factor;

When canopy evaporation happens only for a fraction of the time step (f), the transpiration during that time step has two parts as described by

$$E_t = (1 - f) E_p \frac{r_w}{r_w + r_0 + r_c} + f.(1 - (\frac{W_i}{W_{im}})^{2/3}) E_p \frac{r_w}{r_w + r_0 + r_c} \quad \text{..... (4.35)}$$

The vegetation transpiration from a certain vegetation tile is the total contribution from all three soil layers, weighted by the fractions of roots in each layer.

The bare soil evaporation only occurs on the top thin layer. When the surface soil is saturated, it evaporates at potential evaporation rate. When the topsoil is not saturated, its evaporation rate (E_1) is calculated using the ARNO formulation by Franchini and Pacciani (1991). The infiltration capacity (i) uses the spatially heterogeneous structure described by the Xianjiang Model (Zhao et al., 1980), which is expressed as,

$$i = i_m (1 - (1 - A)^{\frac{1}{b_i}}) \quad \text{..... (4. 36)}$$

where, i_m = maximum infiltration capacity (mm) and is calculated using the equation as given by,

$$i_m = (1 + b_i).\theta_s.|z| \quad \text{..... (4.37)}$$

where, A = fraction of area for which the infiltration capacity is less than i; b_i = infiltration shape parameter; $\boldsymbol{\theta}_s$ = soil porosity; z = soil depth (m);

All these variables are for the top thin soil layer.

The bare soil evaporation is described as,

$$E_1 = E_p \left[\int_0^{A_s} dA + \int_{A_s}^{1} \frac{i_0}{i} dA \right] \quad \text{..... (4.38)}$$

where, A_s = fraction of the bare soil that is saturated; i_0 = corresponding point infiltration capacity

For 'infiltration' estimation, VIC model uses the variable infiltration curve (Zhao et al., 1980) to account for the spatial heterogeneity of runoff generation. It assumes that surface runoff from the upper two soil layers is generated by those areas for which the precipitation, when added to the soil moisture storage at the end of the previous time step, exceeds the storage capacity of the soil. The formulation of subsurface runoff follows the Arno model conceptualization.

VIC model assumes that there is no lateral flow in the top two layers and therefore the movement of moisture is characterized by the Richards 1-D equation as given by,

$$\frac{\partial \emptyset}{\partial t} = \frac{\partial}{\partial z}(D(\emptyset)\frac{\partial \emptyset}{\partial t}) + \frac{\partial K(\emptyset)}{\partial z} \quad \text{..... (4.39)}$$

where, K(φ) = hydraulic conductivity (mm d^{-1}); z = soil depth (m); Φ = volumetric soil moisture content; D = soil water diffusivity (mm^2 d^{-1});

By including the atmospheric forcing, the integrated soil moisture for the top two soil layers (Mahrt and Pan, 1984) can be described as:

$$\frac{\partial \theta_i}{\partial t}.z_i = I - E - K(\theta)|_{-z_1} + D(\theta)\frac{\partial \theta}{\partial z}|_{-z_1} \quad \text{..... (4.40)}$$

where, I = infiltration rate (mm d-1) (It is the difference between precipitation (and through fall if there is vegetation coverage) and the direct runoff Q_d; z_1 and z_2 are soil depth for layer 1 and layer 2 respectively.
The infiltration rate I is the difference between the precipitation (or throughfall if there is vegetation coverage) and the direct runoff Q_d.

For the lower soil layer, an empirical formulation derived from large-scale catchment hydrology is used in which the drainage and subsurface drainage are lumped together as base flow (Q_b). The soil moisture for the soil layer is described by the water balance equation including diffusion between the soil layers as given by,

$$\frac{\partial \theta_3}{\partial t}.(z_3 - z_2) = K(\theta)|_{-Z_2} + D(\theta)\frac{\partial \theta}{\partial z}|_{-Z_2} - E - Q_b \quad \text{..... (4.41)}$$

If it is bare soil, the evapotranspiration term E is zero because there is no evaporation from the lower soil layer. Otherwise, if the vegetation roots go through into the lower soil layer, the evapotranspiration term E needs to be considered.

The total runoff Q is expressed as given by,

$$Q = \sum_{n=1}^{N+1} C_n.(Q_{d,n} + Q_{b,n}) \quad \text{..... (4.42)}$$

where, $Q_{d,n}$ (mm) and $Q_{b,n}$ (mm) are the direct surface runoff and base flow for the n^{th} land cover tile, respectively; C_n is the vegetation fractional coverage.

Since the top thin soil layer has a very small water holding capacity, the direct surface runoff (Q_d) within each time step, is calculated for the entire upper layer (layer 1 and layer 2) (Liang et al., 1996) as given by,

$$Q_d = \begin{cases} P - z_2.(\theta_s - \theta_2) + z_2\theta_s(1 - \frac{i_0 + P}{i_m})^{1+b_i}, & P + i_0 \le i_m \\ P - z_2(\theta_s - \theta_2), & P + i_0 \ge i_m \end{cases} \quad \text{..... (4.43)}$$

where, infiltration capacity associated terms (i_0, i_m, $\boldsymbol{\theta}_s$ and b_i) are explained previously.

The formulation of base flow (sub-surface runoff, Q_b), which used the Arno model formulation is expressed as given by,

$$Q_b = \begin{cases} \frac{D_S D_m}{W_S \theta_S}\theta_3, & 0 \le \theta_3 \le W_s\theta_s \\ \frac{D_S D_m}{W_S \theta_S}\theta_3 + (D_m - \frac{D_S D_m}{W_S})(\frac{\theta_3 - W_S\theta_S}{\theta_S - W_S\theta_S})^2, & \theta_3 \ge W_S\theta_S \end{cases}$$

…… (4.44)

where, D_m = maximum subsurface flow (mm d^{-1}); D_s = fraction of D_m; W_s = fraction of maximum soil moisture; $\boldsymbol{\theta}_s$= soil porosity

The base flow recession curve is linear below a threshold ($W_s\boldsymbol{\theta}_s$) and nonlinear above the threshold. The first derivative at the transition from linear to nonlinear drainage is continuous.

4.6.1 Routing in VIC

To simulate the 'horizontal routing process within grid cells', the fast and slow components of the measured discharge are separated with the linear model described in Duband et al., (1993) as given by,

$$\frac{dQ^S(t)}{dt} = -k.Q^S(t) + b.Q^F(t)$$

…… (4.45)

where, $Q^S(t)$ is the slow flow, $Q^F(t)$ is the fast flow, and Q(t) is the total flow with $Q(t) = Q^S(t) + Q^F(t)$;

The ratio of b over k represents the ratio of water in the slow flow over water in the fast flow. The fast and slow components are analytically connected as given by,

$$Q^S(t) = b\int_0^t \exp\big(-k(t-\tau)\big)\,Q^F(\tau)d\tau + Q^S(0)\exp(-kt)$$

…… (4.46)

The equation shows that the initial condition $Q^S(0)$ decays exponentially with the mean residence time of water in the flow (1/k) and the half-life decay is $T_{1/2}$ = (ln2)/k. With discrete data, the discharge equation can be solved as given below,

$$Q^S(t) = \frac{\exp(-k.\triangle t)}{1+b.\triangle t}Q^S(t-\triangle t) - \frac{b.\triangle t}{1+b.\triangle t}Q(t)$$

…… (4.47)

It is assumed that there exists a linear relationship between the measured stream flow and P^{eff} which is the part of the precipitation that contributes to stream flow.

With the above-stated assumption, the unit hydrograph and the P^{eff}, with the impulse response function one can iteratively be solved as given by,

$$Q^F(t) = \int_0^{t_{max}} UH^F(\tau)\, P^{eff}(t-\tau)d\tau$$

..... (4.48)

where, $UH^F(\boldsymbol{\tau})$ = unit hydrograph for the fast flow component; t_{max} = time taken for all fast processes to decay.

The equation below can be solved iteratively for the calculation of $UH^F(\boldsymbol{\tau})$

$$\begin{pmatrix} Q_m^F \\ \vdots \\ Q_n^F \end{pmatrix} = \begin{pmatrix} P_m^{eff} & \cdots & P_1^{eff} \\ \vdots & \ddots & \vdots \\ P_n^{eff} & \cdots & P_{n-m+1}^{eff} \end{pmatrix} \begin{pmatrix} UH_0^F & \cdots & \\ \vdots & \ddots & \vdots \\ UH_{m-1}^F & \cdots & \end{pmatrix}$$

..... (4.49)

After each of the iteration steps the following constraint is applied:

$$\sum_{i=0}^{m-1} UH_i^F = \frac{1}{1+\frac{b}{k}}$$

..... (4.50)

with $UH_i^F \geq 0\ \forall i$

As regards the channel routing, the transport of water in channels is described using a simple linear river routing model, which follows the linearized Saint-Venant equation. The model assumes that water is transported out of the grid box only in the form of river flow. The following is the linearized Saint-Venant equation, where C and D are parameters that denote wave velocity and diffusivity respectively.

$$\frac{\partial Q}{\partial t} = D\,\frac{\partial^2 Q}{\partial x^2} - C\frac{\partial Q}{\partial t}$$

..... (4.51)

Either from measurements or by estimation from geographical data of the river bed, C and D are regarded as effective parameters since there is often more than one river in one grid cell. This way each grid cell ultimately ends up with one C and one D value, which characterizes the water transport within the cell.

The Saint-Venant equation is solved with convolution integrals as given by,

$$Q(x,t) = \int_0^t U(t-s)h(x,s)ds$$

..... (4.52)

where,

$$h(x,t) = \frac{x}{2t\sqrt{\pi t D}} \exp\left(-\frac{(Ct-x)^2}{4Dt}\right) \quad \text{..... (4.53)}$$

is the impulse response function of the Saint-Venant equation with h(x,0)=0 when x>0 and h(0,t) = δ(t) for t ≥ 0. Because this solution scheme is linear and numerically stable, the influence from human activities (e.g., dams, irrigation water use) can be easily implemented in each node.

4.6.2 VIC-Reservoir Model

VIC-Res is a coupled version of the VIC model and Reservoir given by Thang et al. In this model, along with the flow direction file, the location of the reservoirs in addition to the operation strategies carried by that individual is required. The four different operation strategies mentioned in the model are the Rule curve, Simplified rule curve, Operating rule and the predefined time series curve method. Depending upon the data availability, either of the four operation strategies can be chosen. The initial two methods are the same except for the fact that in the first method we use only the Hmax, Hmin and the pre-defined number of days where this level should be reached. However, in the second method, all 12 monthly target water levels should be reached. The third method is similar to Standard Linear Operation Policy (SLOP) operation strategy. The graphical representation of VIC's spatial domain, selection of dam cell, reservoir cells, cells with other land use and Seasonal Rule Curve is given in Figure 4.6.

For reservoir simulation, the VIC-Res model implements the following mass balance equation at each simulation time step t (and for each reservoir) as given by,

$$S_{t+1} = S_t + Q_t - E_t - R_t$$

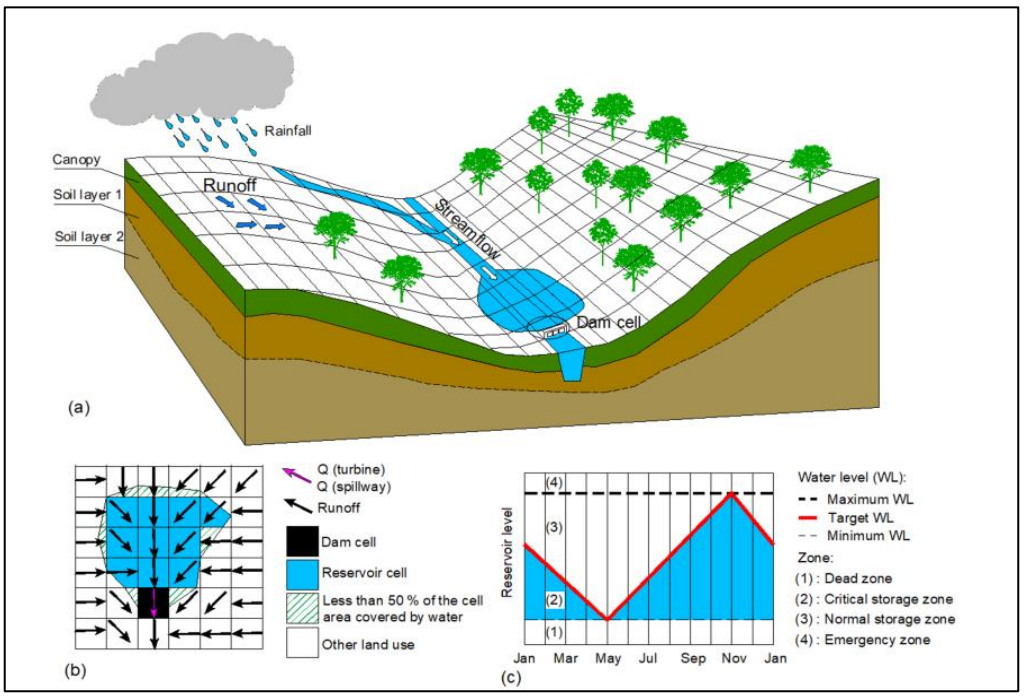

Figure 4.6: (a) Graphical representation of VIC's spatial domain (b) selection of dam cell (black), reservoir cells (blue), and cells with other land use (remaining) (c) Seasonal Rule Curve

$$0 \leq S_t \leq S_{cap}$$

$$0 \leq R_t \leq \min\left(S_t + Q_t - E_t, R_{max}\right) \quad \text{..... (4.54)}$$

where, S_t is the reservoir storage at time t; Q_t is the inflow volume; E_t is the evaporation loss; and R_t is the water released from the reservoir.

Both storage S_t and R_t discharge is constrained by the design specifications of each reservoir. Specifically, the storage cannot exceed the reservoir capacity S_{cap}, while the discharge is bounded by the water availability and capacity of the turbine R_{max}.

The excess water, if any, is spilled as given by,

$$Spill_t = \max(0, S_t + Q_t - R_{max} - E_t - S_{cap}) \quad \text{..... (4.55)}$$

The above equation thus represents the release dynamics when the reservoir water level is in Zone 4.

Zone 1, 2 and 3 are represented by the following equations as given below,

- **Zone 1 :**

$$if\ S_t \leq S_d \qquad \boldsymbol{R_t = 0}$$

..... (4.56)

- **Zone 2, Case 1:**

$$if\ S_d \leq S_t \leq S_{ts.t_{modT}}\ \text{and}\ S_t + Q_t - E_t \leq S_{ts,t_{modT}} \qquad \boldsymbol{R_t = 0}$$

..... (4.57)

- **Zone 2, Case 2:**

$$if\ S_d \leq S_t \leq S_{ts.t_{modT}}\ \text{and}\ S_t + Q_t - E_t > S_{ts,t_{modT}}$$

$$\boldsymbol{R_t = S_{ts,t_{modT}} - (S_t + Q_t - E_t)}$$

..... (4.58)

- **Zone 3, Case 1:**

$$if\ S_{ts,t_{modT}} \leq S_t \leq S_{cap} \quad \text{and} \quad S_t + Q_t - E_t - R_{max} \leq S_{ts,t_{modT}}$$
$$\boldsymbol{R_t = (S_t + Q_t - E_t) - S_{ts,t_{modT}}}$$

..... (4.59)

- **Zone 3, Case 2:**

$$if\ S_{ts,t_{modT}} \leq S_t \leq S_{cap} \quad \text{and} \quad S_t + Q_t - E_t - R_{max} > S_{ts,t_{modT}}$$
$$\boldsymbol{R_t = (R_{max})}$$

..... (4.60)

where, S_d is the storage corresponding to the dead water level and $S_{ts,t_{modT}}$ is the target storage at time t_{modT}.

From Figure 4.6 part (c), it can be observed that the whole water storage is divided into four zones viz., dead storage zone, critical storage zone, normal storage zone and the emergency zone by three water levels. These water levels are the dead water level, the target water level and lastly, the maximum water level.

i) If the water level falls below the dead water level i.e., Zone 1 then the turbines are not operated.

ii) If the water level falls in between the dead zone and the critical storage zone i.e. Zone 2, then the model solves the mass balance equation to check whether the water level goes beyond the target water level. If the level goes beyond the targeted water level, then the model releases through the turbines else the turbines are not operational.

iii) If the water level reaches Zone 3 which is in between the target and the maximum water level, then the turbines are used at their maximum capacity till the water level comes back to the target level.

iv) In Zone 4, which is above the maximum water level, in addition to the use of turbines at their fullest, spillways are also opened.

4.7 Hydrological Modelling using HEC-HMS

HEC-HMS is hydrologic modelling software developed by the US Army Corps of Engineers. It is a physically based, conceptual semi-distributed model designed to simulate the rainfall-runoff processes in large river basins to small natural and urban watersheds. The system encompasses losses, runoff transform, open channel routing, and analysis of meteorological data, rainfall-runoff simulation and parameter estimation. HEC-HMS uses separate models to represent each component of the runoff process, including models that compute runoff volume, models of direct runoff, and models of base flow (Figure 4.7). Each model run combines a basin model, meteorological model and control specifications with run options to obtain results. Several studies have been conducted using the HEC-HMS model in different regions under different soil and climatic conditions.

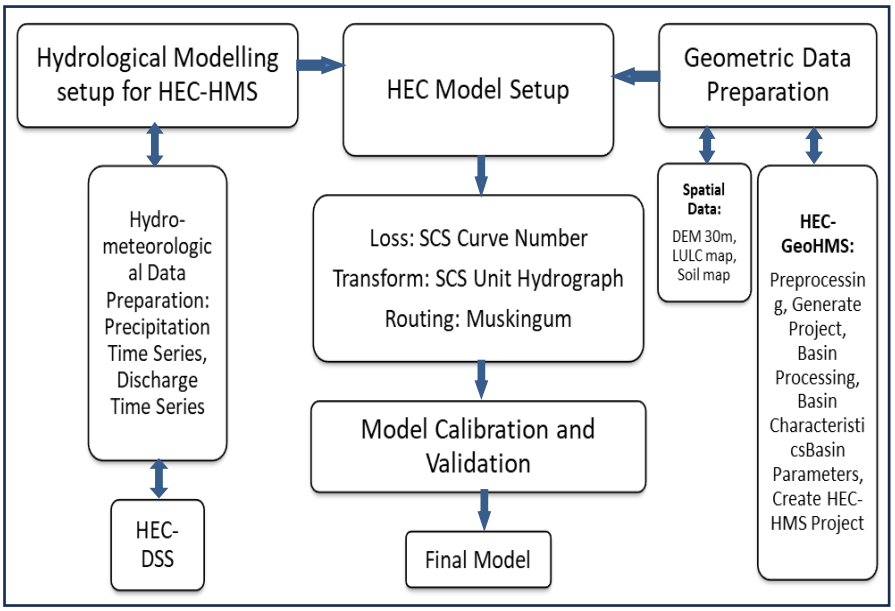

Figure 4.7: HEC-HMS operational flow chart

There exist multiple components in HEC-HMS via Basin Model, Meteorological Model, Control Specification, Time series data, and Paired data manager. 'Basin Model' represents the physical basin area with hydrologic elements (subbasins, junctions, reach, reservoirs) and drainage network of the catchment. The hydrologic elements are connected in a dendritic network to simulate runoff processes. The elements available include subbasin, reach, junction, reservoir, diversion, source and sink. Computation proceeds from upstream elements in the downstream direction. 'Meteorological Model' deals with information regarding meteorological components such as temperature, precipitation evapotranspiration, sunshine hours, wind speed, humidity, snow melt. HEC-HMS provides a variety of options to define each meteorological element. The historical precipitation can be analysed by four different methods. The 'user-specified hyetograph' can be used for precipitation data analysed outside the program. The 'gage-weights' method uses an unlimited number of recording and non-recording rain gauges. The 'gridded precipitation' option can be used for radar rainfall data or other gridded rainfall products.

Control Specification manages starting date and time, ending date and time and computational time step for the simulations. Time series data incorporates real time series data for all the meteorological elements defined in meteorological model which are fed in this part. Apart from above mentioned meteorological elements, the discharge data can also be supplied for calibration and validation of the developed model. It can be supplied to the software manually or in the form of HEC-DSS, the Hydrologic Engineering Center Data Storage System. Paired Data holds meteorological data in tabular/graphical form, (Scharffenberg, 2016). The potential evapotranspiration can be estimated using the 'Hargreaves' and 'Hamon' methods which require temperature data only. However, 'Priestly Taylor' method and the 'Penman Monteith' method are also available, but require more atmospheric parameters. There are few more methods and even a user-specified method can be used with data developed from analysis outside the program.

There are multiple options provided by HEC-HMS for loss method viz., Green-Ampt, Deficit and Constant, SCS Curve Number method, Smith Parlange, Initial Constant, and Exponential. Continuous simulation methods include the one-layer Deficit Constant, Layered Green and Ampt, and Soil Moisture

Accounting methods. The soil moisture accounting (SMA) method is mostly suitable for river systems with deep aquifer source of water.

Soil moisture accounting is an empirical model in HEC-HMS that allows for long term simulation of hydrologic processes that occurs over time in a catchment. It accounts for both wet and dry behavior. It simulates water movement and storage through both surface and subsurface layers. Storage components include canopy interception and depression storage on surface layer while subsurface layer include soil profile and groundwater layer. The flow components included in this method are precipitation, evapotranspiration and surface runoff on the surface and infiltration and percolation in the subsurface layer. SMA depicts the real hydrological processes. The schematic of the soil loss method is given in Figure 4.8.

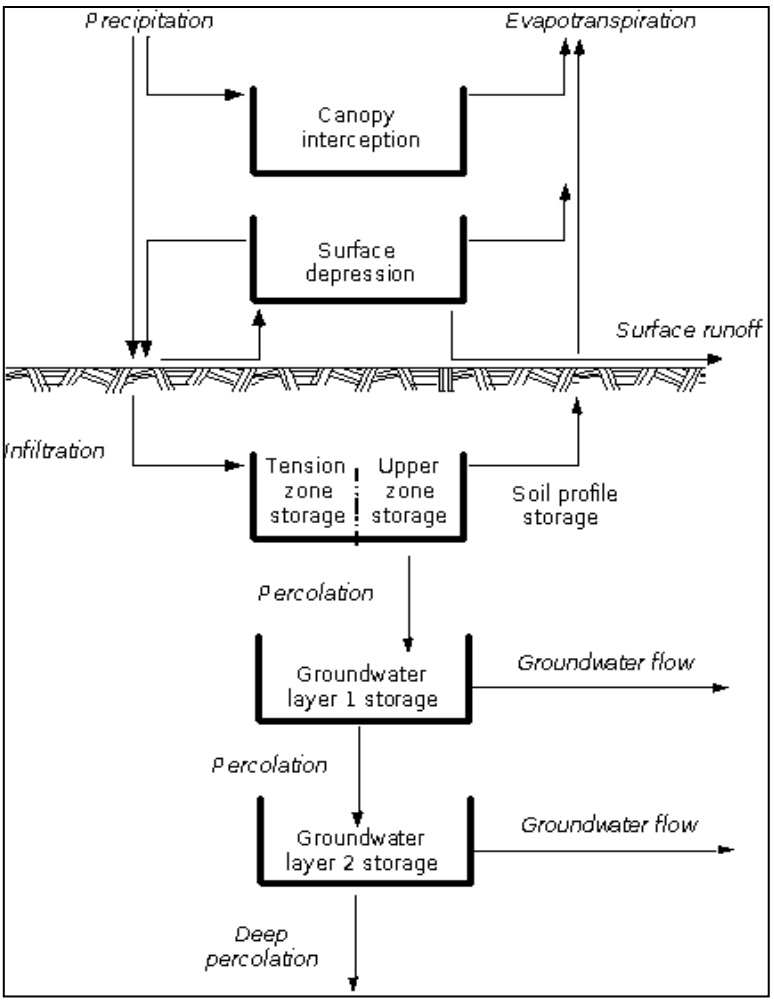

Figure 4.8: Process schematic of SMA Loss Method (Source: Scharffenberg et al, 2018)

Canopy and Surface components can also be added when needed to represent interception and capture processes. There are eight methods used for transforming excess precipitation into surface runoff. The unit hydrograph methods include the Clark, Snyder, and SCS techniques. However, the user specified unit hydrograph or S-graph ordinates can also be used. The modified Clark method, ModClark, a linear quassi-distributed unit hydrograph can also be used with gridded data. Also, an implementation of the kinematic wave method with multiple planes and channels is also included. A 2D diffusion wave transform option is available which utilizes the same 2D engine as used in HEC-RAS.

There are five methods that have been included for representing baseflow contributions to the subbasin outflow. The 'recession' method gives an exponentially decreasing baseflow from a single event or multiple sequential events. The 'constant monthly' method generally performs well for the continuous simulation. The 'Linear Reservoir' method conserves mass by routing infiltrated precipitation to the channel. The nonlinear 'Boussinesq' method provides a response similar to the 'Recession' method but the parameters can be estimated from measurable qualities of the watershed. Two methods are available for specifying the initial baseflow condition viz., a) initial discharge and b) initial discharge per area (Scharffenberg et al, 2006). Also, two different methods are available for determining the baseflow during a storm event viz., a) ratio to peak and b) threshold flow (Scharffenberg et al, 2006).

The linear reservoir base flow method, as its name implies, uses a linear reservoir to model the recession of base flow after a storm event. Infiltration computed by the loss method is connected as the inflow to the linear reservoir. It can be used with the soil moisture accounting or gridded soil moisture accounting methods; the infiltration is connected to the lateral outflow of the groundwater layers. For all other loss methods, the computed infiltration is separated equally between the two layers defined in the base flow method. Subsurface flow in the catchment is illustrated by baseflow in HEC-HMS. Baseflow comprises of interflow and flow in groundwater aquifer. There is insignificant contribution of baseflow in case of short rainfall event, so it can be ignored. While in case of long rainfall event, the base-flow contributes to the recession limb of hydrograph and has a significant contribution in flood volume, (Cunderlik and Simonovik, 2004).

Nine hydrologic routing methods are available in HEC-HMS for simulation of flow in open channels. Routing with no attenuation can be modelled with the 'Lag' method. Routing with constant or variable attenuation and translation can be modelled with the 'Lag and K' method. The traditional 'Muskingham' method is included along the 'Straddle Stagger' method for simple approximations of attenuation. The 'Modified Puls' method can be used to model a reach as a series of cascading, level pools with user-specified storage-discharge relationship. Channels with trapezoidal, rectangular or circular cross-sections can be modelled with 'Kinematic Wave' or 'Muskingham-Cunge' methods. The 'Constant Loss' method can be added to any routing method while the 'Percolation' method can be used only with the 'Modified Puls' or 'Muskingum Cunge' methods.

The Muskingum-Cunge routing method is based on the combination of the conservation of mass and the diffusion representation of the conservation of momentum. It is sometimes referred to as a variable coefficient method because the routing parameters and the flow depth. It represents the attenuation of flood waves and can be used in reaches with a small slope, (Scharffenberg et al, 2018). Water impoundments can also be represented in HEC-HMS. Lakes are usually represented by a user-entered storage discharge relationship. Reservoirs can be simulated by describing the physical spillway and outlet structures. Also, the diversion structures can also be represented if necessary for which the methods available include 'user-specified function', 'lateral weir', 'pump station' and 'observed diversion flows'.

The ArcHydro tool available in ArcGIS has many features for data pre-processing to make the data ready for further use in HEC-GeoHMS. Some of the important features include 'fill sinks function' which has been used to fill the sinks in a DEM grid.; 'flow direction function' which has been used to compute the flow direction; 'flow accumulation function' which has been used to compute the flow accumulation grid that contains the accumulated number of cells upstream of a cell, for each cell in the input grid; 'stream definition function' which has been used to compute a stream grid based on a flow accumulation grid and a user specified threshold; 'stream segmentation function' which has been used to create a grid of stream segments that have a unique identification; 'catchment grid delineation' which has been used to create a grid, in which each cell carries a value (grid code) indicating, to which catchment, the cell belongs; and 'catchment polygon

processing function' which has been used to convert the catchment grid it into catchment polygon feature class.

The other features include 'drainage line processing', 'adjoining catchment processing', 'drainage point processing', 'pore point', 'watershed processing' and 'flow path tracking' and 'terrain pre-processing'. The data extraction has been carried out using HEC-GeoHMS and the extraction process starts with specifying an outlet location at the river. With the use of terrain pre-processing dataset, HEC-GeoHMS uses the dataset upstream the outlet location, to run the flow analysis. The ArcHydro tool in ArcGIS with the features for data pre-processing viz., 'fill sinks function', 'flow direction', flow accumulation', 'stream definition', 'catchment grid delineation', stream segmentation', catchment polygon processing', 'drainage line processing', adjoining catchment processing', 'drainage point processing', 'pour point', and 'watershed processing' to make the data ready for further use in HEC-GeoHMS.

The HEC-GeoHMS is generally used to extract all the data necessary for the creation of HEC-HMS model for any area. The extraction process starts with specifying an outlet location at the river. With the use of terrain pre-processing dataset, HEC-GeoHMS will use the dataset upstream the outlet location, to run the flow analysis. The HEC-HMS model sensitive parameters and their ranges are given in Table 4.3.

Table 4.3: Sensitive parameters of HEC-HMS model

Model parameter	Description	Parameter range
Soil Storage	Max. amount of water that could be held by the soil profile, mm	400 - 550 mm
Soil Percolation	Average rate of the percolation of water from soil into the GW1 layer, mm/hr.	0.10 – 2.5 mm/hr
Maximum Infiltration	Maximum rate at which water can enter the soil profile, mm/hr	4.0 – 75.0 mm/hr
Tension Storage	Portion of the soil storage from which water in this storage is lost through evapotranspiration only, mm	50 – 180 mm

Canopy Storage	Max. storage that can be intercepted by canopy mm	1.50 – 5.50 mm
GW1 Percolation	Percolation rate to GW2 layer, mm/hr	0.10 – 2.0 mm/hr
Surface Storage	Maximum storage in depression storages before runoff starts, mm	1.0 – 12.7 mm
GW2 Percolation	Deep percolation from GW2 layer, mm/hr	0.10 – 2.0 mm/hr

4.8 Groundwater Recharge using WetSpass

The original WetSpass model is a quasi-steady state spatially distributed water balance model scripted in Avenue and used to predict hydrological processes at seasonal and annual time step. With rising popularity of Python programming language in the scientific and research areas, the model has been scripted in Python and using own spatial library Hydrology and Hydraulic Programming Library. This newer version of the model has the ability to simulate interception from vegetated surfaces, runoff from the landscape, evapotranspiration, soil water balance, and recharge at monthly time step. The model can simulate using long-term monthly average values or unique monthly values for many years.

WetSpass is a GIS based, spatially distributed hydrological model for estimating the spatially distributed yearly and seasonal actual evapotranspiration, surface runoff, and groundwater recharge. The model accounts for the spatial variation in the groundwater recharge, which is the result of distributed land use, soil type, slope, etc. Figure 4.9 gives a schematic water balance of a hypothetical grid cell for WetSpass from Batelaanb & De Smedt (2001). This allows accounting for the non-uniformity of the land use depending on the resolution of the grid cell. The model treats a basin or region as a regular pattern of raster cells. Every raster cell is further sub-divided in a vegetated, bare soil, open water, and impervious surface fraction, for which independent water balances are preserved.

Since the model is a distributed model, the water balance computation is performed at a raster cell level. Individual raster water balance is obtained by summing up independent water balances for the vegetated, bare soil, open- water,

and impervious fraction of a raster cell. The total water balance of a given area is thus calculated as the

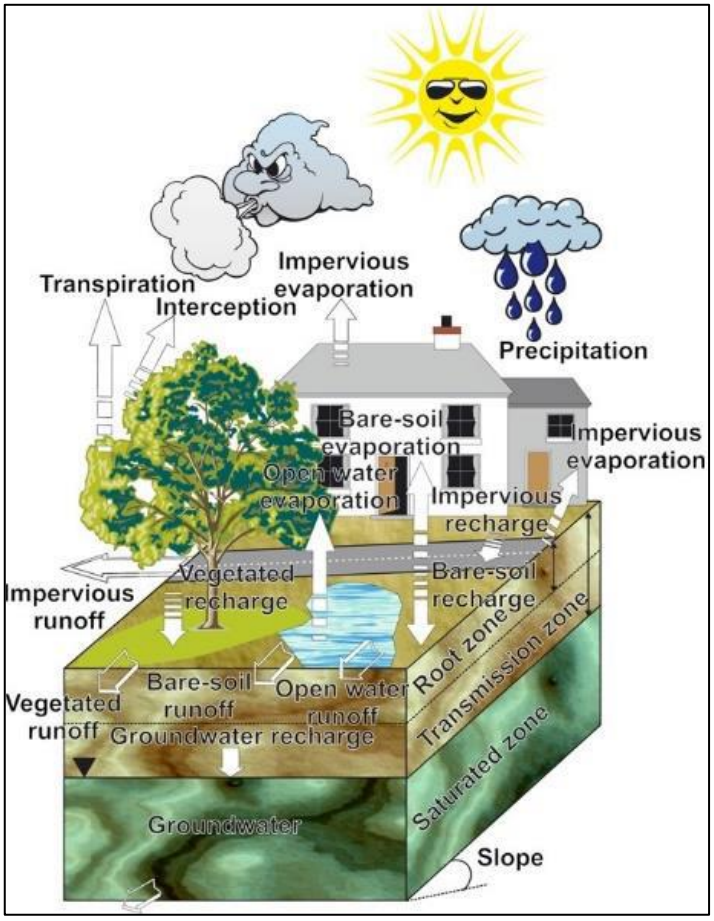

Figure 4.9: Schematic water balance of a hypothetical raster cell. (Source: Batelaan & De Smedt, 2001).

summation of the water balance of each raster cell. The water balance for vegetated surfaces which depends on the average seasonal precipitation *(*P*)*, interception fraction *(*I*)*, surface runoff *(*Sv*)*, actual transpiration *(*Tv*)*, and groundwater recharge *(Rv)* is calculated as given by,

$$P = I + S_v + T_V + R_v \qquad \text{..... (4.61)}$$

where, P is the average seasonal precipitation [LT^{-1}], $\boldsymbol{I}$ is the interception by vegetation [LT^{-1}], *Sv*is runoff over land surface beneath vegetation [LT^{-1}], Tv is the actual transpiration [LT^{-1}] and *R*v is groundwater recharge [LT^{-1}]. The term actual evapotranspiration, ET_v, is used here for the sum of the transpiration, Tv, and the evaporation from the bare soil between the vegetation, ET_{tot}, the total actual

evapotranspiration is the sum of the evaporation of water intercepted by vegetation, *I*, and the actual evapotranspiration, ETv.

$$ET_{tot} = I + T_v + ES$$

..…….…… (4.62)

where, ET_{tot} is the total actual evapotranspiration, 'I' is evaporation of water intercepted by vegetation, T_V transpiration of vegetation cover, and *E*S is evaporation from the bare soil between the vegetation.

The interception fraction has been shown to be reasonably constant at a given annual precipitation value and exhibits a consistent decrease with increasing annual rainfall total (Roberts, 1983). Therefore, the intercepted value is parameterized as a constant percentage from precipitation, dependent on the vegetation type (Batelaan & De Smedt, 2001). Depending on the type of vegetation, the interception fraction represents a constant percentage of the annual precipitation value. Thus, the fraction decreases with an increase in an annual total rainfall amount (since the vegetation cover is assumed to be constant throughout the simulation period) (Batelaan and Woldeamlak, 2003).

Surface runoff is calculated in relation to precipitation amount, precipitation intensity, interception and soil infiltration capacity. The surface runoff, S_v, is calculated in two stages. Initially, the potential surface runoff ($S_{v\text{-}pot}$) is calculated as:

$$S_{v-pot=}C_{sv}(P - I)$$

..…….…… (4.63)

where, *C*sv is a surface runoff coefficient for vegetated infiltration areas. CS_v is a function of vegetation type, soil type and slope. In groundwater discharge areas, saturated surface runoff is occurring. Here, the surface runoff coefficient is very high and assumed to be constant, due to its reduced dependency on soil and vegetation type and the generally near to river position of the runoff producing areas.

The water balance components of vegetated, bare-soil, open-water and impervious surfaces are used to calculate the total water balance of a raster cell. The total evapotranspiration, surface runoff and groundwater recharge of a raster cell have been calculated using equations given below (Batelaan and De Smedt, 2001):

$$ET_{raster=av\,ET_V} + asE_s + aoE_o + aiE_i \quad \text{..... (4.64)}$$

$$S_{raster=avS_V} + asS_s + aoS_o + aiS_i \quad \text{..... (4.65)}$$

$$R_{raster=avR_V} + asR_s + aoR_o + aiR_i \quad \text{..... (4.66)}$$

where, ET_{raster}, S_{raster}, R_{raster} are the total evapotranspiration, surface runoff, and groundwater recharge of a raster cell respectively, each having a vegetated, bare-soil, open-water and impervious area component denoted by av, as, ao, and ai, respectively.

Precipitation is taken as starting point for the computation of the water balance for each of the above-mentioned components of a raster cell. The other processes (interception, runoff, evapotranspiration, and recharge) have been calculated in an orderly manner; which becomes a prerequisite for the seasonal time scale to quantify the processes.

The WetSpass model requires five classes of input data viz., climatic, catchment configuration, vegetation, soil properties and boundary conditions. The climatic data includes precipitation, temperature, potential evapotranspiration, wind speed and Penman coefficient and number of rainy days per month, while catchment configuration considers land use types, leaf area index (LAI), slope and groundwater depth. The soil parameters consist of hydraulic properties etc. The basic input requirements for the WetSpass model consist of model parameter tables, meteorological data, land use, soil elevation and slope data for model calibration and simulation. For the case of calculating PET by the Penman-Monteith equation, additional meteorological data are required, including air temperature, radiation, relative humidity and wind speed. The schematic representation of the input data is given in Figure 4.10.

The WetSpass model uses grid maps, prepared on the basis of both, seasonal (summer and winter) and without seasonal time scales. The grid maps of topography (elevation), slope and soil type are fundamentally non-seasonal that does not show any variability according to the seasonal changes. On the other hand, land use, precipitation, temperature, potential evapotranspiration, wind speed and groundwater depth are variable in nature when the season changes. Therefore, these

data were prepared separately in winter, summer and annual time scales, so as to show the existing feature of the watershed that may appear when the season changes through time. The input grid maps must have similar number of columns and rows with the same cell size for the model to run correctly.

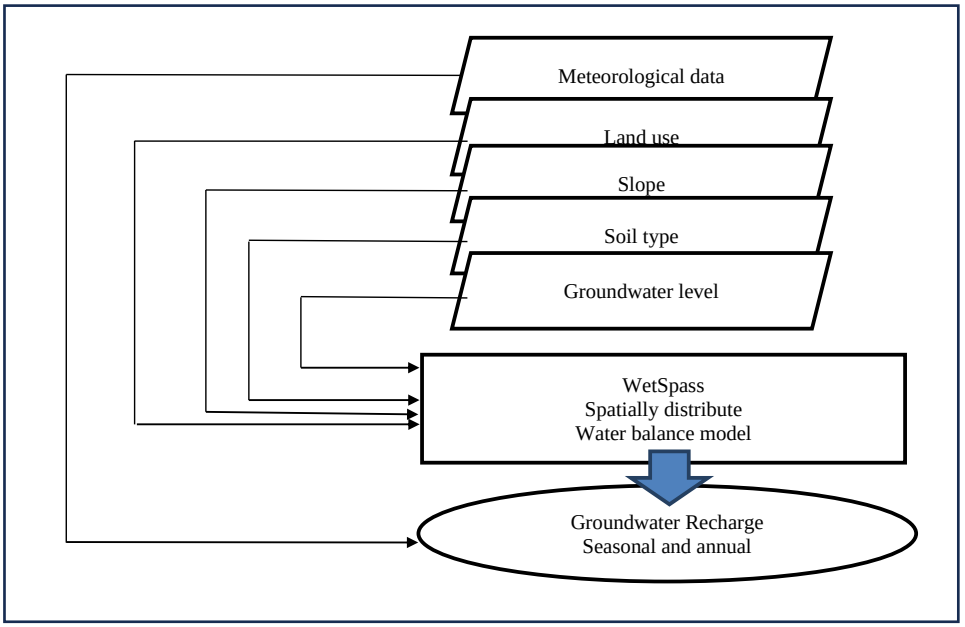

Figure 4.10: Schematic representation of the input data

4.9 Groundwater Modelling using Visual MODFLOW Flex

MODFLOW is a computer program that numerically solves the three-dimensional ground-water flow equation for a porous medium by using a finite-difference method (McDonald and Harbaugh, 1988). MODFLOW-2000 is designed to accommodate the solution of equations in addition to the ground-water flow equation. MODFLOW-2000 allows definition using parameter values, which can be applied to data input for many grid-cell which make it much easier to modify data input values for large parts of a model. Visual MODFLOW supports all the recent public domain and proprietary version of MODFLOW and MT3D for simulating the groundwater flow. In Visual MODFLOW, these programs are referred to as numeric engines because they perform the numeric calculations required to solve the finite difference equations of groundwater flow. The numeric engine support by Visual MODFLOW includes MODFLOW-96 (USGS) and MODFLOW-2000 (USGS) for groundwater flow simulation. In the study,

MODFLOW-2000 has been selected for groundwater flow modelling.

The basic three-dimensional groundwater flow equation is given by,

$$\frac{\partial}{\partial x}\left(Kx\frac{\partial h}{\partial x}\right)+\frac{\partial}{\partial y}\left(Ky\frac{\partial h}{\partial y}\right)+\frac{\partial}{\partial z}\left(Kz\frac{\partial h}{\partial z}\right)\pm W=Ss\frac{\partial h}{\partial t}$$

..……..…… (4.67)

where, K_x, K_y, K_z = hydraulic conductivity values along the x, y, z axes [LT^{-1}]; h= hydraulic head [L]; W = source/sink terms [T^{-1}]; S_s = specific storage coefficient [L^{-1}].

The hydraulic conductivity is the ease with which water can move through an aquifer. It can be determined by dividing aquifer transmissivity by aquifer thickness. The hydraulic conductivity can vary in a geological unit over relatively short distance. The hydraulic conductivity parameter in the model includes K_x i.e. the hydraulic conductivity in the x- direction, K_y i.e. the hydraulic conductivity in y-direction and K_z i.e. hydraulic conductivity in z-direction. The average hydraulic conductivity (K) is calculated using the following equation as given by,

$$K = T/b$$

..……..…… (4.68)

where, K= average hydraulic conductivity of the aquifer material from top to its bottom (m/day); b = thickness of the aquifer (m); T = transmissibility expressed (m^2/day).

The storage parameter of the model includes specific storage (S_s), specific yield (S_y), effective porosity (Eff. Por.) and total porosity (Tot. Por.). The specific storage (S_s) is defined as the amount of water per unit volume of a saturated formation that is stored or expelled from storage owing to the compressibility of the mineral skeleton and the pore water under unit change in head. The specific yield of the aquifer is the amount of water per unit volume that will drain from an aquifer under the influence of gravity. The specific yield is usually larger than specific storage. In very fine-grained units, the S_s component is ignored and storativity is considered equivalent to specific yield. For sand gravel aquifers, specific yield is generally equal to the porosity.

MODFLOW uses S_y to determine storage volumes in unconfined layer, whereas for a confined layer, S_s are used. The effective porosity, p_e, also called the kinematic porosity, of a porous medium is defined as the ratio of the part of the pore volume where the water can circulate to the total volume of a representative sample of the medium. This is used by MODPATH to determine the average linear groundwater velocities for use in time dependent capture zones and times marker along path lines but this term is not used in MODFLOW. The specific storage has been calculated considering the storage coefficient and thickness of each layer. The following equation has been used.

$$S_s = S/t \qquad \text{..……..…… (4.69)}$$

where, S_s = the specific storage per m, t = the thickness (m), S = the storage coefficient

Various other parameters of the study area such as average recharge and constant head are computed using standard procedures and given to the model for evaluating its performance. Visual MODFLOW 2011.1 model is the modified version of MODFLOW and Visual MODFLOW. It allows considerable flexibility in modelling environment for practical applications in 2D and 3D groundwater flow and contaminant simulation from a multilayer aquifer of different types of groundwater basins. It is a fully integrated package that combines with the powerful analytical tools and a logical menu structure which allows users to (i) quickly dimension the model domain and select units, (ii) conveniently assign model properties and boundary conditions, (iii) run model simulations for flow, (iv) calibrate the model using manual or automated techniques, (v) optimize pumping and remediation well rates and locations, and (vi) visualize the results using 2D or 3D graphics. The model input parameters and results can be visualized in 2D (cross-section and plain view) or 3D at any time during the development of the model or displaying of the results. The flow chart depicting the model setup and model simulation is given in Figure 4.11.

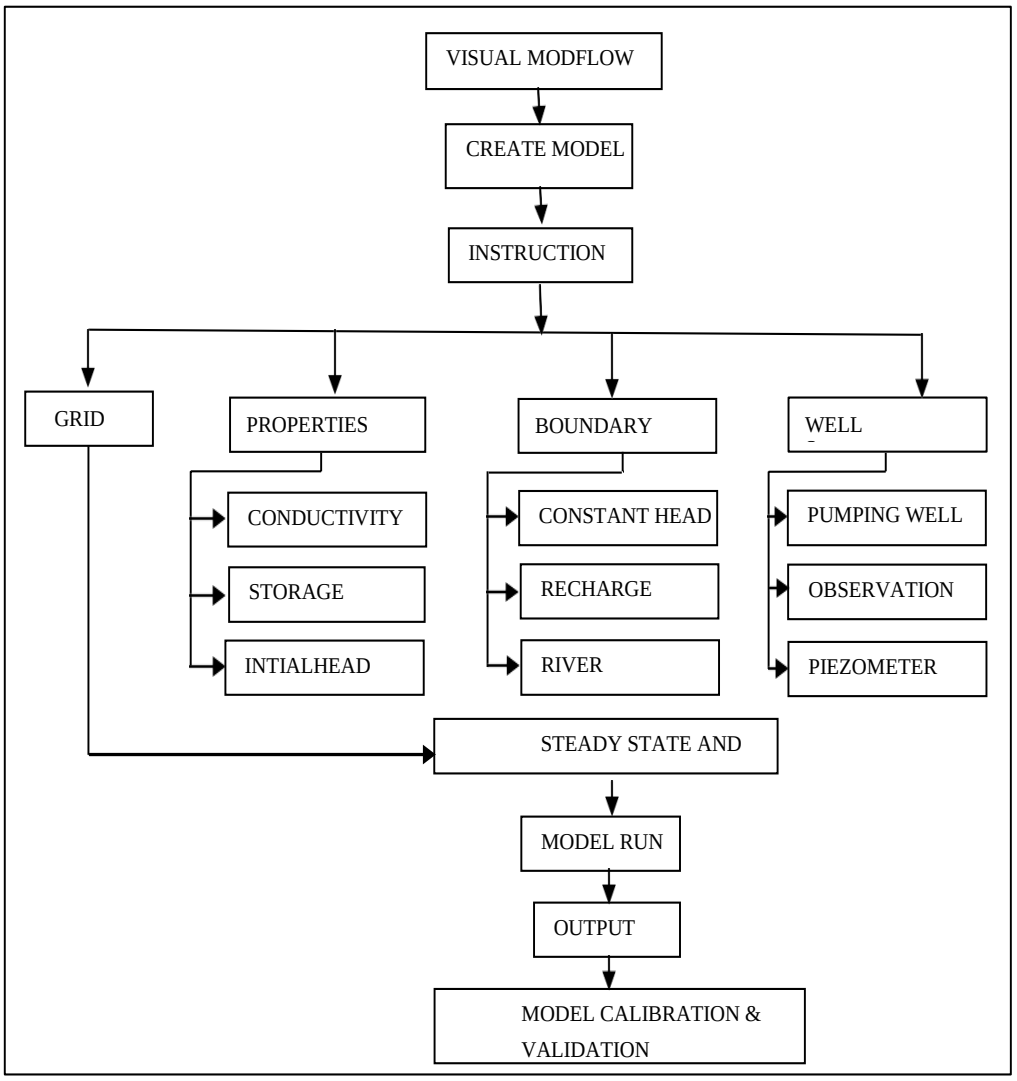

Figure 4.11: Visual MODFLOW application process

The boundary conditions for the groundwater flow and mass transport models are assigned and edited in the 'Boundaries' module of the 'Input' section. Each boundary condition has the same set of graphical tools on the left-hand toolbar for assigning, editing, erasing, and copying the model boundary conditions. The boundary conditions considered in this study are (i) Recharge and (ii) Constant head. Each group of boundary condition grid cells requires a minimum of one time period of data containing a start time, a stop time and complete set of data for the selected boundary condition type.

For steady state simulations, Visual MODFLOW requires data for a single time period only, whereas for transient simulations, Visual MODFLOW can accommodate unlimited number of time periods. If the steady state flow option is selected, Visual MODFLOW prepares the dataset for a steady-state flow

simulation and automatically uses data from the first stress period of each boundary condition and pumping well defined in a project. If the transient flow option is selected, Visual MODFLOW prepares the data set for a transient flow simulation. During this process, Visual MODFLOW automatically merges all of the different time period data defined for each pumping well and boundary condition into the stress period format required by the different versions of MODFLOW.

The Visual MODFLOW model is divided into three main sections viz., a) input, b) run and c) output. The 'Input' section allows the user to graphically assign all necessary input parameters for building a three-dimensional groundwater flow and contaminant transport model. The input section of Visual MODFLOW is used to

(i) Refine 3D finite difference grid,

(ii) Assign boundary condition locations and attributes.

The 'Run' section, allows the user to modify the various MODFLOW, MODFLOW-SURFACT, MODPATH, MT3D/RT3D, MGO and WinPEST parameters and options which are run-specific. The 'Output' section allows the user to display all of the modelling and calibration results for MODFLOW, MODFLOW-SURFACT, MODPATH, Zone Budget, and MT3D/RT3D. The Output Menus allows selecting, customizing, overlying the various display options, and exporting images for presenting the modelling results.

4.9.1 Visual MODFLOW Flex Calibration and Validation

The model was calibrated is generally carried out in two stages, which involves a steady state condition and a transient state (pumping) condition. Monthly values of discharge of pumping wells (m^3/day) and head of observation wells (m), screen top and bottom, conductivity, specific storage, specific yield, effective porosity, total porosity, recharge and evapotranspiration are assigned for different zones and layers of the study area and this is used for the calibration of the model. The calculated head is compared with the observed values using various methods such as mathematical, graphical, linear regression and statistical tests of significance. The model needs to be subsequently validated with comprising of groundwater level data of independent observation levels not considered for the

calibration so as to test the confidence in the calibrated model.

4.10 Groundwater Modelling using MUSE

Model MUSE has also been developed by the U.S. Geological Survey (USGS), and is a widely used groundwater modeling software known for its user-friendly interface, robust numerical algorithms, and flexibility in model construction (Niswonger et al., 2011). It incorporates various modeling components, including MODFLOW for flow simulations, MT3DMS for transport modeling, and PEST for parameter estimation (Hill et al., 2000). Model Muse has been applied in diverse hydrogeological settings, such as aquifer characterization (Abd-Elhamid et al., 2010), and analysis of managed aquifer recharge (Niswonger et al., 2013). Its versatility allows for the simulation of complex hydrogeological processes, including groundwater-surface water interactions (Morway et al., 2016) and multi-phase flow (Thorne et al., 2015). The flow chart depicting the groundwater flow modelling process is given in Figure 4.12.

The conceptualization of the MUSE includes defining the study area in the model, and identifying hydrogeological units, such as aquifers, confining layers, and recharge/discharge areas and characterizing geological, hydrological, and hydrogeological properties through field investigations, geological surveys, well logs and geophysical data. Mesh generation is an important step for creating a numerical mesh/grid representing the study area with appropriate resolution. Mesh refinement is also possible in areas of interest or complex hydrogeological features. The boundary conditions include river head boundaries, specified flux boundaries, and no-flow boundaries based on field observations and conceptual understanding.

The hydraulic properties to be incorporated into the model include

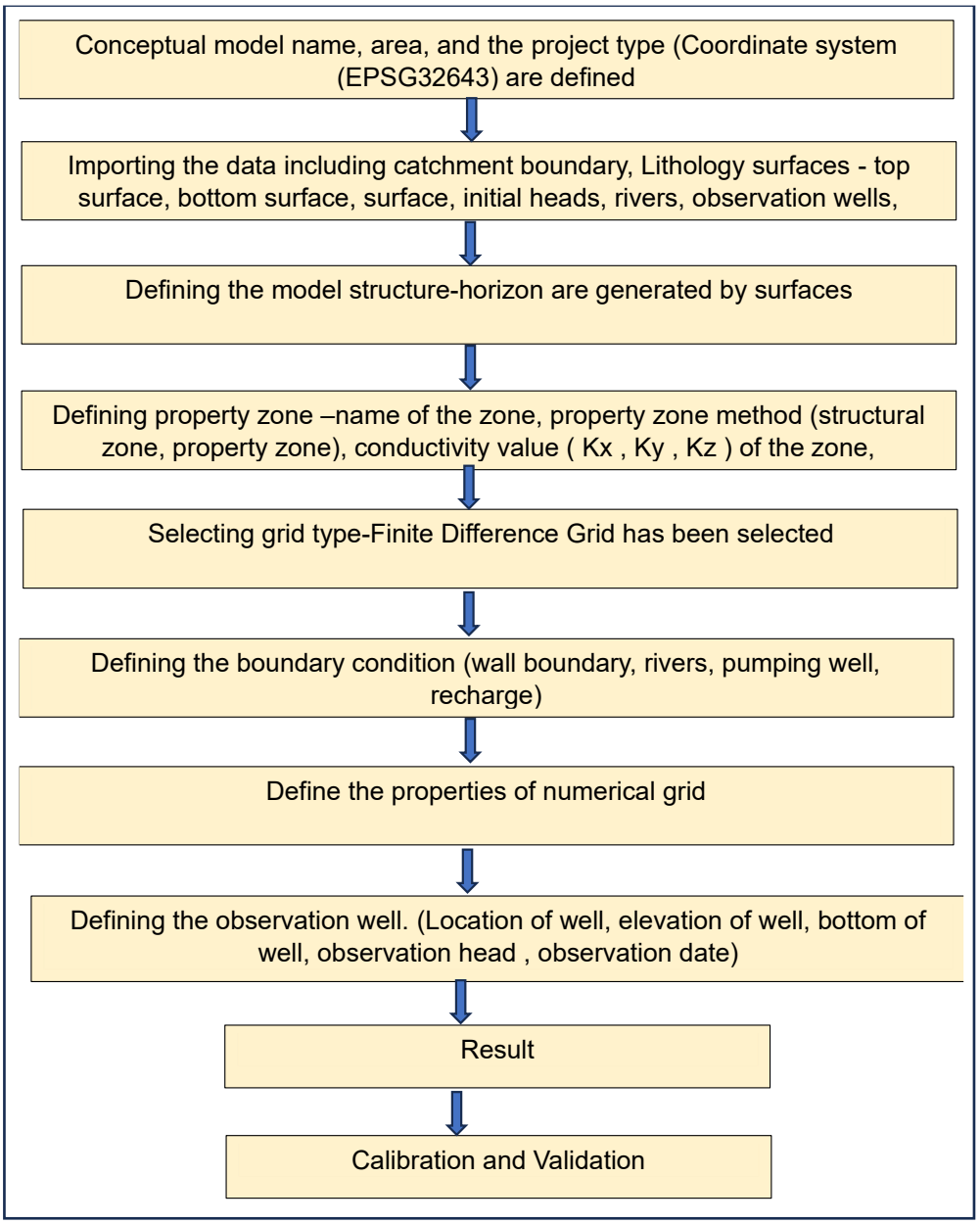

Figure 4.12: MUSE groundwater flow modelling process

hydraulic conductivity, specific yield, porosity, to hydrogeological units. The range of these hydraulic properties for calibration is carried out through field measurements, pumping tests, and literature values.

4.10.1 Model MUSE Calibration and Validation

The model was calibrated using the head of observation wells (m), discharge data of pumping wells (m^3/day), conductivity, specific storage, specific yield, screen top and bottom, effective porosity, total porosity, recharge and evapotranspiration assigned to the various zones and layers. The computed and

observed heads have been compared using various performance evaluation criteria. The confidence in the calibrated model is evaluated through model validation with independent groundwater level of those observation levels that were not considered for the calibration.

4.11 Flood Plain Mapping using HEC-RAS

The U.S. Army Corps of Engineers Hydrologic Engineering Center's River Analysis System (HEC-RAS) offers an optimal platform for conducting one-dimensional steady water surface profile computations, one- and two-dimensional unsteady flow simulation, movable boundary sediment transport computations, generalized water quality modelling. All these four components use a common geometric data representation and common geometric and hydraulic computation routines. Also, the system has several hydraulic design features that can be invoked once the basic surface profiles are computed. The software also supports spatial mapping of many computed parameters (depth, water surface elevation, velocity, etc.). Typically, the model outcomes from HEC-RAS find application in floodplain management initiatives and flood insurance studies to assess the impacts of floodway encroachments.

The steady water surface profiles modelling component can be used for computing water surface profiles for 'steady gradually varied flow' for single river reach, a dendritic system or a full network of channels. This component is capable of modelling subcritical, supercritical and mixed flow regime water surface profiles. The computational procedure is based on the solution of the one-dimensional energy equation. Energy losses are evaluated by Manning's equation (friction) and contraction/expansion coefficient multiplied by the change in velocity head. The momentum equation is used where the water surface profile is 'rapidly varied' which may include 'mixed flow regime' calculations such as hydraulic jumps, hydraulics of bridges and evaluating profiles at river confluences (stream junctions). The steady flow system is designed for application in flood plain management and flood insurance studies to evaluate floodway encroachments. It is also capable of assessment of changes in the water surface profiles due to channel improvements and levees. The assumptions or limiting conditions that are implicit

in the analytical expressions include a) flow is steady (time dependent terms are not included) and gradually varied except at bridges, culverts, weirs etc., flow is one dimensional which mean that velocity component is calculated only in the direction of flow (total energy head is assumed to be same for all points in a cross-section); and river channels have small and gentle slopes (less than 1:10).

The unsteady water surface profiles modelling component can be used for simulating one-dimensional unsteady flow, two-dimensional unsteady flow or combined 1D and 2D unsteady flow modelling through a full network of open channels. The ID unsteady flow components have been developed for subcritical flow regime calculations. The 2D unsteady flow equation solver was developed to facilitate combined 1D and 2D hydrodynamic modelling. Upstream boundary conditions are required at the upstream end of all reaches that are not connected to other reaches or storage areas. This upstream boundary condition is applied as flow hydrograph of discharge versus time. Similalrly, the downstream boundary conditions are required at the downstream end of all reaches which are not connected to other reaches or storage areas. The downstream boundary conditions that can be applied include stage hydrograph, flow hydrograph, single-valued rating curve or normal depth from Manning's equation. The hydraulic computations for cross-sections, bridges, culverts and other hydraulic structures are also incorporated in the unsteady flow module. The unsteady flow module also has the capability to model storage areas and hydraulic connections between storage areas, 2D flow areas and between stream reaches.

Flood inundation modelling comprises hydrologic modelling, hydraulic modelling, and terrain analysis (Jung, 2011). Hydrologic modelling involves estimating flow discharges, either by employing regression equations to compute peak-flow data (e.g., Bisese, 1995; Austin *et al.*, 2011) or by conducting detailed rainfall simulations across the watershed drainage area to generate runoff hydrographs (e.g., Bravo *et al.*, 2012; Kingston, 2012). Hydraulic modelling utilizes these discharge data to calculate water surface elevations and the spatial extent of flood inundation. It offers an accurate depiction of flow routing through the modelled river network, taking into account the backwater effects of floodplains in moderating and delaying peak flows (Bravo *et al.*, 2012). Terrain analysis involves

outlining the inundated floodplain areas in conjunction with Digital Terrain Models (DTM).

4.11.1 One-dimensional (1D) hydrodynamic modelling

HEC-RAS possesses the capacity to model one-dimensional (1D) water surface profiles in steady and unsteady conditions for both natural and artificial channels. The calculation of water surface profiles occurs between consecutive cross-sections of the channel through the iterative solution of the energy equation, employing the standard method. The governing physical laws for water flow in a stream are expressed through the principles of conservation of mass and conservation of momentum. These principles are formulated as partial differential equations commonly known as continuity and momentum equations, and collectively referred to as Saint-Venant's equations. In this study, the simulation of one-dimensional gradually varied flow is conducted by applying the continuity and momentum equations.

In 1D hydraulic modelling, flow is assumed to move downstream solely in the longitudinal direction. The terrain in a 1D model is represented as a transversal system, with results estimated at each cross-section for average velocity and water depth. In the present study, one dimensional unsteady gradually varied flow simulation has been performed with the help of continuity and momentum equations.

$$\frac{\partial A}{\partial t} + \frac{\partial Q}{\partial x} = 0 \qquad \text{..... (4.70)}$$

$$\frac{\partial Q}{\partial t} + \frac{\partial \frac{Q^2}{A}}{\partial x} + gA\frac{\partial H}{\partial x} + gA\,(S_o - S_f) = 0 \qquad \text{..... (4.71)}$$

where, A = cross-sectional area normal to the flow; Q = lateral inflow/outflow of the channel; H = water surface elevation, also called stage; S_f = friction slope; x = longitudinal coordinate; Q = discharge; g = acceleration of gravity; S_o = bed slope; t = temporal coordinate.

The flow chart for the 1D hydrodynamic modelling in HEC-RAS is given in Figure 4.13. The development of the 1D hydrodynamic model setup within the

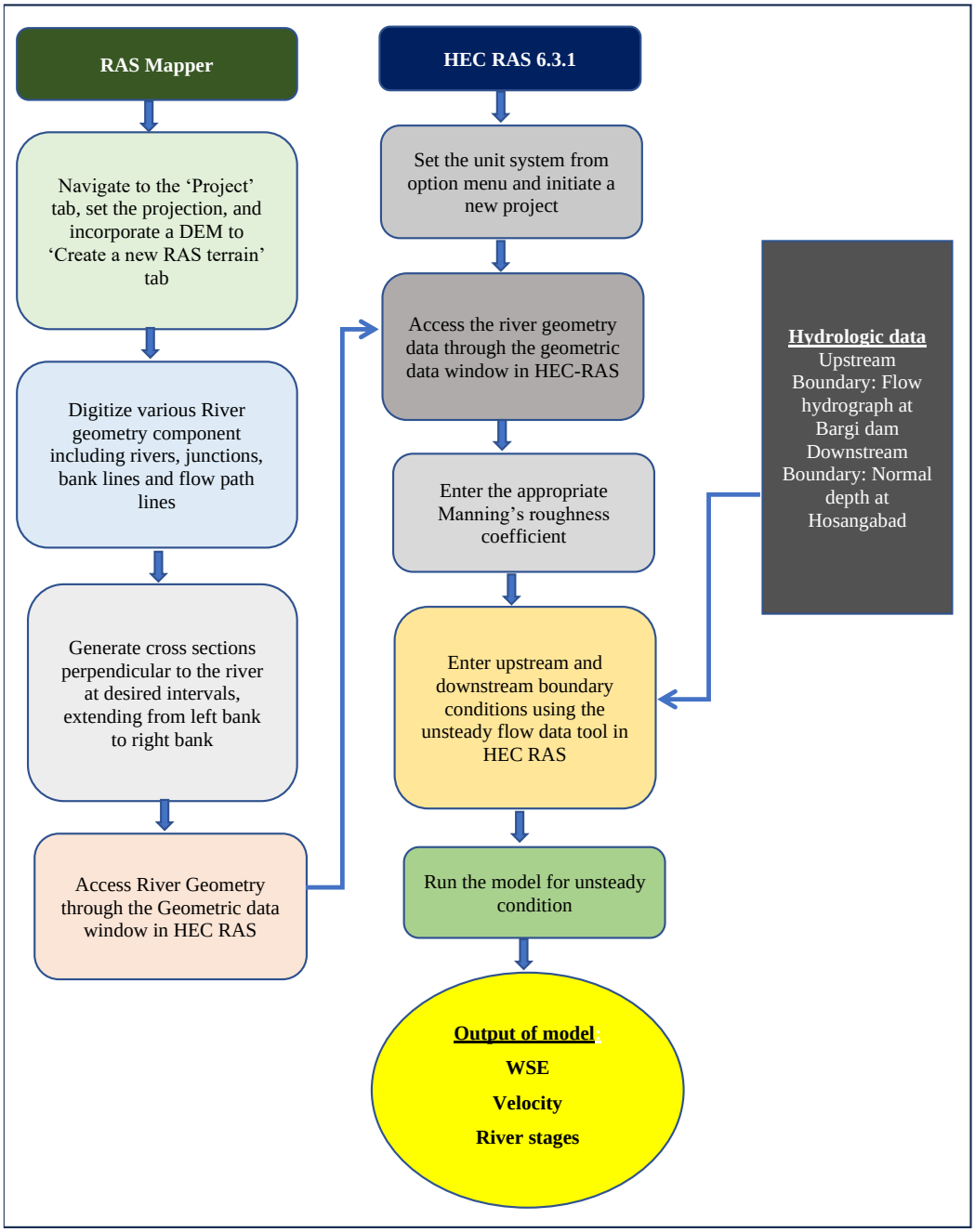

Figure 4.13: Flow chart for the 1D hydrodynamic modelling in HEC-RAS

HEC-RAS environment includes creating a new terrain model by importing the DEM using RAS mapper; adding geometry using RAS mapper by sequentially creating by digitizing various HEC-RAS layers viz., stream centre line, banks, flow paths and cross-sections; and assigning appropriate river code and reach code to streams; entering Manning's n value for channel and banks; assigning appropriate upstream and downstream boundary conditions and applying the specified conditions for the 1D model; ; selecting the desired equation for simulation and executing the program at the desired computation interval.

4.11.2 Two-dimensional (2D) hydrodynamic modelling

The primary channel and adjacent floodplain areas constitute a river system mixture. During flood events exceeding the main channel depth, water surface elevations extend into the floodplains. In the concept of 2D modelling, the river and adjoining floodplain area are subdivided into grid cells. A cell face serves as the interface between two grid cells, comprising ground elevations derived from GIS cells. Hydraulically a cell face resembles a cross-section facilitating the calculation of various properties such as hydraulic radius cross-sectional area wetted perimeter, and conveyance for desired water surface elevations. Two-dimensional models consider the ground as a constant surface, while 1D model focus solely on river and inland geometries at specific locations along the channel length. The use of a constant terrain enables two-dimensional models to more accurately depict lateral flow interactions between the main channel and floodplains, including their impacts on floodplain storage.

To develop a 2D hydrodynamic model in HEC-RAS, the entire study area must be delineated by a continuous polygon covering the river, banks and floodplain, referred to as the "2D flow area" corresponding to the entirely of the simulated model. This 2D flow area is subdivided into a grid, with each compartment serving as a control volume for inflow and outflow calculations based on respective velocities. In developing a 2D model, a computational mesh is established for the main river reach, extending from upper most reservoir or beginning of the main river to a considerable area downstream the area of interest which is prone to floods and the flood plain mapping needs to be carried out.

The newer version of HEC-RAS 6.3.1 offers the option to develop a model using either the full momentum equation, known as the 2D Saint Venant's equation, or the 2D diffusive wave equation, as illustrated by equations (3), (4), and (5) (Gary W. Brunner, 2016; Quirogaa et al., 2016a; Patel *et al.*, 2017).

$$\frac{\partial \zeta}{\partial t} + \frac{\partial p}{\partial x} + \frac{\partial q}{\partial y} = 0$$

..... (4.72)

$$\frac{\partial p}{\partial t} + \frac{\partial}{\partial x}\left(\frac{p^2}{h}\right) + \frac{\partial}{\partial y}\left(\frac{pq}{h}\right) = -\frac{n^2 p g\sqrt{p^2+q^2}}{h^2} - gh\,\frac{\partial \zeta}{\partial x} + pf + \frac{\partial}{p\partial x}\,(h\tau_{xx}) + \frac{\partial}{p\partial y}\left(ht_{xy}\right)$$

$$\frac{\partial p}{\partial t}+\frac{\partial}{\partial y}\left(\frac{q^2}{h}\right)+\frac{\partial}{\partial y}\left(\frac{pq}{h}\right)=-\frac{n^2 q g\sqrt{p^2+q^2}}{h^2}-gh\frac{\partial \zeta}{\partial y}+qf+\frac{\partial}{p\partial y}\left(h\tau_{yy}\right)+\frac{\partial}{p\partial y}\left(ht_{xy}\right)$$

..... (4.73)

where, h is the depth of water in meter; p and q are the explicit flow in the x and y directions (m^2 s^{-1}); g is the acceleration due gravity (m s^{-2}); n is the Manning roughness coefficient, is the water density (kg m^{-3}); xx, yy and xy are the components of the effective shear stress and f is the Coriolis (s^{-1}).

The program solves either the 2D Shallow Water equations (with optional momentum additions for turbulence, wind forces, mud and debris flows, and Coriolis effects) or the 2D Diffusion Wave equations. This is user selectable, giving modelers more flexibility. In general, the 2D Diffusion Wave equations allow the software to run faster and have greater stability properties. The 2D Shallow Water equations are applicable to a wider range of problems. However, many modelling situations can be accurately modelled with the 2D Diffusion Wave equations. Because users can easily switch between equation sets, each can be tried for any given problem to see if the use of the 2D Shallow Water equations is warranted over the Diffusion Wave equations. When opting for the diffusive wave equation, the primary terms of momentum the above last two equations are disregarded. While the default setting in HEC-RAS software is the diffusion wave equation.

The development of the 2D computational mesh within the HEC-RAS environment includes specifying the desired values for 2D flow area computation points and setting both DX and DY values for the simulation; partitioning the 2D flow area into grid cells of desired grid size; importing land use information into HEC-RAS in shape file and gridded formats, generating land cover information using RAS Mapper and integrating it with the selected 2D geometric data of the floodplain; applying a spatially varying Manning's n based on National Land Cover Database (NLCD) guidelines; providing upstream and downstream boundary conditions outside the 2D area and applying the specified conditions for the 2D model; selecting the desired equation for simulation and executing the program at the desired computation interval. The flow chart for the 2D hydrodynamic modelling in HEC-RAS is given in Figure 4.14.

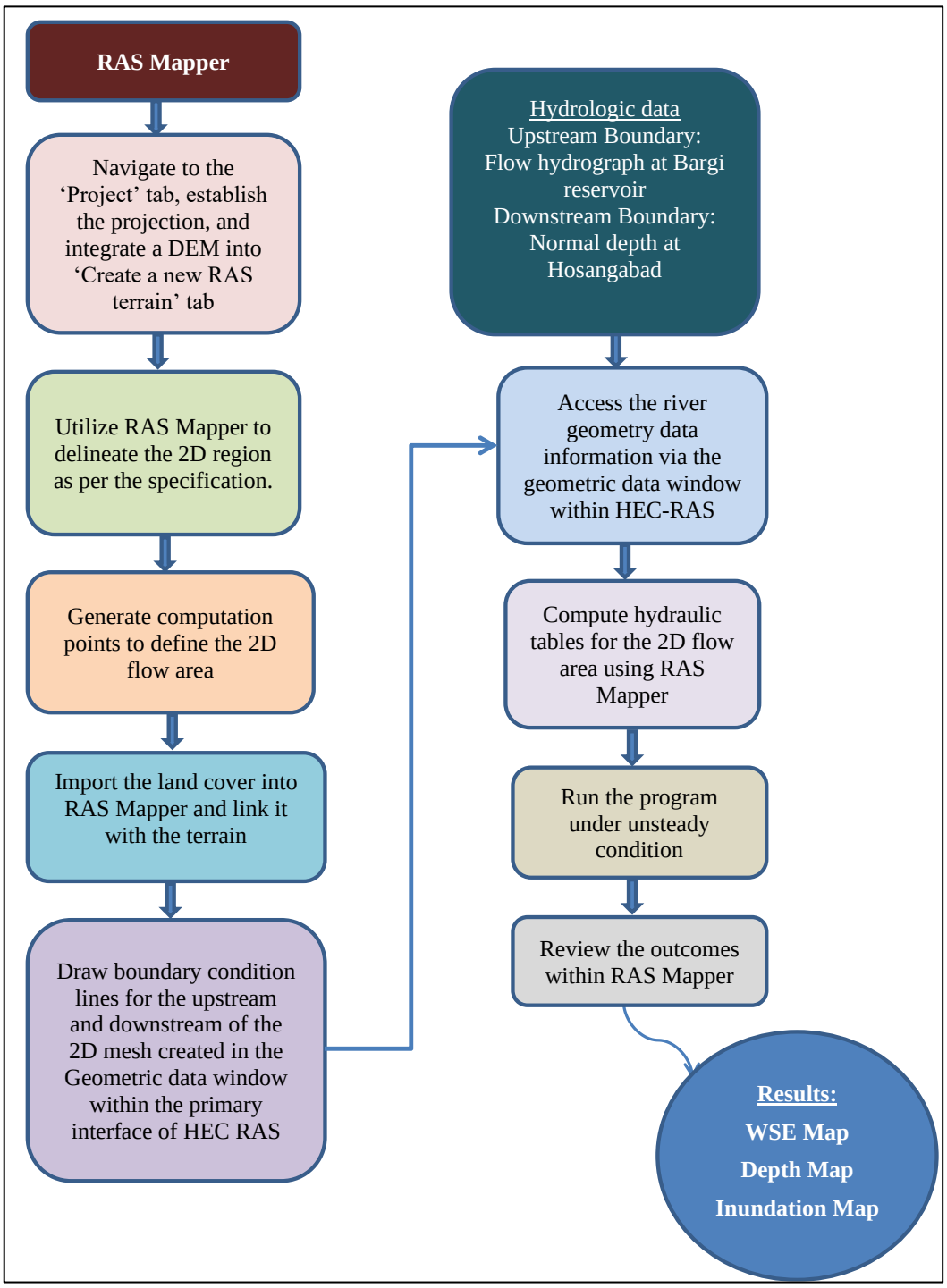

Figure 4.14: Flow chart for the 2D hydrodynamic modelling in HEC-RAS

The mapping of the inundated area and animations of the flooding can be done inside of HEC-RAS using the RAS Mapper features. The mapping of the 2D flow areas is based on the detailed underlying terrain which means that the wetted area will be based on the details of the underlying terrain, and not the computational mesh cell size. The 2D flow area computational solution has been programmed to

take advantage of multiple processors on a computer (referred to as parallelization), allowing it to run much faster than on a single processor.

There are three basic model data requirements viz., a) geometric data, b) steady flow data and c) unsteady flow data. Accurately representing ground surface elevations is fundamental for developing hydrodynamic models, whether 1D or 2D. A high-quality terrain model precisely depicts river and floodplain elevations, incorporating physical features like channel banks, channel beds, and high ground elements such as roadways and levees that influence flow. The geometric data consists of establishing the connectivity of river system (river system schematic), cross-section data, reach lengths, energy loss coefficients (friction losses, contraction and expansion losses), stream junction information, storage areas, and 2D flow areas. Information on other hydraulic structures like bridges, culverts, spillways, weirs etc. can also be included.

The steady flow data required to perform the steady water surface profile computations include flow regime, boundary conditions, and discharge data (peak flow or flow data from specific instance in time). The unsteady flow data required to perform the unsteady water surface profile computations include internal and external boundary conditions as well as initial conditions. The open ends of the river system can be modelled with either of the boundary conditions viz., flow hydrograph (most upstream boundary condition), stage hydrograph or flow and stage hydrograph. The downstream ends of the river system can be modelled with either of these boundary conditions viz., rating curve, normal depth (Manning's equation), stage hydrograph, flow hydrograph or stage and flow hydrograph. Additionally, gated structures defined within the river system (inline, lateral or between storage areas and/or 2D flow areas) could have these boundary conditions viz., time series of gate openings, elevation-controlled gate, navigation dam, rules or internal observed stage and flow.

4.12 Evaluation of Drought Characteristics

Standardized Precipitation Index (SPI) is most widely used to evaluate the meteorological drought characteristics. SPI is based on an equiprobability transformation of aggregated monthly precipitation into a standard normal variable.

In practice, computation of the index requires fitting a probability distribution to aggregated monthly precipitation series (k = 1, 3, 6, 12, 24 months); computing the non-exceedance probability related to such aggregated values; and defining the corresponding standard normal quantile as the SPI. McKee et al. (1993) assumed the aggregated precipitation to be gamma distributed and used a maximum likelihood method to estimate the parameters of the distribution. Although, McKee et al. (1993) originally proposed a classification restricted only to drought periods, it has become customary to use the index to classify the wet periods as well.

This permits it use to compare both dry and wet periods at different locations. Moreover, since it is based on precipitation alone, a drought assessment is possible even if other meteoro-hydrological data are not available, which is generally the case in developing countries. The negative values of the standardized normal variable are compared with the boundaries of different classes of drought proposed by McKee et al. (1993) which helps to identify the severity level of the drought event. Among users, there is a general consensus about the fact that the SPI on shorter time scales (3 or 6 months) describes drought events affecting agricultural practices, while on the longer ones (12 or 24 months) it is more suitable for water resources management purposes. The computation of the SPI is accomplished as per the following equations,

$$\bar{X}_{ln} = \frac{\sum \ln X}{N} \quad \text{..... (4.74)}$$

$$\beta = \frac{1}{4U}\left[1 + \sqrt{\frac{4U}{3}}\right] \quad \text{..... (4.75)}$$

$$\alpha = \frac{\bar{X}}{\beta} \quad \text{..... (4.76)}$$

where, U is the constant given by,

$$U = \ln(\overline{X}) - \bar{X}_{ln} \quad \text{..... (4.77)}$$

The resulting parameters are then used to find the cumulative probability of an observed precipitation event for the given month and time scale for the station. The cumulative probability as given by Gamma distribution is given by,

$$G(x) = \frac{1}{\alpha^{\beta}\,\Gamma\beta}\int_0^x x^{\beta-1}e^{\frac{-x}{\alpha}}\,dx \quad \text{..... (4.78)}$$

Letting t = $\frac{-x}{\alpha}$, this equation becomes the incomplete gamma function,

$$G(x) = \frac{1}{\Gamma\beta}\int_0^{t\alpha} t^{\beta-1}e^{-t}\ dt \quad \text{..... (4.79)}$$

Since the gamma function is undefined for x = 0 and a precipitation distribution may contain zeros, the cumulative probability becomes,

$$H(x) = q + (1-q)G(x) \quad \text{..... (4.80)}$$

where, 'q' is the probability of a zero.

However, the three-parameter gamma distribution is considered to produce more robust values of SPI. If 'm' is the number of zeros in a precipitation time series, states that 'q' can be estimated by 'm/N' and used tables of incomplete gamma function to determine cumulative probability H(x). The cumulative probability is then transformed to the standard normal random variable Z with mean zero and variance one, which is the value of the SPI. The Z or SPI values are more easily obtained computationally using an approximation provided by Abramowitz & Stegun (1972) that converts cumulative probability to the standard normal random variable Z.

$$Z = SPI = -\left[t - \frac{c_{0+}c_1t+c_2t^2}{1+d_1t+d_2t^2+d_3t^3}\right] \quad \text{for } 0< H(x) \leq 0.5 \quad \text{..... (4.81)}$$

$$Z = SPI = +\left[t - \frac{c_{0+}c_1t+c_2t^2}{1+d_1t+d_2t^2+d_3t^3}\right] \quad \text{for } 0.5 < H(x) \leq 1.0 \quad \text{..... (4.82)}$$

where,

$$t = \sqrt{ln\left\{\frac{1}{(H(x))^2}\right\}} \text{ for } 0< H(x) \leq 0.5 \text{ and} \quad \text{..... (4.83)}$$

$$t = \sqrt{ln\left\{\frac{1}{(1.0-H(x))^2}\right\}} \quad \text{for } 0.5 < H(x) \leq 1.0 \quad \text{..... (4.84)}$$

$$c_0 = 2.515517\ , c_1 = 0.802853\ and\ c_2 = 0.010328$$

$$d_1 = 1.432788, d_2 = 0.189269\ and\ d_3 = 0.001308$$

A drought event continues during the period when SPI is continuously negative and reaches an intensity of -1.0 or less. The event ends when the SPI become positive. As the SPI is normally distributed it can also be helpful to find out

the dry event as well as wet event. The frequency, duration and intensity (magnitude) of drought are the characteristics that can be calculated with SPI. The positive sum of the SPI for all the months within a drought event is termed as drought magnitude. The division of magnitude by its duration is the intensity of drought for that particular duration. In order to evaluate of drought severity in different areas using SPI, one of the most commonly used classification presented by (Hayes et al., 1999), at the National Drought Mitigation Center (NDMC) is given in Table 4.4.

Table 4.4: Standard ranges of SPI values and their classification

S. No.	SPI range	Classification	Occurrence probability (%)
1.	2.0 ≥	Extremely wet	2.3
2.	1.5 to 1.99	Very wet	4.4
3.	1.0 to 1.49	Moderately wet	9.2
4.	0.0 to 0.99	Mild wet	34.1
5.	0.0 to -0.99	Mild drought	34.1
6.	-1.0 to -1.49	Moderate drought	9.2
7.	-1.5 to-1.99	Severe drought	4.4
8.	-2.0 ≤	Extreme drought	2.3

In summary, the SPI allocates a single numeric value to the precipitation (-3 to 3), which can be compared across regions with different climates. Thus, an SPI of 2 or more happens about 2.3% of the time and a mild drought (SPI between 0 and -0.99) happens 34.1% of the time. The SPI was designed to state that it is possible to simultaneously experience wet conditions on one or more-time scales, and dry conditions at other time scales. Table 4.5 gives the SPI and its corresponding cumulative probability.

Table 4.5: SPI and corresponding cumulative probability

S. No.	SPI	Cumulative probability	S. No.	SPI	Cumulative probability
1.	-3.0	0.0014	7.	0.0	0.5000
2.	-2.5	0.0062	8.	+0.5	0.6915
3.	-2.0	0.0228	9.	+1.0	0.8413
4.	-1.5	0.0668	10.	+1.5	0.9332
5.	-1.0	0.1587	11.	+2.0	0.9772

6.	-0.5	0.3085	12.	+2.5	0.9938

The SPI for a month/year in the period of record is dependent upon the timescale. SPI can be evaluated for various time scales of 1, 3, 6 and 12 months. A 3-month SPI is used for a short-term or seasonal drought index and 12-month SPI is used for an intermediate-term drought index. 24-month and 48-month SPI is used as long-term drought index. The SPI has been favourably evaluated and compared with others indices (Keyantash and Dracup, 2004) and is now integrated in the set of indices used by the Drought Monitor in the USA (Svoboda et al., 2002). The SPI can be used on all stations having more than 30-year rainfall data (Hayes et al., 1999).

4.13 Model performance evaluation

The rainfall-runoff model performance has been evaluated using the goodness of fit statistics given by Nash Sutcliffe Efficiency (NSE) (Nash and Sutcliffe, 1970), Root Mean Square Error (RMSE), Percent Bias (PBias), coefficient of determination (r^2) and RMSE-Observations Standard Deviation Ratio (RSR) as suggested by (Moriasi et al., 2007). The NSE is a normalized statistic that determines the relative magnitude of residual variance in comparison to the observed data variance and varies between - to 1, 1 indicating a perfect match.

However, the NSE is more biased towards high flows. (Moriasi et al., 2007) suggested that NSE values should be greater than 0.50 in order for model results to be judged satisfactory on a monthly time step simulation. The NSE has been computed from the following equation,

$$NSE = 1.0 - \left[\frac{\sum_{i=1}^{n}(Y_i^{obs} - Y_i^{sim})^2}{\sum_{i=1}^{n}(Y_i^{obs} - Y_{mean}^{obs})^2}\right] \quad \text{..... (4.85)}$$

The coefficient of determination (r^2) describes the proportion of the total variance in the observed data that can be explained by the model, and ranges between 0 and 1, with higher values indicating a better fit. However, this correlation-based measure is more sensitive to the extreme values (Willmott, 1981). The r^2 can be computed from the following equation,

$$r^2 = \left(\frac{\sum_{i=0}^{n}(Y_i^{obs} - Y_{mean}^{obs})(Y_i^{sim} - Y_{mean}^{sim})}{\sqrt{\sum_{i=1}^{n}(Y_i^{obs} - Y_{mean}^{sim})^2}\sqrt{\sum_{i=1}^{n}(Y_i^{sim} - Y_{mean}^{sim})^2}}\right)^2$$

..... (4.86)

The root mean square error (RMSE) has also been used to assess the model performance. The lower values of RMSE indicate a better fit of the simulated data with the observed data. The RMSE is given by,

$$RMSE = \left\{1/n\sqrt{\sum_{i=1}^{n}(Y_i^{obs} - Y_i^{sim})^2}\right\}$$

..... (4.87)

The Mean Square Error (MSE) and RMSE are many a times used as objective function for minimization in hydrological models to narrow (minimize) the gap between the observed and simulated flow values. The Percent Bias (PBias) measures the average tendency of the simulated data to be larger or smaller than their observed counterparts. The best value of PBias is zero, with low values indicating a perfect model simulation, whereas the positive values indicate model underestimation and negative values indicate overestimation (Gupta et al., 1999). The PBias has been calculated by using following equation,

$$PBias = \left[\frac{\sum_{i=1}^{n}(Y_i^{obs} - Y_i^{sim})}{\sum_{i=1}^{n} Y_i^{obs}} X100\right]$$

..... (4.88)

The RMSE-observations Standard deviation Ratio (RSR) has been proposed by(Singh et al., 2004) which standardizes the RMSE using the Observation standard deviation and it combines both an error index and the additional information recommended by (Legates and McCabe, 1999). RSR is calculated as the ratio of the RMSE and standard deviation of the observed data, and has been computed using the following equation,

$$RSR = \frac{RMSE}{STDEV_{obs}} = \left[\frac{\sqrt{\sum_{i=1}^{n}(Y_i^{obs} - Y_i^{sim})^2}}{\sqrt{\sum_{i=1}^{n}(Y_i^{obs} - Y_i^{mean})^2}}\right]$$

..... (4.89)

The lower RSR values are indicative of lower RMSE and better will be the model performance (Moriasiet al., 2007). In the above equations,$Y_i^{obs}$is the ith observed data, $Y_{mean}^{obs}$is mean of observed data, $Y_i^{sim}$is the ith simulated value, $Y_{mean}^{sim}$is the mean of model simulated value, and *n* is the total number of events. The model performance rating of the evaluation statistics at monthly time step according to Moriasi et al. (2007) is given in Table 4.6.

Table 4.6: Performance rating for evaluation statistics at monthly time step

Performance rating	RSR	NSE	PBIAS (%)
Very Good	0.00 ≤ RSR ≤ 0.50	0.75 < NSE ≤ 1.00	PBIAS < ± 10
Good	0.50 < RSR ≤ 0.60	0.65 < NSE ≤ 0.75	± 10 ≤ PBIAS < ± 15
Satisfactory	0.60 < RSR ≤ 0.70	0.50 < NSE ≤ 0.65	± 15 ≤ PBIAS < ± 25
Unsatisfactory	RSR > 0.70	NSE ≤ 0.50	PBIAS ≥ ±25

Source: Moriasi et al., (2007)

5.0 RESULTS AND DISCUSSIONS

The modelling studies have been carried out to understand the various components of hydrology, wherein modelling efforts have been directed towards simulation of surface water flow, groundwater flow, demand-supply scenario and droughts thereby using the various calibrated and validated models to evaluate the impacts of climate change on the overall water availability scenario. Also, the flood planning mapping at Hoshangabad which is prone to frequently flood has been carried out to understand the flood scenario in the region. The details of the various models including the brief theoretical background have been briefly explained in the previous section on Methodology.

5.1 Investigation of Climate Change Signals in Historical Time Period

5.1.1 Changes in Precipitation

The investigation of historical climate datasets of precipitation, maximum and minimum temperature is essential to detect the presence any relevant signals of climate change. This helps to assess the extent to which the variables responsible for climate change have already started impacting the vulnerable regions within the study area. The investigation of the climate change signals has been evaluated for the complete Narmada basin to understand its spatial variability in the various zones of this elongated river basin. The indices used to assess the changes in the precipitation include average annual rainfall, decadal rainfall, annual rainy days, 1-day maximum rainfall, heavy rainfall (daily rainfall > 50 mm), very heavy rainfall (daily rainfall > 100 mm), and extreme rainfall (daily rainfall > 200 mm). It has been observed that the average annual rainfall is decreasing marginally in the basin as depicted in Figure 5.1.

The average annual rainfall over the basin is 1119.19 mm (1991-2015) which varied between 676.9 mm in 1965 and 1682.7 mm in 1944. The analysis was thereafter extended to longer time slices of 30 years and the variation of the average rainfall during these 30-year time horizons are given in Table 5.1. It can be observed that the average annual rainfall in the present time horizon (1991-2015) is limited to 1060.02 mm whereas it was 1102.35 mm during the baseline period (1961-1990). 93 grids out of 130 grids covering the basin area depicted a

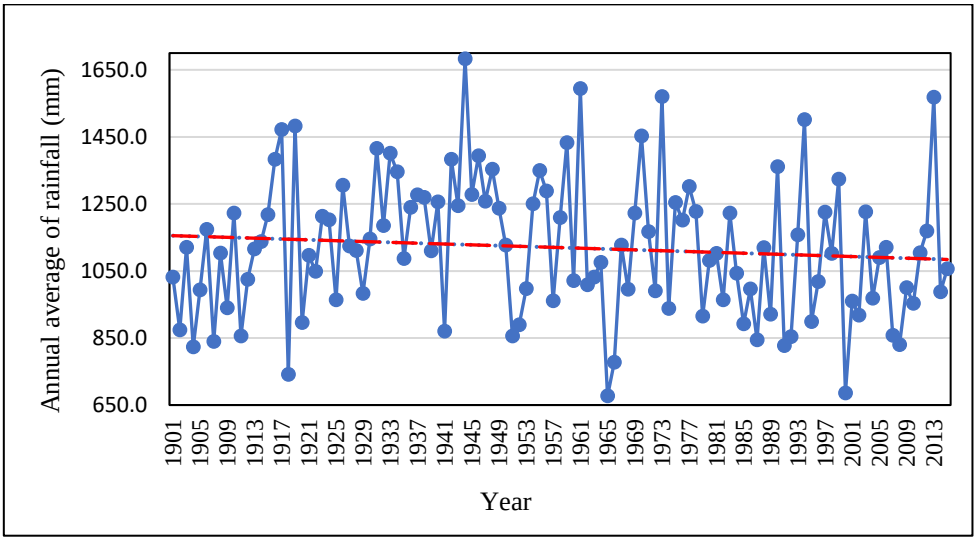

Figure 5.1: Temporal variation of the average annual rainfall in Narmada basin

Table 5.1: Variation in the average rainfall during 30-yr time horizons

S. No.	Time horizon	Mean annual rainfall (mm)
1.	1901-30	1087.92
2.	1931-60	1222.15
3.	1961-90	1102.35
4.	1991-15	1060.02

decreasing annual rainfall pattern during the present time period (1991- 2015) as compared to the baseline period (1961-1990). Also, the average annual rainfall is decreasing in most of the districts during the present period as compared to the baseline period. The comparison of the average decadal rainfall during the last few decades also depicts a similar pattern of decrease in the average annual rainfall from 1125.27 mm during1951-60 to 992.31mm during 2001-10 (Figure 5.2). The average seasonal rainfall during the monsoon season is 1053.70 mm.

The spatial variation of the average annual rainfall in the study area is given in Figure 5.3. The average annual rainfall varies spatially between 600 to 800 mm in Dhar and Barwani districts, 800 to 1000 mm rainfall is seen in some parts of Dhar and Khargone, Indore and Khandwa which thereafter increases to 1000 to1200 mm in the districts of Harda, Sehore, Raisen, Narshinghpur and major parts of Hoshangabad and Chhindwara. It further increases between 1200 to 1400 mm at Betul, Jabalpur, Mandla and some parts of Katni, Hoshangabad and Balaghat districts.

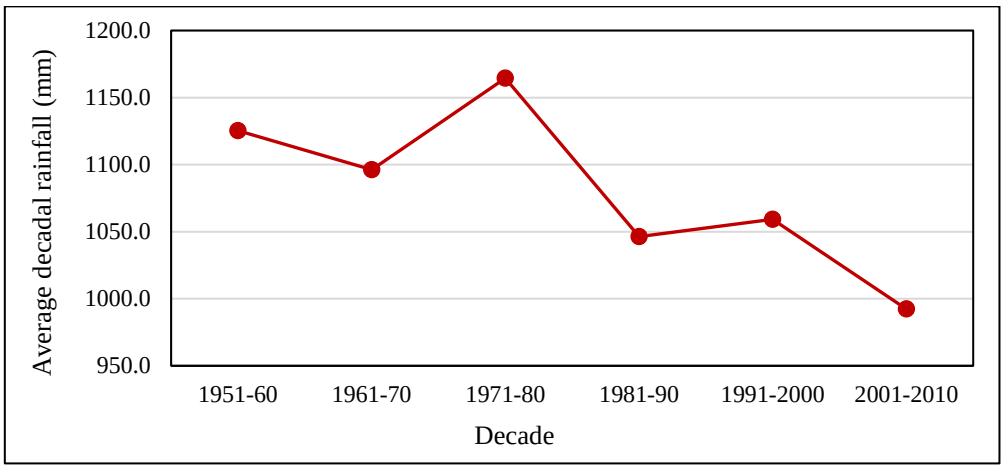

Figure 5.2: Temporal variation of annual average rainfall during last few decades

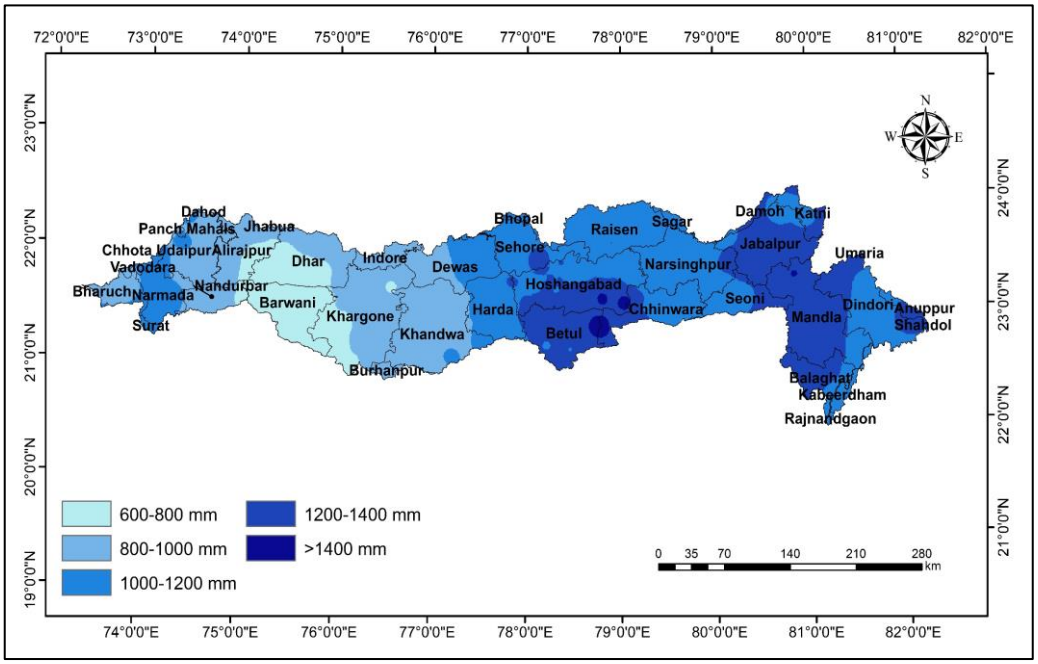

Figure 5.3: Spatial variation of the changes in the average annual rainfall between the baseline and present period in Narmada basin

A day which records a rainfall of 2.50 mm or more has been considered as a rainy day. The annual number of rainy days has been extracted from the daily rainfall time series spanning 1901-2015 for all the 130 blocks in the study area. The plot showing the temporal variation of the annual number of rainy days is given in Figure 5.4. There are 59 rainy days on an average and the number of rainy days in any year varies between 43 to 79 days. The changes in the number of rainy days between the baseline period (1961-1990) and the present time period (1991-2015) is given in Figure 5.5. It can be seen that the number of rainy days has decreased in almost all the districts in the study area.

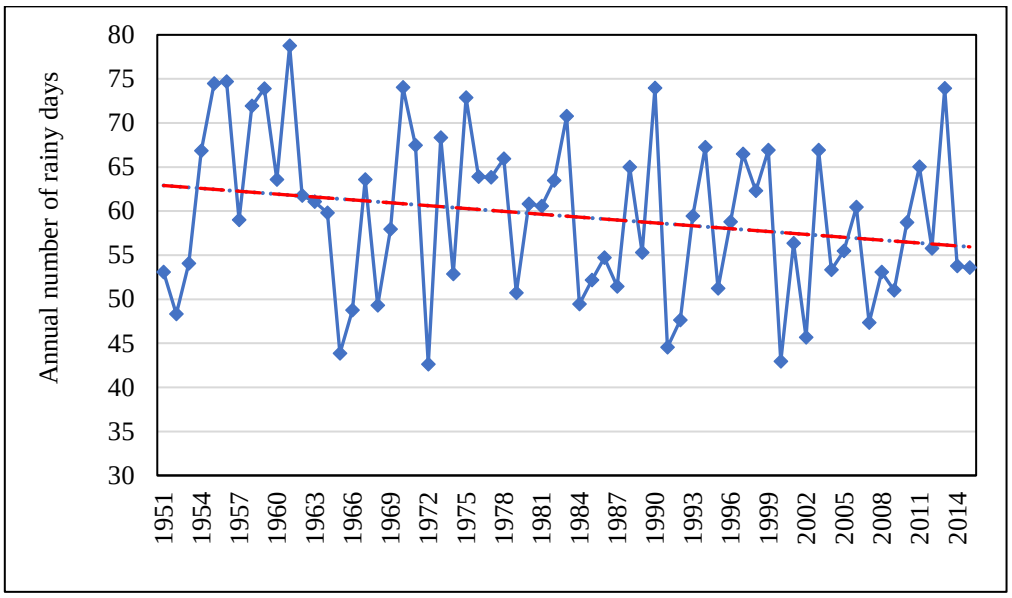

Figure 5.4: Temporal variation of annual number of rainy days in Narmada basin

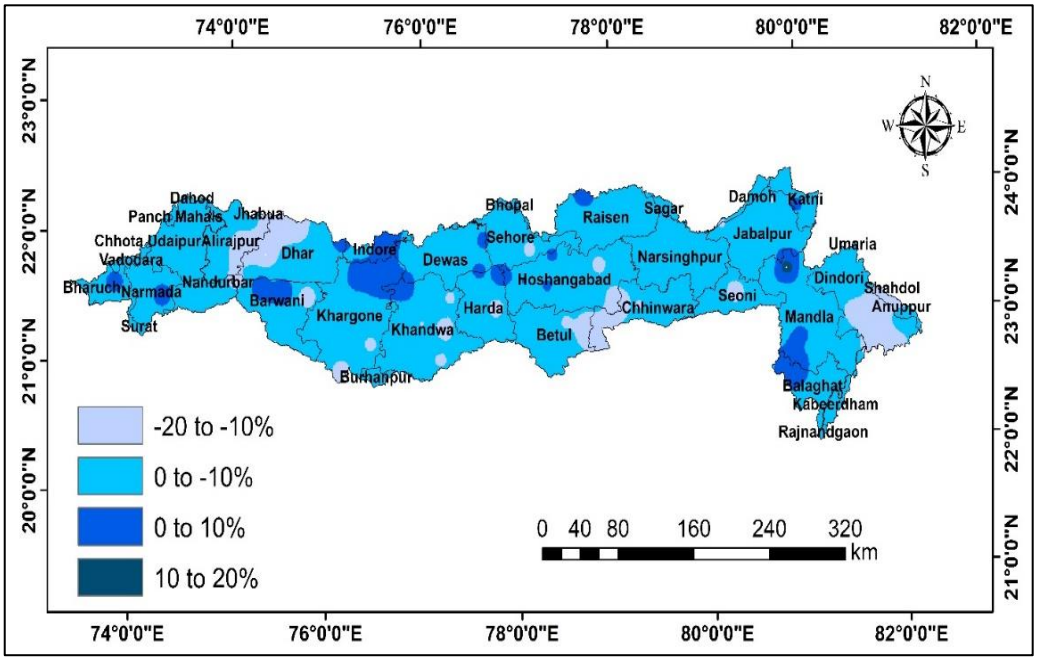

Figure 5.5: Spatial variation of the changes in the annual number of rainy days between the baseline and present period in Narmada basin

The 1-day maximum rainfall varied between 131.40 mm and 716.10 mm. The temporal variation of the 1-day maximum precipitation is given in Figure 5.6. An increasing trend in the 1-day maximum rainfall can be seen from the plot. However, even though the 1-day maximum rainfall increased in 64 grids, at the same time it has also decreased in 66 grids. The spatial variation of the changes in 1-day maximum rainfall between the baseline and current periods is given in Figure 5.7. The 1-day maximum rainfall has increased in the districts of Betul,

Narsinghpur, Seoni, Sehore, Harda, Chhota Udaipur, Chhindwara and some parts of Jabalpur, Mandla, Dhar, Barwani, Khargone, Khandwa, Indore and Bhopal districts.

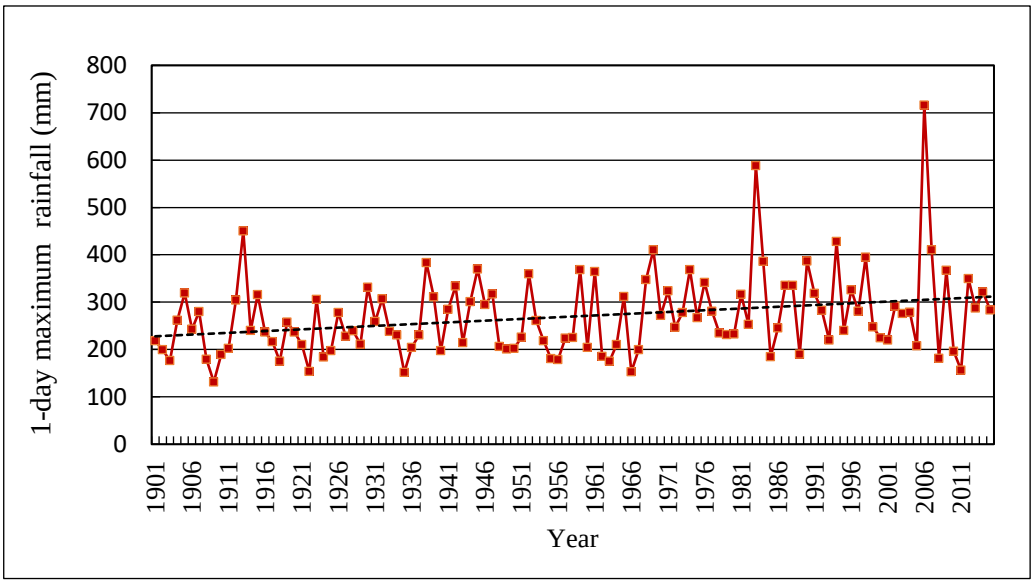

Figure 5.6: Temporal variation of 1-day maximum rainfall in Narmada basin

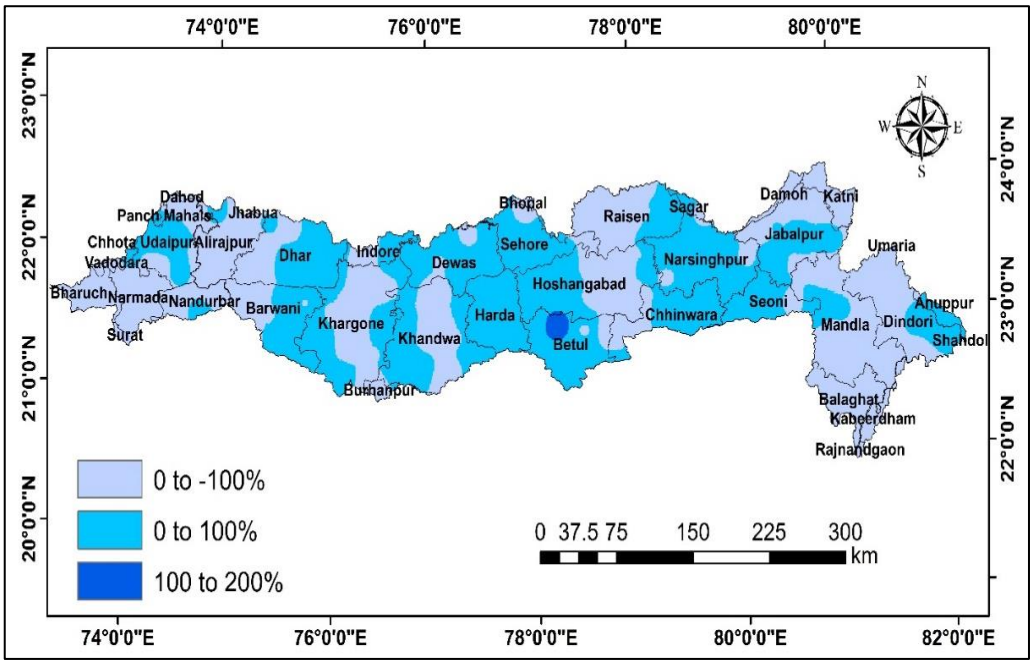

Figure 5.7: Spatial variation of the changes in the 1-day maximum rainfall between the baseline and present period in Narmada basin

To understand the changes in the extreme rainfall event pattern, the rainfall has been categorized into three categories viz., heavy rainfall with daily rainfall > 50 mm/day; very heavy rainfall with daily rainfall > 100 mm/day; and extreme rainfall with rainfall > 200 mm/day. A maximum of 8 heavy rainfall events occurred

and the maximum rainfall contribution to the annual rainfall from the heavy rainfall event was 652.79 mm in 1944. A minimum number 2 heavy rainfall events occurred and the minimum annual rainfall obtained from the heavy rainfall events was 112.18 mm in 1909. On an average the basin received 3 heavy rainfall events with an annual contribution of 313.66 mm from such events. A insignificant increase in contribution from heavy rainfall events to the annual rainfall was observed.

The comparison of the changes in the heavy rainfall events between the baseline and the present period is given Figure 5.8. A mixed trend has been observed with increase in heavy rainfall recorded in the Upper Narmada region, whereas the Middle and Lower Narmada have witnessed a decrease in the heavy rainfall. Some parts in districts of Middle Narmada have seen a decrease of more than 50% in the heavy rainfall contribution to the annual rainfall. The number of rainy days with heavy rainfall showed an increase in 72 grids and a decrease in 58 grids during the present time period as compared to the baseline period. The increase in the heavy rainfall events have been observed at the districts of Raisen, Narshinghpur, Chhindwara, Sehore, Sagar, Seoni and Mandla whereas a decrease in the heavy rainfall events have been observed at Bharuch, Chhota Udaipur, Indore, Panch Mahal, Vadodara, Dahod and Jhabua districts.

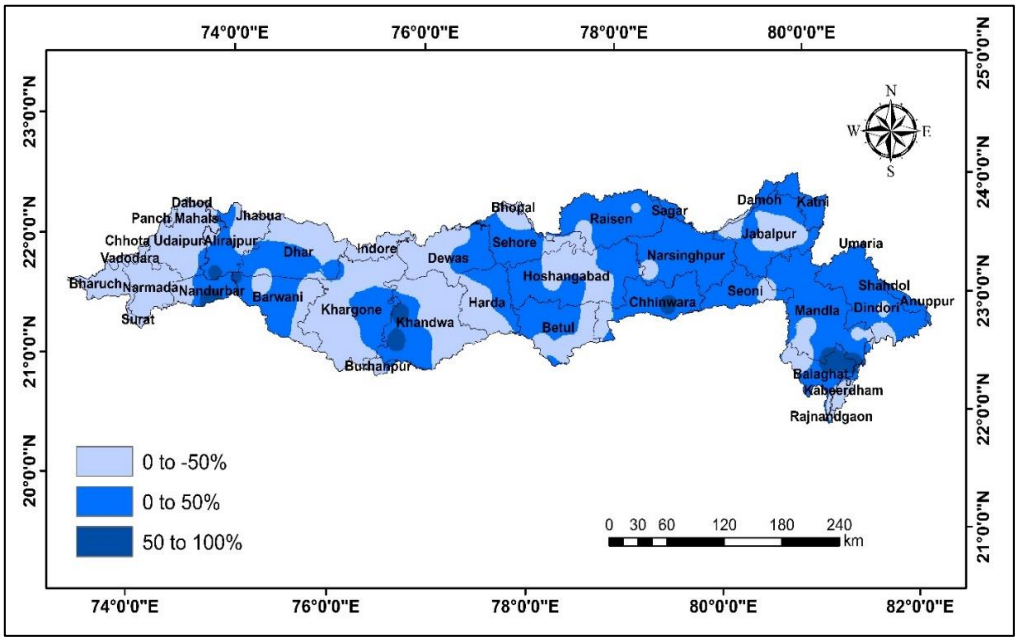

Figure 5.8: Spatial variation of the changes in the heavy rainfall between the baseline and present period in Narmada basin

An increasing trend has been observed in the rainfall obtained from very heavy rainfall events (rainfall > 100 mm). The contribution to annual rainfall from very heavy rainfall events is 97.9 mm. The spatial variation of the very heavy rainfall is given in Figure 5.9. It can be observed that the very heavy rainfall has increased in Dhar, Barwani, Indore Khargaone, Alirajpur, Jhabua, Panch Mahal, Dahod, Betul Jabalpur, Chhindwara districts and some parts of Raisen and Mandla districts whereas it has decreased in the remaining districts. Out of the 130 grids, 79 grids show an increase in the very heavy rainfall events. This indicates that the occurrences of the very heavy rainfall events have increased in substantial parts of the study area.

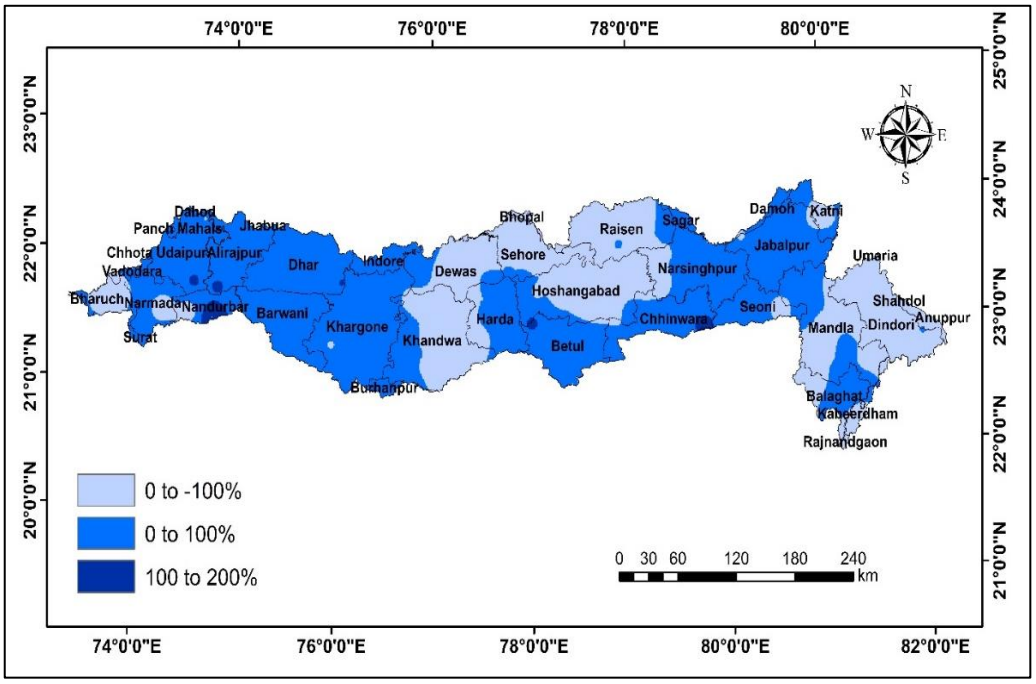

Figure 5.9: Spatial variation of the changes in the very heavy rainfall between the baseline and present period in Narmada basin

Similarly, an increasing pattern has been observed in the maximum extreme rainfall in the basin. The temporal variation of the maximum of extreme rainfall in Narmada basin is given in Figure 5.10. Also, the comparison of the changes in annual maximum extreme rainfall between the present and baseline period is given in Figure 5.11. It can be observed that the maximum extreme rainfall has decreased almost for the entire study area except some parts of middle Narmada. More than 25% decrease has been observed in the districts of Bharuch, Vadodara, Chhota Udaipur, Panch Mahal, Dahod, Surat, Jhabua, Alirajpur, Seoni, Jabalpur, Damoh,

Katni, Mandla, Balaghat, Dindori, Umariya parts of Dhar, Khargone, Khandawa, Dewas, Sehore and Hoshangabad.

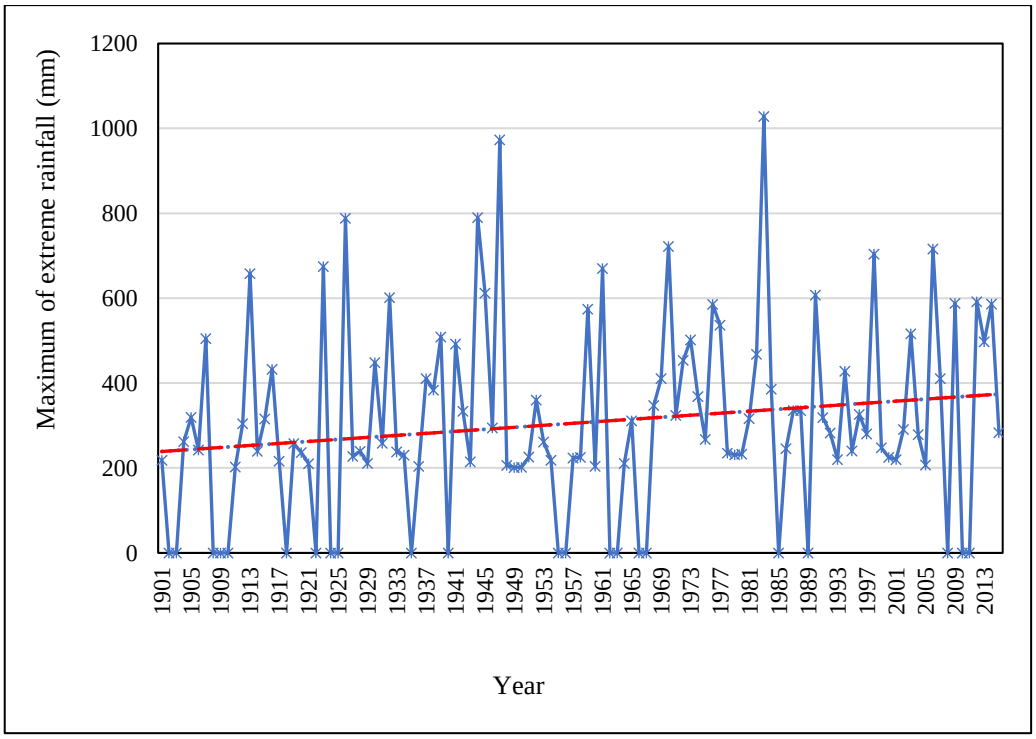

Figure 5.10: Temporal variation of maximum of extreme rainfall in Narmada basin

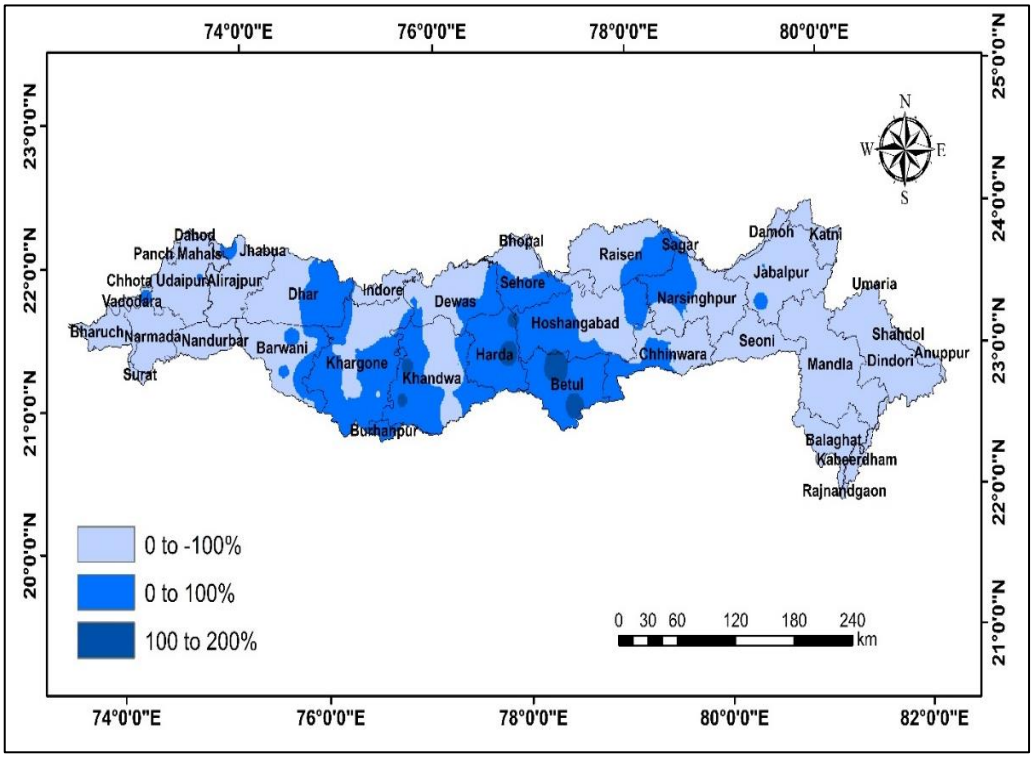

Figure 5.11: Spatial variation of the changes in the maximum of extreme rainfall between the baseline and present period in Narmada basin

5.1.2 Changes in Maximum and Minimum Temperature

The indices used to assess the changes in the maximum temperature include 1-day maximum temperature, very hot days (MaxT > 40ºC) and hot days (MaxT >35ºC). The analysis pertaining to the minimum temperature comprises of four indices viz., 1-day maximum of minimum temperature, very hot nights (MinT > 25ºC) and hot nights (MinT > 20ºC) and cold nights (MinT <10ºC).

The annual one-day maximum temperature has been extracted from the timer series of the daily maximum temperature (MaxT) available during the period 1951-2015. The temporal variation of the 1-day maximum of MaxT is given in Figure 5.12. It can be observed that there is a substantial increase in the 1-day maximum temperature in the basin. The average maximum temperature during 1961-1990 was 43.40ºC which thereafter increased to 44.06ºC during 1991-2013. The average increase in the MaxT has been 0.75ºC/100 years, which is quite significant and in tune with the IPCC warming predictions.

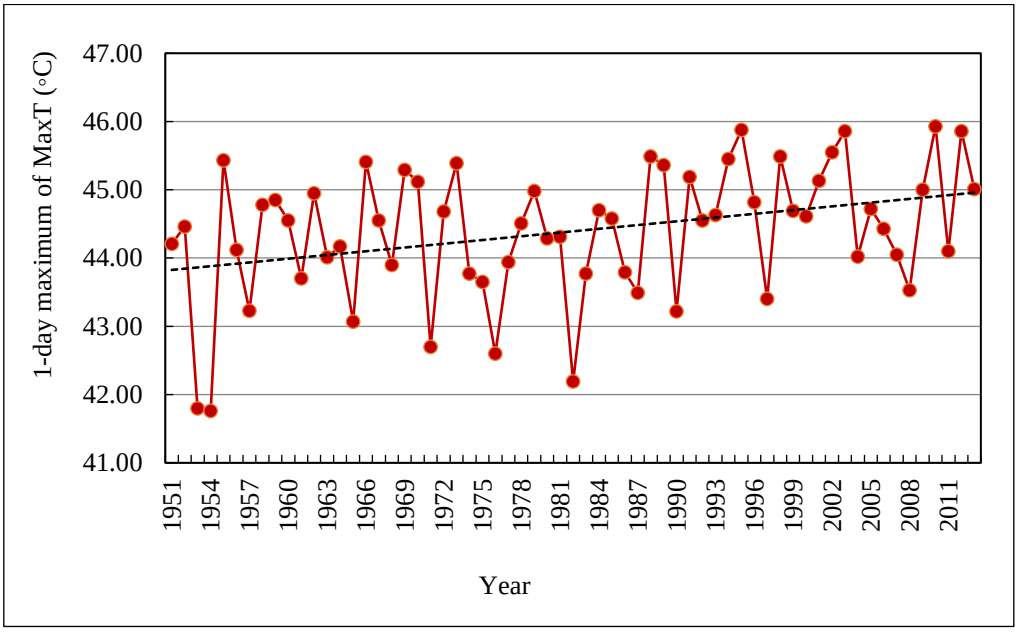

Figure 5.12: Temporal variation of 1-day maximum of MaxT in Narmada basin

The spatial plot showing the comparison of the changes in 1-day maximum of MaxT between the baseline and present period is given in Figure 5.13. The complete basin has witnessed an increase in 1-day maximum temperature with the middle regions of the basin comprising of the districts of Raisen, Bhopal, Sehore, Sagar, Narsinghpur, Hoshangabad, Betul, Chhindwara and parts of Seoni, Dewas,

Harda, Dhar, Alirajpur, Jhabua and Dahod witnessing an increase of more than 1% whereas the maximum temperature in the remaining districts falling in the basin increased between 0 to 1%.

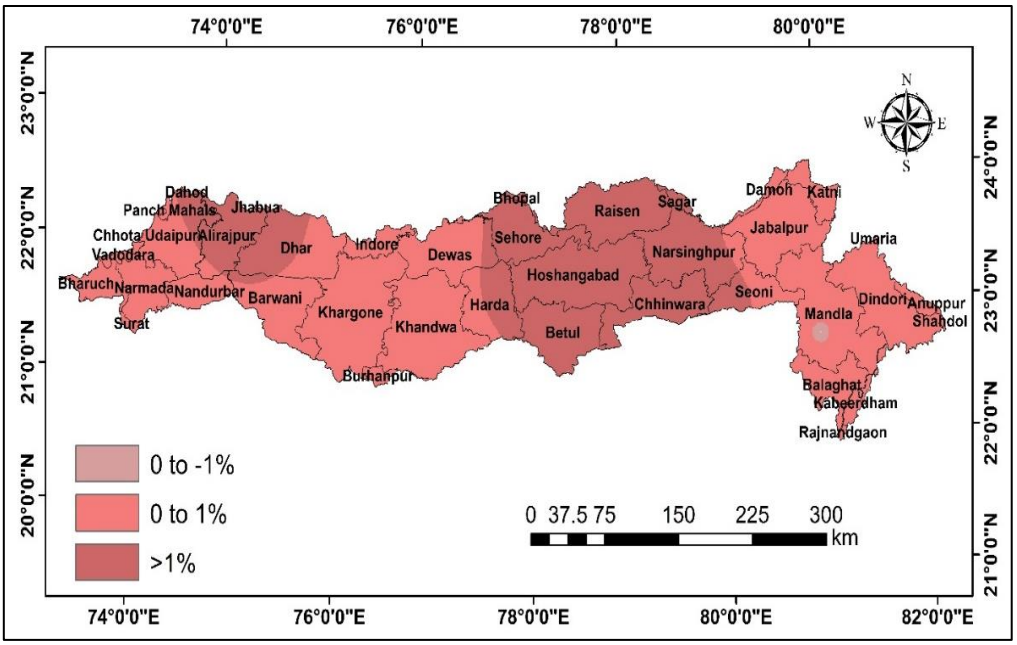

Figure 5.13: Spatial variation in the changes in 1-day maximum temperature between the baseline and present period in Narmada basin

A very hot day has been classified as day during which the maximum temperature is greater than 40°C. The number of very hot days is increasing steadily in the basin with 10 out of 13 grids depicting an increase in the very hot days. The spatial variation in changes in the number of very hot days is given in Figure 5.14. The numbers of very hot days are also increasing steadily in the basin in line with the increase in the very hot day temperatures. On an average, there are 37 very hot days in the basin. It has been observed that increase in the number of very hot days is maximum (>3%) between the baseline and present period in coastal districts of Vadodara, Bharuch, Narmada and Surat and also in mainland districts including Hoshangabad, Betul, Sehore, Bhopal, Raisen, Harda, Dewas, Narshinghpur, Chhindwara, Jabalpur, Sagar, Seoni, Damoh, Katni, Mandla, Shahdol, Dindori, and Anuppur. The number of very hot days have also decreased in some regions of the basin including parts of Khargone, Burhanpur, Khandwa and Barwani districts.

A hot day has been classified as day during which the maximum temperature is greater than 35°C. The maximum temperature is increasing steadily

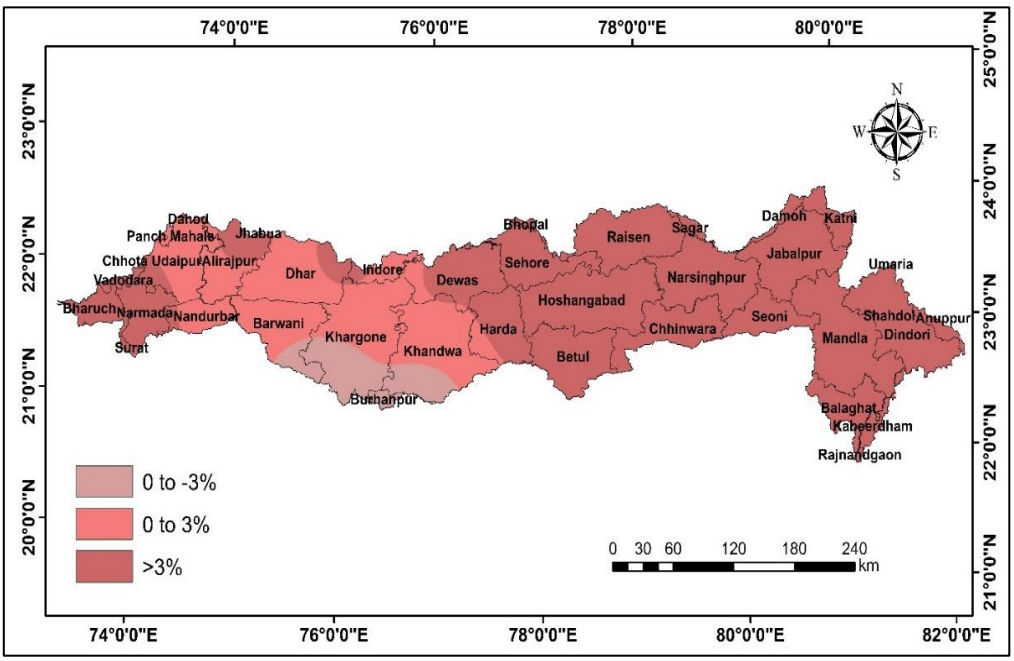

Figure 5.14: Spatial variation in the changes in number of very hot days between the baseline and present period in Narmada basin

during the hot days and all the 13 grids in the basin have depicted an increase in the maximum temperature during hot days. On an average, there are 102 hot days in the study area. The spatial variation in changes in the number of hot days between the baseline and present period is given in Figure 5.15. The average number of hot days increased in 4 grids whereas it decreased in 9 grids. It can be observed that the number of hot days is increasing from east to west, the being maximum in the Upper Narmada region comprising of Mandla, Dindori, Balaghat and Shahdol districts.

The annual one-day maximum of the minimum temperature has been extracted from the time series of the daily minimum temperature (MinT) during 1961-2015. It can be observed that there is no trend in the 1-day maximum of the minimum temperature in the basin. The spatial variation in changes in 1-day maximum of MinT between the baseline and present period is given in Figure 5.16. Major portions of the Narmada basin, particularly all districts in the Upper Narmada region have witnessed increase in the minimum temperature. 11 grids have depicted an increase in the 1-day maximum of the minimum temperature time series. The districts of Balaghat, Mandla, Dindori, Shahdol, Anuppur, Umaria, Seoni, Jabalpur, Chhindwara, Narsinghpur, Raisen, Sagar, Damoh, Katni and some parts of Middle Narmada region have seen an increase of more than 3% as compared to the baseline period.

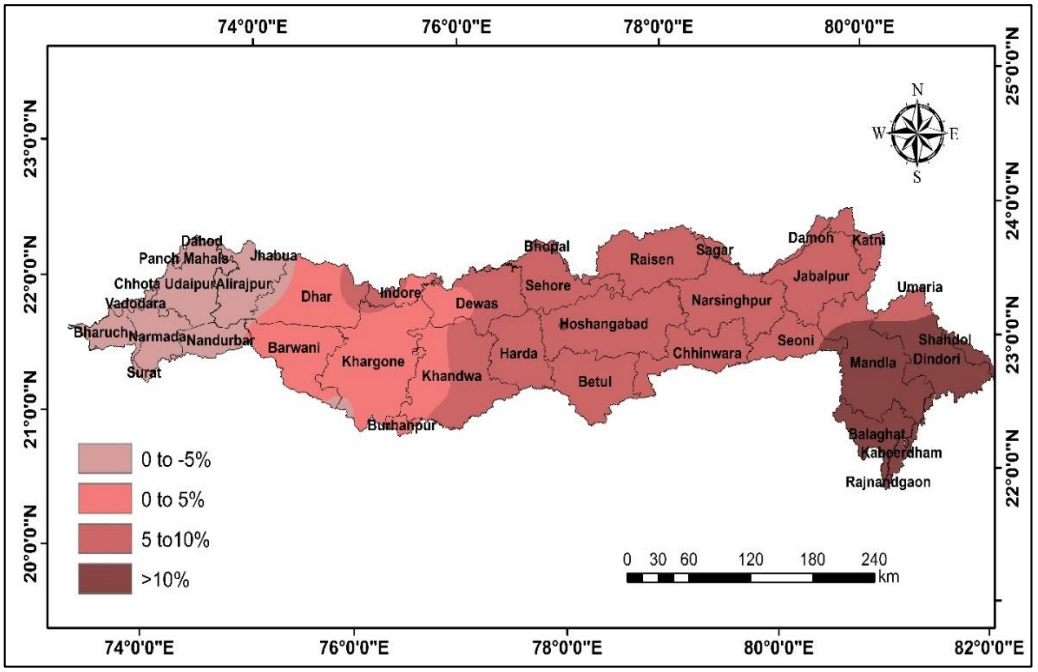

Figure 5.15: Spatial variation in the changes in number of hot days between the baseline and present period in Narmada basin

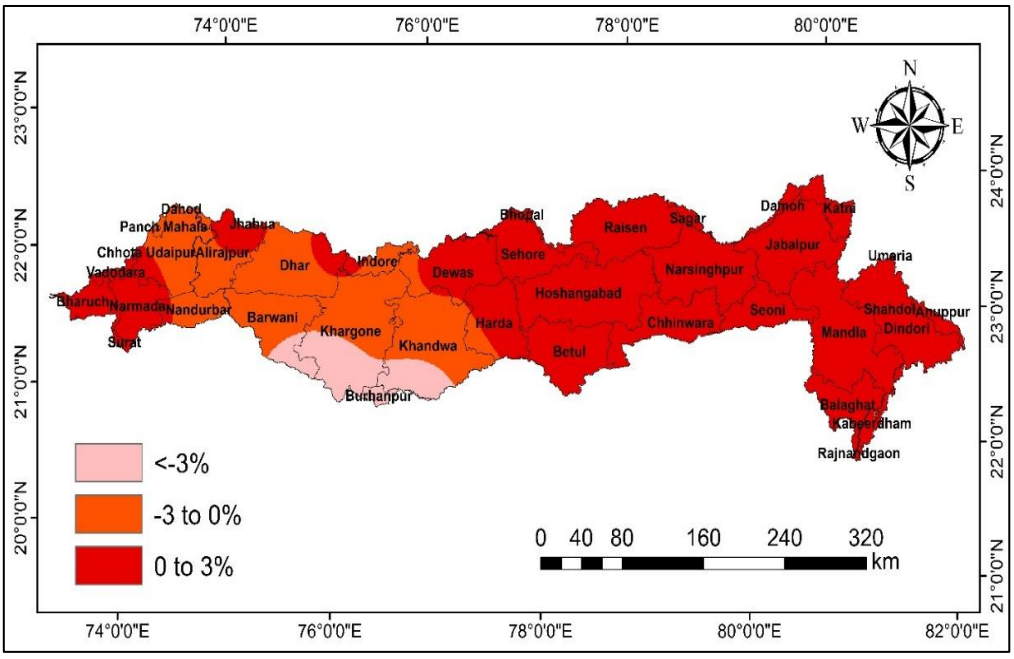

Figure 5.16: Spatial variation in the changes in 1-day maximum of MinT between the baseline and present period in Narmada basin

A very hot night has been classified as day during which the minimum temperature is greater than 25ºC. The comparison of the average minimum temperature during the very hot nights between the baseline and present time period shows a mixed trend. Similarly, the number of very hot nights was extracted from

the time series of the minimum temperature and on an average, there are 42 very hot nights in the basin. The spatial variation in changes in number of very hot nights between the baseline and present period is given in Figure 5.17.

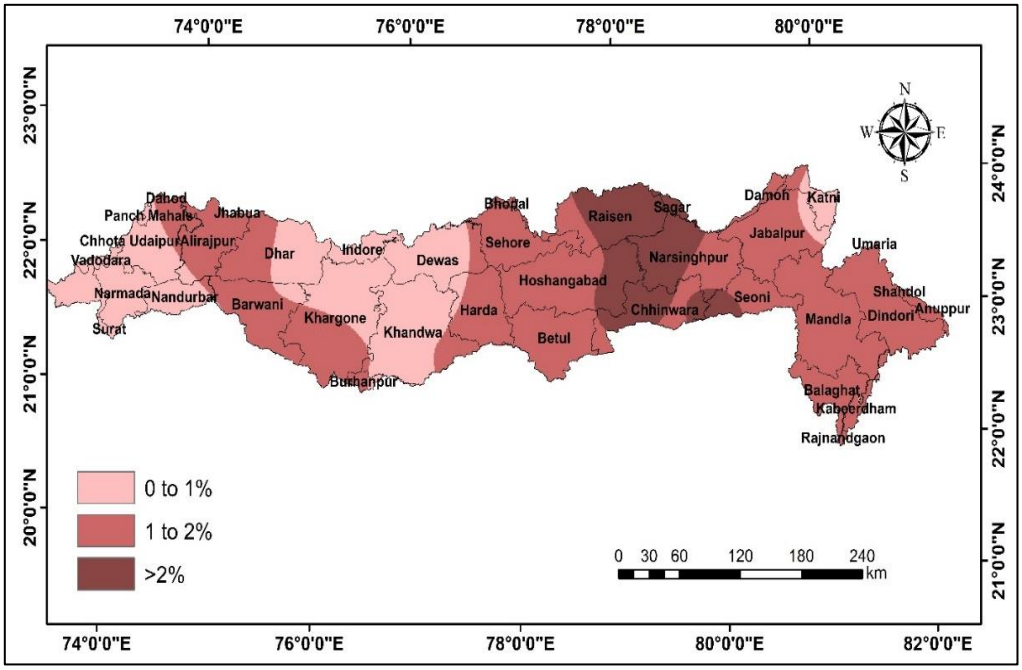

Figure 5.17: Spatial variation in the changes in number of very hot nights between the baseline and present period in Narmada basin

The number of very hot days increased in all the 13 grids covering the study area. Some parts of districts have seen an increase in the number of very hot nights, with highest increase in Raisen, Sagar, Chhindwara (>2%) whereas Anuppur, Dindori, Balaghat, Mandla, Jabalpur, Katni, Damoh, Seoni, Hoshangabad, Betul, Sehore,Harda, Alirajpur and parts of Khargone, Barwani, Dhar has witnessed and increase between 1 and 2% and the remaining districts of the Narmada basin have seen an increase of 0 to 1%.

A hot night has been classified as day during which the minimum temperature is greater than 20ºC. All the 13 grids have shown an increase in the minimum temperature during the hot nights during the present time period. On an average there are 194 hot nights in the study area. The number of hot nights has also increased substantially in all the 13 grids covering the Narmada basin. The spatial variation in changes in number of hot nights between the baseline and present period is given in Figure 5.18. The number of hot nights increased by more than 2% in the parts of Raisen, Narsinghpur, Hoshangabad and Chhindwara districts

followed by an increase between 1 to 2% in the districts of Balaghat, Dindori, Mandla, Shahdol, Anuppur, Jabalpur, Damoh, Seoni, Betul, Sehore, Harda, Alirajpur and parts of Raisen, Narsinghpur, Hoshangabad, Chhindwara, Khargone, Dhar and Dahod districts.

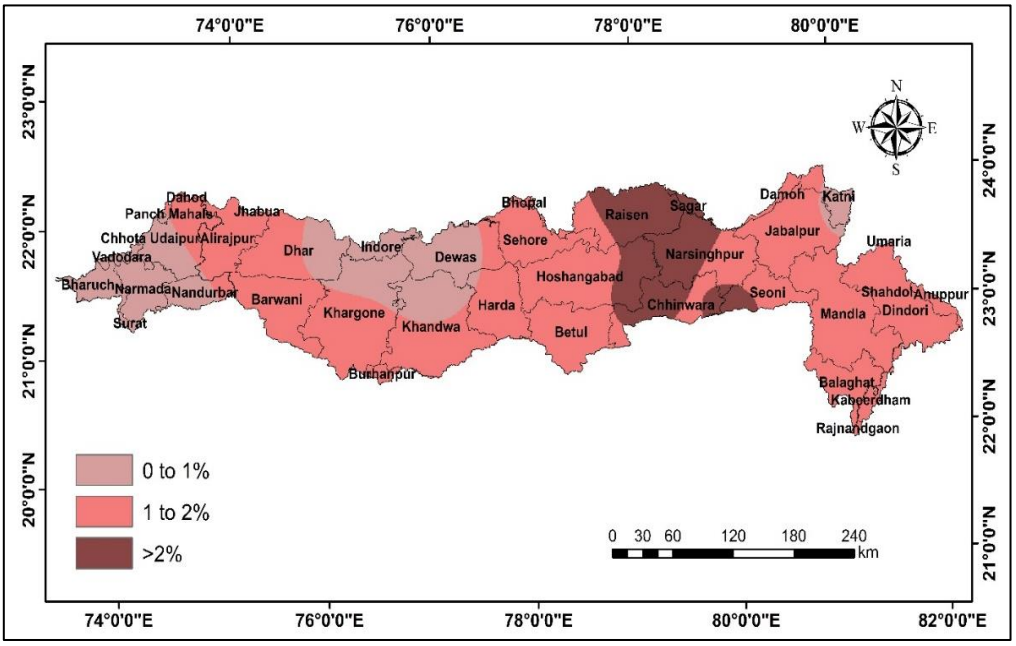

Figure 5.18: Spatial variation in the changes in number of hot nights between the baseline and present period in Narmada basin

A cold night has been classified as day during which the minimum temperature is less than 10^{o}C. The number of cold nights has also been extracted from the minimum temperature time series. On an average there are 333 cold nights in the basin. The spatial variation in changes in number of hot nights between the baseline and present period is given in Figure 5.19. The number of cold nights has decreased by more than 20% during the present period in the coastal districts of Vadodara, Bharuch, Narmadapuram and Surat whereas it has decreased by 10 to 20% in the districts of Balaghat, Mandla, Shahdol, Seoni, Jabalpur, Narsinghpur, Sagar, Raisen, Betul, Betul, Khargone, Dhar, Barwani, Dhar and Alirajpur. The remaining parts of the basin also witnessed a decrease in the number of cold nights during the present period ranging between 0 to 10%.

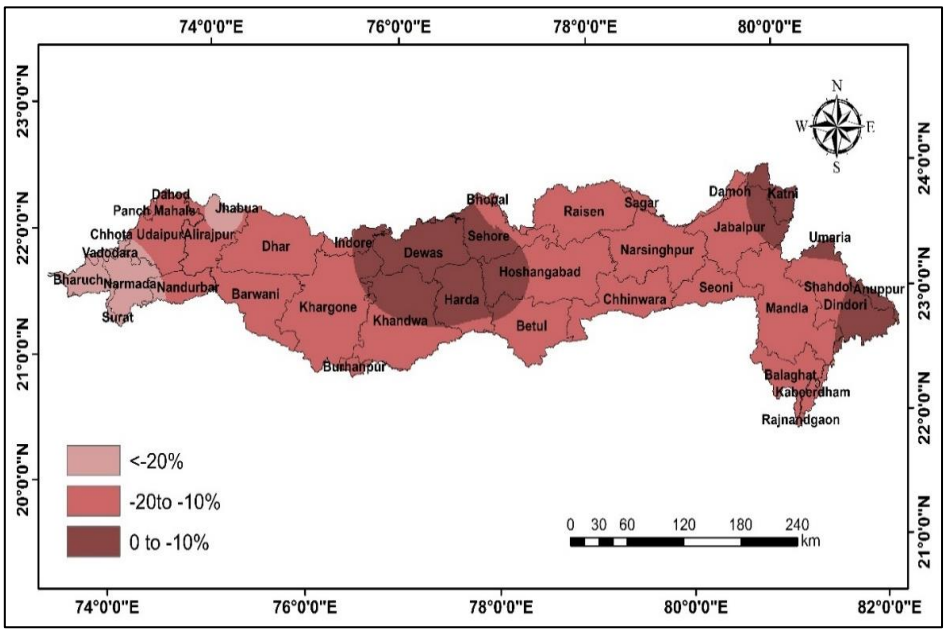

Figure 5.19: Spatial variation in the changes in number of cold nights between the baseline and present period in Narmada basin

5.2 Evaluation of Hydrological Soil Properties

The hydrological soil properties including infiltration, saturated and unsaturated hydraulic conductivity have been evaluated using field experiments as explained in the previous section. The details of the test sites which were selected based on different soil-crop combinations are given in Figure 5.20. The results of these tests are given in Table 5.2.

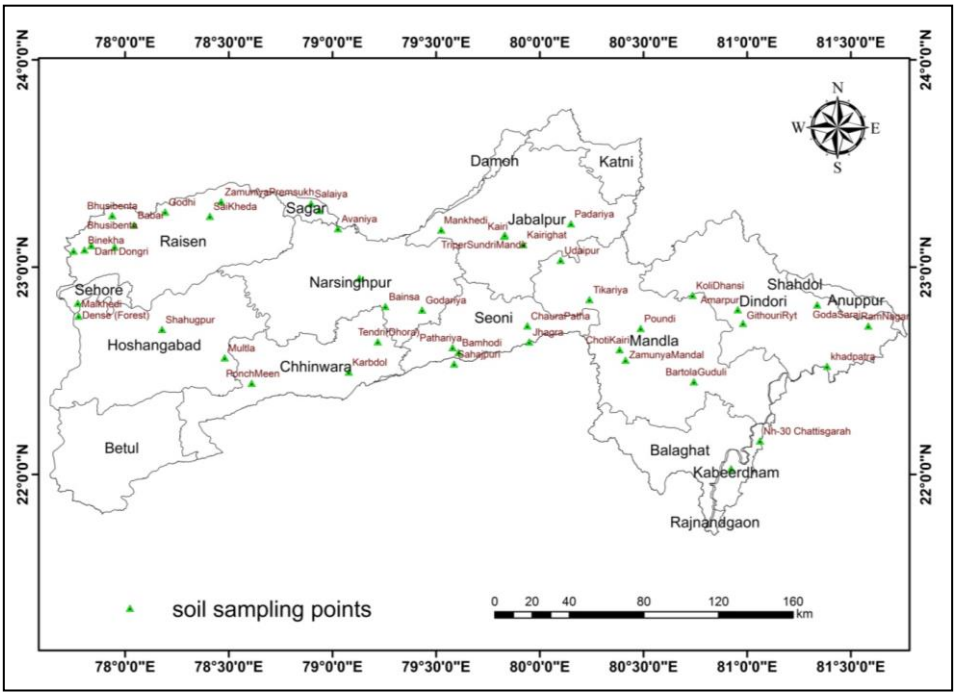

Figure 5.20: Soil test sites in Upper Narmada basin

Table 5.2: Hydrological soil properties at different test sites of Upper Narmada basin

S. No.	Test site	Latitude	Longitude	Unsaturated hydraulic conductivity (cm /sec)	Saturated hydraulic conductivity (cm/sec)	Infiltration rate (cm/hr)
1.	Zamuniya Mandla	22.5514	80.4139	0.0007369	0.000043	3.2
2.	Saikheda	23.2454	78.4089	0.0020894	0.0000504	8.9
3.	Poundi	22.7042	80.4867	0.0000756	0.0000947	2.1
4.	Bhusibenta	23.2405	77.9376	0.0004092	0.0001786	0.5
5.	Khairi	23.2535	79.7596	0.0001797	0.0010948	5.5
6.	Udaipur	23.0329	80.1011	0.0008283	0.0001242	5.1
7.	GhatPipaliya	22.7158	81.5846	0.0019258	--	3.8
8.	Zamuniya Raisen	23.0775	77.7515	0.0007038	0.0007279	7.7
9.	Padariya	23.0775	77.7515	0.0005134	0.0000176	7.2
10.	Tendni	22.6440	79.2186	0.0004739	0.0010889	5.5
11.	Bartula	22.4472	80.7432	0.0005042	0.0006134	5.6
12.	Banhodi	22.5882	79.6081	0.0016791	0.0004872	2.3
13.	Muttki	22.5624	78.4804	0.0017658	0.0002465	5.7
14.	TripurSundri Mandir	23.1545	79.8314	0.0004874	0.0001184	2.3
15.	Kathotiya	22.9458	79.1299	0.0004041	0.0006516	2.4
16.	Gandhi	23.2668	78.1935	0.0006867	0.0001728	0.5
17.	Talpura	22.0280	80.923	0.000368	0.0035719	4.0
18.	Avariya	23.1857	79.0266	0.0007648	0.0000499	0.8
19.	ChouraPatha	22.7170	79.9400	0.0002563	0.000198	--
20.	Malakhedi	22.7462	77.7456	0.0010573	0.0007279	--

The infiltration was evaluated at 18 test sites in the Upper Narmada basin for different soil-crop combinations. The infiltration rate varied between 0.50 to 8.90 cm/hr. The maximum infiltration rate of 7.7 cm/hr and 8.9 cm/hr was found at Zamuniya Raisen and Saikheda respectively in Raisen district of Madhya Pradesh the basic whereas the minimum infiltration rate of 0.5 cm/hr was found at Bhusibenta and Gandhi test sites, indicating the presence of hard and compact layer below the soil strata. The field photograph of the infiltration test at Bhusibenta in Upper Narmada basin is given in Figure 5.21.

Figure 5.21: Infiltration test at Bhusibenta in Upper Narmada basin

The saturated hydraulic conductivity in Upper Narmada basin was evaluated at 20 test sites using Guelph Permeameter and the map showing the saturated hydraulic conductivity at the test sites is given in Figure 5.22. It has been found that the average hydraulic conductivity is 0.000539876 (cm/sec) and ranges between a maximum of 0.003571895 (cm/sec) in Kabeerdham district of Chhattisgarh and a minimum of 0.00001761 (cm/sec) in Raisen district of Madhya Pradesh. The field photograph of the Guleph Permeameter test for evaluation of saturated hydraulic conductivity at Malakhedi in Upper Narmada basin is given in Figure 5.23.

The unsaturated hydraulic conductivity in Upper Narmada basin was evaluated at 20 test sites using Mini Disk Infiltrometer and the map showing the unsaturated hydraulic conductivity at the test sites is given in Figure 5.24. It has been found that the average unsaturated hydraulic conductivity is 0.000539876 (cm/sec) and ranges between a maximum value is 0.002089 (cm/sec) which in Raisen district of Madhya Pradesh and a minimum of 0.000075 (cm/sec) in Mandla district of Madhya Pradesh.

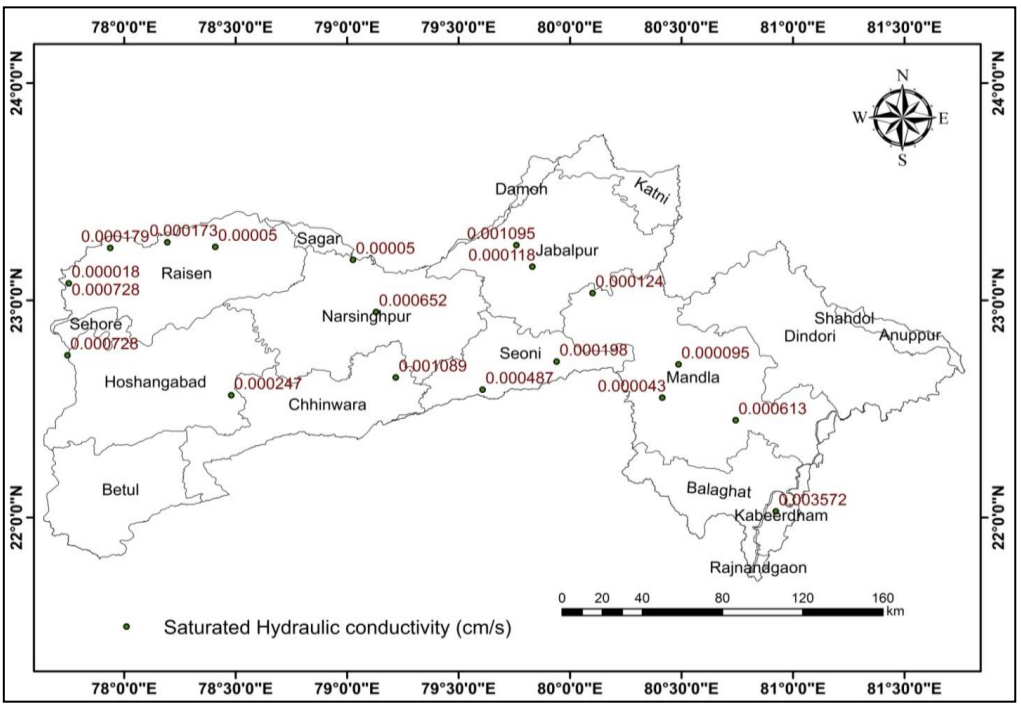

Figure 5.22: Saturated hydraulic conductivity of soils in Upper Narmada basin

Figure 5.23: Guelph Permeameter test for evaluation of saturated hydraulic conductivity at Malakhedi in Upper Narmada basin.

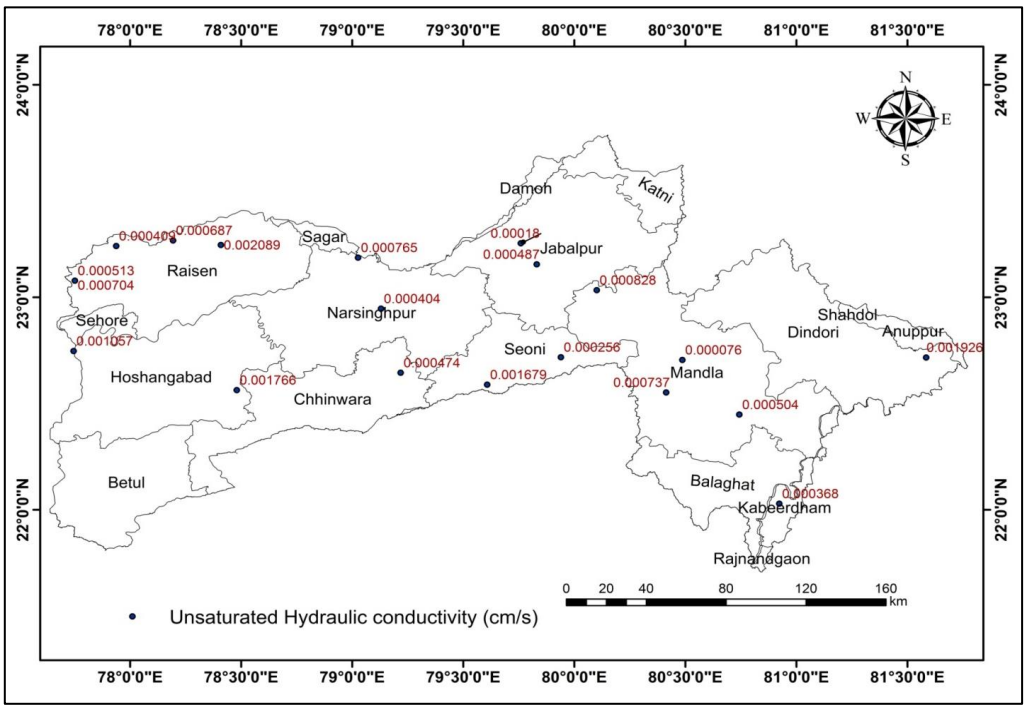

Figure 5.24: Unsaturated hydraulic conductivity of soils in Upper Narmada basin

5.3 Ground-truth verification and Collection of field information

The general information about the study area including the various types of crops grown, the crop yields, water management practices, reservoir operation and demand management, ground-truth verification have been collected using field visits. Figure 5.25 shows the interaction with the farmers about the crops adopted and water requirements for crops in their fields. Figure 5.26 depicts the interaction with the Bargi Reservoir Project authorities on the reservoir operation and management at the Bargi Dam. The ground truth verification of the wheat farm of Jawaharlal Nehru Krishi Vishwa Vidyala (JNKVV) after crop harvesting is given in Figure 5.27. Similarly, the ground truth verification of the sugarcane field at Natwara village, wheat field in Narsinghpur and paddy field at Dhondi is given in Figure 5.28 to Figure 5.30.

5.4 Hydrological Modelling using SWAT

The ArcSWAT extension for ArcGIS10.4 has been used for simulating the hydrology in Narmada basin up to Hoshangabad. The study area has been limited to the Upper Narmada basin extending up to Hoshangabad, as most of proposed watershed interventions in the form of upcoming and proposed dams are planned

Figure 5.25: Interaction with farmers

Figure 5.26: Interaction at Bargi Reservoir

Figure 5.27: Ground truth verification of the wheat field of J.N.K.V.V. after crop harvesting

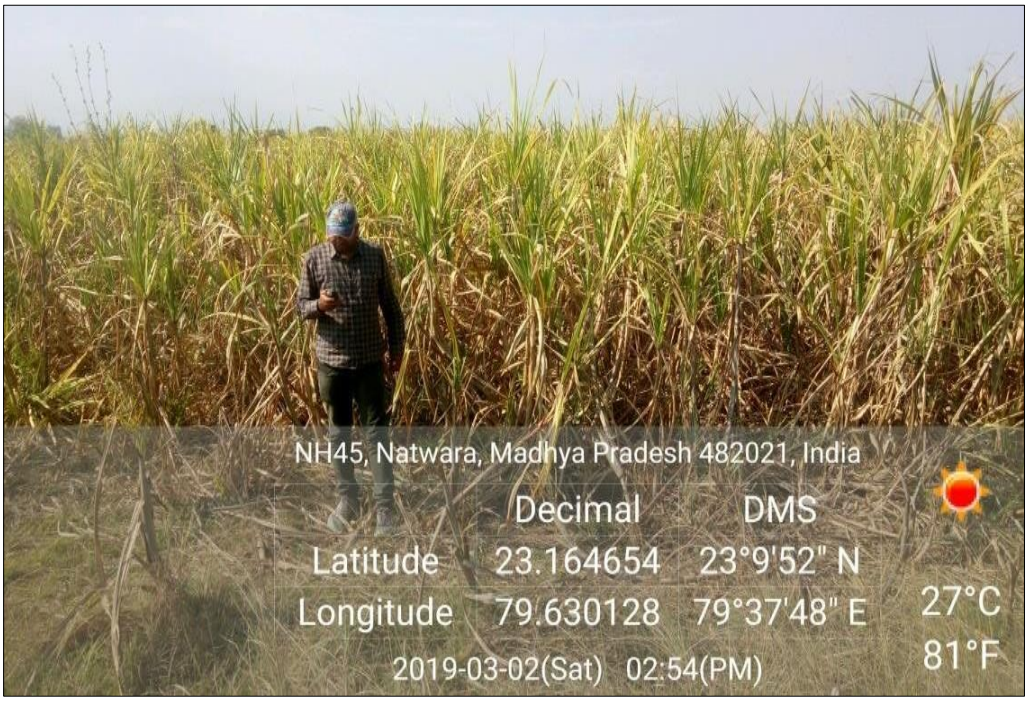

Figure 5.28: Ground truth verification of the sugarcane field at Natwara village

Figure 5.29: Ground truth verification of the sugarcane field in Narsinghpur

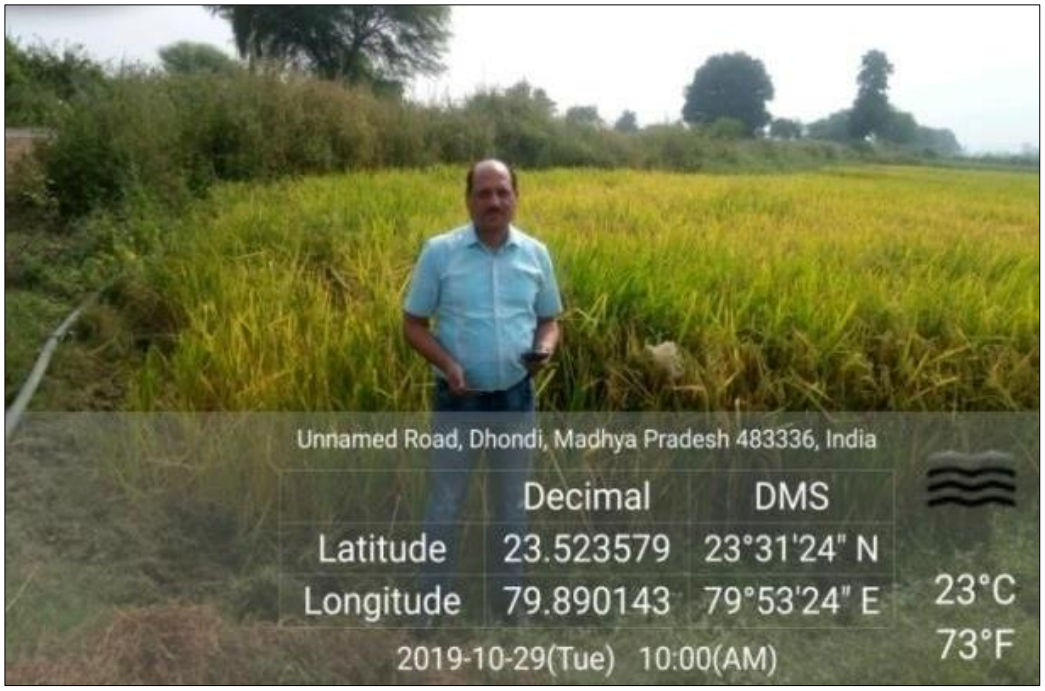

Figure 5.30: Ground truth verification of the paddy field in Dhondi village

in this region. Moreover, the rainfall and base flow from the upper regions is responsible for sustaining the flows in the Narmada basin round the year making Narmada River, the largest perennial west flowing river in central India. The Rain Avanti Bai Lodhi Sagar (RABLS) Multipurpose Project, Tawa Project and Barna

Irrigation Project are the three existing projects in the study area with more few dams being planned on the main river and its tributaries.

The SRTM-DEM at 30 m resolution downloaded from CGIAR consortium for spatial information (CGIAR-CSI) website (http://srtm.csi.cgiar.org/); land use/land cover map prepared from the multispectral satellite data from National Remote Sensing Centre (NRSC) LISS IV satellite data; soil characteristics based on the Food and Agricultural Organization's (FAO) Harmonized World Soil Database (HWSD) prepared by International Institute for Applied Systems Analysis (IIASA) have been used to represent the spatial distribution of the topography, land use and soil properties in the study area. Thereafter three slope classes, seventeen SWAT land use classes and seven soil classes have been considered for the derivation of HRUs with threshold values for the sub-basins as 20%, which resulted in 272 subbasins and 1020 HRUs. The maps showing the study area with the location of dam sites and gauging sites, along with DEM, land use and soil type etc. is given in Figure 5.31 to Figure 5.36.

The high resolution ($0.25^o \times 0.25^o$) daily gridded rainfall data (Rajeevan et al., 2005), and the ($1^o \times 1^o$) gridded minimum and maximum temperature (Srivastava et al., 2005) prepared by IMD have been imported into the model framework. The remaining weather data for running SWAT viz., wind speed, relative humidity, solar radiation and sunshine hours have been generated using the weather generator available in SWAT at daily time steps. Thus, the input database for the setup of SWAT model is explained below.

The basic model setup with the high-resolution climate data, DEM, soil, and land use/land cover along with the manual insertion of additional nodes at gauging sites and dam sites have been used for simulation of the hydrology pertaining to the virgin condition of the basin, as the reservoir properties have not yet been incorporated in the model setup. The default run assumes the basin to be

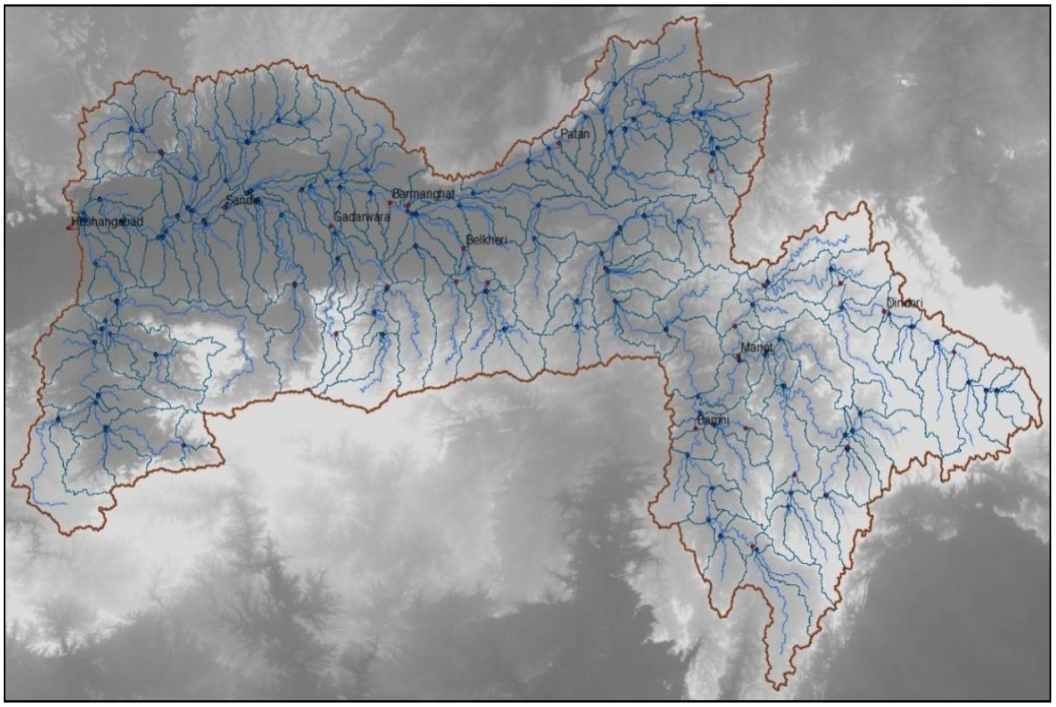

Figure 5.31: Digital Elevation Model (DEM) of Narmada up to Hoshangabad G/D site

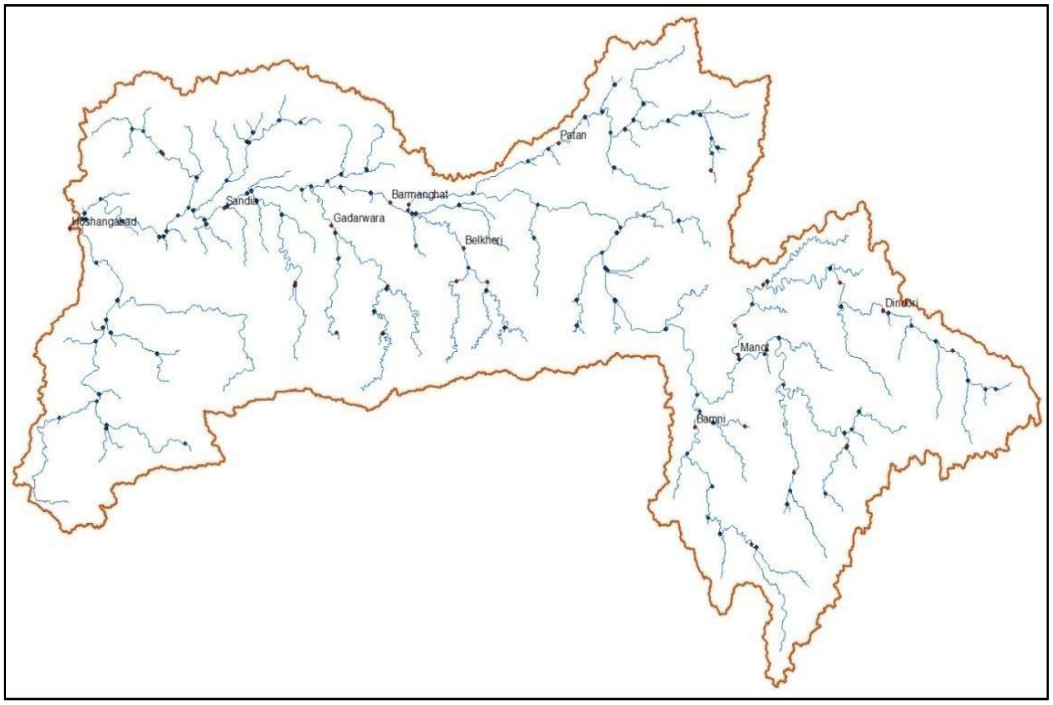

Figure 5.32: Drainage map of Narmada up to Hoshangabad G/D site

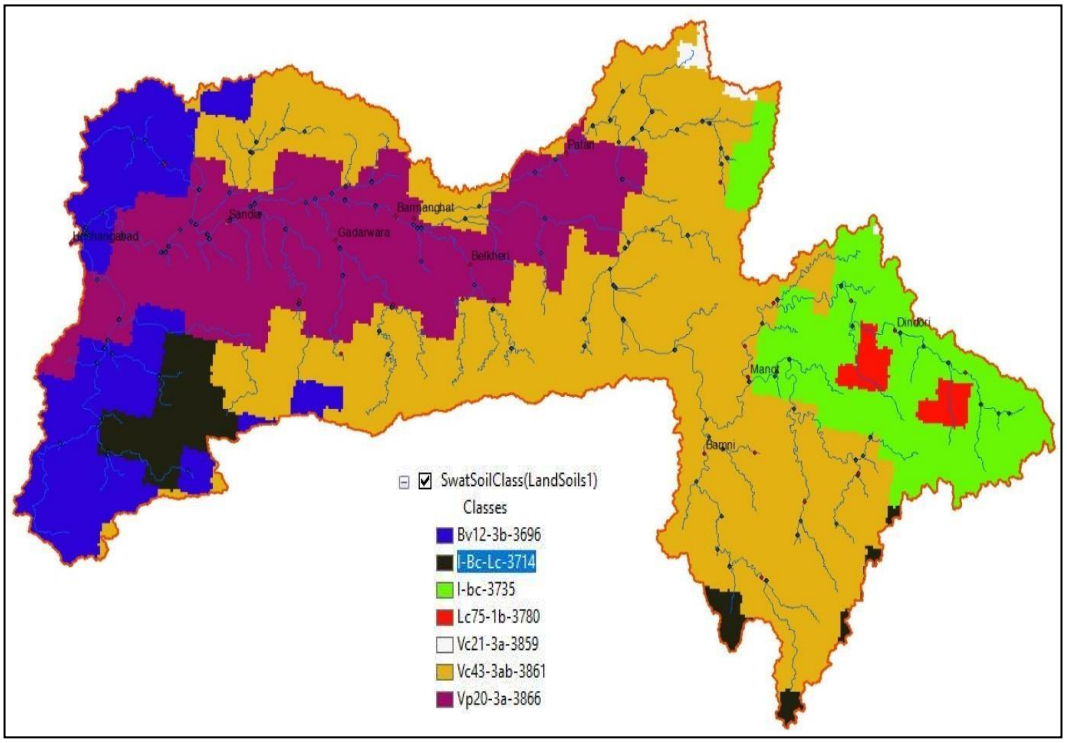

Figure 5.33: Soil map of Narmada up to Hoshangabad G/D site

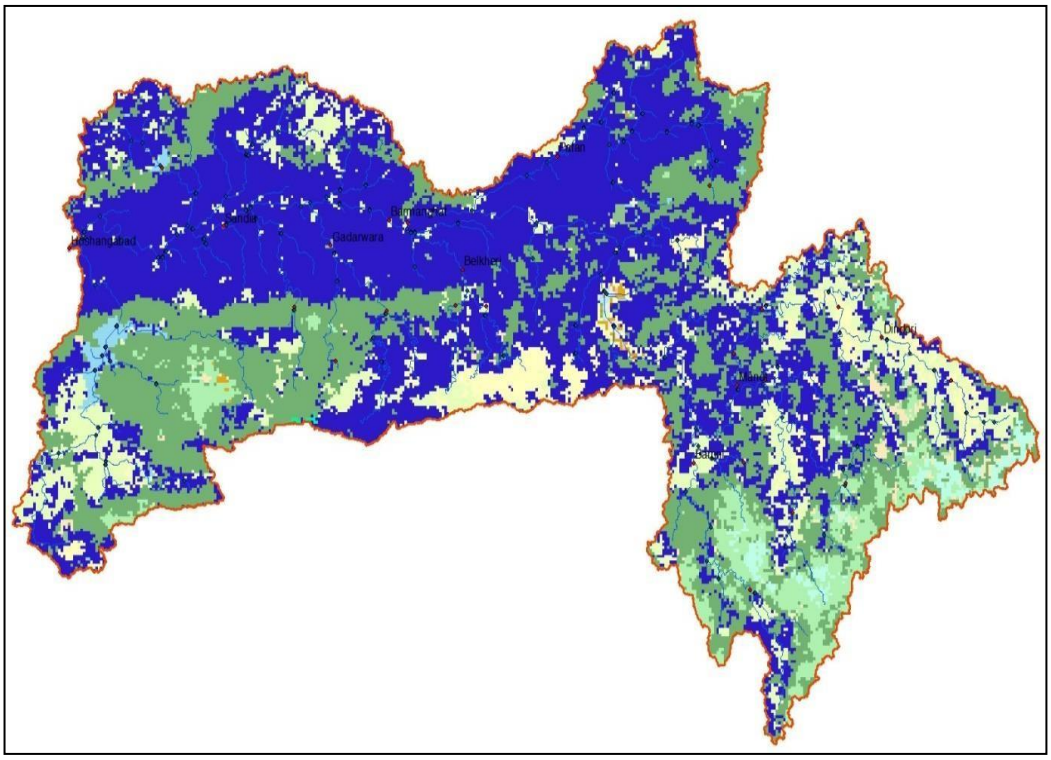

Figure 5.34: LULC map of Narmada up to Hoshangabad G/D site

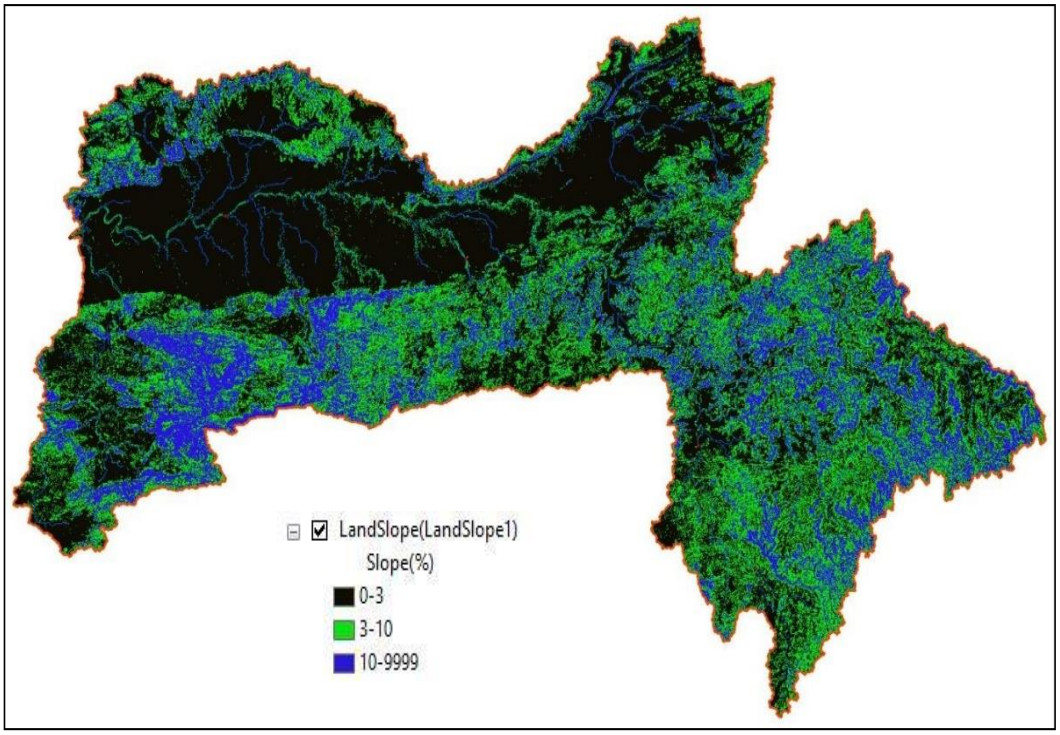

Figure 5.35: Slope map of Narmada up to Hoshangabad G/D site

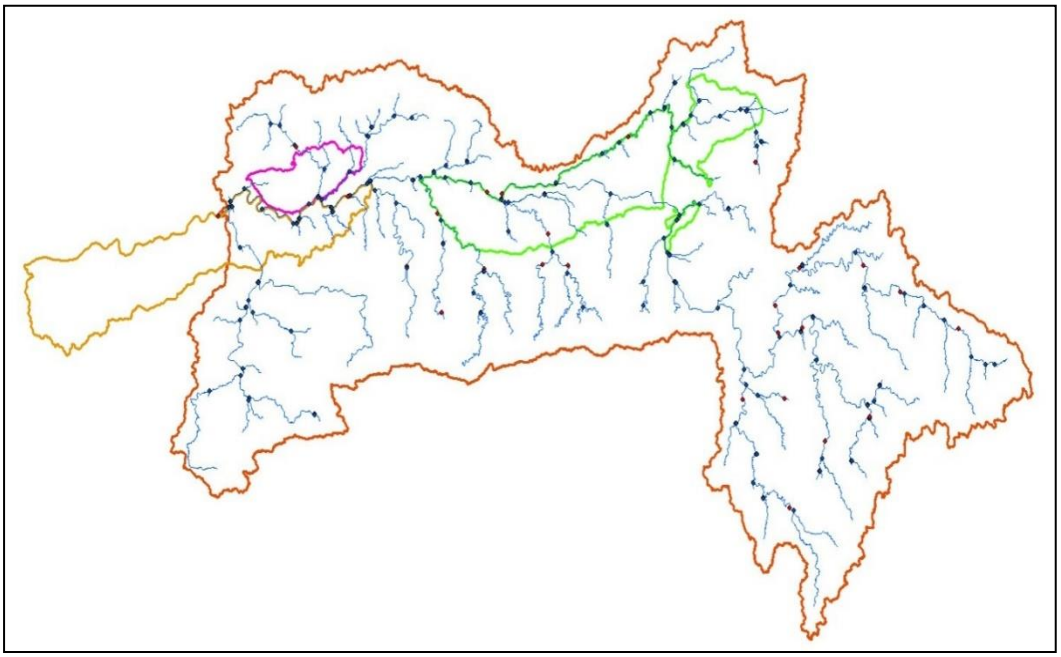

Figure 5.36: Command area of existing projects in Narmada basin up to Hoshangabad

virgin with no watershed interventions. The daily discharge data at Dindori, Manot, Mohgaon, Patan, Belkheri, Barmanghat, Sandia and Hoshangabad provided by the Central Water Commission (CWC) has been used to compare the SWAT simulated

discharge with the observed discharge. Subsequently, the management operations including irrigation by groundwater etc. have been input into the model depending on the actual field conditions and the model run have been carried out. The workflow of the setup and modelling process is given in Figure 5.37.

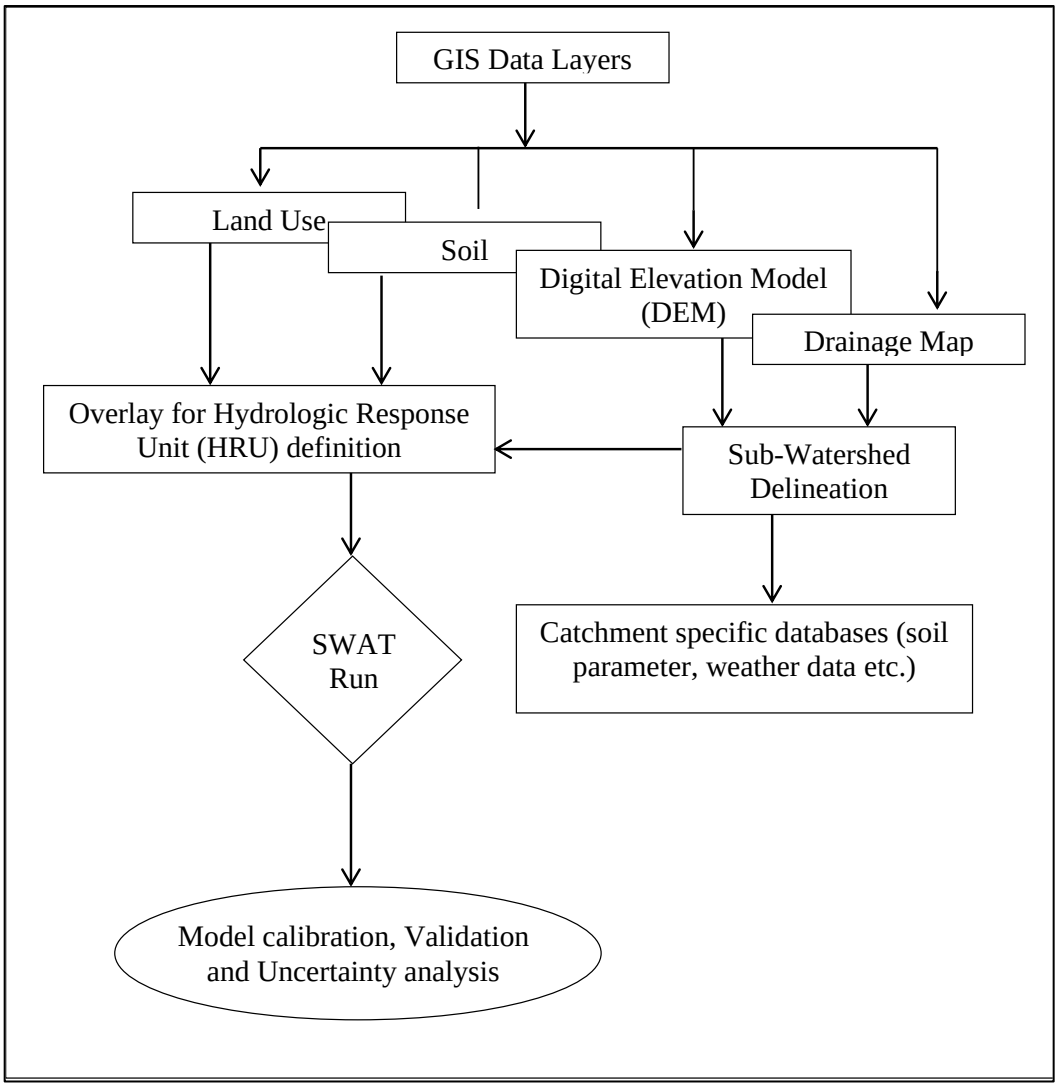

Figure 5.37: Workflow of the SWAT setup

The gauge-discharge sites where daily discharge data is available and flow simulated is given below,

1. Manot
2. Mohgaon
3. Belkheri
4. Patan
5. Barmanghat
6. Gadarwara
7. Sandia
8. Hoshangabad.

The discharge sites at Manot, Mohgaon, Belkheri, Patan, and Gadarwara are on tributaries whereas Barmanghat, Sandia and Hoshangabad are on the main Narmada River. The gauging site at Barmanghat and Sandia are located on the main river downstream and discharge at both these gauging sites are influenced by the releases from the Bargi dam. Similarly, the gauging site at Hoshangabad is located on the main river and downstream of Bargi, Tawa and Barna dams and the flow at Hoshangabad is influenced by the releases from all these three dams.

The comparison of the observed and simulated virgin discharges during the default run is given in Figure 5.38. The reservoir properties including the full supply level, gross storage capacity, emergency spillway level, dead storage level, dead storage capacity, water spread area at full supply level, etc., have been used to set up the model and was extracted from the detailed project reports of the respective dams, provided by Narmada Valley Development Authority (NVDA) and Water Resources Department (WRD), Govt. of Madhya Pradesh. The monthly outflows from the existing reservoirs viz., RABLS Project, Tawa Project, Barna Project and Matiyari dam along with the management operations viz., irrigation from reservoir, shallow aquifer and deep aquifer have been added and model runs performed at the daily and monthly time steps from 2003 to 2012, with warm-up period of 4 years.

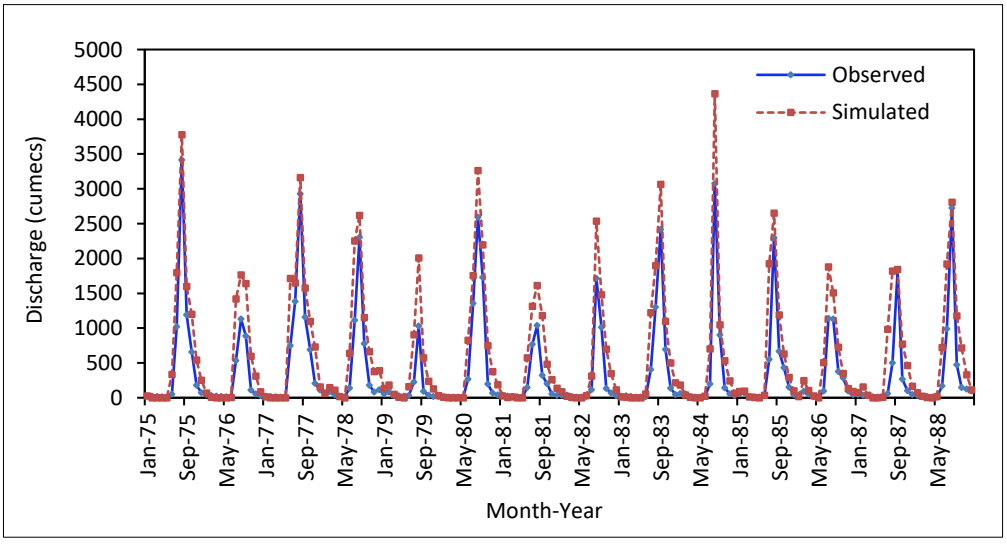

Figure 5.38: Comparison of observed and simulated virgin flows at Barmanghat

The multi-site calibration of SWAT model has been carried using the SUFI-2 algorithm in the SWAT-CUP software which combines parameter calibration and uncertainty prediction. The input parameter uncertainty is represented by uniform

distributions whereas the model output uncertainty is quantified by the 95 Percent Prediction Uncertainty (95PPU). The multi-site calibration has been performed using the daily stream flow data at Dindori, Manot, Mohgaon, Patan, Belkheri, Barmanghat, Sandia and Hoshangabad for the period from 2008 to 2012. The initial uncertainty ranges were assigned to each parameter globally and the model runs were made with 1000 simulations. The global sensitivity analysis and one at a time sensitivity analysis was used to identify the most sensitive parameters and the non-sensitive parameters were then eliminated based on the p-values and t-statistic. The curve number (CN2) is the most sensitive parameter followed by groundwater delay (GWDELAY), groundwater revap coefficient (GW_REVAP) and threshold depth of water in the shallow aquifer required for return flow to occur (GWQMN). The other important parameters are available water capacity of the soil layer (SOL_AWC), base flow alpha factor (ALPHA_BF) and soil evaporation compensation factor (ESCO). The results of the global sensitivity analysis of the SWAT parameters are given in Figure 5.39 whereas the final calibrated parameter values and their adopted ranges are given in Table 5.3.

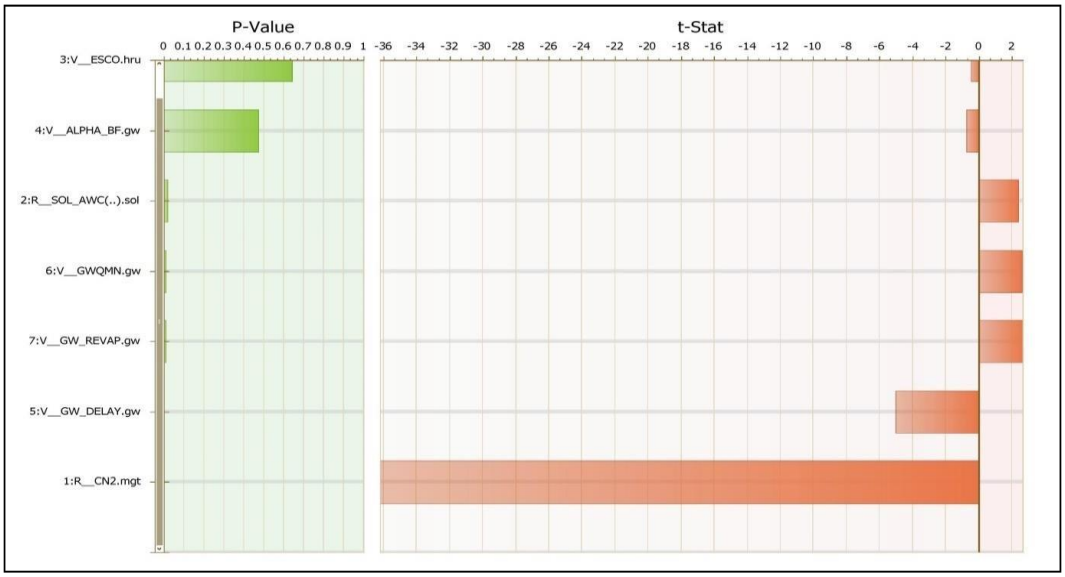

Figure 5.39: Results of the global sensitivity analysis of SWAT parameters for Narmada

Table 5.3: SWAT parameters with respective range and calibrated values

Name	Description	Lower Bound	Upper Bound	Process	Default	Calibrated	Rank

v_ESCO.hru	Soil evaporation compensation factor	0	1	Evaporation	0.95	0.848	7
v_ALPHA_BF.gw	Baseflow alpha factor (1/days)	0	1	Ground water	-	0.544	6
r_SOL_AWC.sol	Available water capacity of the soil layer (mm/mm of soil)	0	1	Soil	0.223	0.212	5
v_GWQMN.gw	Threshold depth of water in the shallow aquifer required for return flow to occur (mm)	0	5000	Ground water	0	178.1	4
v_GW_REV AP.gw	Groundwater revap coefficient	0.02	0.20	Ground water	-	0.169	3
v_GW_DELAY.gw	Groundwater delay (days)	0	50	Ground water	-	33.99	2
r_CN2.mgt	SCS runoff CN for AMC II	35	98	Runoff	83	68.64	1

The model parameter and input data uncertainty are represented by the 95PPU band and quantified by the P-factor and R-factor. The 95PPU band ideally gets smaller with subsequent iteration during the calibration process. A balance is maintained between the P- factor and R-factor such that the P-factor does not become too small while the R-factor remains high. The desired parameter ranges are obtained when the P-factor and the R-factor does not change in the subsequent iterations. The water balance components have also been checked during the calibration process to make sure that the simulations are reasonable for the basin.

The model evaluation statistics during the calibration for all the gauging sites are given in Table 5.4. The comparison of the observed and simulated daily

discharges at Manot is given in Figure 5.40. The model is able to simulate the flows reasonably well at Manot as the peaks as well as the rising and recession limbs of the simulated and observed hydrographs closely resemble each other. The time to peak as well as the magnitude of the peak flow has also been simulated satisfactorily. The NSE of 0.60 and PBias of +5.50, indicates a good simulation at Manot. Similarly, the RSR (0.63) also indicates only satisfactory simulation at the Manot. However, the performance of the monthly simulation is much better with NSE of 0.92, RSR of 0.29 and PBias limited to +2.07 only.

Table 5.4: SWAT performance for daily and monthly runoff simulation during calibration

S. No.	Gauging site	Daily			Monthly		
		NSE	RSR	PBIAS	NSE	RSR	PBIAS
1.	Manot	0.60	0.63	+5.50	0.92	0.29	+2.07
2.	Mohgaon	0.55	0.67	+8.76	0.79	0.46	+5.84
3.	Belkheri	0.50	0.70	-41.22	0.63	0.53	-29.01
4.	Patan	0.52	0.68	-39.88	0.77	0.48	+14.87
5.	Gadarwara	0.62	0.62	+17.49	0.80	0.45	+10.36
6.	Barmanghat	0.52	0.67	-28.43	0.68	0.51	-22.96
7.	Sandia	0.65	0.60	-20.37	0.75	0.50	-18.83
8.	Hoshangabad	0.61	0.62	-23.91	0.82	0.43	-21.60

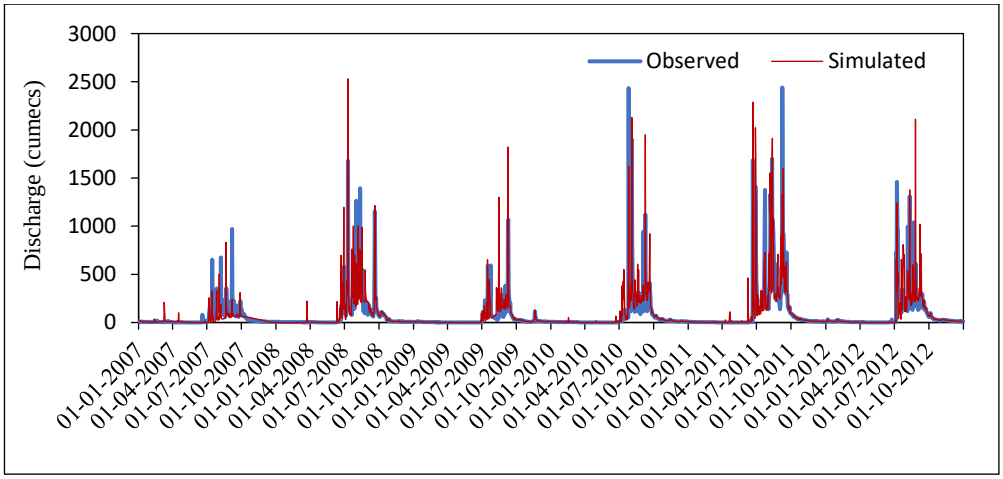

Figure 5.40: Comparison of observed and simulated daily flows at Manot during calibration

Similarly, the simulation at Mohgaon during calibration also indicates a very good monthly simulation with NSE of 0.79 (very good: $0.75 < \text{NSE} \leq 1.00$);

RSR of 0.46 (very good: 0.00 ≤ RSR ≤ 0.50) and PBIAS of +5.84 (very good: PBIAS < ± 10). However, the model performance for the monthly runoff simulation is better as compared to the daily runoff simulation during calibration at Mohgaon. The model performance during calibration for the monthly runoff simulation at Belkheri (Figure 5.41) suggests a satisfactory simulation NSE of 0.63 (satisfactory: 0.50 < NSE ≤ 0.65); RSR of 0.53 (good: 0.50 ≤ RSR ≤ 0.60) and PBIAS of -29.01 (unsatisfactory: PBIAS < ± 25). The model performance during calibration for the daily runoff simulation at Belkheri is comparable with that of the monthly simulation but with lower performance with NSE of 0.50. RSR of 0.70 and PBIAS of -41.22. Belkheri is the smallest headwater catchment and the model is underestimating the runoff except for few peaks only.

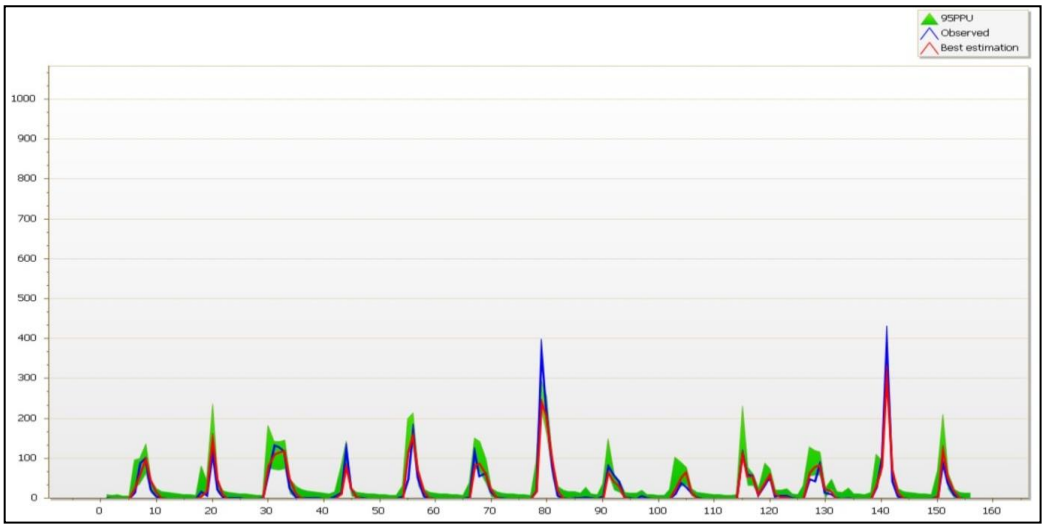

Figure 5.41: Comparison of the observed and simulated monthly flows along with the 95PPU band at Belkheri

The performance of SWAT model for the monthly runoff simulation at Patan during calibration is good with NSE of 0.77 (good: 0.65 < NSE ≤ 0.75); RSR of 0.48 (very good: 0.00 ≤ RSR ≤ 0.50) and PBIAS of +14.87 (good: ± 10 ≤ PBIAS < ± 15). The performance of the model for simulation of daily runoff during calibration is NSE: 0.52, RSR: 0.68 and PBIAS: -39.88 which suggest much lower performance for daily runoff simulation. The performance of SWAT model for the monthly runoff simulation at Gadarwara during calibration is good with NSE of 0.80 (very good: 0.75 < NSE ≤ 1.00); RSR of 0.45 (very good: 0.00 ≤ RSR ≤ 0.50) and PBIAS of +10.36 (good: ± 10 ≤ PBIAS < ± 15). The performance of the model for simulation of daily runoff during calibration is NSE: 0.62, RSR: 0.62 and

PBIAS: +17.49 which suggest marginally lower performance for daily runoff simulation.

The model has been able to simulate the flows at Barmanghat with considerable accuracy considering the complexities due to the releases from the Bargi dam and the irrigation in the command areas. The performance of the model during calibration for monthly flow simulation with NSE of 0.68 (good: $0.65 < NSE \leq 0.75$); RSR of 0.51 (good: $0.50 < RSR \leq 0.60$) and PBIAS of -22.96 (satisfactory: $\pm 15 \leq PBIAS < \pm 25$) suggests a good simulation at this gauging site. The performance of the model for simulation of daily runoff during calibration is NSE: 0.52, RSR: 0.67 and PBIAS: +28.43 suggests lower performance for daily runoff simulation as compared to monthly runoff simulation.

The model has been able to simulate the flows for Narmada River at Sandia with considerable accuracy considering the complexities due to the releases from the Bargi dam, irrigation in the command areas along with the joining of few major tributaries also. The performance of the model during calibration for monthly flow simulation with NSE of 0.75 (good: $0.65 < NSE \leq 0.75$); RSR of 0.50 (good: $0.50 < RSR \leq 0.60$) and PBIAS of -18.83 (satisfactory: $\pm 15 \leq PBIAS < \pm 25$) suggests a good simulation at Sandia. The performance of the model for simulation of daily runoff during calibration is NSE: 0.65, RSR: 0.60 and PBIAS: -20.37 suggests lower performance for daily runoff simulation as compared to monthly runoff simulation.

The model has been able to simulate the flows for Narmada River at Hoshangabad with considerable accuracy considering the complexities due to the releases from three major dams viz, Bargi dam, Barna dam and Tawa dam, irrigation in the command areas along with the joining of few major tributaries also. The performance of the model during calibration for monthly flow simulation with NSE of 0.82 (very good: $0.75 < NSE \leq 1.00$); RSR of 0.43 (very good: $0.00 \leq RSR \leq 0.50$) and PBIAS of -21.60 (satisfactory: $\pm 15 \leq PBIAS < \pm 25$) suggests a very good simulation at Hoshangabad. The performance of the model for simulation of daily runoff during calibration is NSE: 0.61, RSR: 0.62 and PBIAS: -23.91 suggests lower performance for daily runoff simulation as compared to monthly runoff simulation.

Based on the model evaluation criteria estimated at all the gauging sites, it can be observed that at except at Belkheri, the model is able to simulate the flows with fair degree of accuracy at all other gauging sites, with the quality of simulation ranging between satisfactory and very good. Apart from the better simulations in the headwater catchments, the model is able to perform equally well for the gauging sites on the main river too. This indicates that the model has been calibrated by taking into consideration the model parameter uncertainties and input data uncertainties, which can be confirmed, based on the results of the validation with the independent data sets. The calibrated model has been run with the independent data for the period of three years from 2013 to 2015 after incorporating the calibrated parameters for validating the model setup for the study area. The model evaluation statistics during the validation for all the gauging sites is given in Table 5.5.

Table 5.5: SWAT performance for daily and monthly runoff simulation during validation

S. No.	Gauging site	Daily			Monthly		
		NSE	RSR	PBIAS	NSE	RSR	PBIAS
1.	Manot	0.57	0.66	-18.56	0.75	0.50	-24.37
2.	Mohgaon	0.62	0.62	-16.00	0.72	0.53	+1.15
3.	Gadarwara	0.61	0.62	+8.79	0.80	0.45	+10.36
4.	Patan	0.48	0.70	+10.26	0.65	0.60	+5.73
5.	Belkheri	0.56	0.61	-12.38	0.87	0.36	-5.05
6.	Barmanghat	0.50	0.68	-29.97	0.63	0.52	-24.88
7.	Sandia	0.53	0.65	-25.44	0.68	0.51	-16.59
8.	Hoshangabad	0.58	0.63	-26.82	0.77	0.46	-24.87

The comparison of the observed and simulated flows at Manot during validation period is given in Figure 5.42. It can be observed that the calibrated model is able to simulate the flows reasonably well during the validation period with the independent datasets, as the rising limbs, peaks and falling limbs of the simulated hydrographs resemble with observed hydrographs. This is also

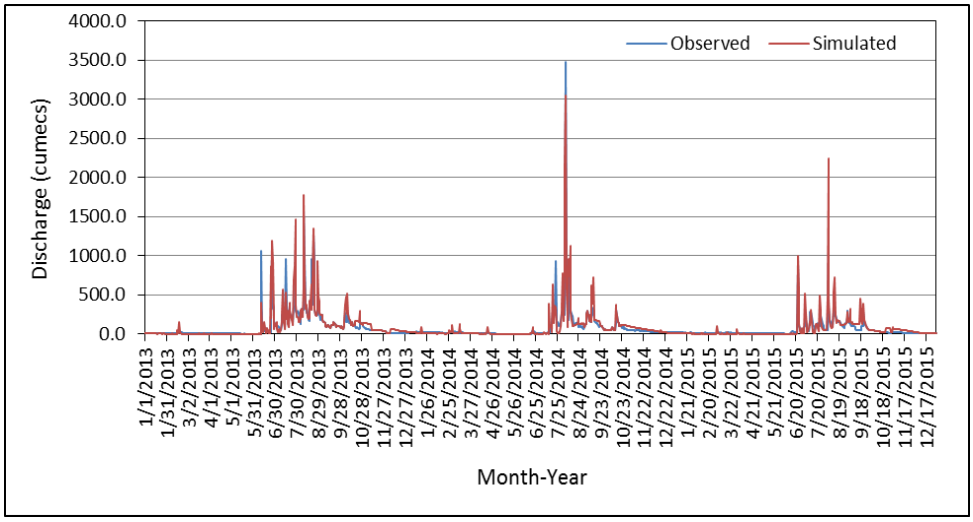

Figure 5.42: Comparison of the observed and simulated monthly flows at Manot during validation

substantiated by the model evaluation statistics at Manot for the monthly runoff simulation during validation with NSE of 0.75 (good: $0.65 < NSE \leq 0.75$); RSR of 0.50 (good: $0.50 < RSR \leq 0.60$) indicates good simulation whereas PBIAS of -24.37 (satisfactory: $\pm 15 \leq PBIAS < \pm 25$) indicates good simulation results during validation at Manot G/D site. The performance of the model for simulation of daily runoff during validation is NSE: 0.57, RSR: 0.66 and PBIAS: -18.56 suggests slightly lower performance for daily runoff simulation as compared to monthly runoff simulation.

The performance of the model during validation for monthly flow simulation at Mohgaon is good with NSE of 0.72 (good: $0.65 < NSE \leq 0.75$); RSR of 0.53 (good: $0.50 < RSR \leq 0.60$) and PBIAS of +1.15 (very good: $PBIAS < \pm 10$) suggests a good simulation at Mohgaon. The performance of the model for simulation of daily runoff during validation is NSE: 0.62, RSR: 0.62 and PBIAS: -16.00 suggests lower performance for daily runoff simulation as compared to monthly runoff simulation. The comparison of the observed and simulated flows at Mohgaon during validation period is given in Figure 5.43.

The performance of the model during validation for monthly flow simulation at Belkheri is good with NSE of 0.87 (very good: $0.75 < NSE \leq 1.00$); RSR of 0.36 (very good: $0.00 \leq RSR \leq 0.50$) and PBIAS of -5.05 (very good: $PBIAS < \pm 10$) suggests a good simulation at Mohgaon. The performance of the model for simulation of daily runoff during validation is NSE: 0.56, RSR: 0.61 and

PBIAS: -12.38 suggests lower performance for daily runoff simulation as compared to monthly runoff simulation.

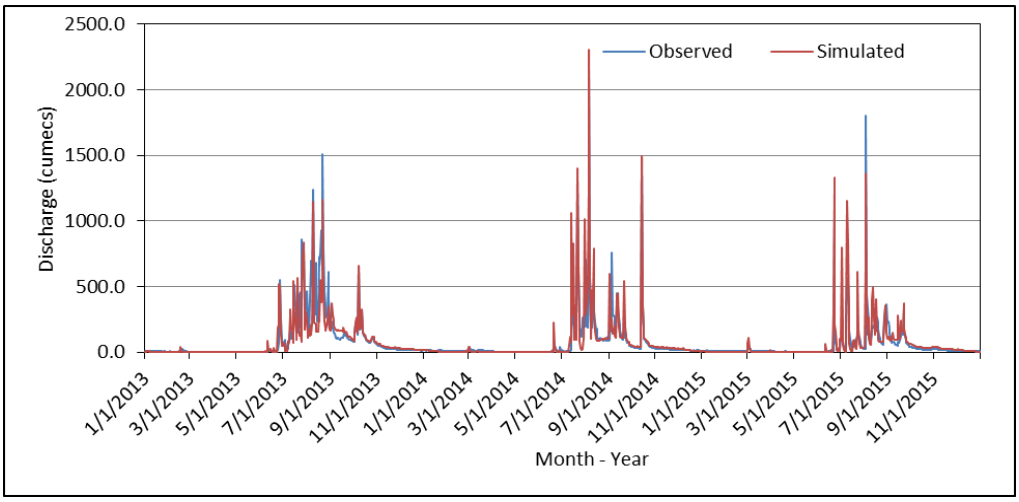

Figure 5.43: Comparison of the observed and simulated monthly flows at Mohgaon during validation

The performance of the model during validation for monthly flow simulation at Patan is good with NSE of 0.65 (satisfactory: $0.50 < NSE \leq 0.65$); RSR of 0.60 (good: $0.50 < RSR \leq 0.60$) and PBIAS of +5.73 (very good: PBIAS < ± 10) suggests a satisfactory simulation at Patan. The performance of the model for simulation of daily runoff during validation is NSE: 0.48, RSR: 0.70 and PBIAS: +10.26 suggests lower performance for daily runoff simulation as compared to monthly runoff simulation. The performance of the model during validation for monthly flow simulation at Gadarwara is very good with NSE of 0.80 (very good: $0.75 < NSE \leq 1.00$); RSR of 0.45 (very good: $0.00 \leq RSR \leq 0.50$) and PBIAS of +10.36 (good: $\pm 10 \leq PBIAS < \pm 15$) suggests a good simulation at Gadarwara. The performance of the model for simulation of daily runoff during validation is NSE: 0.61, RSR: 0.62 and PBIAS: +8.79 suggests lower performance for daily runoff simulation as compared to monthly runoff simulation.

The performance of the model during validation for monthly flow simulation at Barmanghat is satisfactory with NSE of 0.63 (satisfactory: $0.50 < NSE \leq 0.65$); RSR of 0.52 (good: $0.50 < RSR \leq 0.60$) and PBIAS of -24.88 (satisfactory: $\pm 15 \leq PBIAS < \pm 25$) suggests a satisfactory simulation at Barmanghat. The performance of the model for simulation of daily runoff during validation is NSE: 0.50, RSR: 0.68 and PBIAS: -29.97 suggests lower performance for daily runoff

simulation as compared to monthly runoff simulation. The performance of the model during validation for monthly flow simulation at Sandia is good with NSE of 0.68 (good: $0.65 < NSE \leq 0.75$); RSR of 0.51 (good: $0.50 < RSR \leq 0.60$) and PBIAS of -16.59 (satisfactory: $\pm 15 \leq PBIAS < \pm 25$) suggests a good simulation at Sandia. The performance of the model for simulation of daily runoff during validation is NSE: 0.53, RSR: 0.65 and PBIAS: -25.44 suggests lower performance for daily runoff simulation as compared to monthly runoff simulation.

The performance of the model during validation for monthly flow simulation at Hoshangabad is good with NSE of 0.77 (satisfactory: $0.50 < NSE \leq 0.65$); RSR of 0.46 (good: $0.50 < RSR \leq 0.60$) and PBIAS of -24.87 (satisfactory: $\pm 15 \leq PBIAS < \pm 25$) suggests a satisfactory simulation at Hoshangabad. The performance of the model for simulation of daily runoff during validation is NSE: 0.58, RSR: 0.63 and PBIAS: -26.82 suggests lower performance for daily runoff simulation as compared to monthly runoff simulation.

The performance of the model based on the performance indicators at the remaining gauging sites vary between satisfactory to good. Therefore, the model is able to simulate the flows at all the gauging sites with reasonable degree of accuracy and the model can be considered to be calibrated suitable for the study area. After the incorporation of the major dams in the study area, the model can be effectively used to assess the impacts of climate change on the water resources in the Upper Narmada basin.

The performance evaluation of the SWAT model for the monthly and daily runoff simulation shows that model is capable of simulating the flows in headwater catchments as well as the main river catchments with fair degree of accuracy. In the headwater catchments the model efficiency (NSE) during daily calibration varied between 0.50 at Belkheri and 0.62 at Gadarwara. The difference in volume between computed and observed discharge varied between -39.88% at Patan to +17.49% at Gadarwara. Similarly, during validation in headwater catchments, the NSE varied between 0.48 at Patan and 0.62 at Mohgaon. Even though the NSE at Belkheri was 0.50 during calibration, it improved to 0.56 during the validation period. The performance of the model for monthly streamflow simulation is far better, during

both calibration and validation in the headwater catchments and NSE varied between 0.63 at Belkheri and 0.92 at Manot during calibration, whereas NSE varied between 0.65 at Patan to 0.87 at Belkheri. Therefore, the performance of SWAT model for simulation of river flows in the headwater catchments is reasonably good to very good for monthly runoff simulations and satisfactory to good for daily runoff simulations .

The performance of SWAT model at the main river catchments is also similar considering that effect of the few major dams that have been incorporated also comes into play. The streamflow for Narmada at Barmanghat has the influence of Bargi dam, which is a major reservoir and has releases from spillway during floods and also the flows from the river bed powerhouse. The NSE at Barmanghat for daily runoff simulation during the calibration is 0.52 and 0.50 during validation. The results of the monthly simulation are far better when compared to the model performance during daily simulation. The stream flows for Narmada at Hoshangabad has the influence of three major dams viz, Bargi dam, Tawa dam and Barna dam along with the contribution of the tributaries later on. The performance of SWAT model for daily runoff simulation at Hoshangabad is reasonably good with NSE of 0.61 during calibration and 0.58 during validation. The performance of the model for monthly streamflow simulation is far better in the main river catchments too, with NSE of 0.82 during calibration and 0.77 during validation for Narmada at Hoshangabad. Therefore, the performance of SWAT model for simulation of river flows in the main river catchments is equally good as well.

5.5 Hydrological Modelling using WEAP

WEAP based hydrological modelling has been conducted in the study area in a part to whole manner. The schematic view of the study area as setup in WEAP model is given in Figure 5.44. For setting up an ‘area’ of the catchment, ‘years’ and ‘time steps’ have been defined. The model simulation was initiated from 2008 and as such 2008 has been considered as current account year for

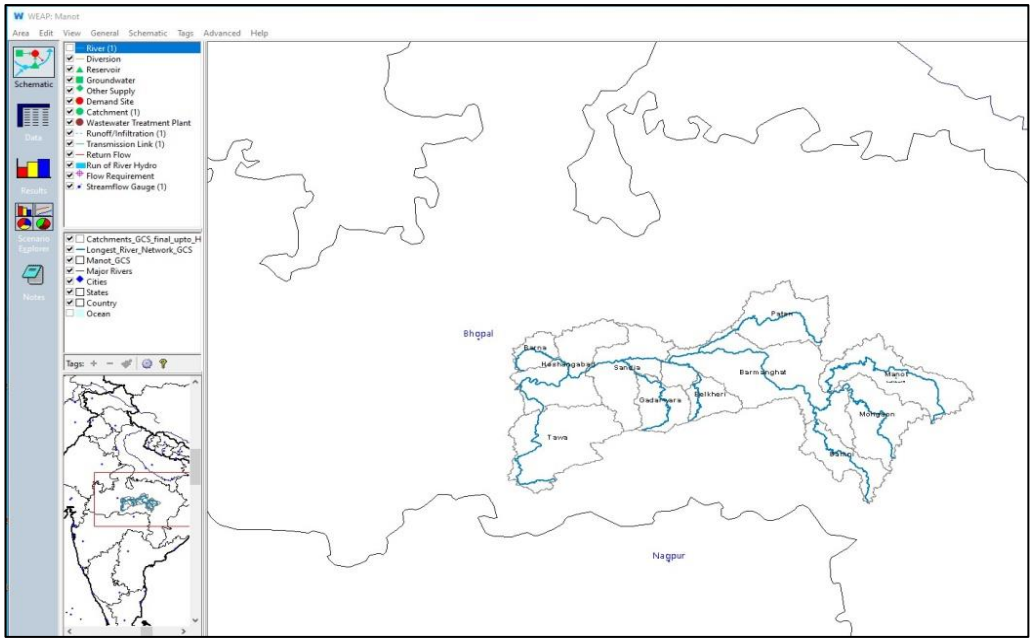

Figure 5.44: Schematic view of catchments of Narmada River basin up to Hoshangabad

which the model parameters are defined and the last year scenario up to which 'area' (catchment) is modelled is 2012. Simulation has been carried out at daily time step including leap days having time step boundary based on the calendar month. Thereafter the 'units' for the different input and output parameters have been assigned. The river network for the study area, already delineated using ArcGIS 10.4 has been added to the model schematic as given in Figure 5.45 which has the network of Narmada River and its tributaries up to Hoshangabad. This GIS layer serves the purpose of visualisation only and the river and its primary elements have to be drawn manually.

Similarly, the GIS layer of the catchment boundary has also been added to the schematic but only for the purposes of visualisation. The catchment is defined in WEAP as a 'node' and not as a boundary shape. However, catchment area and all other relevant catchment properties have been defined in the "Data View" of WEAP interface. The agricultural land with irrigation within the catchment is connected to the river network through the "Transmission Link" provided in the element window whereas the return flow from the catchment is transmitted through the "Runoff/Infiltration" link back to the river network.

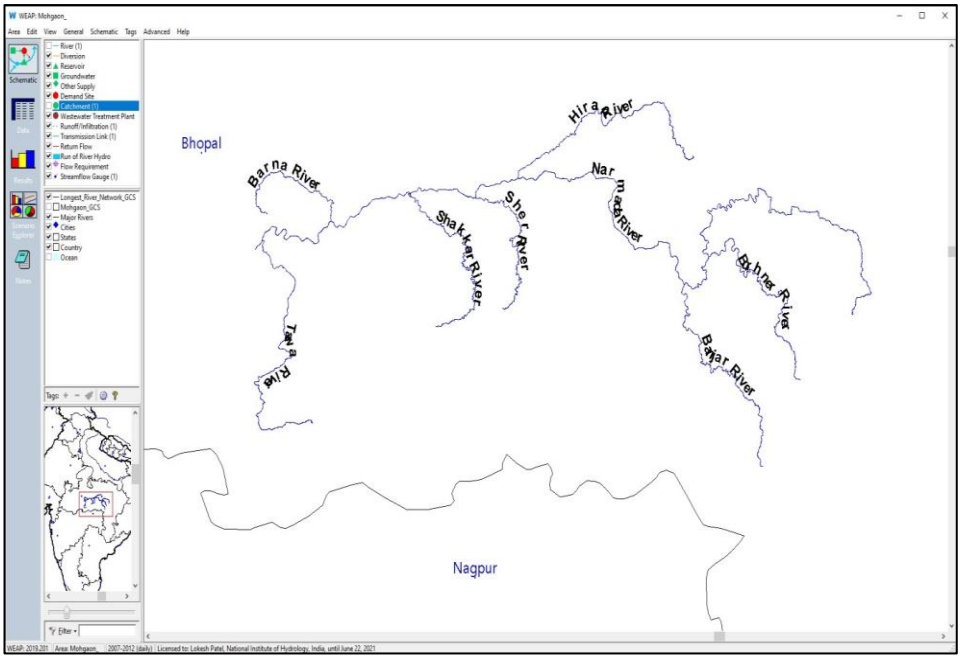

Figure 5.45: River network of Narmada River basin up to Hoshangabad

The stream flow gauge located in WEAP element window has been placed to map window at the outlet of the catchment. Therefore, the catchment setup has a 'River network', 'Catchment node', 'Transmission link', 'Runoff/Infiltration link', and 'Stream flow Gauge'. Figure 5.46 gives the typical setup of Manot catchment which is one of the upstream catchments of the study area. After the setup of the catchment in WEAP, the input data to the model had to be added from the 'Data View' of WEAP interface. The data has been entered step by step for each of the element provided in the schematic for two scenarios viz., a) 'Current Accounts' which is responsible for the first year of model calibration and b) 'Reference Scenario' for remaining years of model calibration. The catchment can be further sub-divided into many more branches, viz., Land Use/Land Cover classes as the sub-branch for catchment. For the catchment representing the study area, data pertaining to land use, climate and irrigation has been input to the model. The model parameters are can be calibrated include, i) soil water capacity, ii) deep water capacity, iii) runoff resistance factor, iv) root zone conductivity, v) deep conductivity, vi) preferred flow direction, vii) initial Z1 and viii) Initial Z2. As the total catchment area is further divided into sub-catchments, the total area of the catchment and percentage of the sub classes have been defined. The crop coefficient (K_c) values for different crop types have also been incorporated in the model.

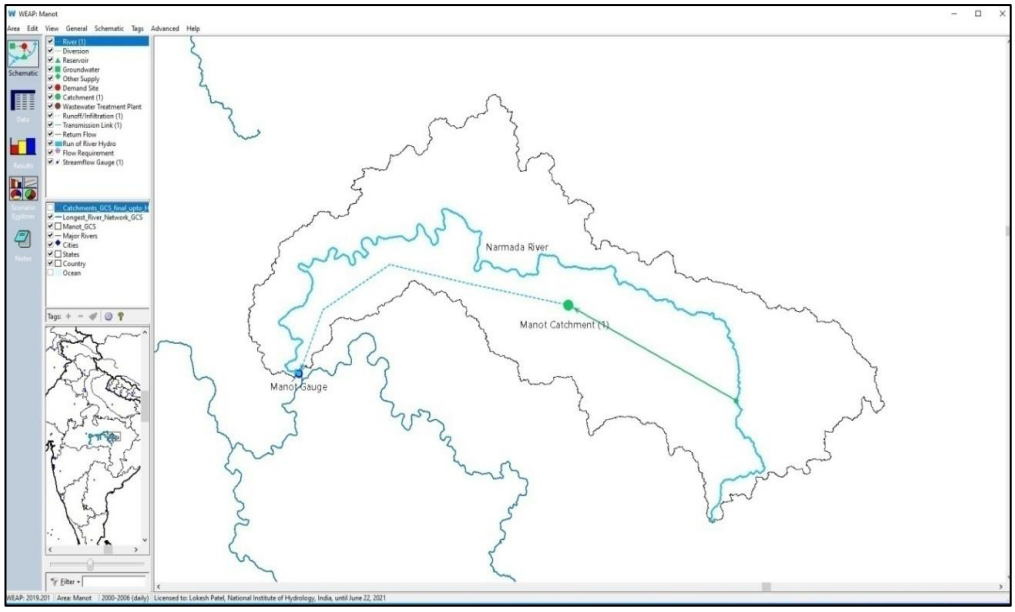

Figure 5:46: Typical setup of Manot catchment in WEAP Schematic

Subsequently the climatic data viz. precipitation, temperature, humidity, wind speed etc., K_c values and discharge data are provided as model inputs. The IMD gridded daily precipitation data at a resolution of 0.25 degree along with the temperature, humidity and wind speed was retrieved from the Data Access Viewer of NASA at the same resolution of 0.25-degree grid at daily time steps. These climate data along with the K_c values and the daily observed discharge have been provided as model inputs. The observed daily discharge data is provided for the gauge input. Irrigation has been provided for the agricultural area only. The main river and its tributaries and the corresponding catchments which have been considered for calibration and validation include a) Narmada River at Manot, b) Burhner River at Mohgaon, c) Sher River at Belkheri, d) Hiran River at Patan, d) Narmada River at Barmanghat, e) Shakkar River at Gadarwara, f) Narmada River at Sandia, and g) Narmada River at Hoshangabad. The models have been calibrated from 2008 to 2012 and validated from 2013 to 2015.

Manot is the upper most catchment of the Narmada River Basin, having hilly region in the catchment with the gauging site at Manot with a catchment area of 4467 km^2. The land use/ land cover of the Manot catchment has been classified into five categories viz., agriculture (56.95%), forest (29.55%), shrub land (13.35%), urban (0.01%), and water (0.14%). The performance of the model during calibration and validation at Manot is given in Table 5.6. For daily runoff

Table 5.6: WEAP performance for daily and monthly runoff simulation during calibration and validation for Narmada at Manot

	Daily		Monthly	
Parameters	Calibration	Validation	Calibration	Validation
NSE	0.63	0.600	0.931	0.85
PBias (%)	5.39	-21.26	5.48	-21.22
RSR	0.60	0.63	0.27	0.38

simulation at Manot, the model was able to achieve the Nash-Sutcliff efficiency (NSE) of 0.63 during calibration and 0.60 during validation, PBias was accounted for as 5.39% during calibration and -21.26% during validation, and RSR was 0.60 during calibration and 0.63 during validation. However, at a monthly time step, the model was able to achieve better NSE of 0.93 during calibration and 0.85 during validation, PBias was for 5.48% during calibration and -21.22% during validation, RSR was 0.27 during calibration and 0.38 during validation. The comparison of the observed and simulated daily and monthly discharge at Manot during calibration and validation is given in Figure 5.47 and Figure 5.48 respectively. Mohgaon is another headwater catchment of one of the tributaries viz., Burhner adjoining the Manot catchment, with the gauging site located at Mohgaon and a catchment area of 4090 km^2. The land use/ land cover of the Mohgaon catchment has been classified into five categories viz., agriculture (44.65%), forest (41.67%), grassland (0.26%), shrub land (13.33%), and water (0.09%).

The performance of the model during calibration and validation at Mohgaon is given in Table 5.7. For the daily runoff simulation at Mohgaon, the model was able to achieve the NSE of 0.58 during calibration and 0.67 during validation, PBias was -11.84% during calibration and -20.20% during validation, and RSR was 0.65 during calibration and 0.58 during validation. However, at a monthly time step, the model was able to achieve better NSE of 0.87 during calibration and 0.78 during validation, PBias was for -11.73% during calibration and -20.42% during validation, RSR was 0.36 during calibration and 0.47 during validation. The comparison of the observed and simulated daily discharge for Burhner River at Mohgaon during calibration and validation is given in Figure 5.49.

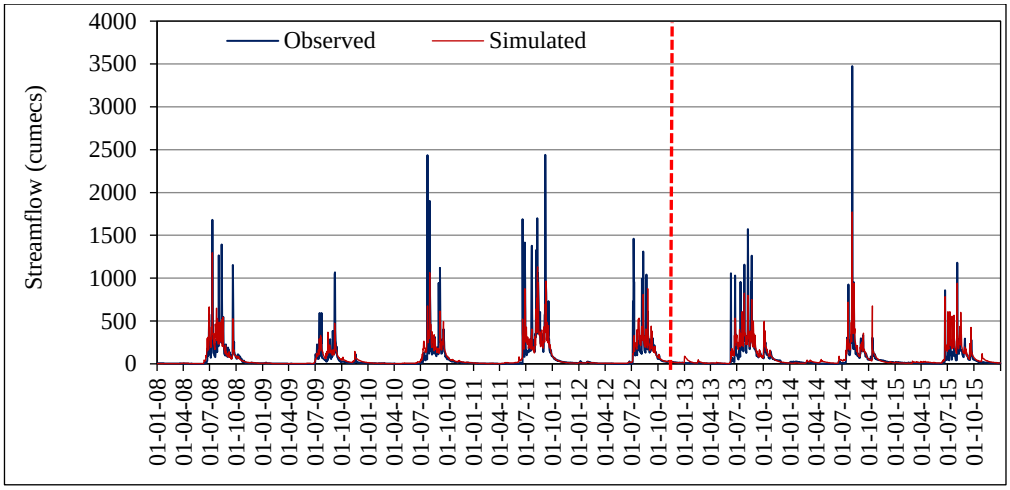

Figure 5.47: Comparison of daily observed and simulated stream flow during calibration and validation for R. Narmada at Manot

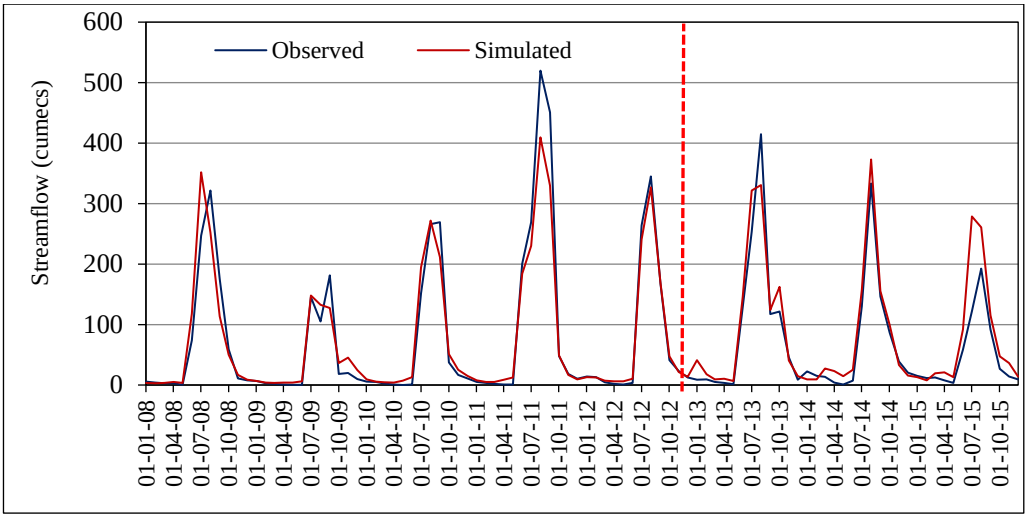

Figure 5.48: Comparison of monthly observed and simulated stream flow during calibration and validation for R. Narmada at Manot

Table 5.7: WEAP performance for daily and monthly runoff simulation during calibration and validation for Burhner at Mohgaon

Parameters	Daily Time Step		Monthly Time Step	
	Calibration	Validation	Calibration	Validation
NSE	0.58	0.67	0.87	0.78
PBias (%)	-11.84	-20.20	-11.73	-20.42
RSR	0.65	0.58	0.36	0.47

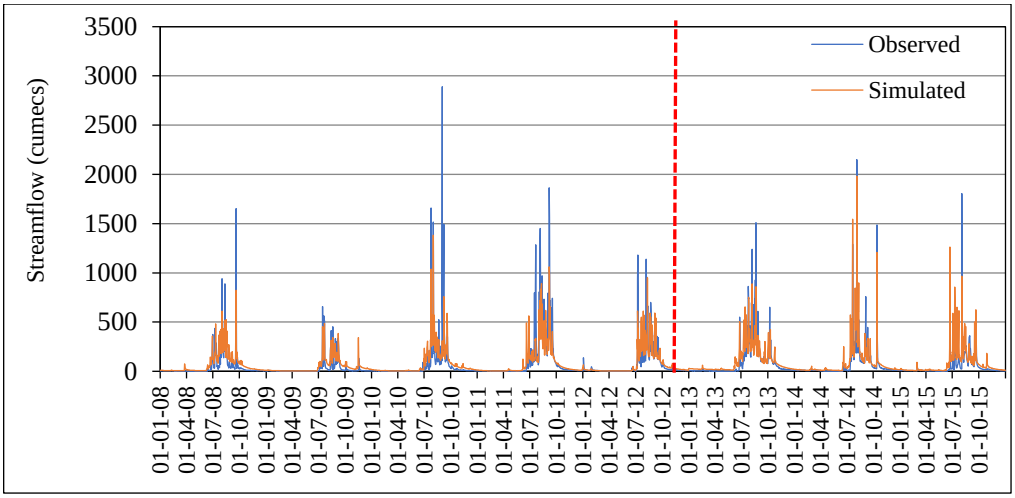

Figure 5.49: Comparison of daily observed and simulated stream flow during calibration and validation for R. Burhner at Mohgaon

Belkheri is another headwater catchment of one of the tributaries viz., Sher River having some part of foothills of the Satpura Range in its catchment area, with the gauging site located at Belkheri and a catchment area of 1508 km^2. The land use/land cover of the Belkheri catchment has been classified into five categories viz., agriculture (67.89%), barren (0.42%), forest (3.95%), grassland (0.12%), shrub land (27.38%), and water (0.24%). The performance of the model during calibration and validation at Belkheri is given in Table 5.8. For the daily runoff simulation at Belkheri, the model was able to achieve the NSE of 0.64 during calibration and 0.67 during validation, PBias was -9.16% during calibration and -2.02% during validation, and RSR was 0.60 during calibration and 0.57 during validation. However, at the monthly time step, the model was able to achieve better NSE of 0.91 during calibration and 0.95 during validation, PBias was for -9.04% during calibration and -2.14% during validation, RSR was 0.30 during calibration and 0.22 during validation. The comparison of the observed and simulated daily discharge for Sher River at Belkheri during calibration and validation is given in Figure 5.50.

Table 5.8: WEAP performance for daily and monthly runoff simulation during calibration and validation for Sher at Belkheri

	Daily		Monthly	
Parameters	Calibration	Validation	Calibration	Validation
NSE	0.64	0.67	0.91	0.95
PBias (%)	-9.16	2.02	-9.04	2.14
RSR	0.60	0.57	0.30	0.22

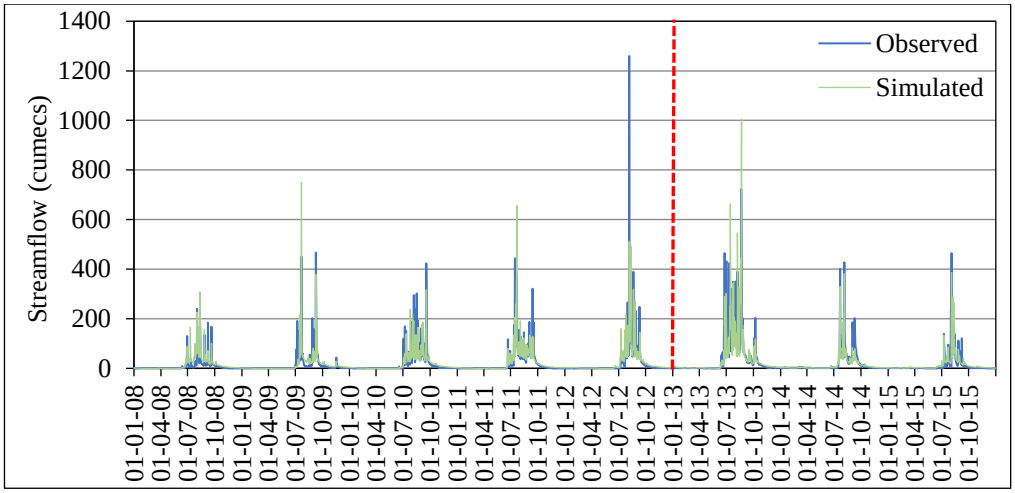

Figure 5.50: Comparison of daily observed and simulated stream flow during calibration and validation for R. Sher at Belkheri

Patan is another headwater catchment of one of the longest tributaries viz., Hiran River having Vindhyachal Range as its northern boundary, with the gauging site located at Patan and a catchment area of 3950 km^2. The land use/land cover of the Patan catchment has been classified into seven categories viz., agriculture (61.44%), barren (0.02%), forest (4.39%), grassland (0.31%), shrub land (31.25%), urban (1.88%) and water (0.71%). The performance of the model during calibration and validation at Patan is given in Table 5.9. For the daily runoff simulation at Patan, the model was able to achieve the NSE of 0.63 during calibration and 0.65 during validation, PBias was -9.61% during calibration and +2.44% during validation, and RSR was 0.61 during calibration and 0.59 during validation. However, at the monthly time step, the model was able to achieve better NSE of 0.85 during calibration and 0.82 during validation, PBias was for -9.52% during calibration and +2.23% during validation, RSR was 0.39 during calibration and 0.42 during validation. The comparison of the observed and simulated daily discharge for Hiran River at Patan during calibration and validation is given in Figure 5.51.

Table 5.9: WEAP performance for daily and monthly runoff simulation during calibration and validation for Hiran at Patan

	Daily		Monthly	
Parameters	Calibration	Validation	Calibration	Validation
NSE	0.63	0.65	0.85	0.82
PBias (%)	-9.61	2.44	-9.52	2.23
RSR	0.61	0.59	0.39	0.42

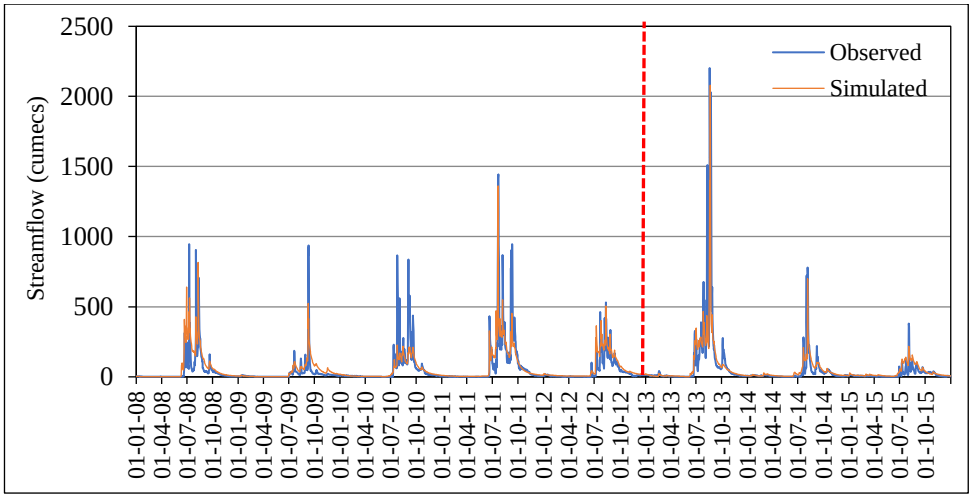

Figure 5.51: Comparison of daily observed and simulated stream flow during calibration and validation for R. Hiran at Patan

Barmanghat catchment is located on Narmada River and also comprising of headwater catchments of Manot, Mohgaon, Bamni, Belkheri and Patan. Apart from these headwater catchments, it also has its own catchment area of 10574 km^2, which makes a total catchment area of Narmada up to Barmanghat as 26453 km^2. The land use/land cover of the Barmanghat catchment has been classified into seven categories viz., agriculture (52.34%), barren (0.03%), forest (24.76%), grassland (2.33%), shrub land (18.36%), urban (0.48%) and water (1.69%). The performance of the model during calibration and validation at Barmanghat is given in Table 5.10. At a daily time-step at Barmanghat, the model was able to achieve the NSE of 0.56 during calibration and 0.59 during validation, PBias was -16.39% during calibration and -9.48% during validation, and RSR was 0.66 during calibration and 0.64 during validation. However, at the monthly time step, the model was able to achieve better NSE of 0.84 during calibration and 0.87 during validation, PBias was for -16.26% during calibration and -9.65% during validation, RSR was 0.39 during calibration and 0.36 during validation.

Table 5.10: WEAP performance for daily and monthly runoff simulation during calibration and validation for Narmada at Barmanghat

	Daily		Monthly	
Parameters	Calibration	Validation	Calibration	Validation
NSE	0.56	0.59	0.84	0.87
PBias (%)	-16.39	-9.48	-16.26	-9.65
RSR	0.66	0.64	0.39	0.36

The comparison of the observed and simulated daily discharge for Narmada River at Barmanghat during calibration and validation is given in Figure 5.52. Gadarwara is another headwater catchment of Shakkar River, with the gauging site located at Gadarwara and a catchment area of 2270 km^2. The land use/land cover of the Gadarwara catchment has been classified into five categories viz., agriculture (70.56%), forest (4.06%), grassland (1.84%), shrub land (23.49%), and water (0.05%).

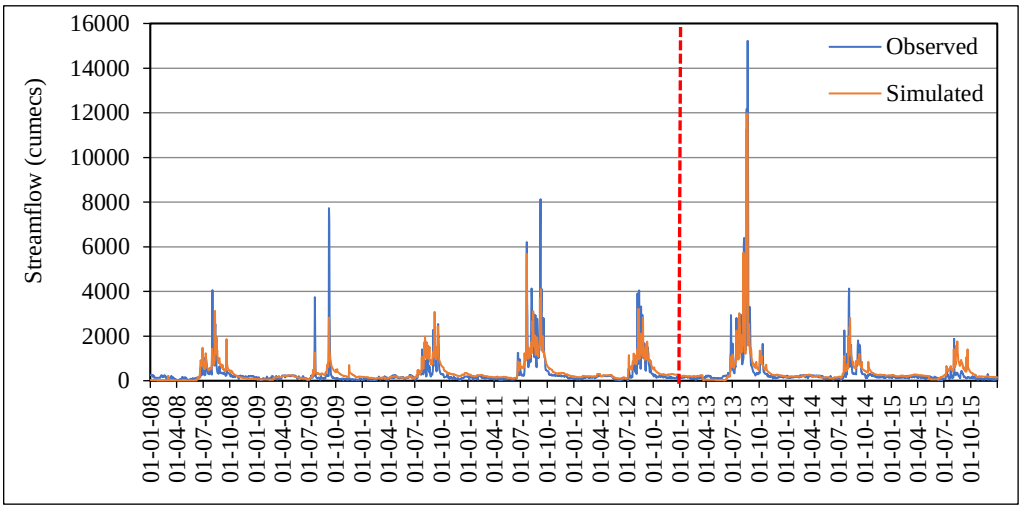

Figure 5.52: Comparison of daily observed and simulated stream flow during calibration and validation for R. Narmada at Barmanghat

The performance of the model during calibration and validation at Gadarwara is given in Table 5.11. For the daily runoff simulation at Gadarwara, the model was able to achieve the NSE of 0.68 during calibration and 0.61 during validation, PBias was 14.41% during calibration and -1.30% during validation, and RSR was 0.56 during calibration and 0.63 during validation. However, at the monthly time step, the model was able to achieve better NSE of 0.75 during calibration and 0.86 during validation, PBias was for 14.54% during calibration and -1.42% during validation, RSR was 0.50 during calibration and 0.37 during validation. The comparison of the observed and simulated daily discharge for Shakkar River at Gadarwara during calibration and validation is given in Figure 5.53.

Sandia catchment is located on Narmada River and also comprising of headwater catchments of Manot, Mohgaon, Bamni, Belkheri, Patan and Gadarwara along with the catchment up to Barmanghat. Apart from these

Table 5.11: WEAP performance for daily and monthly runoff simulation during calibration and validation for Shakkar at Gadarwara

Parameters	Daily		Monthly	
	Calibration	Validation	Calibration	Validation
NSE	0.68	0.618	0.75	0.86
PBias (%)	14.41	-1.30	14.54	-1.42
RSR	0.56	0.63	0.50	0.37

catchments, it also has its own catchment area of 5230.5 km^2, which makes a total catchment area of Narmada up to Sandia as 33953.5 km^2. The land use/land cover of the Sandia catchment has been classified into seven categories viz., agriculture (55.54%), barren (0.03%), forest (21.45%), grassland (2.60%), shrub land (18.55%), urban (0.39%) and water (1.45%).

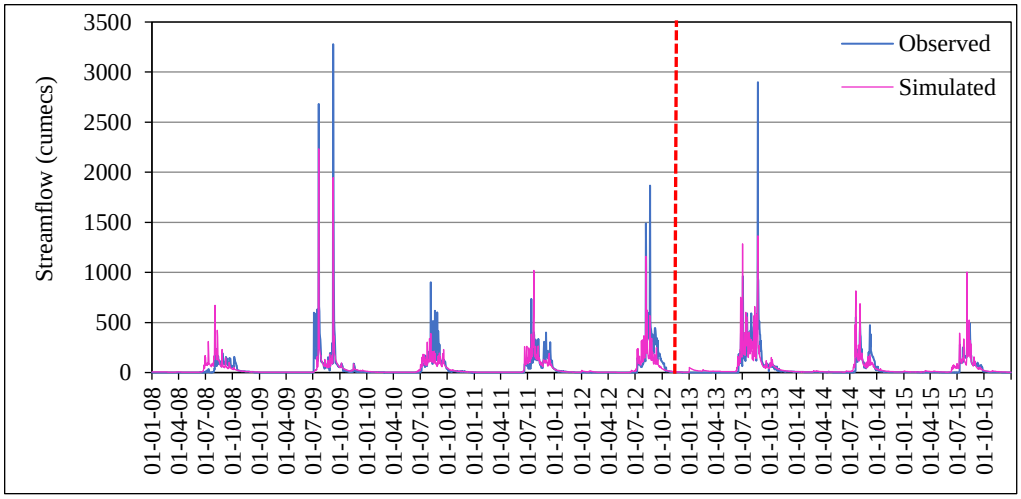

Figure 5.53: Comparison of daily observed and simulated stream flow during calibration and validation for R. Shakkar at Gadarwara

The performance of the model during calibration and validation at Sandia is given in Table 5.12. For the daily runoff simulation at Sandia, the model was able to achieve the NSE of 0.57 during calibration and 0.59 during validation, PBias was -8.48% during calibration and -11.54% during validation, and RSR was 0.66 during calibration and 0.64 during validation. However, at the monthly time step, the model was able to achieve better NSE of 0.82 during calibration and 0.91 during validation, PBias was for -8.23% during calibration and -11.45% during validation, RSR was 0.43 during calibration and 0.31 during validation. The comparison of the observed and simulated daily discharge for Narmada River at Sandia during calibration and validation is given in Figure 5.54.

Table 5.12: WEAP performance for daily and monthly runoff simulation during calibration and validation for Narmada at Sandia

Parameters	Daily		Monthly	
	Calibration	Validation	Calibration	Validation
NSE	0.57	0.59	0.82	0.91
PBias (%)	-8.48	-11.54	-8.23	-11.45
RSR	0.66	0.64	0.43	0.31

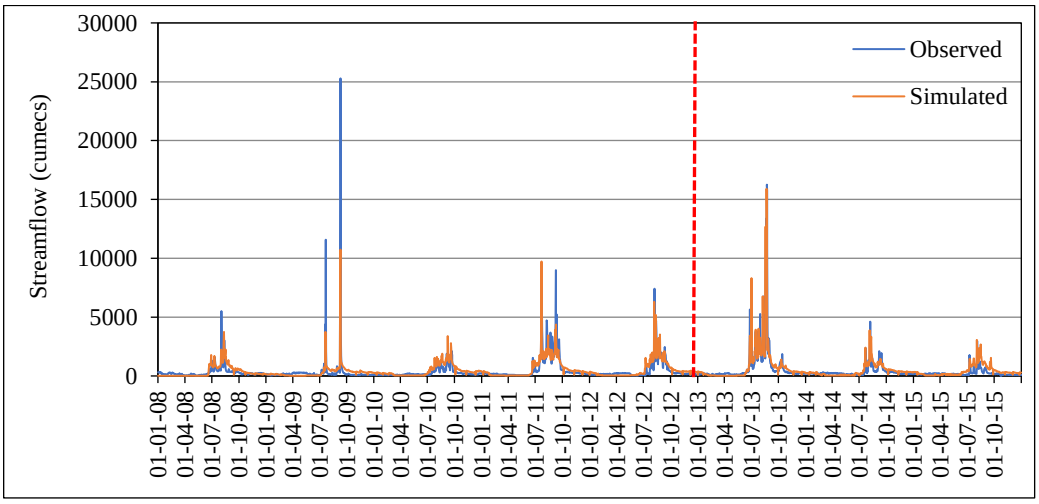

Figure 5.54: Comparison of daily observed and simulated stream flow during calibration and validation for R. Narmada at Sandia

Hoshangabad catchment is located on Narmada River and also comprising of headwater catchments of Manot, Mohgaon, Belkheri, Patan, Gadarwara and along with the catchment up to Sandia. Apart from these catchments, it also has its own catchment area of 10594.5 km^2, which makes a total catchment area of Narmada up to Hoshangabad as 44548.0 km^2. The land use/land cover of the Hoshangabad catchment has been classified into seven categories viz., agriculture (55.11%), barren (0.05%), forest (20.91%), grassland (3.45%), shrub land (18.32%), urban (0.33%) and water (1.84%). The performance of the model during calibration and validation at Hoshangabad is given in Table 5.13. For the daily runoff simulation at Hoshangabad, the model was able to achieve the NSE of 0.63 during calibration and 0.62 during validation, PBias was -4.12% during calibration and -14.12% during validation, and RSR was 0.61 during calibration and 0.62 during validation. However, at the monthly time step, the model was able to achieve better NSE of 0.90 during calibration and 0.92 during validation, PBias was for -3.87% during calibration and -14.08% during validation, RSR was 0.32

Table 5.13: WEAP performance for daily and monthly runoff simulation during calibration and validation for Narmada at Hoshangabad

Parameters	Daily		Monthly	
	Calibration	Validation	Calibration	Validation
NSE	0.63	0.62	0.90	0.92
PBias (%)	-4.12	-14.12	-3.87	-14.08
RSR	0.61	0.62	0.32	0.29

during calibration and 0.29 during validation. The comparison of the observed and simulated daily discharge for Narmada River at Hoshangabad during calibration and validation is given in Figure 5.55.

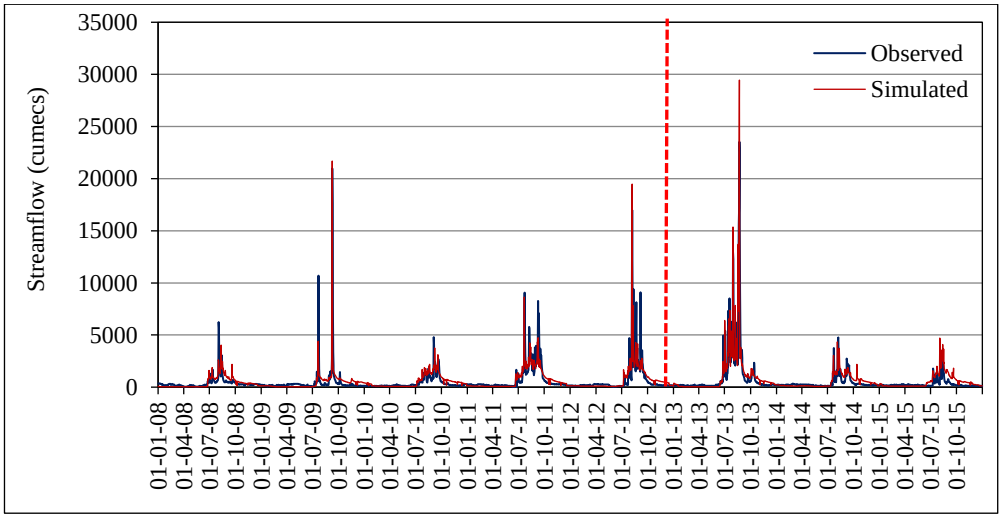

Figure 5.55: Comparison of daily observed and simulated stream flow during calibration and validation for R. Narmada at Hoshangabad

The performance evaluation of the WEAP model for the daily stream simulation shows that model is capable of simulating the flows in headwater catchments as well as the main river catchments with good degree of accuracy. In the headwater catchments the model efficiency (NSE) during daily calibration varied between 0.58 at Mohgaon and 0.68 at Gadarwara. The difference in volume between computed and observed discharge varied between –11.84% at Mohgaon to +14.41% at Gadarwara. Similarly, during validation in headwater catchments, the NSE varied between 0.60 at Manot and 0.67 at Mohgaon. Even though the NSE at Mohgaon was 0.58 during calibration, it considerably improved to 0.67 during the validation period. The performance of the model for monthly streamflow

simulation is far better, both during calibration and validation. Therefore, the performance of WEAP model for simulation of river flows in the headwater catchments is reasonably good.

The performance of WEAP model at the main river catchments is also similar considering that few major dams have been incorporated. The streamflow for Narmada at Barmanghat has the influence of Bargi dam, which is a major reservoir and has releases from spillway during floods and also the flows from the river bed powerhouse. The NSE at Barmanghat is 0.56 during calibration and 0.59 validation. The streamflow for Narmada at Hoshangabad has the influence of three major dams viz, Bargi dam, Tawa dam and Barna dam along with the contribution of the tributaries later on. The performance of WEAP model at Hoshangabad is reasonably good with NSE of 0.63 during calibration and 0.62 during validation whereas the difference in volume between the observed and computed flow is limited to -4.12% during calibration and -14.12% during validation. The performance of the model for monthly streamflow simulation is far better validation in the man river catchments also, with NSE of 0.90 during calibration and 0.92 during validation for Narmada at Hoshangabad. Therefore, the performance of WEAP model for simulation of river flows in the main river catchments is equally good as well.

5.6 Hydrological Modelling using MIKE11-NAM

In the MIKE11-NAM, the model parameters and variables represent average values for the entire catchment. For some parameters a range of likely values can be estimated on the basis of physiographic, climatic and soil characteristics of the catchment. However, as most of them are of empirical or conceptual nature, it implies that the final estimation must be carried out by calibration against the observed hydrological observations. An automatic calibration procedure was developed for the MIKE11-NAM model (Madsen, 2000). It is based on a multiple-objective strategy, where different calibration objectives can be optimized simultaneously (water balance, overall hydrograph shape, peak flows and low flows). MIKE-11 NAM recommends to consider a time series of 3 to 5 years data for model calibration and validation.

In the present study, the daily rainfall, discharge and evaporation for during 2008 to 2015 of Narmada basin have been used for model calibration and validation. In the present study, calibration was carried out in two steps, viz., a) initially the model was calibrated using the in-built auto-calibration facility to obtain a set of model parameters and b) after obtaining a set of model parameters, a trial-and-error method was subsequently adopted to optimize each of the model parameters by varying each of them within their physically permissible range. The reliability of the MIKE11-NAM was evaluated based on the performance indicators viz., NSE, RSR and PBIAS. The performance evaluation of MIKE11-NAM evaluated during calibration is given in Table 5.14.

Table 5.14: MIKE11 NAM performance for daily runoff simulation during calibration

S. No.	Gauging site	Daily			Monthly		
		NSE	RSR	PBias (%)	NSE	RSR	PBias (%)
1.	Manot	0.72	0.53	-4.23	0.90	0.31	-4.35
2.	Mohgaon	0.57	0.66	-2.34	0.85	0.38	-2.31
3.	Gadarwara	0.63	0.61	+26.38	0.71	0.53	+26.42
4.	Patan	0.69	0.56	+2.34	0.89	0.32	+12.34
5.	Belkheri	0.52	0.69	-21.58	0.63	0.60	-21.99

For the daily simulation during calibration, NSE is 0.72, RSR is 0.53 and PBias is -4.23% which improves further for monthly simulation with NSE of 0.90, RSR as 0.31 and PBias is -4.35%. The performance of MIKE11-NAM at Mohgaon is satisfactory with NSE of 0.57, RSR of 0.66 and PBias of -2.34% for daily simulation and NSE of 0.85, RSR of 0.38 and PBias of -2.31% for monthly simulation. The performance of MIKE11-NAM at Gadarwara good with NSE of 0.63, RSR of 0.61 and PBias of +26.38% for daily simulation and NSE of 0.71, RSR of 0.53 and PBias of +26.42% for monthly simulation. The performance at Patan is also good with NSE of 0.69, RSR of 0.56 and PBias of +2.34% for daily simulation and NSE of 0.89, RSR of 0.32 and PBias of +12.34% for monthly simulation. The performance of MIKE11 NAM at Belkheri is satisfactory with NSE of 0.52, RSR of 0.69 and PBias of -21.52% for daily simulation and NSE of 0.63,

RSR of 0.60 and PBias of -21.99% for monthly simulation.

The comparison of the observed and simulated daily flows during calibration at Manot is given in Figure 5.56 to Figure 5.58 respectively.

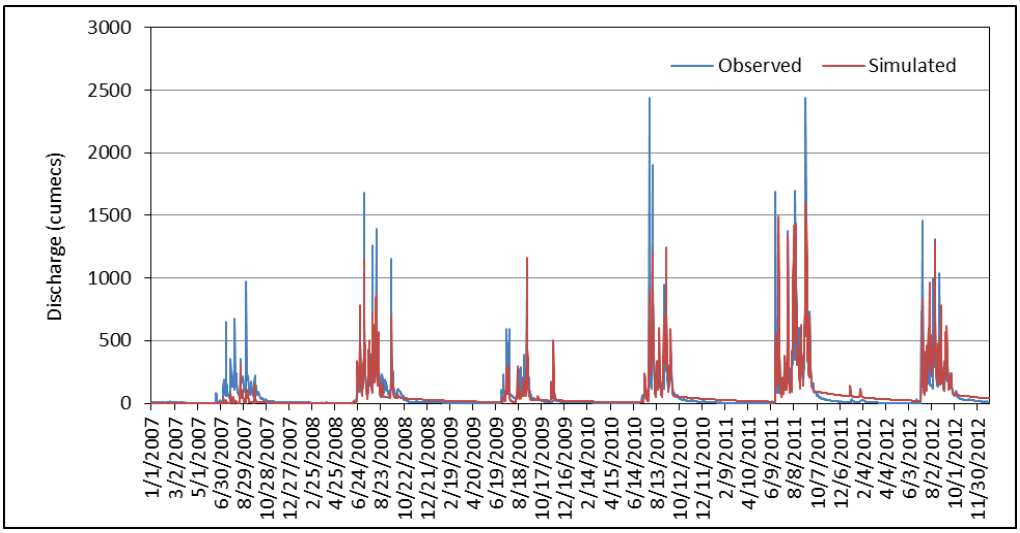

Figure 5.56: Comparison of observed and simulated flows during calibration for Narmada at Manot

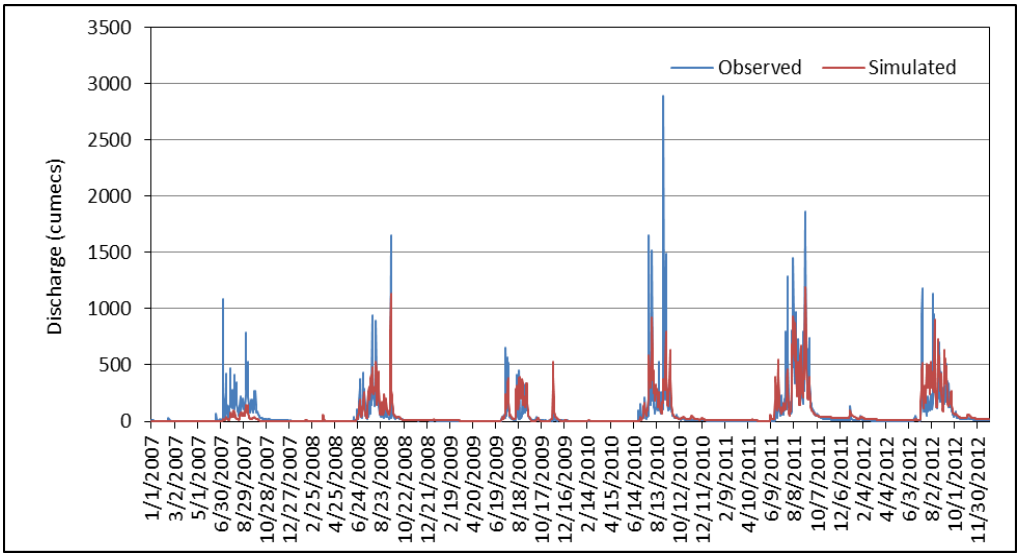

Figure 5.57: Comparison of observed and simulated flows during calibration for Burhner at Mohgaon

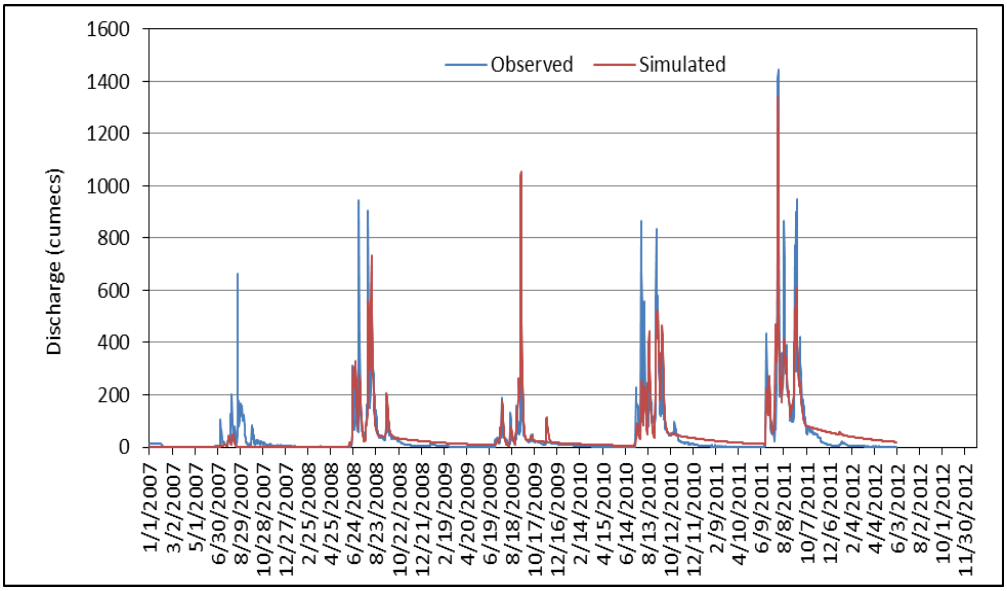

Figure 5.58: Comparison of observed and simulated flows during calibration for Hiran at Patan

It can be observed that the performance of the MIKE11-NAM in simulating the daily flow varies between satisfactory and good except at Belkheri. The model is not able to simulate the peaks of the hydrograph and at the same time the lean period flows are being overestimated. The model performance during the validation period is given in Table 5.15. The comparison of the observed and simulated flows at Manot and Mohgaon during validation is given in Figure 5.59 and Figure 5.60 respectively. The performance of MIKE11-NAM at Manot is good as indicated by the performance indicators.

Table 5.15: MIKE11-NAM performance for daily runoff simulation during validation

S. No.	Gauging site	Validation (daily)			Validation (monthly)		
		NSE	RSR	PBIAS	NSE	RSR	PBIAS
1.	Manot	0.59	0.64	-15.11	0.89	0.32	-15.02
2.	Mohgaon	0.66	0.58	-11.46	0.83	0.40	-11.57
3.	Gadarwara	0.57	0.62	+14.50	0.86	0.31	+14.56
4.	Patan	0.47	0.73	+24.12	0.56	0.66	+27.37
5.	Belkheri	0.55	0.67	+0.44	0.65	0.59	+0.05

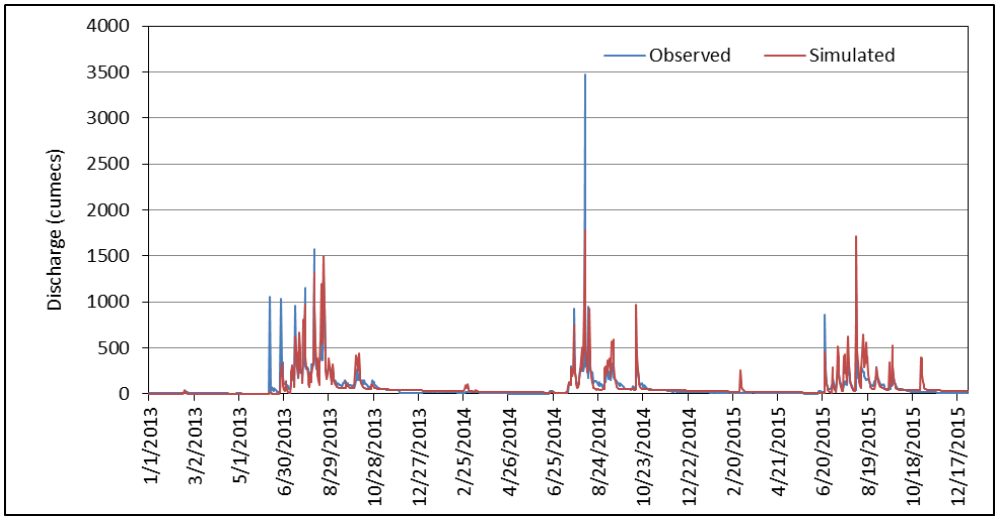

Figure 5.59: Comparison of observed and simulated flows during validation for Narmada at Manot

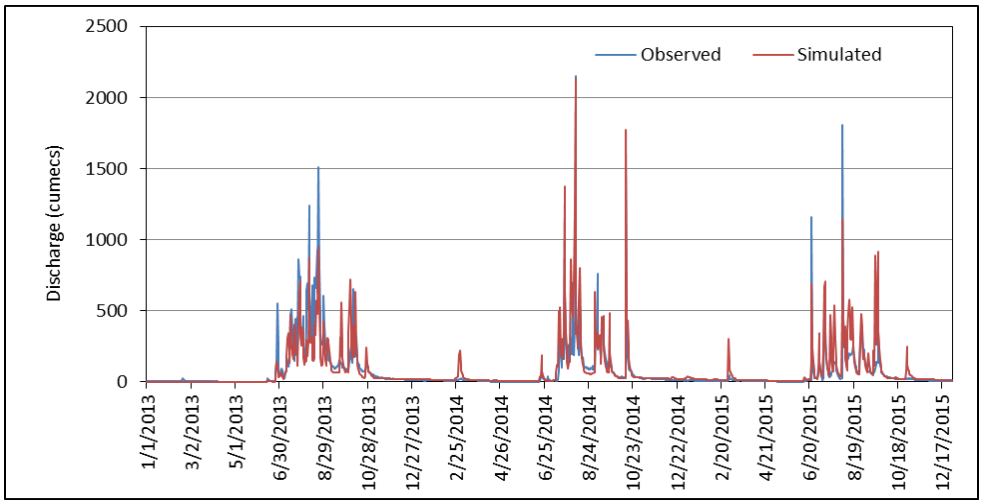

Figure 5.60: Comparison of observed and simulated flows during validation for Burhner at Mohgaon

For the daily simulation, NSE is 0.59, RSR is 0.64 and PBias is -15.11% which improves for monthly simulation with, NSE as 0.89, RSR with NSE of 0.57, RSR of 0.62 and PBias of +14.50% for daily simulation and NSE of 0.86, RSR of 0.31 and PBias of +14.56% for monthly simulation. However, the performance at Patan is not satisfactory as compared to other gauging sites with NSE of 0.47, RSR of 0.73 and PBias of +24.12% for daily simulation and NSE of 0.56, RSR of 0.66 and PBias of +27.37% for monthly simulation. The performance of MIKE11-NAM at Belkheri is satisfactory with NSE of 0.55, RSR of 0.67 and PBias of +0.44% for daily simulation and NSE of 0.65, RSR of 0.59 and PBias of +0.50% for monthly simulation. It can be observed that the performance of the MIKE11-NAM in

simulating the daily flow varies between satisfactory and good.

The MIKE11-NAM model has been applied in this study and its performance is satisfactory as far as the simulations in the headwater catchments is considered. The NSE during the daily runoff calibration varied between 0.52 at Belkheri to 0.72 at Manot whereas it varied between 0.47 at Patan to 0.66 at Mohgaon. The performance on the monthly scale is also good and the NSE varied between 0.63 at Belkheri to 0.90 at Manot during calibration whereas the NSE varied between 0.56 at Patan to 0.89 at Manot during validation for the monthly runoff simulations. However, the incorporation of the reservoirs is not possible in main-river catchments, wherein Barmanghat has the influence of Bargi dam and Hoshangabad has the influence of Bargi, Tawa and Barna dams.

5.7 Hydrologic Modelling using VIC

The Upper Narmada Basin (UNB) was delineated using the 30 m resolution SRTM DEM after according the necessary projection system to the DEM. After delineation, the shape file of the Upper Narmada basin was extracted. Thereafter, a fishnet of 0.125° x 0.125° spatial resolution was imposed on this shapefile covering the complete study area. 612 grids have been generated comprising of 18 rows and 34 columns. The additional information including grid number, run grid, latitude, longitude, slope (%), elevation (m), average annual rainfall (mm), and soil texture were added in the attribute table of the grid file. Run grids are those grids that fall under the shape file and numbered as 1 else remaining is numbered as 0. The soil parameter file and the vegetation parameter have been then created using the attribute table of the fishnet file.

Since the VIC model has been developed to run on LINUX and UNIX platforms so, a separate tool known as CYGWIN is required to compile and run the model. The source code directory path is assigned in the Cygwin window and then the model has been compiled and after running the compile program, the fluxes get generated for each grid cell. After the fluxes get generated for each individual grid cells, the VIC routing model has to be compiled and run using the input file along with the other datasets.

The parameters sensitive to the surface runoff include depth of the second soil layer (z2), the depth of the third soil layer (z3) and the variable infiltration capacity parameter (b_infilt) whereas the parameters sensitive to the base flow are Ws, Ds and Dsmax. Ds, Ws and Dsmax determine the shape of the base flow curve, which relates the soil moisture in the lower layer to the amount of baseflow. The list of sensitive parameters of VIC model are given in Table 5.16.

Table 5.16: Sensitive parameters of VIC

S. No.	Parameter	Description
1.	b_infilt	• It governs the shape of the variable capacity curve and effectively controls the partitioning of rainfall into surface runoff and infiltration. • A higher value indicates low infiltration and yields high surface runoff. • Generally, the range is 10^{-5}-0.4
2.	z2 & z3 (m)	• Controls the amount of water for transpiration and baseflow. • A thicker bottom soil layer causes higher ET, longer soil moisture retention and higher baseflow
3.	Dsmax (mm/day)	• Max baseflow velocity of the lowest soil layer
4.	Ds	• Fraction of Dsmax, where the rapidly increasing non-linear baseflow starts • A higher value of Ds causes higher baseflow
5.	Ws	• Fraction of the max soil moisture of the lowest soil when the rapidly increasing baseflow begins • A higher value of Ws tends to delay the peak runoff

The VIC model has been setup for the study area and multi-site calibration has been carried out for simulation of daily flow for Narmada River and its tributaries at the gauging sites of main river at Manot and its tributaries at Mohgaon, Patan, Belkheri and Gadarwara. The model was calibrated and validated from 2008-12 and 2013-15 respectively for the study. The soil parameters are the most sensitive parameters and thus the model was calibrated by adjusting the sensitive parameters identified from the sensitivity analysis. The headwater catchments have been calibrated initially followed by the gauging sites on the main Narmada River viz., Barmanghat, Sandia and Hoshangabad after implementation of the major reservoirs located on the main river. The performance evaluation of the VIC model

for daily runoff simulation during the calibration and validation Table 5.17. Similarly, the performance evaluation for monthly runoff simulation during the calibration and validation is given in Table 5.18.

During the daily runoff simulation at Manot, the model was able to achieve the NSE of 0.64 during calibration and 0.57 during validation and PBias was +16.6% during calibration and +0.02% during validation.

Table 5.17: VIC performance for daily runoff simulation during calibration and validation

Stations	Calibration		Validation	
	NSE	PBIAS (%)	NSE	PBIAS (%)
Manot	0.64	16.6	0.57	0.2
Mohgaon	0.54	5.95	0.58	2.10
Belkheri	0.53	-15.4	0.57	9.43
Patan	0.68	-4.05	0.82	8.27
Gadarwara	0.62	15.7	0.58	0.1
Barmanghat	0.65	-23.96	0.74	-17.78
Sandia	0.80	-16.16	0.84	-22.69
Hoshangabad	0.77	-8.22	0.86	-24.19

Table 5.18: VIC performance for monthly runoff simulation during calibration and validation

Stations	Calibration		Validation	
	NSE	PBIAS (%)	NSE	PBIAS (%)
Manot	0.90	16.48	0.94	0.6
Mohgaon	0.86	5.98	0.79	1.95
Belkheri	0.87	-15.5	0.84	9.5
Patan	0.89	-4.16	0.92	8.12
Gadarwara	0.82	15.82	0.87	0.5
Barmanghat	0.83	-23.91	0.88	-17.78
Sandia	0.88	-16.13	0.90	-22.69
Hoshangabad	0.89	-8.28	0.88	-24.19

However, for the monthly simulation, the model was able to achieve higher performance with NSE of 0.90 during calibration and 0.94 during validation, whereas PBias was for 16.48% during calibration and +0.60% during validation.

The comparison of the observed and simulated daily runoff at Manot during calibration and validation is given in Figure 5.61.

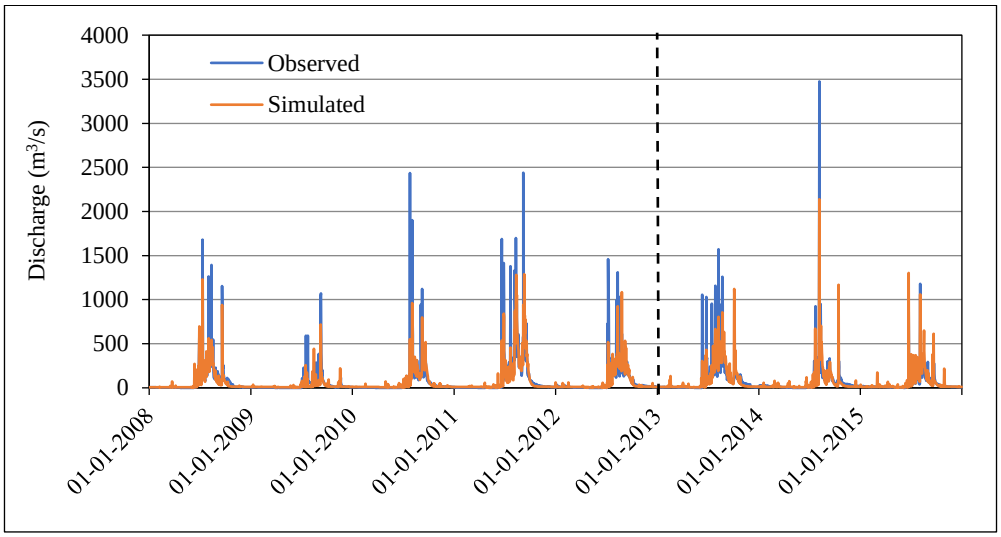

Figure 5.61: Comparison of daily observed and simulated stream flow during calibration and validation for R. Narmada at Manot

During the daily runoff simulation at Mohgaon, the model was able to achieve the NSE of 0.54 during calibration and 0.58 during validation and PBias was +5.95% during calibration and +2.10% during validation. However, for the monthly simulation, the model was able to achieve higher performance with NSE of 0.86 during calibration and 0.79 during validation, whereas PBias was for 5.98% during calibration and +1.95% during validation. The comparison of the observed and simulated daily runoff at Mohgaon during calibration and validation is given in Figure 5.62.

During the daily runoff simulation at Belkheri, the model was able to achieve the NSE of 0.53 during calibration and 0.57 during validation and PBias was -15.40% during calibration and +9.43% during validation. However, for the monthly simulation, the model was able to achieve higher performance with NSE of 0.87 during calibration and 0.84 during validation, whereas PBias was for -15.50% during calibration and +9.50% during validation. The comparison of the observed and simulated daily runoff at Belkheri during calibration and validation is given in Figure 5.63.

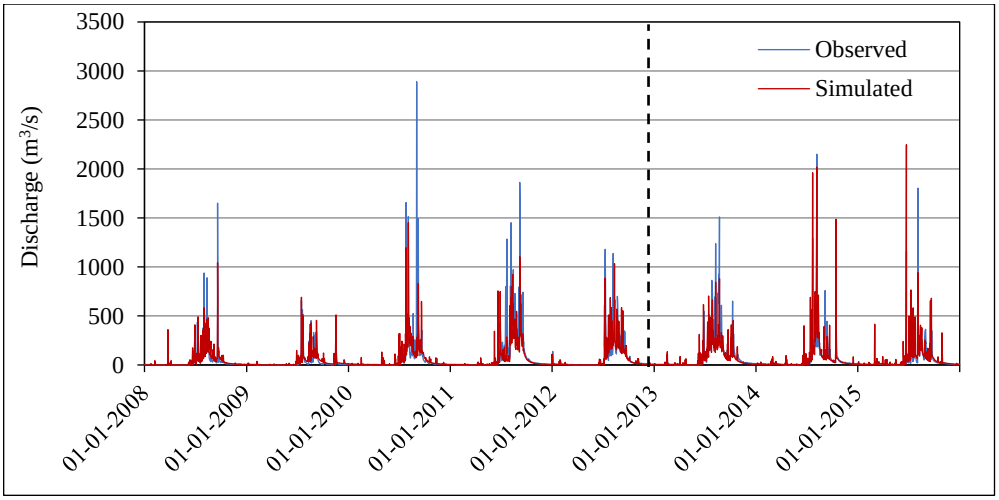

Figure 5.62: Comparison of daily observed and simulated stream flow during calibration and validation for R. Burhner at Mohgaon

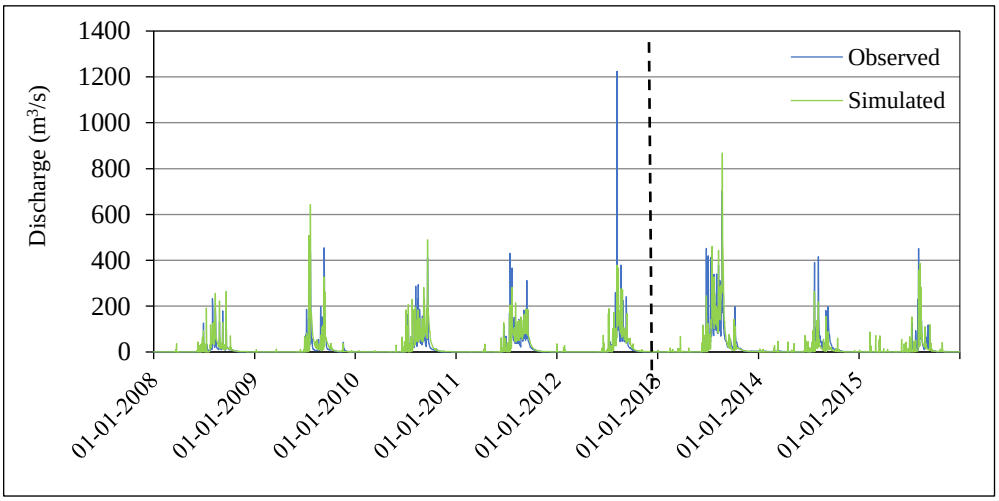

Figure 5.63: Comparison of daily observed and simulated stream flow during calibration and validation for R. Sher at Belkheri

During the daily runoff simulation at Patan, the model was able to achieve the NSE of 0.68 during calibration and 0.82 during validation and PBias was -4.05% during calibration and +8.27% during validation. However, for the monthly simulation, the model was able to achieve higher performance with NSE of 0.89 during calibration and 0.92 during validation, whereas PBias was for -4.16% during calibration and +8.12% during validation. The comparison of the observed and simulated daily runoff at Patan during calibration and validation is given in Figure 5.64.

During the daily runoff simulation at Gadarwara, the model was able to achieve the NSE of 0.62 during calibration and 0.58 during validation and PBias

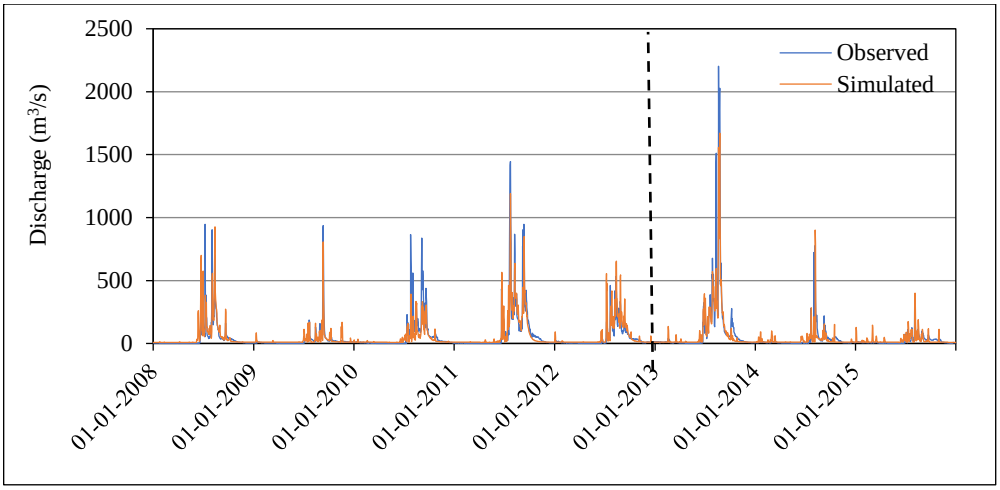

Figure 5.64: Comparison of daily observed and simulated stream flow during calibration and validation for R. Hiran at Patan

was +15.7% during calibration and +0.10% during validation. However, for the monthly simulation, the model was able to achieve higher performance with NSE of 0.82 during calibration and 0.87 during validation, whereas PBias was for 15.82% during calibration and +0.50% during validation. The comparison ofthe observed and simulated daily runoff at Gadarwara during calibration and validation is given in Figure 5.65.

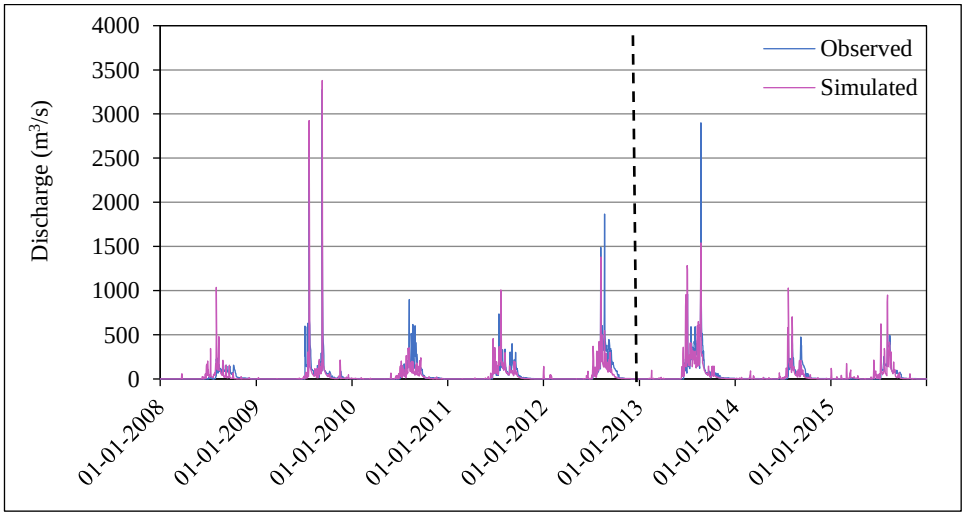

Figure 5.65: Comparison of daily observed and simulated stream flow during calibration and validation for R. Shakkar at Gadarwara

During the daily runoff simulation at Barmanghat, the model was able to achieve the NSE of 0.65 during calibration and 0.74 during validation and PBias was -23.96% during calibration and -17.78% during validation. However, for the monthly simulation, the model was able to achieve higher performance with NSE

of 0.83 during calibration and 0.88 during validation, whereas PBias was for -23.91% during calibration and -17.78% during validation. The comparison of the observed and simulated daily runoff at Barmanghat during calibration and validation is given in Figure 5.66.

During the daily runoff simulation at Sandia, the model was able to achieve the NSE of 0.80 during calibration and 0.84 during validation and PBias was -16.16% during calibration and -22.69% during validation. However, for the monthly simulation, the model was able to achieve higher performance with NSE of 0.88 during calibration and 0.90 during validation, whereas PBias was for -16.13% during calibration and -22.69% during validation. The comparison of the observed and simulated daily runoff at Sandia during calibration and validation is given in Figure 5.67. During the daily runoff simulation at Hoshangabad, the model was able to achieve the NSE of 0.77 during calibration and 0.82 during validation and PBias was -8.22% during calibration and -24.19% during validation. However, for the monthly simulation, the model was able to achieve higher performance with NSE of 0.89 during calibration and 0.88 during validation, whereas PBias was for -8.28% during calibration and -24.19% during validation. The comparison of the observed and simulated daily runoff at Hoshangabad during calibration and validation is given in Figure 5.68.

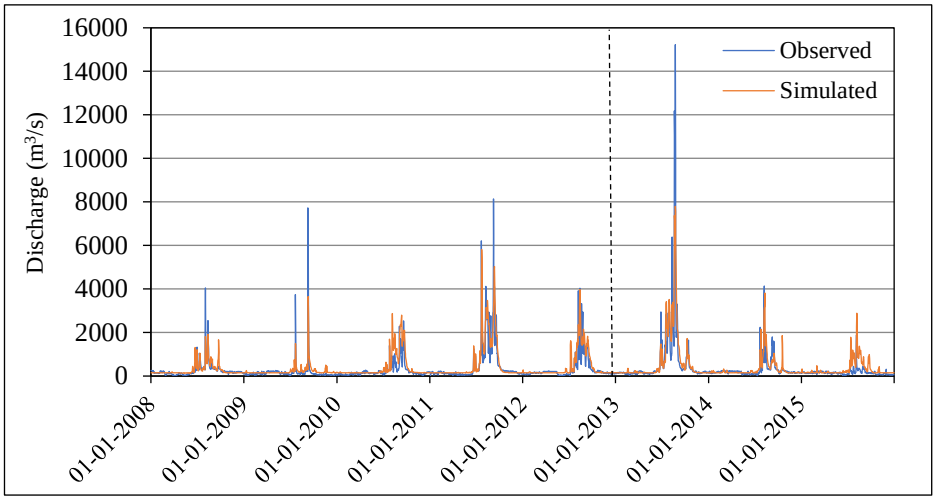

Figure 5.66: Comparison of daily observed and simulated stream flow during calibration and validation for R. Narmada at Barmanghat

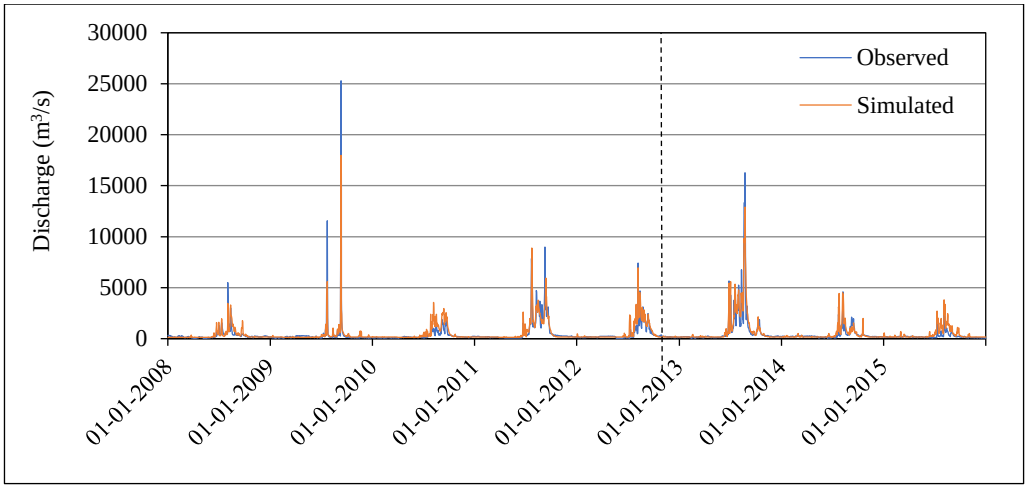

Figure 5.67: Comparison of daily observed and simulated stream flow during calibration and validation for R. Narmada at Sandia

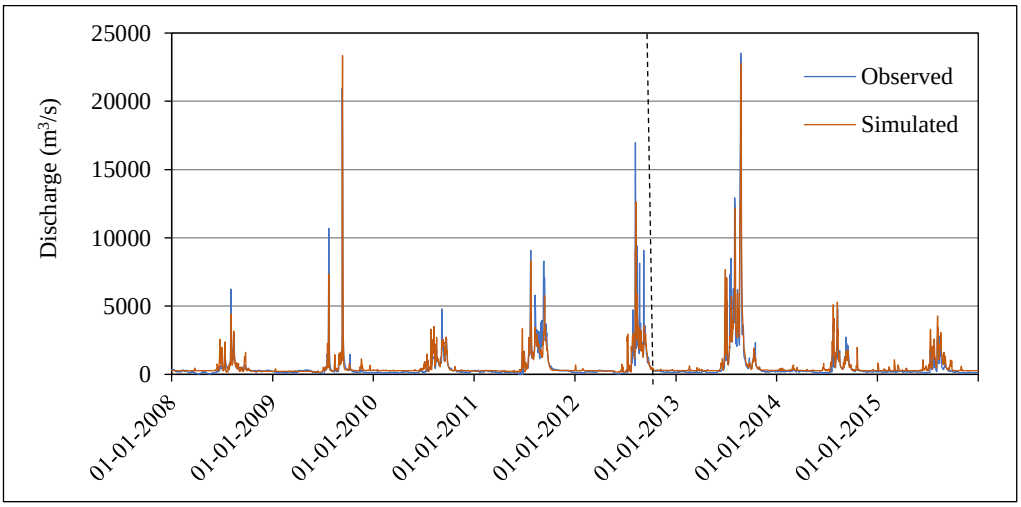

Figure 5.68: Comparison of daily observed and simulated stream flow during calibration and validation for R. Narmada at Hoshangabad

The performance evaluation of the VIC model for the daily stream simulation shows that model is capable of simulating the flows in headwater catchments as well as the main river catchments with good degree of accuracy. In the headwater catchments the model efficiency (NSE) during daily calibration varied between 0.53 at Belkheri and 0.68 at Patan. The difference in volume between computed and observed discharge varied between –4.05% at Patan to +16.60% at Manot. Similarly, during validation in headwater catchments, the NSE varied between 0.57 at Belkheri and Manot and 0.82 at Patan. Even though the NSE at Belkheri was 0.53 during calibration, it marginally improved to 0.57 during the validation period. The performance of the model for monthly streamflow

simulation is far better both during calibration and validation. Therefore, the performance of VIC model for simulation of river flows in the headwater catchments is reasonably good.

The performance of VIC model at the main river catchments is good considering the incorporation of few major dams. The streamflow for Narmada at Barmanghat has the influence of Bargi dam, which is a major reservoir and has releases from spillway during floods and also the flows from the river bed powerhouse. The NSE at Barmanghat is 0.65 during calibration and 0.74 validation. The streamflow for Narmada at Hoshangabad has the influence of three major dams viz, Bargi dam, Tawa dam and Barna dam along with the contribution of the tributaries later on. The performance of VIC model at Hoshangabad is reasonably good with NSE of 0.77 during calibration and 0.86 during validation whereas the difference in volume between the observed and computed flow is limited to -8.22% during calibration and -24.19% during validation. Therefore, the performance of VIC model for simulation of river flows in the main river catchments is reasonably good as well.

5.8 Hydrological Modelling using HEC-HMS

HEC-GeoHMS has been used to extract all the data necessary for the creation of HEC-HMS model for the study area. The ArcHydro tool available in ArcGIS has been used for data pre-processing to make the data ready for further use in HEC-GeoHMS. The sub-basins of UNB for the HEC-HMS model setup is given in Figure 5.69. Once the model has been created and imported in HEC-HMS environment, the rain gauges have been assigned to the respective sub- basins. The Thiessen Polygon method has been used for computation of the areal rainfall. The soil type and land use / land cover (LULC) data have been assigned to understand the response of model with ‘Curve Number (CN) method’ initially, to get an idea about flow simulation. The results obtained by CN method showed that the incorporation of a more complex method, which includes properties and contribution of deep aquifer systems, may improve the simulation results considerably. Therefore, the ‘Soil Moisture method’ has been adopted for flow simulation in UNB.

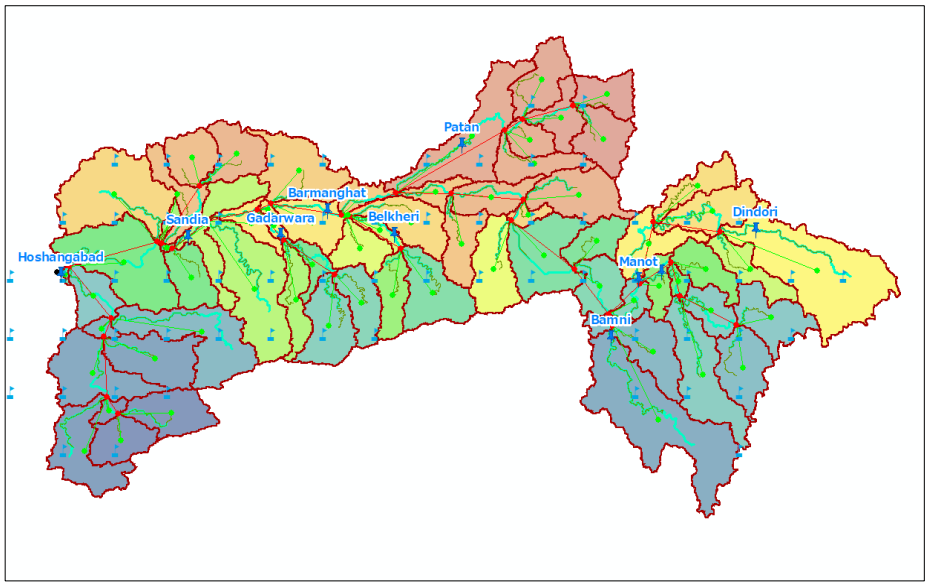

Figure 5.69: HEC-HMS setup of Upper Narmada basin

The 'Soil Moisture Accounting' (SMA) method has been used as the loss model for flow simulation in UNB model. The loss models basically compute the catchment runoff from rainfall by subtracting losses such as interception, infiltration, evaporation, transpiration and surface storage etc. for each time step. The 'transformation model' is used for calculating direct runoff at the outlet of watershed area due to the excess rainfall falling over it. The principle of unit hydrograph has been used for the transformation of excess rainfall to direct runoff for the UNB model.

Baseflow methods accounts for the subsurface flow in model. Generally short rainfalls do not contribute much from baseflow, and thus can be ignored. Baseflow is the sum of interflow and flow from the groundwater aquifer. In case of a long rainfall event, the baseflow contributes to the recession limb of hydrograph and has a significant contribution in flood volume, Cunderlik and Simonovik, 2004. There exist five 'baseflow models' in HEC- HMS and the 'Linear Reservoir' baseflow method has been adopted for UNB model.

For development of basin model for UNB, the 'Soil Moisture Accounting (SMA) loss method', 'SCS Unit Hydrograph Transformation method', and 'Linear Reservoir baseflow method' have been utilized for continuous simulation of daily runoff. The soil moisture accounting loss method uses five layers to represent the dynamics of water movement, both above and within the soil matrix. The layers

include canopy interception, surface depression storage, soil, upper groundwater zone, and lower groundwater zone. The soil layer is subdivided into tension storage zone and gravity storage zone (Scharffenberg et al, 2006. HEC-HMS Reference Manual, 2000).

The lag time parameter has been defined in the SCS Unit Hydrograph transformation used for the development of the translation hydrograph. The Linear Reservoir baseflow method uses a linear reservoir to model the recession of baseflow after a storm event by conserving the mass within the sub-basin. The inflow to the linear reservoir is taken as the infiltration which has been computed by the loss method. The infiltration is also connected to the lateral outflow of the groundwater layers. The 'initial discharge method' has been selected for specifying the initial baseflow condition. The 'ratio to peak' method was selected after several trials for determining the baseflow during a storm event for the UNB model.

The 'Muskingum routing method' has been used for flow routing, which uses a simple conservation of mass approach to route flow through the stream reach. The Muskingum K is essentially the travel time through the reach and is the weighting between inflow and outflow influence which can be estimated from the cross-sectional properties and flow properties. The K and X values for reaches are obtained by iteration method. The values of K and X derived based on the iteration have been found to be satisfactory with respect to the temporal distribution of peaks and the quantities of flow.

The model runs have been performed after incorporating the appropriate model properties and reservoir. The model has been developed for nine different subbasins based on the available gauging sites up to Hoshangabad. The calibration has been carried out during 2008 to 2012 and thereafter it has been validated during 2013 to 2015. The model performance was analyzed based upon NSE, RSR and PBIAS. Sensitivity analysis performed for this study showed groundwater coefficient, groundwater percolation, groundwater storage, and percentage imperviousness as the sensitive parameters. The performance evaluation indicators of the model during the calibration at the various gauging sites is given in Table 5.19. The performance indicators of the HEC-HMS model simulation during the validation period is given in Table 5.20. The performance of the model during

calibration at these gauging sites varied between satisfactory and good.

Table 5.19: HEC-HMS performance for daily runoff simulation during calibration

S. No.	Gauging site	NSE	PBias (%)
1.	Manot	0.67	3.00
2.	Mohgaon	0.53	7.45
3.	Belkheri	0.52	18.31
4.	Patan	0.67	-0.99
5.	Gadarwara	0.69	13.49
6.	Barmanghat	0.45	18.16
7.	Sandia	0.59	6.59
8.	Hoshangabad	0.65	0.36

Table 5.20: HEC-HMS performance for daily runoff simulation during validation

S. No.	Gauging Site	NSE	PBias (%)
1.	Manot	0.56	12.20
2.	Mohgaon	0.54	13.23
3.	Belkheri	0.69	-0.80
4.	Patan	0.63	-7.50
5.	Gadarwara	0.56	28.83
6.	Barman Ghat	0.45	14.50
7.	Sandia	0.57	8.05
8.	Hoshangabad	0.60	4.77

During the daily runoff simulation at Manot, the HEC-HMS model was able to achieve the NSE of 0.67 during calibration and 0.56 during validation and PBias was +3.00% during calibration and +12.20% during validation. The comparison of the observed and simulated daily runoff at Manot during calibration and validation is given in Figure 5.70 and Figure 5.71 respectively.

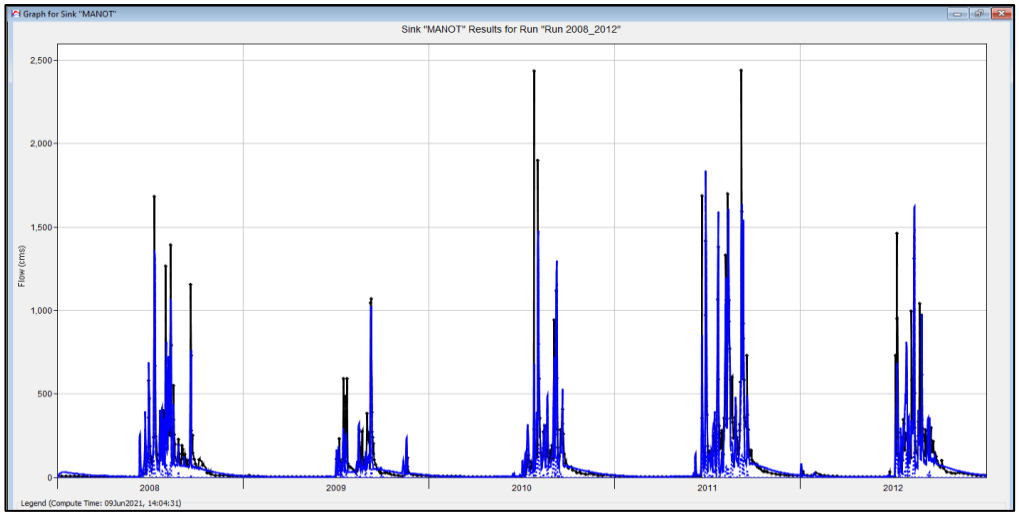

Figure 5.70: Comparison of observed and simulated flows during calibration at Manot

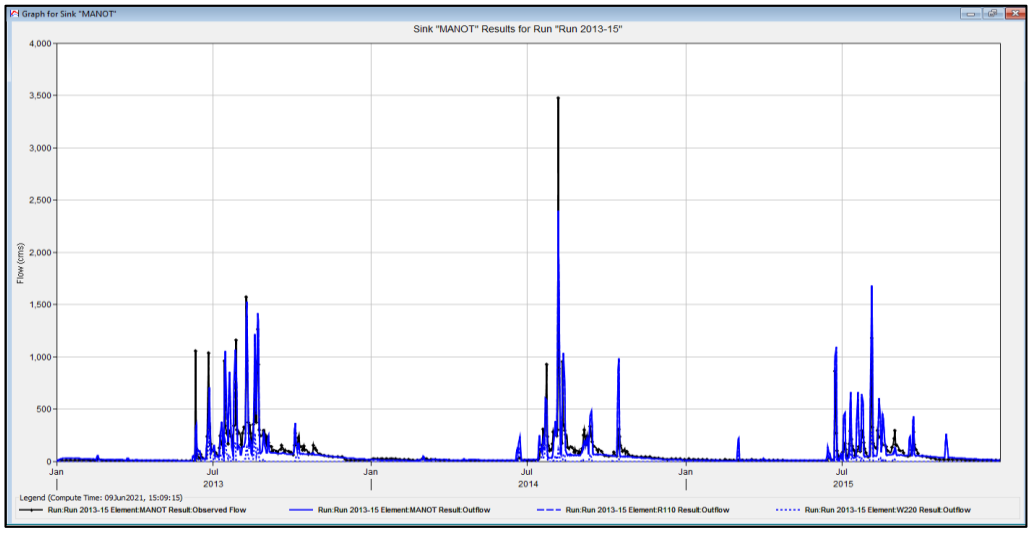

Figure 5.71: Comparison of observed and simulated flows during validation at Manot

During the daily runoff simulation at Mohgaon, the HEC-HMS model was able to achieve the NSE of 0.53 during calibration and 0.54 during validation and PBias was +7.45% during calibration and +13.23% during validation. The comparison of the observed and simulated daily runoff at Mohgaon during calibration and validation is given in Figure 5.72 and Figure 5.73 respectively. During the daily runoff simulation at Belkheri, the HEC-HMS model was able to achieve the NSE of 0.52 during calibration and 0.69 during validation and PBias was +18.31% during calibration and -0.80% during validation. The comparison of the observed and simulated daily runoff at Belkheri during calibration and validation is given in Figure 5.74 and Figure 5.75 respectively.

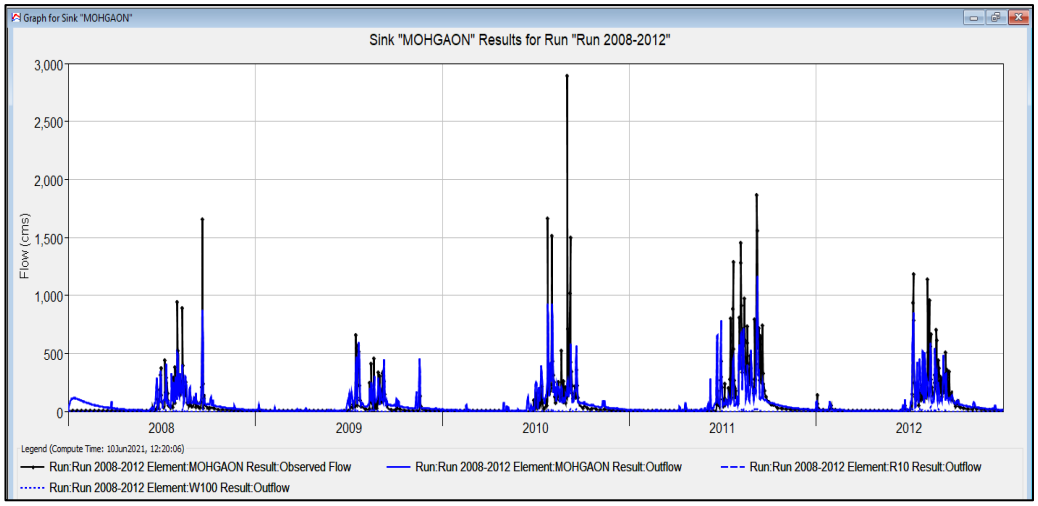

Figure 5.72: Comparison of observed and simulated flows during calibration at Mohgaon

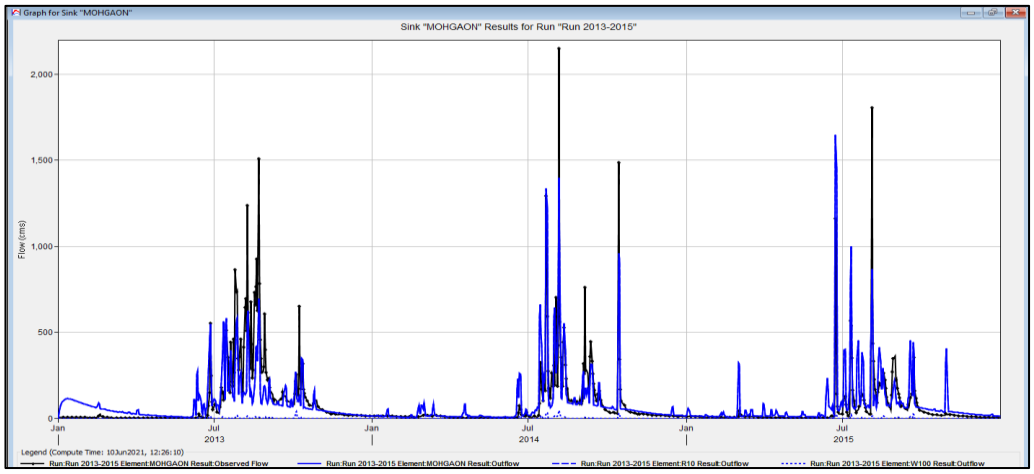

Figure 5.73: Comparison of observed and simulated flows during validation at Mohgaon

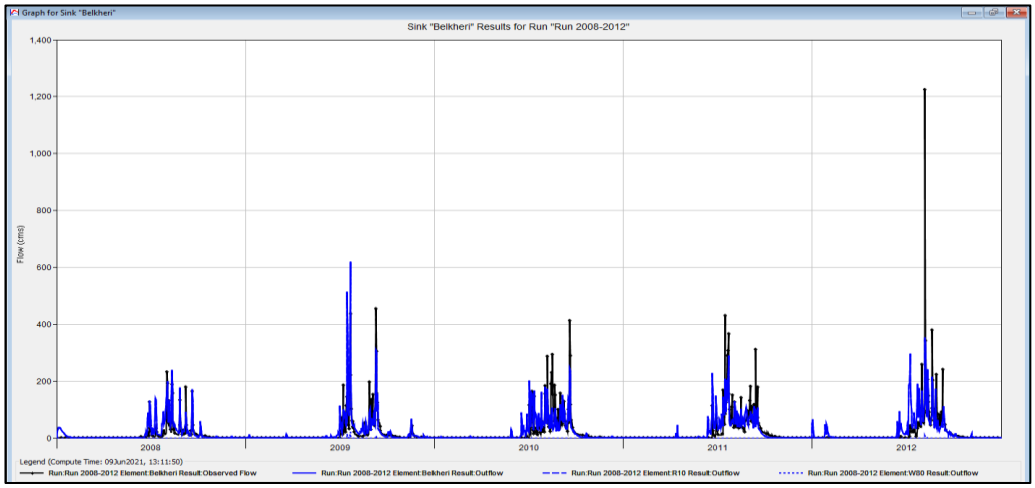

Figure 5.74: Comparison of observed and simulated flows during calibration at Belkheri

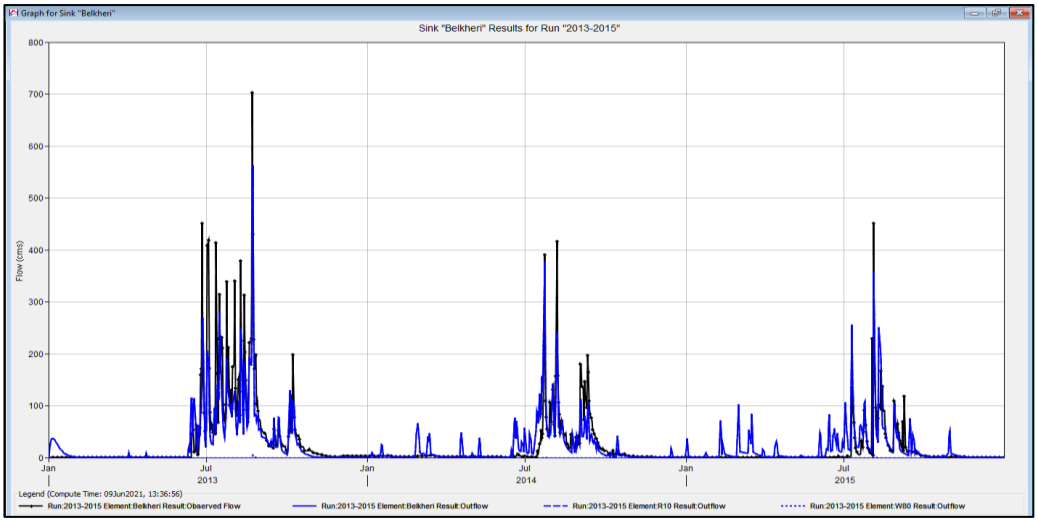

Figure 5.75: Comparison of observed and simulated flows during validation at Belkheri

During the daily runoff simulation at Patan, the HEC-HMS model was able to achieve the NSE of 0.67 during calibration and 0.63 during validation and PBias was -0.99% during calibration and -7.50% during validation. The comparison of the observed and simulated daily runoff at Patan during calibration and validation is given in Figure 5.76 and Figure 5.77.

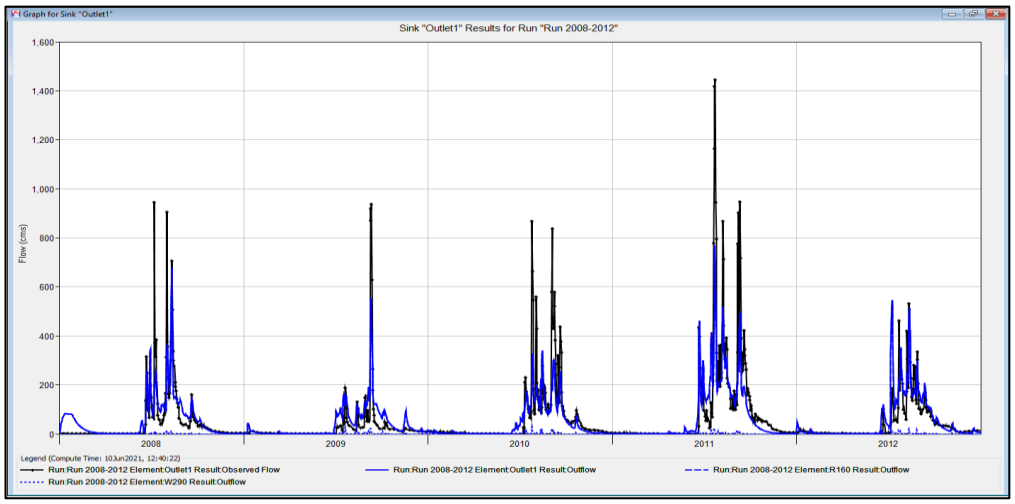

Figure 5.76: Comparison of observed and simulated flows during calibration at Patan

During the daily runoff simulation at Gadarwara, the HEC-HMS model was able to achieve the NSE of 0.69 during calibration and 0.56 during validation and PBias was +13.49% during calibration and +28.83% during validation. The comparison of the observed and simulated daily runoff at Gadarwara during calibration and validation is given in Figure 5.78 and Figure 5.79.

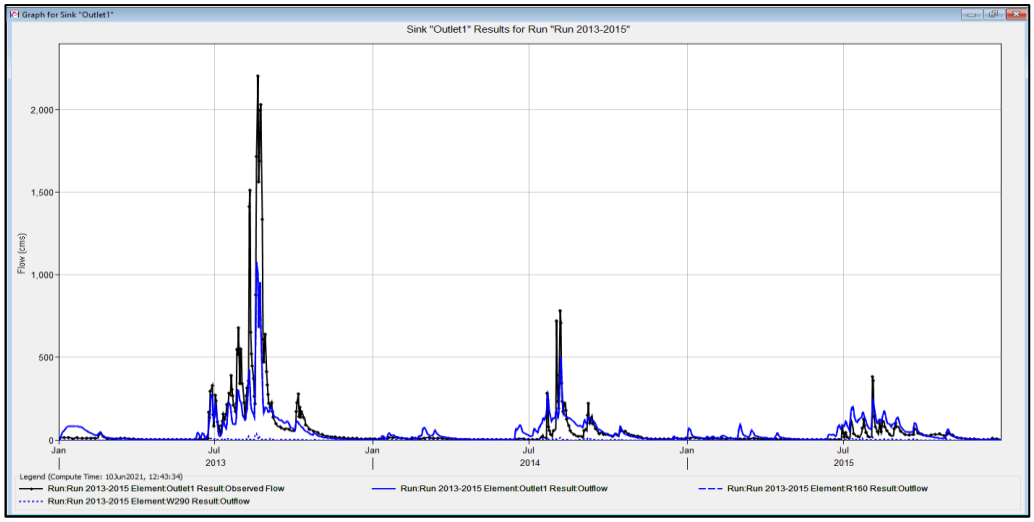

Figure 5.77: Comparison of observed and simulated flows during validation at Patan

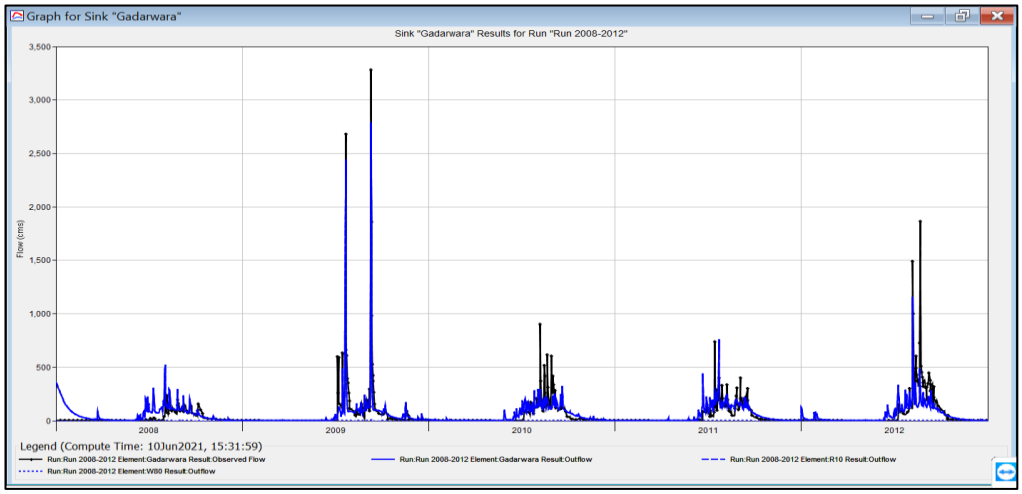

Figure 5.78: Comparison of observed and simulated flows during calibration at Gadarwara

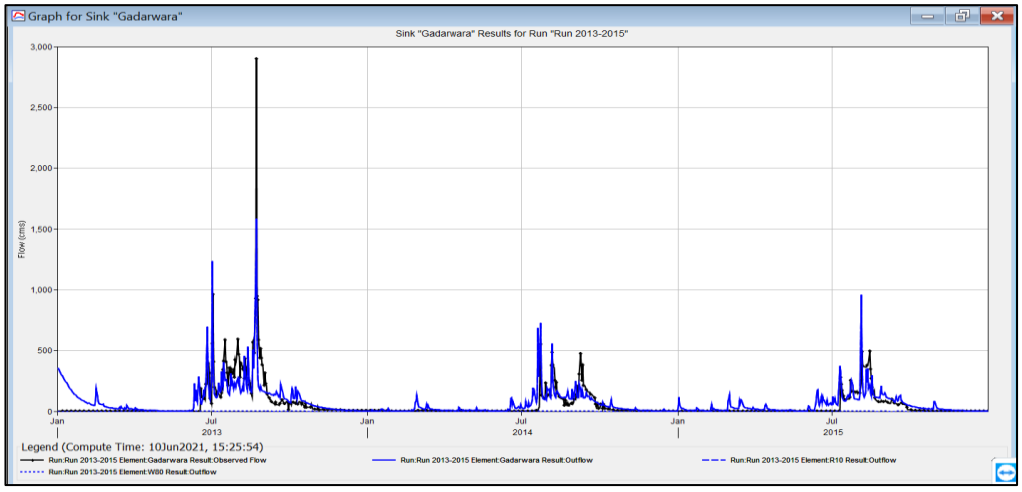

Figure 5.79: Comparison of observed and simulated flows during validation at Gadarwara

During the daily runoff simulation at Barmanghat, the HEC-HMS model was able to achieve the NSE of 0.45 during calibration and 0.45 during validation and PBias was +18.16% during calibration and +14.50% during validation. The comparison of the observed and simulated daily runoff at Barmanghat during calibration and validation is given in Figure 5.80 and Figure 5.81.

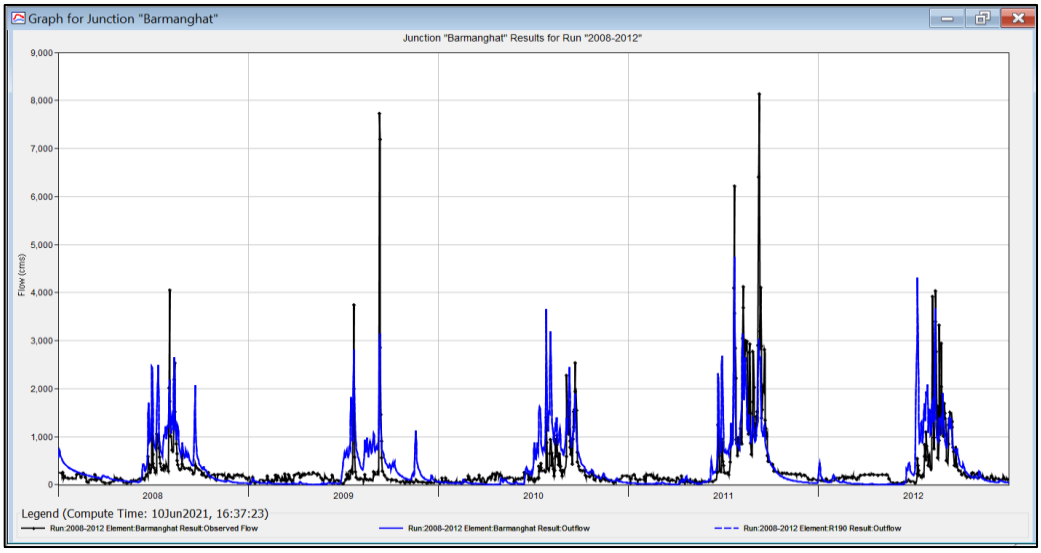

Figure 5.80: Comparison of observed and simulated flows during calibration at Barmanghat

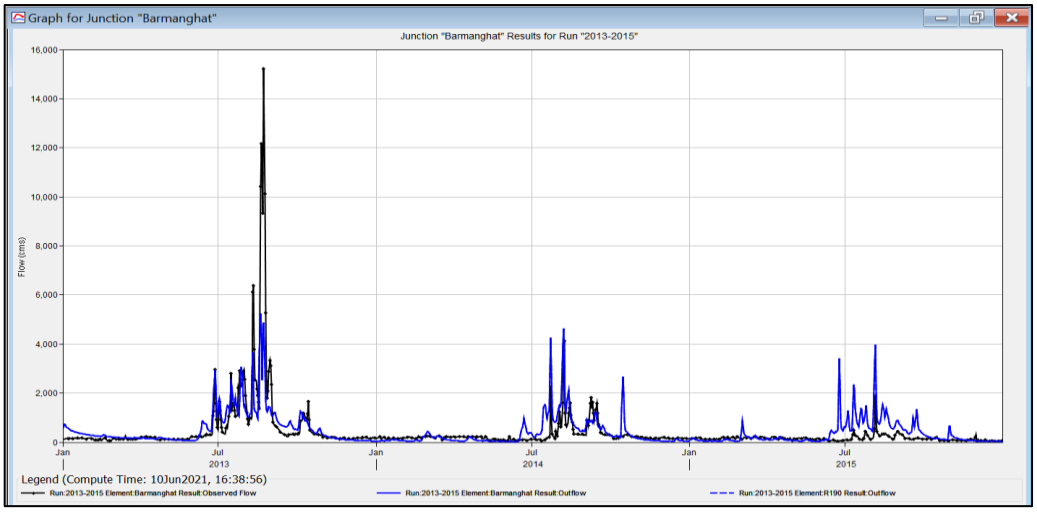

Figure 5.81: Comparison of observed and simulated flows during validation at Barmanghat

During the daily runoff simulation at Sandia, the HEC-HMS model was able to achieve the NSE of 0.59 during calibration and 0.57 during validation and PBias was +6.59% during calibration and +8.05% during validation. The comparison of

the observed and simulated daily runoff at Sandia during calibration and validation is given in Figure 5.82 and Figure 5.83.

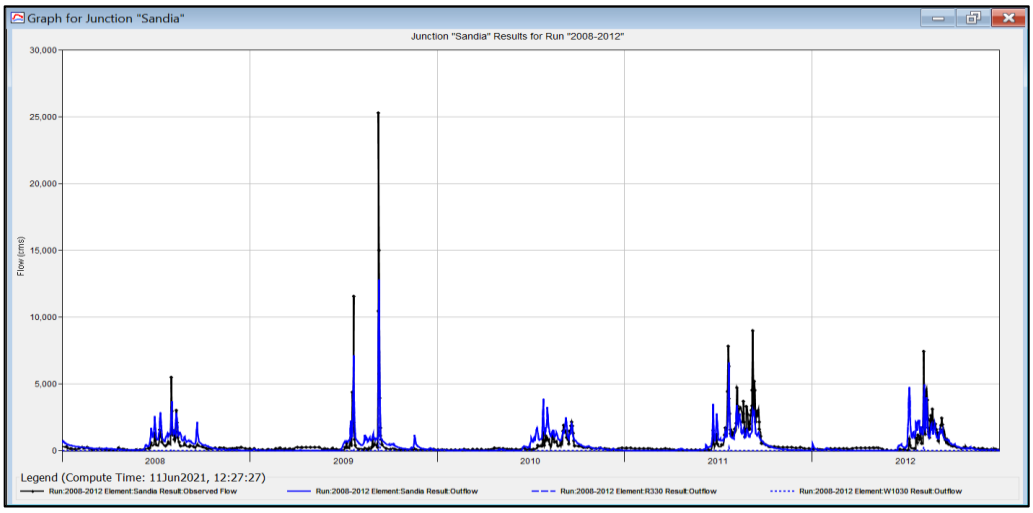

Figure 5.82: Comparison of observed and simulated flows during calibration at Sandia

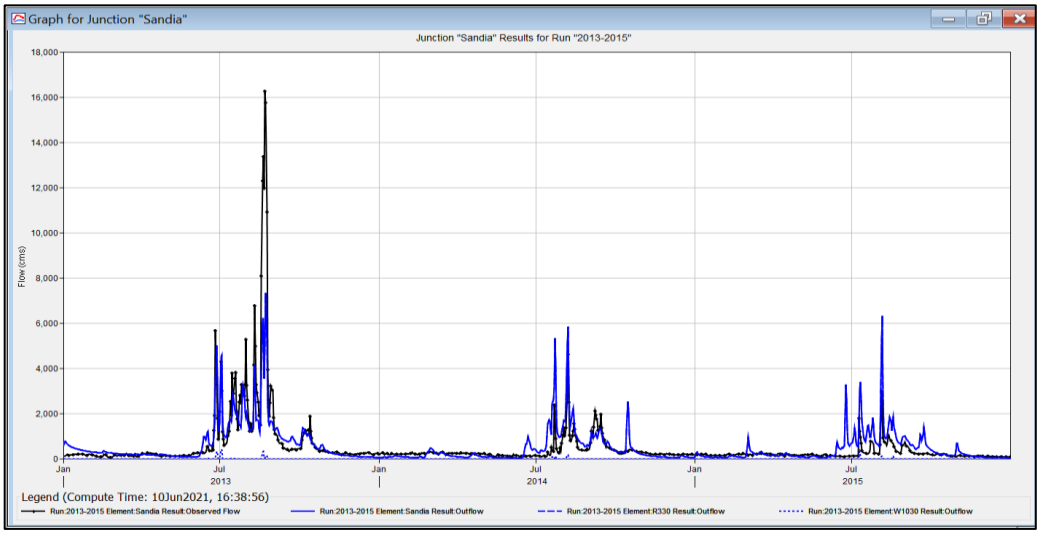

Figure 5.83: Comparison of observed and simulated flows during validation at Sandia

During the daily runoff simulation at Hoshangabad, the HEC-HMS model was able to achieve the NSE of 0.65 during calibration and 0.60 during validation and PBias was +0.36% during calibration and +4.77% during validation. The comparison of the observed and simulated daily runoff at Hoshangabad during calibration and validation is given in Figure 5.84 and Figure 5.85.

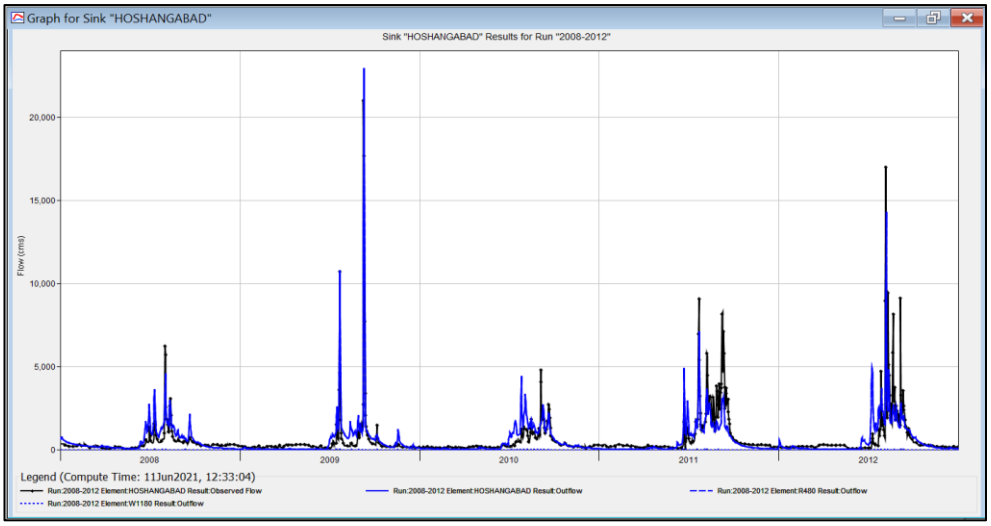

Figure 5.84: Comparison of observed and simulated flows during calibration at Hoshangabad

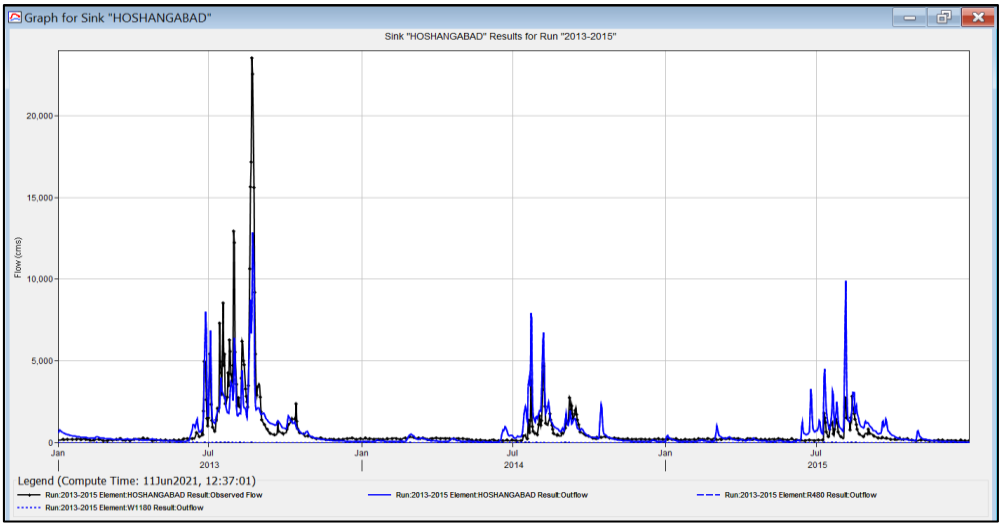

Figure 5.85: Comparison of observed and simulated flows during validation at Hoshangabad

The performance evaluation of the HEC-HMS model for the daily stream simulation shows that model is capable of simulating the flows in headwater catchments as well as the main river catchments with good degree of accuracy. In the headwater catchments the model efficiency (NSE) during calibration varied between 0.52 and 0.53 at Belkheri and Mohgaon, 0.67 at Manot and Patan and 0.69 at Gadarwara. The difference in volume varied between -0.99% at Patan to +18.31% at Belkheri. Similarly, during validation in headwater catchments, the NSE varied between 0.54 at Mohgaon to 0.69 at Belkheri. Even though the NSE at Belkheri was 0.53 during calibration, it considerably improved to 0.69 during the

validation period. As such, the performance of HEC-HMS in simulation of daily river flows in the headwater catchments is reasonably good.

The performance of HEC-HMS at the main river catchments is good considering the incorporation of few major dams. The streamflow for Narmada at Barmanghat has the influence of Bargi dam, which is a major reservoir and has releases from spillway during floods and also the flows from the river bed powerhouse. The NSE is lowest at Barmanghat (0.45) during both calibration and validation. The streamflow for Narmada at Hoshangabad has the influence of three major dams viz, Bargi dam, Tawa dam and Barna dam along with the contribution of the tributaries later on. The performance of HEC-HMS at Hoshangabad is reasonably good with NSE of 0.65 during calibration and 0.60 during validation whereas the difference in volume is limited to +0.36% during calibration and +4.77% during validation.

Based on the application of various hydrological models for runoff simulation, it is rather difficult to suggest one particular model best suited for the study area, as each model has its own set of capabilities and limitations. The major advantage of SWAT model includes, a) it is available freely in public domain and can be used with ArcGIS of QGIS software, b) considerable effort has been put for making the SWAT datasets freely available in the public domain, c) both of these factors have led to the extensive application of the model by the researchers and well as decision makers for water resources management, d) used extensively for impact assessment of climate change and land use change or changes in water resources management, e) has the capability to incorporate reservoirs and ponds, f) irrigation and management practices being carried out in the watershed can be included, g) various sources of water can be assigned to meet demands in each subbasin, depending on whether it falls in the canal command or else irrigation demands are met from shallow or deeper aquifers, h) continuous model development is underway and SWAT has been linked with MODFLOW, grid-based SWAT etc. are available but for a price, i) SWAT-CUP software is available to carry out the sensitivity analysis, calibration and uncertainty analysis, j) back-end support from the developers and SWAT user-groups helps to address the model setup and run issues in a timely manner.

The major disadvantages of SWAT model includes, a) requires extensive data to model the runoff, sediments, and water quality of river basins to generate accurate results, which may be generally available or accessible in many regions, b) observed data on rainfall, climatic variables, runoff, sediment, watershed interventions, irrigation management practices and water quality, c) also requires high resolution DEM, LULC and soil datasets in digital format, which is used by the model to delineate the watershed, subbasins and HRUs and assign model parameters, d) large number of parameters viz, 14 flow parameters and 9 sediment parameters need to assigned realistic parameter values within the prescribed parameter ranges, e) understanding the physical meaning and importance of each parameter and its contribution to the variable being simulated is of utmost concern to obtain meaningful results, f) very good model for studying the overall water availability in river basins but performance of the model in simulating the peak events is just satisfactory, g) model performance deteriorates as the modelling efforts progress from runoff to sediment and lastly to water quality.

The major advantages of VIC model include, a) source code is freely available in public domain, b) VIC can be run at various time intervals, c) sub-grid heterogeneity is represented statistically, d) open-source status allows user to modify the source code as per project requirements, e) availability of tools and scripts to manipulate model data in multiple ways, f) reservoirs can be added and modelled through a separate routine, g) availability of global data sets for model inputs and parameters, h) good user-group and detailed user-manuals, i) model can perform studies on continental scale and j) climate change and land cover change impact assessments can be carried out.

The major disadvantages of VIC model includes, a) it is not supported for Microsoft Windows operating system, b) cannot process geospatial data, c) each grid cell is treated independently except for routing, d) water can only enter a grid cell via the atmosphere, e) non-channel flow between grid cells is ignored, f) once water reaches the channel network, it is assumed to stay in the channel (it cannot flow back into the soil), g) grid cells are simulated independently of each other, h) routing of stream flow is performed separately from the land surface simulation

using a separate model, and i) not much applicable for small watersheds as it is intended for large regions.

The advantages of WEAP model includes, a) limited number of soil and land use-related parameters (seven), b) it is adaptable to whatever data is available to describe the water resources system, whether daily, weekly, monthly, or annual time-steps, c) it is user-friendly windows based application, d) simulation time is very less for policy making and scenario development, e) can assess the water supply-demand scenario, f) model can be used for multiple scenarios of water demand, supply, runoff, stream flows, storage, pollution generation, treatment and discharge and instream water quality, g) can be linked to groundwater model, h) can be linked to energy models, i) can be used for water quality modelling and ecosystem preservation, j) reservoirs can be incorporated in the model and k) model available freely for research with temporary license for one year, l) model can be used for climate change and land use change impact assessments. The disadvantages of WEAP model includes, a) model is not applicable for detailed design, b) data has to be imported into the model, c) source code is not available, d) cannot model reservoir water quality, and e) cannot account for stream attenuation.

The advantages of HEC-HMS model includes, a) HEC-GeoHMS can process geospatial data in ArcGIS, b) calibration is performed using an optimization algorithm, c) compatible with other HEC-programs due to common data storage system, d) allows for discharge output values as well as all internal state variables at user defined grid locations, e) widely used across the world, f) detailed technical report and user's manual is available and g) applicable for flood studies, reservoir spillway design, streamflow forecasting, urban drainage, future urbanization impacts, water quality, erosion and sediment transport. The disadvantages of HEC-HMS model include, a) cannot model branching or looping stream networks, b) cannot model backwater in the stream network, c) supplemental tool HEC-GeoHMS requires ArcGIS with the Spatial Analyst extension, d) source code is not publicly available, and e) usually selected for event-based modelling like simulating flood hydrographs or in the design of flood estimation.

MIKE 11-NAM is a lumped conceptual model with continuous accounting of moisture content in sub-surface zones, which simulates the rainfall-runoff process and has nine model parameters. The advantages of the MIKE 11-NAM model include, a) model is simple to use with limited data requirement, b) used for inflow forecasting to rivers and reservoirs, c) runoff impact assessments for land use changes, d) climate change scenario analysis and e) long-term water resources analysis and planning, e) model outputs can be used for hydrodynamic modelling in HEC-RAS. The disadvantages of MIKE 11-NAM includes, a) it can be used as a planning tool, b) can only be used in unregulated river basins or in headwater catchments of major river systems, c) reservoirs cannot be incorporated, d) licensed software and e) not available in public domain.

As far as the applicability of these models in Upper Narmada basin, the SWAT and VIC models are sophisticated process based hydrologic models and able to model the runoff reasonably well along with other important water balance components. The calibration and validation results of both these models as comparable even though SWAT is based on the concept of HRUs whereas VIC is grid-based model. Both models can be effectively used for climate change impact assessments and also to assess the impacts of developmental activities on the basin hydrology. But the major difference between both models lies in the fact that VIC model is generally designed for large scale river basins with large grid sizes whereas the SWAT model can be used for a very small watershed or even at field level and even for very large river basins with equally good performance. Looking into the easy availability of the spatial datasets for Indian river basins, SWAT model can be applied with ease and lesser expertise as compared to VIC model.

As the Narmada River basin is a highly regulated river basin with many major and medium dams, MIKE 11-NAM has its limitations due to the absence of adding dams in the model and can therefore be used to simulate the runoff only in tributaries of headwater catchments. The performance of the HEC-HMS model is satisfactory in Upper Narmada basin and the model is quite versatile as there are many options available to model each component of the basin hydrology. The water infrastructure can be incorporated along with the gate operations for the better representation of the actual hydrology during the runoff generation. The major

advantage of the HEC-HMS model is that the model outputs can be used for flood studies using hydrodynamic models for which HEC-RAS can be used along with HEC-HMS. The event-based modelling can be carried out in HEC-HMS for flood studies and linked with reservoir operation models for flood control operation of major reservoirs.

Even though WEAP model is a simple and easy to use model available in public domain, its performance in Upper Narmada basin has been found to be satisfactory for the daily and monthly runoff simulations. The model apart from being used for climate change impact assessment in the study area was also used for the changes in the supply demand scenario in future and the possibility of unmet demands and measures needed to be adopted to minimise the unmet demands in future. The WEAP model can be linked to groundwater models and energy models in future to assess the changes in the groundwater availability and energy demands in future under the projected climate change scenarios. Therefore, the applicability of the model greatly depends on the objective of the study, availability of datasets, free availability of the model, and the size of the river basin and desired accuracy in modelling.

5.9 Groundwater Modelling using Visual MODFLOW Flex

The groundwater flow modelling has been carried out for Narsinghpur district located in Upper Narmada basin using Visual MODFLOW Flex. In this district there has been a major shift in the cropping pattern with drastic changes in the crop water demands for irrigating the recently introduced water intensive crops. There has been a multi-fold increase in the area under wheat and sugarcane with corresponding decrease in the area under chick pea. The cultivation of sugarcane and wheat is expanding rapidly with increase in wheat cultivation by more than 100% since 2005 and increase in sugarcane cultivation by more than double. The changes in the cropping pattern in Narsinghpur district is given in Figure 5.86. Since the crop water requirement at most of the blocks except Gotegaon is met through groundwater, there is a possibility of changes in the groundwater availability at present and in future also.

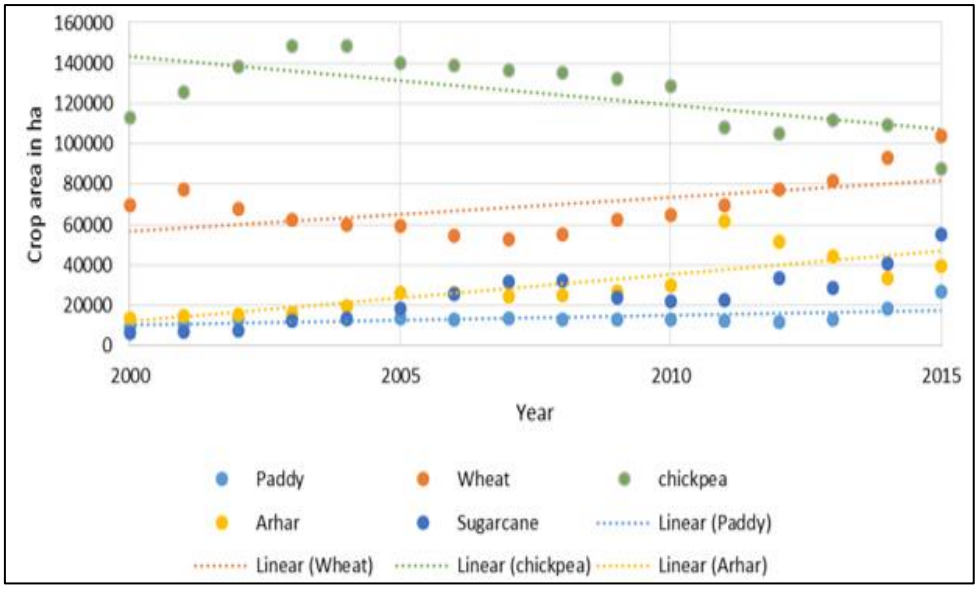

Figure 5.86: Changes in the cropping pattern in Narsinghpur district

The groundwater level data required for groundwater flow simulation in Narsinghpur district has been obtained from State Water Data Centre, Water Resources Department, Govt. of Madhya Pradesh. The groundwater level data spanning over a period of 16 years (2000 – 2016) at 100 observation wells and 16 piezometers have been used for the groundwater model calibration and validation. The location map of the observation wells and piezometers in Narsinghpur district is given in Figure 5.87 and Figure 5.88 respectively. The details of observation wells and piezometers located in the various blocks are given Table 5.21.

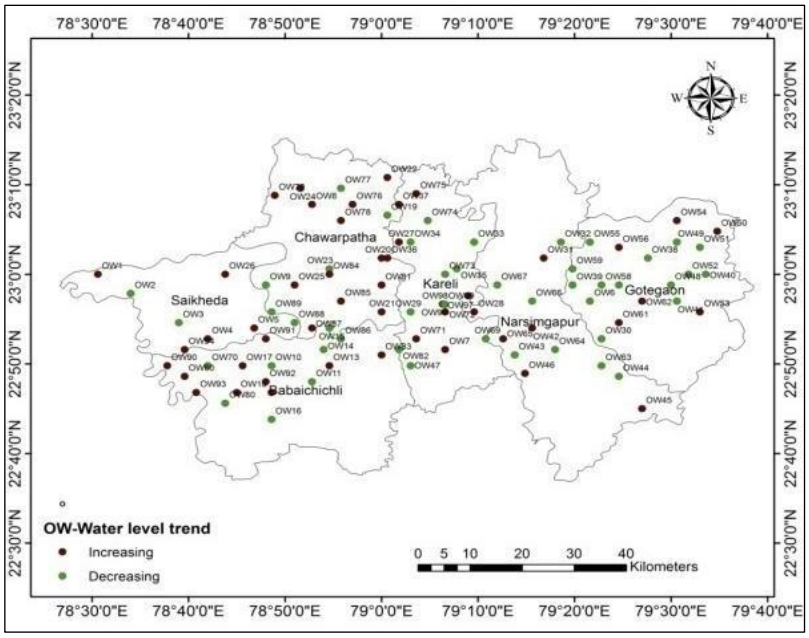

Figure 5.87: Observation wells in Narsinghpur district

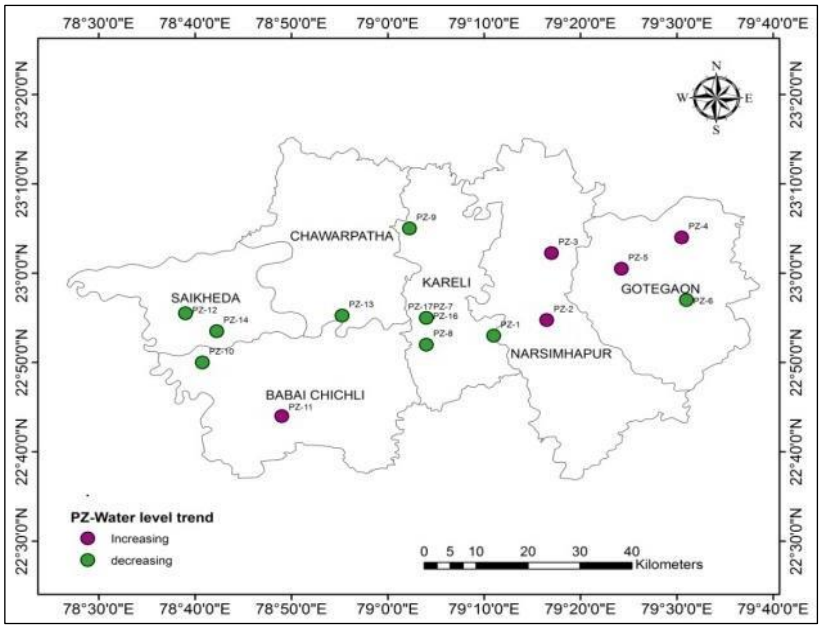

Figure 5.88: Piezometers in Narsinghpur district

The geology is one of the major factors which play an important role in the distribution and occurrence of groundwater. The porosity and permeability in aquifer rocks is based on the geology. Moreover, the rock type which gets exposed at the surface significantly affects the groundwater recharge. The

Table 5.21: Details of observation wells and piezometers Narsinghpur district

Block	Observation wells	Piezometers
Saikheda	OW1, OW2, OW26, OW3, OW4, OW5, OW94	PZ12, PZ 4
Chawarpatha	OW19, OW20, OW21, OW22, OW23, OW24, OW25, OW36, OW76, OW77, OW78, OW79, OW8, OW81, OW84, OW85, OW87, OW89, OW9	PZ13
Babaichichli	OW10, OW11, OW12, OW13, OW14, OW15, OW16, OW17, OW18, OW60, OW70, OW80, OW83, OW86, OW90, OW91, OW92, OW93	PZ10, PZ11
Kareli	OW100, OW27, O 29, OW33, OW34, OW35, OW37, OW47, OW7, OW71, OW72, OW73, OW74, OW75, OW95, OW96, OW97, OW98, OW99	PZ1, PZ16, PZ17, PZ7, PZ8, PZ9
Narsighpur	OW28, OW 30 OW, 31, OW 32, OW 42, OW 43, OW 44, OW45, OW46, OW63, OW64, OW65, OW66, OW67	PZ2, PZ3
Gotegaon	OW30, OW 38, OW 39, OW 40, OW 41, OW 48, OW 49, OW 50, OW51, OW52, OW53, OW54, OW55, OW56, OW57, OW58, OW59, OW6, OW61, OW62	PZ4, PZ5, PZ6

Narsinghpur district falls in alluvium, Deccan Trap basalts, Gondwana, Vindhyan Sandstone, Bijawars and Archeans as can be seen from the geological map of Narsinghpur district given in Figure 5.89.

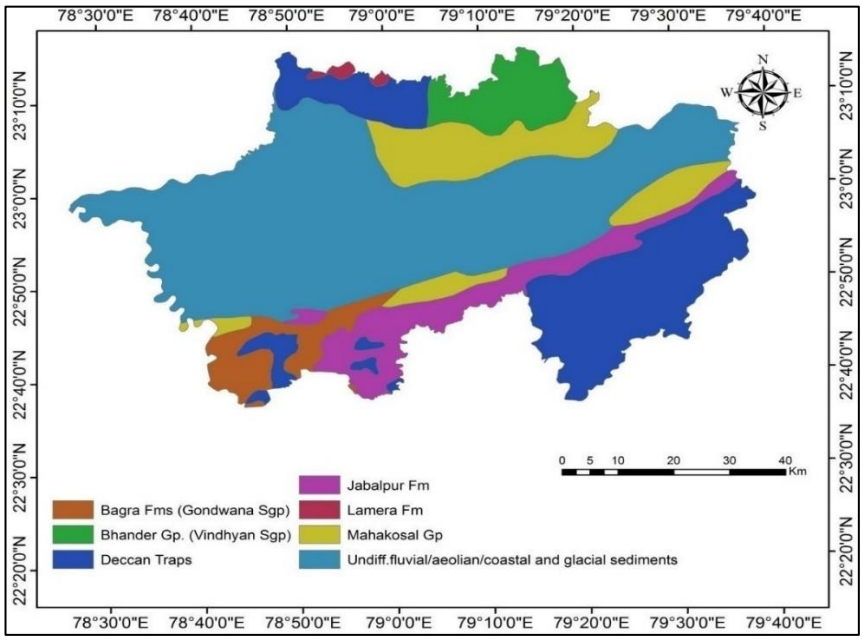

Figure 5.89: Geological map of Narsinghpur district

The geomorphology is another important factor from the groundwater point of view and it mainly depends on the structural evolution of geological formations. The Narsinghpur district is broadly divided into three sectors namely, a) Narmada valley alluvial plain, b) Satpura range in the southern parts, and c) Vindhyan range in the north. The geomorphological of Narsinghpur district is given in Figure 5.90. The alluvial plain of Narmada valley stretches from east to west throughout the district on the both sides of the Narmada River. The regional slope of the area is westward.

The initial stage in developing the groundwater flow model involves defining the region of interest and establishing appropriate boundary conditions as existing on ground. The Narmada River may become effluent and influent depending on the flows and surrounding groundwater conditions which has been simulated by the ‘River Package’. The assumptions made for conceptualization of the groundwater flow regime includes, no flow occurs across the catchment

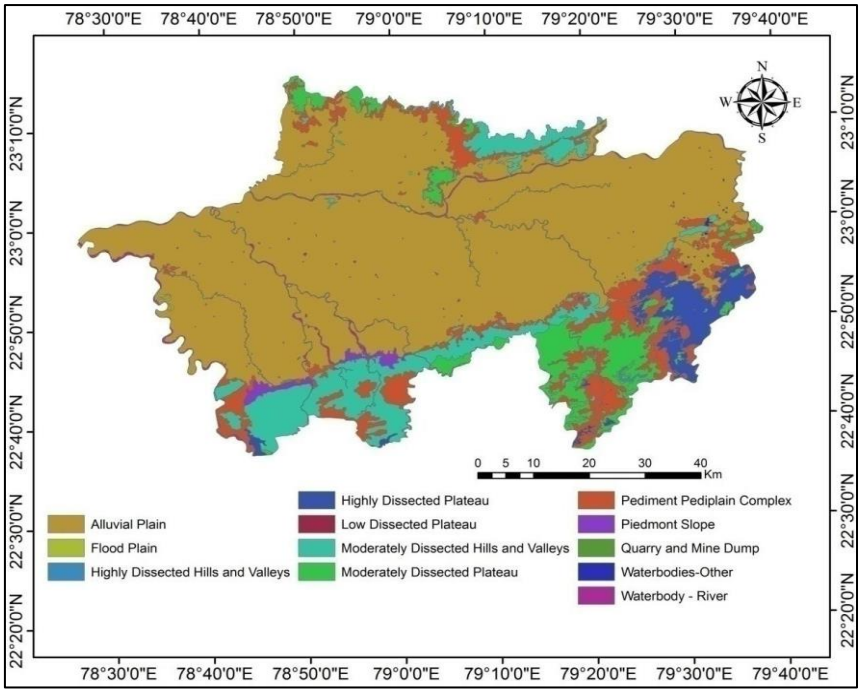

Figure 5.90: Geomorphological map Narsinghpur district

boundaries, as these boundaries are coinciding approximately with groundwater divide and there will be continuous leakage to the fracture zone from the overlying weathered zone, seepage from the surface water bodies and streams are additional input to the recharging system, and the delay in recharge to aquifer is inappreciable and the hydrogeological parameters do not change during the period for which the aquifer is being simulated.

The simulated model domain of study area is divided into a grids consisting of 79 rows and 128 columns which is two layered aquifer model, covering an area of 79000 m x 128000 m (Figure 5.91). The resulting mesh consists of square blocks of 1000 m x 1000 m. The grid is a finite difference block-centered grid, i.e., nodes are located at the center of the block. The water level data measured at 100 observation wells during May 2000 to June 2015 have been used to prepare the water level contours initially. The aquifer simulation was carried out by using Visual MODFLOW Flex software package. The objective of the mathematical modelling is to simulate the spatial and temporal variation in groundwater levels across the study area.

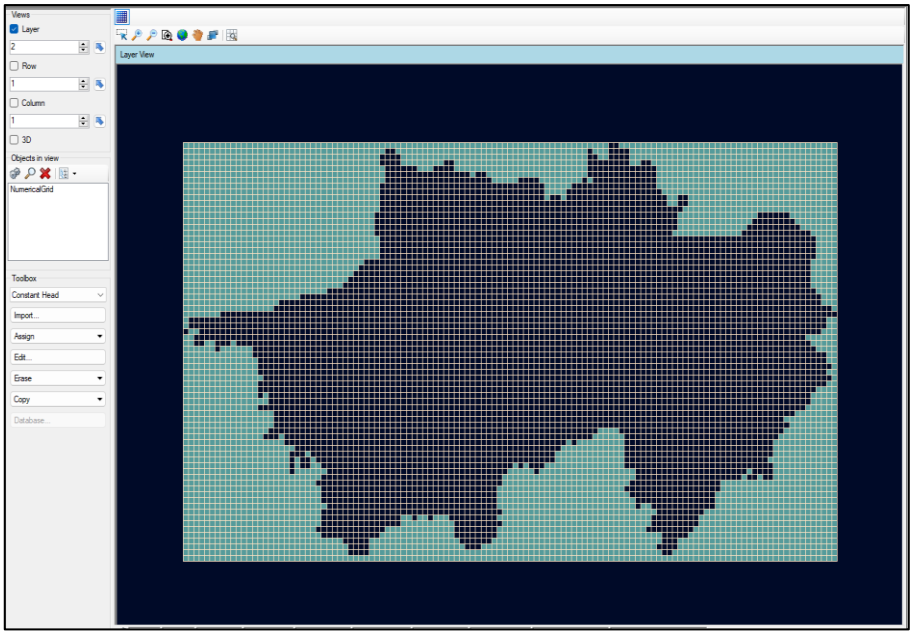

Figure 5.91: Grid map of Narsinghpur district

A two-layer model has been considered based on the analysis of lithological data of Narsinghpur district. The first layer mostly consists of 80 m alluvium zone and underlain by 80 to 190 m thick Gondwana formation with fracture zone as given in Figure 5.92. The simulated vertical section has a total thickness of about 190 m. The top layer is representing alluvium portion in the system which is typically designated as unconfined layer and the second layer is representing the Gondwana formation fracture zone and assumed as comprising of semi-confined to confined conditions with variable T and S. The hydraulic conductivity and specific yield are given as inputs to the model. MODFLOW calculates the transmissivity of the layer by multiplying the thickness of the aquifer with the hydraulic conductivity.

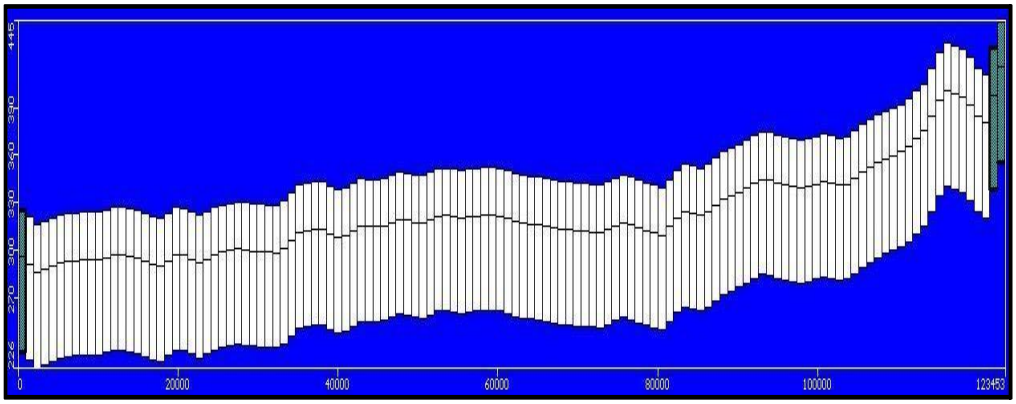

Figure 5.92: Vertical cross section of aquifer layer

The location of hydraulic heads given to the model based on the observed groundwater levels is given in Figure 5.93. The recharge to the groundwater regime due to monsoon rainfall, seepage from surface water bodies and irrigation return flow from fields contributes as inputs to the aquifer system. The outflow occurs mainly through groundwater withdrawal/draft from wells for irrigation.

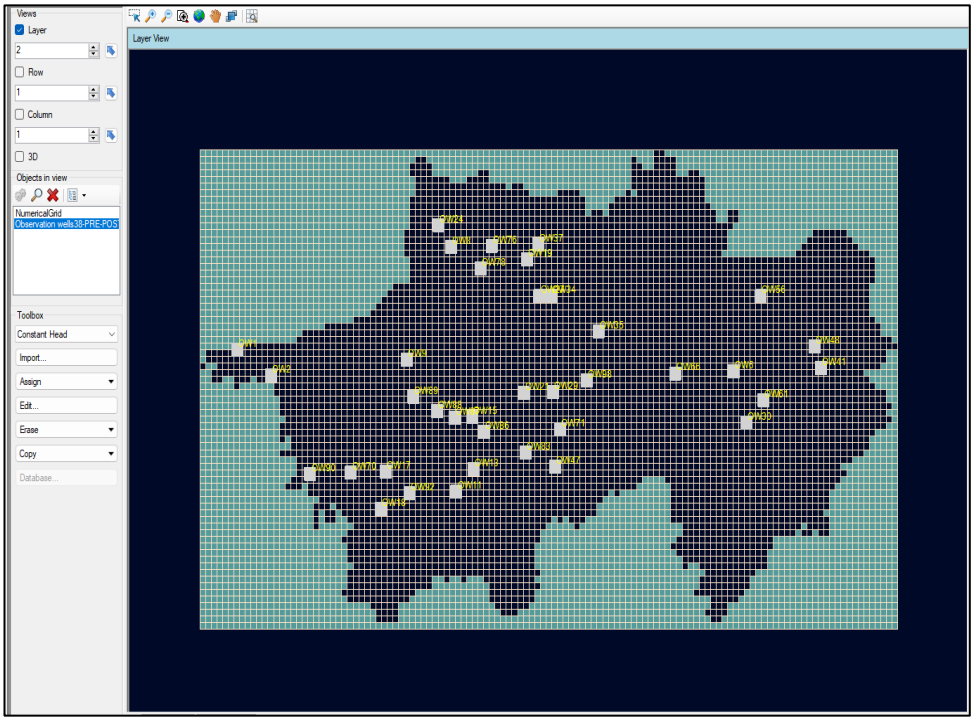

Figure 5.93: Location of hydraulic head input points

The initial conditions refer to the hydraulic head distribution everywhere in the groundwater system at the beginning of simulation and thus boundary conditions are finite. The zone wise initial head map is given in Figure 5.94. The rate of groundwater recharge is found to be higher in rainy season (June to September) which is the principal rainy months of the south-west monsoon season. Furthermore, the rates of groundwater recharge are also found to be dependent on the land use land cover type. The results of the analysis show that precipitation is the most important hydrologic process which is responsible for the groundwater recharge and other hydrological processes in the study area.

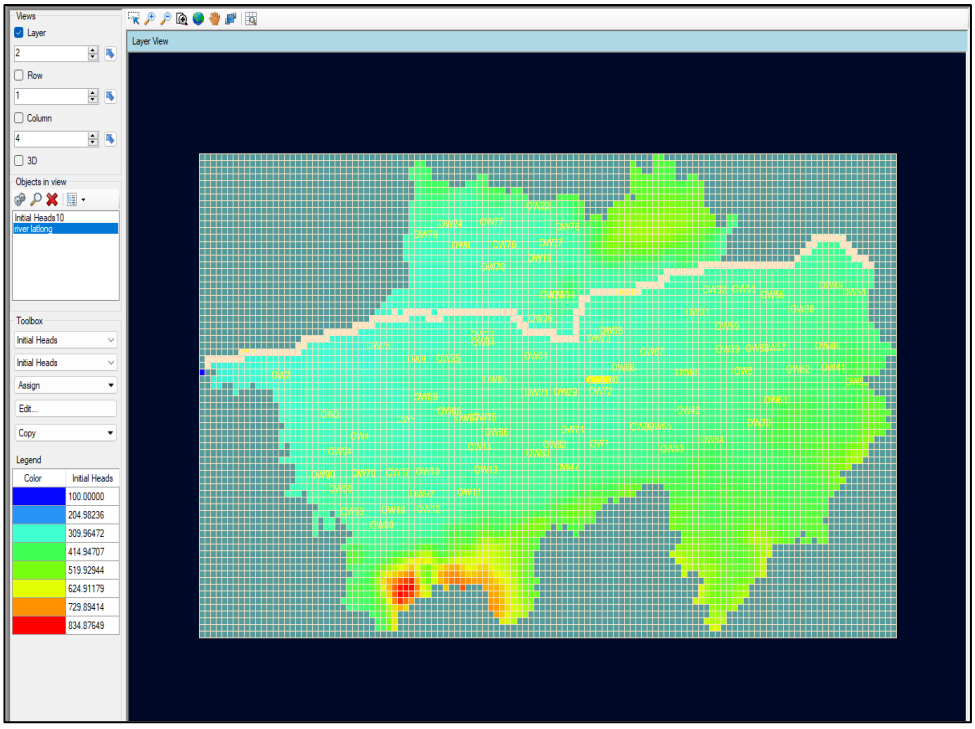

Figure 5.94: Initial head map

Also, the amount of infiltration depends on many factors such as vegetation cover, ground slope, soil type, water table depth, geology and hydrogeology etc. Recharge is more related to the regions with natural vegetation cover, flat topography, permeable soils, and deep-water table and others. groundwater recharge has been estimated using WetSpass model. The model determines the long-term average spatially distributed recharge as a spatial variable depending on soil texture, land use, slope, and meteorological conditions. The spatial distribution of groundwater recharge shown in Figure 5.95. Similarly, the groundwater recharge has been estimated for the year 2005, the results of which are given in Figure 5.96. The variation rainfall quantum causes a large variation in recharge particularly during the monsoon months.

The groundwater recharge during the monsoon months of 2005 have been estimated as 25-65 mm in June, 20-40 mm in July, 50-80 mm in August, and 15-25 mm September. has been estimated in the year. The spatial variability of groundwater recharge computed for 2010 is presented in Figure 5.97. The groundwater recharge varied between 25-30 mm June, 50-70 mm in July, 40-80 mm in August, and 10-35 mm in September. During 2015, the groundwater recharge varied between 30-60 mm June, 20-50mm in July, 35-60 mm in August,

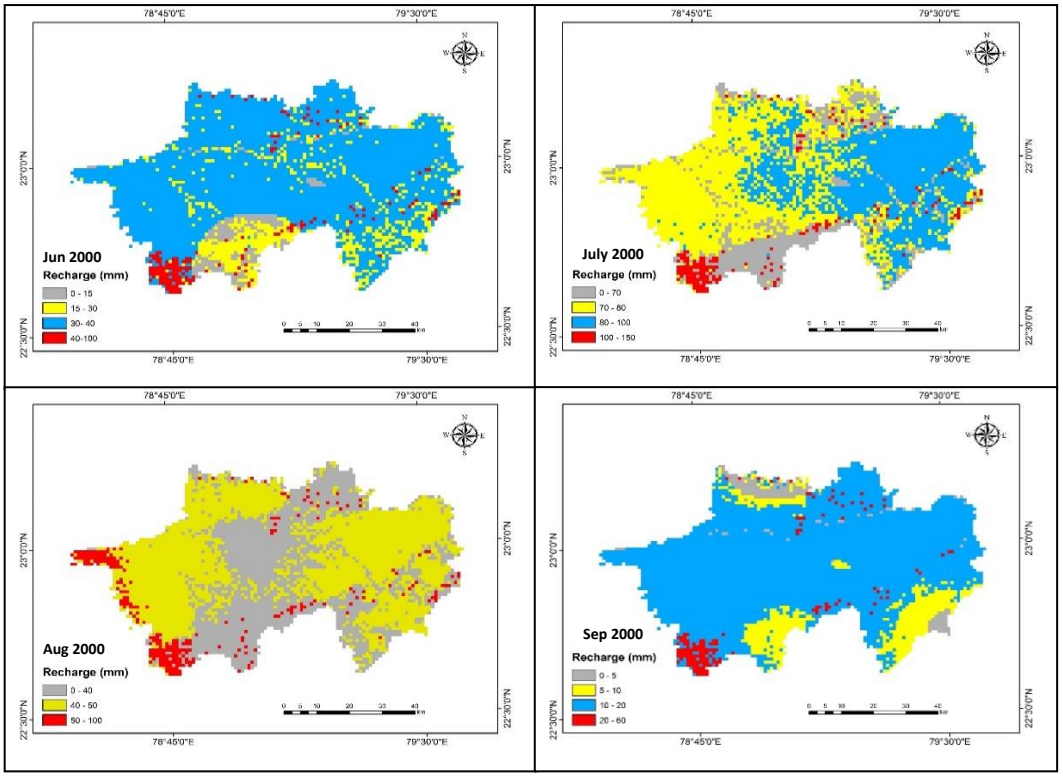

Figure 5.95: Spatial distribution of groundwater recharge year 2000

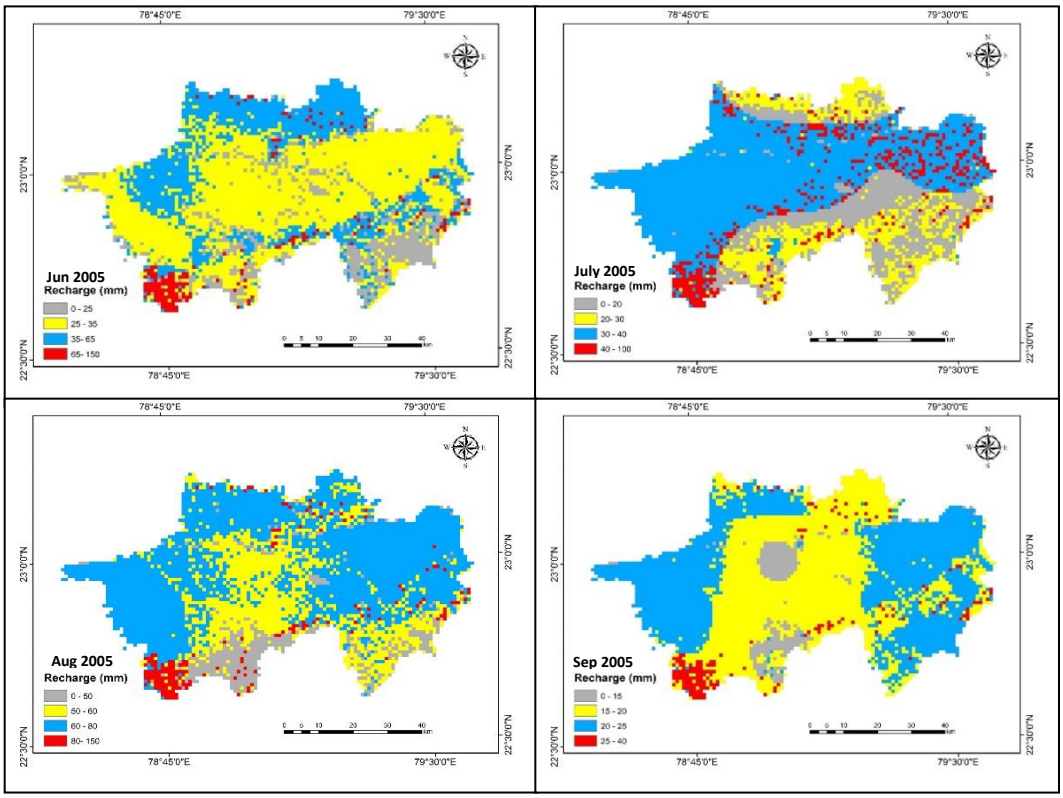

Figure 5.96: Spatial distribution of groundwater recharge in 2005

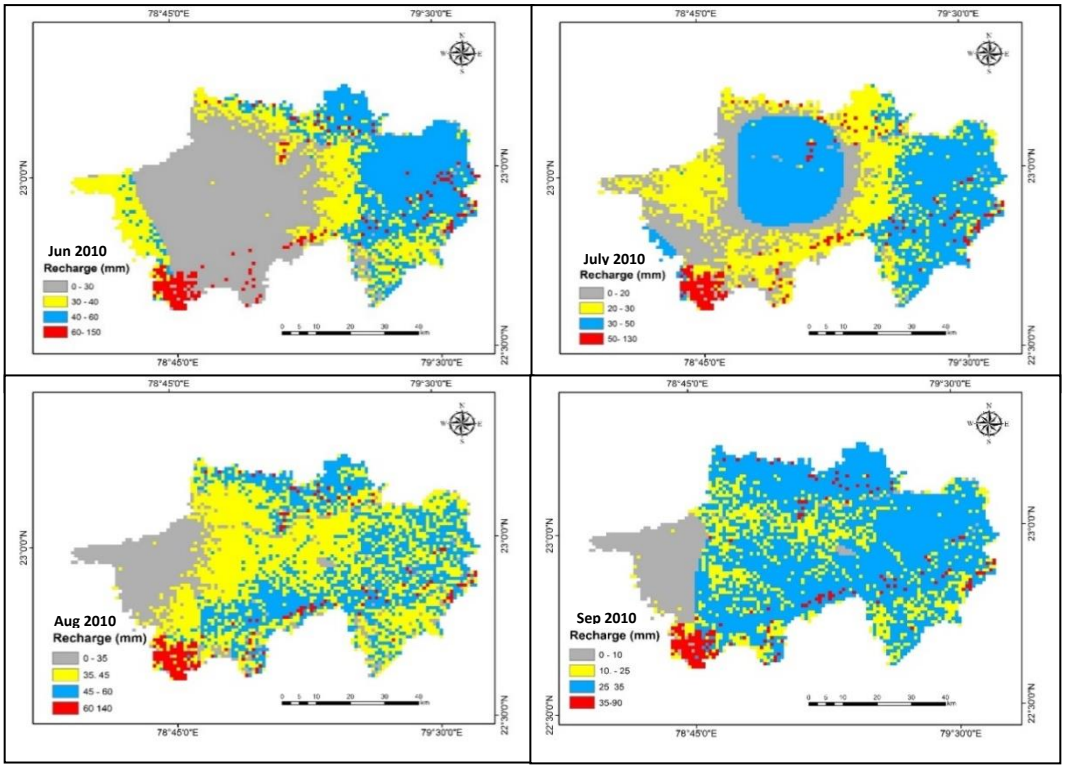

Figure 5.97: Spatial distribution of groundwater recharge in 2010

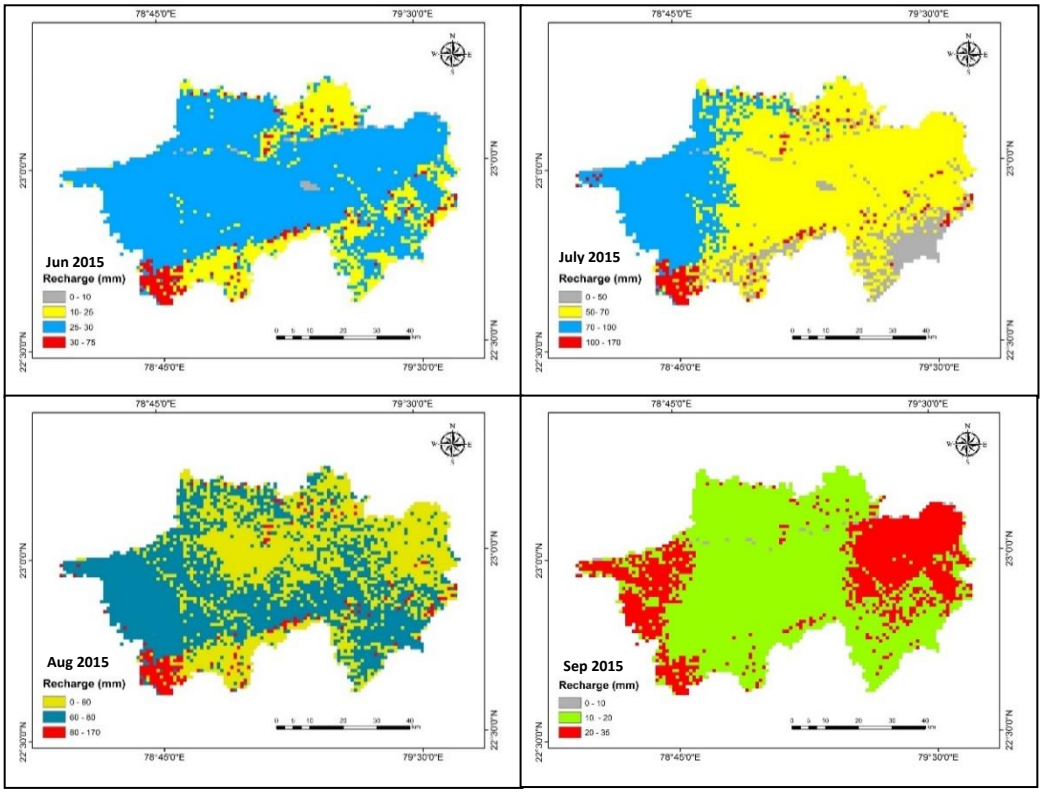

Figure 5.98: Spatial distribution of ground water recharge year 2015

and 10-20 mm in September. The spatial variability of the groundwater recharge

during 2015 is given in Figure 5.98.

The collection of ground-truth data at various locations, enables validation of land use classes which have been identified from the remote sensing data. During the field survey, the GPS points, direct observations and photo documentation approach was adopted while interpreting major crops which are grown in Narsinghpur district both in kharif season and rabi season. For the crop type identification, the intensive field survey was conducted at different locations in Narsinghpur district. Crops are generally grown during kharif and rabi seasons. During field survey, the major crops identified were paddy, pigeon pea and sugarcane in kharif season and wheat and gram in rabi season. The crop signatures were taken along with GPS locations at the reference sample sites. This information has been used for the supervised classification which were interpreted though GIS platform.

The crop map has been prepared for both kharif and rabi seasons for Narsinghpur district and is given in Figure 5.99 and Figure 5.100 respectively. This information has been used to assess the spatially varying crop water requirement in the study area. The entire study area has been divided into uniform grids of 79 rows and 128 columns, with each grid representing 1 km^2 area. As per the crop map, wheat and paddy are the most predominant crops grown in the study area in rabi and kharif season respectively. The major crops viz., paddy,

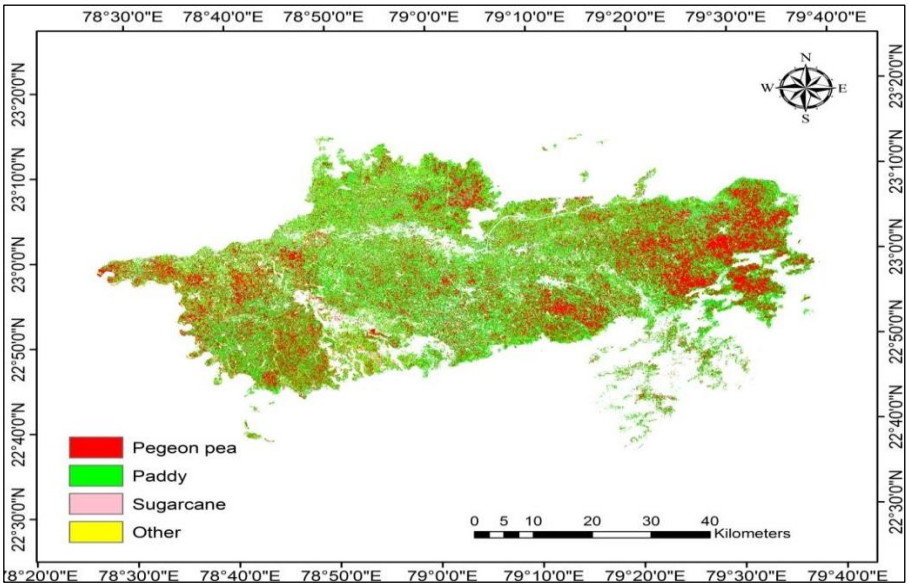

Figure 5.99: Crop map of kharif season

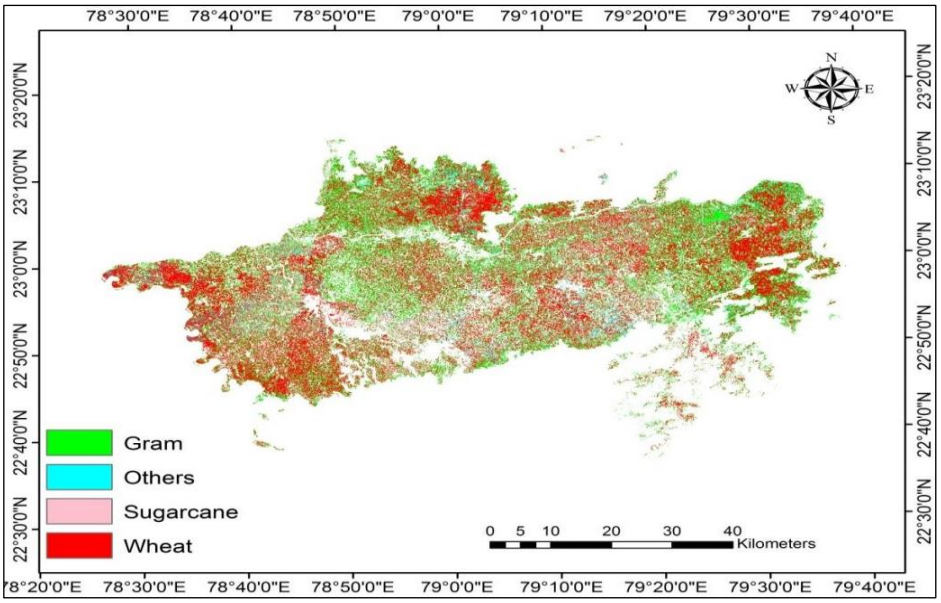

Figure 5.100: Crop map of rabi season

pigeon pea, sugarcane, wheat and gram contribute to the total kharif and rabi cropped area in the district.

Considering the crop map as the base map, the location of pumping wells has been considered to be distributed all over the study area as shown in Figure 5.101. There are 4063 pumping wells in Narsinghpur district and this has been represented by the red colored symbols. The flow boundaries have been assigned to the model based on the actual field conditions of the district. The Narsinghpur district is surrounded by hills on both the south and the north. The topography is undulating with forests which is dominating in this area. The eastern part of the district is having a plain topography with Narmada River flowing from almost the middle of the district. Here, the flow boundaries are marked as constant outflow boundary at different locations. The rest of the grid on periphery has been marked as no flow boundary. The river head boundary is shown in Figure 5.102 in white whereas constant head boundary is shown in Figure 5.103 in red.

5.9.1 Model calibration and validation

Transient simulations are needed to analyze time-dependent problems. A transient simulation typically begins with steady state initial condition and ends before or when a new steady state is reached. Transient simulations produce a set of heads for each time step, whereas steady state simulation generates only one set of heads. Transient head data can be displayed using a series of contour maps or

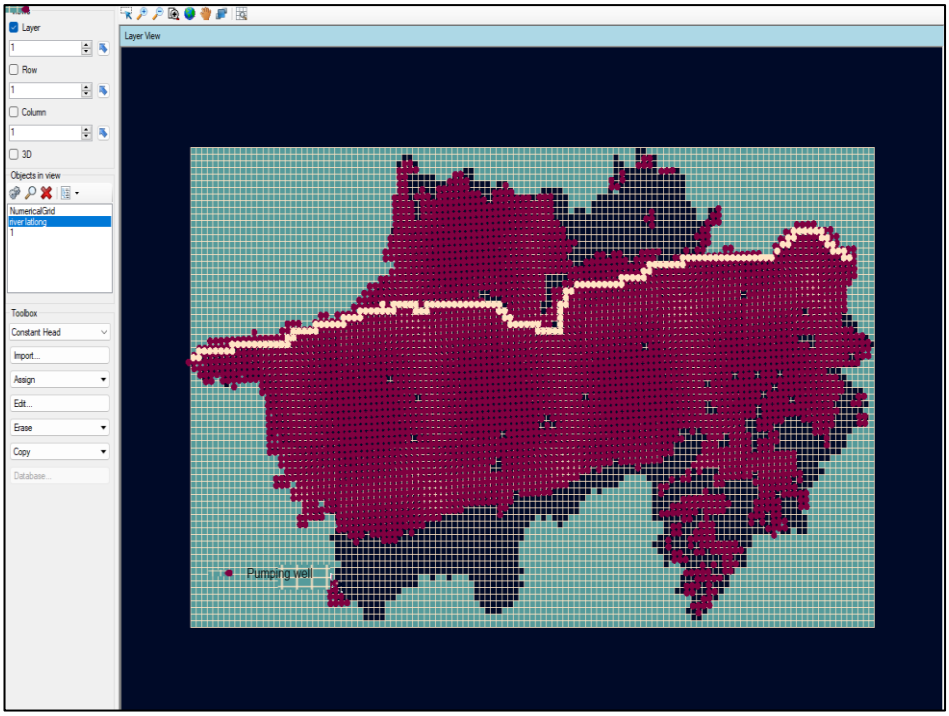

Figure 5.101: Pumping wells in Narsinghpur district

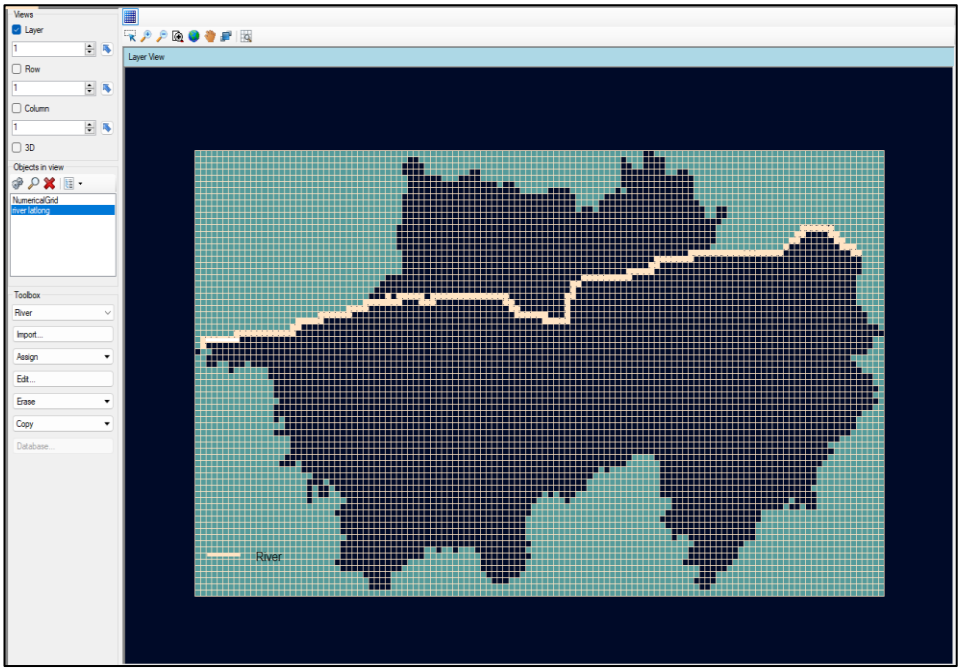

Figure 5.102: River head boundary of study area

hydrographs to show the transient variation of water level at selected nodes. In the present model, storage coefficient has been considered as 0.0001 for the basaltic terrain and 0.001 for alluvium areas, based on CGWB reference studies conducted for Narsinghpur district. The dynamic variation of recharge estimated as explained previously has been fed to the aquifer modelling for quarterly time steps for the

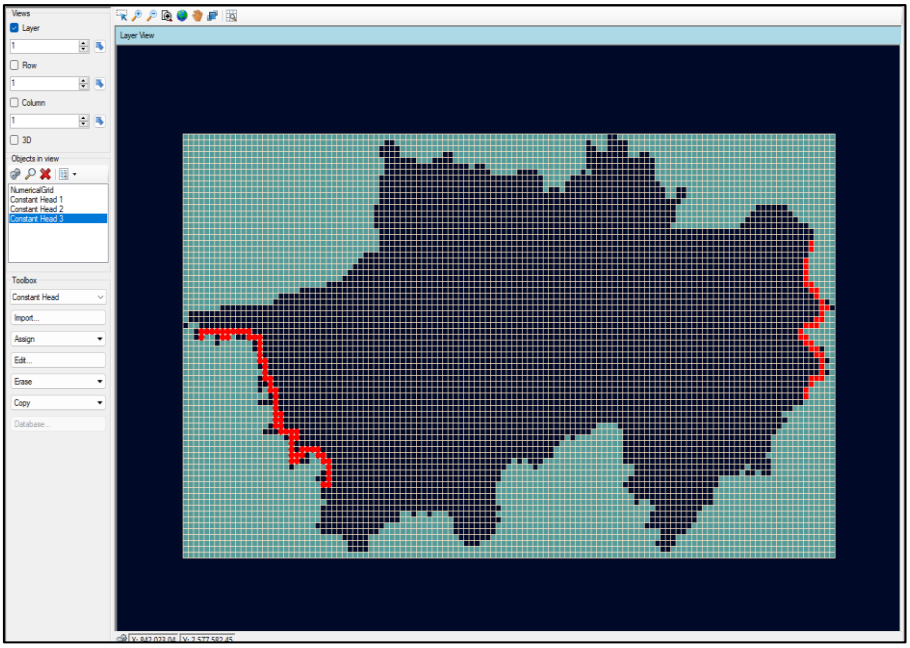

Figure 5.103: Constant head boundary of study area

kharif, rabi and summer seasons. The groundwater flow model has been calibrated and validated for the sixteen-year period spanning June 2000 to November 2015. The comparison of the observed and simulated heads during the pre-monsoon and post-monsoon seasons during the calibration period (2000 to 2011) is given in Figure 5.104. The comparison of the observed and simulated heads during the pre-monsoon and post-monsoon seasons during the validation period (2011 to 2015) is given in Figure 5.105. The model performance during calibration and validation in transient condition is given in Table 5.22.

Table 5.22: Model performance during calibration and validation Visual MODFLOW Flex

S. No.	Performance indicators	Calibration (2000-2010)	Validation (2011-2015)
1.	Normalized RMS %	2.73	3.74
2.	Standard error of estimate (m)	0.08	0.16
3.	Correlation coefficient	0.99	0.98

The model performance during the calibration and validation suggests that the Visual MODFLOW Flex is able to simulate the groundwater flow in the Narsinghpur district with a fair degree of accuracy. The calibrated model will be driven with the future climate data and future demands to study the future groundwater scenario in the Narsinghpur district.

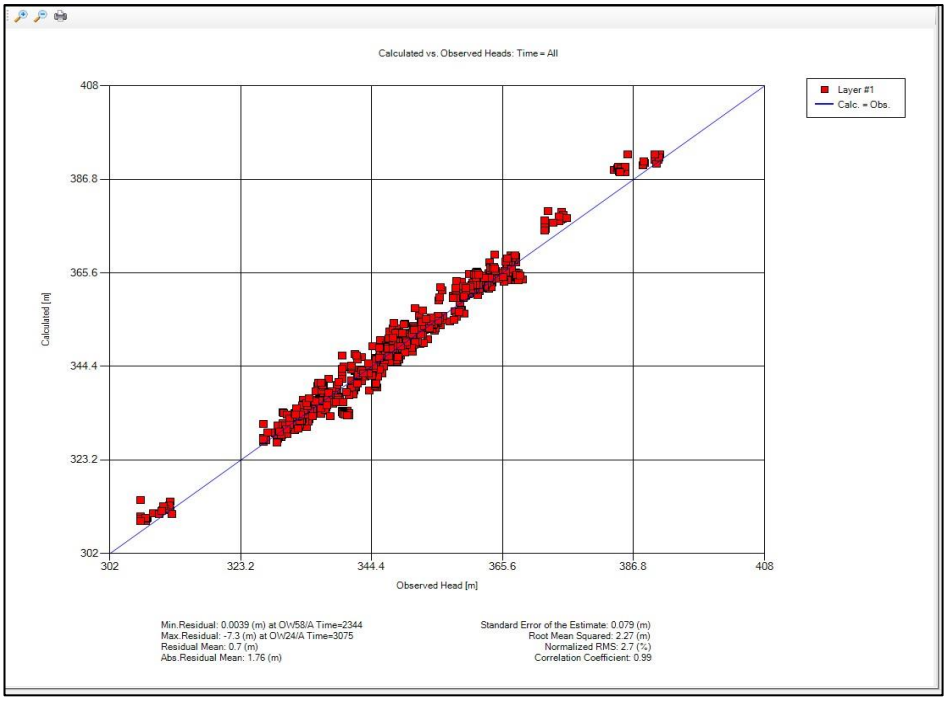

Figure 5.104: Comparison of computed and observed heads during calibration for the pre-monsoon and post-monsoon seasons

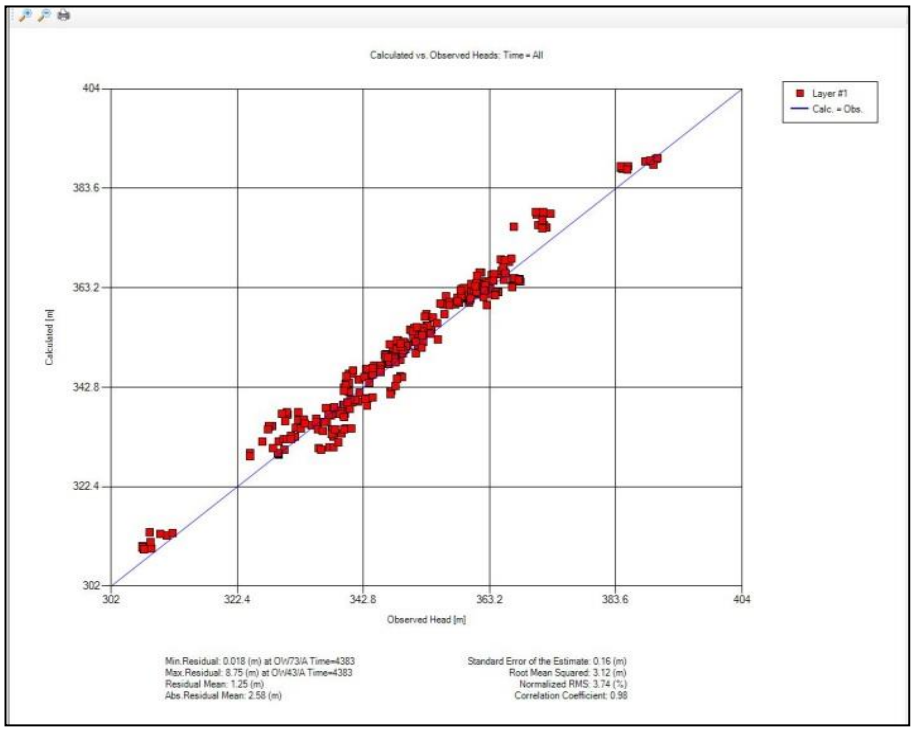

Figure 5.105: Comparison of computed and observed heads during validation for the pre-monsoon and post-monsoon seasons

5.10 Groundwater Modelling using Model MUSE

The groundwater flow modelling has been carried out for Narsinghpur district located in Upper Narmada basin using Model MUSE. After preparing the boundaries for the study area, the region was discretized and sub-divided into a number of square grids. The model setup was similar to Visual MODFLOW Flex after identifying hydrogeological units, such as aquifers, confining layers, and recharge/discharge areas, the numerical/mesh/grid was created along with the boundary conditions representing the actual field conditions. The hydraulic properties such as hydraulic conductivity, specific yield, porosity, to hydrogeological units were assigned to the hydrogeological units along with the initial conditions at the beginning of the simulation period. The input data including aquifer properties such as storage coefficient and transmissibility was assigned for each grid block. The IMS iterative Model Solution solver is used to perform the groundwater flow modelling in Model MUSE.

The geologic profile of the study area is depicted in Figure 5.106. The study area has a double-layered aquifer system with an unconfined and confined aquifer based on the lithology of the study area. Alluvium is the forming material of the aquifer. One of the most important aspects in the modelling process is the building of a conceptual model, which includes identifying the study region, selecting appropriate boundary conditions, creating a three-dimensional model (3D in general) of the hydrogeological system, and estimating sources and sinks. It's crucial that the conceptual model accurately represents the key hydrogeological conditions. The numerical modelling is built on the conceptualization of the system.

The numerical model's dimension and grid design are determined by the nature of the conceptual model. Defining the area and characteristics of the aquifer system, as well as building an understanding of groundwater flow directions, are all part of a conceptual model. The conceptual model for the area is developed using hydro stratigraphy, well logs and geophysical logs, a geologic map, and a geologic cross-section. For the phreatic aquifer, groundwater recharge is a key supply of water. GIS was utilized extensively in this project to create a database and to map the spatial distribution of rainfall used in developing a conceptual groundwater model for the Narsinghpur district based on WRD and CGWB data and reports.

Subsequently, developed conceptual model has been converted to mathematical model modular Finite Difference Model (McDonald and Harbaugh, 1988).

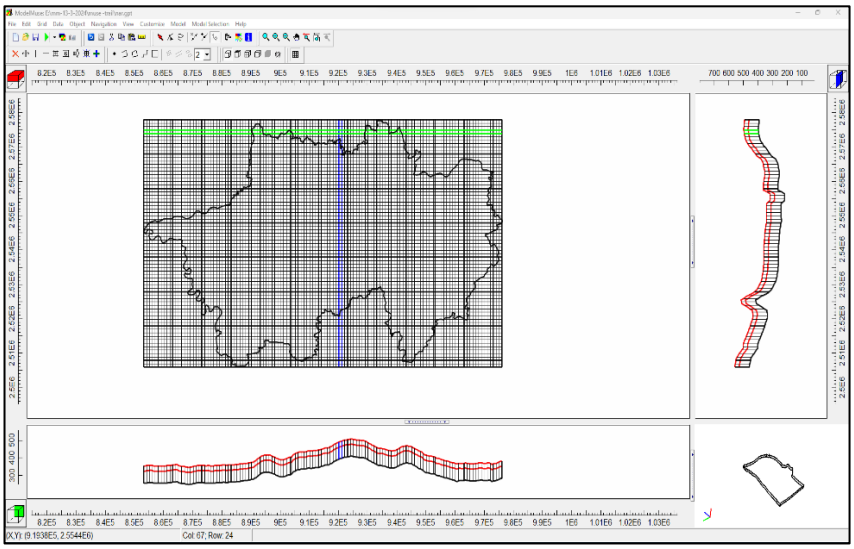

Figure 5.106: Grid map of study area

The simulated model domain of study area is divided into grids consisting of 79 rows and 123 columns which is two layered aquifer model, covering an area of 79000m x 123000 m (Figure 5.107). The resulting mesh consists of square blocks of 1000 m x 1000 m. Based on the analysis of lithological data of the study area, a two-layer model has been considered. The first layer mostly consists of 80 m alluvium zone and underlain by 80-190 m thick Gondwana and fracture zone as given in Figure 5.108. The simulated vertical section has a total thickness of about 190 m. The top layer is representing alluvium portion in the system which is typically designated as unconfined layer and the second layer is representing the Gondwana and fractured zone and assumed as semi-confined to confined conditions with variable T and S.

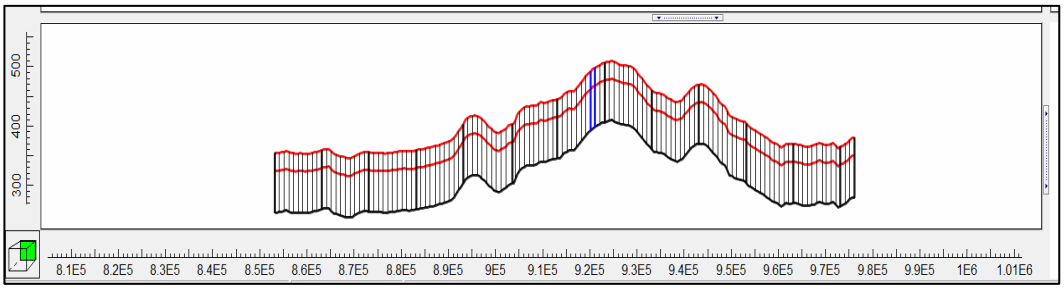

Figure 5.107: Vertical cross section of aquifer layer

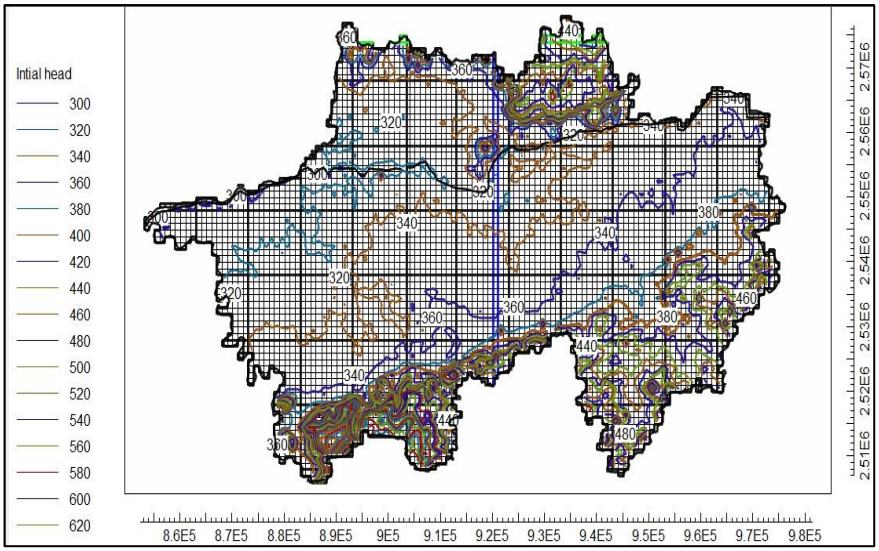

Figure 5.108: Initial head contours of study area

The initial head conditions are time domain boundary conditions that describe how hydraulic head is distributed in the system at the start of the simulation (Anderson & Woessner, 1992). In numerical groundwater models, starting conditions are initial head distributions that must be established for the numerical groundwater model as well as for model calibration. The convergence criteria of the model numerical approach are not met without an initial head. The static water level records of the wells obtained from CGWB and WRD were used in this case. The initial head map is given in Figure 5.109.

Considering the crop map as the base map, the location of pumping wells has been considered to be distributed all over the study area as shown in Figure 5.110. The black colored symbols represent the pumping locations and there are 4063 pumping wells in Narsinghpur district. All the river stretches were assigned river stage at various time steps, river bed level, river bed conductivity, river bed thickness, and river breadth at upstream and downstream sites. The river kit is designed to handle seepage from a river into an aquifer. The most variation in river stage is in August, followed by July, September, October, and June. The monthly river stage varies relatively little from November to May due to limited rain and water diversion into canals for agricultural and other purposes. The Narmada River has been assigned to the conceptual model of the study area.

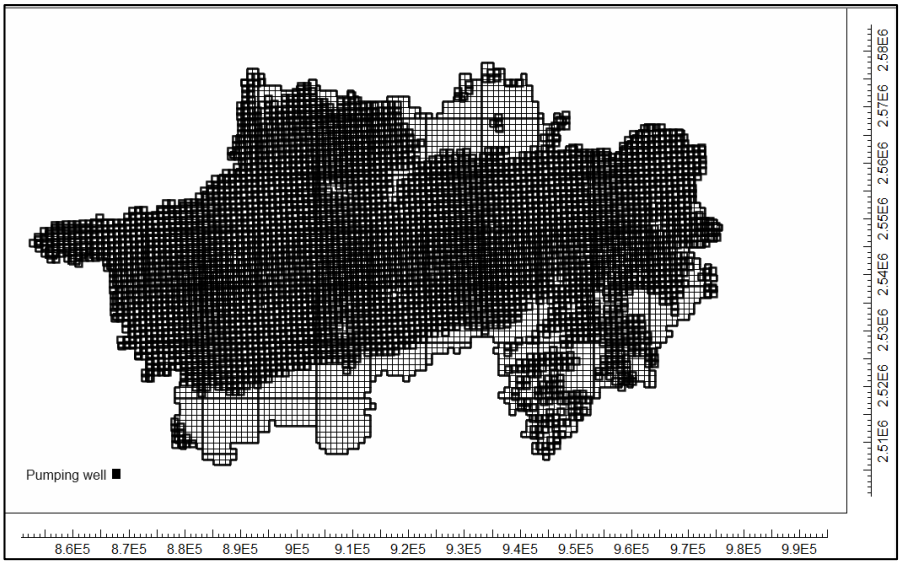

Figure 5.109: Pumping wells in Narsinghpur district

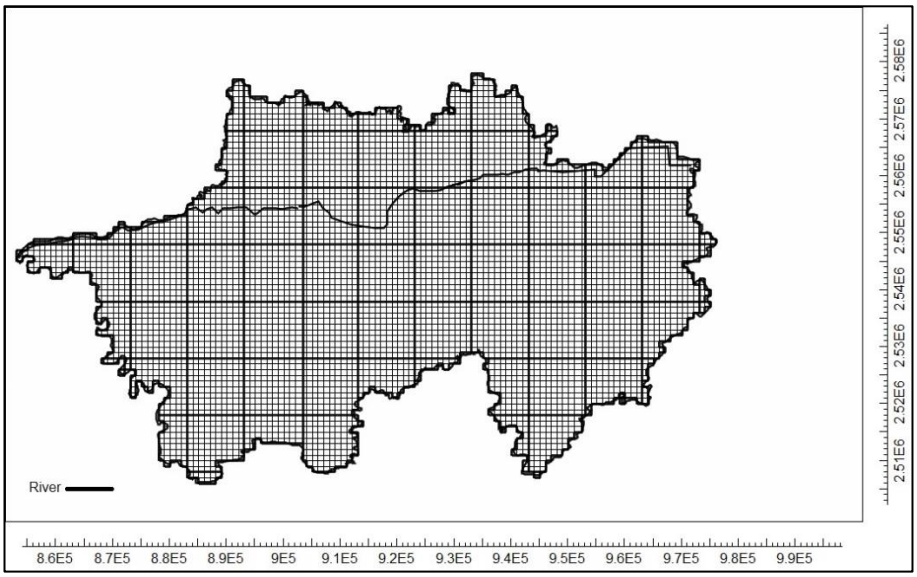

Figure 5.110: Narmada river in the study area

5.10.1 Calibration and Validation of Model MUSE

The hydraulic features of the hydro stratigraphic units, such as hydraulic conductivity, specific storage, and specific yield, have been used as calibration parameters for the transient groundwater model flow simulation. The process of altering the values of specified model input parameters to obtain a sufficient match between simulated and actual field-measured measurement of the simulated variable, within an acceptable range is known as model calibration. A mixture of automated and trial-and-error calibration procedures have been used to calibrate the groundwater-flow model in the study area. In this study, the groundwater-flow

model was optimized for transient flow modelling. The transient calibration was carried out utilizing observed groundwater-level data from 2000 to 2010 as given in Figure 5.111. The model validation has been carried out with the observed groundwater level data from 2011 to 2015 and is given in Figure 5.112. The computed results consist of hydraulic head at each of the grid blocks throughout the aquifer. These spatial distributions of hydraulic heads have been determined at each of the sequence of time interval covering the period of interest. The model performance evaluation statistics during calibration and validation is give in Table 5.23. The final head distribution over the different layers in the model is given in Figure 5.113.

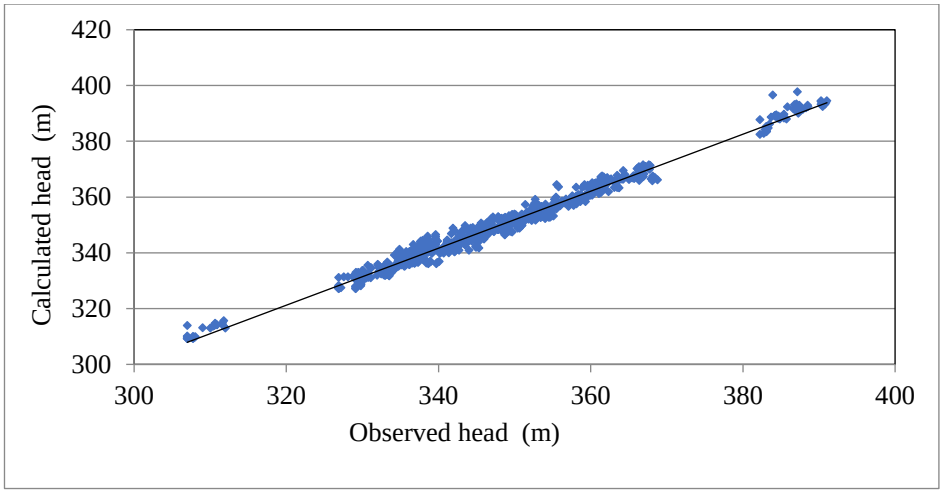

Figure 5.111: Model performance during calibration period

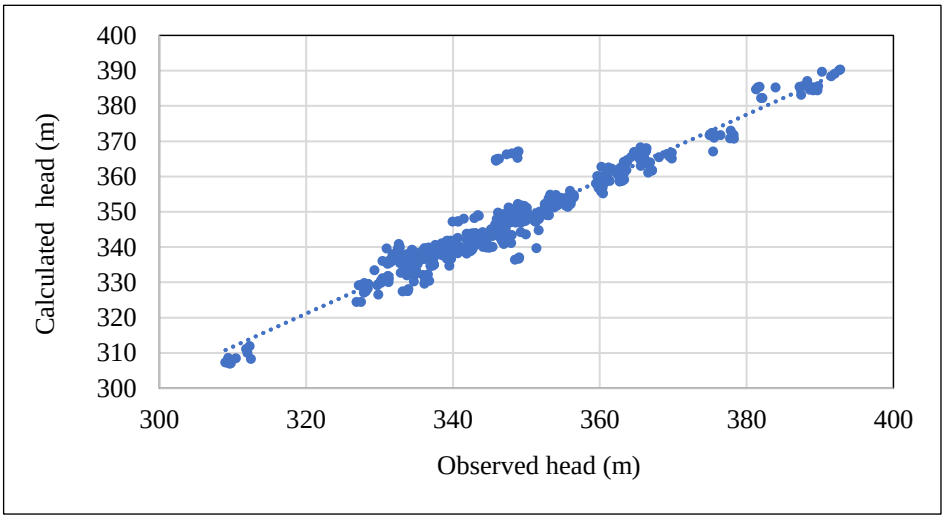

Figure 5.112: Model performance during validation period

Table 5.23: Model performance during calibration and validation Model MUSE

S. No.	Performance indicators	Calibration (2000-2010)	Validation (2011-2015)
1.	Normalized RMS %	2.40	4.11
2.	Standard error of estimate (m)	0.04	0.12
3.	Correlation coefficient	0.98	0.92

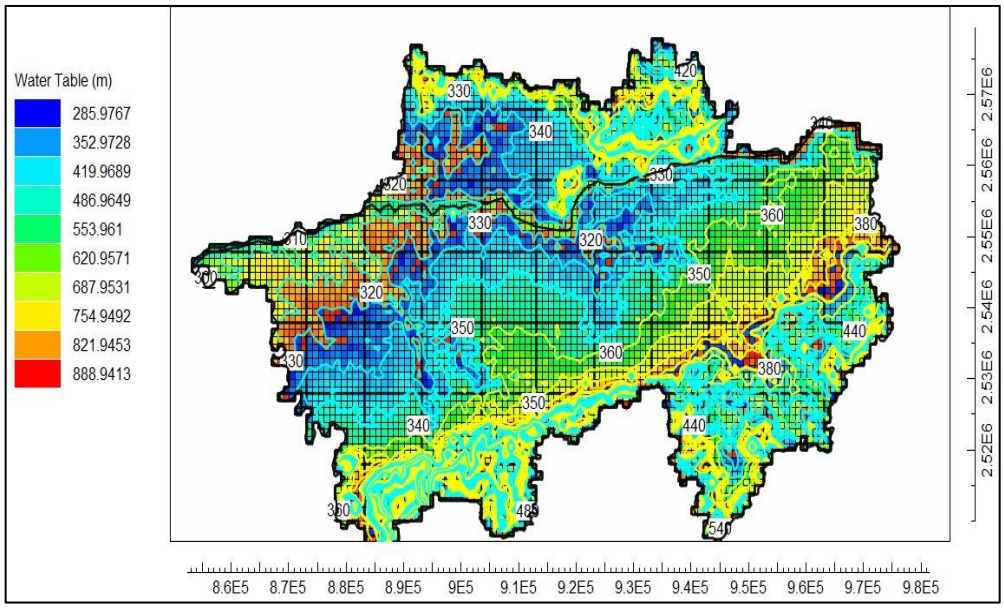

Figure 5.113: Distribution of final heads in the study area

The model performance during the calibration and validation suggests that the Model MUSE is able to simulate the groundwater flow in the Narsinghpur district with a fair degree of accuracy. The calibrated model will be driven with the future climate data and future demands to study the future groundwater scenario in the Narsinghpur district.

Both Model MUSE and MODFLOW can be used for groundwater flow modelling and contaminant transport modelling. However, Model MUSE may lack some of the advanced features and capabilities found in Visual MODFLOW Flex as it is primarily focused on providing a user-friendly interface for building and visualizing model simulation results and may not include features for complex analyses. Model MUSE can be beneficial for new users or those who need to quickly build and visualize groundwater models but advance users may find the interface limiting in terms of flexibility and options for model setup and analysis.

The available resources and documentation for Model MUSE may not be as extensive or detailed compared to commercial software packages. As such, Model MUSE may have a smaller user community which can impact the availability of online forums, user groups, and other resources for troubleshooting issues or sharing knowledge and experiences.

MODFLOW is the best suited model for simulation of groundwater flow in the Upper Narmada basin. The spatial variability of the groundwater recharge was captured using the WetSpass model. The spatially varying groundwater recharge was given as model input to MODFLOW along with the other model parameters and boundary condition to simulate te groundwater heads. The performance of MODFLOW was satisfactory for the Narsinghpur district in the Upper Narmada basin.

5.11 Flood Plain Mapping using HEC-RAS

The HEC-RAS software was used to independently simulate floodplain and water level in downstream side of the study area at Sethani Ghat in Hoshangabad. The area is prone to heavy flooding whenever the flood waters are relased from the three major dams viz., Bargi, Tawa and Barna. Residential areas and agricultural fields located near the river are more vulnerable to the threat of flooding. Generally, releases from the dams are synchronised in such a manner that heavy sumergence can be avoided in these flood prone areas through mutual interaction between the project authorities and timely depletion of reservoirs and adopting time-delays in releasing flood waters based on the time of travel of the flood water to reach the area of interest. Also, the areas near the confluence of Tawa River with the Narmada river witnesses flood plains and silting issues but the issue is of much lesser importance as sompared to the flooding near Sethani Ghat areas which is very heavily populated.

The flood hydrographs have been computed for all the contributing tributaries based on the CWC Flood Estimation Report for Sub-zone 3c. The actual releases from the dams have been considered for few days before, during and after the flood related submergence dates in the area of interest. The 2D model of HEC-RAS has been setup in the Upper Narmada basin from Rani Avanti Bai Sagar

(Bargi) Dam up to the village Pathoda, which is more than 10 km downstream of the area of interest, to simulate the flood inundations within the city of Hoshangabad. However, in Hoshangabad, the gauging site of Central Water Commission (CWC) is located at Sethani Ghat, but to get the full picture of flood inundation including the backwater effects of local nalas which confluence after the Sethani Ghat the downstream boundary was considered 10 km further downstream.

The distances top Sethani Ghat from Tawa dam is 54.197 km; 119.46 km from Barna dam and 324.285 km from Bargi dam. The average time of travel is generally about 8 hours from Tawa dam, 10 to12 hours from Barna dam and 36 to 40 hours from Bargi dam. The areas near Sethani Ghat are at much higher elevations, but the backwater effect from the local nalas merging with Narmada River during the times when the river is in spate is significant. The major nine tributaries of River Narmada include River Soner, River Sher, River Shakkar, River Dudhi and River Tawa joining River Narmada on the left flank and River Hiran, River Sendhor, River Tendoni, River Barna on the right flank of the main river. River Ghoghra is a tributary of River Barna which confluences with it downstream of the Barna dam.

The model setup for the study area included the creation of the 2D flow area which defines the boundary for which 2D computations will occur in which a computational mesh (grid) of size 100 m x 100 m was created. The FABDEM of 30 m resolution has been used for the flood modelling exercise which is a modified version of Copernicus DEM. The terrain has been created from the FABDEM. The boundary conditions have been defined. Figure 5.114 shows the 2D computational mesh and terrain of the study area for flood modelling. The upstream boundary conditions comprised of the flow hydrographs at the various tributaries and actual spillway releases due to opening of gates to release flood waters whereas normal depth was considered as the downstream condition. Sentinel 10 m land use / land cover data has been used to generate the various land cover information using RAS Mapper and integrated it with the geometric data of the flood plain (Figure 5.115). The LULC codes (FID) had been changed

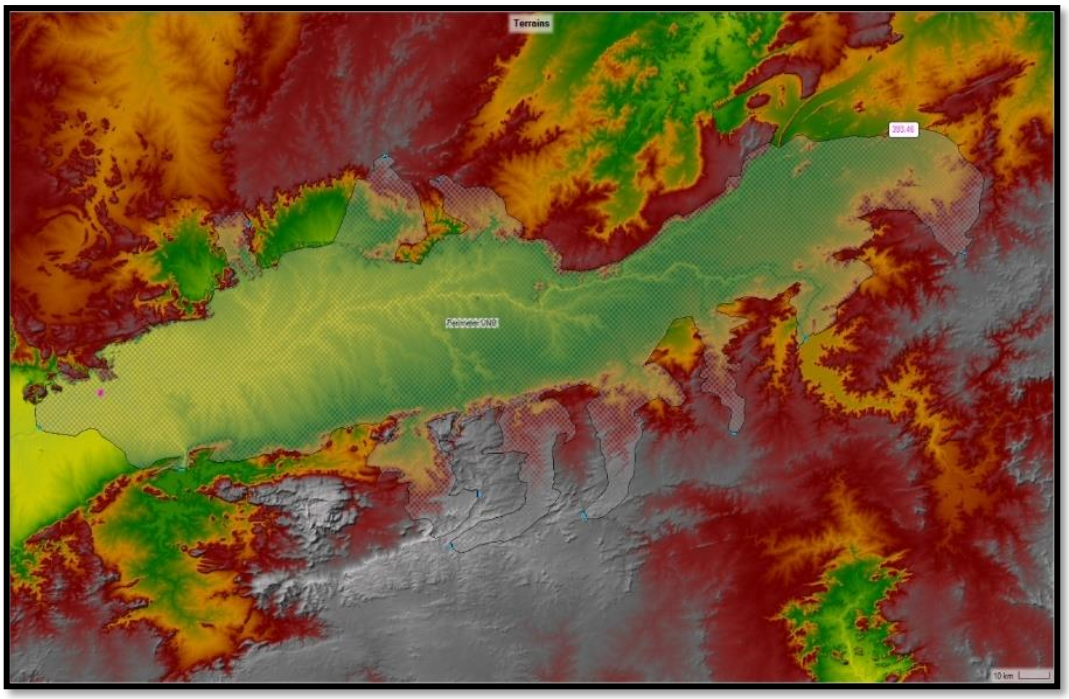

Figure 5.114: Generation of 2D computation mesh (100 x 100 m) for study area

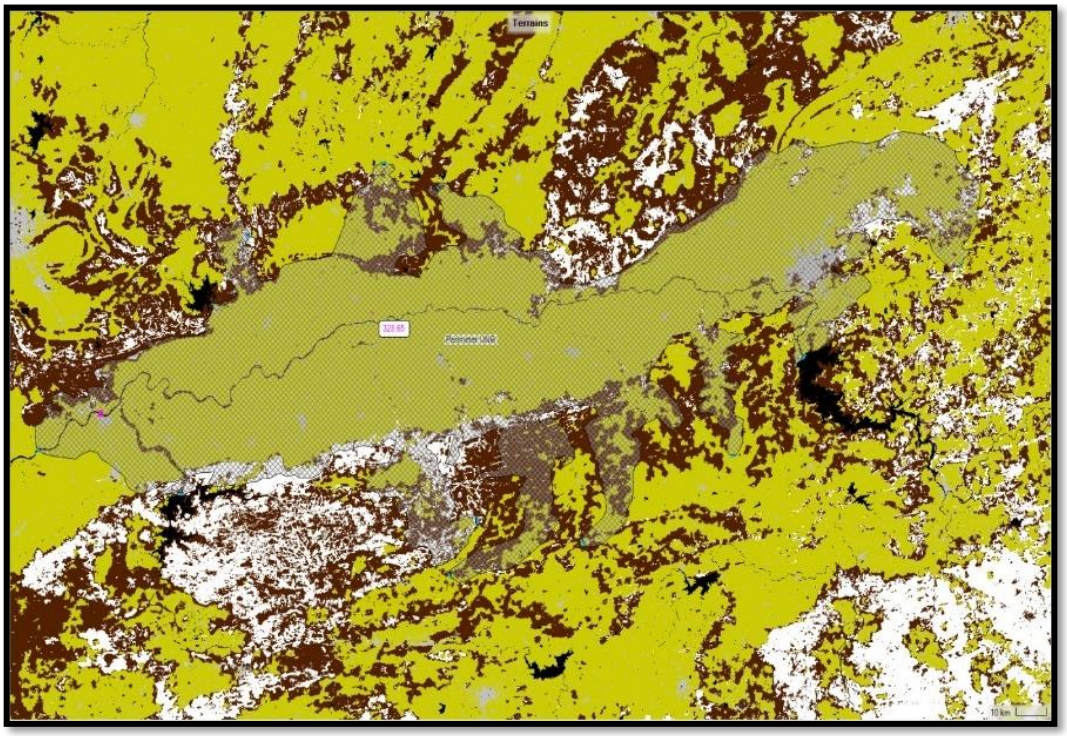

Figure 5.115: Land cover associated with 2D flow area

previously in ArcGIS to match with the FID of the HEC-RAS as HEC-RAS has its own FID system through which the model understands the various types of land cover based on its FID. The Manning's 'n' has been provided to the model as

suggested in the HEC-RAS Manual (Table 5.24). The location of Sethani Ghat and Tawa-Narmada confluence is given in Figure 5.116.

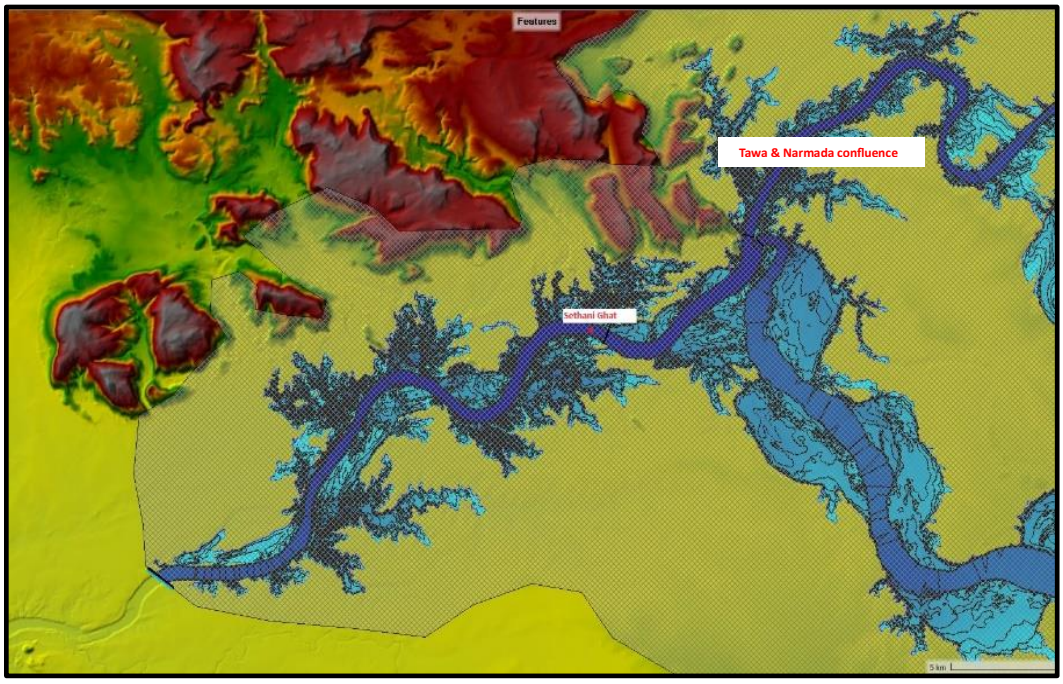

Figure 5.116: Location of Sethani Ghat in Hoshangabad and Tawa River confluence

Table 5.24: Land cover-based Manning's 'n'

S. No.	LULC	Manning's n
1.	No data	99
2.	Open water	0.026
3.	Built up (open)	0.035
4.	Built up (low intensity)	0.05
5.	Built up (medium intensity)	0.055
6.	Built up (high intensity)	0.065
7.	Barren/Rocky/Sandy/Clay	0.03
8.	Deciduous Forest	0.18
9.	Evergreen Forest	0.16
10.	Mixed Forest	0.19
11.	Shrub / Scrub	0.10
12.	Grassland / Herbaceous	0.07
13.	Pasture / Hay	0.06
14.	Cultivated Crops	0.055
15.	Woody wetlands	0.08
16.	Herbaceous Wetlands	0.07

The terrain layer and the land cover layer were associated with the geometry user the 'layer associations' tool in 'manage layer associations. The slope of the energy gradient line has also been evaluated using RAS Mapper and provided in the model. The full momentum equation, water surface tolerances and storage area elevation tolerance has been provided to the model. The unsteady flow analysis has been carried out for the study area with a computation interval of 1 minute for the various model runs based on actual flooding in the study area and also based on 4hypothetical scenarios that may occur in future. The flood plains have been mapped for the flood inundations resulting from the contribution of these nine tributaries and the actual releases from the three major dams in the study area viz., Bargi Dam, Barna Dam, and Tawa Dam. Three select historical major flood events that occurred at Hoshangabad have been simulated as flood scenarios for the various dates of flood occurrence on 06th August 2012, 23rd August 2013, and 30th August 2020.

5.11.1 Flood Scenario on 06th August 2012

In this scenario, apart from the individual contribution from various tributaries, the maximum releases (actual) from Tawa dam were 15682.9 cumecs and the actual maximum releases from Barna dam was 886.5 cumecs, while there were no releases from Bargi dam. This information along with the necessary model parameters have been provided to the 2D model setup for the study area. The simulation results indicate that the resultant flood waters reached up to the Mangalwara Ghat road near Dussehra Maidan in Hoshangabad, which has been ascertained from the field authorities. The flood water encroached a distance of about 1.2 km from the left bank of River Narmada along the Lediya Nala. The flood inundation map showing the submergence in the vicinity of Sethani Ghat is given in Figure 5.117. The details of the inundation in the various villages can be seen from the administrative block map overlayed over this flood inundation map.

The water depth contours have been extracted at an interval of 1 meter from the model results. The depth contours plotted for the flood scenario on 06th August 2012 depicts that the maximum water depths lie in the main river channel and also in the local nala, while the water that encroached in the city has a depth limited to 1 meter only. The depth contours for the flood scenario on 06th August

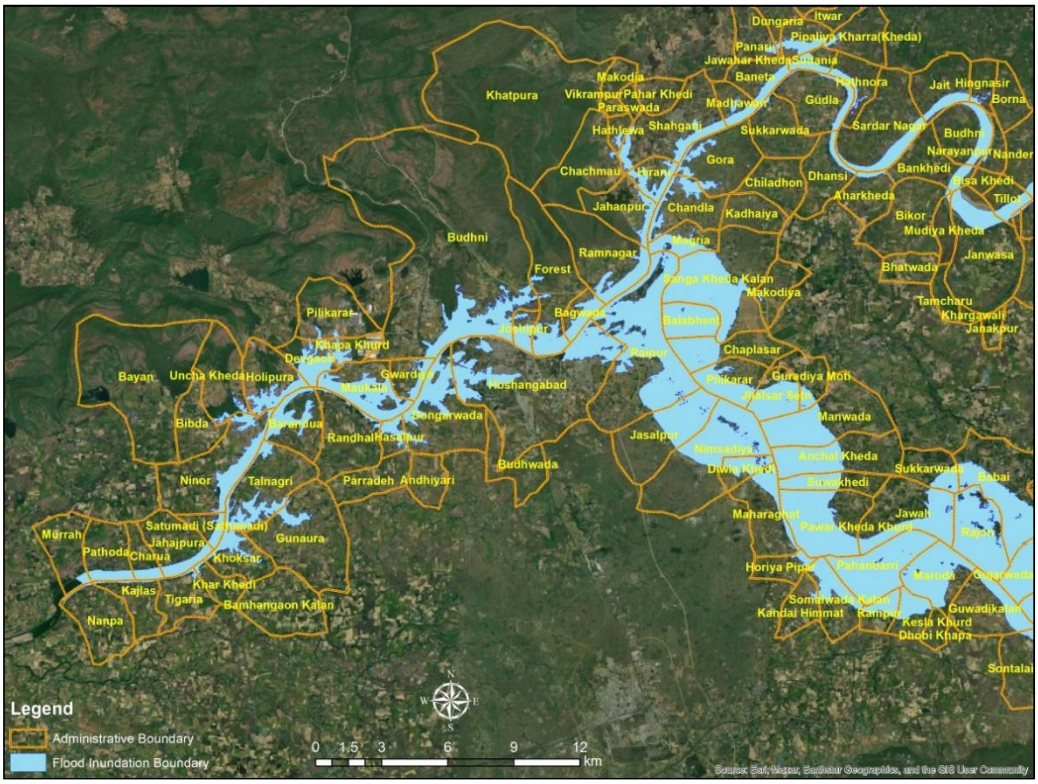

Figure 5.117: Flood inundation map for flood Scenario of 06th August 2012

2012 is given in Figure 5.118. The water surface elevations have also been mapped for the simulation of the same flood event of 06th August 2012. The maximum water surface level achieved by the flood event on 06th August 2012 at

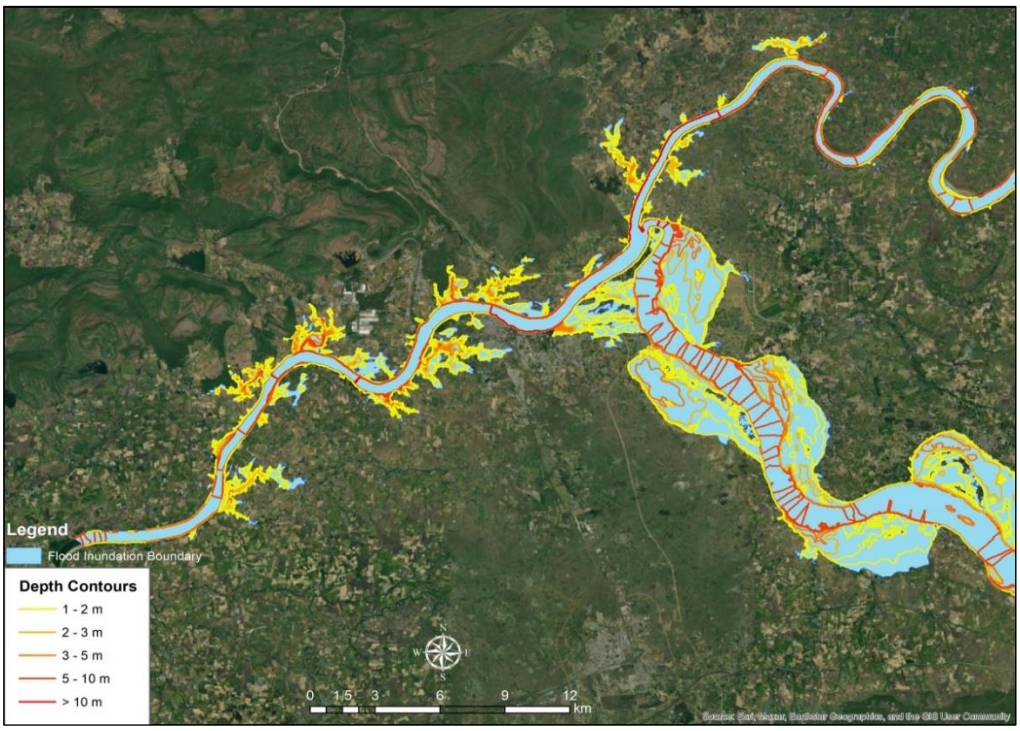

Figure 5.118: Depth contour map of the flood scenario of 06th August 2012

Sethani Ghat in Hoshangabad was found to be 297.5 m above msl, while at the confluence of River Tawa and River Narmada at Bandrabhan the water surface elevation was found to be 299 m above msl. The water surface elevation map for the flood scenario on 06th August 2012 is given in Figure 5.119.

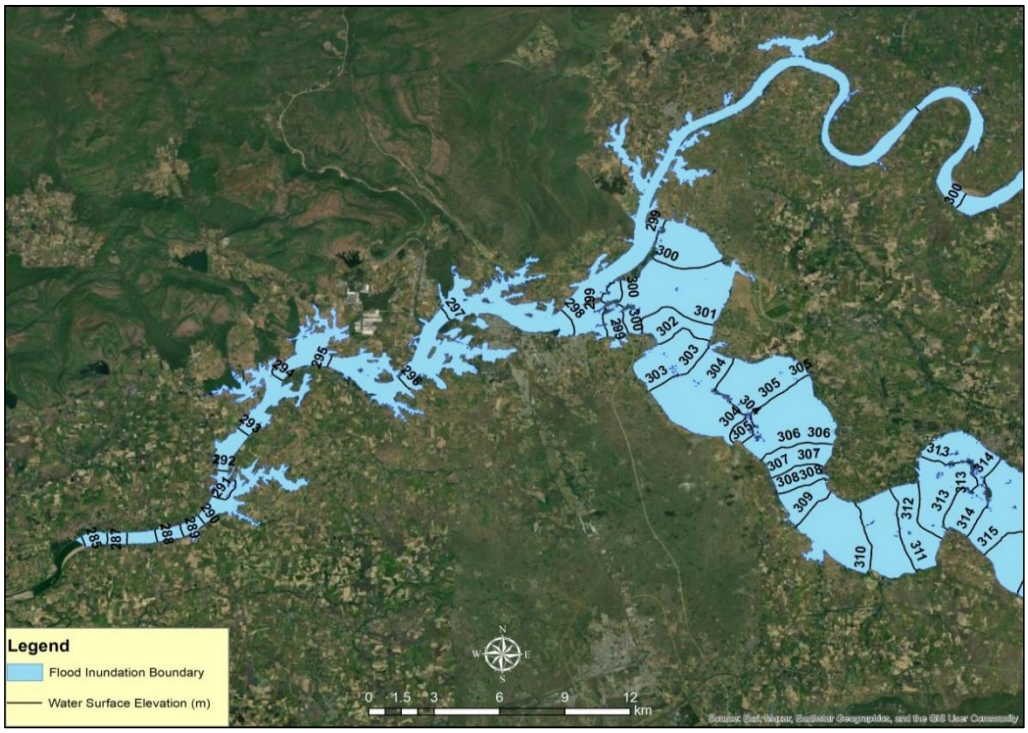

Figure 5.119: Water surface elevation map fort flood scenario of 06th August 2012

5.11.2 Flood Scenario on 23rd August 2013

In this scenario apart from the contribution of tributaries, the actual maximum releases from Tawa dam were 17420.28 cumecs, maximum releases from Barna dam were 1317.47 cumecs while the actual maximum releases from the Bargi dam was 5032 cumecs. This is the second highest release that has taken place from Tawa dam and the reservoirs were operated in such a manner so as to minimise the flood situation in Hoshangabad. The simulation results indicated that the resultant flood waters reached up to the Jaystambh Chowk in Hoshangabad which has been ascertained from the field authorities at Hoshangabad. The flood waters encroached for a distance of about 1.525 km from the left bank of River Narmada along the Lediya Nala. The flood inundation map is given in Figure 5.120.

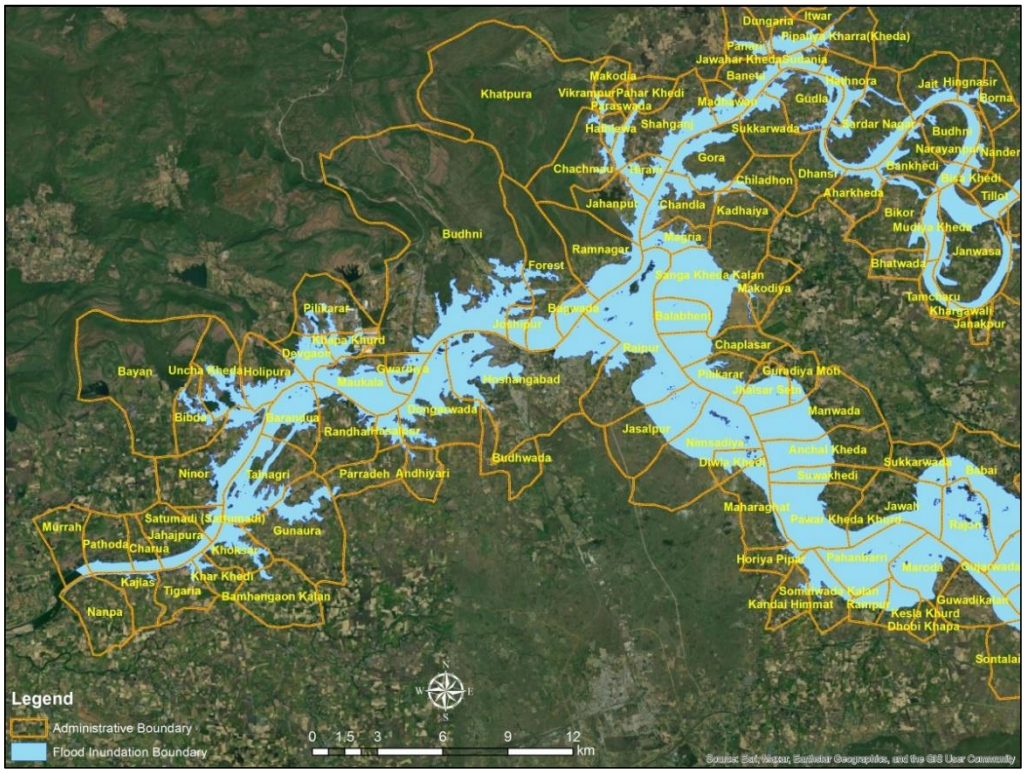

Figure 5.120: Flood inundation map for flood scenario of 23rd August 2013

The water depth contours has been extracted from the model results at an interval of 1 meter. The depth contours plotted for the flood scenario on 23rd August 2013 depicts that the maximum depths lie in the main river channel and also in local nala, while the depth of water which encroached up to Jaystambh Chowk has the depth of 1 meter only. The depth contours for the flood scenario of 23rd August 2013 is given in Figure 5.121. The water surface elevations have also been mapped for simulation of the same flood event of 23rd August 2013. The maximum water surface level achieved during the flood event on 23rd August 2013 at Sethani Ghat in Hoshangabad was found to be 299.5 m above msl, while at the confluence of River Tawa and River Narmada at Bandrabhan it was found to be 301 m above msl. The water surface elevation map for the flood scenario of 23rd August 2013 is given in Figure 5.122.

5.11.3 Flood Scenario on 30th August 2020

In this scenario apart from the contribution of tributaries, the actual maximum releases from Tawa dam were 17429.9 cumecs, which is the maximum water released so far from Tawa dam, the maximum releases from Bargi dam was

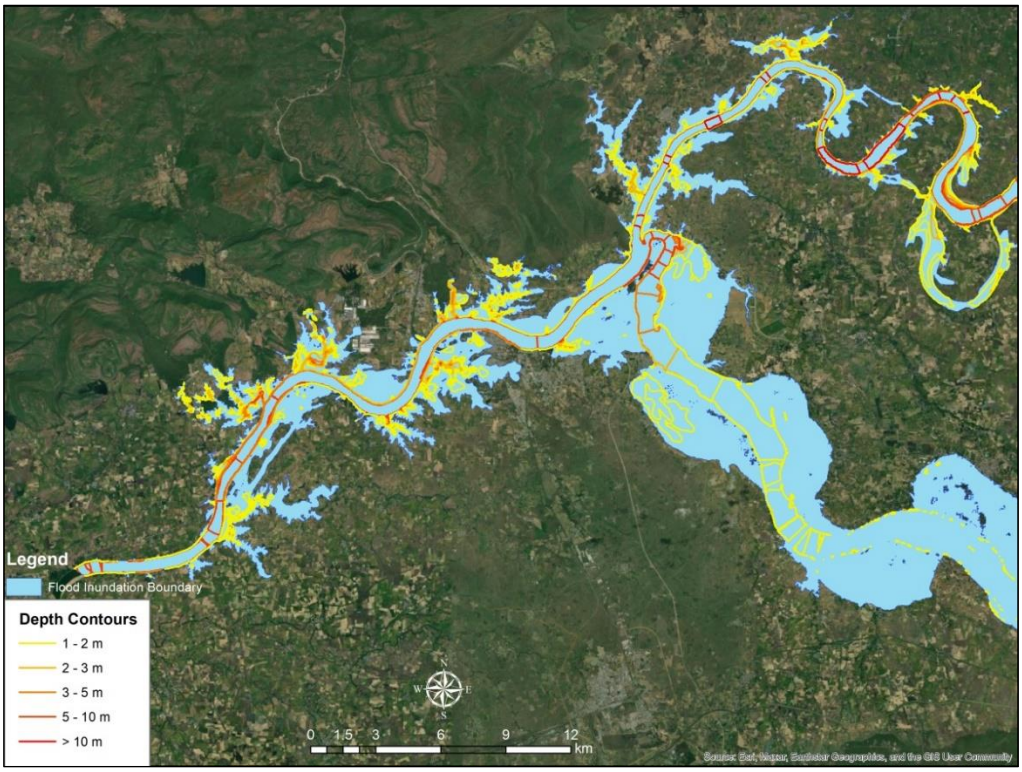

Figure 5.121: Depth contour map of the flood scenario on 23rd August 2013

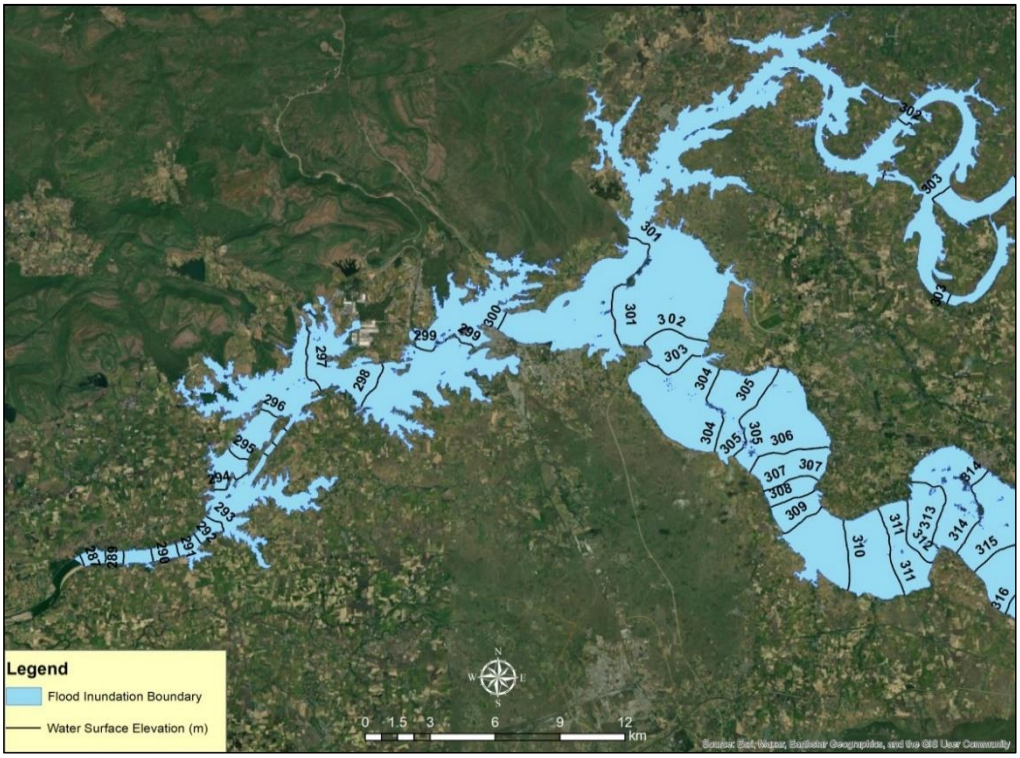

Figure 5.122: Water surface elevation map for flood scenario of 23rd August 2013

6601 cumecs, which also the maximum among the three scenarios considered here in this study, while there was no releases from Barna dam. The resultant flood waters reached up to the Anjuman Middle School in Hoshangabad. The flood water encroached a distance of about 1.447 km from the left bank of River Narmada along the Lediya Nala. The flood inundation map is given in Figure 5.123.

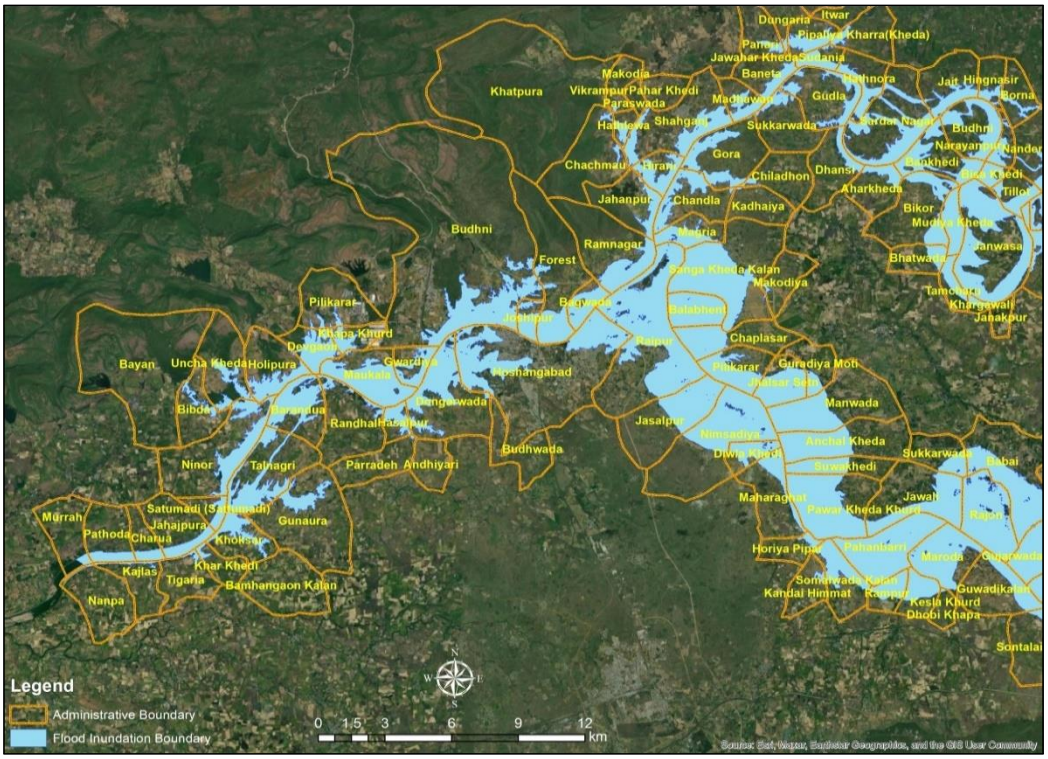

Figure 5.123: Flood inundation map for flood scenario of 30th August 2020

The water depth contours has been extracted from the model results at an interval of 1 meter. The depth contours plotted for the flood scenario of 30th August 2020 depicts that the maximum depths lie in the main river channel and in local nala, while the water depth of the encroached water up to Anjuman Middle School is limited to 1 meter. The depth contours for the flood scenario of 30th August 2020 is given in Figure 5.124.

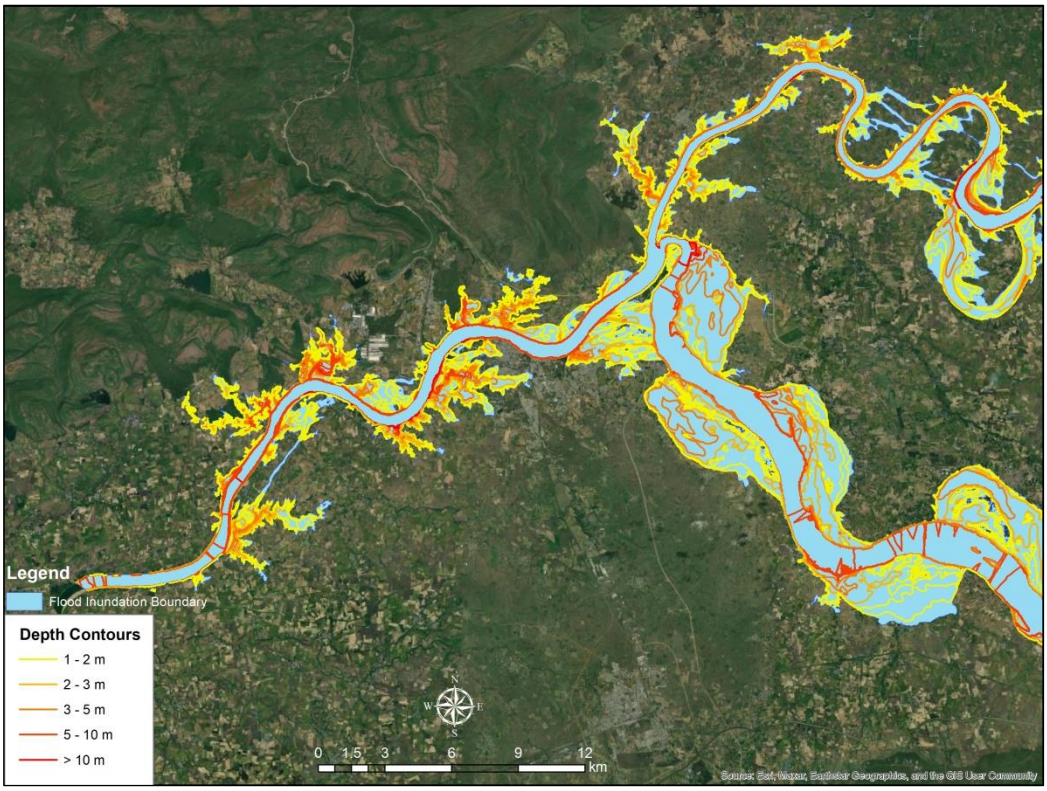

Figure 5.124: Depth contour map of the flood scenario of 30th August 2020

The water surface elevations have also been mapped for the flood scenario of 30th August 2020. The maximum water surface level achieved by the flood event on 30th August 2020 at Sethani Ghat in Hoshangabad was found to be 299.0 m above msl, while at the confluence of River Tawa and River Narmada at Bandrabhan the depth was found to be 300 m above msl. The water surface elevation map for the flood scenario of 30th August 2020 is given in Figure 5.125.

5.11.4 Hypothetical Scenario for simultaneous effect of dam releases

In this scenario, the actual maximum releases made from Bargi, Barna and Tawa dams were synchronized in such a way that the effects of these releases 'responds simultaneously' at Sethani Ghat in Hoshangabad to get the flood encroachment area that could be possible in the city, if ever such a scenario was ought to happen. Based on the model simulations, the resultant flood water can reach up to the Jaystambh Chowk in Hoshangabad along the Lediya nala. The flood water can encroach up to a distance of about 1.6 km from the left bank of River Narmada along the Lediya Nala, and also the flood water can encroach up to Pahadiya Road

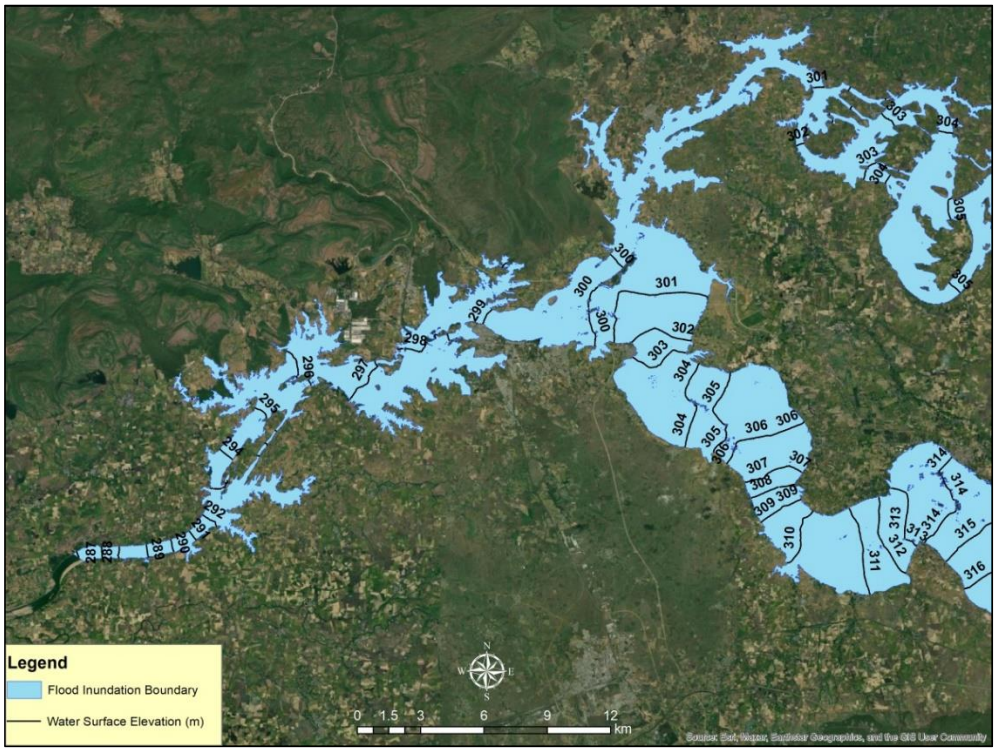

Figure 5.125: Water surface elevation map for flood scenario of 30th August 2020

near Narayan Nagar in Hoshangabad along the dried Sukthwa River. The flood inundation map for the simultaneous response scenario is given in Figure 5.126.

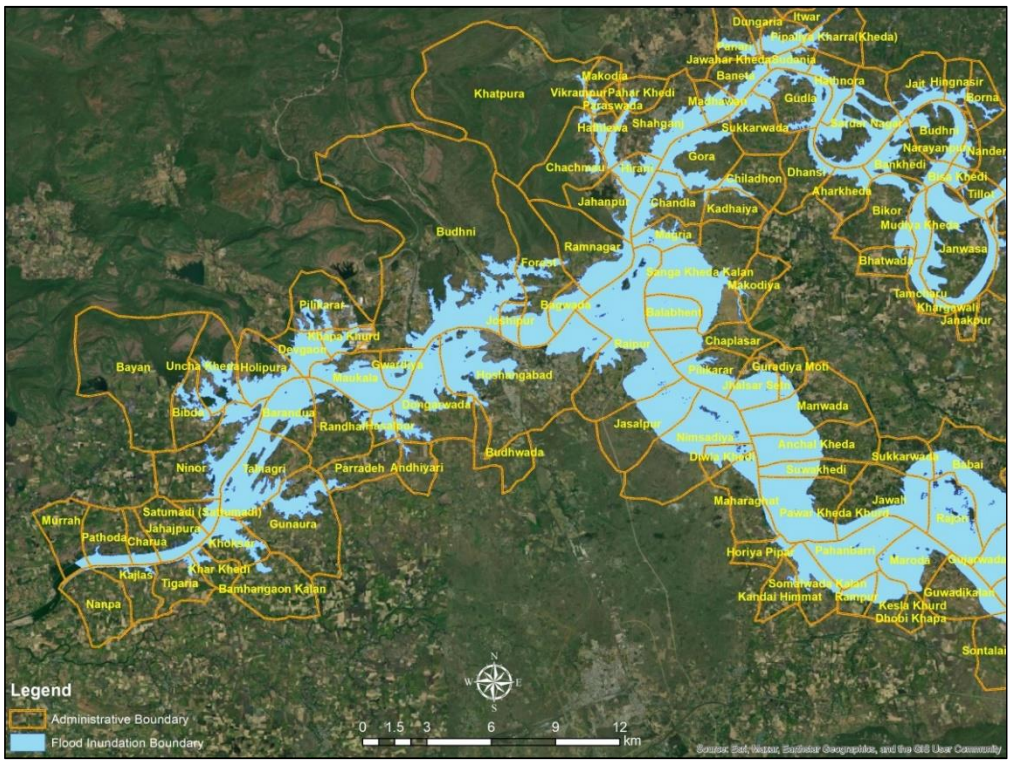

Figure 5.126: Flood inundation map for the simultaneous response scenario of all dams

The water depth contours has been extracted from the model results at an interval of 1 meter. The depth contours plotted for the hypothetical scenario for simultaneous effect of dam releases, depicts that the maximum depths lie in the main river channel and in local nalas, while the water can encroach up to Jaystambh Chowk with a depth limited to 1 meter. The depth of flood water along dried Sukthwa River can reach up to Pahadiya Road near Narayan Nagar can also has a depth up to 1 meter there, which gradually gets deeper towards its confluence with the main River Narmada, which has depth about 3 meters before the confluence. The depth contours for the hypothetical scenario for simultaneous response of all three dam releases along with the individual tributary contributions is given in Figure 5.127. The water surface elevations has also been mapped for the simultaneous response scenario of all dams. The maximum water surface level achieved by the flood generated at Sethani Ghat in Hoshangabad will be 300.5 m above msl, while at the confluence of River Tawa and River Narmada at Bandrabhan it was found to be 301.5 m above msl. The water surface elevation map for the simultaneous response scenario of all dams is given in Figure 5.128.

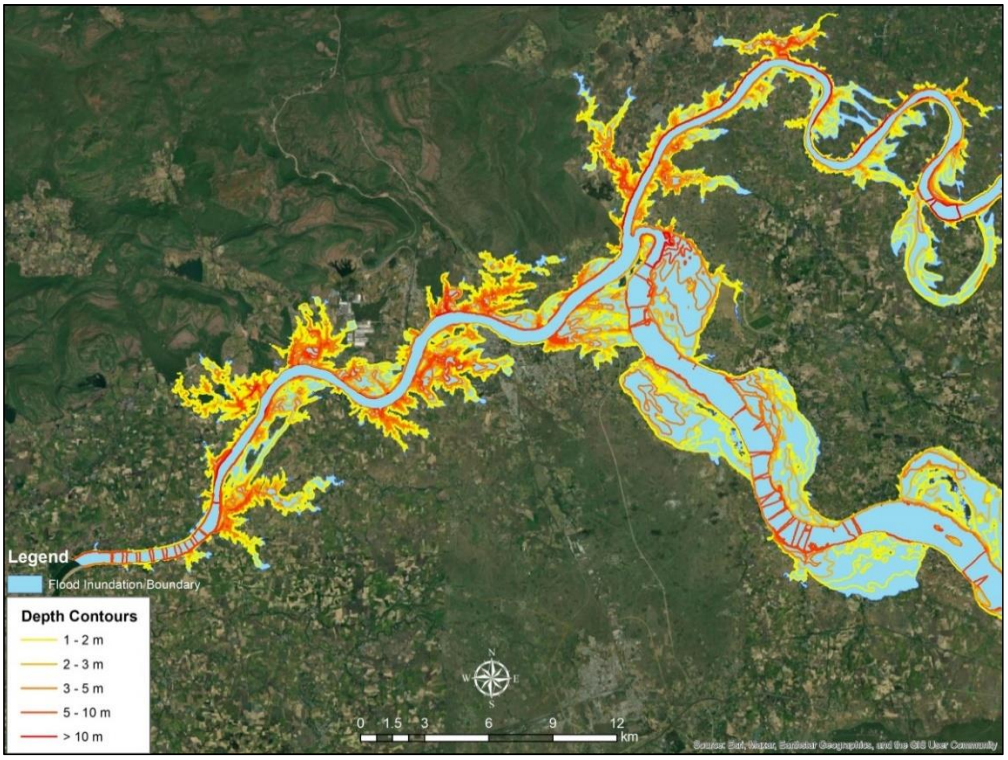

Figure 5.127: Depth contour map for simultaneous response scenario of all dams

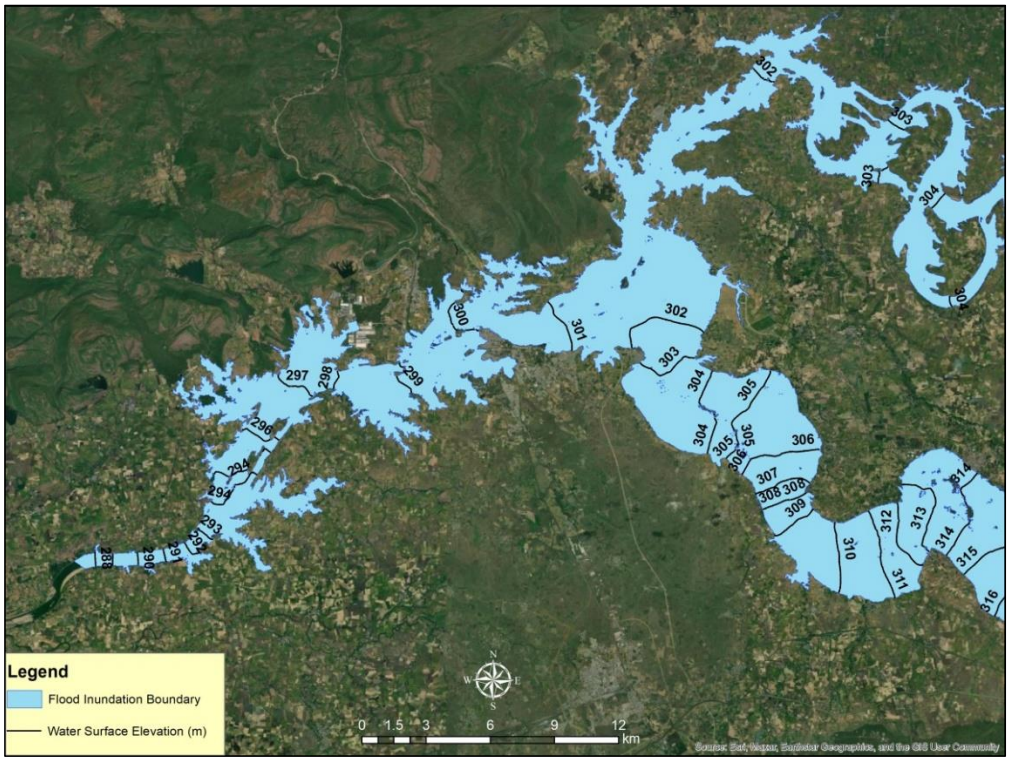

Figure 5.128: Water surface elevation map for simultaneous response scenario of all dams

5.11.5 Hypothetical Scenario for Bargi dam maximum releases

In this hypothetical scenario, the maximum releases that can be made from Bargi dam if all 21 gates were to be opened, which is equal to the maximum spillway capacity of 43000 cumecs has been assumed to be released hypothetically in gradually increasing order, while no releases have been considered from Barna and Tawa dams. By considering such a hypothetical scenario, the impact of maximum possible individual dam releases from Bargi dam, can be mapped at Sethani Ghat in Hoshangabad. The results of the model simulations, shows that the resultant flood waters, may enter in the city due to the backwater influence of Lediya Nala that ultimately joins the left bank of River Narmada near Home Science PG College and making an island near Sethani Ghat. The flood water that may enter along the dried Sukthwa River may encroach up to St. Joseph college of Nursing at Rasuliya in Hoshangabad. The flood inundation map for maximum Bargi dam spillway releases scenario is given in Figure 5.129.

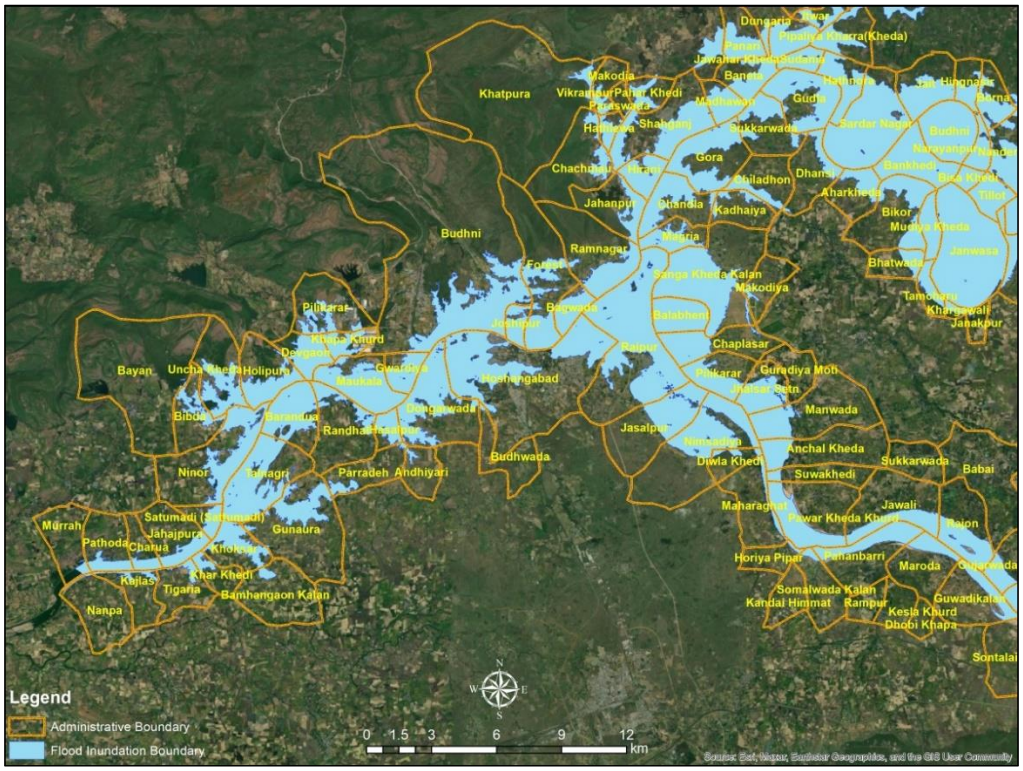

Figure 5.129: Flood inundation map for maximum Bargi dam spillway releases scenario

The water depth contours has been extracted from the model simulation results at an interval of 1 meter. The depth contours plotted for this hypothetical scenario for Bargi dam spillway maximum releases, depicts that the maximum depths lie in the main river channel and in local nalas. The depth of water that may encroach the city through Lediya Nala may have a maximum depth of 3 m along the Nala. The flood water along Sukthwa River may reach up to St. Joseph college of Nursing at Rasuliya has the maximum depth up which gradually gets deeper towards its confluence with main River Narmada, which has depth about 3 to 5 meters before the confluence. The depth contours for the hypothetical maximum Bargi dam spillway releases scenario is given in Figure 5.130. The water surface elevations has also been mapped for the maximum Bargi dam spillway releases scenario. The maximum water surface level achieved by the flood that may be generated at Sethani Ghat in Hoshangabad is found to be 301.25 m above msl, while at the confluence of River Tawa and River Narmada at Bandrabhan it was found to be 302.5 m above msl. The water surface elevation map for maximum Bargi dam spillway releases scenario is given in Figure 5.131.

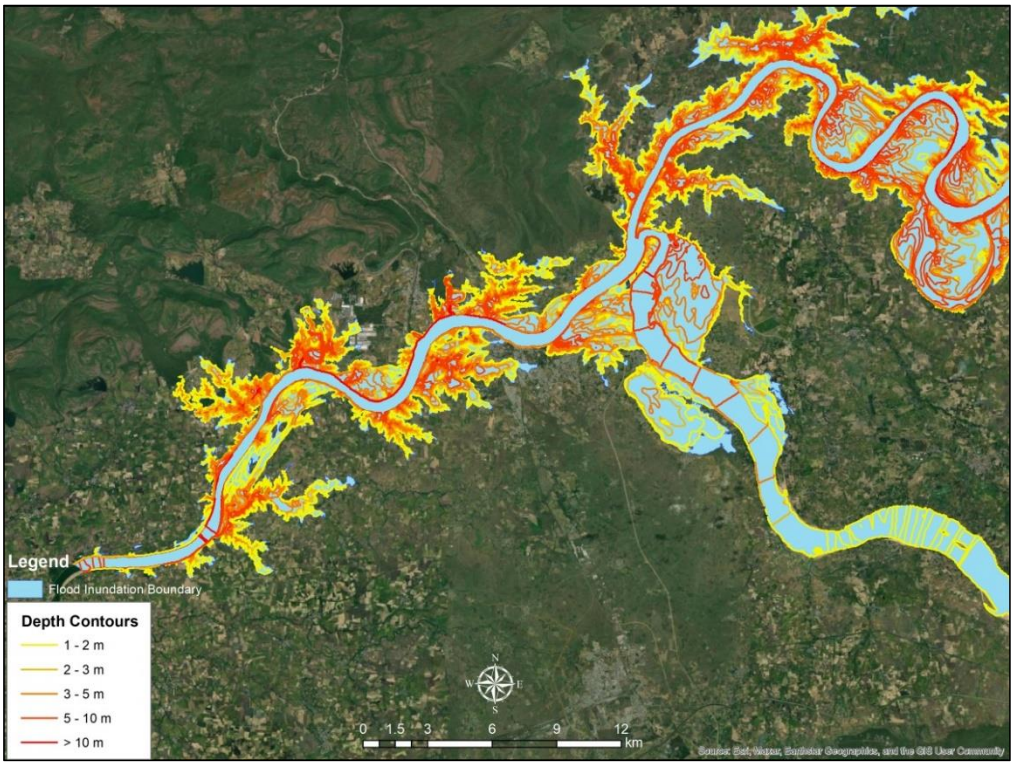

Figure 5.130: Depth contour map for maximum Bargi dam spillway releases scenario

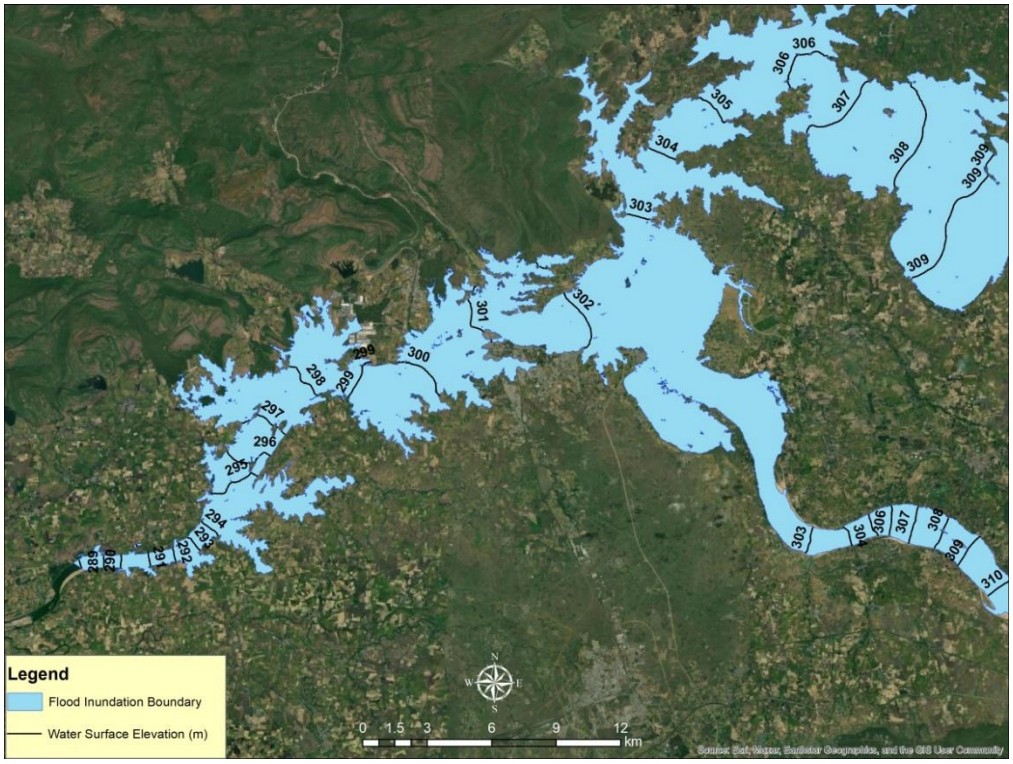

Figure 5.131: Water surface elevation map for maximum Bargi dam spillway releases scenario

5.11.6 Hypothetical Scenario for Barna dam maximum spillway releases

In this scenario, for Barna dam maximum spillway releases only scenario, which corresponds to the opening of all gates of Barna dam, is equal to the spillway capacity of 13556 cumecs, has been considered to be released hypothetically in gradually increasing order, while no releases have been considered from other two dams viz., Bargi and Tawa. By doing this the impact of maximum releases from Barna dam can be mapped at Sethani Ghat in Hoshangabad. After the model simulations, the flood water may enter in the city as backwater of Lediya Nala and can encroach up to the Dusshera maidan. The flood water may also enter along the dried Sukthwa River and encroach up to the railway track near Bengali colony. The flood inundation map for the hypothetical Barna dam maximum spillway releases only scenario is given in Figure 5.132.

The water depth contours has been extracted from the model simulation results at an interval of 1 meter. The depth contours plotted for this hypothetical scenario for Barna dam maximum spillway releases, depicts that the maximum depths lie in the main river channel and in local nalas. The water may encroach the city through Lediya Nala with a maximum depth of 1 meter along the Nala. The flood water along Sukthwa River can reach up to the railway track near Bengali Colony with a maximum depth there which will gradually get deeper towards its confluence with the main River Narmada, which has depth about 2 meters before its confluence. The depth contours for the hypothetical scenario for Barna dam maximum releases is given in Figure 5.133. The water surface elevations has also been mapped for the this hypothetical scenario. The maximum water surface level achieved by the flood generated at Sethani Ghat in Hoshangabad was found to be298 m above MSL, while at the confluence of River Tawa and River Narmada at Bandrabhan it was found to be 299.5 m above MSL. The water surface elevation map for Barna dam maximum releases scenario is given in Figure 5.134.

5.11.7 Hypothetical Scenario for Tawa dam maximum releases

In this hypothetical scenario, the maximum spillway releases that can be made from Tawa dam if all gates are opened, which equals to the maximum

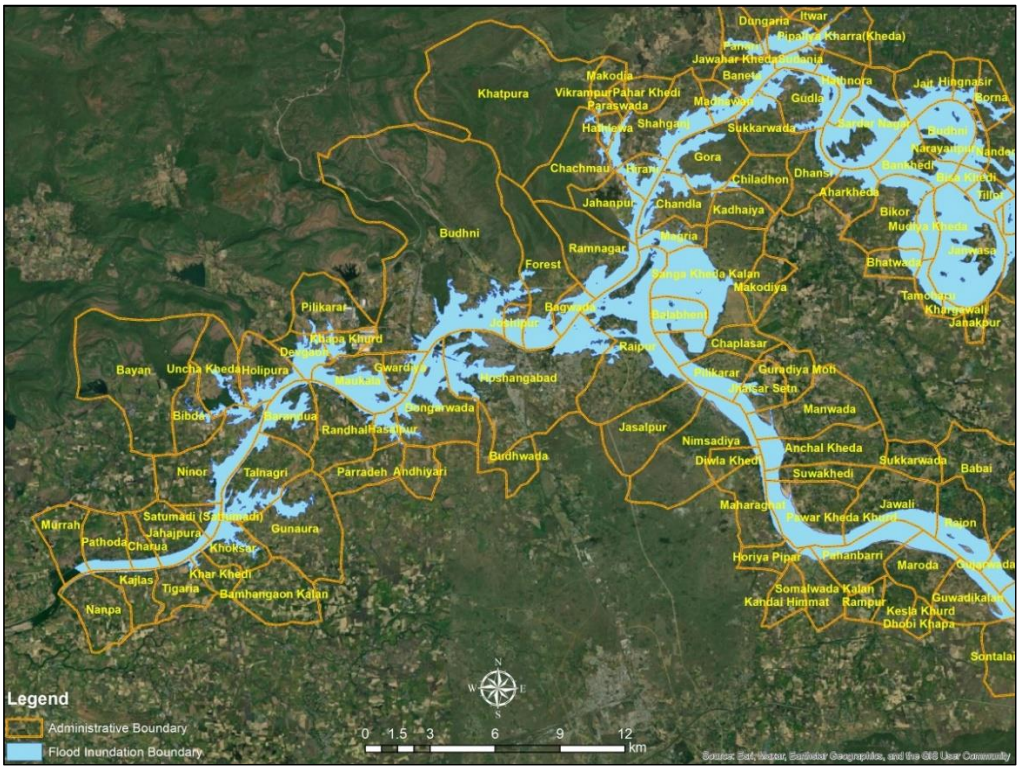

Figure 5.132: Flood inundation map Barna dam maximum spillway releases scenario

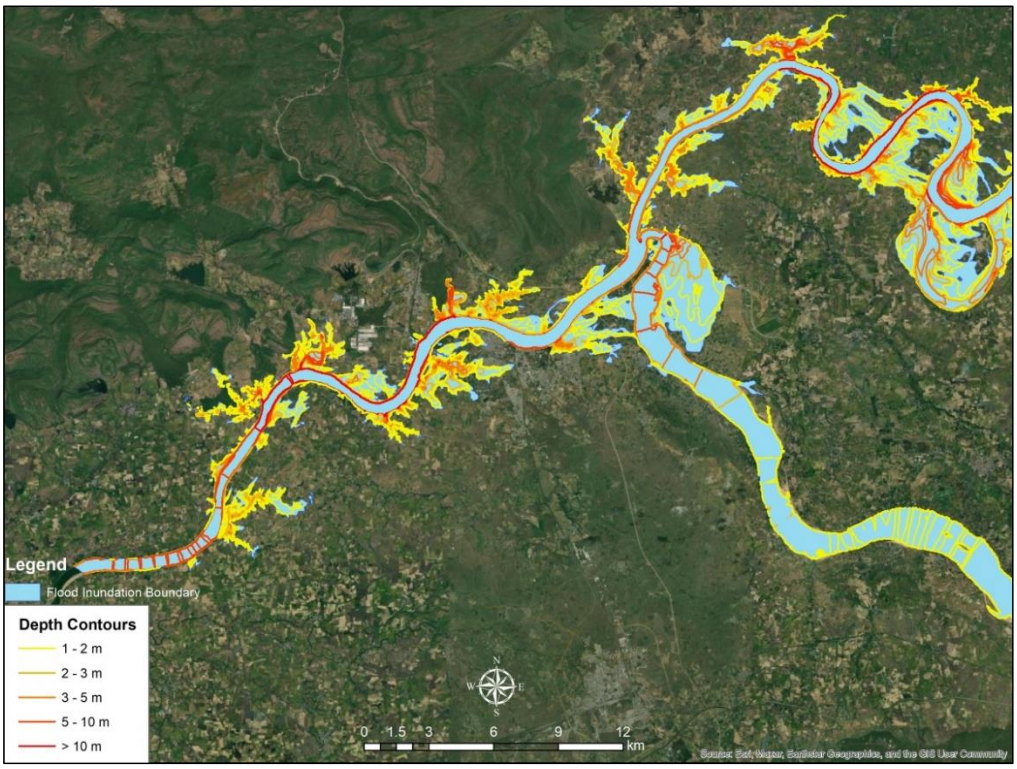

Figure 5.133: Depth contour map for Barna dam maximum spillway releases scenario

Figure 5.134: Water surface elevation map for Barna dam maximum spillway releases scenario

spillway capacity of 30800 cumecs, has been considered to be released in gradually increasing order, while no releases have been considered from other two dams of Bargi and Barna. By doing this the impact of maximum releases from Tawa dam can be mapped at Sethani Ghat in Hoshangabad. Moreover, as Tawa dam is located nearest to the Sethani Ghat and Hoshangabad, and also has a large spillway capacity, its influence is seen to be maximum on the downstream floods. This was observed based on the simulations based on actual releases from these three dams and was also confirmed from the project authorities too. The results of

the model simulations indicate that releases from Tawa dam have the maximum impacts among all the three major dams in Upper Narmada basin. The resultant flood water may enter the city as back water of Lediya Nala which may join the left bank of River Narmada again at Home Science PG College thus creating an island like situation near Sethani Ghat. The flood water will also enter along the Sukthwa River which may encroach up to the Abhimanyu Little Angels School in Kalika Nagar. The flood inundation map for the Tawa dam maximum spillway releases scenario is given in Figure 5.135.

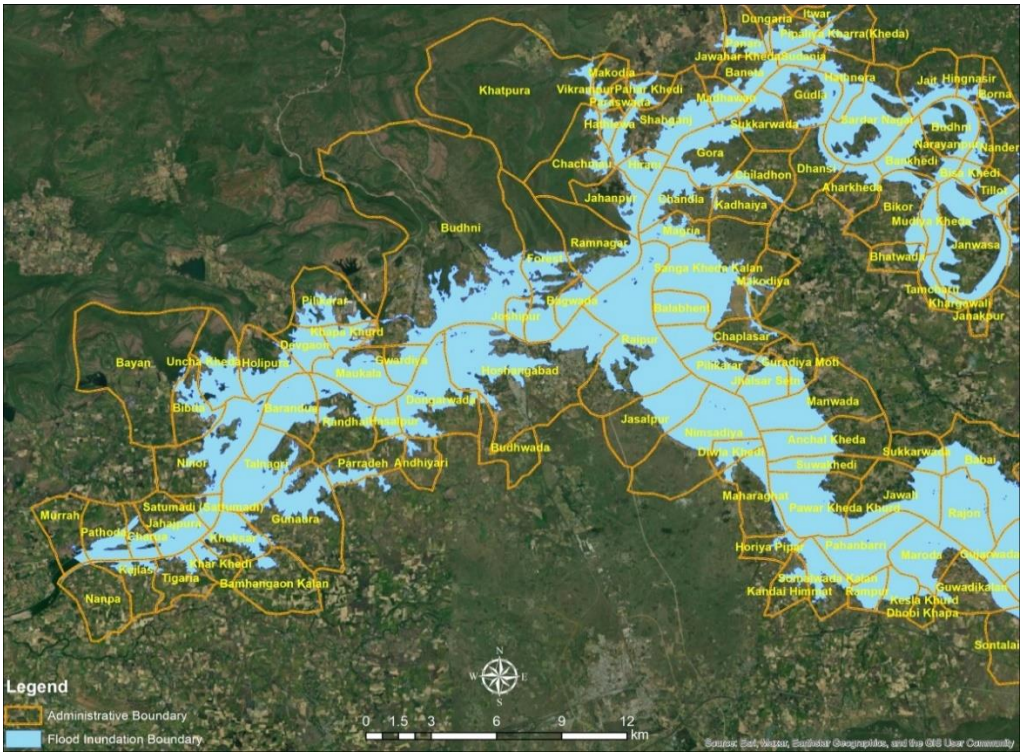

Figure 5.135: Flood inundation map for Tawa dam maximum spillway releases scenario

The water depth contours have been extracted from the model results at an interval of 1 m. The depth contours plotted for this hypothetical scenario for Tawa dam maximum releases, depicts that the maximum depths lie in the main river channel and in local nalas, while the water encroached in the city through Lediya Nala has the maximum depth of 3 m along the Nala. The flood water along Sukthwa River which reached up to the Abhimanyu little Angels School in Kalika Nagar has the maximum depth up to 1 m at Kalika Nagar and gradually gets deeper towards the confluence with the main River Narmada which has depth about 5 m before the confluence. The depth contours for the hypothetical Tawa dam maximum spillway releases scenario is given in Figure 5.136.

The water surface elevations has also been mapped for the Tawa dam maximum releases scenario. The maximum water surface level that may be achieved by the flood generated at Sethani Ghat in Hoshangabad was found to be 302 m above msl, while at the confluence of River Tawa and River Narmada at Bandrabhan it was found to be 303.5 m above msl. The water surface elevation map for Tawa dam maximum releases scenario is given in Figure 5.137.

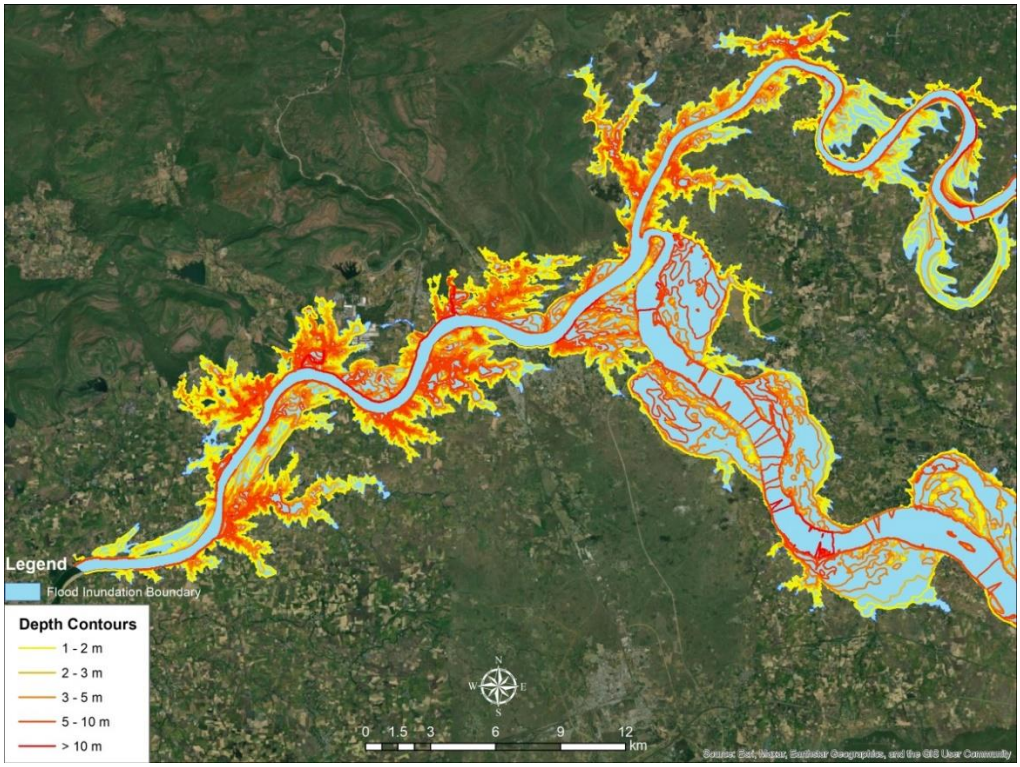

Figure 5.136: Depth contour map for Tawa dam maximum spillway releases scenario

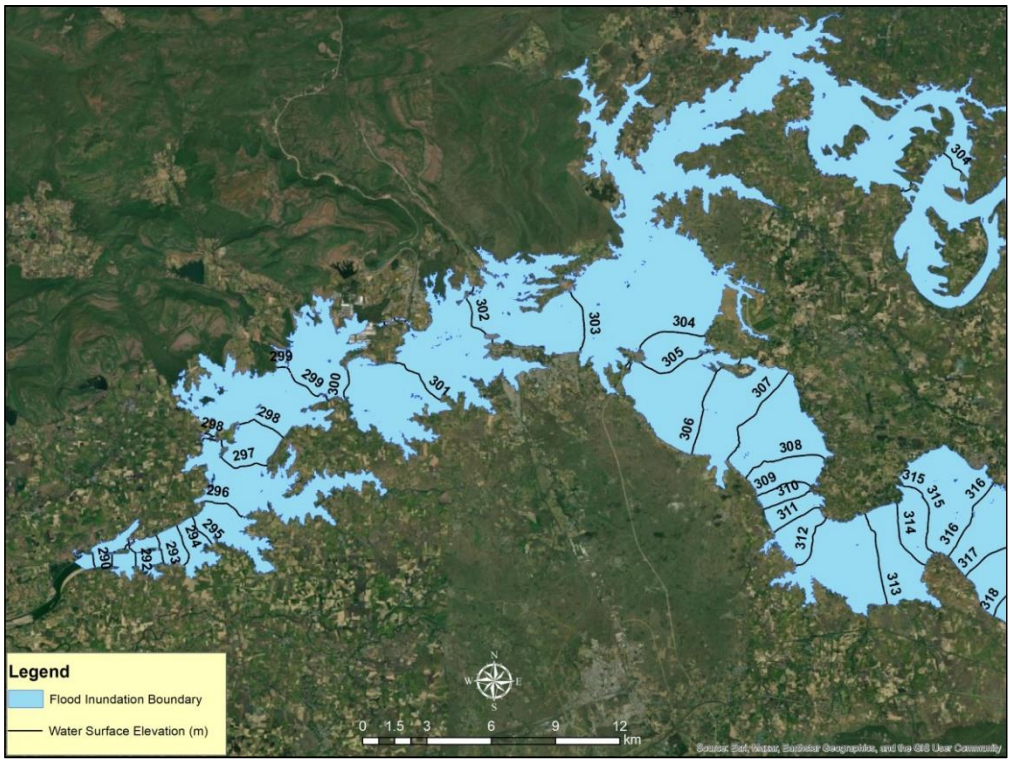

Figure 5.137: Water surface elevation map for Tawa dam maximum spillway releases scenario

The model simulations have thus been carried out for three actual flood events that caused heavy flooding in Hoshangabad and four interesting hypothetical what-if scenarios which may occur in future, if circumstances so warrant, even though the project authorities operate these dams in tandem to minimize the flood risk downstream at Hoshangabad. The comparison of the three actual flood events viz. flood of 06 August 2012, 23 August 2013 and 30 August 2020 indicates that all these three events are distinct but also do have some similarities between them. It can be observed that all these flood events occurred in August which is the time by which the reservoirs get filled-up to their maximum capacities subject to favorable inflows from good rainfall occurring during the months of June, July and August. Generally, to avoid devastating flood scenario downstream at Hoshangabad, the dam releases are carried out in a staggered manner. Also, depending on the rainfall and flood forecasts based on the rainfall occurring in the catchment, the dam storages are depleted accordingly in advance, so as to avoid all three dam releases reaching Hoshangabad at the same time. It takes considerable time for the flood waters released from Bargi dam to reach Sethani Ghat as compared to the flood releases from Barna and Tawa dams which are located much near to the flood area. The maximum flood impact is observed to be from the releases made from the Tawa dam during all the three major flood events that occurred at Hoshangabad.

The worst flood scenario occurred on August 23, 2013 when releases were made from all the three major reservoirs and flood waters reached up to the Jaystambh Chowk located in the main city in Hoshangabad along the Lediya Nala into the city for a distance of about 1.525 km from the left bank of River Narmada with the maximum water surface elevation of 299.5 m above msl at Sethani Ghat in Hoshangabad and 301.0 m above msl at Bandrabhan, the confluence of River Tawa and River Narmada. The second worst flood scenario occurred on August 30, 2020 when releases were made from Tawa and Bargi dams only and flood waters reached up to Anjuman Middle School in Hoshangabad along the Lediya Nala into the city for a distance of about 1.447 km from the left bank of River Narmada with the maximum water surface elevation of 299.0 m above msl at Sethani Ghat in Hoshangabad and 300.0 m above msl at Bandrabhan. The third worst flood scenario occurred on August 06, 2012 when releases were made from Tawa and Barna dams

only and flood waters reached up to Mangalwara Ghat road near Dussehra Maidan in Hoshangabad along the Lediya Nala into the city for a distance of about 1.20 km from the left bank of River Narmada with the maximum water surface elevation of 297.5 m above msl at Sethani Ghat in Hoshangabad.

The four hypothetical what-if scenarios were also considered. The first hypothetical scenario was what would be the flood scenario at Hoshangabad, if such a situation arose wherein the staggering of releases from the three dams was not possible due the dams being at FRL with regular inflows coming into the reservoirs due to the incessant rainfall occurring in the catchments of these dams. The simulation results showed that the resultant flood water can reach up to the Jaystambh Chowk in Hoshangabad along the Lediya nala and also up to Pahadiya Road near Narayan Nagar in Hoshangabad along the dried Sukthwa River with water elevation of 300.5 m above msl at Sethani Ghat and 301.5 m above msl at Bandrabhan. The other three scenarios were simulated to understand as to what would happen if all the gates of only one reservoir was opened. It can be seen that there would be severe flooding at Hoshangabad in all these scenarios with formation of islands in the areas in the vicinity of the main river and through backwater effects from Lediya nala and Sukthwa River. However, the worst condition will be encountered, if ever, all the gates of Tawa dam were to be opened.

To minimize the chances of occurrence of such flood events both non-structural and structural measures need to be considered. The non-structural measures include flood management through development of real-time flood forecasting and early warning systems with short-period lead times (3 to 5 days), supervisory control and data acquisition (SCADA) systems for gate openings, modernization in collection of real-time hydrometeorological data, updating of reservoir rule-curves in accordance with the changing rainfall and demand patterns, flood proofing, emergency preparedness, response and recovery and learning (adapt) and adjust accordingly to live with floods through land regulations and other measures. The integrated operation of reservoirs for flood control can provide realistic solutions to the flooding problem at Hoshangabad.

The structural measures can include removal of the obstruction in the pathway of free flow of water in the main river downstream of the study area near

Gwari Ghat, structural measures to protect long stretches of the Tawa river banks which is prone to both soil erosion and silt deposition, remove encroachments in the natural detention basins and all along the flood plains prone to regular flooding, prohibition of unplanned development in wetlands and natural depressions and studying the possibility of inter-basin transfer of flood water to other river basins in Ganga, Wainganga or Tapti river systems based on detailed feasibility studies.

5.12 Water Allocation Planning and Management

Another capability of the WEAP model is that it can be used for water allocation planning based on the future water availability and future water demands. There are two major categories of demands in the study area viz., domestic and agricultural water demand. The domestic water requirement and the water needs of the livestock have been projected for the future time periods using the Logistic curve method. The projections for the future domestic demands is based on the census data of 1991, 2001 and 2011 whereas the projections for the future livestock demands is based on the livestock census of 2007, 2012 and 2017. The agricultural water requirement which is the other major water demand which needs to be categorized depending on the available water sources and their water availability for fulfilling the agriculture water demands. The agricultural land in the study area has been mapped into following types for the catchments of the various gauging sites viz., a) agriculture in the command area being fed through reservoir releases, b) cropped areas nearby and adjoining the streams and rivers, and c) groundwater fed agricultural area falling outside the command areas.

The three major dams existing the study area namely Bargi reservoir, Tawa reservoir and Barna dam have their canal command network in many of the sub-catchments of various gauging sites located in the study area. The agricultural land intersecting with the canal command network has been mapped as canal command area. The agricultural land near by the stream considered as the ‘river water take-off area’ limited to a distance of 200 m from the stream, for which pumping of river water is economically feasible too. The remaining agricultural land is taken as the area which needs to be irrigated through groundwater. The catchment wise details of these categorized agricultural lands are provided below.

The Dindori sub-catchment has total agricultural area of 112583 ha, out of which 109526 ha requires to be irrigated through groundwater, while the remaining 3057 ha agricultural area uses water directly from river water take-off. There is no command area of any dam falling in this catchment. The Manot sub-catchment has total agricultural area of 168026 ha, out of which 163568 ha needs to be irrigated by groundwater, while the remaining 4458 ha uses water directly from river water take-off. There is no command area of any dam falling in this catchment. Mohgaon sub-catchment has total agricultural area of 177725 ha, out of which 173782 ha needs irrigated through groundwater source, while 3943 ha agricultural area uses water directly from river water take-off. In this catchment too, there is no command area of any dam. Belkheri sub-catchment has total agricultural area of 100509 ha, out of which 98083 ha requires to be irrigated through groundwater source. The remaining 2426 ha agricultural area uses water directly from river water take-off. In Belkheri catchment also, there is no command area of any dam. The agricultural lands categorized in Dindori, Manot, Mohgaon, Belkheri, Patan, Barmanghat, Gadarwara, Sandia and Hoshangabad sub-catchments is shown in Figure 5.138.

Patan sub-catchment has total agricultural area of 246395 ha, out of which 205278 ha needs to be irrigated through groundwater and the remaining 4388 ha uses water directly from river water take-off. In Patan sub-catchment, there is existence of canal command network of Bargi dam, which irrigates 36729 ha of area of the sub-catchment. The individual sub-catchment at Barmanghat has total agricultural area of 543460 ha, out of which 338261 ha need irrigation from groundwater and 3386 ha agricultural area uses water directly from river water take-off. As the Barmanghat sub-catchment is located at the downstream of Bargi dam, the agricultural area under the canal command network is 201813 ha. The Gadarwara sub-catchment has total agricultural area of 156189 ha, out of which 144072 ha needs irrigation through groundwater source, 7764 ha comes under the canal command network of Bargi dam and the remaining 4353 ha uses water

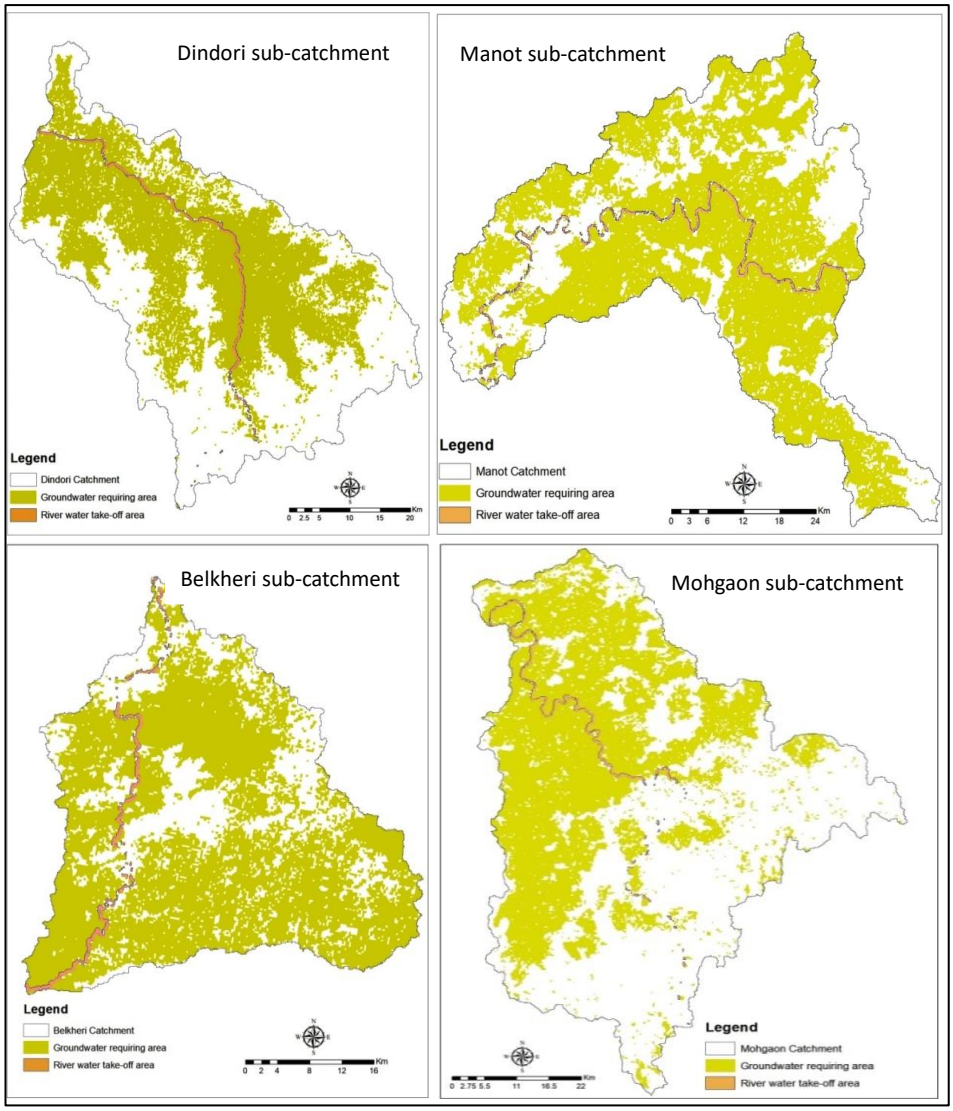

Figure 5.138: Agricultural land categorized in Dindori, Manot, Belkheri and Mohgaon sub-catchments

directly from river water take-off.

The individual sub-catchment of Sandia has total agricultural area of 292161 ha, out of which 235883 ha requires to be irrigated through groundwater, 1730 ha through water directly from river water take-off. Apart from this the Sandia catchment has a canal command network of both Bargi and Tawa dams, which in total cover 54548 ha of individual sub-catchment area of Sandia. The Hoshangabad sub-catchment has its individual agricultural area of 653049 ha. Within this, 448784 ha is irrigated through groundwater, 6280 ha through water directly from river water take-off, while 197985 ha comes under the canal command network of Tawa and Barna dams. The agricultural lands categorized in Patan, Barmanghat, Gadarwara, Sandia and Hoshangabad sub-catchments is shown in Figure 5.139. The combined

agricultural land categorized for the whole Upper Narmada basin up to Hoshangabad is given in Figure 5.140.

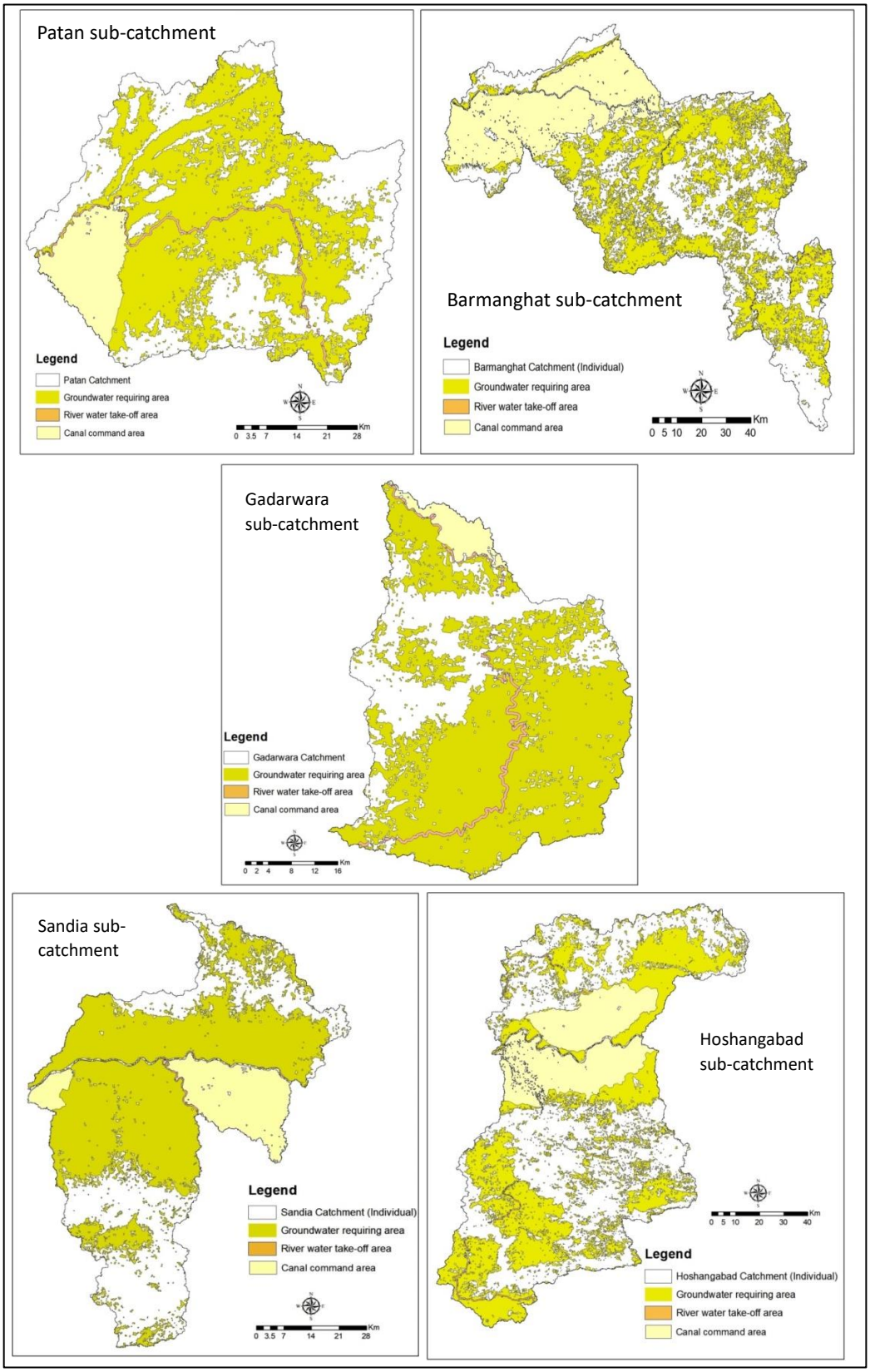

Figure 5.139: Agricultural land categorized in Patan, Barmanghat, Gadarwara, Sandia and Hoshangabad sub-catchments

The supply and demand analysis has been performed using WEAP with the agricultural, domestic and livestock water demands in the sub-catchment areas of the gauging sites located at tributaries and the main river up to Hoshangabad. The analysis for agricultural demand and supply has been performed separately considering two scenarios viz., a) with soybean and wheat as kharif and rabi crops respectively and b) with paddy as kharif crop and wheat as rabi crop. These two scenarios have been considered as a major shift is seen in the cropping pattern with soyabean being replaced by paddy extensively in many sub-catchments particularly in command areas and where abundant groundwater is available. The supply-demand analysis has been carried out separately for the domestic sector and livestock sector. The analysis has been performed for five time zones viz., baseline (1961-1990), present (1991-2019), near-term (2020-2040), mid-term (2041-2070), and end-term (2071-2100) for the two future climate scenarios viz., SSP245 and SSP585.

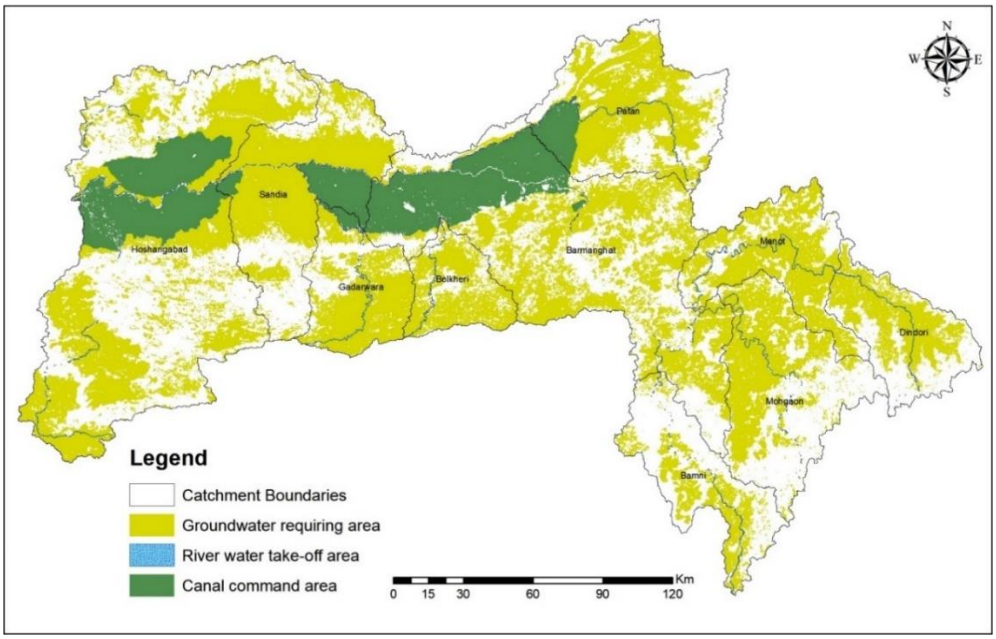

Figure 5.140: Agricultural land categorized in Upper Narmada basin up to Hoshangabad

5.12.1 Supply-Demand Scenario in Agricultural Sector

5.12.1.1 Soyabean–Wheat Scenario

The annual average **'agricultural water demand'** for 'soybean–wheat' scenario for the headwater sub-catchments under SSP245 and SSP585 future climate scenarios is given in Table 5.25. It has been observed that the agricultural

demand in case of 'soybean–wheat' scenario is highest during the present time period (1991-2019) for all the sub-catchments in the study area. A decreasing trend in agricultural water demand is observed for all future time periods due to higher effective rainfall availability for crop water requirement as a consequence of higher rainfall projected for future time periods.

The agricultural water demands for the soyabean-wheat combination are the highest in Gadarwara sub-catchment with 1450.04 MCM during the baseline which is projected to vary between 1233.46 MCM to 1295.08 MCM during future time periods under SSP245 scenario and is projected to vary between 1182.08 MCM to 1276.82 MCM during future time periods under SSP585 scenario. The agricultural water demands for the soyabean-wheat combination are lowest in Belkheri sub-catchment which varied between 491.30 MCM during baseline period and 514.72 MCM during the present period and projected to vary between 424.09 MCM to 444.80 MCM during future time periods under SSP245 scenario and is also projected to vary between 405.22 MCM to 442.84 MCM during the future time periods under SSP585 scenario. A similar scenario is seen for the sub-catchments on the main river system with the maximum irrigation water demands at Hoshangabad sub-catchment and minimum demand at Barmanghat sub-catchment. Also, the water demands are higher in case of SSP245 future climate scenario as compared to SSP85 scenario during all future time periods. The comparison of the agricultural water demand in the headwater sub-catchments under SSP245 future climate scenario is provided in Figure 5.141.

Table 5.25: Annual average water demand for 'soybean–wheat' scenario in the headwater sub-catchments under SSP245 and SSP585 future climate scenarios

(in MCM)	Dindori	Manot	Mohgaon	Belkheri	Patan	Gadarwara
Baseline (1961-1990)	477.60	626.26	757.38	491.30	1691.78	1450.04
Present (1991-2019)	512.45	672.08	822.76	514.72	1704.50	1475.98
SSP245						
Near-term (2020-2040)	448.03	561.28	681.62	444.80	1527.47	1295.08
Mid-term (2041-2070)	442.43	566.83	671.77	434.42	1466.02	1278.78

End-term (2071-2100)	432.18	553.20	665.25	424.09	1443.64	1233.46
SSP585						
Near-term (2020-2040)	447.10	564.47	684.53	442.84	1527.04	1276.82
Mid-term (2041-2070)	439.67	556.00	671.55	415.97	1425.17	1258.83
End-term (2071-2100)	421.41	544.24	652.34	405.22	1418.50	1182.08

 # All units are in MCM

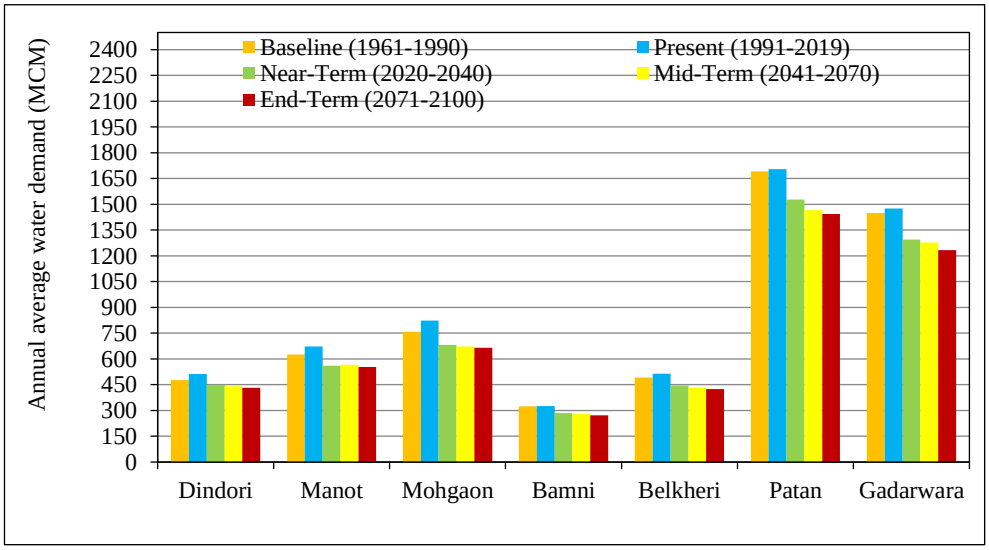

Figure 5.141: Annual average water demand for 'soybean–wheat' scenario in headwater sub-catchments under SSP245 future climate scenario

The average annual **'agricultural supply delivered'** for 'soybean–wheat' scenario for the headwater river sub-catchments is given in Table 5.26 and for main river sub-catchments in Table 5.27 under SSP245 and SSP585 future climate scenarios. It can be observed that the water supply delivered at Dindori can meet he full agricultural water demands, whereas marginal shortfalls limited to a maximum of 5 to 6% have been observed Manot, Mohgaon, Belkheri and Patan sub-catchments. The water supplies delivered for agricultural demand in case of 'soybean–wheat' scenario is lowest in Gadarwara sub-catchment during the present time period (1991-2019) which is about 44%. However, the water supplies are projected to improve in future time periods in Gadarwara sub-catchment with 50 to 55% under SSP245 scenario and 51 to 60% under SSP585 scenario.

Table 5.26: Annual average supply delivered for 'soybean–wheat' scenario in headwater sub-catchments under SSP245 and SSP585 future climate scenarios

(in %)	Dindori	Manot	Mohgaon	Belkheri	Patan	Gadarwara
Baseline (1961-1990)	100.0	100.00	99.53	100.00	94.87	44.43
Present (1991-2019)	100.0	100.00	100.00	100.00	100.0	43.61
SSP245						
Near-term (2020-2040)	100.0	98.46	97.39	99.20	93.57	50.25
Mid-term (2041-2070)	100.0	96.23	98.17	100.00	100.0	50.25
End-term (2071-2100)	100.0	94.22	95.49	96.62	98.53	54.03
SSP585						
Near-term (2020-2040)	100.0	98.97	97.93	99.50	93.14	51.77
Mid-term (2041-2070)	100.0	96.15	98.17	100.00	100.0	51.17
End-term (2071-2100)	100.0	94.12	95.40	96.47	98.51	59.86

 # All units are in %

Table 5.27: Annual average supply delivered for 'soybean–wheat' scenario in the main river sub-catchments using SSP245 and SSP585 future climate scenarios

Time period	Barmanghat	Sandia	Hoshangabad
Baseline (1961-1990)	95.87	89.15	90.22
Present (1991-2019)	100.00	93.25	94.56
SSP245			
Near-Term (2020-2040)	94.07	88.16	89.11
Mid-Term (2041-2070)	99.58	93.66	94.87
End-Term (2071-2100)	98.75	93.57	94.79
SSP585			
Near-Term (2020-2040)	94.11	88.38	89.28
Mid-Term (2041-2070)	99.56	93.69	94.89
End-Term (2071-2100)	98.71	94.26	95.35

 # All units are in %

Similarly, small shortfalls in water supply are also noticed in Sandia and Hoshangabad sub-catchments which varies at Sandia sub-catchment between 89.2% during baseline period and 93% during the present period which is projected to increase to 93.6% during the end-term under SSSP245 scenario and 94.3%

during the end term under SSP585 scenario. The water supplies are projected to improve in all future time zones under both SSP245 and SSP585 future climate scenarios with higher water supplies that can be delivered under SSP585 future climate scenario.

The annual average **'unmet agricultural demands'** for the agricultural demand in 'soybean–wheat' scenario for the headwater river catchments is given in Table 5.28 and given in Table 5.29 for the main river sub-catchments under SSP245 and SSP585 climate scenarios. It can be observed that there are no unmet agricultural demands at Dindori sub-catchment during any time periods. Marginal unmet agricultural demands at projected for all future time periods at Manot, Mohgaon, and Belkheri sub-catchments. Marginally higher unmet agricultural demands have been observed during the baseline period (5.13%) and projected to vary between 1 to 7% under both future climate scenarios.

Table 5.28: Annual average unmet demand for 'soybean–wheat' scenario in the headwater sub-catchments under SSP245 and SSP585 future climate scenarios

(in %)	Dindori	Manot	Mohgaon	Belkheri	Patan	Gadarwara
Baseline (1961-1990)	0.00	0.00	0.47	0.00	5.13	55.57
Present (1991-2019)	0.00	0.00	0.00	0.00	0.00	56.39
SSP245						
Near-term (2020-2040)	0.00	1.53	2.61	0.80	6.43	49.75
Mid-term (2041-2070)	0.00	3.77	1.83	0.00	0.00	49.75
End-term (2071-2100)	0.00	5.78	4.51	3.38	1.46	45.97
SSP585						
Near-term (2020-2040)	0.00	1.03	2.07	0.51	6.86	48.23
Mid-term (2041-2070)	0.00	3.85	1.83	0.00	0.00	48.83
End-term (2071-2100)	0.00	5.88	4.60	3.54	1.49	40.14

 # All units are in %

Table 5.29: Annual average unmet demand for 'soybean–wheat' scenario in the main river sub-catchments under SSP245 and SSP585 future climate scenarios

(in %)	Barmanghat	Sandia	Hoshangabad
Baseline (1961-1990)	4.13	10.85	9.78
Present (1991-2019)	0.00	6.75	5.44
SSP245			
Near-Term (2020-2040)	5.93	11.84	10.89
Mid-Term (2041-2070)	0.42	6.34	5.13
End-Term (2071-2100)	1.25	6.43	5.21
SSP585			
Near-Term (2020-2040)	5.89	11.62	10.72
Mid-Term (2041-2070)	0.44	6.31	5.11
End-Term (2071-2100)	1.29	5.74	4.65

 # All units are in %

The unmet agricultural demand in case of 'soybean–wheat' scenario is highest in Gadarwara sub-catchment during the present time period (1991-2019) which is around 56% of the water requirement. However, the unmet agricultural demands are projected to get lower in all future time zones and decrease up to 40% during the end-term (2071-2100) in Gadarwara sub-catchment. The unmet demands are higher in Gadarwara sub-catchment as compared to other catchments and varies between 40% and 56% of the water requirement while unmet demand in other sub-catchments varies only between 0 to 11%. It is also due to the reason that Gadarwara sub-catchment has practically no canal command and is located on a tributary river, which has its major flows only during monsoon season. It also has dense population as a big town of Gadarwara is located within it, raising a considerable domestic and livestock water demands apart from the agricultural water requirements. It has also been noticed that the unmet demands are projected to be lower under SSP585 scenario. The comparison of the annual average unmet demands for main river sub-catchments under SSP245 future climate scenario is given in Figure 5.142.

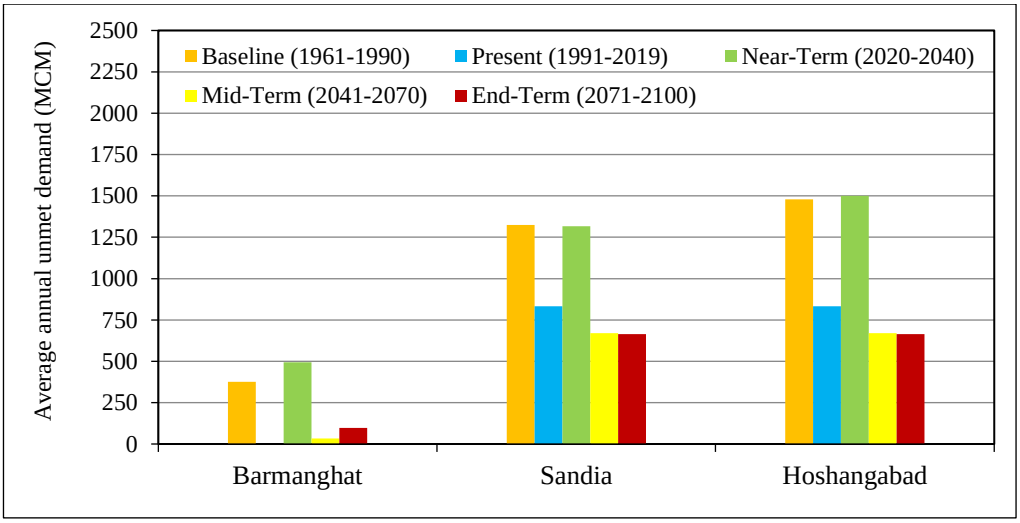

Figure 5.142: Annual average unmet demand for 'soybean–wheat' scenario in the main river catchments under SSP245 future climate scenario

5.12.1.2 Paddy – Wheat Scenario

The annual average **'agricultural water demand'** for 'paddy–wheat' scenario for the headwater sub-catchments under SSP245 and SSP585 future climate scenarios is given in Table 5.30. It has been observed that the agricultural water demand for the 'paddy-wheat' scenario is highest during present time period (1991-2019) for all the sub-catchments in the study area. A decreasing trend in agricultural water demand is observed for all future time periods due to higher effective rainfall availability for crop water requirement as a consequence of higher rainfall projected for future time periods.

The agricultural water demands for the paddy-wheat combination are the highest in Patan sub-catchment with 1708.70 MCM during the baseline period and 1737.77 MCM during the present period which is projected to vary between

Table 5.30: Annual average water demand for 'paddy–wheat' scenario in the headwater sub-catchments under SSP245 and SSP585 future climate scenarios

Time period	Dindori	Manot	Mohgaon	Belkheri	Patan	Gadarwara
Baseline (1961-1990)	486.26	642.09	770.51	501.91	1708.7	1478.72
Present (1991-2019)	530.01	677.11	857.33	526.34	1737.77	1491.15
SSP245						
Near-Term (2020-2040)	456.39	575.99	698.22	458.37	1550.54	1309.68

Mid-Term (2041-2070)	454.19	585.02	693.27	447.32	1487.71	1291.66
End-Term (2071-2100)	442.58	570.10	683.62	447.81	1487.72	1246.52
SSP585						
Near-Term (2020-2040)	457.03	579.63	696.75	452.50	1541.41	1288.69
Mid-Term (2041-2070)	448.90	573.15	692.44	425.94	1452.12	1271.47
End-Term (2071-2100)	430.32	560.57	668.48	427.94	1451.82	1195.25

 # All units are in MCM

1487.72 MCM to 1550.54 MCM during future time periods under SSP245 scenario and is projected to vary between 1451.82 MCM to 1541.41 MCM during future time periods under SSP585 scenario. The agricultural water demands for the soyabean-wheat combination are lowest in Belkheri sub-catchment which varied between 501.91 MCM during baseline period and 526.34 MCM during the present period and projected to vary between 447.81 MCM to 458.37 MCM during future time periods under SSP245 scenario and is also projected to vary between 427.94 MCM to 452.50 MCM during the future time periods under SSP585 scenario. A similar scenario is seen for the sub-catchments on the main river system with the maximum irrigation water demands at Hoshangabad sub-catchment and minimum demand at Barmanghat sub-catchment. Also, the agricultural water demands are lower under SSP585 future climate scenario as compared to SSP245 scenario for all future time periods. The comparison of the agricultural water demand in the headwater sub-catchments under SSP245 future climate scenario is provided in Figure 5.143.

The average annual **'agricultural supply delivered'** for 'paddy–wheat' scenario for the headwater river sub-catchments is given in Table 5.31. It can be observed that for the 'paddy-wheat' scenario, the water supply delivered at Dindori can meet the full agricultural water demands, whereas marginal shortfalls limited to a maximum of 5 to 8% have been observed Manot, Mohgaon, Belkheri and Patan sub-catchments. The supply delivered is lowest for the Gadarwara sub-catchment during the present time period (1991-2019), which is only about 42%

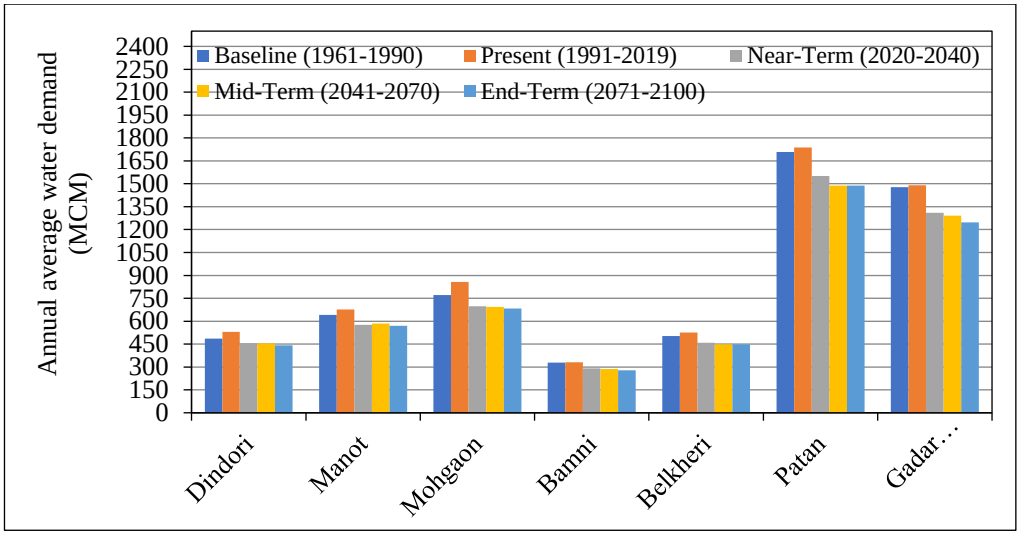

Figure 5.143: Annual average water demand for 'paddy–wheat' scenario in the headwater sub-catchments under SSP245 future climate scenario

of the agricultural water requirement during the baseline and present time periods. However, the water supplies are projected to improve in all future time periods in Gadarwara sub-catchment with 49 to 53% under SSP245 scenario and 50 to 59% under SSP585 scenario.

Table 5.31: Annual average supply delivered for 'paddy–wheat' scenario in the headwater sub-catchments under SSP245 and SSP585 future climate scenario

Time period	Dindori	Manot	Mohgaon	Belkheri	Patan	Gadarwara
Baseline (1961-1990)	100.0	100.0	99.54	100.0	94.92	42.63
Present (1991-2019)	100.0	100.0	100.00	100.0	100.0	42.16
SSP245						
Near-Term (2020-2040)	100.0	97.60	97.23	99.10	93.67	49.24
Mid-Term (2041-2070)	100.0	95.14	97.12	100.0	100.0	49.15
End-Term (2071-2100)	100.0	93.20	94.82	92.55	96.18	52.85
SSP585						
Near-Term (2020-2040)	100.00	97.84	97.66	99.49	93.18	50.81
Mid-Term (2041-2070)	100.00	95.04	97.12	100.00	100.00	50.14
End-Term (2071-2100)	100.00	93.08	94.71	92.21	96.08	58.67

 # All units are in %

The average annual 'agricultural supply delivered' for 'paddy–wheat' scenario for main river sub-catchments is given in Table 5.32 under SSP245 and SSP585 future climate scenarios Similarly, small shortfalls in water supply are also noticed in Sandia and Hoshangabad sub-catchments which varied at Sandia sub-catchment between 89% during baseline period and 93% during the present period and is projected to be 92.8% during the end-term under SSSP245 scenario and 93.5% during the end-term under SSP585 scenario. The shortfall in the Hoshangabad catchment varied between 90% during baseline period and 95% during the present period and is projected to be 94.2% during the end-term under SSSP245 scenario and 94.7% under SSP585 scenario during the end-term.

Table 5.32: Annual average supply delivered for 'paddy–wheat' scenario in the main river sub-catchments under SSP245 and SSP585 future climate scenario

Time period	Barmanghat	Sandia	Hoshangabad
Baseline (1961-1990)	95.92	88.98	90.09
Present (1991-2019)	100.00	93.11	94.48
SSP245			
Near-Term (2020-2040)	94.08	88.11	89.10
Mid-Term (2041-2070)	99.40	93.45	94.71
End-Term (2071-2100)	97.94	92.89	94.23
SSP585			
Near-Term (2020-2040)	94.09	88.32	89.27
Mid-Term (2041-2070)	99.39	93.49	94.73
End-Term (2071-2100)	97.86	93.51	94.74

 # All units are in %

The annual average **'unmet agricultural demands'** for the agricultural demand in 'paddy–wheat' scenario for the headwater river catchments is given in Table 5.33 and given in Table 5.34 for the main river sub-catchments under SSP245 and SSP585 climate scenarios. It can be observed that there are no unmet agricultural demands at Dindori sub-catchment during any time periods. Marginal

unmet agricultural demands at projected for all future time periods at Manot, Mohgaon, Belkheri and Patan sub-catchments.

The unmet demands in case of 'paddy–wheat' scenario are higher in Gadarwara sub-catchment as compared to other catchments and varies between 40% and 56% of the water requirement while unmet demand in other sub-catchments varies only between 0 to 11%. The unmet demands are highest in Gadarwara sub-catchment as compared to other catchments and varies between 42% and 58% of the water requirement while unmet demand in other sub-catchments varies only between 0 to 8%. The unmet agricultural demand is highest in Gadarwara sub-catchment during the present time period (1991-2019)

Table 5.33: Annual average unmet demand for paddy – wheat scenario in headwater sub-catchments under SSP245 and SSP585 future climate scenarios

Time period	Dindori	Manot	Mohgaon	Belkheri	Patan	Gadarwara
Baseline (1961-1990)	0.00	0.00	0.46	0.00	5.08	57.37
Present (1991-2019)	0.00	0.00	0.00	0.00	0.00	57.84
SSP245						
Near-Term (2020-2040)	0.00	2.40	2.77	0.90	6.33	50.76
Mid-Term (2041-2070)	0.00	4.86	2.88	0.00	0.00	50.85
End-Term (2071-2100)	0.00	6.80	5.18	7.44	3.82	47.15
SSP585						
Near-Term (2020-2040)	0.00	2.16	2.34	0.51	6.82	49.19
Mid-Term (2041-2070)	0.00	4.96	2.88	0.00	0.00	49.86
End-Term (2071-2100)	0.00	6.92	5.29	7.79	3.92	41.33

 # All units are in %

Table 5.34: Annual average unmet demand for paddy–wheat scenario in the main river sub-catchments under SSP245 and SSP585 future climate scenarios

Time period	Barmanghat	Sandia	Hoshangabad
Baseline (1961-1990)	4.08	11.02	9.91
Present (1991-2019)	0.00	6.89	5.52
SSP2-45			

Near-Term (2020-2040)	5.92	11.89	10.90
Mid-Term (2041-2070)	0.60	6.55	5.29
End-Term (2071-2100)	2.06	7.11	5.77
SSP5-85			
Near-Term (2020-2040)	5.91	11.68	10.73
Mid-Term (2041-2070)	0.61	6.51	5.27
End-Term (2071-2100)	2.14	6.49	5.26

 # All units are in %

which is around 58% of the water requirement. However, for the future time zones, unmet agricultural demands are lower in the Gadarwara sub-catchment as compared to the baseline period, lowest being during the end-term under both scenarios. The comparison of the annual average unmet demands for main river sub-catchments under SSP245 future climate scenario is given in Figure 5.144.

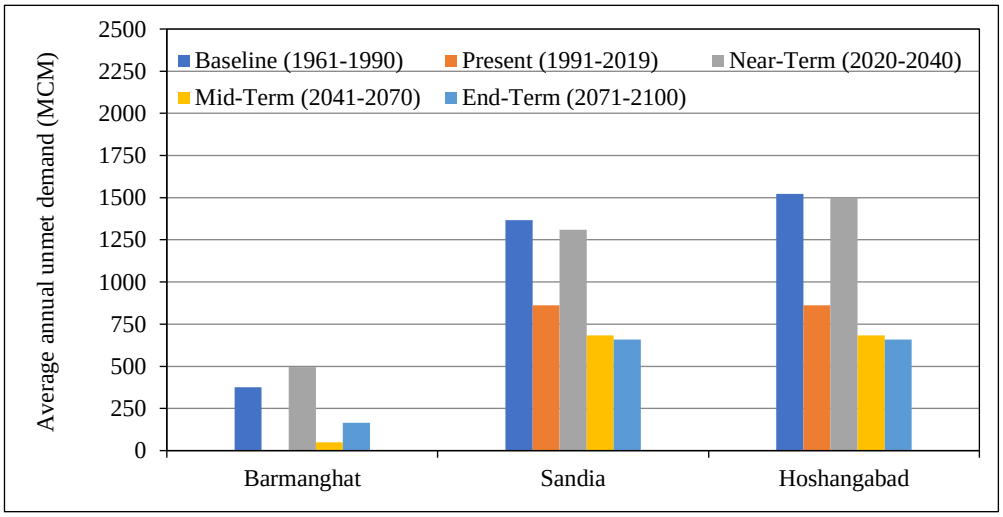

Figure 5.144: Annual average unmet demand for paddy – wheat scenario in the main river catchments under SSP585 future climate scenario

The cropping pattern in the various sub-catchments of the Upper Narmada basin is fast changing with more and more areas coming under paddy cultivation which is also a water intensive crop and requires substantial quantum of water. The command areas have not been designed to cater to the kharif water demands for paddy except for Barna reservoir which supplies water for kharif crop depending on the status of the available storage and inflows during the monsoon season. Even though the crop water requirements of the paddy crop are much higher than the soyabean crop, but owing to the projections of higher rainfall in all future time periods under both future climate scenarios, there are only marginal shortfalls in

meeting the demands except at headwater catchment Gadarwara that has limitations of both surface and groundwater due to which less water intensive crops are grown there. The agricultural water demands in most of the other headwater and main river catchments can be satisfied with the existing water infrastructure, river flows and groundwater.

5.12.2 Supply-Demand Scenario in Domestic Sector

The annual average **'domestic water demand'** in the headwater sub-catchments is given in Table 5.35 and given in Table 5.36 for the main river sub-catchments, under both SSP245 and SSP585 climate scenarios. It can be observed

Table 5.35: Annual average water demand for domestic needs in the headwater sub-catchments under SSP245 and SSP585 scenarios

Time period	Dindori	Manot	Mohgaon	Belkheri	Patan	Gadarwara
Baseline (1961-1990)	7.06	7.39	7.73	4.24	45.56	5.74
Present (1991-2019)	13.56	14.18	14.84	8.14	87.48	11.02
SSP245 & SSP585						
Near-term (2020-2040)	19.58	20.48	21.43	11.75	126.4	15.91
Mid-term (2041-2070)	23.96	25.06	26.22	14.38	154.6	19.47
End-term (2071-2100)	26.67	27.90	29.19	16.01	172.1	21.67

 # All units are in MCM

Table 5.36: Annual average water demand for domestic needs in the main river sub-catchments under SSP245 and SSP585 scenarios

Time period	Barmanghat	Sandia	Hoshangabad
Baseline (1961-1990)	115.07	139.05	180.51
Present (1991-2019)	220.95	267.00	346.60
SSP245 and SSP585			
Near-term (2020-2040)	319.13	385.64	500.62
Mid-term (2041-2070)	390.49	471.88	612.57
End-term (2071-2100)	434.69	525.29	681.90

 # All units are in MCM

that the water requirement for domestic needs is increasing continuously during each time period due to population growth in all sub-catchments. As such it is projected to be maximum during the end-term (2071-2100). However, there is no difference in on the domestic water demands under both SSP245 and SSP585 climate scenarios, as domestic demands are only dependent on the population and per capita water requirement in each time period and is therefore same.

The domestic water demands are maximum in Patan sub-catchment which is projected to increase from 45.56 MCM during the baseline period to 172.10 MCM during the end-term due to the population growth in the villages, towns and major cities. One of the major city Jabalpur is located within the Patan sub-catchment. Similarly, the domestic water demands are lowest in Belkheri sub-catchment which is also the smallest sub-catchment and the domestic demand is projected to increase from 4.24 MCM during the baseline period to 16.01 MCM during the end-term.

For the main river sub-catchments, the domestic water demands are projected to increase from 115.07 MCM during the baseline period to 434.69 MCM during the end-term at Barmanghat sub-catchment, from 139.05 MCM during baseline period to 425.29 MCM during the end-term at Sandia sub-catchment and from 180.51 MCM during the baseline period to 681.90 MCM during the end-term at Hoshangabad sub-catchment. The comparison of the domestic water demand in headwater sub-catchments and for the main river sub-catchments are given in Figure 5.145 and Figure 5.146 respectively.

The annual average **'domestic supply delivered'** under SSP245 and SSP585 climate scenarios is given in Table 5.37 for the headwater sub-catchments. Based on the supplies delivered, it has been observed that the water supplies delivered for domestic purpose has met almost all the water demands in all sub-catchments during all the time periods except at Dindori sub-catchment. Full supplies could be delivered at Manot, Mohgaon, and Belkheri sub-catchments during the baseline and all future time periods. Marginal shortfalls in supplies are projected for Patan and Gadarwara sub-catchments. Dindori which is the most upstream sub-catchment of the Narmada River has the lowest supply delivered,

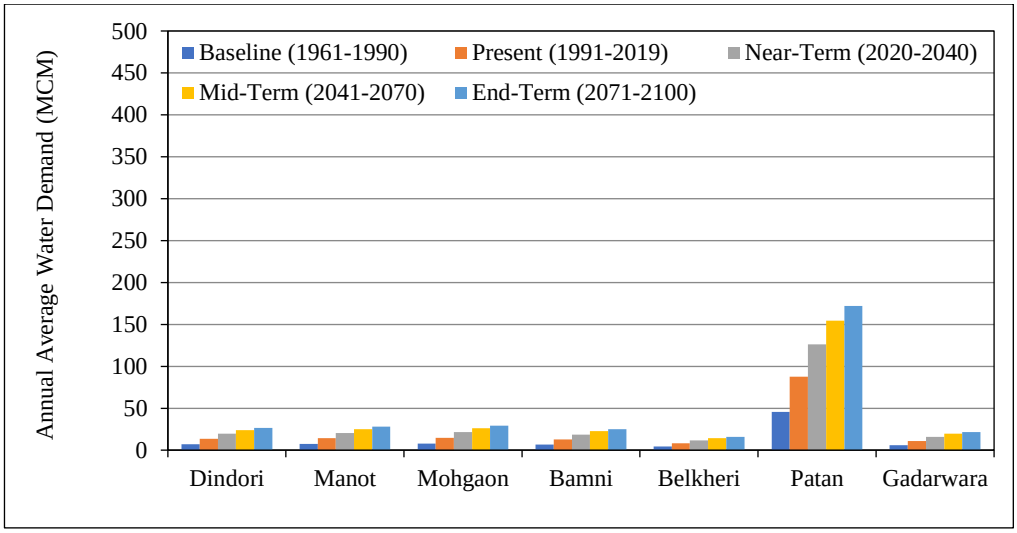

Figure 5.145: Annual average water demand for domestic needs in the headwater sub-catchments

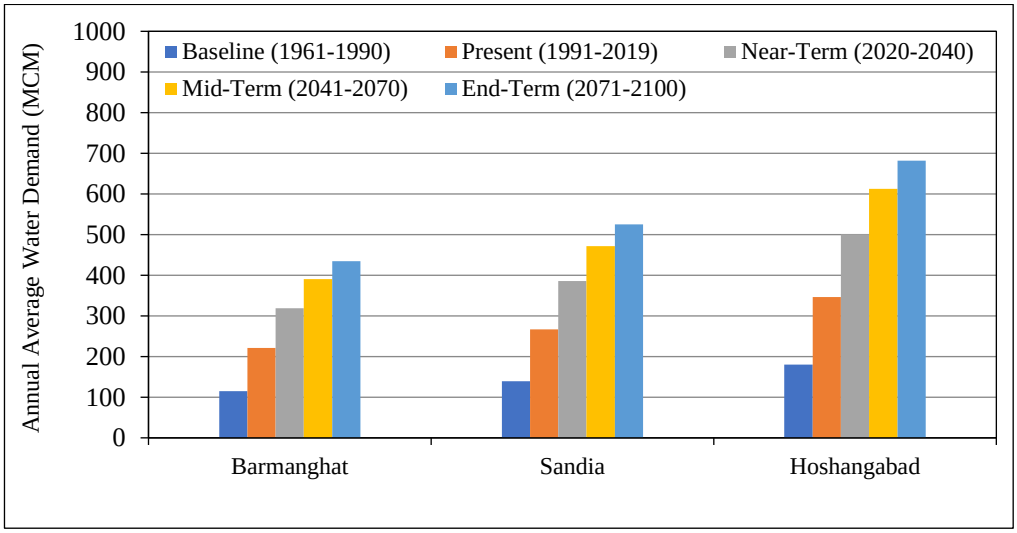

Figure 5.146: Annual average water demand for domestic needs in the main river sub-catchments

about 74% of the total domestic water demands. This may be due to the lack of sufficient water in the first to second order streams in the catchment area and also due to lack of sufficient groundwater availability as it is located on the hilly and undulating topography. The water supplies are marginally higher under SSP585 scenario as compared to SSP245 scenario. The comparison of the annual average water supplies delivered domestic needs for headwater sub-catchments under SSP245 climate scenario is given in Figure 5.147. Similarly, the comparison of the annual average water supplies delivered for headwater sub-catchments under SSP585 climate scenario are provided in Figure 5.148.

Table 5.37: Annual average supply delivered for domestic purpose using SSP245 and SSP585 in the headwater sub-catchments

Time period	Dindori	Manot	Mohgaon	Belkheri	Patan	Gadarwara
Baseline (1961-1990)	73.80	100.00	100.00	100.00	99.98	99.30
Present (1991-2019)	73.16	100.00	100.00	100.00	100.00	98.91
SSP245						
Near-term (2020-2040)	74.31	100.00	100.00	100.00	99.97	94.41
Mid-term (2041-2070)	73.16	100.00	100.00	100.00	100.00	94.04
End-term (2071-2100)	73.19	99.96	99.97	100.00	99.97	94.55
SSP585						
Near-term (2020-2040)	74.31	100.00	100.00	100.00	99.96	94.59
Mid-term (2041-2070)	73.16	100.00	100.00	100.00	100.00	94.09
End-term (2071-2100)	73.19	99.96	99.97	100.00	99.97	96.08

 # All units are in %

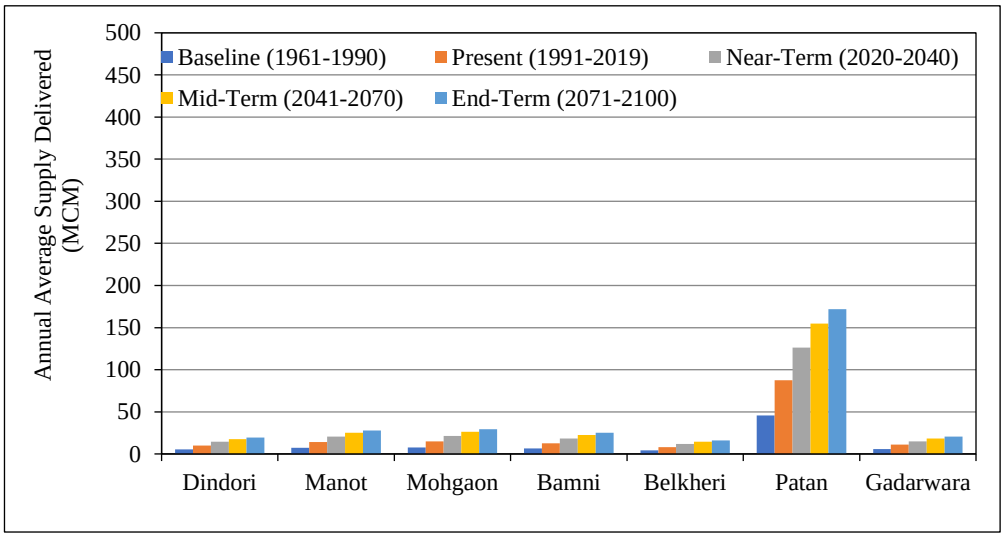

Figure 5.147: Annual average supply delivered for domestic purpose using SSP245 in the headwater sub-catchments

The annual average **'unmet domestic demands'** for the main river sub-catchments under SSP245 and SSP585 climate scenarios is given in Table 5.38. Diverse situation has been observed for the unmet demands for domestic needs in the various headwater sub-catchments. There are not unmet demands neither in the baseline and present periods nor projected for any of the future time periods. However, there is very marginal unmet demand at Patan sub-catchment varying between 0.02% during the baseline period and projected to vary between 0.02 and0.03% under both SSP245 and SSP585 scenarios. The unmet demand at Gadarwara is slightly higher and varied between 0.07% during the baseline period

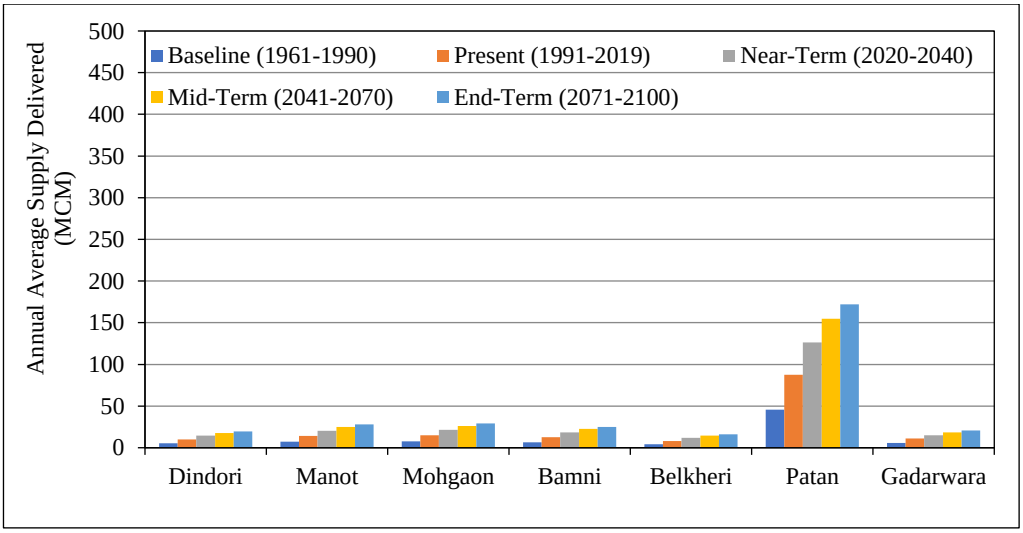

Figure 5.148: Annual average supply delivered for domestic purpose using SSP585 in the headwater sub-catchments

which increased marginally to 1.09% during the present period due to the actual increase in population.

Table 5.38: Annual average unmet demand for domestic needs in the main river sub-catchments under SSP245 and SSP585 scenarios

Time period	Barmanghat	Sandia	Hoshangabad
Baseline (1961-1990)	1.62	1.37	1.05
Present (1991-2019)	1.65	1.40	1.08
SSP245			
Near-Term (2020-2040)	1.59	1.55	1.19
Mid-Term (2041-2070)	1.65	1.61	1.24
End-Term (2071-2100)	1.63	1.60	1.23
SSP585			
Near-Term (2020-2040)	1.59	1.54	1.19
Mid-Term (2041-2070)	1.65	1.61	1.24
End-Term (2071-2100)	1.61	1.54	1.18

 # All units are in %

Further, the unmet demands at Gadarwara under SSP245 scenario are projected to be higher at 5.59% during near-term, 5.96% during mid-term and 5.49% under end-term. The unmet demands at Gadarwara under SSP585 scenario is projected to be higher than that during the baseline and present periods, but marginally lower than that under SSP245 scenario with 5.41% during near-term, 5.91% during mid-term and 3.92% during the end-term. The only sub-catchment with unmet demands more than 5% is the Dindori sub-catchment. The unmet

domestic demands at the main river sub-catchments are less and ranges between 1.59% to 1.62% at Barmanghat, between 1.37% and 1.61% at Sandia and between 1.05% and 1.24% at Barmanghat. The unmet domestic demand in all the sub-catchments is lesser under SSP585 climate scenario as compared SSP245 scenario. The comparison of the annual average unmet water demand of domestic needs for main river sub-catchments under SSP245 climate scenario is given in Figure 5.149.

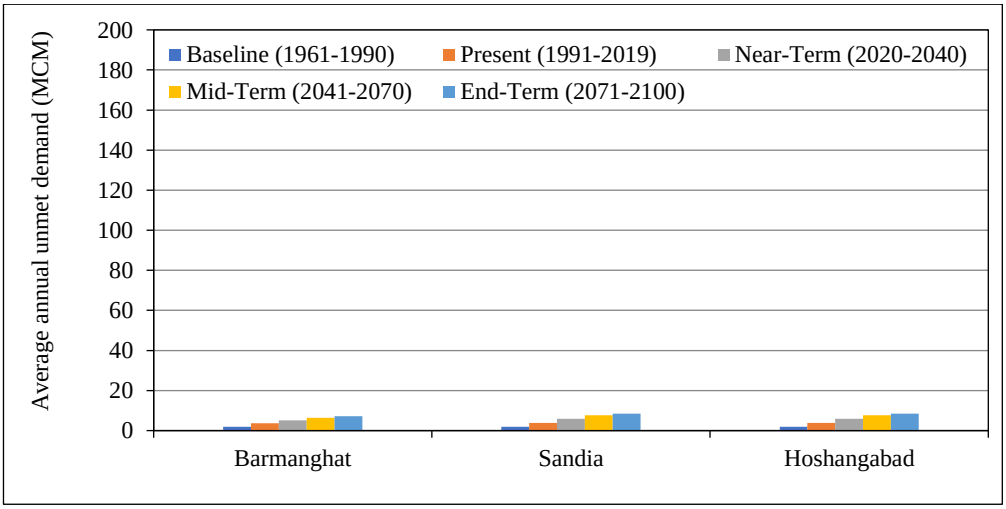

Figure 5.149: Annual average unmet demand for domestic needs in the main river sub-catchments under SSP245 scenario

The domestic water demands in most of the headwater and main river catchments can be satisfied with the groundwater and existing water infrastructure.

5.12.3 Supply-Demand Scenario in Livestock Sector

The annual average **'livestock water demand'** under SSP245 and SSP585 climate scenarios is given in Table 5.39 for the headwater sub-catchments and in Table 5.40 for the sub-catchments on the main river. From these demand tables, it has been observed that the livestock water requirements are increasing continuously during all time periods in a similar manner as that of domestic water needs for all sub-catchments. The livestock water demands are projected to be maximum during the end-term (2071-2100). Not much livestock growth projected for the future as the rural population is gradually minimising their dependence on livestock, except for meeting their own requirements, as the feed and fodder for nurturing animals and poultry has become very costly off late. Also, there is not much of a difference in livestock demands between the SSP245 and SSP585

Table 5.39: Annual average water demand for livestock purpose using SSP245 and SSP585 in the headwater sub-catchments

Time period	Dindori	Manot	Mohgaon	Belkheri	Patan	Gadarwara
Baseline (1961-1990)	0.68	0.30	0.96	0.71	1.12	0.81
Present (1991-2019)	1.27	0.56	1.79	1.31	2.07	1.51
SSP245 & SSP585						
Near-Term (2020-2040)	1.35	0.60	1.91	1.40	2.21	1.61
Mid-Term (2041-2070)	1.36	0.60	1.92	1.41	2.22	1.61
End-Term (2071-2100)	1.36	0.60	1.92	1.41	2.22	1.62

 # All units are in MCM

Table 5.40: Annual average water demand for livestock in the main river sub-catchments under SSP245 and SSP585 scenarios

Time period	Barmanghat	Sandia	Hoshangabad
Baseline (1961-1990)	6.80	9.93	14.88
Present (1991-2019)	12.61	18.42	27.61
SSP245 & SSP585			
Near-Term (2020-2040)	13.46	19.66	29.46
Mid-Term (2041-2070)	13.53	19.76	29.61
End-Term (2071-2100)	13.54	19.77	29.62

 # All units are in MCM

climate scenarios. The comparison of the livestock water demand in the headwater sub-catchments are provided in Figure 5.150.

The average annual **'livestock supply delivered'** under SSP245 and SSP585 climate scenarios for the headwater sub-catchments is given in Table 5.41 and for the sub-catchments located on main river is given in Table 5.42. From these tables, it can can be observed that the water supplies delivered for livestock purpose was generally sufficient to meet most of the livestock demands almost all the sub-catchments during all the time periods except for marginal short supplies in Gadarwara sub-catchment, where the supplies could meet only about 95% of the total livestock water demands. In this catchment, the water supply was sufficient during the baseline period (1961-1990), but there have been shortfalls in the delivered water supply from present time period (1991-2019) and projected to

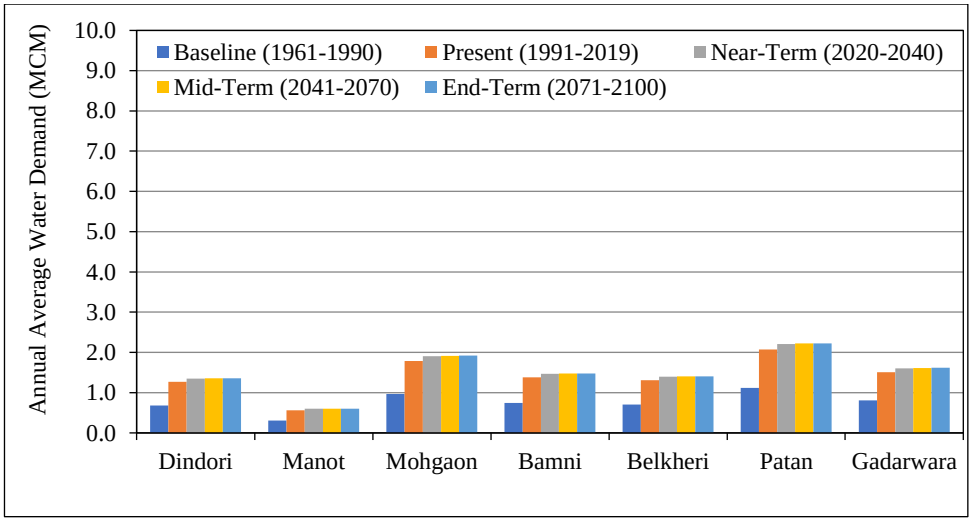

Figure 5.150: Annual average water demand for livestock in the headwater sub-catchments

Table 5.41: Annual average supply delivered for livestock in the headwater sub-catchments using SSP245 and SSP585 scenarios

Time period	Dindori	Manot	Mohgaon	Belkheri	Patan	Gadarwara
Baseline (1961-1990)	100.0	100.0	100.0	100.0	100.0	100.0
Present (1991-2019)	100.0	100.0	100.0	100.0	100.0	98.68
SSP245						
Near-term (2020-2040)	100.0	100.0	100.0	100.0	100.0	94.41
Mid-term (2041-2070)	100.0	100.0	100.0	100.0	100.0	94.41
End-Term (2071-2100)	100.0	100.0	100.0	100.0	100.0	94.44
SSP585						
Near-term (2020-2040)	100.0	100.0	100.0	100.0	100.0	94.41
Mid-term (2041-2070)	100.0	100.0	100.0	100.0	100.0	94.41
End-term (2071-2100)	100.0	100.0	100.0	100.0	100.0	95.68

 # All units are in %

continue up to end-term (2071-2100).

Similarly for the sub-catchments on the main river, the water supplies were sufficient to meet the livestock demands at Barmanghat for all time periods under both SSP245 and SSP585 scenarios. However, marginal shortfall in water supplies

Table 5.42: Annual average supply delivered for livestock in the main river sub-catchments under SSP245 and SSP585 scenarios

Time period	Barmanghat	Sandia	Hoshangabad
Baseline (1961-1990)	100.0	100.0	100.0
Present (1991-2019)	100.0	99.95	99.93
SSP245			
Near-term (2020-2040)	100.0	99.54	99.69
Mid-term (2041-2070)	100.0	99.49	99.66
End-term (2071-2100)	100.0	99.54	99.70
SSP585			
Near-term (2020-2040)	100.0	99.54	99.69
Mid-term (2041-2070)	100.0	99.49	99.66
End-term (2071-2100)	100.0	99.70	99.80

 # All units are in %

was seen at Sandia and Hoshangabad sub-catchments limited to less than 0.05% during the present time period and projected to continue up to the end-term time periods. Generally, the water supplies are projected to be marginally higher under the SSP585 scenario.

The average annual **'unmet livestock demands'** for the headwater sub-catchments under SSP245 and SSP585 climate scenarios is given in Table 5.43. There are not much unmet demands in sub-catchments as it can be seen from the table mentioned below. with practically no unmet demands in all the sub-catchments except for Gadarwara sub-catchment where it is limited to 5.6% only. It can be observed that for the Gadarwara sub-catchment under SSP245 and SSP585, there have been no unmet demands during the baseline period (1961-1990) but is projected to increase marginally to a maximum 5.59% during the near-term (2020-2040) and decrease marginally during the mid-term (2041-2070) and end-term (2071-2100).

The unmet demand for the livestock needs is projected to be lower during the end-term under SSP585 scenario (4.32%). Also, there are only marginal shortfalls of water supplies in the Sandia and Hoshangabad sub-catchments too, which raises unmet demands in these sub-catchments but it is negligible as these unmet demands are quite less and lie below 1% of the total water demands for livestock. The comparison of the annual average unmet water demand for

Table 5.43: Annual average unmet demand for livestock needs in the headwater sub-catchments under SSP245 and SSP585 scenarios

Time period	Dindori	Manot	Mohgaon	Belkheri	Patan	Gadarwara
Baseline (1961-1990)	0.00	0.00	0.00	0.00	0.00	0.00
Present (1991-2019)	0.00	0.00	0.00	0.00	0.00	1.32
SSP245						
Near-Term (2020-2040)	0.00	0.00	0.00	0.00	0.00	5.59
Mid-Term (2041-2070)	0.00	0.00	0.00	0.00	0.00	5.57
End-Term (2071-2100)	0.00	0.00	0.00	0.00	0.00	5.56
SSP585						
Near-Term (2020-2040)	0.00	0.00	0.00	0.00	0.00	5.59
Mid-Term (2041-2070)	0.00	0.00	0.00	0.00	0.00	5.59
End-Term (2071-2100)	0.00	0.00	0.00	0.00	0.00	4.32

 # All units are in %

livestock needs is given in Figure 5.151 for the main river sub-catchments under SSP245 climate scenario and in Figure 5.152 under the SSP585 climate scenario.

The livestock water demands in most of the headwater and main river catchments can also be satisfied with the groundwater and existing water infrastructure. Therefore, the supply demand scenario in the study area is projected to be favourable and most of the water demands including the domestic, livestock, agricultural and other demands can be satisfactorily met with the available water resources in the basin.

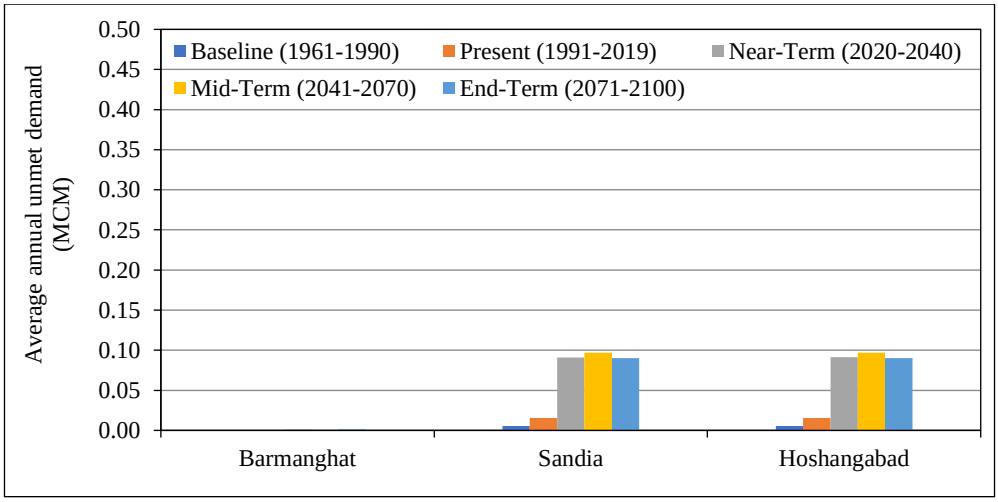

Figure 5.151: Annual average unmet demand for livestock in the main river sub-catchments under SSP245 scenario

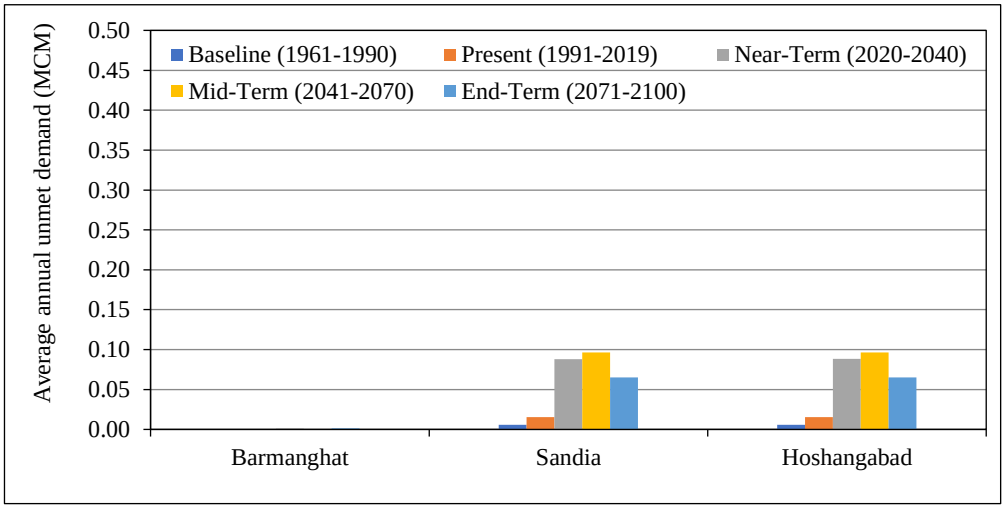

Figure 5.152: Annual average unmet demand for livestock in the main river sub-catchments under SSP585 scenario

5.13 Climate Change Impact Assessment on Water Resources

5.13.1 Climate Change Impact on Temperature

5.13.1.1 Impact on Maximum Temperature

The annual average maximum temperature (MaxT) under the SSP245 scenario is also projected to increase from 32.3ºC during the baseline period (1961-1990) to 32.99ºC during the near-term (2020-2040), 33.9ºC during the mid-term (2041-2070) and 34.3ºC during the end-term (2071-2100). A much higher increase of maximum temperature (MaxT) is projected under the SSP585 scenario, from 32.3ºC during the baseline period (1961-1990) to 33.0ºC during the near-term (2020-

2040), to 34.2ºC during the mid-term (2041-2070) and to 35.7ºC during the end-term (2071-2100). Therefore, the average maximum temperature is projected increase at the rate of 1.58ºC/100 year under SSP245 scenario and 2.61ºC/100 year under SSP585 scenario. The comparison of the average annual maximum temperature (ensemble mean) during various time periods, under both SSP25 and SSP585 scenarios in the Upper Narmada basin is given in Figure 5.153.

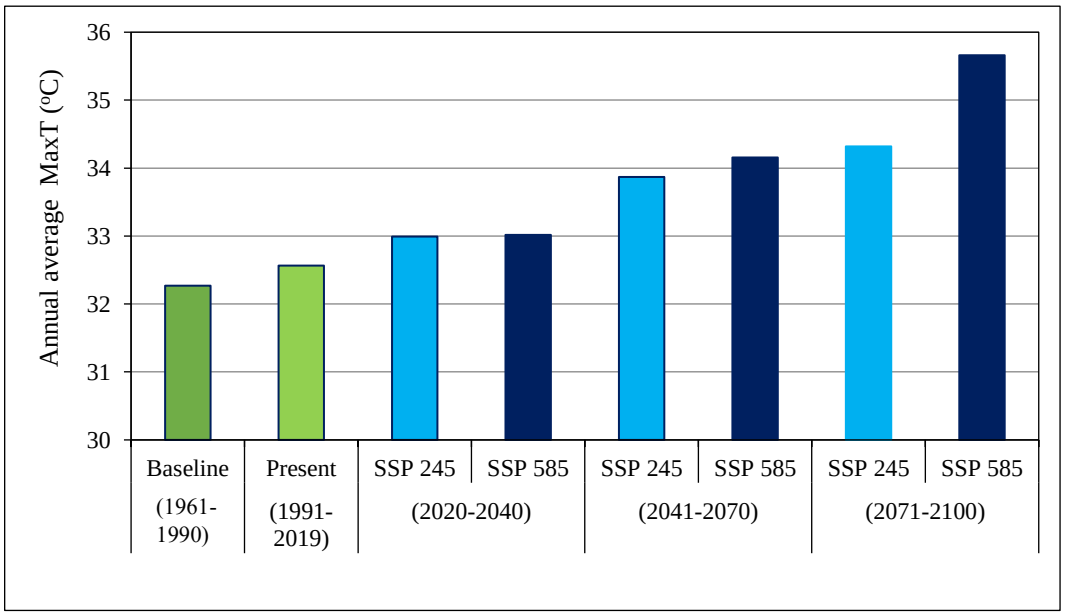

Figure 5.153: Annual average Maximum Temperature (ensemble mean) under SSP245 and SSP585 scenarios

The extreme heat events as represented by the 1-day MaxT under SSP245 scenario is projected to increase from 43.31ºC during the baseline period (1961-1990) and 43.84ºC during the present period (1991-2019) to 44.21ºC during near-term (2020-2040), 44.96ºC during the mid-term (2041-70) and 45.46ºC during the end-period (2071-2100). Similarly, the extreme heat events under SSP585 scenario are projected to increase at a slightly higher rate from 43.31ºC and 43.84ºC during the baseline period (1961-1990) and present period (1991-2019) respectively to 44.28ºC during near-term period (2020-2040), 45.25ºC during the mid-term (2041-70) and 46.85ºC during the end-period (2071-2100). The comparison of the 1-day maximum temperature (ensemble mean) during various time periods, both under SSP25 and SSP585 scenarios in Upper Narmada basin is given in Figure 5.154.

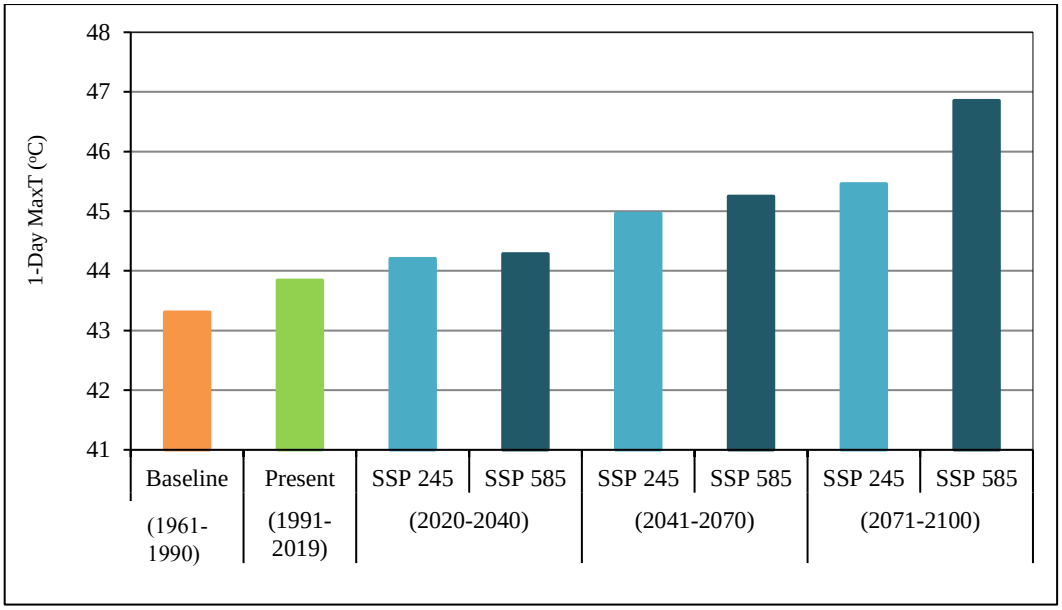

Figure 5.154: 1-day maximum of Maximum Temperature (ensemble mean) under SSP245 and SSP585 scenarios

The average number of very hot days represented by the days with MaxT> 40ºC under SSP245 scenario is projected to increase from 36 days during the baseline period (1961-1990) and 40 days during the present period (1991-2019) to 51 days during near-term period (2020-2040), 68 days during the mid-term (2041-70) and 76 days during the end-period (2071-2100). Similarly, the average number of very hot days under SSP585 scenario is projected to increase at a higher rate from 36 days during the baseline period (1961-1990) and 40 days during the present period (1991-2019) to 53 days during near-term period (2020-2040), 74 days during the mid-term (2041-70) and 102 days during the end-period (2071-2100). The comparison of the average annual very hot day events (ensemble mean) during the various time periods under SSP25 and SSP585 scenarios in Upper Narmada basin is given in Figure 5.155. Therefore, it can be seen that under the average maximum temperature in the Upper Narmada basin is projected to increase substantially along with the increase in the 1-day maximum temperature. This is ought to result in heat waves and increased water demands for consumptive water requirement for agriculture and water other water dependent sector. The comparison of the number of very hot days (MaxT>40ºC) and number of hot days (MaxT>35ºC) are also projected to increase substantially in future, but the rate of increase is higher under SSP585 scenario as compared to SSP245.

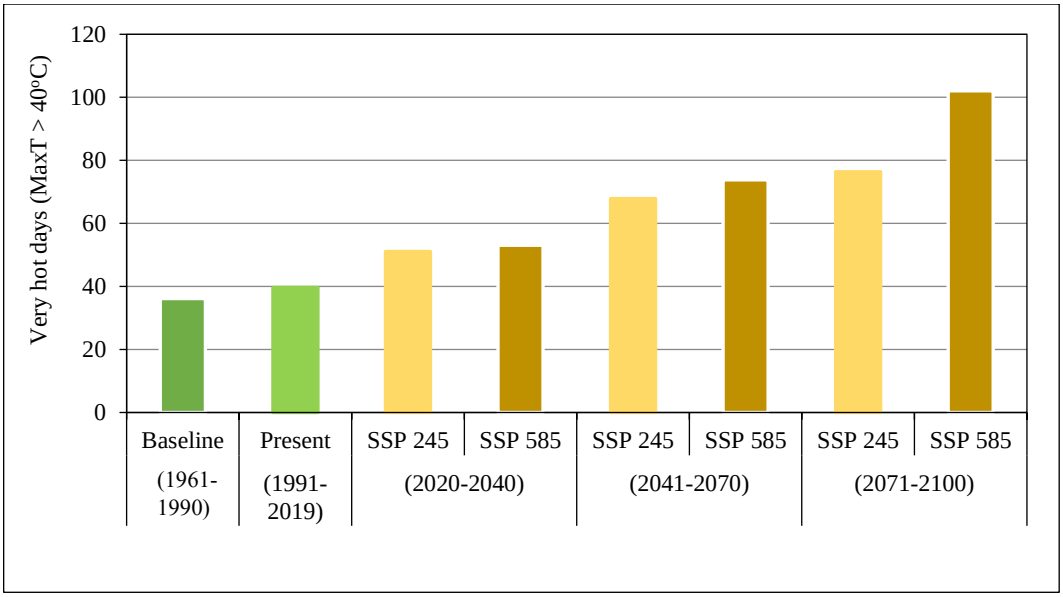

Figure 5.155: Comparison of very hot days (ensemble mean) under SSP245 and SSP585 scenarios

5.13.1.2 Impact on Minimum Temperature

The annual average minimum temperature (MinT) under SSP245 scenario is also projected to increase from 18.94°C during the baseline period (1961-1990) to 20.04°C during the near-term (2020-2040), 21.01°C during the mid-term (2041-2070) and 21.72°C during the end-term (2071-2100). A much higher increase of minimum temperature (MinT) is projected under the SSP585 scenario, from 18.94°C during the baseline period (1961-1990) to 20.09°C during the near-term (2020-2040), to 21.63°C during the mid-term (2041-2070) and to 23.65°C during the end-term (2071-2100). Therefore, the average minimum temperature is projected increase at the rate of 2.14°C/100 year under SSP245 scenario and 3.62°C/100 year under SSP585 scenario. It can be observed that the increase in the annual average minimum temperature (MinT) is highest during the end term as compared to the baseline period. Also, the increase during the end term under SSP585 scenario is substantially higher as compared to the SSP245 scenario. The comparison of the annual average minimum temperature (ensemble mean) during the various time periods under SSP25 and SSP585 scenarios in the Upper Narmada basin is given in Figure 5.156.

The lowest (minimum) of the minimum temperature (MinT) under SSP245 scenario is projected to increase from 6.31°C and 6.14°C during the baseline period

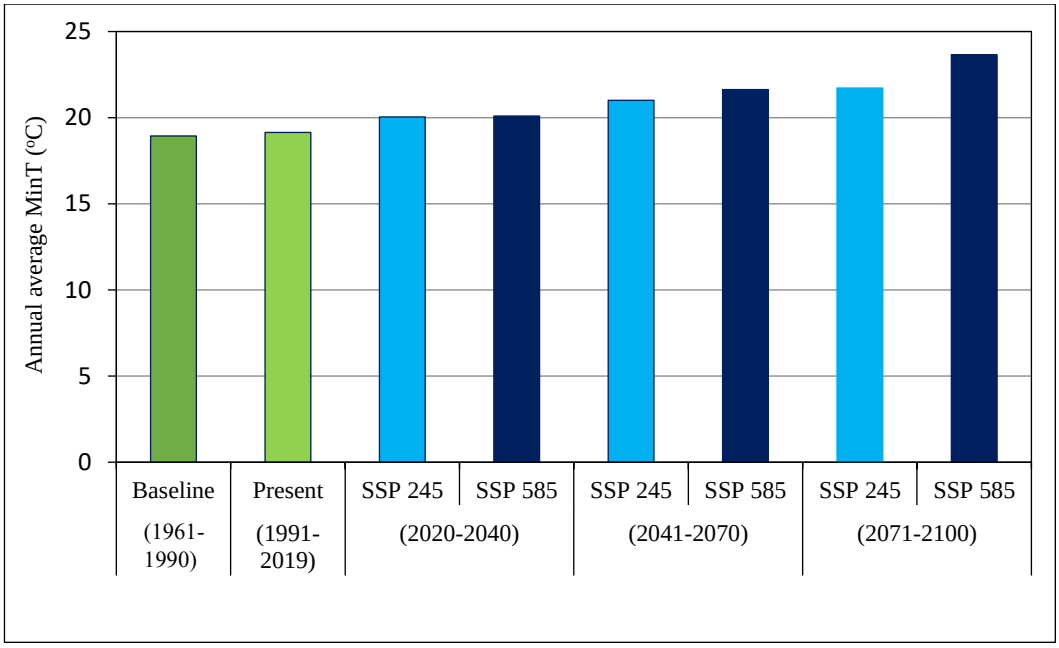

Figure 5.156: Annual average minimum temperature (ensemble mean) under SSP245 and SSP585 scenarios

(1961-1990) and present period (1991-2019) respectively to 7.44°C during near-term period (2020-2040), 8.20°C during the mid-term (2041-70) and 9.03°C during the end-period (2071-2100). Similarly lowest of the minimum temperature (MinT) under SSP585 scenario is projected to increase at a much higher rate from 6.31°C and 6.14°C during the baseline period (1961-1990) and present period (1991-2019) respectively to 7.41°C during near-term period (2020-2040), 8.90°C during the mid-term (2041-70) and 11.13°C during the end-period (2071-2100). It can be observed that the increase in the lowest of MinT is the highest during the end term as compared to the baseline period. Also, the increase in the end term is substantially higher as under SSP585 scenario compared to the SSP245 scenario. The annual lowest of the minimum temperature (ensemble mean) during the various time periods under SSP25 and SSP585 scenarios in the Upper Narmada basin is given in Figure 5.157.

The average number of very hot night events represented by the days with MinT> 25°C is projected to increase from 42 days during the baseline period (1961-1990) and 46 days during the present period (1991-2019) to 76 days during near-term period (2020-2040), 97 days during the mid-term (2041-70) and 113 days during the end-period (2071-2100) under SSP245 scenario. Similarly, the average

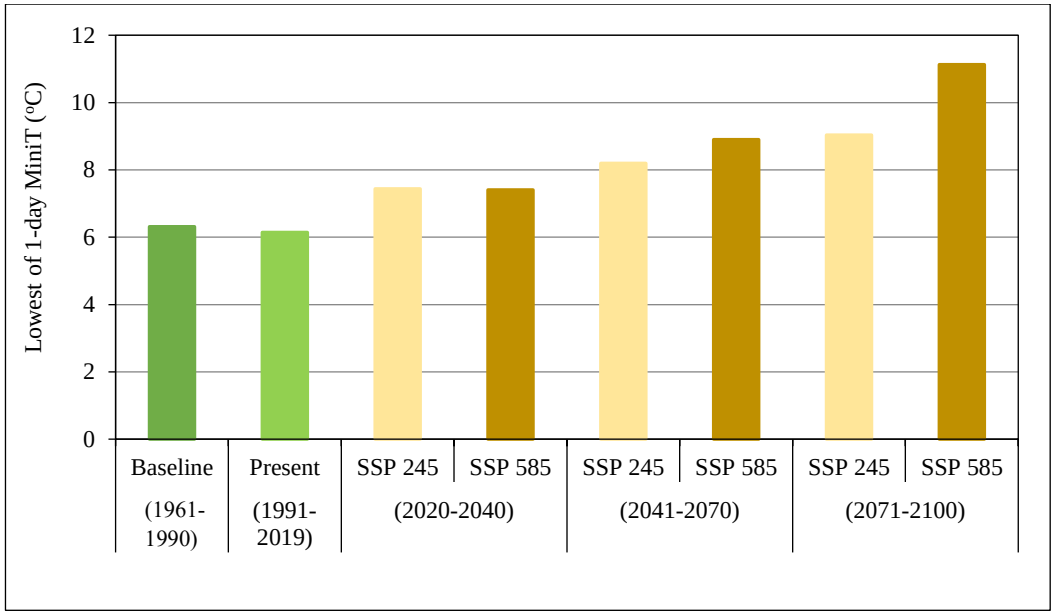

Figure 5.157: Lowest 1-day minimum temperature (ensemble mean) under SSP245 and SSP585 scenarios

number of very hot events under SSP585 scenario is projected to increase at a higher rate from 42 days during the baseline period (1961-1990) and 46 days during the present period (1991-2019) to 78 days during near-term period (2020-2040), 111 days during the mid-term (2041-70) and 157 days during the end-period (2071-2100). It can be seen that the average number of very hot night events are projected to be highest during the end term. Also, the increase during the end term is substantially higher under SSP585 scenario as compared to the SSP245 scenario. The comparison of the average annual very hot events (ensemble mean) during various time periods, under SSP25 and SSP585 scenarios in Upper Narmada basin is given in Figure 5.158.

The average number of cold nights represented by the days with MinT> 10ºC is projected to decrease from 32 days during the baseline period (1961-1990) and 28 days during the present period (1991-2019) to 20 days during near-term period (2020-2040), 13 days during the mid-term (2041-70) and 9 days during the end-period (2071-2100) under SSP245 scenario. Similarly, the average number of cold nights under SSP585 scenario is projected to decrease from 32 days during the baseline period (1961-1990) and 28 days during the present period (1991-2019) to 21 days during near-term period (2020-2040), 9 days during the mid-term (2041-70) and 2 days during the end-period (2071-2100). It can be observed that the

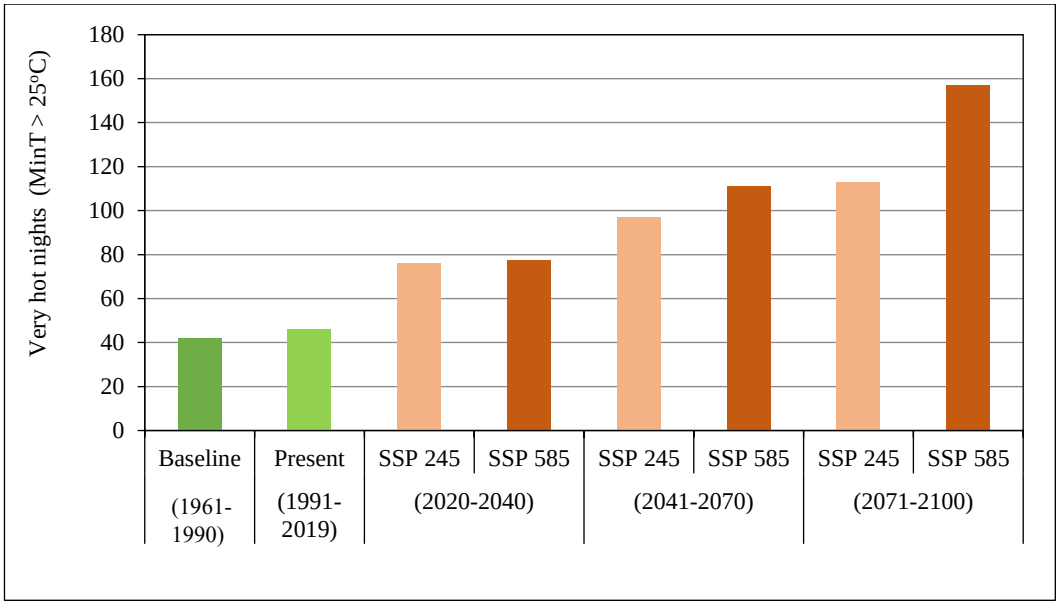

Figure 5.158: Comparison of very hot nights (ensemble mean) under SSP245 and SSP585 scenarios

average number of cold nights are projected to be the lowest during the end term. Also, the decrease in cold nights during the end term is substantially higher under SSP585 scenario as compared to the SSP245 scenario. The comparison of the average annual cold nights (ensemble mean) during various time periods under SSP25 and SSP585 scenarios in Upper Narmada basin is given in Figure 5.159.

This indicates that the future temperature changes linked to global warming may be characterized by a marked asymmetry between daytime maxima and night time minima. The increases in both maximum and minimum temperature will have significant impacts on the water demands viz., increase in water demands for the domestic, agricultural and other water dependent sectors, considerable impacts on crop growth and crop yields, intensification of the hydrological cycle, increased spatio-temporal variability in the precipitation distribution leading to higher water deficits and water surplus scenarios.

5.13.2 Climate Change Impact on Precipitation

The projected changes in future precipitation during near-term (2020-2040), mid-term (2041-70) and end-period (2071-2100) have been assessed relative to the baseline period (1961–1990). The average annual precipitation projections across all GCMs show an increase during all future time periods, the increase

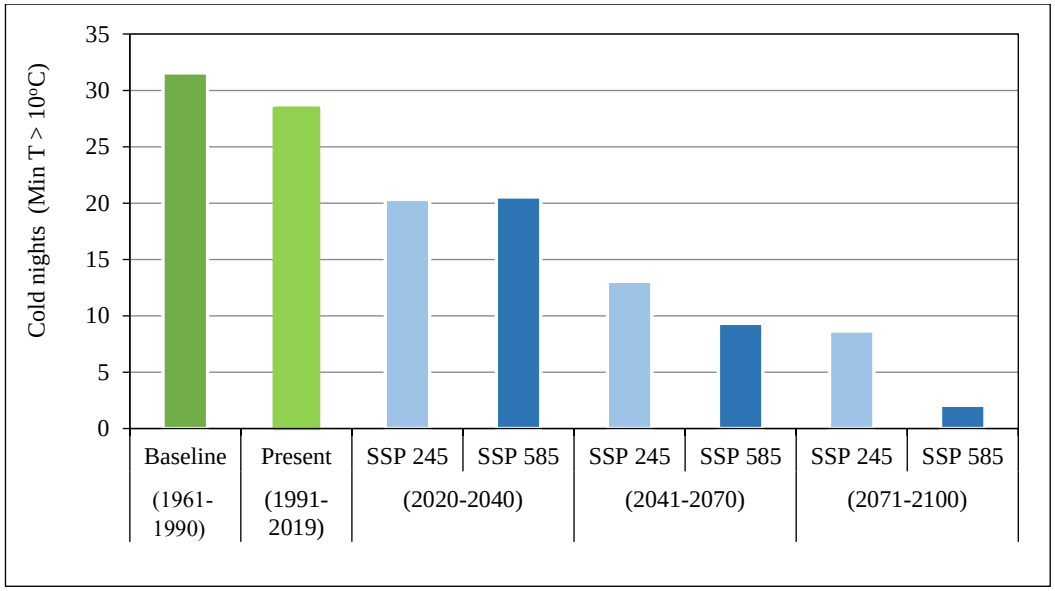

Figure 5.159: Comparison of cold nights (ensemble mean) under SSP245 and SSP585 scenarios

being more predominant during the end-term. There is considerable variation in mean annual precipitation between the individual GCMs with CanESM5 predicting substantially higher increase in annual average precipitation as compared to other GCMs. The mean annual precipitation during baseline period is 1120.0 mm which is projected to increase in future by all the GCMs, the largest increase being projected by CanESM5 as 1710 mm during 2020-2100. The ensemble average annual precipitation under the SSP245 scenario during the near-term (2020-2040), mid-term (2041-70) and end-term (2071-2100) is projected to increase to 1280.7 mm, 1364.6 mm and 1493.1 mm respectively.

Similarly, the ensemble average annual precipitation under SSP585 scenario during the near-term (2020-2040), mid-term (2041-70) and end-term (2071-2100) is projected to increase to 1285.9 mm, 1457.1 mm and 1831.3 mm respectively. The comparison of the annual average precipitation during the various future time periods with the present and baseline period is given in Figure 5.160. Therefore, the future is projected to be wetter with considerable increase in the annual average precipitation in the Upper Narmada basin. The projected increase in the average annual precipitation may result in higher water availability in the basin, which can be ascertained through hydrologic modelling exercise. The comparison of the 1-day maximum precipitation (ensemble mean) during the various time periods under SSP25 and SSP585 scenarios in the Upper Narmada basin is given in Figure 5.161.

The extreme rainfall represented by the average of the1-day maximum precipitation under SSP245 scenario is projected to increase from109.4 mm and 107.0 mm during the baseline period (1961-1990) and present period (1991-2019) respectively to 104.0 mm during near-term period (2020-2040), 109.0 mm during the mid-term (2041-70) and 117.4 mm during the end-period (2071-2100). Similarly, the 1-day maximum precipitation under SSP585 scenario is projected to increase at a slightly higher rate from 109.4 mm and 107.0 mm during

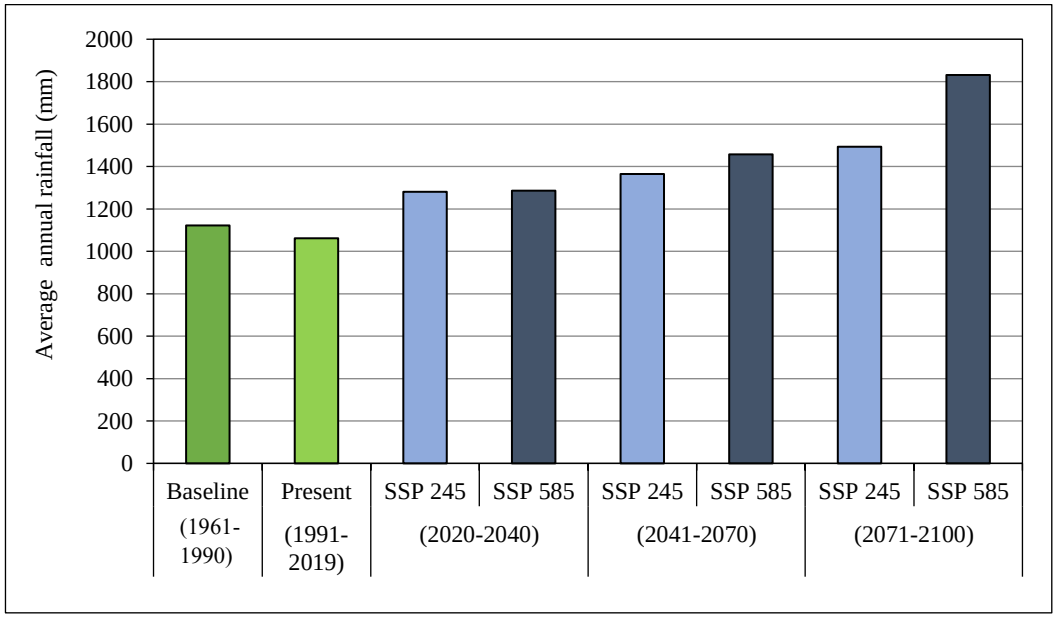

Figure 5.160: Comparison of average annual rainfall (ensemble mean) under SSP245 and SSP585 scenarios

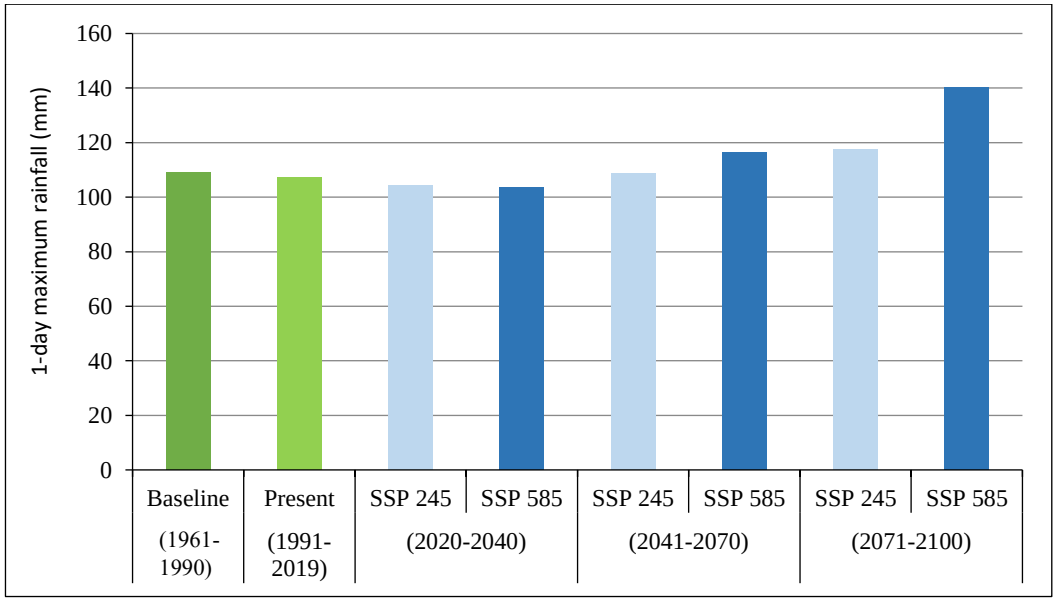

Figure 5.161: Comparison of 1-day maximum rainfall (ensemble mean) under SSP245 and SSP585 scenarios

the baseline period (1961-1990) and present period (1991-2019) respectively to 103.6 mm during near-term period (2020-2040), 116.5 mm during the mid-term (2041-70) and 140.1 mm during the end-period (2071-2100). The increase in the 1-day maximum precipitation will translate into increase in flood events of higher flood magnitude in the future.

The 3-day consecutive precipitation represents the antecedent moisture conditions responsible for generating high volume runoff. The maximum 3-day consecutive rainfall in the study area is projected to increase from 182.4 mm during the baseline period (1961-1990) and 177.7 mm during the present period (1991-2019) to 209.1 mm during near-term (2020-2040), 218.2 mm during mid-term (2041-2070) and 237.3 mm during end-term (2071-2100) under SSP245 scenario which is a fair increase. Similarly, the maximum 3-day consecutive rainfall is projected to increase at a higher rate from 182.4 mm during the baseline period (1961-1990) and 177.7 mm during the present period (1991-2019) to 207.0 mm during near-term (2020-2040), 233.4 mm during mid-term (2041-2070) and 284.7 mm during end-term (2071-2100) under SSP585 scenario, which is a substantial increase that will get translated into higher stream flow volumes during these continuous storm events in future. The comparison of the maximum 3-day consecutive precipitation (ensemble mean) during the various time periods under SSP25 and SSP585 scenarios in the Upper Narmada basin is given in Figure 5.162.

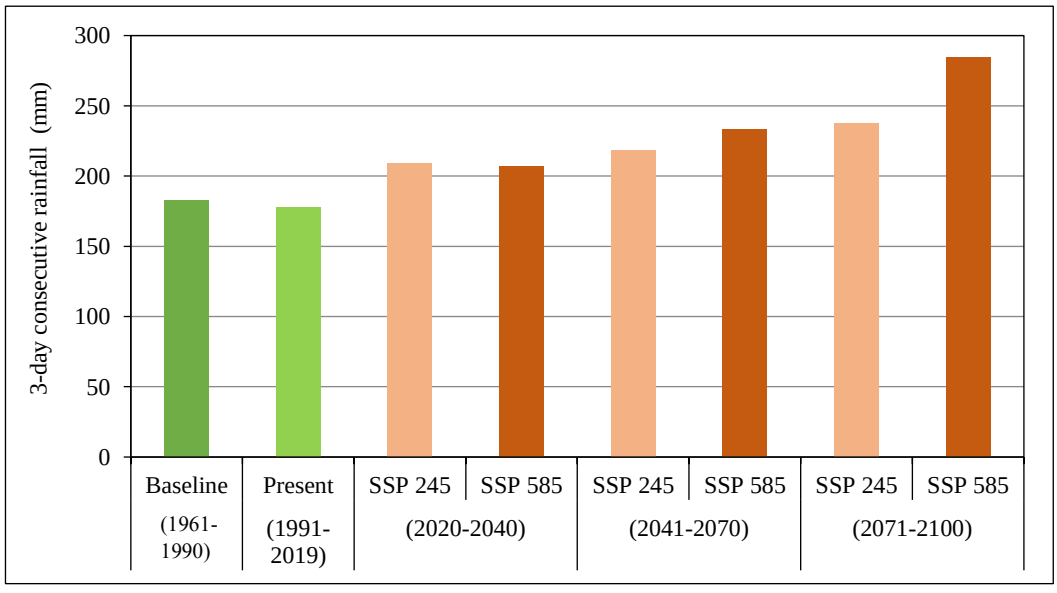

Figure 5.162: Comparison of 3-day consecutive rainfall (ensemble mean) under SSP245 and SSP585 scenarios

The average rainfall intensity, which is the ratio of the rainfall occurring during the rainy days to the number of rainy days, is also projected to increase from 17.97 mm/day and 18.0 mm/day during the baseline period (1961-1990) and present period (1991-2019) respectively to 18.49 mm/day under SSP245 scenario and 20.66 mm/day under SSP585 scenario by the end-term (2071-2100). The average 1-day maximum rainfall is projected to increase from 108.14 mm during 1961-2019 to 110.13 mm during 2020-2100 (SSP245) and 120.04 mm during 2020-2100 (SSP585). The comparison of the average rainfall intensity (ensemble mean) during the various time periods under SSP25 and SSP585 scenarios in the Upper Narmada basin is given in Figure 5.163.

The comparison of the heavy rainfall events (ensemble mean) during various time periods, under SSP25 and SSP585 scenarios in Upper Narmada basin is given in Figure 5.164. The number of heavy rainfall events represented by the days with daily rainfall > 50 mm/day under SSP245 scenario is projected to increase from 83 days during the baseline period (1970-1990) and 110 days during the present period (1991-2019) to 93 days during near-term period (2020-2040), 145 days during the mid-term (2041-70) and 167 days during the end-period (2071-2100). Similarly, the number of very hot events under SSP585 scenario is projected to increase at a higher rate from 83 days during the baseline period (1970-1990)

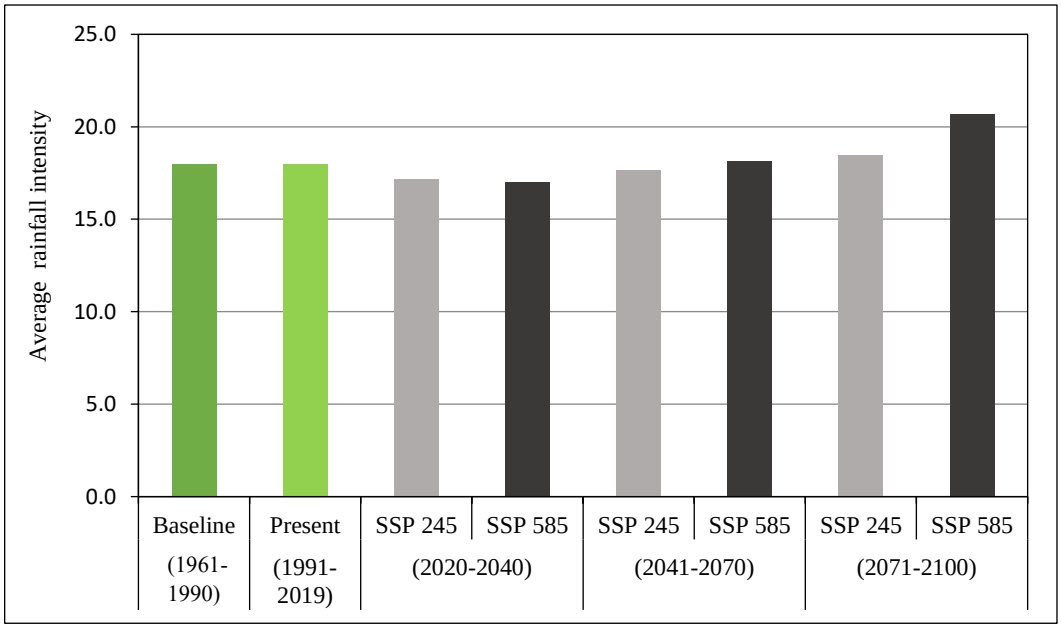

Figure 5.163: Comparison of average rainfall intensity (ensemble mean) under SSP245 and SSP585 scenarios

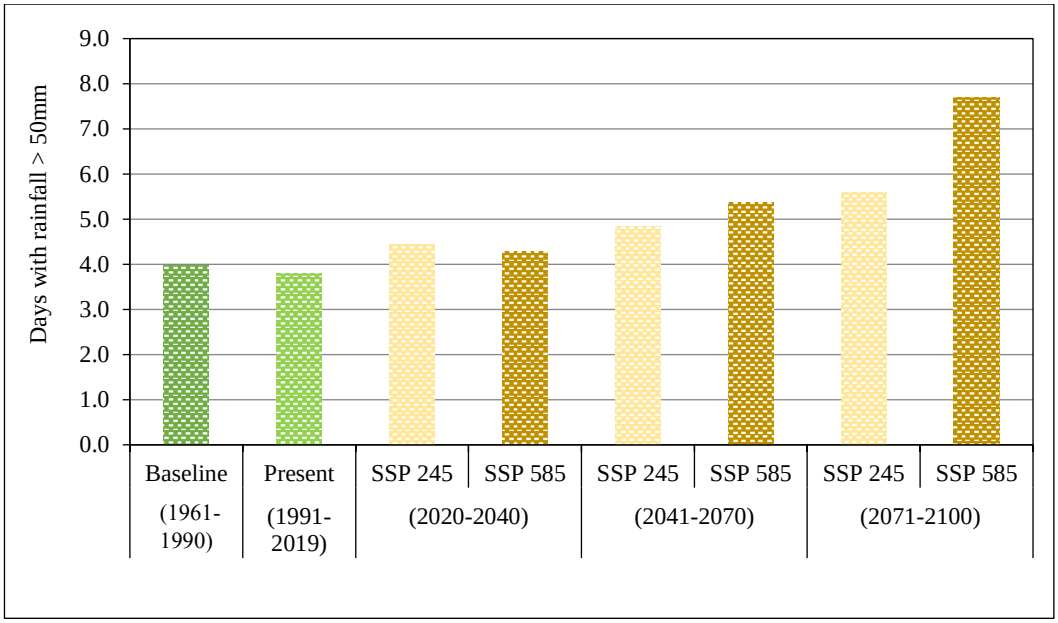

Figure 5.164: Comparison of heavy rainfall events (ensemble mean) under SSP245 and SSP585 scenarios

and 110 days during the present period (1991-2019) to 90 days during near-term period (2020-2040), 161 days during the mid-term (2041-70) and 224 days during the end-period (2071-2100). A substantial increase in the heavy rainfall events is projected for the future which will result in high stream flow volumes in the rivers.

The number of very heavy rainfall events represented by the days with daily rainfall > 100 mm/day under SSP245 scenario is projected to increase from 18 days during the baseline period (1970-1990) and 22 days during the present period (1991-2019) to 20 days during near-term period (2020-2040), 30 days during the mid-term (2041-70) and 39 days during the end-period (2071-2100). Similarly, the number of very hot events under SSP585 scenario is projected to increase at a higher rate from 18 days during the baseline period (1970-1990) and 22 days during the present period (1991-2019) to 19 days during near-term period (2020-2040), 38 days during the mid-term (2041-70) and 66 days during the end-period (2071-2100). The comparison of the very heavy rainfall events (ensemble mean) during various time periods, under SSP25 and SSP585 scenarios in Upper Narmada basin is given in Figure 5.165. A substantial increase in the very heavy rainfall events projected for the future will result in higher flood events of higher magnitudes in future.

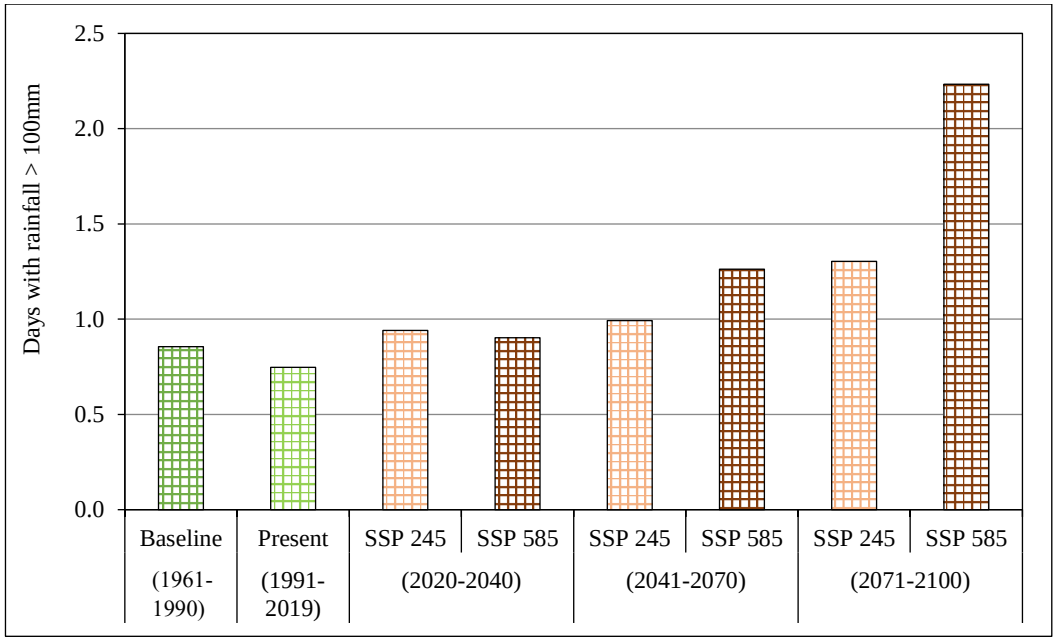

Figure 5.165: Comparison of very heavy rainfall days (ensemble mean) under SSP245 and SSP585 scenarios

5.13.3 Climate Change Impact on Surface Water

5.13.3.1 Climate Change impact on Average Flows

The climate change impacts on the surface water runoff has been determined by driving the calibrated and validated hydrological models with the high resolution (0.25º x 0.25º) bias corrected future climate data of 13 CMIP6 GCMs for two future climate scenarios viz., SSP245 and SSP585. The simulation of the hydrological models with the bias corrected future climate data from 13 GCMs provides 13 sets of future stream flows for each SSP scenario and helps to understand the uncertainty in the projected future stream flows so as to get a range within which the flows are expected to vary in future. The hydrolgical models used to simulate the future stream flows include SWAT, WEAP, VIC, MIKE11-NAM and HEC-HMS. The results from each of the hydrological model simulations points towards the same trend with marginally differeing magnitudes. As such, the hydrological model outputs from any one hydrological model will be discussed in details, whereas the brief summary shall be given for the future stream flow simulation from the remaining four hydrological models. The comparison of the mean daily discharge during the baseline period (1961-1990), present period (1991-2019), near-term (2020-2040), mid-term (2041-2070) and end-term (2071-2100) has been carried out

for the gauging sites located at the outlet of headwater catchments and also located in the main river channel. The initial results are based on SWAT model simulations.

The average daily discharge at Manot is projected to increase slightly from 133.15 cumecs during the baseline period (1961-1990) and 119.26 cumecs during present period (1991-2019) to 133.52 cumecs during the near-term (2020-2040), 140.56 cumecs during the mid-term (2041-2070) and155.89 cumecs during the end-term (2071-2100) under SSP245 scenario. Similarly, the average daily discharge at Manot is projected to increase from 133.15 cumecs during the baseline period (1961-1990) and 119.26 cumecs during present period (1991-2019) to 143.30 cumecs during the near-term (2020-2040), 164.69 cumecs during the mid-term (2041-2070) and 206.57 cumecs during the end-term (2071-2100) under SSP585 scenario. The comparison of the average daily discharge under SSP245 and SSP585 scenarios for Narmada River at Manot, during the various time periods is given in Figure 5.166. Therefore, this headwater catchment of Narmada River up to Manot GD site is expected to have a wetter future with higher average stream flow in the sub-basin.

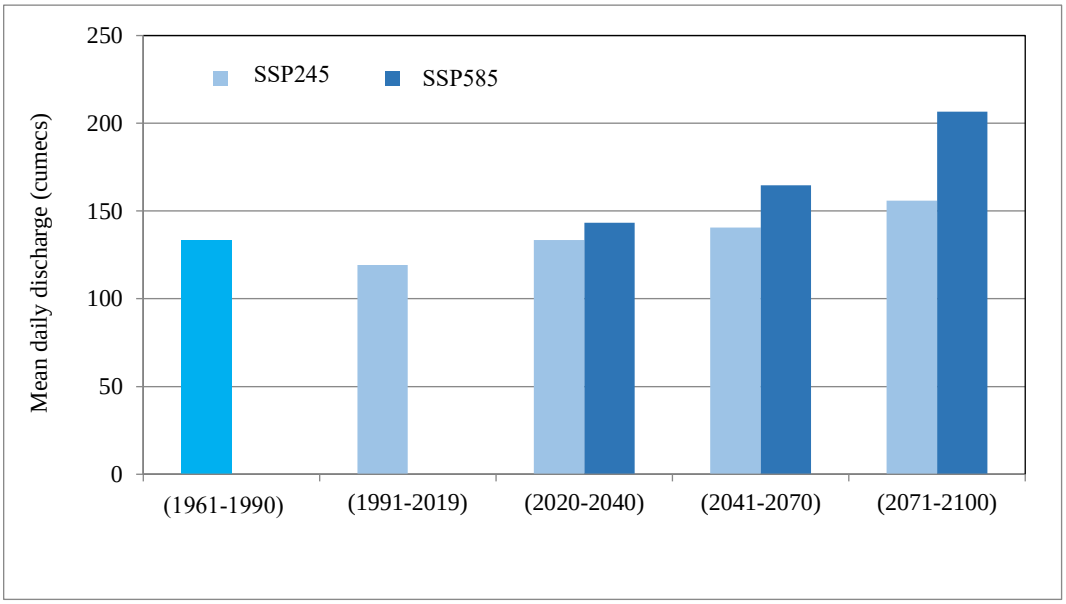

Figure 5.166: Comparison of average daily discharge (ensemble mean) for Narmada River at Manot

The average daily discharge for Burhner River at Mohgaon is projected to increase from 96.14 cumecs during the baseline period (1961-1990) and 94.21 cumecs during present period (1991-2019) to 106.07 cumecs during the near-term

(2020-2040), 111.32 cumecs during the mid-term (2041-2070) and 122.59 cumecs during the end-term (2071-2100) under SSP245 scenario. Similarly, the mean daily flow for Burhner River at Mohgaon is projected to increase from 96.14 cumecs during the baseline period (1961-1990) and 94.21 cumecs during present period (1991-2019) to 111.54 cumecs during the near-term (2020-2040), 129.24 cumecs during the mid-term (2041-2070) and 162.89 cumecs during the end-term (2071-2100) under SSP585 scenario. The comparison of the average daily discharge under SSP245 and SSP585 scenarios, which is another major headwater catchment, during the various time horizons is given in Figure 5.167. Therefore, this headwater catchment of Narmada River system for Burhner river at Mohgaon is also expected to have a wetter future with substantially higher average stream flow in the sub-basin.

The average daily flow for Sher River at Belkheri is projected to increase from 33.55 cumecs during the baseline period (1961-1990) and 33.04 cumecs during present period (1991-2019) to 43.55 cumecs during the near-term (2020-

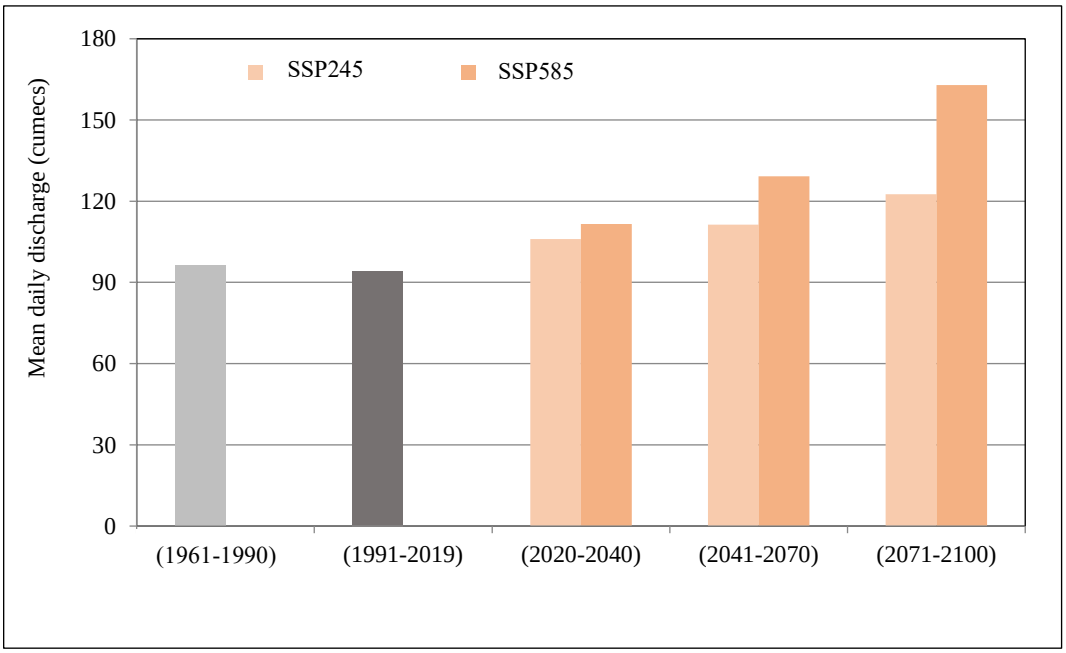

Figure 5.167: Comparison of average daily discharge (ensemble mean) for Burhner River at Mohgaon

2040), 46.44 cumecs during the mid-term (2041-2070) and 52.05 cumecs during the end-term (2071-2100) under SSP245 scenario. Similarly, the average daily flow for Sher River at Belkheri is projected to increase from 33.55 cumecs during the baseline period (1961-1990) and 33.04 cumecs during present period (1991-2019) to 42.33

cumecs during the near-term (2020-2040), 48.24 cumecs during the mid-term (2041-2070) and 62.30 cumecs during the end-term (2071-2100) under SSP585 scenario. The comparison of the mean daily discharge under SSP245 and SSP585 scenarios, for Sher River at Belkheri, which is another left bank headwater catchment, during the various time horizons is given in Figure 5.168. Therefore, this smaller sized left bank headwater catchment of the Narmada River system is expected to have considerably higher average stream flows in the sub-basin.

The average daily flow for Hiran River at Patan is projected to increase from 100.59 cumecs during the baseline period (1961-1990) and 100.41 cumecs during present period (1991-2019) to 118.27 cumecs during the near-term (2020-2040), 126.48 cumecs during the mid-term (2041-2070) and 139.79 cumecs during the end-term (2071-2100) under SSP245 scenario. Similarly, the average daily flow for Hiran River at Patan under SSP585 scenario is projected to increase 100.59 cumecs during the baseline period (1961-1990) and 100.41 cumecs during present period (1991-

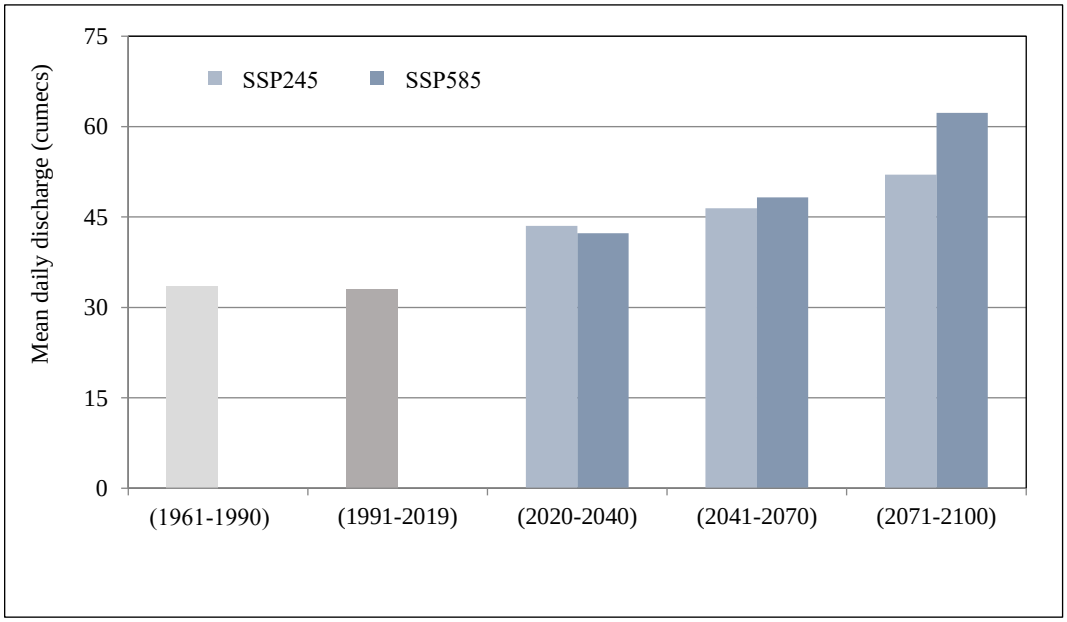

Figure 5.168: Comparison of average daily discharge (ensemble mean) for Sher River at Belkheri

2019)to 116.57 cumecs during the near-term (2020-2040), 135.84 cumecs during the mid-term (2041-2070) and 171.65 cumecs during the end-term (2071-2100). The comparison of the mean daily discharge under SSP245 and SSP585 scenarios for Hiran River at Patan, which is a major right bank headwater catchment, during the various time horizons is given in Figure 5.169.

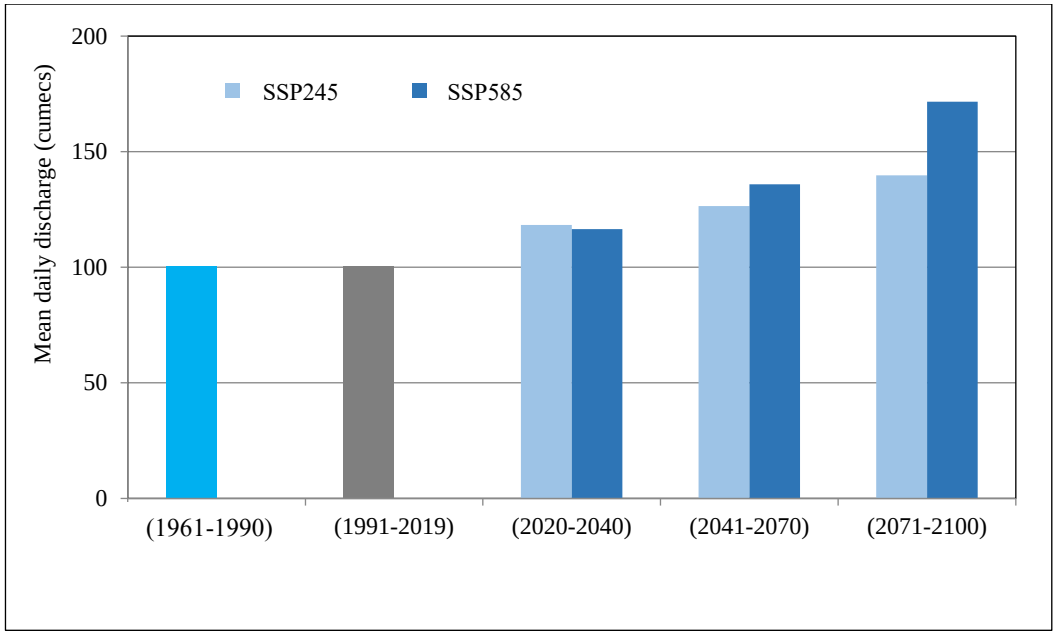

Figure 5.169: Comparison of average daily discharge (ensemble mean) for Hiran River at Patan

The average daily flow for Narmada River up to Barmanghat is projected to increase considerably from 659.37 cumecs during the baseline period (1961-1990) and 637.5 cumecs during present period (1991-2019) to 779.32 cumecs during the near-term (2020-2040), 826.50 cumecs during the mid-term (2041-2070) and 909.51 cumecs during the end-term (2071-2100) under SSP245 scenario. Similarly, the average daily flow is projected to increase slightly from 659.37 cumecs during the baseline period (1961-1990) and 637.50 cumecs during present period (1991-2019) to 990.47 cumecs during the near-term (2020-2040), 1029.82 cumecs during the mid-term (2041-2070) and 1121.79 cumecs during the end-term (2071-2100) under SSP585 scenario. The comparison of the average daily discharge under SSP245 and SSP585 scenarios for Narmada River at Barmanghat during the various time horizons is given in Figure 5.170. Therefore, higher average daily stream flow in future is projected for Narmada River up to Barmanghat GD site which is located downstream of Bargi dam.

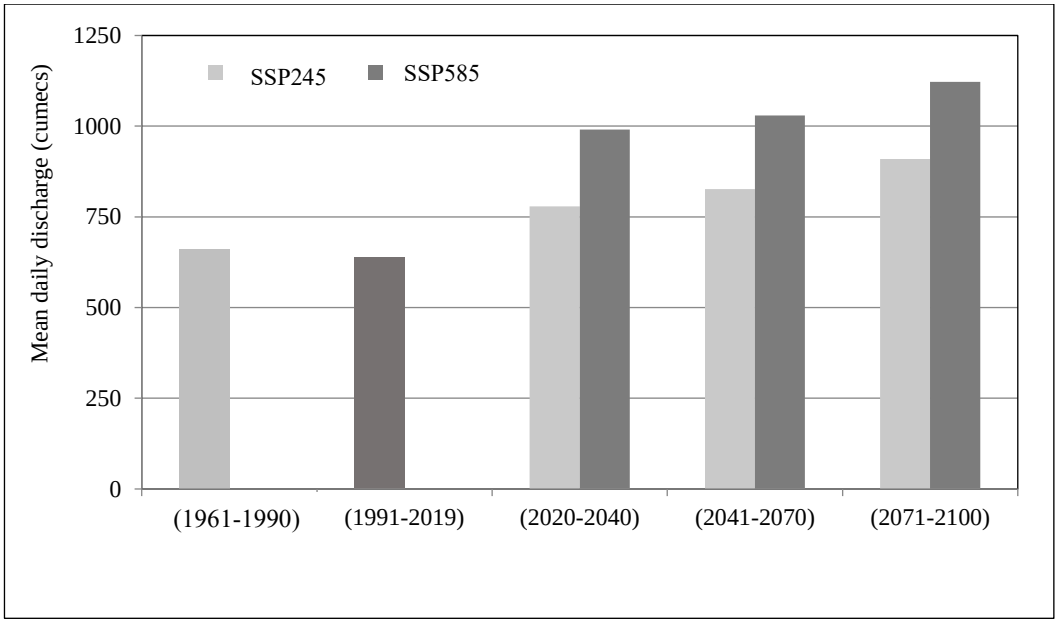

Figure 5.170: Comparison of average daily discharge (ensemble mean) for Narmada at Barmanghat

The average daily flow for Shakkar river at Gadarwara is projected to increase substantially from 49.53 cumecs during the baseline period (1961-1990) and 47.54 cumecs during present period (1991-2019) to 63.61 cumecs during the near-term (2020-2040), 68.02 cumecs during the mid-term (2041-2070) and 75.68 cumecs during the end-term (2071-2100) under SSP245 scenario. Similarly, the average daily flow for Shakkar river at Gadarwara is projected to increase 49.53 cumecs during the baseline period (1961-1990) and 47.54 cumecs during present period (1991-2019) to 63.26 cumecs during the near-term (2020-2040), 74.12 cumecs during the mid-term (2041-2070) and 96.82 cumecs during the end-term (2071-2100) under SSP585 scenario. The comparison of the average daily discharge under SSP245 and SSP585 scenarios, for Shakkar River at Gadarwara, which is a right bank headwater catchment, during the various time horizons is given in Figure 5.171.

The gauging site on the main river at Sandia is located further downstream of the Barmanghat and has the influence of the releases from Bargi dam too. The average daily flow is projected to increase from 824.72 cumecs during the baseline period (1961-1990) and 783.48 cumecs during present period (1991-2019) to 977.88 cumecs during the near-term (2020-2040), 1039.63 cumecs during the mid-term (2041-2070) and 1146.70 cumecs during the end-term (2071-2100) under

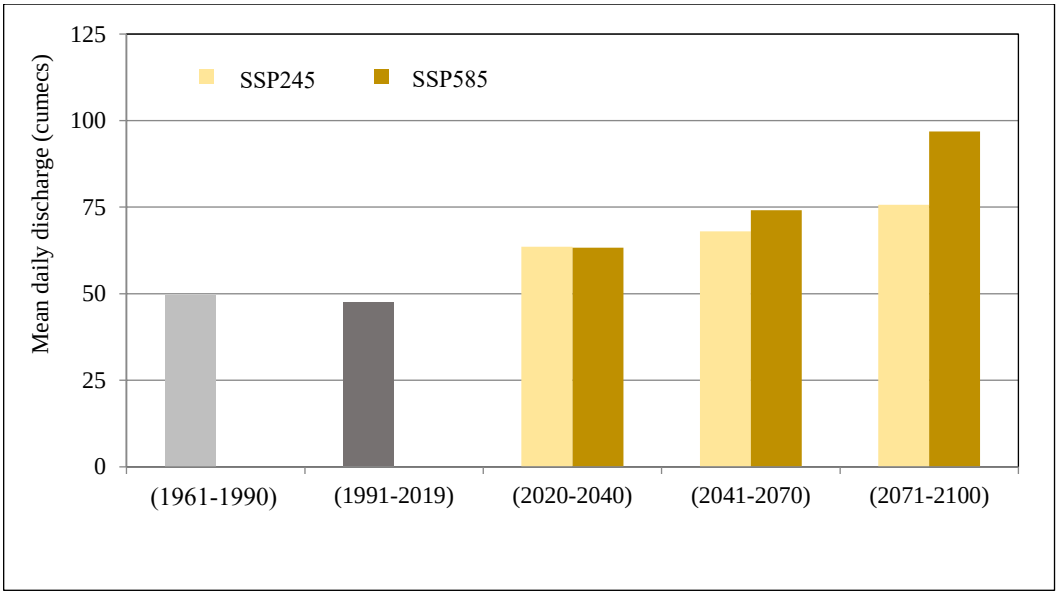

Figure 5.171: Comparison of average daily discharge (ensemble mean) for Shakkar River at Gadarwara

SSP245 scenario. Similarly, the average daily flow is projected to increase slightly from 824.72 cumecs during the baseline period (1961-1990) and 783.48 cumecs during present period (1991-2019) to 952.42 cumecs during the near-term (2020-2040), 1102.08 cumecs during the mid-term (2041-2070) and 1391.97 cumecs during the end-term (2071-2100) under SSP585 scenario. As such, substantially higher average daily stream flow is projected for Narmada River up to Sandia GD site. The comparison of the average daily discharge under SSP245 and SSP585 scenarios, for Narmada River at Sandia located on the main river channel, during the various time horizons is given in Figure 5.172.

This gauging site on Narmada at Hoshangabad which is the last gauging station in the Upper Narmada basin has the influence of the three major dams viz., Bargi dam, Barna dam and Tawa dam. It also has the contribution of the river flows from all the headwater catchments and dam regulations. The average daily flow under SSP245 scenario is projected to increase from 1177.64 cumecs during the baseline period (1961-1990) and 1101.73 cumecs during present period (1991-2019) to 1378.27 cumecs during the near-term (2020-2040), 1466.72 cumecs during the mid-term (2041-2070) and 1620.65 cumecs during the end-term (2071-2100). Similarly, the average daily flow under SSP585 scenario is projected to increase slightly from 1177.64 cumecs during the baseline period (1961-1990) and 1104.73 cumecs during present period (1991-2019) to 1323.06 cumecs during the near-term

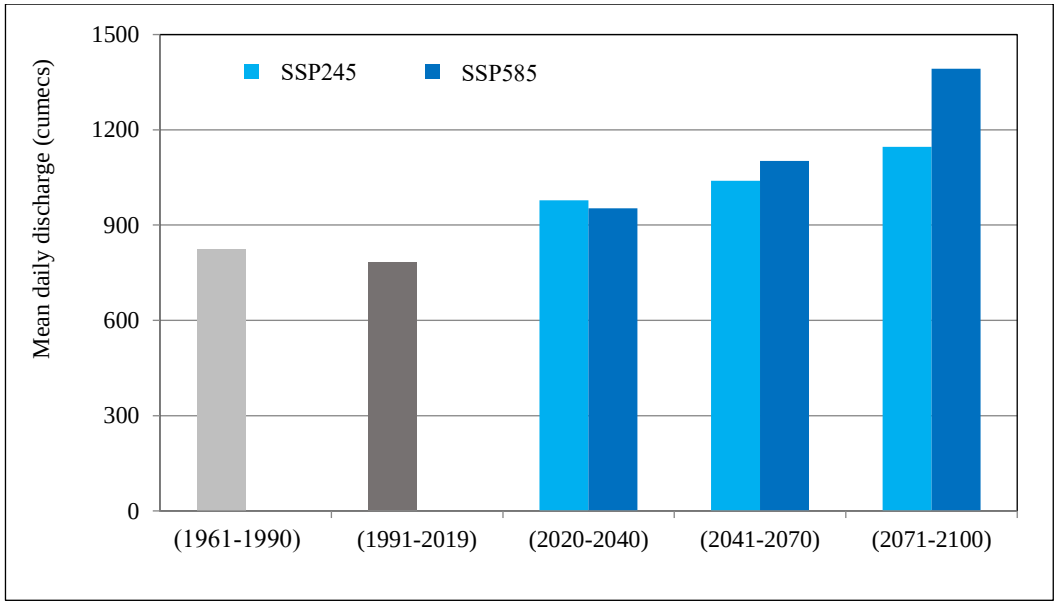

Figure 5.172: Comparison of average daily discharge (ensemble mean) for Narmada at Sandia

(2020-2040), 1529.28 cumecs during the mid-term (2041-2070) and 1934.50 cumecs during the end-term (2071-2100). The comparison of the average daily discharge under SSP245 and SSP585 scenarios, for Narmada River at Hoshangabad during the various time horizons is given in Figure 5.173. Therefore, substantially higher average daily stream flow is projected for all the headwater catchments and main river catchments in the Upper Narmada basin.

5.13.3.2 Climate Change Impact on High Flows

The 1-day maximum stream flow for Narmada River at Manot, which is a headwater catchment from the origin of Narmada River is projected to increase from 3073.51 cumecs during the baseline period (1970-1990) and 2556.56 cumecs during present period (1991-2019) to 3035.29 cumecs during the near-term (2020-2040), 3299.32 cumecs during the mid-term (2041-2070) and 3599.02 cumecs during the end-term (2071-2100) under SSP245 scenario. Similarly, 1-day maximum stream

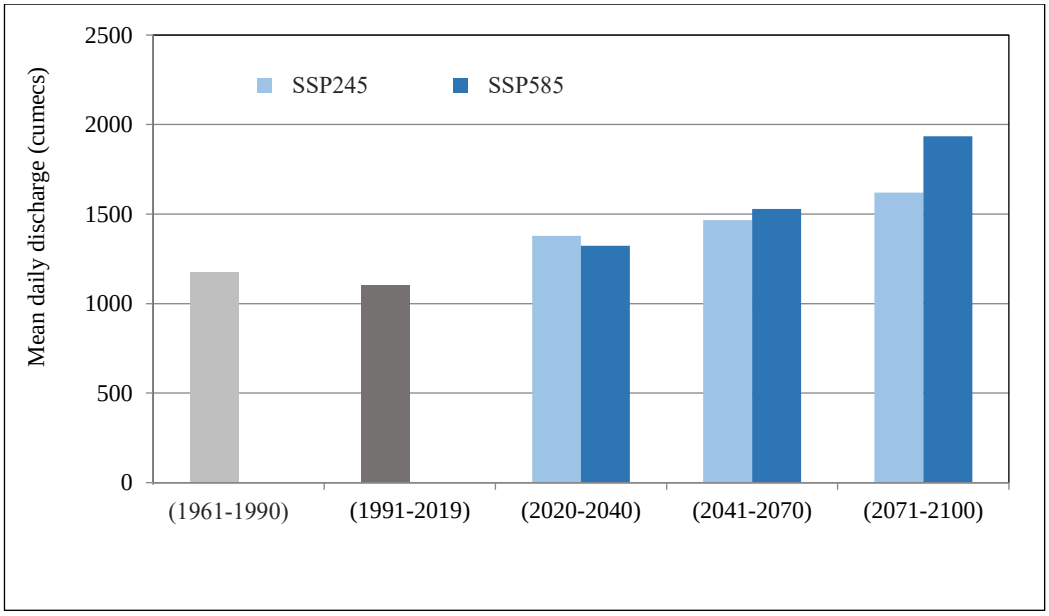

Figure 5.173: Comparison of average daily discharge (ensemble mean) for Narmada at Hoshangabad

flow for Narmada River at Manot under SSP585 scenario is projected to vary between 3073.51 cumecs during the baseline period (1970-1990) and 2556.56 cumecs during present period (1991-2019) to 3291.54 cumecs during the near-term (2020-2040), 3948.57 cumecs during the mid-term (2041-2070) and 4817.79 cumecs during the end-term (2071-2100). The comparison of the 1-day maximum stream flow under SSP245 and SSP585 scenarios for Narmada River at Manot during the various time horizons is given in Figure 5.174.

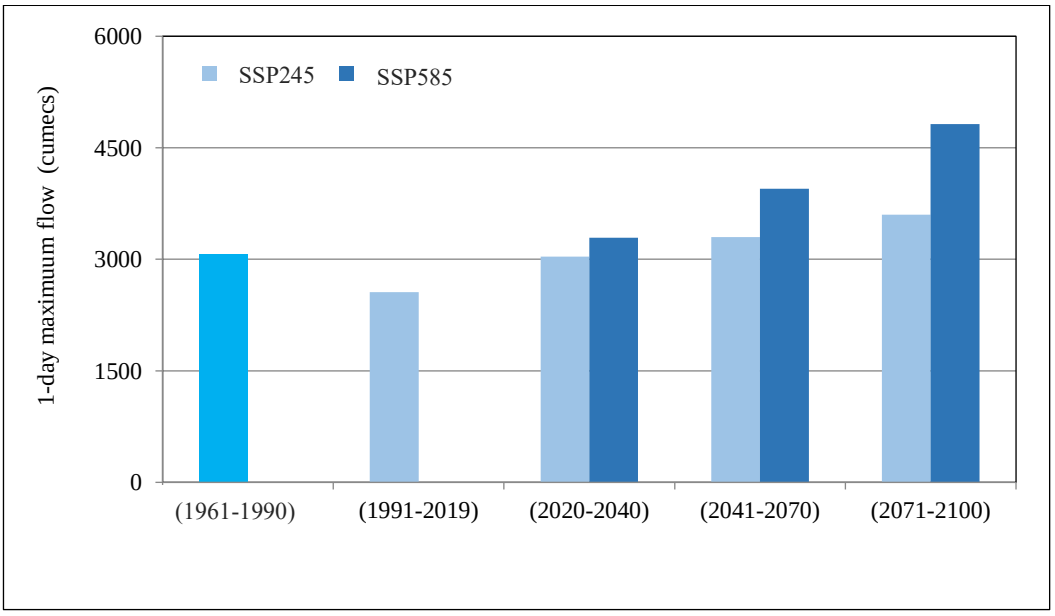

Figure 5.174: Comparison of 1-day maximum flow (ensemble means) for Narmada River at Manot

The high flows represented by the 5% and 10% dependable flows have been computed from the projected future streamflow datasets. The high flows represented by Q5 and Q10, under SSP245 scenario is projected to increase from 6306.84 MCM and 5741.44 MCM respectively during the baseline period (1970-1990) and 6537.67 MCM and 5281.17 MCM respectively, during present period (1991-2019) to 7489.4 MCM and 6793.6 MCM respectively during the near-term (2020-2040), 5823.2 MCM and 5283.3 MCM respectively during the mid-term (2041-2070) and 8575.1 MCM and 7674.6 MCM respectively during the end-term (2071-2100).

Similarly, the high flows represented by Q5 and Q10, under SSP585 scenario is projected to increase from 6306.84 MCM and 5741.44 MCM respectively during the baseline period (1970-1990) and 6537.67 MCM and 5281.17 MCM respectively, during present period (1991-2019) to 8048.1 MCM and 7120.2 MCM respectively during the near-term (2020-2040), 8644.7 MCM and 7955.8 MCM respectively during the mid-term (2041-2070) and 11528.9 MCM and 9996.3 MCM respectively during the end-term (2071-2100). The comparison of the annual dependable flow volumes at 5% and 10% probability of exceedance, Q5 & Q10, which represent the high flows for Narmada River at Manot is given in Figure 5.175. Therefore, this headwater catchment of the Narmada River system is

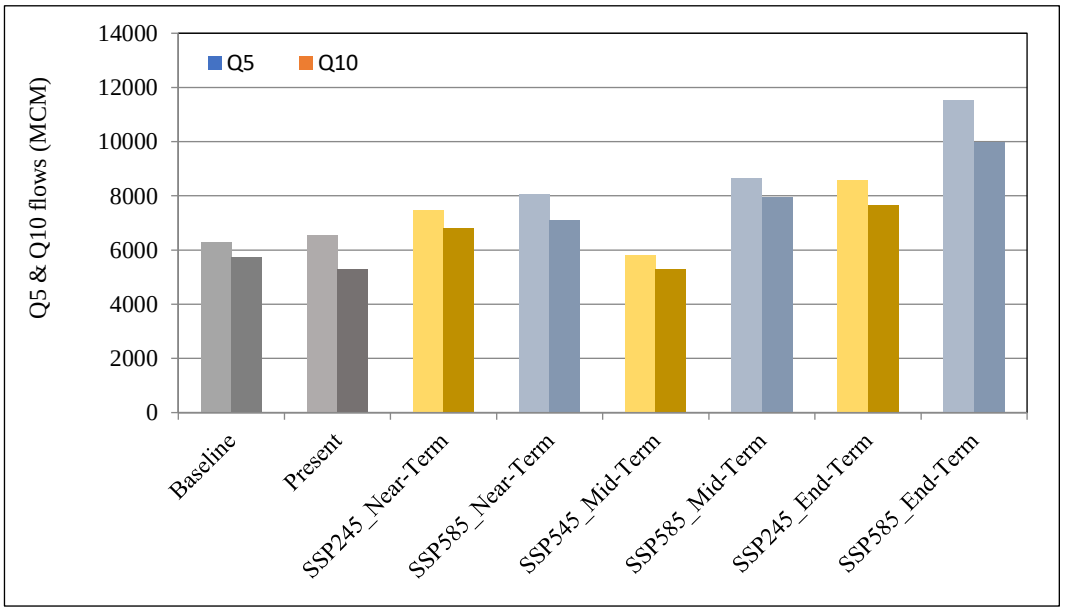

Figure 5.175: Comparison of high flows represented by Q5 & Q10 (ensemble means) for Narmada River at Manot

projected to witness higher magnitude extreme flows as depicted by the increases in the Q5, Q10 and1-day maximum stream flow magnitudes in the future time horizons.

The 1-day maximum stream flow for Burhner river at Mohgaon, another headwater catchment from the upper reaches of the Narmada River basin, is projected to increase from 2087.82 cumecs during the baseline period (1961-1990) and 1788.64 cumecs during present period (1991-2019) to 2521.38 cumecs during the near-term (2020-2040), 2739.37 cumecs during the mid-term (2041-2070) and 3009.30 cumecs during the end-term (2071-2100) under SSP245 scenario. Similarly, the 1-day maximum stream flow for Burhner river at Mohgaon is projected to vary between 2087.72 cumecs during the baseline period (1961-1990) and 1788.64 cumecs during present period (1991-2019) to 2717.57 cumecs during the near-term (2020-2040), 3313.14 cumecs during the mid-term (2041-2070) and 4119.11 cumecs during the end-term (2071-2100) under SSP585 scenario. The comparison of the 1-day maximum stream flow under SSP245 and SSP585 scenarios for Burhner river at Mohgaon during the various time horizons is given in Figure 5.176.

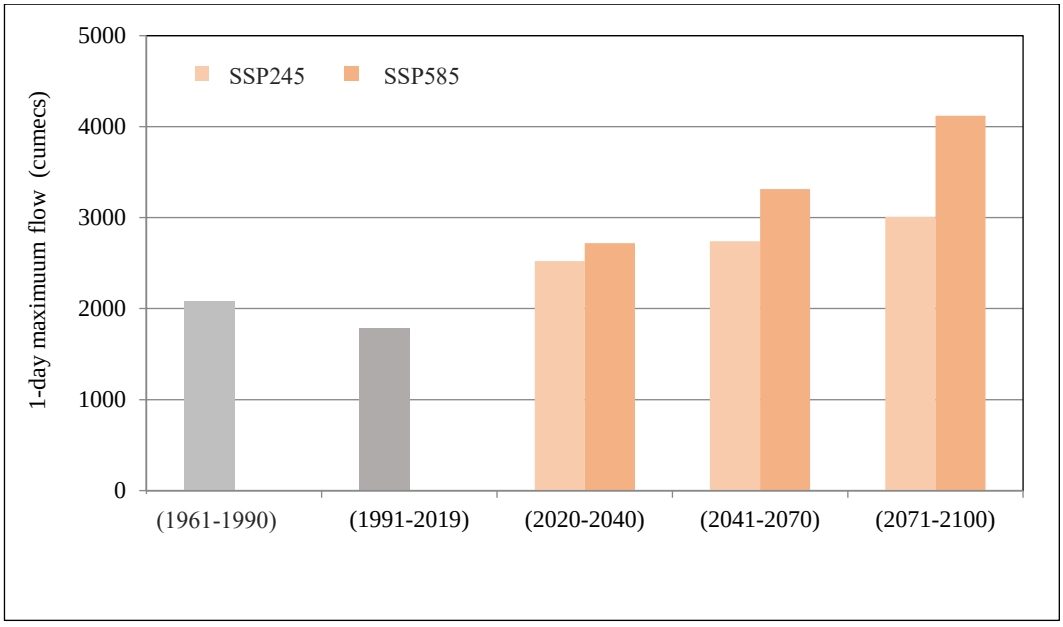

Figure 5.176: Comparison of 1-day maximum flow (ensemble means) for Burhner River at Mohgaon

The high flow based on the annual dependable flow volumes, Q5 and Q10, is projected to increase from 4221.61 MCM and 4126.62 MCM respectively during the baseline period (1961-1990) and 6655.29 MCM and 4546.47 MCM respectively, during present period (1991-2019) to 6297.7 MCM and 5386.4 MCM respectively

during the near-term (2020-2040), 5823.2 MCM and 5283.3 MCM respectively during the mid-term (2041-2070) and 6770.7 MCM and 6021.1 MCM respectively during the end-term (2071-2100) under SSP245 scenario.

Similarly, the high flows based on the annual dependable flow volumes, under SSP585 scenario is projected to increase from 4221.61 MCM and 4126.62 MCM respectively during the baseline period (1961-1990) and 6655.29 MCM and 4546.47 MCM respectively, during present period (1991-2019) to 6343.8 MCM and 5513.6 MCM respectively during the near-term (2020-2040), 6841.5 MCM and 6360.0 MCM respectively during the mid-term (2041-2070) and 9258.1 MCM and 8067.2 MCM respectively during the end-term (2071-2100). Therefore, this major headwater catchment of the Narmada River system is projected to witness higher magnitude extreme flows as depicted by the increases in the Q5, Q10 and 1-day maximum stream flow magnitudes in the future time horizons. The comparison of the annual dependable flow volumes at 5% and 10% probability of exceedance, Q5 & Q10, for Burhner river at Mohgaon is given in Figure 5.177.

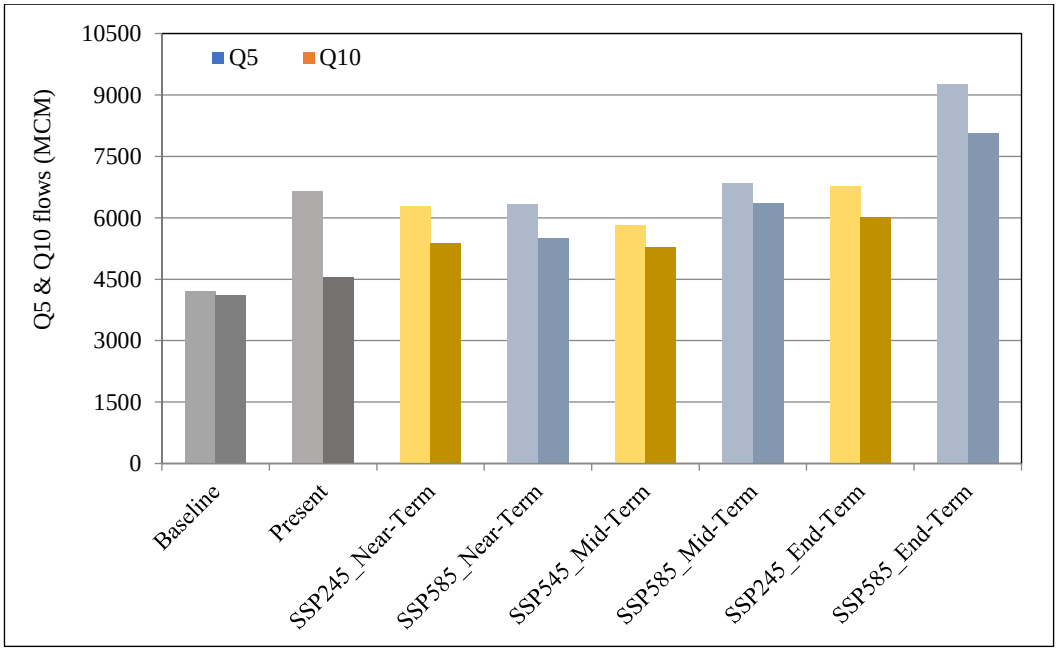

Figure 5.177: Comparison of high flows represented by Q5 & Q10 (ensemble means) for Burhner River at Mohgaon

The 1-day maximum stream flow for Sher River at Belkheri, which is another headwater catchment from the middle reaches of the Narmada River basin, is projected to increase from 1083.72 cumecs during the baseline period (1961-1990)

and 1150.30 cumecs during present period (1991-2019) to 1191.10 cumecs during the near-term (2020-2040), 1279.02 cumecs during the mid-term (2041-2070) and 1435.67 cumecs during the end-term (2071-2100) under SSP245 scenario. Similarly, 1-day maximum stream flow for Sher River at Belkheri is projected to vary between 1083.72 cumecs during the baseline period (1961-1990) and 1150.3 cumecs during present period (1991-2019) to 1153.86 cumecs during the near-term (2020-2040), 1336.07 cumecs during the mid-term (2041-2070) and 1658.33 cumecs during the end-term (2071-2100) under SSP585 scenario. The comparison of the 1-day maximum stream flow under SSP245 and SSP585 scenarios for Sher River at Belkheri during the various time horizons is given in Figure 5.178.

The high flows based on the annual dependable flow volumes, represented by Q5 and Q10, is projected to increase from 1774.2 MCM and 1550.3 MCM respectively during the baseline period (1961-1990) and 1987.1 MCM and 1653.4 MCM respectively, during present period (1991-2019) to 3003.2 MCM and 2335.3

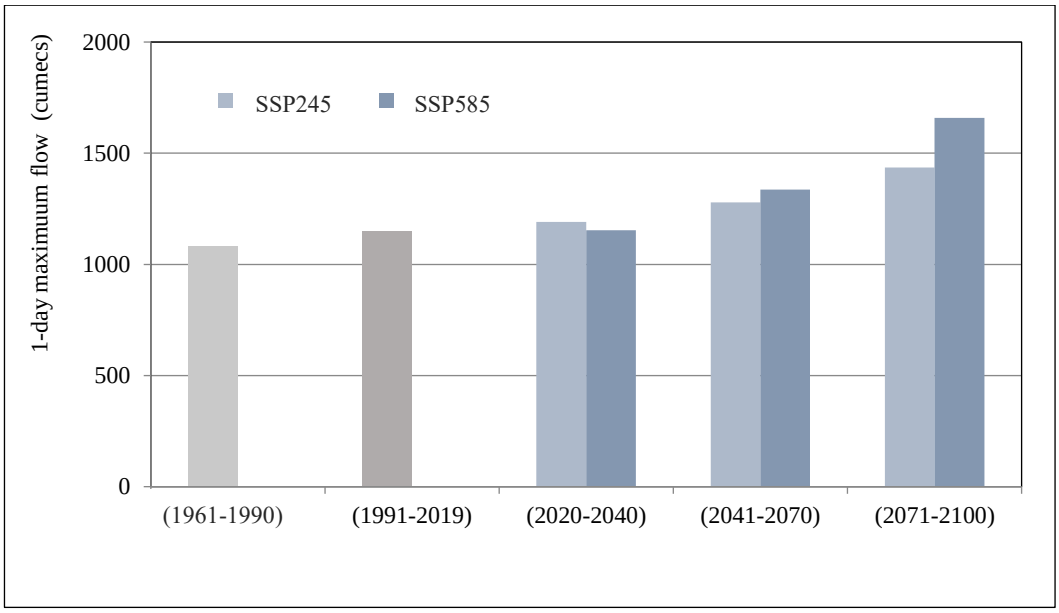

Figure 5.178: Comparison of 1-day maximum flow (ensemble means) for Sher River at Belkheri

MCM respectively during the near-term (2020-2040), 2676.4 MCM and 2340.2 MCM respectively during the mid-term (2041-2070) and 3086.7 MCM and 2623.9 MCM respectively during the end-term (2071-2100) under SSP245 scenario.

Similarly, the high flows based on the annual dependable flow volumes, represented by Q5 and Q10, under SSP585 scenario is projected to increase from 1774.2 MCM and 1550.3 MCM respectively during the baseline period (1961-1990) and 1987.1 MCM and 1653.4 MCM respectively, during present period (1991-2019) to 2599.8 MCM and 2283.0 MCM respectively during the near-term (2020-2040), 2743.2 MCM and 2477.7 MCM respectively during the mid-term (2041-2070) and 3775.9 MCM and 3218.6 MCM respectively during the end-term (2071-2100). Therefore, this smaller left bank headwater catchment of the Narmada River system is projected to witness higher magnitude extreme flows as depicted by the increases in the Q5, Q10 and 1-day maximum stream flow magnitudes in the future time horizons. The comparison of the dependable flow volumes at 5% and 10% probability of exceedance, Q5 & Q10, for Sher River at Belkheri is given in Figure 5.179.

The 1-day maximum stream flow for Hiran River at Patan, which is another headwater catchment from the middle reaches of the Narmada river basin, is

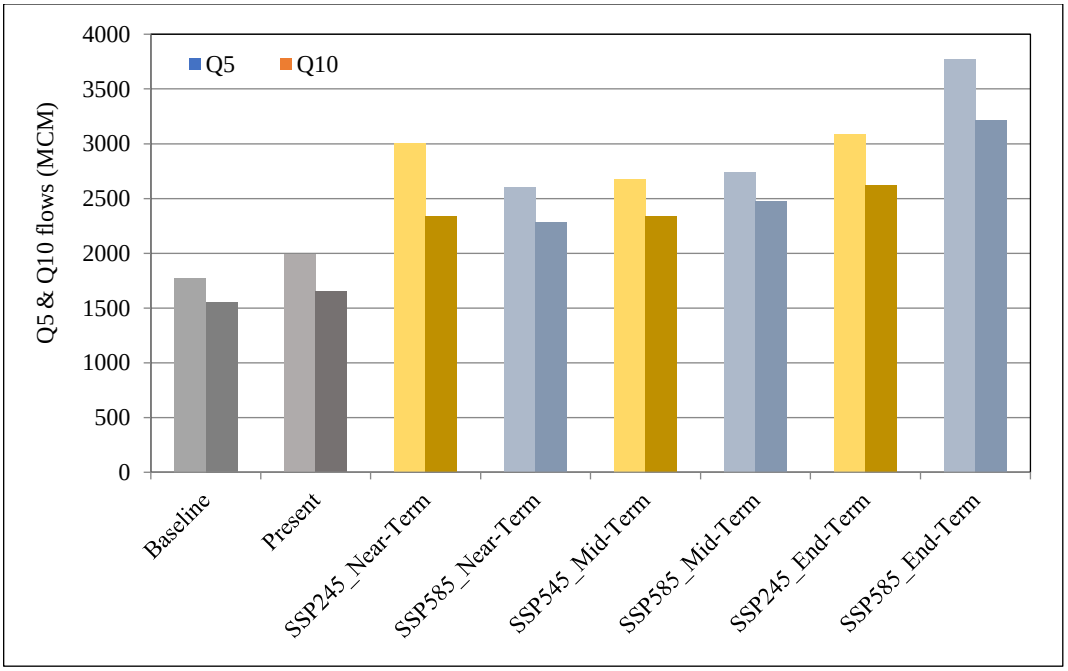

Figure 5.179: Comparison of high flows represented by Q5 & Q10 (ensemble means) for Sher River at Belkheri

projected to increase from 2539.93 cumecs during the baseline period (1961-1990) and 2517.55 cumecs during present period (1991-2019) to 2860.68 cumecs during the near-term (2020-2040), 3091.85 cumecs during the mid-term (2041-2070) and 3378.93 cumecs during the end-term (2071-2100) under SSP245 scenario.

Similarly, 1-day maximum stream flow for Hiran River at Patan under SSP585 scenario is projected to increase from 2539.93 cumecs during the baseline period (1961-1990) and 2517.55 cumecs during present period (1991-2019) to 2870.7 cumecs during the near-term (2020-2040), 3337.8 cumecs during the mid-term (2041-2070) and 3968.7 cumecs during the end-term (2071-2100). The comparison of the 1-day maximum stream flow under SSP245 and SSP585 scenarios for Hiran River at Patan during the various time horizons is given in Figure 5.180.

The high flows based on the annual dependable flow volumes, represented by Q5 and Q10, under SSP245 scenario is projected to increase from 5864.06 MCM and 4685.62 MCM respectively during the baseline period (1961-1990) and 5598.31 MCM and 5160.66 MCM respectively, during present period (1991-2019) to 6927.80 MCM and 6103.30 MCM respectively during the near-term (2020-2040), 6953.80 MCM and 6269.90 MCM respectively during the mid-term (2041-

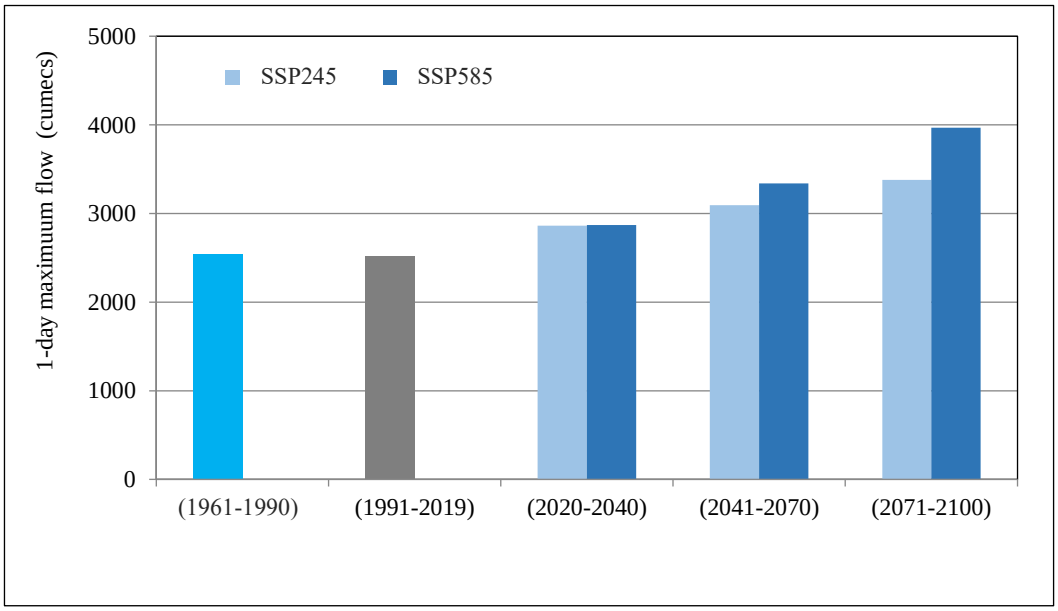

Figure 5.180: Comparison of 1-day maximum flow (ensemble means) for Hiran River at Patan

2070) and 8237.10 MCM and 7197.90 MCM respectively during the end-term (2071-2100).

Similarly, the high flows based on the annual dependable flow volumes, represented by Q5 and Q10, under SSP585 scenario is projected to increase from 5864.06 MCM and 4685.62 MCM respectively during the baseline period (1961-

1990) and 5598.31 MCM and 5160.66 MCM respectively, during present period (1991-2019) to 6974.10 MCM and 6177.10 MCM respectively during the near-term (2020-2040), 7785.20 MCM and 6928.90 MCM respectively during the mid-term (2041-2070) and 10120.2 MCM and 8586.10 MCM respectively during the end-term (2071-2100). The comparison of the annual dependable flow volumes at 5% and 10% probability of exceedance, Q5 & Q10, for Hiran River at Patan is given in Figure 5.181.

The 1-day maximum stream flow for Shakkar river at Gadarwara, which is another headwater catchment located in the middle reaches of the Narmada River basin, under SSP245 scenario is projected to increase from 1748.85 cumecs during the baseline period (1961-1990) and 1838.37 cumecs during present period (1991-2019) to 2010.14 cumecs during the near-term (2020-2040), 2137.31 cumecs during the mid-term (2041-2070) and 2409.48 cumecs during the end-term (2071-2100).

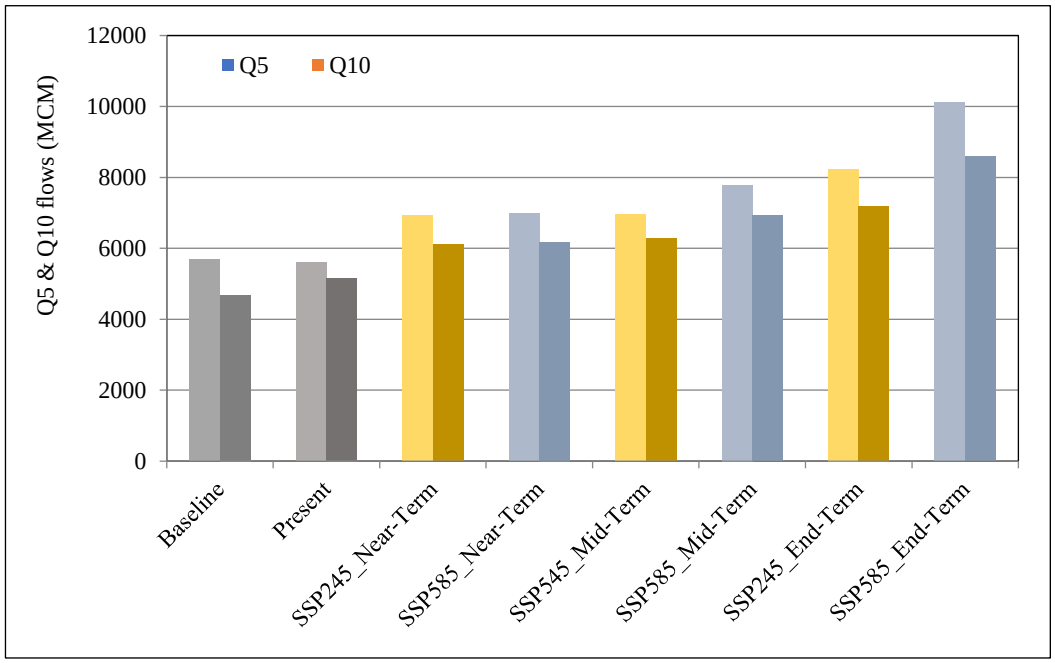

Figure 5.181: Comparison of high flows represented by Q5 & Q10 (ensemble means) for Hiran River at Patan

Similarly, 1-day maximum stream flow for Shakkar river at Gadarwara under SSP585 scenario is projected to increase from 1748.85 cumecs during the baseline period (1961-1990) and 1838.37 cumecs during present period (1991-2019) to 2041.11 cumecs during the near- term (2020-2040), 2364.13 cumecs during the mid-term (2041-2070) and 2937.87 cumecs during the end-term (2071-2100). The comparison of the 1-day maximum stream flow under SSP245 and SSP585 scenarios

for Shakkar river at Gadarwara during the various time horizons is given in Figure 5.182.

The high flows based on the annual dependable flow volumes, represented by Q5 and Q10 for Shakkar river at Gadarwara, under SSP245 scenario is projected to increase from 2622.59 MCM and 2550 MCM respectively during the baseline period (1961-1990) and 3091.73 MCM and 2812.13 MCM respectively, during present period (1991-2019) to 4548.20 MCM and 3503.90 MCM respectively during the near-term (2020-2040), 4145.10 MCM and 3547.50 MCM respectively

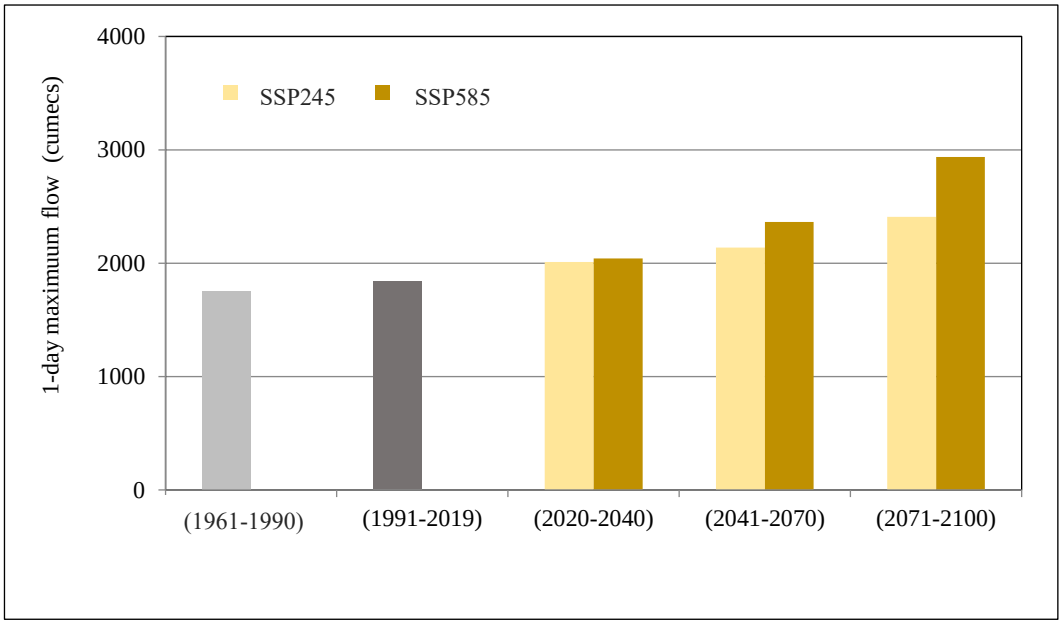

Figure 5.182: Comparison of 1-day maximum flow (ensemble means) for Shakkar river at Gadarwara

during the mid-term (2041-2070) and 4749.50 MCM and 4004.90 MCM respectively during the end-term (2071-2100).

Similarly, the high flows based on the annual dependable flow volumes, represented by Q5 and Q10, under SSP585 scenario is projected to increase from 2622.59 MCM and 2550 MCM respectively during the baseline period (1961-1990) and 3091.73 MCM and 2812.13 MCM respectively, during present period (1991-2019) to 4212.30 MCM and 3486.0 MCM respectively during the near-term (2020-2040), 4368.20 MCM and 3905.50 MCM respectively during the mid-term (2041-2070) and 6031.30 MCM and 5143.20 MCM respectively during the end-term (2071-2100). There (1961-1990) bank headwater catchment of the Narmada River system

is projected to witness higher magnitude extreme flows as depicted by the increases in the Q5, Q10 and 1-day maximum stream flow magnitudes in the future time horizons. The comparison of the annual dependable flow volumes at 5% and 10% probability of exceedance, Q5 & Q10, for Shakkar river at Gadarwara is given in Figure 5.183.

The 1-day maximum stream flow for Narmada River at Barmanghat, which is located on the main Narmada River channel, under SSP245 scenario is projected to increase from 14120.7 cumecs during the baseline period (1961-1990) and

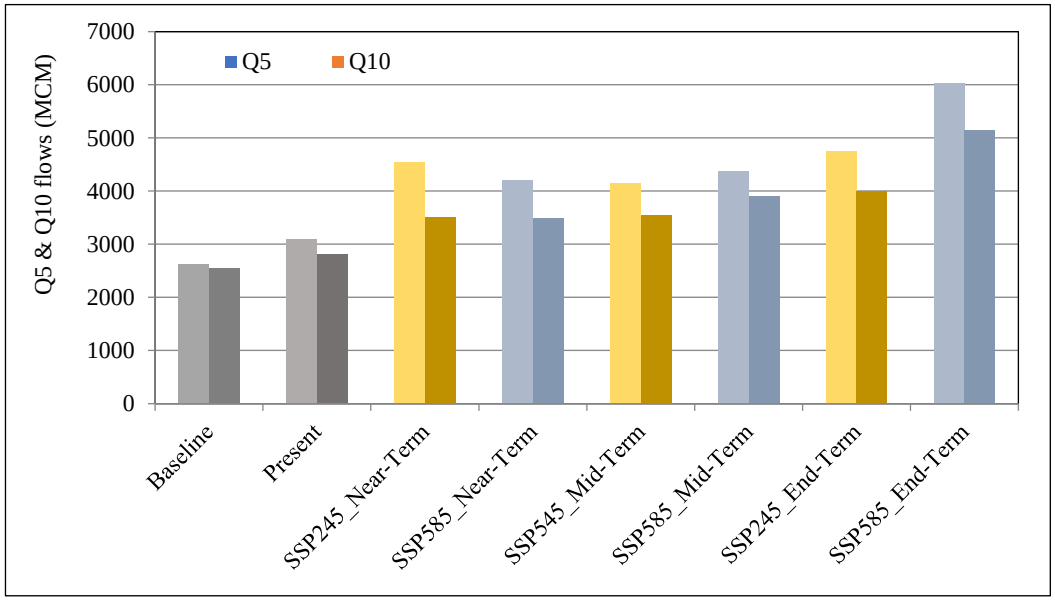

Figure 5.183: Comparison of high flows represented by Q5 & Q10 (ensemble means) for Shakkar river at Gadarwara

11827.0 cumecs during present period (1991-2019) to 17298.91 cumecs during the near-term (2020-2040), 18867.39 cumecs during the mid-term (2041-2070) and 20791.13 cumecs during the end-term (2071-2100). Similarly, 1-day maximum stream flow for Narmada River at Barmanghat under SSP585 scenario is projected to increase from 14120.70 cumecs during the baseline period (1961-1990) and 11827.0 cumecs during present period (1991-2019) to 21520.52 cumecs during the near- term (2020-2040), 22187.42 cumecs during the mid-term (2041-2070) and 24929.21 cumecs during the end-term (2071-2100). The comparison of the average 1-day maximum stream flow under SSP245 and SSP585 scenarios for Narmada River at Barmanghat during the various time horizons is given in Figure 5.184. The high flows based on the annual dependable flow volumes, represented by Q5 and

Q10, for Narmada River at Barmanghat is projected to increase from 28648.30 MCM and 28306.03 MCM respectively during the baseline period (1961-1990) and 33784.35 MCM and 30608.02 MCM respectively during present period (1991-2019) to 45533.9 MCM and 39647.3 MCM respectively during the near-term (2020-2040), 44030.90 MCM and 39318.8 MCM respectively during the mid-term (2041-2070) and 51141.0 MCM and 45249.50 MCM respectively during the end-term (2071-2100) under SSP245 scenario.

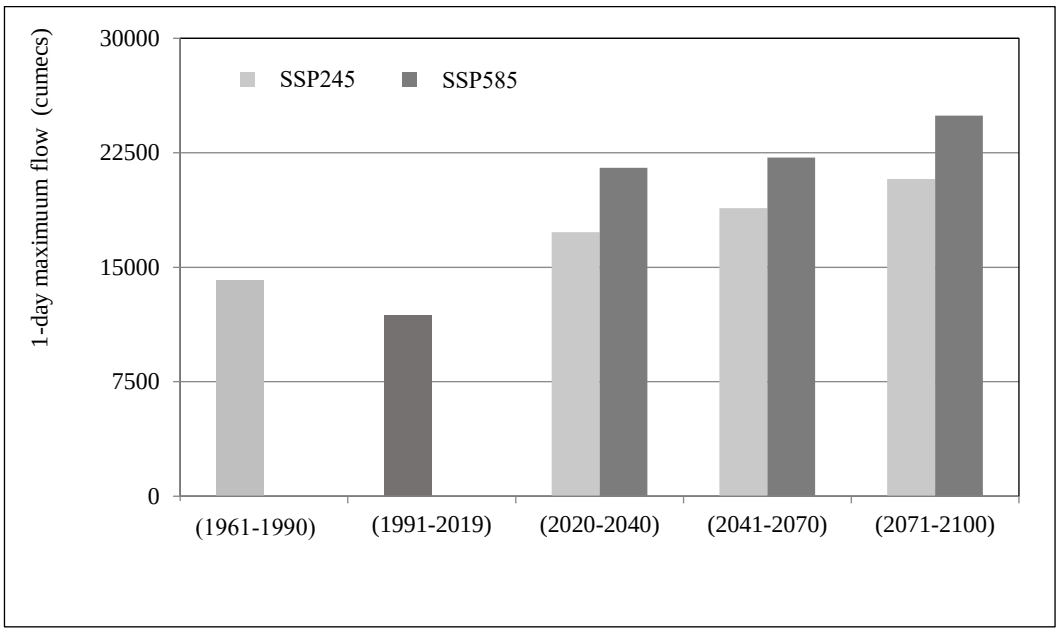

Figure 5.184: Comparison of 1-day maximum flow (ensemble means) for Narmada River at Barmanghat

Similarly, the high flows based on the annual dependable flow volumes, represented by Q5 and Q10, is projected to increase from 28648.30 MCM and 28306.03 MCM respectively during the baseline period (1961-1990) and 33784.35 MCM and 30608.02 MCM respectively, during present period (1991-2019) to 43967.80 MCM and 38776.80 MCM respectively during the near-term (2020-2040), 47962.20 MCM and 43890.40 MCM respectively during the mid-term (2041-2070) and 64054.20 MCM and 55434.10 MCM respectively during the end-term (2071-2100) under SSP585 scenario. The comparison of the annual dependable flow volumes at 5% and 10% probability of exceedance, Q5 & Q10, for Narmada River at Barmanghat is given in Figure 5.185. Therefore, the Narmada River at Barmanghat is projected to witness higher magnitude extreme flows as depicted by the increases in the Q5, Q10 and 1-day maximum stream flow magnitudes in the future time horizons.

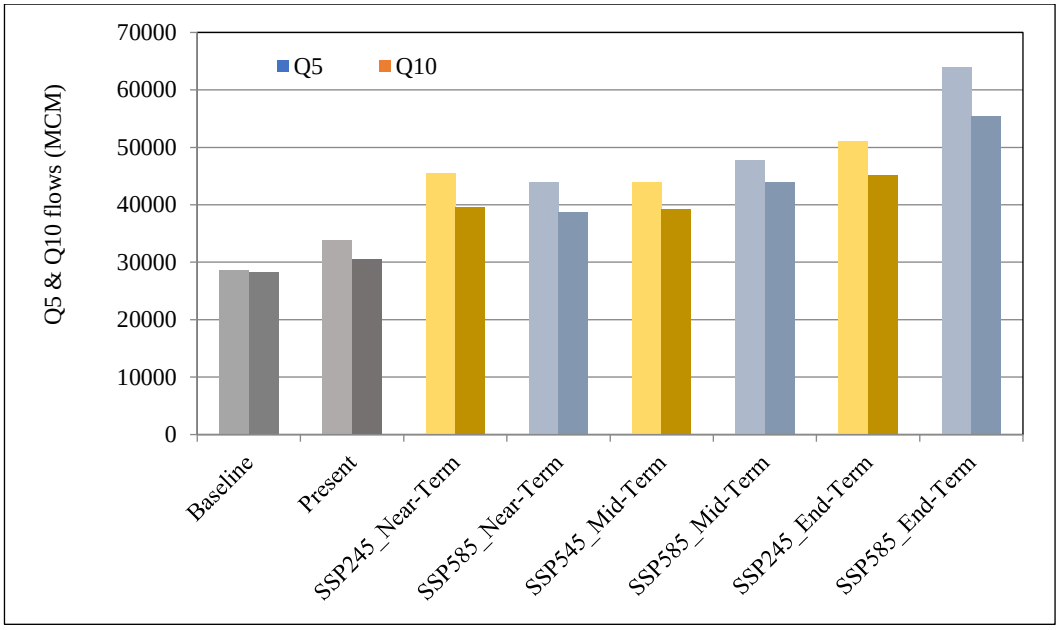

Figure 5.185: Comparison of high flows represented by Q5 & Q10 (ensemble means) for Narmada River at Barmanghat

The 1-day maximum stream flow for Narmada River at Sandia, which is located on the main Narmada River channel, is projected to increase from 17251.40 cumecs during the baseline period (1961-1990) and 15166.00 cumecs during present period (1991-2019) to 19993.74 cumecs during the near-term (2020-2040), 23426.44 cumecs during the mid-term (2041-2070) and 25891.51 cumecs during the end-term (2071-2100) under SSP245 scenario. Similarly, 1-day maximum stream flow for Narmada River at Sandia under SSP585 scenario is projected to increase from 17251.40 cumecs during the baseline period (1961-1990) and 15166.0 cumecs during present period (1991-2019) to 21537.51 cumecs during the near- term (2020-2040), 25015.32 cumecs during the mid-term (2041-2070) and 30513.37 cumecs during the end-term (2071-2100). The comparison of the average 1-day maximum stream flow under SSP245 and SSP585 scenarios for Narmada River at Sandia during the various time horizons is given in Figure 5.186. The 1-day maximum stream flow for Narmada River at Hoshangabad, which is located on the main Narmada River channel, is projected to increase from 23534.30 cumecs during the baseline period (1961-1990) and 22310.70 cumecs during present period (1991-2019) to 29867.19 cumecs during the near-term (2020-2040), 31798.56 cumecs during the mid-term (2041-2070) and 35424.94 cumecs during the end-term

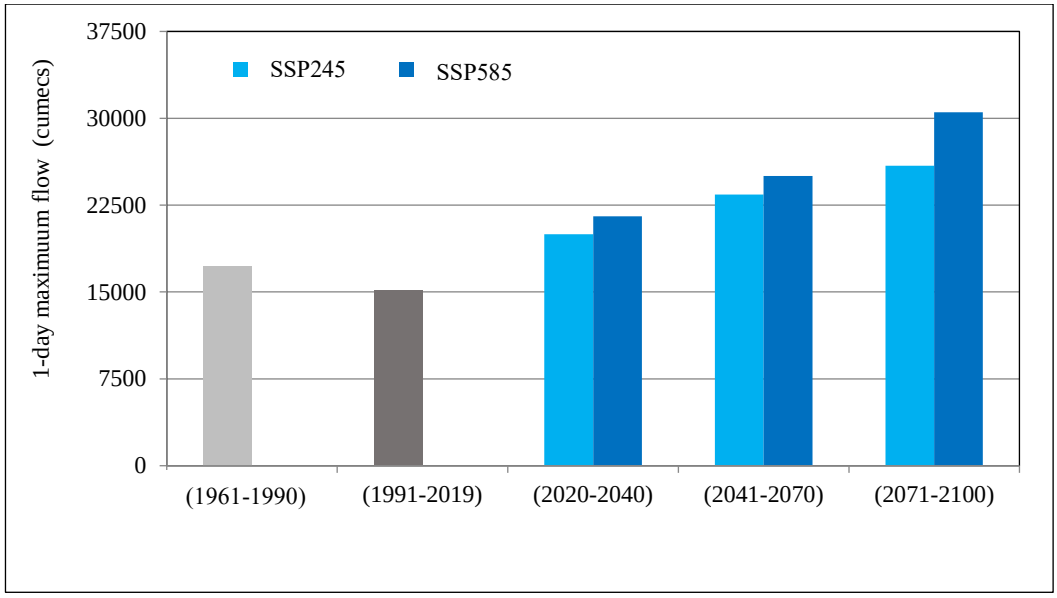

Figure 5.186: Comparison of 1-day maximum flow (ensemble means) for Narmada River at Sandia

(2071-2100) under SSP245 scenario. Similarly, 1-day maximum stream flow for Narmada River at Hoshangabadunder SSP585 scenario is projected to increase from 23534.3 cumecs during the baseline period (1961-1990) and 22310.70 cumecs during present period (1991-2019) to 29280.82 cumecs during the near- term (2020-2040), 33584.36 cumecs during the mid-term (2041-2070) and 41182.01 cumecs during the end-term (2071-2100). The comparison of the average 1-day maximum stream flow under SSP245 and SSP585 scenarios for Narmada River at Hoshangabad during the various time horizons is given in Figure 5.187.

The high flows based on the annual dependable flow volumes, represented by Q5 and Q10, for Narmada River at Hoshangabad under SSP245 scenario is projected to increase from 53860.15 MCM and 49741.87MCM respectively during the baseline period (1961-1990) and 61331.93 MCM and 57085.89 MCM respectively, during present period (1991-2019) to 85929.4 MCM and70275.2 MCM respectively during the near-term (2020-2040), 81509.7 MCM and 71483.6 MCM respectively during the mid-term (2041-2070) and 92735.3 MCM and 81273.6 MCM respectively during the end-term (2071-2100).

Similarly, the high flows based on the annual dependable flow volumes, represented by Q5 and Q10, under SSP585 scenario is projected to increase from

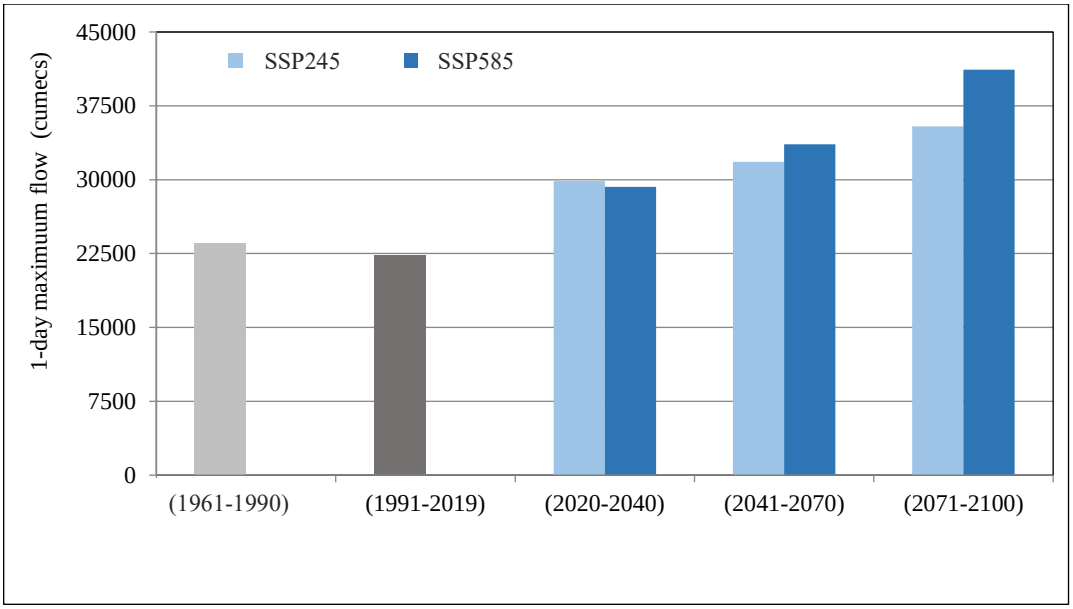

Figure 5.187: Comparison of 1-day maximum flow (ensemble means) for Narmada River at Hoshangabad

53860.15 MCM and 49741.87MCM respectively during the baseline period (1961-1990)and 61331.93 MCM and 57085.89 MCM respectively, during present period (1991-2019) to 78907.70 MCM and 68322.6 MCM respectively during the near-term (2020-2040), 84163.8 MCM and 75422.0 MCM respectively during the mid-term (2041-2070) and 112471.6 MCM and 95937.8 MCM respectively during the end-term (2071-2100).

The comparison of the annual dependable flow volumes at 5% and 10% probability of exceedance (Q5 & Q10), which represent the high flows for Narmada River at Hoshangabad is given in Figure 5.188. Therefore, the Narmada River at Hoshangabad is projected to witness higher magnitude extreme flows as depicted by the increases in the Q5, Q10 and 1-day maximum stream flow magnitudes in the future time horizons.

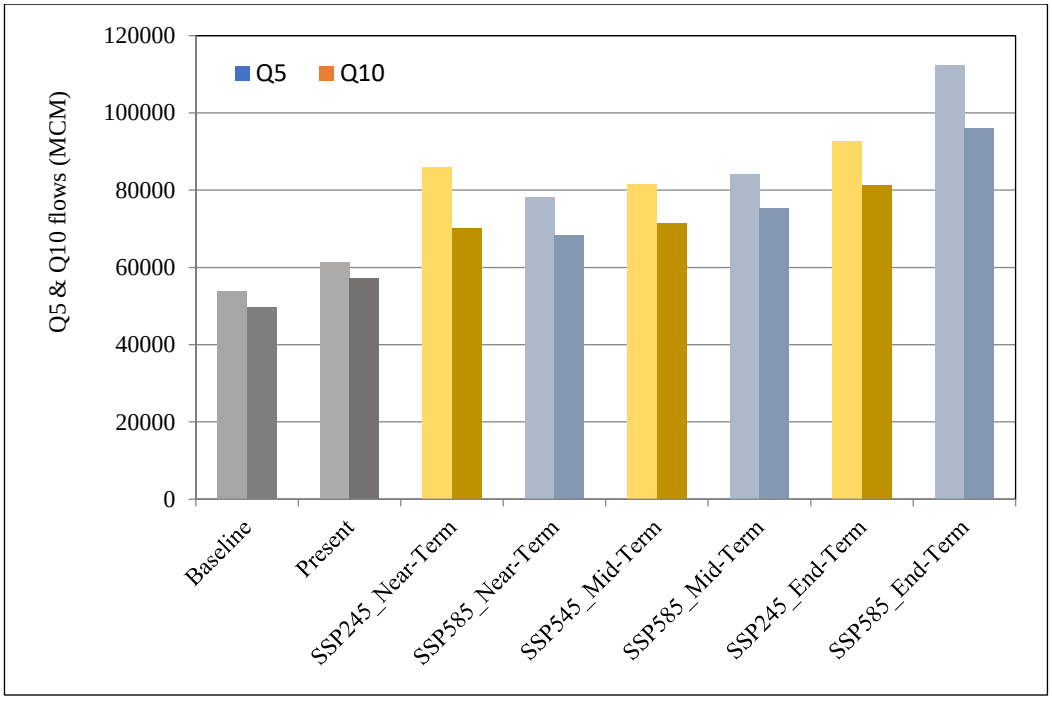

Figure 5.188: Comparison of high flows represented by Q5 & Q10 (ensemble means) for Narmada River at Hoshangabad

5.13.3.3 Climate Change Impact Assessment on Surface Water by Other Models

The impacts of the climate change particularly the precipitation, maximum and minimum temperature on the water availability including mean flows and high flows have been discussed in detail beased on the future SWAT model simulations. Similar analysis has been carried out with all the other surface water models which was calibrated and vlaidated for the the Upper Narmada basin. The other models include WEAP, VIC, HEC-HMS and MIKE11-NAM. The discussions shall be very brief and limited as the direction of the results pertaining to the future water availability can changes in the streamflow pattern are very much similar with the changes only seen in their magnitudes. The resuts of all these models shall be summarised based on the detailed results given above and the brief results from remaining models being explained below in the sections to follow.

5.13.3.3.1 Climate Change Impact Assessment using WEAP

The calibrated and validated WEAP model has been driven with the historical observed data during the baseline period (1961-1900) and present period (1991-2019). Subsequently, the simulations were carried out using the high-

resolution bias corrected future climate data of 13 GCMs for two distinct climate scenarios viz., SSP245 and SSP585. These simulations have been compared to understand the projected changes in the water availability and high flows during various time horizons. The same methodology has been followed for all hydrological models used in the study.

The results of the future WEAP model-based runoff simulation are given in brief in this section. The average daily flows have been estimated for all the headwater catchments as well as the gauging sites on the main River Narmada. The average daily flows are projected to increase marginally in all the tributaries and also in the main river system. The understanding of the average daily streamflow at Hoshangabad which is the last gauging site on river Narmada in Upper Narmada basin helps to understand the overall scenario in the Upper Narmada basin. The comparison of the average daily stream flow for Narmada at Hoshangabad is given in Table 5.44.

It can be observed that under SSP245 scenario, the average daily flows are projected to increase to 973.69 cumecs during the near-term, 963.37 cumecs during the mid-term and 988.51 cumecs during the end-term which is and increase of about 20% and is substantial. Similarly, under SSP585 scenario, the average daily flows are projected to increase to 1030.23 cumecs during the near-term, 1219.49 cumecs during the mid-term and 1583.98 cumecs during the end-term, the increase varying between 27% during the near-term to more than 60% during the end-term. Therefore, it can be observed that the average daily flows are projected to increase in all future time periods under both scenarios, but the increase is substantial under SSP585 scenario and more predominant during the end-term.

The 3-day consecutive flows help to understand the projected changes in the continuous stream flow pattern in the river system and is particularly useful for tributaries and headwater catchments where changes if any in the sustainability of non-stop flows can be an interesting investigation. The 3-day consecutive flows have been computed for all tributaries and gauging sites on

Table 5.44: Average daily stream flow at Hoshangabad from WEAP

Baseline (1961-1990)	809.728 cumecs					
Present (1991-2019)	790.938 cumecs					
Future (cumecs)	Near-term (2020-2040)		Mid-term (2041-2070)		End-term (2071-2100)	
	SSP245	**SSP585**	**SSP245**	**SSP585**	**SSP245**	**SSP585**
ACCESS-CM2	1018.81	925.85	1226.87	1160.86	1295.04	1380.18
ACCESS-ESM1-5	1185.15	749.51	854.91	1127.36	1271.44	1487.17
BCC-CSM2-MR	601.81	660.07	883.76	802.46	911.09	880.11
CanESM5	1005.73	1674.16	1630.51	1964.19	1832.49	3403.48
EC-Earth3	908.54	984.31	1096.51	1288.53	1178.33	1641.73
EC-Earth3-Veg	811.03	795.62	941.96	1074.31	1168.91	1388.60
INM-CM4-8	1020.66	1020.66	859.81	859.81	735.61	735.61
INM-CM5-0	1464.12	1329.64	1365.36	1677.71	1620.07	1939.74
MPI-ESM1-2-HR	954.67	834.30	1184.95	1144.58	1250.72	1918.06
MPI-ESM1-2-LR	805.31	806.79	1155.01	1190.75	1276.91	1972.38
MRI-ESM2-0	774.08	839.44	908.98	706.59	870.82	1034.13
NorESM2-LM	1179.21	940.27	998.81	1099.46	1215.81	1590.97
NorESM2-MM	928.88	963.30	976.82	1053.98	1226.06	1219.56
Ensemble mean	**973.69**	**963.38**	**988.51**	**1030.23**	**1219.49**	**1583.98**

main river system. The 3-day consecutive future flows are projected to increase in all headwater and main river catchments under both future climate scenarios.

The average 3-day consecutive flow simulated for Narmada at Hoshangabad under SSP245 scenario showed an increasing trend from near-term to end-term as compared to that during the baseline and present time periods. The comparison of the 3-day consecutive stream flow for Narmada at Hoshangabad under SSP245 and SSP585 scenarios are given in Figure 5.189 and Figure 5.190 respectively. These results indicate that the 3-day consecutive flows are projected to increase in all future time horizons and generally the increase is highest during the end term. Considerable inter-GCM variability can be seen in the projections under both scenarios, but the highest 3-day consecutive stream flow is projected under SSP585 scenario with the maximum during the end-term.

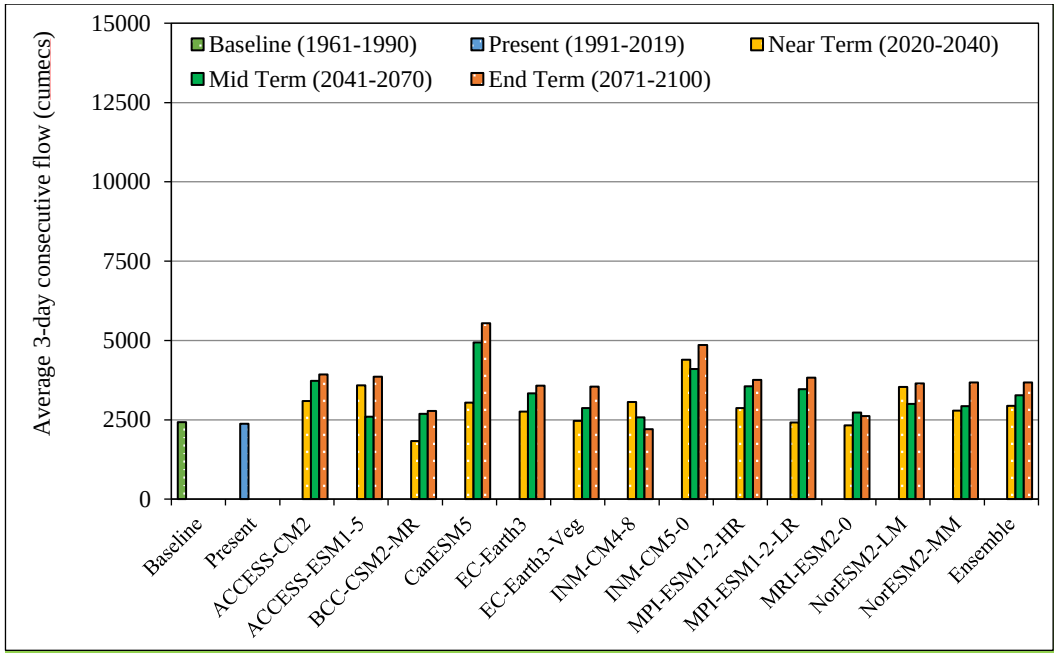

Figure 5.189: Average 3-day consecutive flow Narmada at Hoshangabad under SSP245 scenario

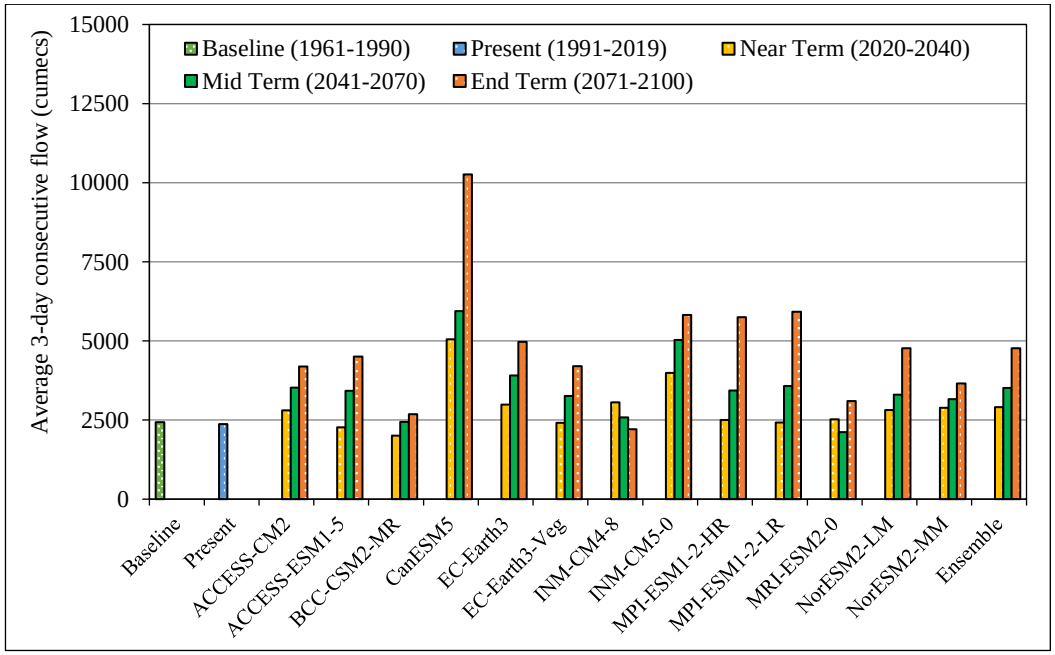

Figure 5.190: Average 3-day consecutive flow for Narmada at Hoshangabad under SSP585 scenario

The average annual peak flow from WEAP simulations have been compared with that during the baseline and present time periods so as to understand the scenario of future high flow in the study area. The average annual peak flows are projected to increase substantially under all future time periods under both future

climate scenarios. The comparison of the average annual peak flows for River Narmada at Hoshangabad under SSP245 and SSP585 scenarios are given in Figure 5.191 and Figure 5.192 respectively. The results indicate that the average annual peak flow is projected to increase in all future time periods and with highest increase projected during the end term. Sizable inter-GCM variability can be seen in the projections under both scenarios, but the highest 3-day consecutive stream flow is projected under SSP585 scenario with the maximum during the end-term.

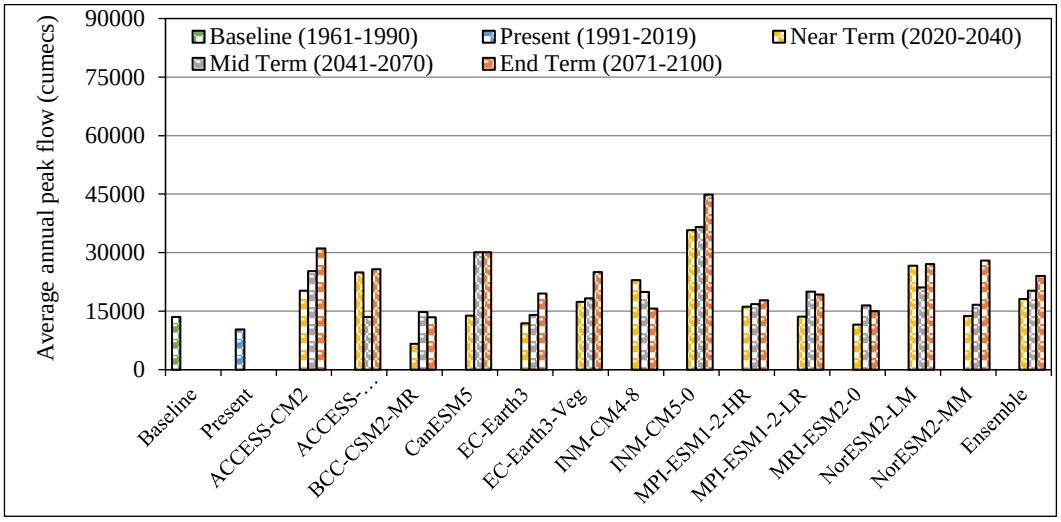

Figure 5.191: Average annual peak stream flow for Narmada at Hoshangabad under SSP245 scenario

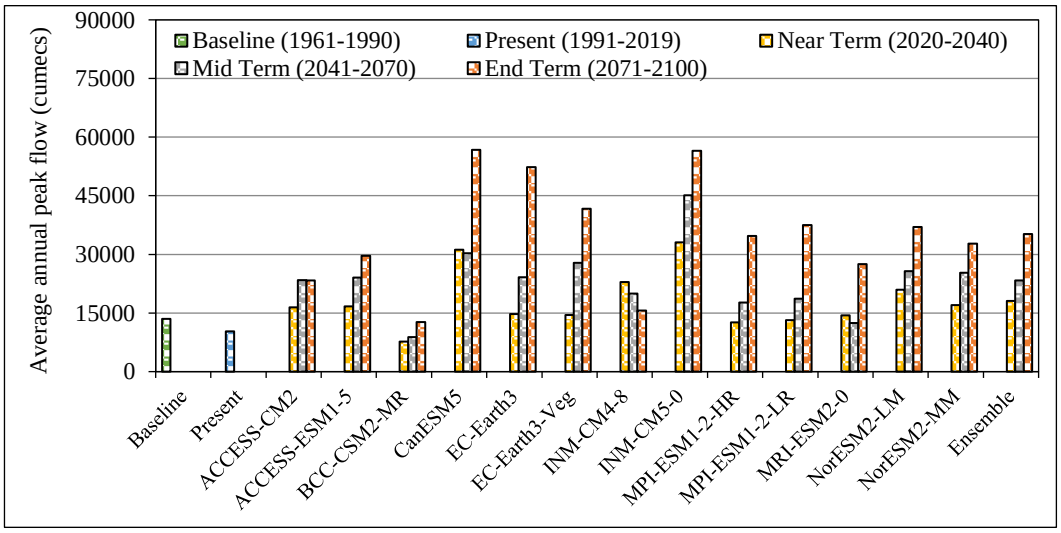

Figure 5.192: Average annual peak stream flow Narmada at at Hoshangabad under SSP585 scenario

The dependable flows at 5%,10%, 50%, 75%, 90%, and 99% probability of exceedance have been computed at all the tributary and main river gauging sites in

the Upper Narmada Basin using WEAP based future flow generated using CMIP6 future climate datasets and observed data during the baseline and present time periods. The dependable flow analysis helps to understand the changes in high flows represented by 5% and 10% dependable flows viz., Q5 & Q10 respectively and the changes in low flows represented by 90% and 95% dependable flows viz., Q90 and Q95 respectively.

The comparison of the dependable flow for River Narmada at Hoshangabad during the baseline and present time period with that during the future time periods under SSP245 and SSP585 scenarios is given Figure 5.193 and Figure 5.194 respectively. In both scenarios, high flows and low flows are projected to increase during the near-term, mid-term, and end-term time periods and compared to the baseline and present periods. However, a substantial increase in the high flows is projected during all future time periods, the maximum increase being projected during the end term under both scenarios. Also, the increase in high flows is projected to be much higher under the SSP585 scenario as compared to SSP245 scenario.

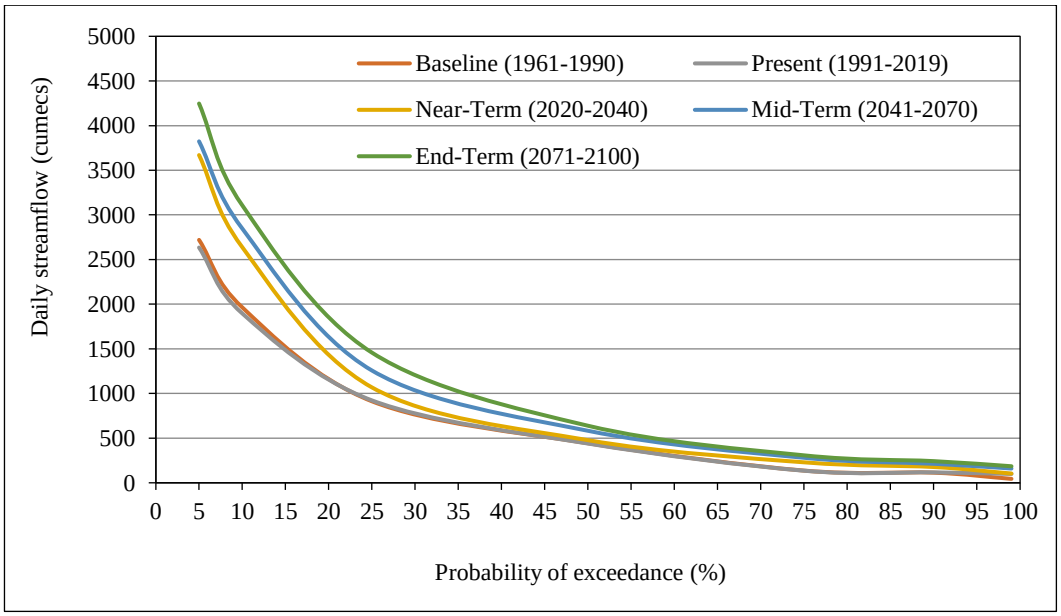

Figure 5.193: Dependable daily stream flow for Narmada at Hoshangabad under SSP245 scenario

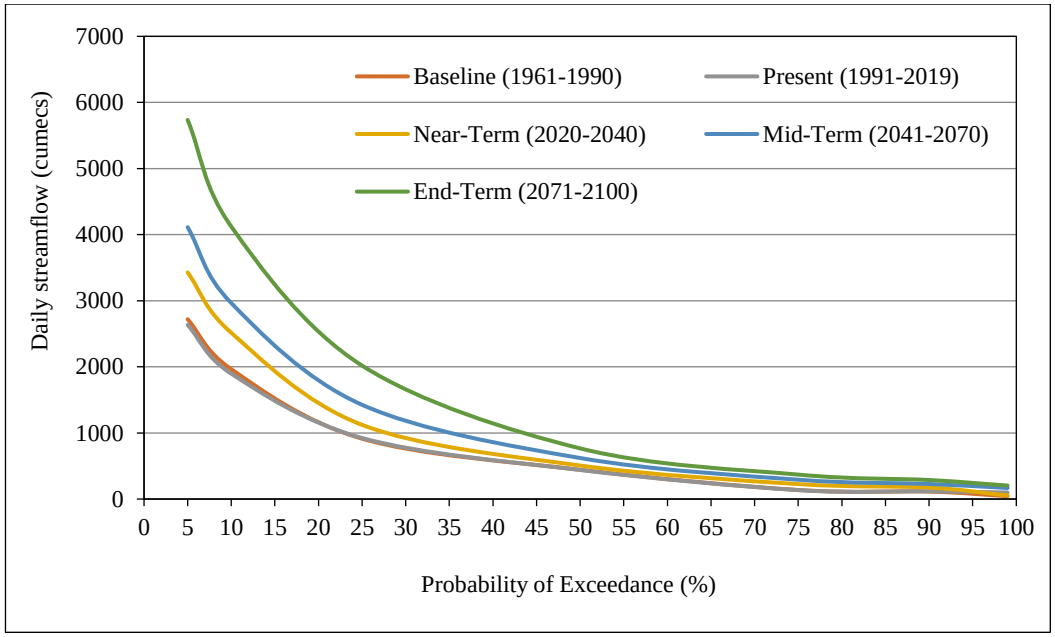

Figure 5.194: Dependable daily stream flow for Narmada at Hoshangabad under SSP585 scenario

5.13.3.3.2 Climate Change Impact Assessment using VIC

The calibrated and validated VIC model has been driven with the historical observed data during the baseline period (1961-1900) and present period (1991-2019). Subsequently, the simulations were carried out using the high-resolution bias corrected future climate data of 13 GCMs for two distinct climate scenarios viz., SSP245 and SSP585. These simulations have been compared to understand the projected changes in the water availability and high flows during various time horizons. The same methodology has been followed for all hydrological models used in the study.

The results are similar to that obtained from other hydrological models and for brevity, only few results are given and discussed in brief. The average daily flow in the headwater catchments as well as the main river catchments are projected to increase in all three future time horizons as compared to the baseline (1961-1990) and present time periods (1991-2019). The highest increase in the average daily flow has been projected during the end-term under both scenarios. Also, the considerably higher increase in the average daily flow is projected under SSP585 scenario as compared to SSP245 scenario.

The comparison of the average 3-day consecutive streamflow for River Narmada at Hoshangabad under SSP245 and SSP585 scenario is given in Figure 5.195 and Figure 5.196 respectively. It can be observed that the average 3-day consecutive flows are also projected to increase in all future time periods, but the increase projected to be higher under SSP585 scenario as compared to SSP245

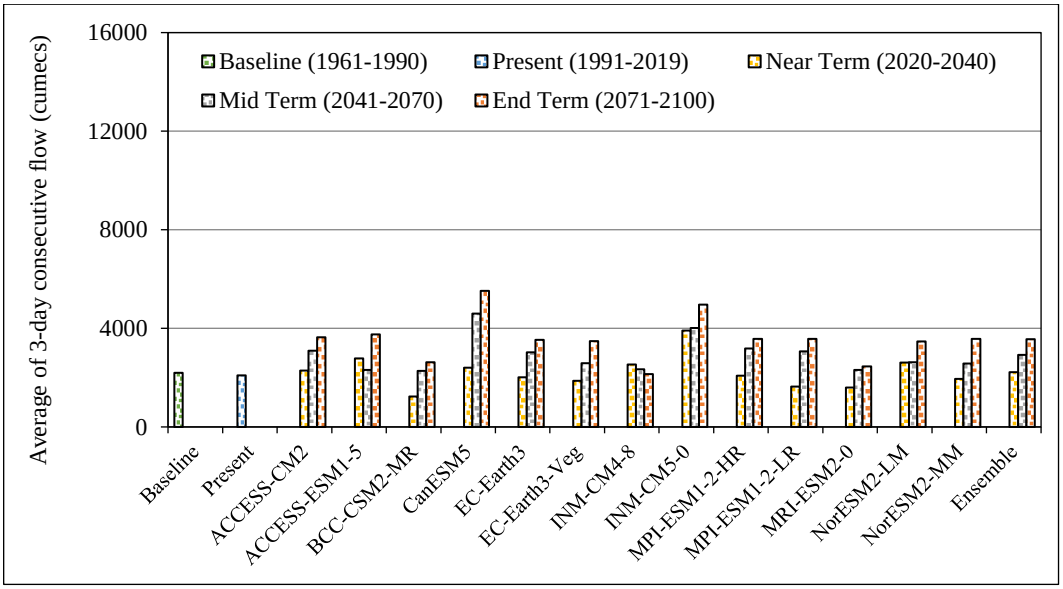

Figure 5.195: Average of 3-day consecutive stream flow for Narmada at Hoshangabad under SSP245 scenario

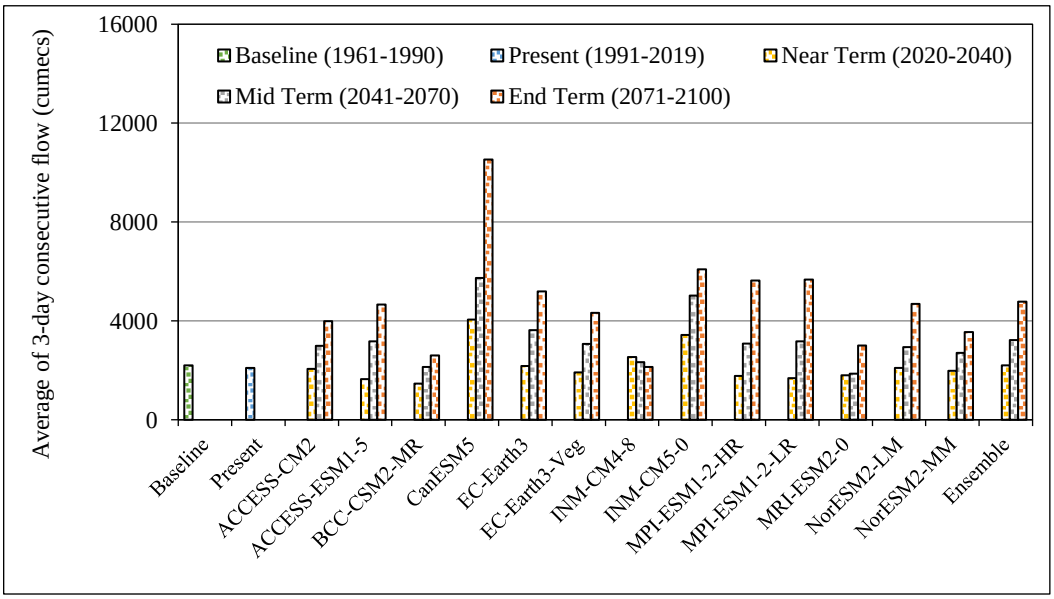

Figure 5.196: Average of 3-day consecutive stream flow for Narmada at Hoshangabad under SSP585 scenario

scenario. Inter-GCM variability can be seen among various GCM projections, but this variability is more pronounced under SSP585 scenario. Higher 3-day consecutive flows are projected during the end-term under both future climate scenarios with predominant increase during the end-term. The comparison of the ensemble mean of the future 3-day consecutive flows with that during the baseline and present time periods for River Narmada at Hoshangabad is given in Figure 5.197. It can be seen very clearly that the 3-day consecutive flows are projected to increase substantially in future.

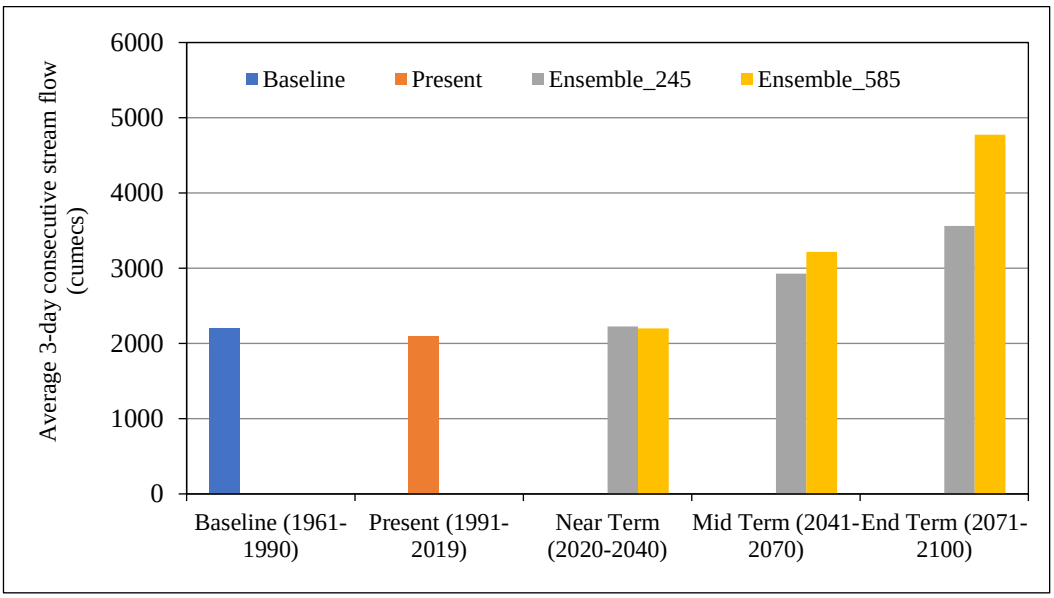

Figure 5.197: Comparison of average of 3-day consecutive stream flow for Narmada at Hoshangabad under SSP245 and SSP585 scenario

The average annual peak flow computed from VIC simulations have been compared with that during the baseline and present time periods so as to understand the scenario of future high flow in the study area. The average annual peak flows have been estimated for at all the tributary and headwater catchments in the study area and it is projected to increase substantially under all future time periods under both future climate scenarios. The comparison of the average annual peak flows for River Narmada at Hoshangabad under SSP245 and SSP585 scenarios are given in Figure 5.198 and Figure 5.199 respectively.

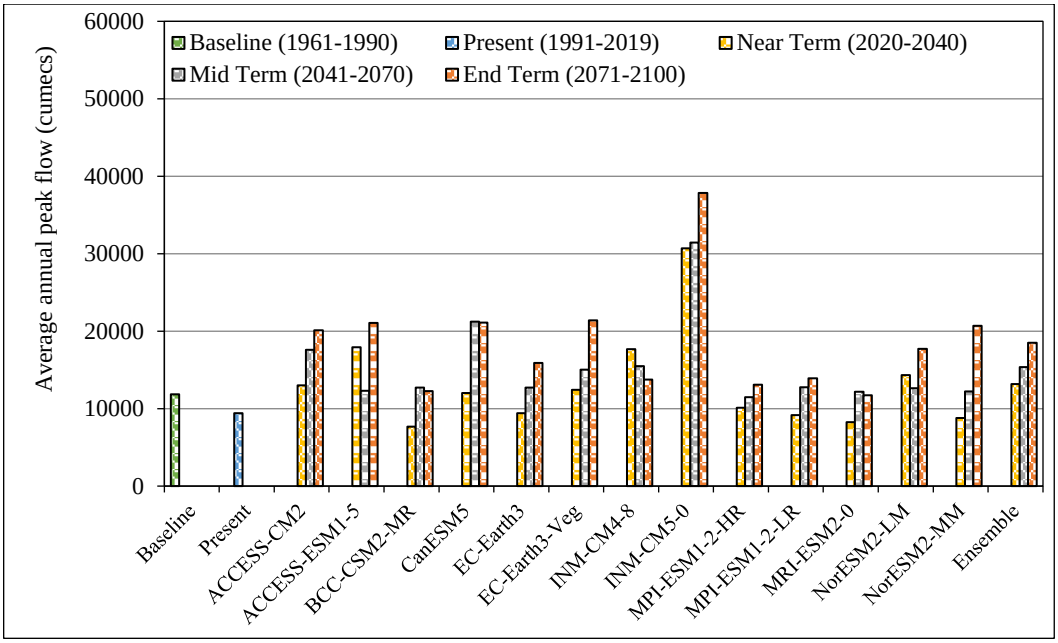

Figure 5.198: Average annual peak flow for Narmada at Hoshangabad under SSP245 scenario

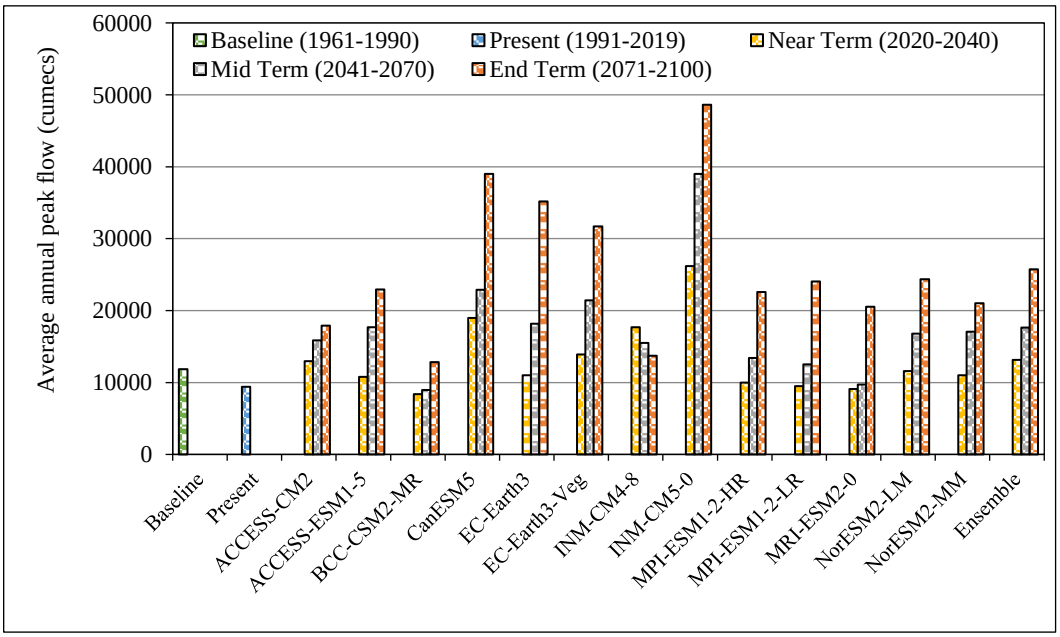

Figure 5.199: Average annual peak flow for Narmada at Hoshangabad under SSP585 scenario

The comparison of the ensemble mean of the future average annual peak low with that during the baseline and present period is given in Figure 5.200. The results indicate that the average annual peak flow at Hoshangabad is projected to increase in all future time periods and with highest increase projected during the end term. Sizable inter-GCM variability can be seen in the projections under both

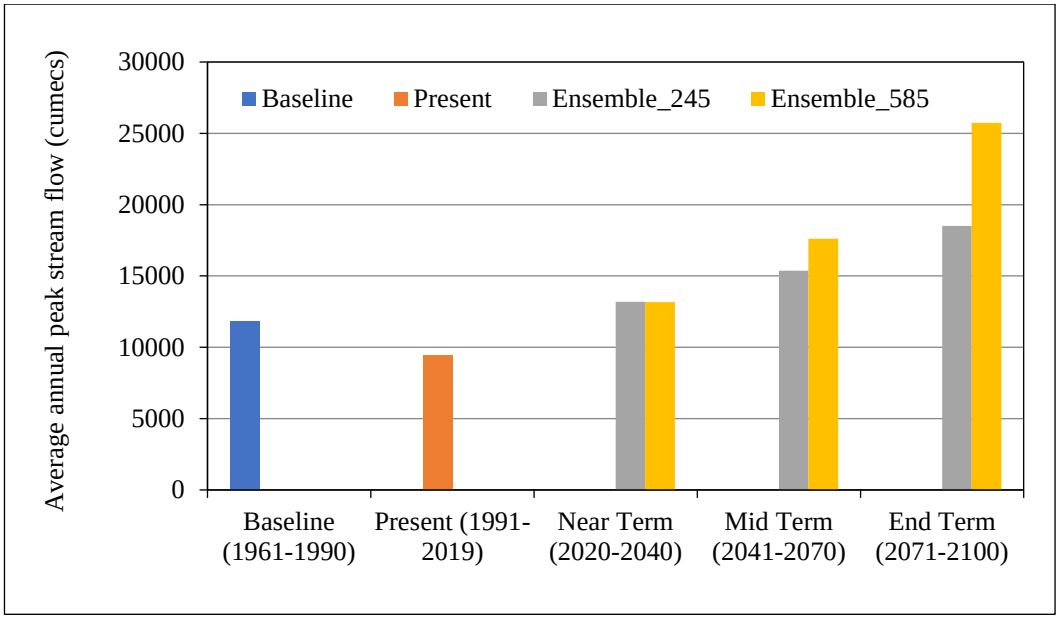

Figure 5.200: Comparison of average annual peak flow for Narmada at Hoshangabad under SSP245 and SSP585 scenarios

scenarios, but the highest 3-day consecutive stream flow is projected under SSP585 scenario with the maximum during the end-term.

The dependable flows at 5%,10%, 90%, and 99% probability of exceedance have been computed at all the tributary and main river gauging sites in the Upper Narmada Basin using VIC based future flows generated using CMIP6 future climate datasets and observed data during the baseline and present time periods. The comparison of the dependable flow for River Narmada at Hoshangabad during the baseline and present time period with that during the future time periods under SSP245 and SSP585 scenarios is given Figure 5.201 and Figure 5.202 respectively. In both scenarios, high flows and low flows are projected to increase during the near-term, mid-term, and end-term time periods and compared to the baseline and present periods. However, a substantial increase in the high flows is projected during all future time periods, the maximum increase being projected during the end term under both scenarios. Also, the increase in high flows is projected to be much higher under the SSP585 scenario as compared to SSP245 scenario.

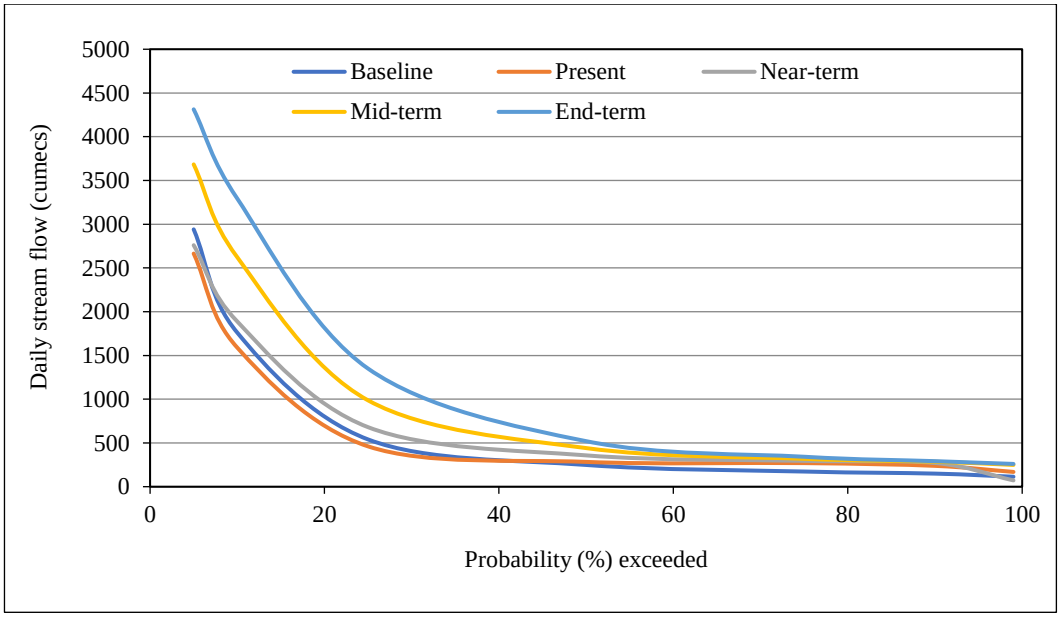

Figure 5.201: Comparison of dependable flow for Narmada at Hoshangabad under SSP245 scenario

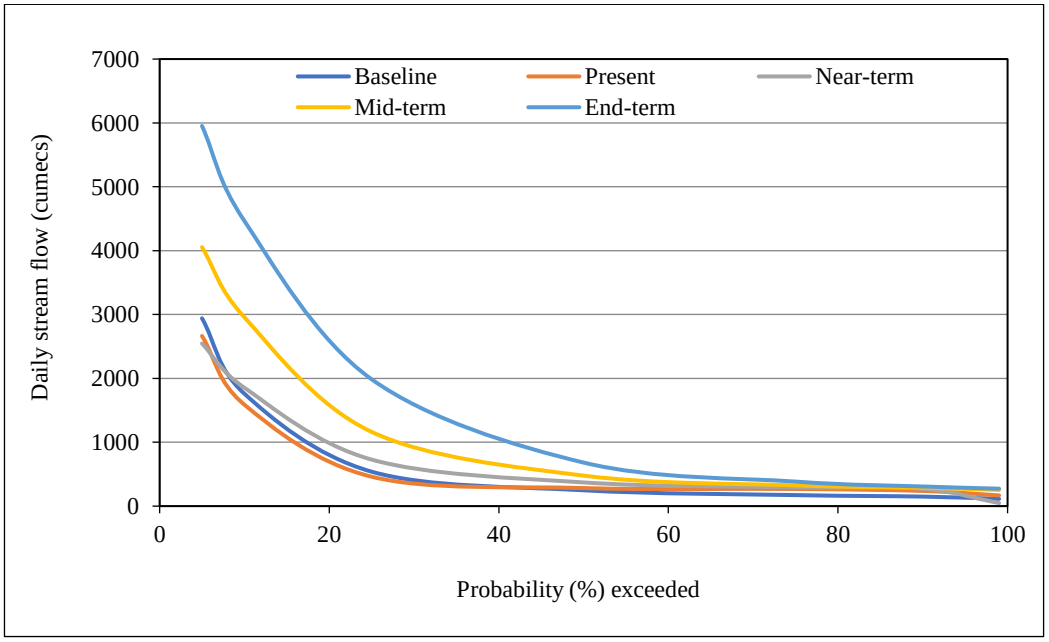

Figure 5.202: Comparison of dependable flows for Narmada at Hoshangabad under SSP585 scenario

5.13.3.3.3 Climate Change Impact Assessment using HEC-HMS

The calibrated and validated HEC-HMS model has been driven with the historical observed data during the baseline period (1961-1900) and present period (1991-2019). Thereafter, the simulations were carried out using the high-resolution bias corrected future climate data of 13 GCMs for two distinct climate scenarios

viz., SSP245 and SSP585. These simulations have been compared to understand the projected changes in the water availability and high flows during various time horizons.

The results are similar to that obtained from other hydrological models and for brevity, only few results are given and discussed in brief. The average daily flow in the headwater catchments as well as the main river catchments are projected to increase in all three future time horizons and the highest increase has been projected during the end-term under both scenarios. Also, the significantly higher increase in the average daily flow is projected under SSP585 scenario.

The comparison of the average 3-day consecutive streamflow for River Narmada at Hoshangabad under SSP245 and SSP585 scenarios is given in Figure 5.203 and Figure 5.204 respectively. Inter-GCM variability can be seen among various GCM projections, but this variability is more pronounced under SSP585 scenario. The average 3-day consecutive flows too are projected to increase during all future time periods, but the increase projected to be higher under SSP585 scenario as compared to SSP245 scenario. Higher 3-day consecutive flows are projected during the end-term under both future climate scenarios with predominant increase during the end-term. It can be observed undoubtedly that the 3-day consecutive flows are projected to increase substantially in future.

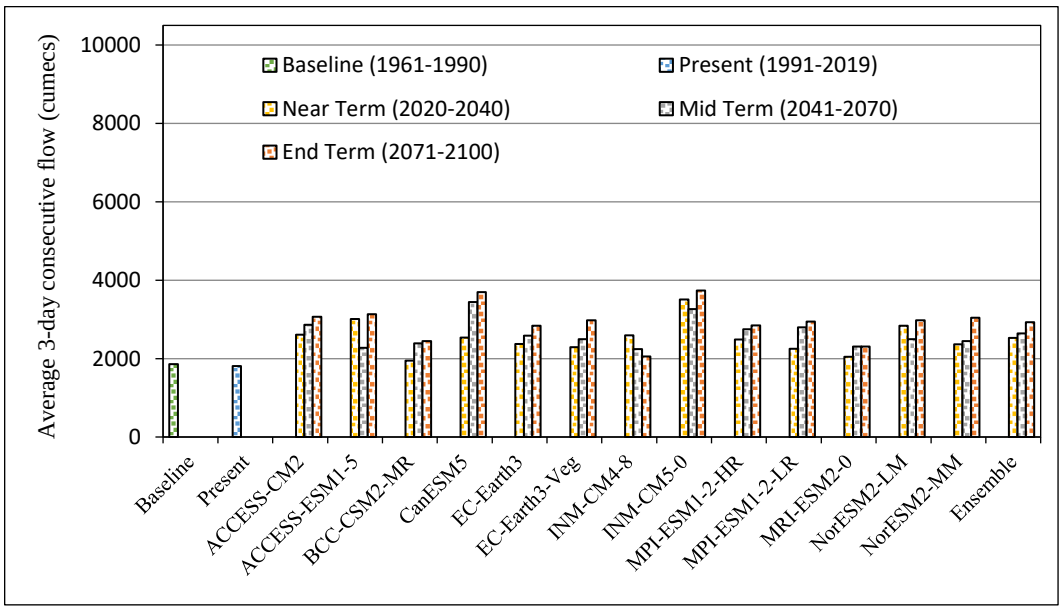

Figure 5.203: 3-Day consecutive flows at Hoshangabad gauging site for SSP245

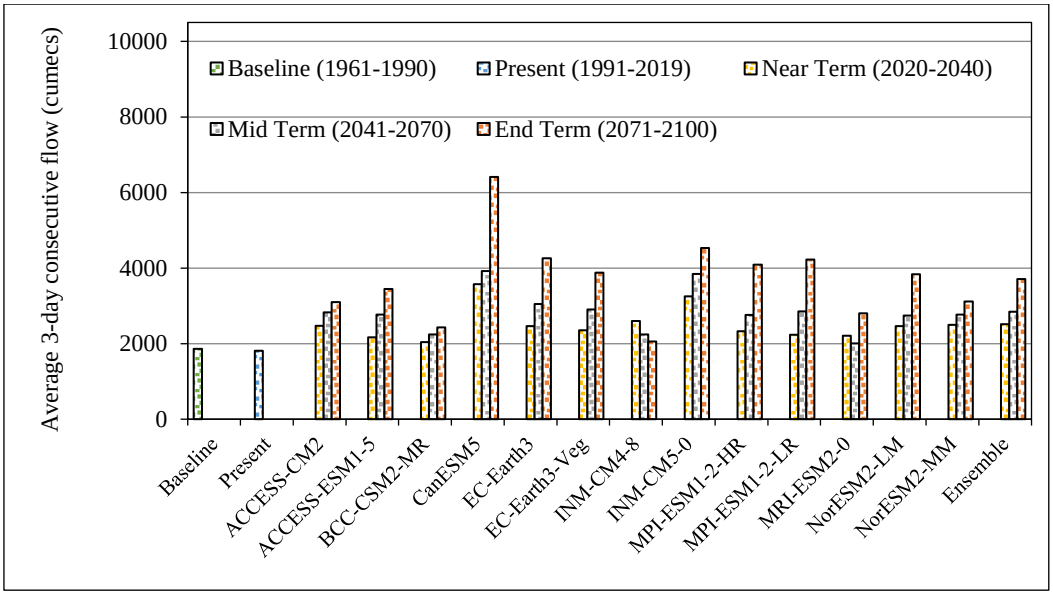

Figure 5.204: 3-day consecutive flows for Narmada at Hoshangabad gauging site for SSP585 scenario

The average annual peak flow computed from HEC-HMS model simulations for all tributary and headwater catchments have been compared with that during the baseline and present time periods. The average annual peak flows is projected to increase substantially under all future time periods under both scenarios. The comparison of the average annual peak flows for River Narmada at Hoshangabad under SSP245 and SSP585 scenarios are given in Figure 5.205 and Figure 5.206 respectively.

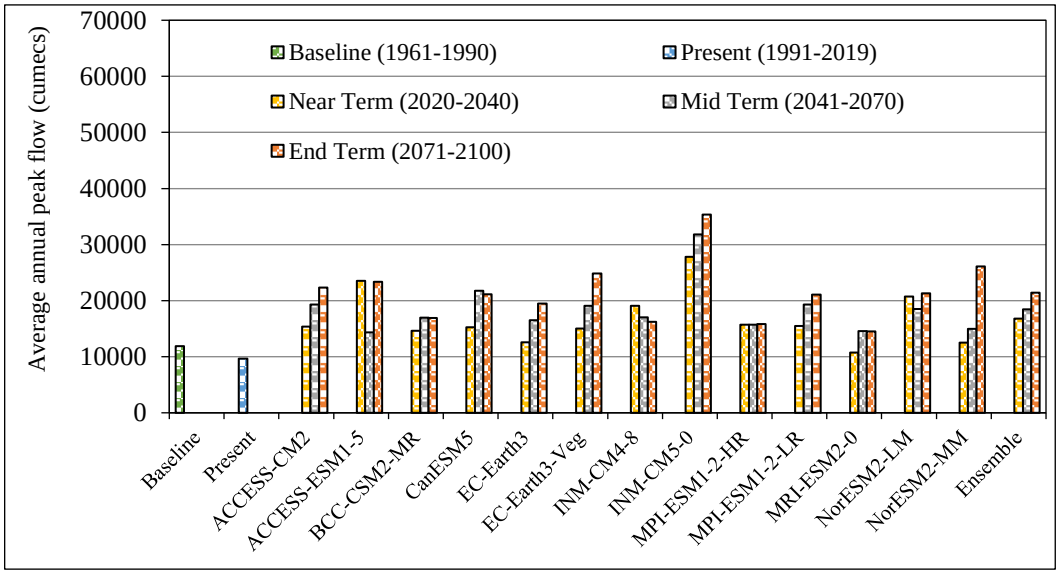

Figure 5.205: Average annual peak flows Narmada at Hoshangabad gauging site for SSP245 scenario

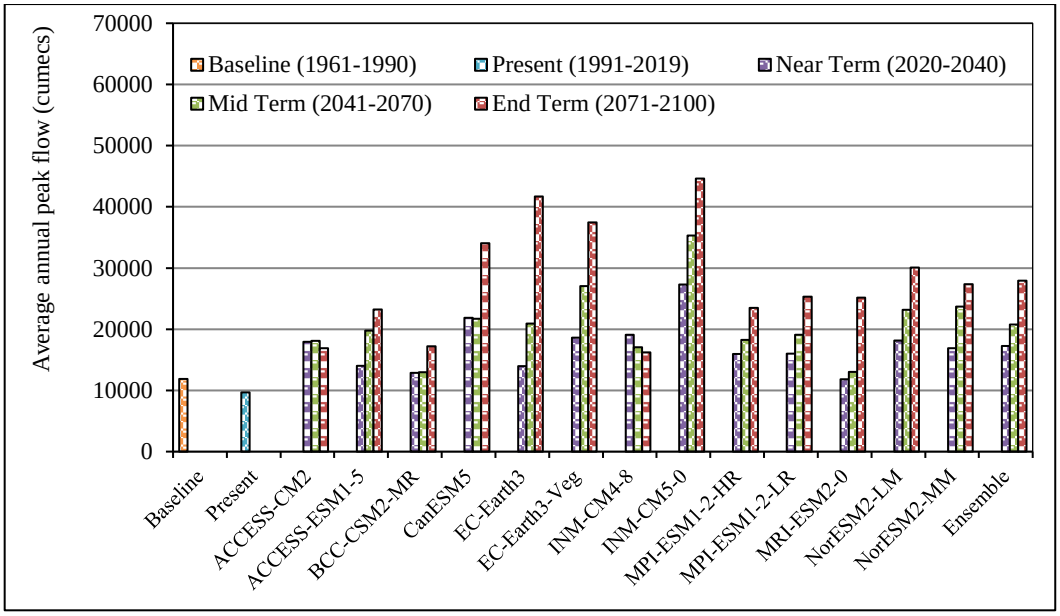

Figure 5.206: Average annual peak flows for Narmada at Hoshangabad gauging site for SSP585 scenario

The dependable flows at 5%,10%, 90%, and 99% probability of exceedance have been computed at all the tributary and main river gauging sites in the Upper Narmada Basin using HEC-HMS based future flows generated using CMIP6 future climate datasets and observed data during the baseline and present time periods. Under SSP245, the 5% dependability daily flows are showing a trend of regular increase in the future time zones, with highest during the end-term period with NT<MT<ET. The 10% dependable flows (Q10) are also having an increasing trend similar to that in Q5. In case of SSP585, Q5 and Q10 are showing similar increasing trend for all future time zones with NT<MT<ET. Similarly, for low flows represented by the 90% dependable flows (Q90) is showing a marginal increase in future with NT<MT<ET. In case of SSP585 too, Q90 and Q95 are showing similar increasing trends for all future time zones with NT<MT<ET. The increase in high flows is projected to be much higher under the SSP585 scenario as compared to SSP245 scenario.

5.14 Climate Change Impact Assessment on Groundwater Flow

The climate change impact assessment on the groundwater flow is carried out by groundwater modelling approaches. The groundwater flow models viz., MODFLOW and MUSE have been setup for the study area and have been calibrated

and validated. These models have been driven by the groundwater recharge estimated using the WetSpass model which have been driven using the high-resolution bias-corrected bias corrected future climate data of 13 CMIP6 GCMs under SSP245 and SSP585 future climate scenarios. The Narsinghpur district located in the Upper Narmada basin has been selected for the reasons mentioned in the earlier section. The future groundwater recharge has been compared with the present time period which is considered as 2000-2015, so as to limit the computational requirements and lack of historical data. Moreover, the groundwater recharge and draft scenario might have been vastly different at that time as compared to what it is today due to the large-scale developmental activities in the study area.

The estimated average annual groundwater recharge during different time periods viz., near-term (2021-2040), mid-term (2041-2070), and end-term (2071-2100) under SSP245 and SSP585 has been compared with the present time horizon (2000–2015) in order to evaluate the changes that have occurred in groundwater recharge in Narsinghpur district in Upper Narmada basin. The annual groundwater recharge during the present time period was 123 mm and has been used for comparing annual groundwater recharge obtained from different GCMs under multiple scenarios. The future annual groundwater recharge has been estimated based on WetSpass runs using CMIP6 future climate datasets.

The future annual groundwater recharge as estimated by WetSpass using ACCESS-CM2 future climate data under SSP245 scenario, projects an increase in annual groundwater recharge during near-term (124 mm), mid-term (164 mm), and end-term (148 mm) under SSP 245 as compared to the present period (123 mm). Similarly, the annual groundwater recharge has been evaluated using ACCESS-CM2 under SSP585 scenario which showed significantly higher annual groundwater recharge during near-term (166 mm), mid-term (205 mm), and end-term (206 mm). The comparison of the annual groundwater recharge under SSP245 and SSP585 scenarios is given in Figure 5.207. It can be observed that under SSP245 scenario, the groundwater recharge is projected to increase steadily till mid-term and thereafter projected to decrease during end-term period. However, in contrast to this, under SSP585 scenario, the groundwater recharge is projected to

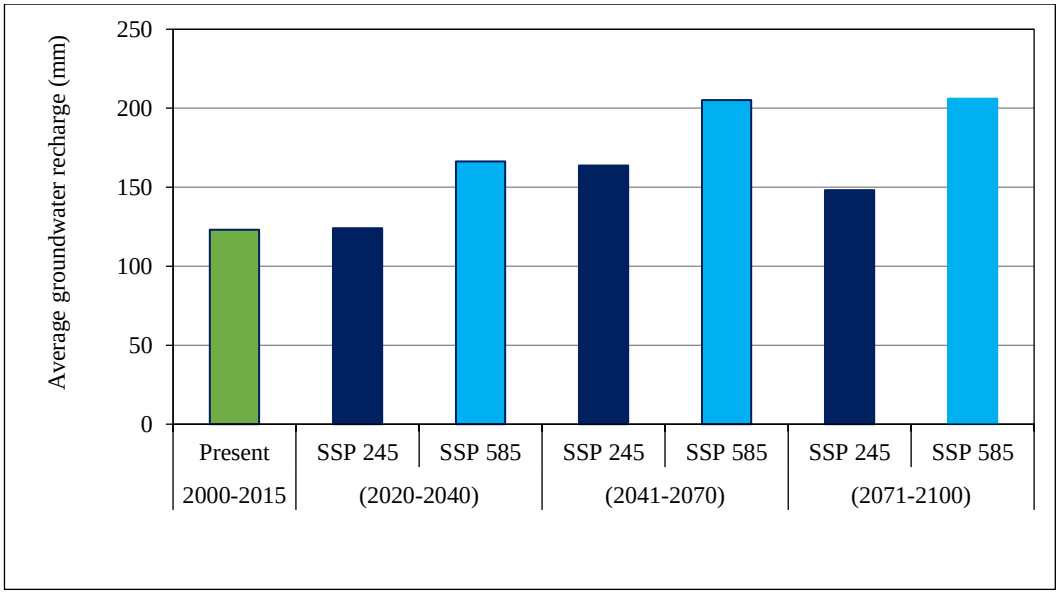

Figure 5.207: Average annual groundwater recharge with ACCESS-CM2 under SSP245 and SSP585 scenarios

increase in all future time periods. The spatial variation of the groundwater recharge has also been evaluated and Figure 5.208 and Figure 5.209 shows the annual groundwater recharge during 2020, 2041, 2071, and 2100 under SSP245 and SSP585 scenarios respectively.

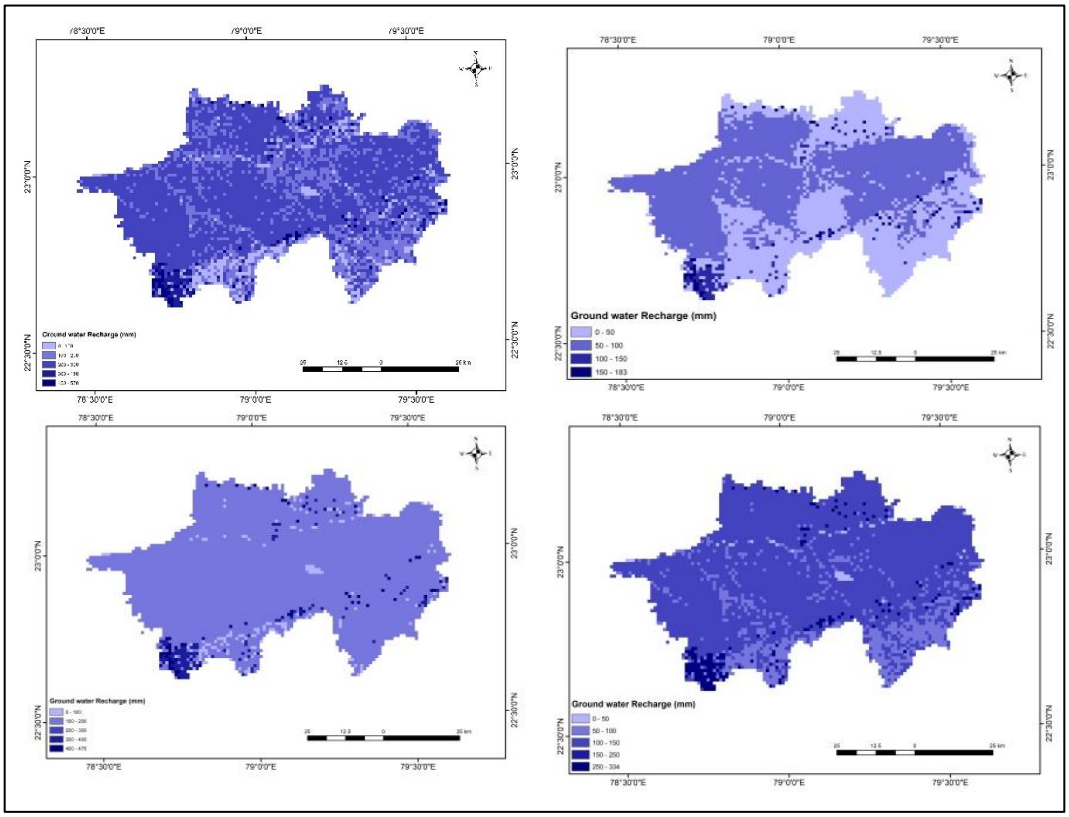

Figure 5.208: Average annual groundwater recharge with ACCESS-CM2 under SSP245 scenario during 2020, 2041, 2071, 2100

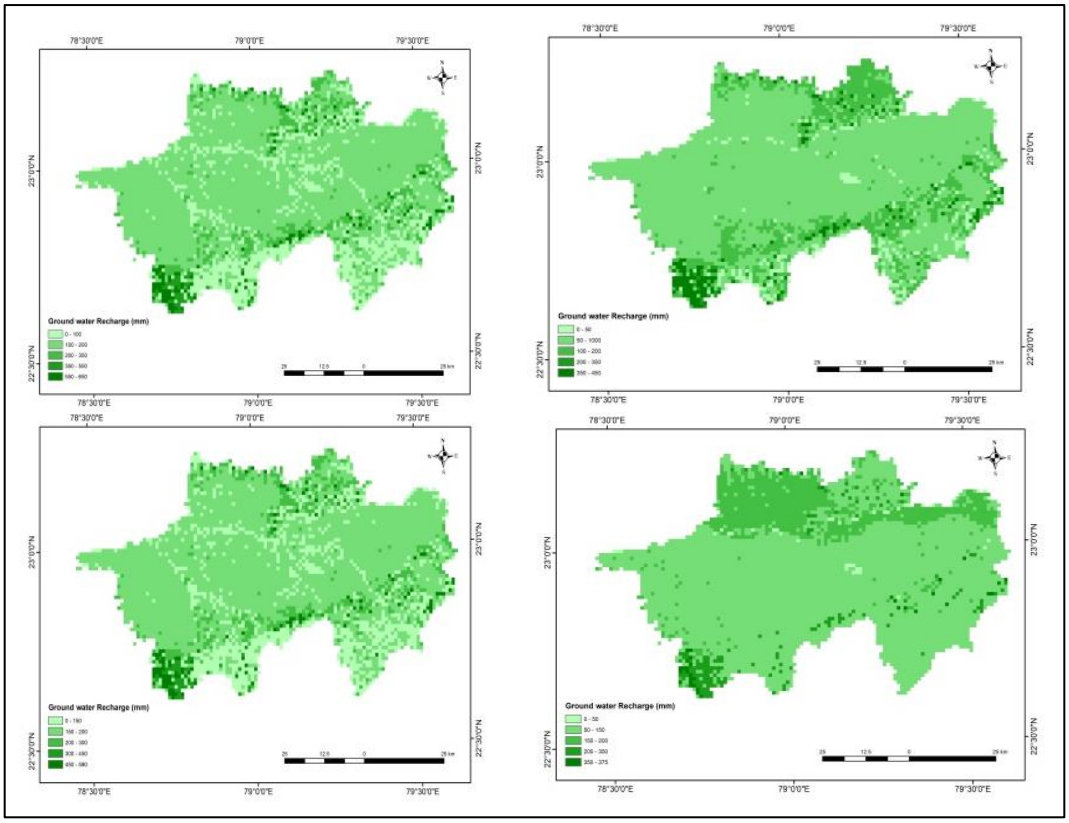

Figure 5.209: Average annual groundwater recharge with ACCESS-CM2 under SSP585 scenario during 2020, 2041, 2071, 2100

The future annual groundwater recharge as estimated by WetSpass using BCC-CSM2-MR future climate data under SSP245 scenario, projects an increase in annual groundwater recharge from 123 mm during the present period to 153 mm during near-term, 217 mm during the mid-term and 178 mm during the end-term under the SSP 245 scenario. Similarly, the annual groundwater recharge has been evaluated using BCC-CSM2-MR under SSP585 scenario which indicated significantly higher annual groundwater recharge during near-term (157 mm), mid-term (201 mm), and end-term (157 mm). The comparison of the annual groundwater recharge under SSP245 and SSP585 scenarios is given in Figure 5.210. It can be observed that under SSP245 scenario, the groundwater recharge is projected to increase steadily till mid-term and thereafter projected to decrease during end-term period. Also, a similar trend resembling that under SSP245 has been observed under SSP585 scenario.

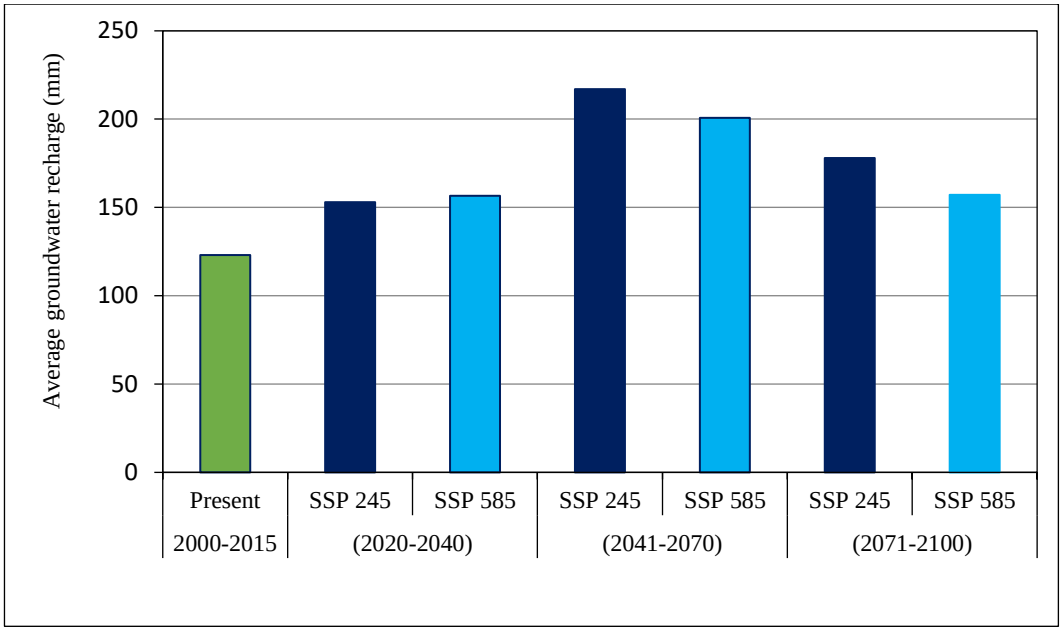

Figure 5.210: Average annual groundwater recharge with BCC-CSM2-MR under SSP245 and SSP585 scenarios

The future annual groundwater recharge as estimated by WetSpass using EC-Earth3-Veg future climate data under SSP245 scenario, projects an increase in annual groundwater recharge from 123 mm during the present period to 188 mm during near-term, 235 mm during the mid-term and 217 mm during the end-term under the SSP 245 scenarios. Similarly, the annual groundwater recharge has been evaluated using EC-Earth3-Veg under SSP585 scenario which indicated significantly higher annual groundwater recharge during near-term (178 mm), mid-term (235 mm), and end-term (210 mm). The comparison of the annual groundwater recharge under SSP245 and SSP585 scenarios is given in Figure 5.211. It can be observed that under SSP245 scenario, the groundwater recharge is projected to increase steadily till mid-term and thereafter projected to decrease marginally during end-term period. Also, a similar trend resembling that under SSP245 has been observed for SSP585 scenario.

Similar analysis has been carried out for estimation of the groundwater recharge using all the 13 CMIP6 GCMs. The results from the various simulations capture the inter-model variability in the simulation of groundwater recharge that is based on the variability in the rainfall and the rainy using different models under diverse future climate scenarios. The results of the average annual groundwater recharge as simulated for all the CMIP6 GCMS has been clubbed together and the

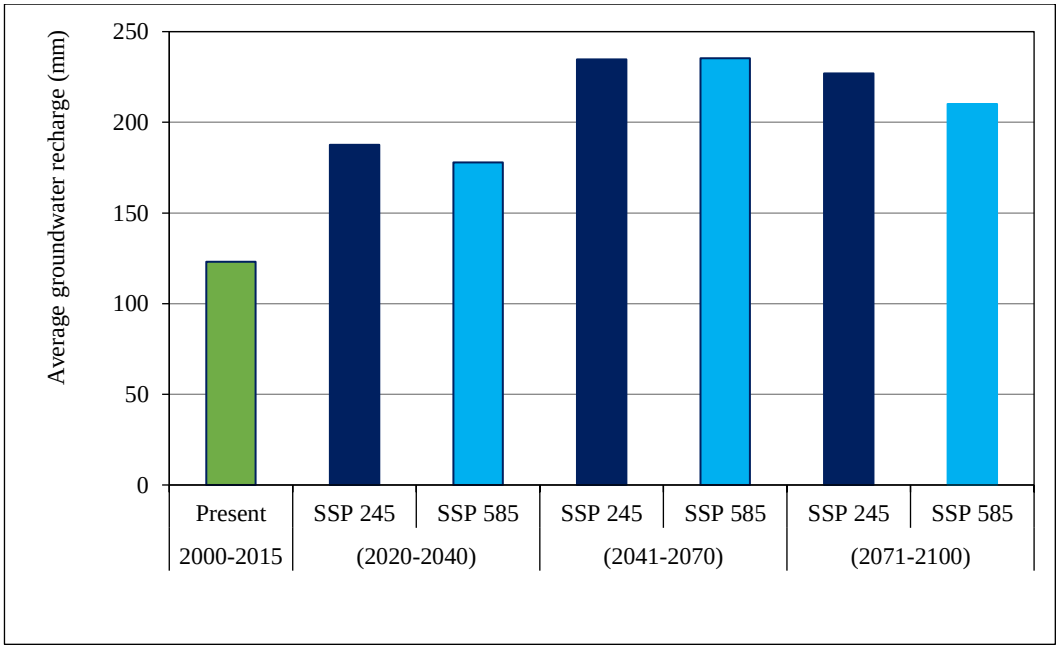

Figure 5.211: Average annual groundwater recharge with EC-Earth3-Veg under SSP245 and SSP585 scenarios

comparison of the present and ensemble mean future annual groundwater recharge is given in Figure 5.212.

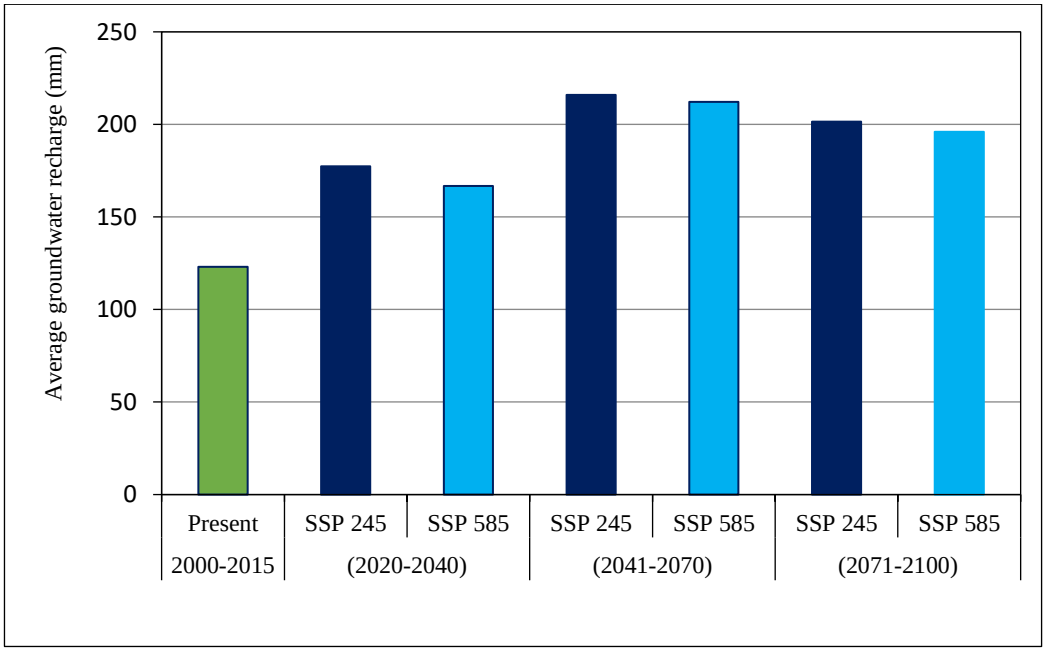

Figure 5.212: Ensemble mean average annual Groundwater recharge under SSP245 and SSP585 scenarios

The ensemble mean results indicate that the average annual groundwater recharge under SSP245 scenario is projected to increase from 123 mm during the

present period to 177 mm during the near-term, 216 mm during the mid-term and 201 mm during the end-term. Also, the average annual groundwater recharge based on the ensemble means under SSP585 scenario is projected to increase to 167 mm during the near-term to 212 mm during the mid-term and 196 mm during the end-term. It can be observed that even though the annual groundwater recharge is projected to increase in all future time periods under both scenarios, but the groundwater recharge under the SSP585 scenario is marginally lower than that under SSP245.

The groundwater flow modelling i.e. simulation of the groundwater heads (levels) has been carried out using the calibrated and validated groundwater models MODFLOW and MUSE. The model MUSE also used the MODFLOW engine for simulations. As such, the detailed results shall be given for the MODFLOW based future simulations whereas only brief discussion of the results shall be given for MUSE based simulations. The future groundwater levels have been estimated for both future climate scenarios viz., SSP245 and SSP585 using the future climate data and groundwater recharge.

The future groundwater level as estimated by MODFLOW using ACCESS-CM2 GCM future climate data under SSP245 scenario, projects an increase in groundwater heads from an average of 347.4 m above m.s.l. during the present time period to 348.0 m during near-term, 349.5 m during the mid-term and 350.6 m above m.s.l. during the end-term under SSP 245 scenario. Similarly, the annual groundwater recharge has been evaluated using ACCESS-CM2 GCM under SSP585 scenario which indicated marginally lower groundwater heads during near-term (348.1 m), mid-term (349.3 m), and end-term (350.3 m). The comparison of the groundwater head under SSP245 and SSP585 scenarios is given in Figure 5.213. It can be observed that under SSP245 scenario, the groundwater recharge is projected to increase during the mid-term and thereafter projected to decrease during mid-term and end-term period. Also, a similar trend resembling that under SSP245 has been observed under SSP585 scenario.

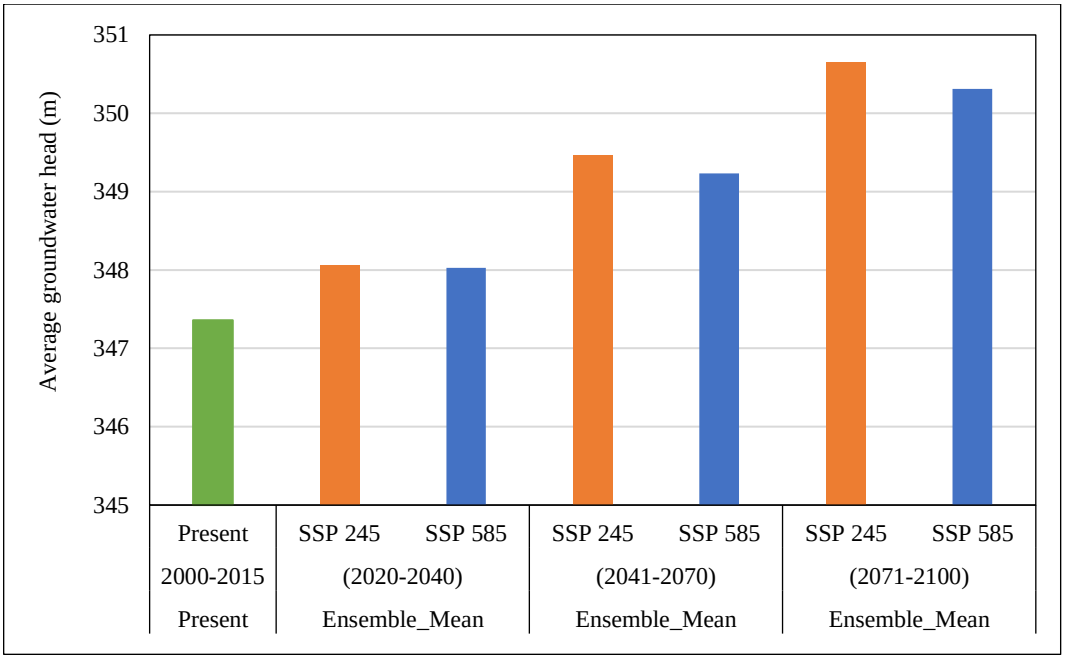

Figure 5.213: Comparison of average groundwater head with ACCESS-CM2 under SSP245 and SSP585 scenarios

The spatial variation of the groundwater levels in the various regions of the district have been studying by plotting the groundwater level contours during various years of the simulation. The spatial variation of the groundwater heads during few years viz., 2020, 2041, 2071, and 2100 using ACCESS-CM2 is given in Figure 5.214 and Figure 5.215 under SSP245 and SSP585 scenarios respectively. It can be observed that there is a distinct variability in the groundwater heads during various years depicted in the study area under both scenarios. It can be observed that the groundwater levels are generally lower in the north-west parts of the district, whereas it is relatively higher in the southern and south-east parts of the district. The groundwater heads are dynamic and varies depending on the groundwater recharge and groundwater draft from the groundwater aquifer and therefore the variability in the groundwater levels can be seen during different years of future simulations.

The future groundwater level as estimated by MODFLOW using BCC-CSM2-MR GCM future climate data under SSP245 scenario, projects an increase in groundwater heads from an average of 347.4 m above m.s.l during the present time period to 348.9 m during near-term, 350.3 m during the mid-term and 350.1 m

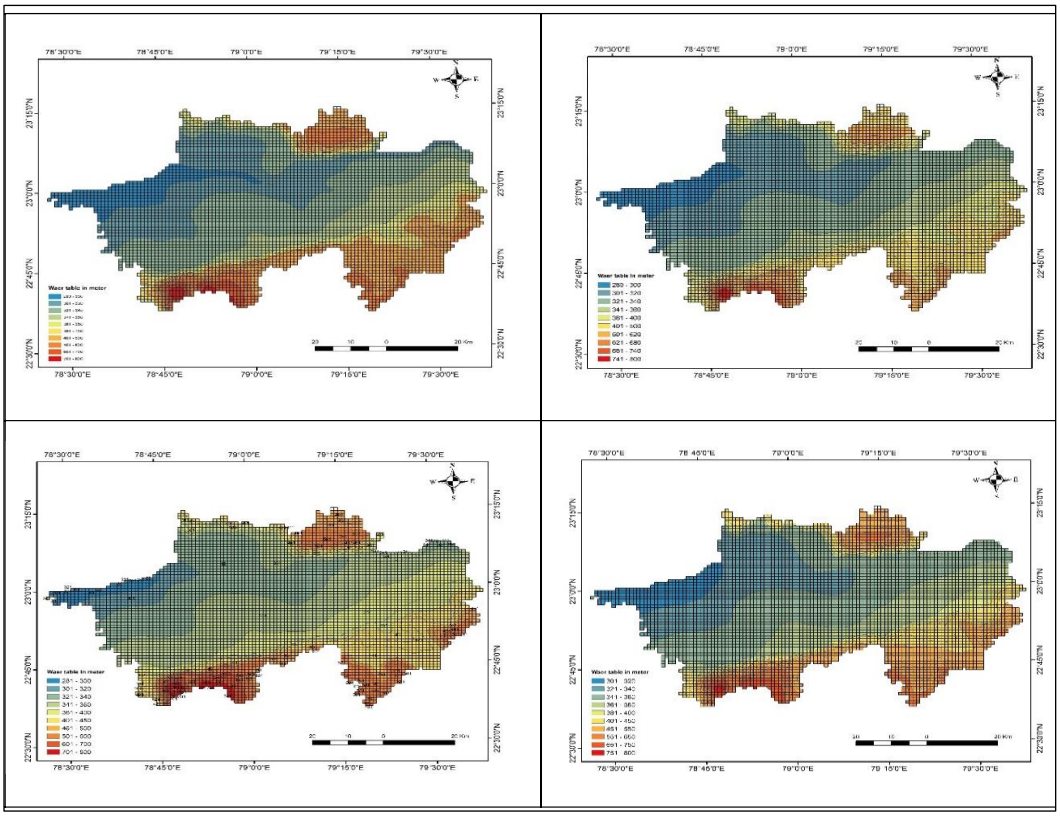

Figure 5.214: Spatial variation of groundwater heads with ACCESS-CM2 during 2020, 2041, 2071, 2100 under SSP245 scenario

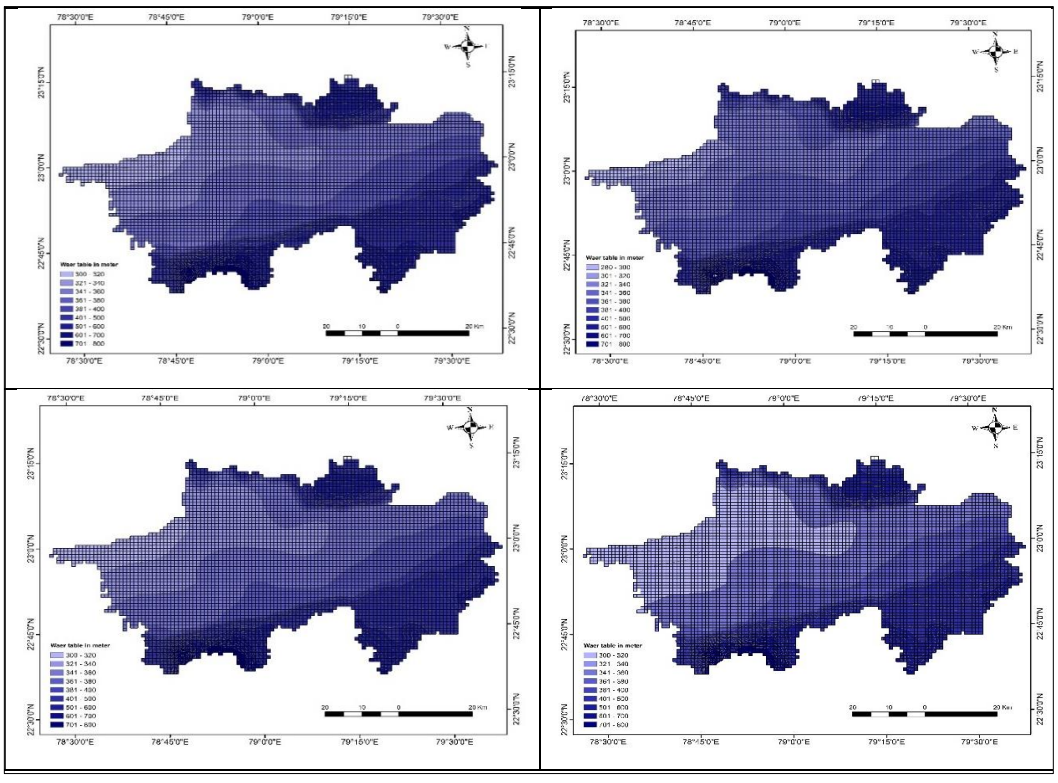

Figure 5.215: Spatial variation of groundwater heads with ACCESS-CM2 during 2020, 2041, 2071, 2100 under SSP585 scenario

above m.s.l. during the end-term under the SSP245 scenario. Similarly, the annual groundwater recharge has been evaluated using BCC-CSM2-MR under SSP585scenario which indicated marginally lower groundwater heads during near-term (349.0 m), mid-term (349.6 m), and end-term (349.5 m). The comparison of the groundwater head under SSP245 and SSP585 scenarios is given in Figure 5.216. It can be observed that under SSP245 scenario, the groundwater recharge is projected to increase during the mid-term and thereafter projected to decrease marginally during mid-term and end-term period. Also, a similar trend resembling that under SSP245 has been observed under SSP585 scenario. Also, the spatial variation of the groundwater levels in the various regions of the district have been studying by plotting the groundwater level contours during various years of the simulation. A similar spatial variability as with ACCESS-CM2 was observed in the spatial variation of the groundwater levels using BCC-CSM2-MR GCM.

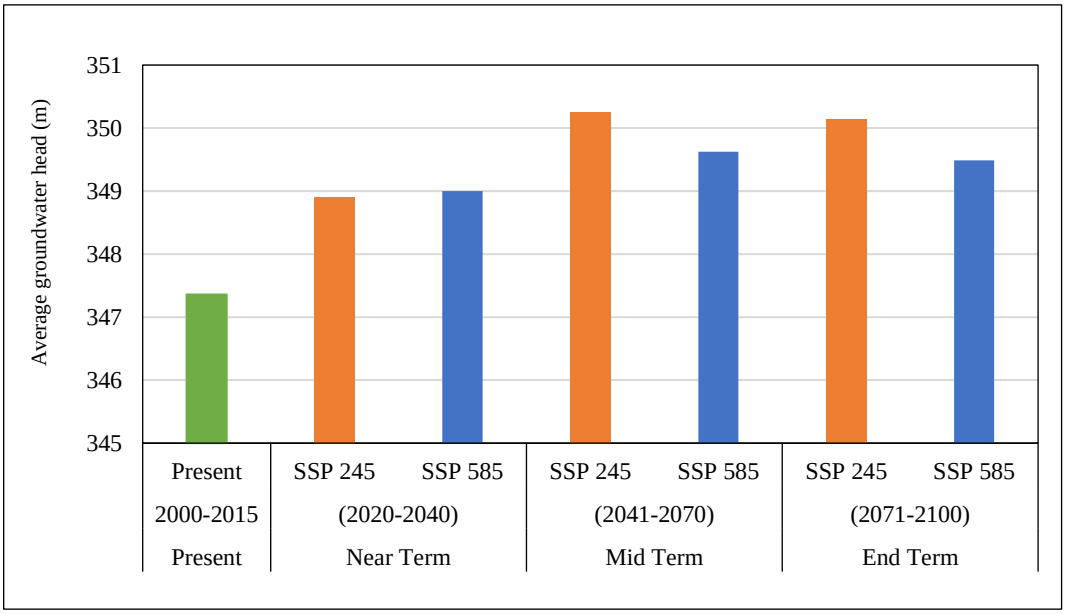

Figure 5.216: Comparison of average groundwater head with BCC-CSM2-MR under SSP245 and SSP585 scenarios

The future groundwater level as estimated by MODFLOW using EC-Earth3-Veg GCM future climate data under SSP245 scenario, projects an increase in groundwater heads from an average of 347.4 m above m.s.l during the present time period to 352.7 m during near-term, 353.8 m during the mid-term and 353.4 m above m.s.l. during the end-term under the SSP245 scenario. Similarly, the annual groundwater recharge has been evaluated using EC-Earth3-Veg GCM under SSP585

scenario which indicated marginally lower groundwater heads during near-term (352.4 m), mid-term (353.6 m), and end-term (353.1 m). The comparison of the groundwater head under SSP245 and SSP585 scenarios is given in Figure 5.217. It can be observed that under SSP245 scenario, the groundwater recharge is projected to increase during the mid-term and thereafter projected to decrease marginally during mid-term and end-term period. Also, a similar trend resembling that under SSP245 has been observed under SSP585 scenario. However, the simulated heads during all three future time periods with EC-Earth3-Veg and EC-Earth3 GCMs are much higher than that found using ACCESS-CM2, ACCESS-ESM1, BCC-CSM2-MR and CanESM5 GCMs. Also, the spatial variation of the groundwater levels in the various regions of the district have been studying by plotting the groundwater level contours during various years of the simulation.

The spatial variation of the groundwater levels using EC-Earth3-Veg GCM under SSP245 and SSP585 scenarios are given in Figure 5.218 and Figure 5.219 respectively. It can be observed that there is a distinct variability in the groundwater heads during various years under both scenarios. It can be observed that the groundwater levels are generally lower in the north-west parts of the district, whereas it is relatively higher in the southern and south-east parts of the district. The groundwater heads are dynamic and varies depending on the groundwater recharge and groundwater draft from the groundwater aquifer and therefore the variability in the groundwater levels can be seen during different years of future simulations.

The simulation of the future groundwater levels has been carried out using the other GCMs including ACCESS-ESM1, CanESM5, EC-Earth3, INM-CNM4-8, INM-CM5-0, MPI-ESM1-2-HR, MPI-ESM1-2-LR, MRI-ESM2-0, NorESM2-LM, NorESM2-MM also. The ensemble mean of the future groundwater levels have been evaluated and compared with the groundwater level during the present period. The comparison of the groundwater head during the present time period with the ensemble mean groundwater levels under SSP245 is given in Figure 5.220. It can be observed that the ensemble mean of the simulated future groundwater levels also indicates higher groundwater heads in all future time periods with 349.0 m during the near-term, 350.2 m during the mid-term and 350.8 m during

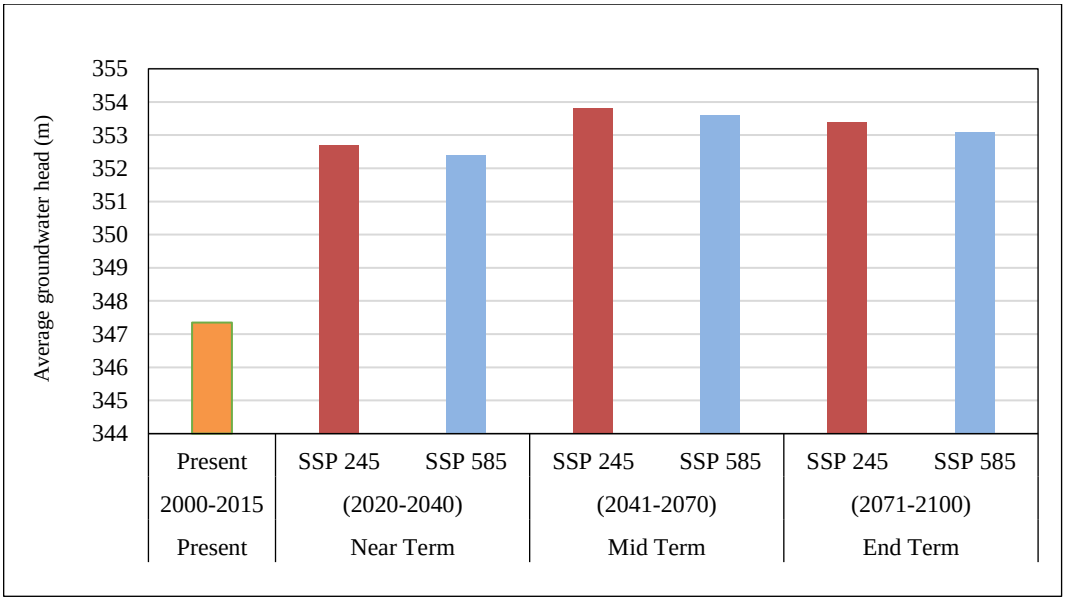

Figure 5.217: Comparison of average groundwater head with EC-Earth3-Veg under SSP245 and SSP585 scenarios

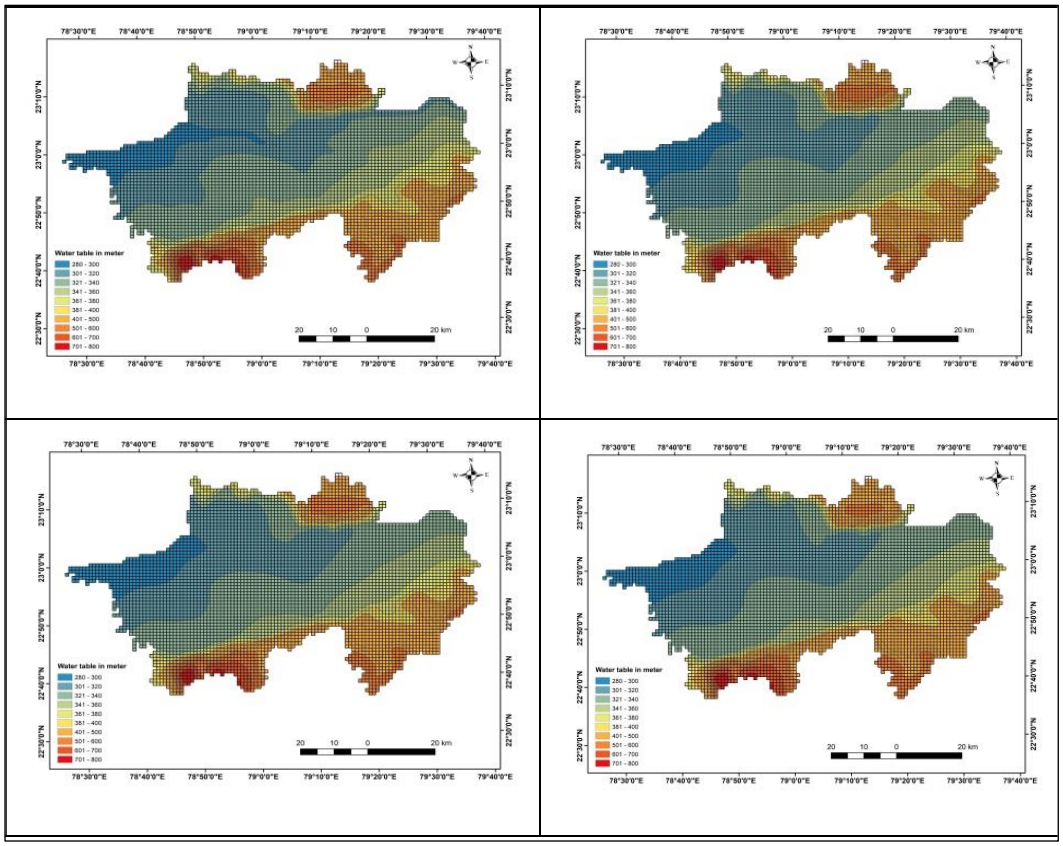

Figure 5.218: Spatial variation of groundwater heads with EC-Earth3-Veg during 2020, 2041, 2071, 2100 under SSP245 scenario

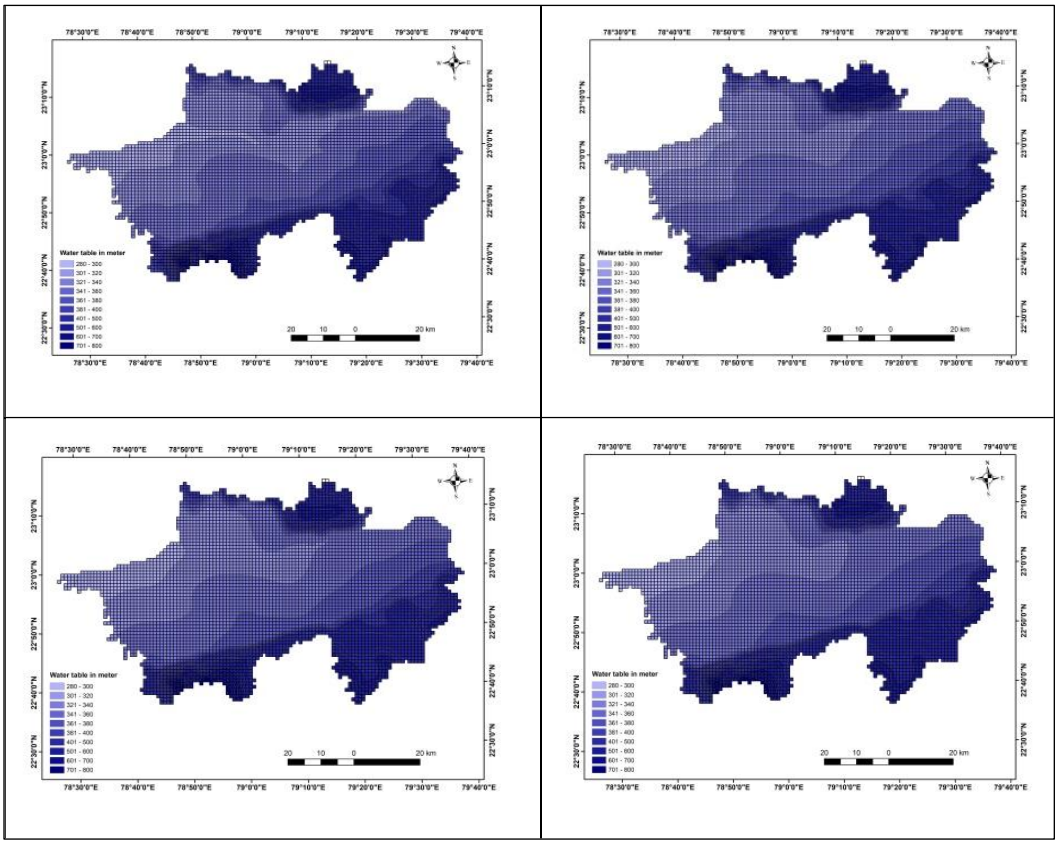

Figure 5.219: Spatial variation of groundwater heads with EC-Earth3-Veg during 2020, 2041, 2071, 2100 under SSP585 scenario

the end-term. The inter-GCM variability can be observed from these plots which depicts that CanESM5 GCM projects a decrease in the groundwater recharge which is possibly due the projections of very high future stream flows. All other GCMs project higher groundwater levels in all future time zones.

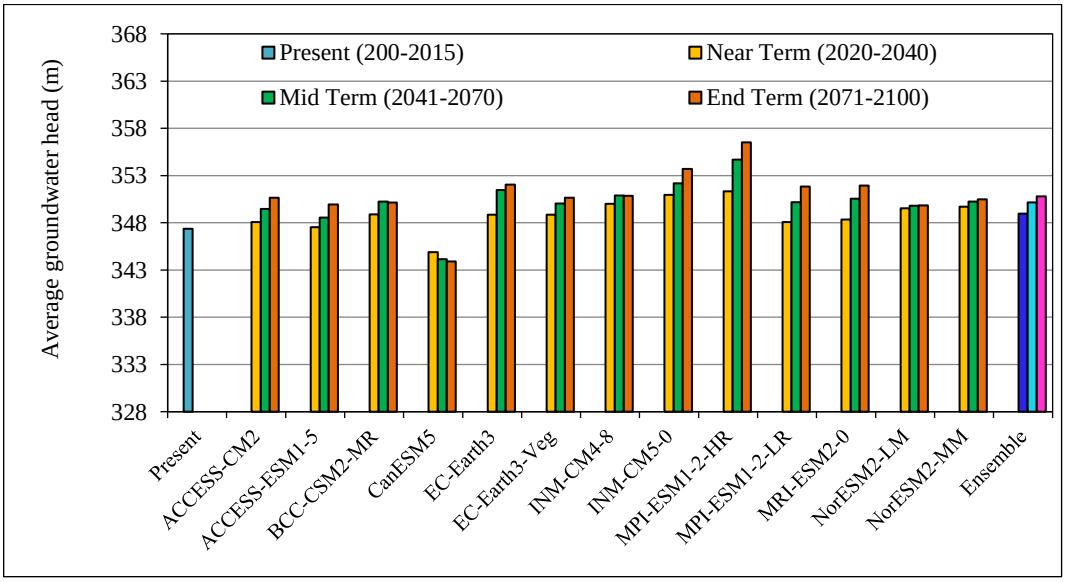

Figure 5.220: Comparison of ensemble mean groundwater head with of that of all individual GCMs under SSP245 scenario

The comparison of the groundwater head during the present time period with the ensemble mean groundwater levels under SSP585 is given in Figure 5.221. The ensemble mean of the simulated future groundwater levels also indicates higher groundwater recharge in all future time periods with 348.85 m during the near-term, 350.55 m during the mid-term and 350.85 m during the end-term. The inter-GCM variability can be observed from these plots and all GCMs project higher groundwater heads in future. The comparison of the ensemble mean projected future groundwater level indicates marginally lower groundwater level in the near-term but marginally higher groundwater levels during the mid-term and end-term under SSP585 scenario.

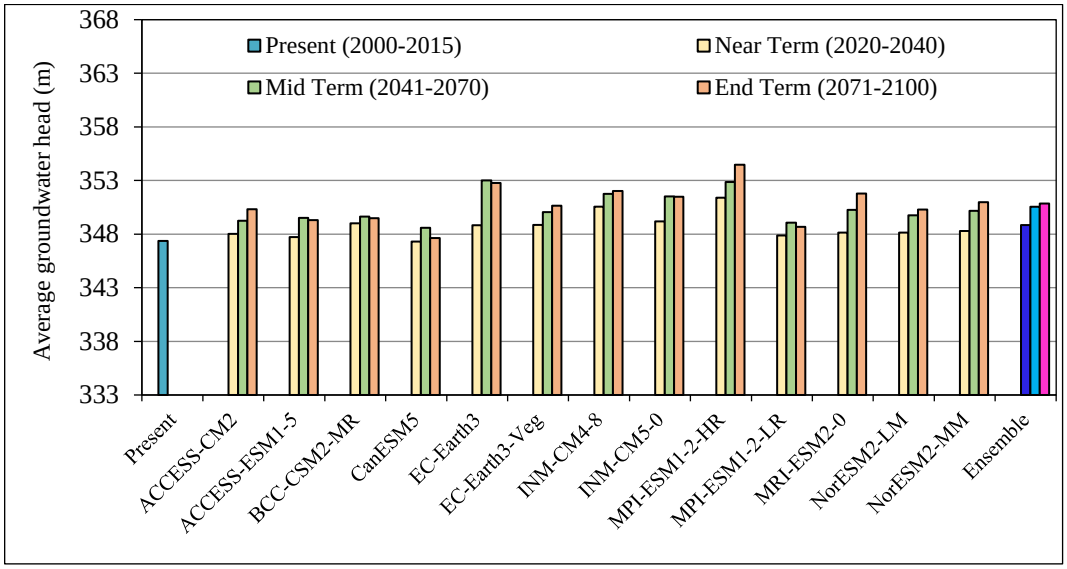

Figure 5.221: Comparison of ensemble mean groundwater head with of that of all individual GCMs under SSP585 scenario

The future groundwater level as estimated by Model MUSE using ACCESS-ESM1 future climate data under SSP245 scenario, projects an increase in groundwater heads from an average of 347.4 m above m.s.l. during the present time period to 349.50 m during near-term, 353.00 m during the mid-term and 355.60 m above m.s.l. during the end-term under SSP 245 scenario. Similarly, the annual groundwater level has been evaluated using ACCESS-ESM1 under SSP585 scenario which indicated marginally lower groundwater heads during near-term (349.48 m), mid-term (352.63 m), and end-term (354.86 m). The comparison of the groundwater head under SSP245 and SSP585 scenarios is given in Figure 5.222. It can be observed that under SSP245 scenario, the groundwater recharge is projected

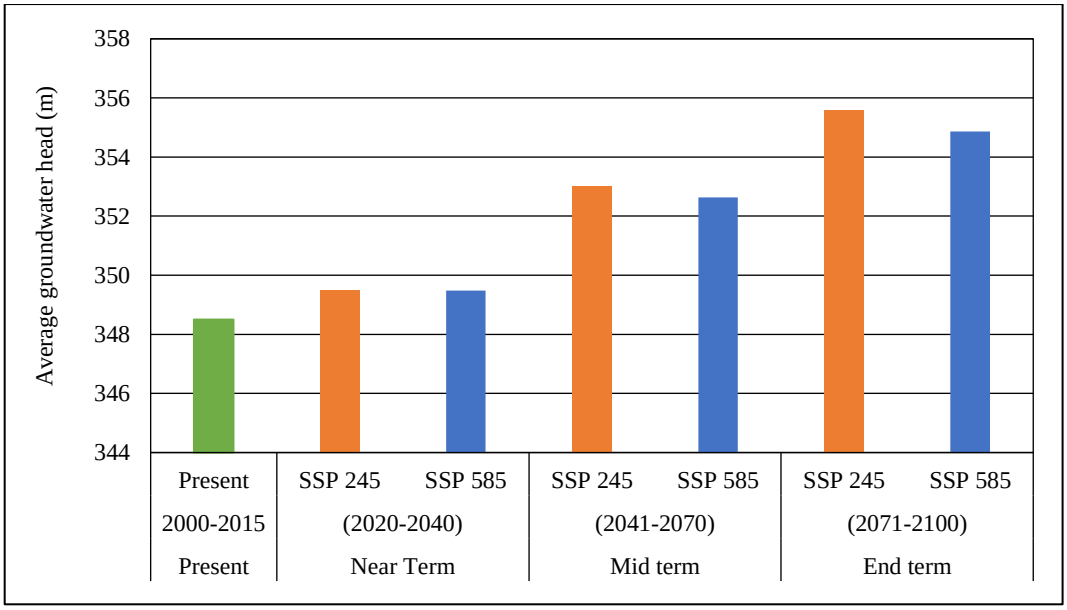

Figure 5.222: Comparison of average groundwater head with ACCESS-ESM1 under SSP245 and SSP585 scenarios

to increase during the mid-term and thereafter projected to decrease during mid-term and end-term period. Also, a similar trend resembling that under SSP245 has been observed under SSP585 scenario. However, the groundwater levels projected under SSP585 scenario are marginally lower than that under SSP245 scenario.

The spatial variation of the groundwater levels using Model MUSE with ACCESS-ESM1 GCM in the various regions of the district have been studying by plotting the groundwater level contours during various years of the simulation. The spatial variation of the groundwater heads during few years viz., 2020, 2041, 2071, and 2100 using ACCESS-ESM1 GCM is given in Figure 5.223 and Figure 5.224 under SSP245 and SSP585 scenarios respectively. It can be observed that there is a distinct variability in the groundwater heads during various years depicted in the study area under both scenarios. It can be observed that the groundwater levels are generally lower in the north-west parts of the district, whereas it is relatively higher in the southern and south-east parts of the district. The groundwater heads are dynamic and varies depending on the groundwater recharge and groundwater draft from the groundwater aquifer and therefore the variability in the groundwater levels can be seen during different years of future simulations.

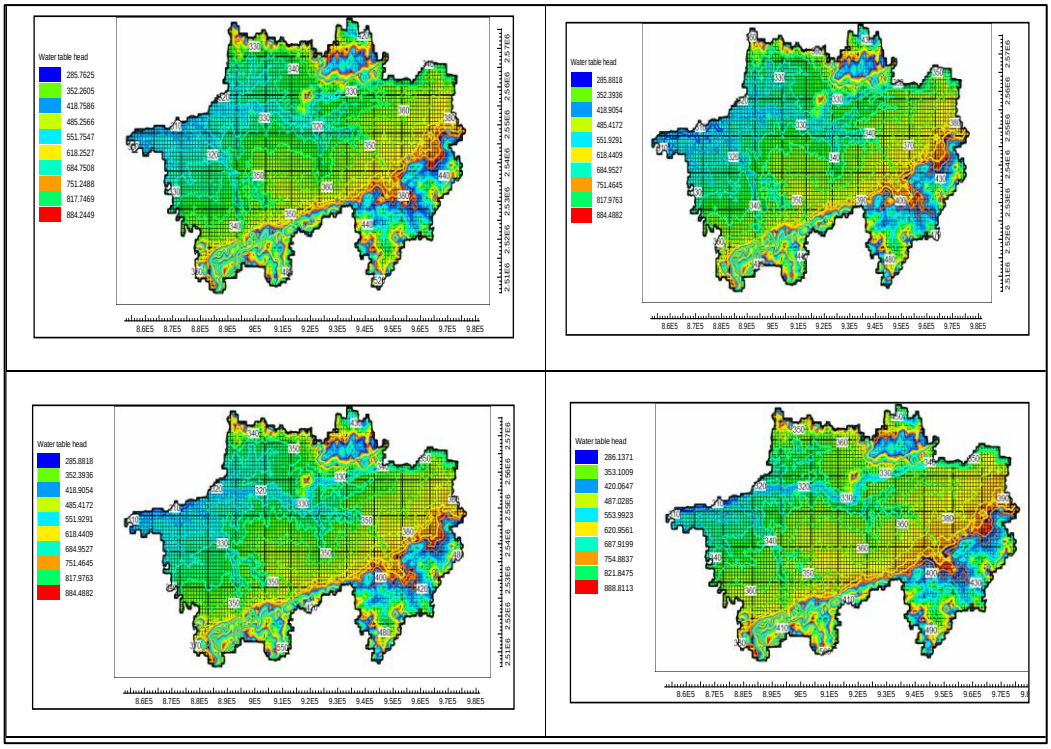

Figure 5.223: Spatial variation of groundwater heads with ACCESS-ESM1 during 2020, 2041, 2071, 2100 under SSP245 scenario

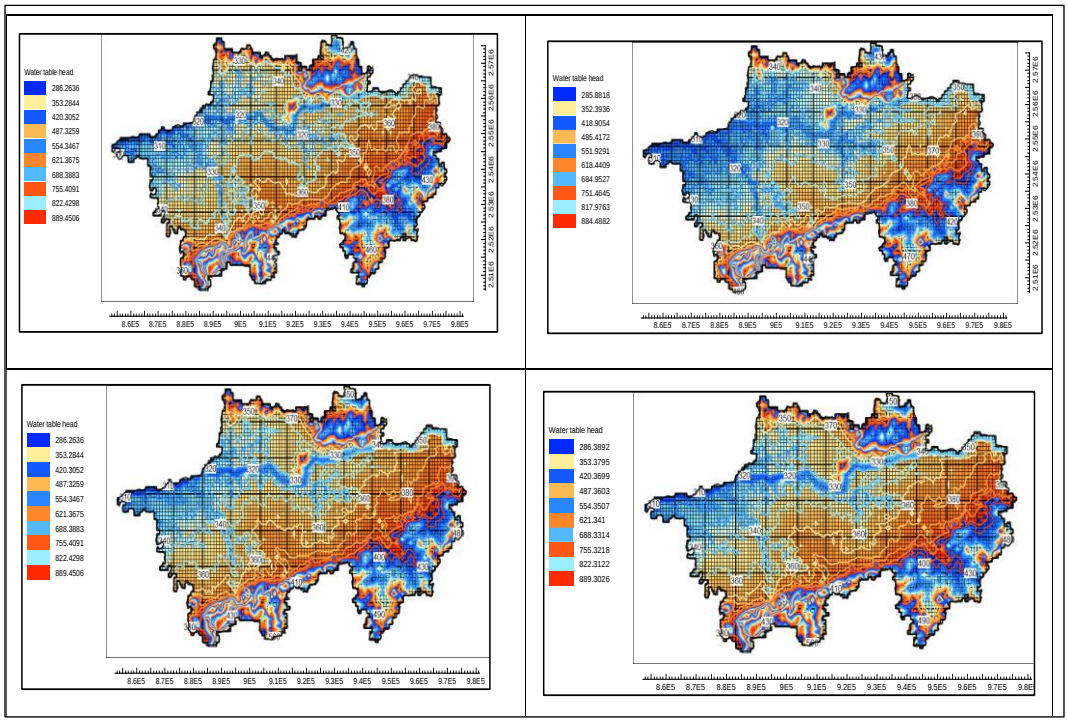

Figure 5.224: Spatial variation of groundwater heads with ACCESS-ESM1 during 2020, 2041, 2071, 2100 under SSP585 scenario

There has been a major shift in the cropping pattern in the district wherein the soyabean crop has largely been replaced by the paddy crop during the kharif season. Paddy is a water intensive crop and the agricultural demands in non-command areas are being met completely from the groundwater. Of-late shift has been observed with more and more farmers adopting sugarcane also in many pockets in the district. Similarly, during the rabi season the area under wheat cultivation is continuously increasing with decrease in gram. Therefore, in non-command areas there is additional water demand to be met directly from the groundwater aquifer and precipitation whenever it become available. However, the projections of higher groundwater levels in future which is mainly due to projected higher rainfall and higher groundwater recharge even after considering the changed cropping pattern augurs well for the agriculture sector in the district particularly in the non-command areas which is completely dependent on groundwater.

5.15 Climate Change Impact Assessment on Future Drought Scenario

The drought characteristics have been evaluated using Standardized Precipitation Index (SPI). The SPI has been evaluated at three different time slices viz., 3-month SPI (3m-SPI), 6-month SPI (6m-SPI) and 12-month SPI (12m-SPI). It has been generally observed from several studies that the 3-m SPI provides a seasonal estimation of the precipitation and also represents the soil moisture availability (short-term moisture conditions), the 6-m SPI represents the surface water availability (medium-term moisture conditions) whereas the 12-m SPI represents the groundwater availability (long-term moisture conditions). Therefore, 3-m SPI has been used as an indicator to evaluate the seasonal precipitation availability and the short-term moisture conditions in the study area. The SPI at time scales of 3, 6 and 12 months have been evaluated for baseline period (1961-1990), present time period (1991-2019), near-term (2020-2040), mid-term (2041-2070) and end-term (2071-2100) at basin scale based on the gridded monthly rainfall data, both historical and future available for the study area.

The total drought severity and total drought duration have been evaluated for each time period for comparison of the changes in drought characteristics in future under the impacts of climate change. The severity for the various types of droughts

[i.e., extreme drought (SPI < -2.0), severe drought (-2.0 < SPI < -1.5), moderate drought (-1.5 < SPI < -1.0)] during the drought years, have been summed to during the various drought events for computing the total drought severity whereas the duration during the various drought events have been summed up to compute the total drought duration. The drought intensity has been computed by dividing the total drought magnitude by drought duration. The comparison of the 3-m SPI based meteorological drought duration during the various time periods in the study area is given in Figure 5.225.

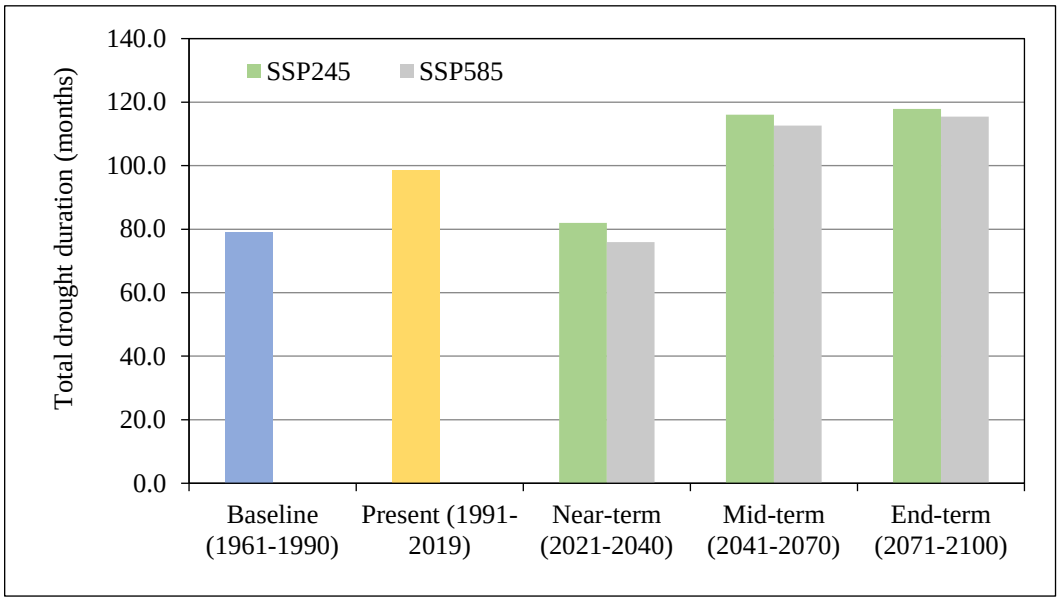

Figure 5.225: Comparison of the drought duration in Upper Narmada basin under SSP245 and SSP585 scenarios

The comparison of the meteorological drought duration during various time periods indicates that the drought duration increased from the baseline period (79.6 months) to the present period (98.5 months). Thereafter, the drought duration is projected to decrease during the near term under both future climate scenarios i.e. 81.9 months under SSP245 scenario and 75.9 months under SSP585 scenario, even though it is higher that during the baseline period. However, the drought duration is projected to increase further from here on during the mid-term with 116 months under SSP245 scenario and 112.6 months under SSP585 scenario. Marginal increase in the drought duration is projected during the end-term as compared to the mid-term with 117.8 months under SSP245 scenario and 115.4 months under the SSP585 scenario.

The comparison of the 3-m SPI based meteorological drought magnitude during the various time periods in the study area is given in Figure 5.226. The comparison of the magnitude of the meteorological drought during various time periods indicates that the drought magnitude increased from the baseline period (83.61) to the present period (101.18). Thereafter, the drought magnitude is projected to decrease during the near term under both future climate scenarios i.e. -89.78 under SSP245 scenario and -80.92 under SSP585 scenario, even though it is higher that during the baseline period. However, the drought magnitude is projected to increase substantially from here on during the mid-term with -126.34 under SSP245 scenario and -122.37 months under SSP585 scenario. Marginal increase in the drought magnitude is projected during the end-term as compared to the mid-term with -127.59 under SSP245 scenario and -124.62 under the SSP585 scenario.

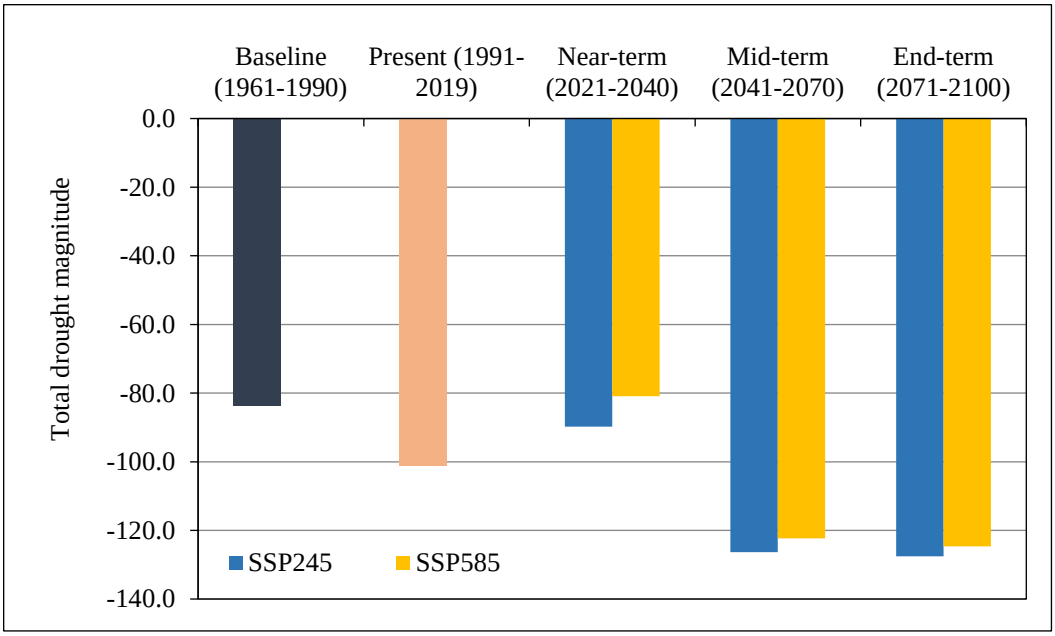

Figure 5.226: Comparison of the drought magnitude in Upper Narmada basin under SSP245 and SSP585 scenarios

The comparison of the intensity of the meteorological drought during various time periods (Figure 5.227) indicates that the drought intensity decreased from the baseline period (1.06) to the present period (1.04). Thereafter, the drought intensity is projected to increase during the near-term under both future climate scenarios i.e. -1.09 under SSP245 scenario and -1.07 under SSP585 scenario, even though it is higher that during the baseline period. However, the drought intensity is projected to marginally decrease during the mid-term to -1.09 under SSP245

scenario and -1.08 under SSP585 scenario. Marginal decrease in the drought intensity is projected during the end-term as compared to the mid-term to -1.08 under SSP245 scenario and -1.08 under the SSP585 scenario.

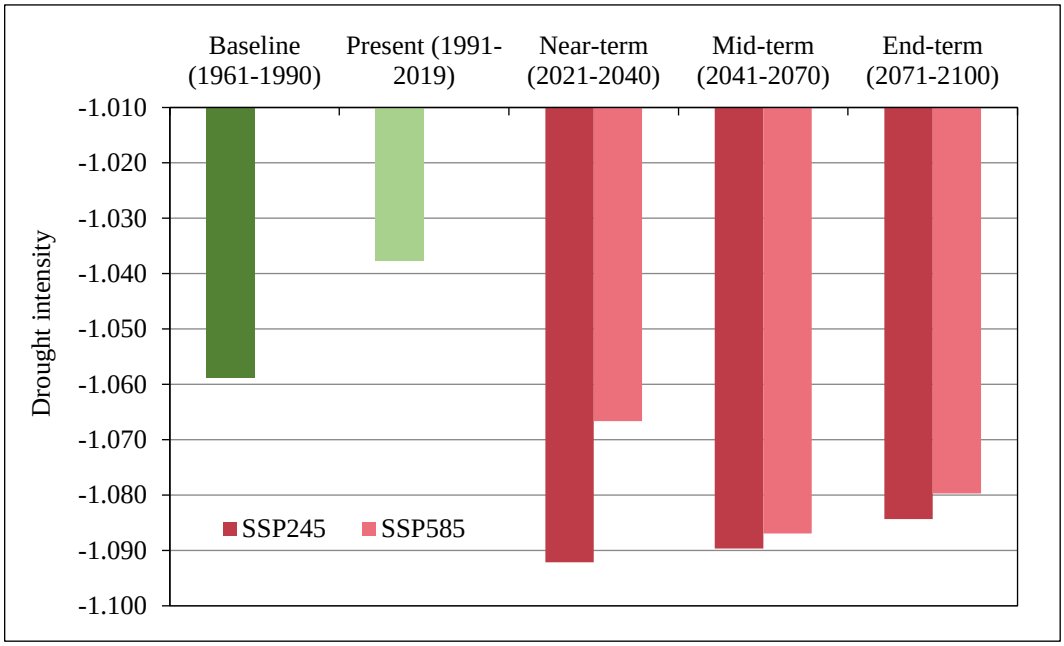

Figure 5.227: Comparison of the drought intensity in Upper Narmada basin under SSP245 and SSP585 scenarios

The 6-m SPI and 12-m SPI based future drought characteristcs have also been evaluated and that too resemble much with the future meteorological drought characterisitcs evaluated based on the 3m-SPI. As such, the impact assessment of the climate change on future meteorological, hydrological and groundwater drought characteristics very clearly indicates that the drought severity as well as the drought duration is projected to increase in all future time periods. As compared to the baseline period (1961-1990), the total drought magnitude duration has increased during the near term but is projected to decrease marginally during the near term under both scenarios. Thereafter the drought magnitude and duration is both projected to increase during the mid-term and end-term time periods. However, the drought magnitude and duration are projected to be marginally lower under SSP585 scenario. The increase in the dry spells and few low rainfall years are largely responsible for the increase in the drought magnitude and durtation in the study area. However, the projected increase is the precipitation and streamflows can be conserved in surface and sub-surface systems and can be utilised during the periods of droughts and dry spells in the basin. Also the projected increase in the average

groundwater recharge and subsequent rise of groundwater levels leading to higher future groundwater availability suggests, the groundwater can be sustainably utilised for meeting out the various demands during droughts in the study area.

5.16 Climate Change Adaptation

Water is the principal sector, through which the impacts of climate change will be translated to other sectors. The comprehensive analysis carried out in this study encompasses the impact of climate change on the surface water and groundwater systems including impacts on future water availability, future groundwater recharge, and extreme events like floods and droughts. Moreover, the input variables viz., precipitation and temperature which are the main drivers of the hydrologic system including water supply and demand is also projected to undergo considerable changes in the future time zones ahead.

Higher average temperatures and changes in precipitation and temperature extremes are projected to affect the availability of water resources through changes in rainfall distribution, soil moisture, river and groundwater flows, which will as will lead to further deterioration of water quality also. The alteration in the patterns of water availability and its distribution, indicates a situation of likely impacts on the water security of the study area. Moreover, the tributaries located in the headwater catchments originating from forested areas on the ridges in Upper Narmada basin are responsible for the perennial nature of stream flows in Narmada River system. As seen from the impact assessment analysis carried out in this study, the changes are projected to escalate further in future time zones, which calls for appropriate adaptation strategies.

Adaptation refers to anticipating the adverse effects of climate change and taking appropriate action to prevent or minimize the damages as well as taking advantages of the opportunities that may arise. Climate change adaptation also refers to the changes to moderate the potential risks associated with climate change. Basically, it is the process of adjusting to the current or projected impacts of climate change. The adaptation solutions will vary from region to region based on the extent and quantum of projected climate change impacts in future. The Fifth Assessment Report of Working Group 2 of the Intergovernmental Panel on Climate Change

(IPCC WGII AR5) has emphasised the role of technology in supporting adaptation to changes in water (IPCC, 2014). Adaptation technology use has been broadly defined as the application of technology in order to reduce the vulnerability, or enhance the resilience, of a natural or human system to the impacts of climate change (UNFCCC, 2005).

The water sector along with the agriculture sector is the critical area of focus for adaptation. However, water is a complex sector, due to the intrinsic linkage between freshwater resources and other sectors and ecosystems. In the water sector, site-specific solutions need to be considered within the broader context of integrated water management approaches. The adaptations measures for climate change impacts can be broadly divided into two aspects viz., a) adaptation for water sector and b) adaptation for agricultural sector. Since India is predominantly an agriculture-based economy, adaptation is necessary for both these sectors to tackle the diverse impacts of climate change on both water and agriculture sectors.

The possible impacts of climate change on the water availability may include changes in spatial and temporal distribution of water as a consequence of climate variability, changes in the flow patterns in the river systems, particularly the flow in tributaries during the non-monsoon season, changes in the groundwater recharge and groundwater storage in aquifers which will directly affect the baseflows and the availability of water during droughts and dry spells. The possible impacts of climate change on flood will include increase in frequency of flood occurrences, urban water flooding in cities, floods in major urban centres located on river banks, erosion of river banks and adjoining agricultural lands affecting the livelihoods and economy of the local population. The possible impacts of climate change on the drought may include crop failures and subsequent loss of livelihoods in the agriculture sector; reduced crop yields with declining income levels resulting in food security issues; fodder shortages for livestock leading to reduced productivity or even cattle death; disposal of cattle, and land in areas vulnerable to drought and out-migration of population in search of alternate livelihoods. Likewise, there shall be environmental impacts including decline in groundwater recharge, lowering of groundwater levels due to overexploitation of groundwater during periods of droughts and extended dry spells. Therefore, appropriate adaptation measures for

management of the water augmentation, water demand management, drought and flood prevention measures being suggested for the study area includes,

- 'Real-time weather monitoring' and 'Advanced weather forecasting systems'. This will help to timely manage the storage in the water resources infrastructure and help in issuing crop advisories for the various agricultural operations.
- 'Improvement of water conveyance system' through lining of canals. The irrigation water use efficiency and crop productivity can be improved greatly by arresting the seepage losses from canals.
- 'Adoption of pressurised irrigation systems' in all upcoming water resources projects. This will help in increasing system efficiency by providing optimal water directly to the root zone of the crop based on the crop water needs and soil moisture status. Moreover, the traditional non-command areas can be brought under command by lift irrigation.
- 'Sensor-based irrigation water scheduling' depending on the soil moisture availability and crop water needs. This will help in water saving and increased crop yields.
- 'Conjunctive use of surface and groundwater'. This will help to optimally use the surface and groundwater resources in tandem, based on the water surplus and deficit of a particular water source in the various river / canal reaches.
- 'Avoiding water intensive crops' viz., rice, sugarcane and banana by importing these products from water rich region, which is basically 'virtual water transfer'.
- 'Reuse of water' by treatment of waste water for agriculture and industries after proper treatment, and also for use during periods of water shortages.
- 'Water use efficient technologies' for domestic sectors by water efficient flushing systems, reuse of grey water from kitchens for toilet flushing and gardening.
- 'Reducing industrial water use' by recycling of water for use in its operations, rainwater harvesting within the industrial complex, limited or no groundwater use by industries etc.

- ‘Management of irrigated agriculture’ by changing of cropping calendar, cropping pattern, adoption of drought-resistant crops, water efficient irrigation systems and regular upkeep of irrigation infrastructure.
- ‘Increasing storage capacity’ by building reservoirs to harness the surplus water during high rainfall periods and utilise it during water deficit periods. Storage can also be enhanced by removal of accumulated sediments in reservoirs, raising dam heights wherever possible, and planning auxiliary reservoirs elsewhere for supplementing water to the main reservoir.
- ‘Soil conservation measures’ in catchment to arrest/reduce soil erosion for preventing the reservoir sedimentation and loss of storage capacity.
- ‘Rainwater harvesting’ to improve groundwater recharge and cultivation in rainfed areas.
- ‘Water conservation’ by construction of check dams, stop dams, farm ponds etc., which will minimise the risks to crop health during dry spells and short-term droughts.
- ‘Enhanced groundwater recharge’ through percolation basins and injection wells thus increasing the climate resilience during periods of critical dry spells and extended droughts.
- ‘Reservoir operation’ for development of revised rule curves for conservation and flood operations of reservoirs.
- ‘Sensor-based reservoir gate operations’ for managing reservoir releases during floods and normal operations.
- ‘Real-time flood forecasting’ and preparation of emergency evacuation plans to prevent/moderate large flood occurrences and reduce damages to life and property.
- ‘Integrated reservoir operation’ for flood control purposes. The depletion and filling of the reservoirs can be considered in tandem so as to prevent large-scale flooding in the downstream areas and prevent flood related damages to life and infrastructure.

- ‘Creation of flood defences’ like construction of flood protection works, flood levees etc.
- ‘Integrated water resources management’ (IWRM) based planning for water management for managing drought, flood, water, agriculture and livelihoods.

6.0 CONCLUSIONS AND SCOPE OF FUTURE WORK

The water resources sector is the key sector based on which the overall development of the agrarian Indian economy is dependent. The livelihood of the rural masses is mostly dependent on the agriculture and farm-based activities. As such their upliftment is directly or indirectly dependent on the availability of water to meet the various demands including domestic, livestock, agricultural and industrial demands. However, the unplanned and overexploitation of both land and water resources has resulted in its degeneration. The transition from limited withdrawal of groundwater to its overexploitation from shallow and deeper aquifers has created an adverse situation resulting in depleting groundwater table and dwindling of baseflow contribution to rivers and lakes in major river basins of the country which are not sustained by snowmelt and glacier melt runoff in non-monsoon season. Coupled with these changes, the highly uncertain climate change is expected to further affect the basin hydrology due to changes in the precipitation pattern, timing and availability along with the unprecedented rise in temperature.

The comprehensive study carried out in Upper Narmada basin falling in Madhya Pradesh, focused mainly on the investigation of the climate change signals, application of semi-distributed and conceptual hydrological models for simulation of runoff and other hydrological processes, application of distributed groundwater models for groundwater flow modelling, hydrodynamic modelling for flood plain mapping, CMIP6 GCMs based climate change impact assessments on water availability, groundwater recharge and drought. These investigations have been carried out for five time zones viz., baseline (1961-1990), present (1991-2015), near-term (2021-2040), mid-term (2041-2070) and end-term (2071-2100). The changes during the various time periods are given below,

- The mean temperature has steadily increased during the historical time periods. The average rise in average annual maximum temperature is at the rate of 0.75^{o}C/100 years during the present time period, which is significant and in tune with IPCC projections. Even though the complete study area has witnessed higher maximum temperature, but the middle regions of Upper Narmada basin i.e. the districts of Raisen, Bhopal, Sehore, Sagar, Narsinghpur, and Hoshangabad have seen the highest increases.

- The average annual maximum temperature is projected to increase from 32.3^{o}C during the baseline period (1961-1990) to 34.3^{o}C and to 35.7^{o}C during the end-term (2071-2100) under SSP245 and SSP585 scenarios respectively. Therefore, the average maximum temperature is projected increase at the rate of 1.58^{o}C/100 year under SSP245 scenario and 2.61^{o}C/100 year under SSP585 scenario. The drastic increase in the projected maximum temperature will result in higher agricultural water demands due to higher evapotranspiration whereas the resulting higher evaporation from the surface water storages in lakes and reservoirs will affect the water supply particularly during the non-monsoon months.

- The average annual minimum temperature is projected to increase from 18.94^{o}C during the baseline period (1961-1990) to 21.72^{o}C and to 23.65^{o}C during the end-term (2071-2100) under SSP245 and SSP585 scenarios respectively. Therefore, the average maximum temperature is projected increase at the rate of 1.58^{o}C/100 year under SSP245 scenario and 2.61^{o}C/100 year under SSP585 scenario. Therefore, the average minimum temperature is projected increase at the rate of 2.14^{o}C/100 year under SSP245 scenario and 3.62^{o}C/100 year under SSP585 scenario. As such, the projected increase in the average annual minimum temperature is considerably higher as compared to the increase in the average annual maximum temperature. The increase in the minimum temperature will have implications for the crop growth and crop yields which may lead to adverse impacts on the food security. Moreover, there may higher demands from the urban and industrial sectors for employing cooling systems in their homes and campuses.

- The very hot days (MaxT>40^{o}C) and hot days (MaxT>35^{o}C) have increased whereas the number of cold nights (MinT<10^{o}C) have decreased considerably during the historical time periods. The increase in the very hot night and hot nights are seen in all the districts falling in Upper Narmada basin. Also, the decrease in the cold night events are more pronounced in the districts of Raisen, Sagar, and parts of Narsinghpur, Chhindwara and Hoshangabad districts.

- The number of very hot days (MaxT>40^{o}C) is projected to increase from 36 days during the baseline period to 51 days, 68 and 76 days during the near-term (2020-2040), mid-term (2041-2070) and end-term (2071-2100) under SSP245 scenario. The number of very hot days are projected to be much higher under SSP585 scenario during the end-term (102 days). This suggests that heatwaves will occur more frequently in future resulting in forest fires, crop failure and making life miserable for human beings and animals.

- The number of very hot night (MinT>25^{o}C) is projected to increase from 42 days during the baseline period to 76 days, 97 and 113 days during the near-term (2020-2040), mid-term (2041-2070) and end-term (2071-2100) under SSP245 scenario. The number of very hot days are projected to be much higher under SSP585 scenario during the end-term (157 days). This suggests that the night will be very warm and unpleasant climatic conditions may prevail leading to adverse effect on the plant and human health.

- The average annual rainfall in the Narmada basin decreases considerably from east to west. The average annual rainfall has been decreasing steadily during the last few decades. The annual average rainfall has seen a steady decrease from 1102.3 mm during baseline period 1961-90 to 1060.2 during 1991-2015.

- The 1-day maximum rainfall varied between 131.4 mm to 716.1 mm, but no significant trends have been detected. The 1-day maximum rainfall has increased in the districts of Narsinghpur, Sehore, and Chhindwara and some parts of Jabalpur, Mandla, and Bhopal districts. The extreme events including the extreme rainfall (>200mm/day), very heavy rainfall (>100mm/day) and heavy rainfall (>50mm/day) have increased in the study area substantially during the historical time periods.

- The average annual rainfall is projected to increase from 1120.0 mm to 1280.7 mm during the near-term, 1364.5 mm during the mid-term and 1493 mm during the ned-term under SSP585 scenario. Similarly, marginal increase in the annual rainfall is projected under SSP585 scenario during the near-term and mid-term but much higher during end-term (1831.3 mm).

- The average annual rainfall is projected to increase from 1120.0 mm to 1280.7 mm during the near-term, 1364.5 mm during the mid-term and 1493 mm during the ned-term under SSP585 scenario. Similarly, marginal increase in the annual rainfall is projected under SSP585 scenario during the near-term and mid-term but much higher during end-term (1831.3 mm).

- The 1-day maximum rainfall is projected to increase from 109.1 mm during baseline period to 117.4 mm under SSP585 scenario and 140.1 mm under SSP585 scenario during the end-term. Similarly, the 3-day consecutive rainfall is also projected to increase from 182.4 mm during baseline period to 237.3 mm under SSP585 scenario and 284.7 mm under SSP585 scenario during the end-term. The projected increase in the magnitudes in the 1-day maximum rainfall along with the increase in magnitude of the 3-day consecutive flows will generate more flash flood occurrences in the urban centres and may also create floods in the rivers, once the reservoirs are full by mid-August. Also, the number of days with heavy rainfall (> 50 mm/day), very heavy rainfall (> 100mm/day) and extreme rainfall (> 200 mm/day) are all projected to increase in all future time periods under both scenarios, the highest being under SSP585 scenario.

- Various hydrological models have been setup for modelling the various hydrologic processes, which have been used after calibration and validation for climate change impact assessments on water resources in the Upper Narmada basin. As far as process-based semi-distributed models are concerned, SWAT and VIC have been applied and the performance of both these models are satisfactory. Both models have their advantages and limitation which have been discussed in detail. Looking into the ease of data availability, applicability in both small watersheds and large river basins, and support from developers and user-groups SWAT has a clear advantage over VIC model. The performance of both models are very good for monthly runoff simulation but the performance is lower for daily runoff simulations.

- WEAP and MIKE11-NAM have the advantage of being easy to apply with few parameters to handle, but at the same time giving good simulation performance. As reservoirs cannot be incorporated in MIKE11-NAM, its

applicability is limited to headwater catchments only. WEAP is a more versatile tool for planning purposes and can incorporate reservoirs also and at the same time linked with groundwater models and energy models. It can also be used to assess the impacts of climate change on the future supply-demand scenario and can be effectively used to conduct scenario analysis for many what-if conditions. WEAP model performance was satisfactory in the study area, and being relatively simple can be used by early-stage modellers too. Decision Support System can also be developed using WEAP.

- The HEC-HMS has the advantage that it can be used for event-based modelling as well as continuous modelling. The model performance was satisfactory for the study area. The outputs from the model can be used for hydrodynamic modelling for flash flood studies and flood plain mapping in flood prone areas. All these calibrated and validated models have been used for climate change impact assessments of the future water availability and extreme events in the Upper Narmada basin.

- MODFLOW is the best model available as of now for modelling the groundwater systems. Its performance was good for its application in Narsinghpur district, which has seen more extraction of groundwater for water intensive crops being adopted there of-late. The calibrated model was used for climate change impact assessment on the groundwater recharge and groundwater levels.

- The climate change impact assessments have been carried out using these calibrated and validated models which have been forced by the bias-corrected future climate data of 13 CMIP6 GCMs for two future climate scenarios viz., SSP245 and SSP585. The analysis of the model outputs has helped to understand how the future might unfold in the Upper Narmada basin regarding the water availability and extreme events are concerned.

- The average daily discharge is projected to increase in all future time periods at all the tributaries in headwater catchments and main river catchments. The increase in the average runoff in the study area is attributed to the overall increase in the annual rainfall. Similarly, high-flows represented by the 1-day

maximum runoff and Q5 & Q10 are also projected to increase substantially in all tributaries and the main river. This is due to the direct consequence of increase in the 1-day maximum rainfall and increase in the extreme, very heavy and heavy rainfall days in the basin. This is an advantageous for the stakeholders as more storages can be created in the study area, particularly on those tributaries that have not been tapped yet or where there is still scope for constructing new reservoirs to store the flood waters for subsequent use during the non-monsoon period.

- The annual peak flow values are also projected to increase substantially in the study area in all future time periods under both future climate scenarios. This will generate floods in the river system and low-lying areas located near the tributaries and the main river. The frequency of occurrence of floods is projected to increase in future. Therefore, it is necessary to conduct flood plain mapping in flood prone areas in the basin. Hoshangabad city is one such important location which warrants such flood plain mapping, so that appropriate measures can be taken to safeguard the area against loss of life and property.

- The high flows (Q5 & Q10) are projected to increase substantially whereas there area only marginal changes projected for low flow during all future time periods. The marginal increase in the low flows (Q90 & Q95) being projected for the future in the tributaries and main river, augurs well for the Narmada River system as it will help to sustain the perennial nature of the river in future also.

- Higher groundwater recharge is projected in future in the Narsinghpur district as evaluated using WetSpass model mainly due to the increase in rainfall in the district. However, the cropping pattern in the district is changing fast with area under sugarcane and paddy seeing a phenomenal increase. Both these crops area water intensive crops and as most of the major blocks of the district are dependent on groundwater for irrigation, the sustainable use of the precious resource is advocated. The higher groundwater recharge is responsible for getting translated into higher groundwater levels in future as evaluated by distributed Visual MODFLOW. The availability of higher groundwater is

advantageous as it can be effectively utilised during periods of extended droughts and long dry spells in future. The groundwater recharge and the groundwater levels are projected to be marginally higher under SSP245 scenario.

- The droughts are expected to increase in future. The drought duration as well as the drought magnitude is expected to increase considerably in all future time periods, the highest increase being projected during the end-term. The increase in the drought characteristics in future makes it necessary for planning additional water storage structures for supplemental irrigation during dry spells and life saving irrigation during drought years. The high flows can be tapped effectively for this purpose and can also be utilised for artificial recharge of groundwater aquifers, which can be tapped during water scarce periods and droughts.

- The supply demand analysis has highlighted the fact that due to the anticipated changes in the future cropping pattern, there will be some areas where all demands cannot be fully satisfied with the available resources. The Gadarwara subbasin is one such example, which has constraints of limited surface water irrigation facility and is mostly dependent on groundwater. The agriculture in the area is mostly dependent on groundwater. Due to this region, arhar dal is grown extensively in the region as it is a low water intensive crop and can sustain near to dry conditions for sufficiently long periods. However, if paddy and sugarcane is adopted in a big way, there may be unmet demands, which have to be satisfied by alternate mechanisms. The potential of lift irrigation and pressurised irrigation systems needs to be explored along with artificial recharge of groundwater in potential recharge zones. Also the farmers should be discouraged from adopting water intensive cash crops and instead incentive need to be passed on to them to continue with the practice of growing dals and other less water intensive crops in the region.

- The scenario of future unmet demands in other parts of the study area, particularly on the main river catchments can be addressed through judicious use of water by switching over to pressurised irrigation systems like drip and sprinkler irrigation, lining of canals to reduce the seepage losses, and reducing

the sediment inflow into the reservoir to prevent reduction in their storage capacity by catchment area treatment works. The sensor-based operation of the reservoirs and irrigation systems will help in substantial water savings in the agriculture sector and can be considered as a good adaptation measure to enhance climate resilience in the area.

- The occurrence of floods at Hoshangabad has become a regular phenomenon of-late. Hoshangabad is a very important city located on the banks of the main Narmada River and has much religious importance. The flood scenario has been generally observed during late August by which the major reservoirs Bargi, Barna and Tawa are near their FRLs. Subsequent heavy rainfall in their respective catchments leads to heavy inflows to these reservoirs. Moreover, the Narmada River already has substantial inflows in the main river and contribution from various tributaries joining from the left and right banks.

- The operation of these three reservoirs is done in a manner that all released flows do not reach Hoshangabad at the same time, to avoid massive flooding and havoc there. The hydrodynamic modelling was attempted and the flood plain mapping was carried out to model the three worst ever flood scenarios that have occurred there. HEC-RAS model was applied and the model effectively carried out the analysis and the flood mapping based on the actual field conditions including the depth of flood water, its discharge and the areal extent to which the flood water entered into the city. Few hypothetical scenarios of full spillway capacity releases from each dam and the subsequent flooding were explored.

- The flood control operation of the three major reservoirs needs to be studied in detail to develop rule curves for the flood operations. Also, the flooding in the city that generally occurs through ingress of backwater through Lediya Nala and Sukhtwa River should be addressed through installation of proper mechanisms to stop flood water entry from the main river to these small nalas and rivers which is ultimately responsible for the flooding scenario. Looking into the future scenario of high flows as shown by the increase in the 1-day maximum flows and Q5 and Q10 flow, it shall be prudent to have real time weather and flood forecasting systems for the river basin. The depletion of the

reservoirs in advance based on accurate and reliable short-term weather forecast will be helpful in addressing the flood related issues at Hoshangabad.

Various strategies for climate change adaptation have been explained in detail based on the future climate change impacts assessed from this comprehensive study. The measures suggested for climate change adaptation and resilience in the water sector which is the primary driving resources for all other water related sectors include, increasing surface water storage capacity by provision of additional water infrastructure, removal of sediments from existing reservoirs, water diversions, diversifying the options for water supply, lining of canals, adoption of pressurized irrigation systems, sensor based irrigation water scheduling and reservoir gate operations, real-time weather monitoring, real-time flood forecasting, integrated water resources management, adoption of water use efficient technologies for domestic and industrial sectors, recycle and reuse of water and promoting groundwater recharge for increasing the climate resilience. Efforts should be initiated in full earnest to implement the recommendations given for climate change adaptation, which will ensure a sustainable development of the region.

The future scope of work can include the assessment of the impact of climate change on the future water quality, both surface and groundwater quality, contaminant transport modelling, sedimentation studies to assess the likely impact of climate change on sediment inflow, impact of the new projects being envisaged on the river system, the impact of inter-basin transfer of water to Shipra, Son, Chambal and drinking water supplies outside the basin to cities including Bhopal, Indore etc., and impact of climate change on forest fires and the subsequent impact of forest fires on basin hydrology.

REFERENCES

1. Abbaspour, K. C., Yang, J., Maximov, I., Siber, R., Bogner, K., Mieleitner, J. and Srinivasan, R. (2007). Modelling hydrology and water quality in the pre-alpine/alpine Thur watershed using SWAT, Journal of Hydrology, 333(2-4): 413-430.
2. Abdessamed, D. and Abderrazak, B. (2019). Coupling HEC-RAS and HEC-HMS in rainfall– runoff modeling and evaluating floodplain inundation maps in arid environments: case study of Ain Sefra city, Ksour Mountain. SW of Algeria. Environmental Earth Sciences, 78(19):586.
3. Adams III, T. E., Chen, S. and Dymond, R. (2018). Results from operational hydrologic forecasts using the NOAA/NWS OHRFC Ohio River Community HEC-RAS Model. Journal of Hydrologic Engineering, 23(7): 04018028.
4. Agarwal, A., Patil, J. P., Goyal, V. C. and Jayakumar, K. V. (2018). A review on WEAP21 model for managing water resources. J. Indian Water Resour. Soc, 38(4).
5. Agarwal, P., Husain, S., Wankhede, S. and Sharma, D. (2018). Rectus abdominis detrusor myoplasty (RADM) for acontractile / hypocontractile bladder in spinal cord injury patients: Preliminary report. Journal of Plastic, Reconstructive & Aesthetic Surgery, 71(5):736-742.
6. Agrawal, A. and Perrin, N. (2009). Climate adaptation, local institutions and rural livelihoods. Adapting to climate change: thresholds, values, governance, 350-367.
7. Mustafa A. K. and El-Naqa, A. (2013). GIS based spatial Groundwater recharge estimation in the Jafr basin, Jordan-application of WetSpass models for arid regions, Revista Mexicana de Ciencias Geológicas, 30. (1): 96-109.
8. Alslevavni, I. N. and Almohseen, K. A. (2017). Integrated application of (MODFLOW) and (WEAP) Model in Nineveh Province. Journal of Duhok University, 680-690.
9. Aliye, M. A., Aliye, M. A., Aga, A. O., Tadesse, T. and Yohannes, P. (2020). Evaluating the performance of HEC-HMS and SWAT hydrological models in simulating the rainfall-runoff process for data scarce region of Ethiopian Rift valley lake basin. open Journal of Modern Hydrology, 10(04):105.
10. Anlon, B. R., Healy, R. W. and Cook, P. G. (2002). Choosing appropriate techniques for quantifying Groundwater recharge. Hydrogeology Journal (10): 18-39. http:// dx.doi.org/10.1007/s10040-0010176-2.
11. Arnold, J. G., Srinivasan, R., Muttiah, R. S. and Allen, P. M. (1999). Continental scale simulation of the hydrologic balance, J. Am. Water Resour. Assoc., 35 (5): 1037-1051.
12. Arnold J. G., Moriasi, D. N., Gassman, P. W., Abbaspour, K. C., White, M. J., Srinivasan, R., Santhi, C., Harmel, D., Griensven, A. V., Kanna, N. and Jha, M. K. (2012). SWAT: Model use, calibration, and validation,

Transactions of the ASABE 55(4): 1491-1508

13. Arsiso, B. K., Tsidu, G. M., Stoffberg, G. H. and Tadesse, T. (2017). Climate change and population growth impacts on surface water supply and demand of Addis Ababa, Ethiopia. Climate Risk Management, 18: 21-33.

14. Assefa, K. A. and Woodbury, A. D. (2013). Transient, spatially varied Groundwater recharge modeling. Water Resources Research, 49(8): 4593-4606.

15. Aufhammer, M., Ramanathan, V. and Vincent, J. R. (2012). Climate change, the monsoon, and rice yield in India. Clim. Change., 111:411-424. https://doi.org/10.1007/s10584-011-0208-4.

16. Baig, I. A., Chandio, A. A., Ozturk, I., Kumar, P., Khan, Z. A. and Salam, M. A. (2022). Assessing the long- and short-run asymmetrical effects of climate change on rice production: empirical evidence from India. Environ. Sci. Pollut. Res., 29: 34209-34230. https://doi.org/10.1007/s11356-021-18014-z.

17. Bailey, R. T., Park, S., Bieger, K., Arnold, J. G. and Allen, P. M. (2020). Enhancing SWAT+ simulation of Groundwater flow and Groundwater-surface water interactions using MODFLOW routines. Environmental Modelling & Software, 126: 104660.

18. Bazzi, H., Ebrahimi, H. and Aminnejad, B. (2021). A comprehensive statistical analysis of evaporation rates under climate change in Southern Iran using WEAP (Case study: Chahnimeh Reservoirs of Sistan Plain). Ain Shams Engineering Journal, 12(2), 1339-1352.

19. Batchelor, C. H., Rama Mohan Rao, M. S. and Manohar Rao, S. (2003). Watershed development: A solution to water shortages in semi-arid India or part of the problem. Land Use and Water Resources Research, 3(1732-2016-140278).

20. Batelaan, O., Wang, Z. M. and De Smedt, F. (1996). An adaptive GIS toolbox for hydrological modeling, in Kovar, K., Nachtnebel, H.P. (eds.), Application of Geographic Information Systems in Hydrology and Water Resources Management: International Association of Hydrological Sciences, Publication No. (235): 3-9

21. Batelaan, O., De Smedt, F., (2001). WetSpass: A flexible, GIS based, distributed recharge methodology for regional groundwater modelling, In: Gehrels, H., Peters, J., Hoehn, E., Jensen, K., Leibundgut, C., Griffioen, J., Webb, B., Zaadnoordijk, W-J. (eds.), Impact of Human Activity on Groundwater Dynamics: International Association of Hydrological Sciences, Publication No. 269, 11-17.

22. Batelaan, O. and Woldeamlak, S. (2003). ArcView Interface for WetSpass, User Manual, Version 1.1. Department of Hydrology and Hydraulic Engineering, Vrije Universiteit, Brussel.

23. Batelaan, O. and De Smedt, F. (2007). GIS-based recharge estimation by coupling surface–subsurface water balances. Journal of Hydrology, 337(3-4), 337-355. https://doi.org/10.1016/j.jhydrol.2007.02.001

24. Batelaan, O., De Smedt, F. and Aish, A. M. (2010). Distributed recharge estimation for groundwater modeling using WetSpass model, case study - Gaza Strip, Palestine, The Arabian Journal for Science and Engineering, (35): 55-163.

25. Bera, S. (2017). Trend analysis of rainfall in Ganga Basin, India during 1901-2000. Am. J. Clim. Chang., 6:116–131. https://doi.org/10.4236/ajcc.2017.61007.

26. Berredjem, A. and Hani, A. (2017). Modelling current and future supply and water demand in the northern region of the Seybouse Valley, Journal of Water and Land Development 33(1): DOI:10.1515/jwld-2017-0016

27. Beven, K. (2001). How far can we go in distributed hydrological modelling Hydrology and Earth System Sciences, 5(1): 1-12.

28. Bhan, S. C. (2010). Climate change: an overview of observed trends in rainfall and temperature over India. Haryana J. Hortic. Sci., 39(1-2):42-47.

29. Bhardwaj, M., Kumar, P., Kumar, S., Dagar, V. and Kumar, A. (2022). A district level analysis for measuring the effects of climate change on production of agricultural crops, i.e., wheat and paddy: evidence from India. Environ Sci. Pollut. Res., (29):31861–31885. https://doi.org/10.1007/s11356-021-17994-2.

30. Bhatti G.H., and Patel H.M. (2015). Irrigation scheduling strategies for cotton crop in semi-arid climate using WEAP model. Journal of Indian Water Resources Society.

31. Blondin, C. (1991). Parameterization of land-surface processes in numerical weather prediction, in Land Surface Evaporation: Measurements and Parameterization, edited by T.J. Schmugge and J.C. Andre,p p. 31-54, Springer-Verlag New York.

32. Brown, J. L., and Yoder, A. D. (2015). Shifting ranges and conservation challenges for lemurs in the face of climate change. Ecology and Evolution, 5(6): 1131-1142.

33. Chea, S. and Oeurng, C. (2017). Flow simulation in an ungauged catchment of Tonle Sap Lake Basin in Cambodia: Application of the HEC-HMS model. Water Utility Journal, (17):3-17.

34. Cunderlik, J. and Simonovic, S. P. (2004). Calibration, verification and sensitivity analysis of the HEC-HMS hydrologic model. Department of Civil and Environmental Engineering, The University of Western Ontario.

35. Das, P., Behera, M. D., Patidar, N., Sahoo, B., Tripathi, P., Behera, P. R., Srivastava, S. K., Roy, P. S., Thakur, P., Agrawal, S. P. and Krishnamurthy, Y. V. N. (2018). Impact of LULC change on the runoff, baseflow and evapotranspiration dynamics in eastern 2 Indian River basins during 1985-2005 using Variable Infiltration Capacity Approach, Journal of Earth System Science 127(2):1-29. DOI:10.1007/s12040-018-0921-8.

36. Dash, S. K. and Hunt, J. C. R. (2007). Variability of climate change in India. Curr. Sci., 93(6): 782-788.

37. Dash S. S., Sahoo, B. and Raghuwanshi, N. S. (2020). How reliable are

the evapotranspiration estimates by Soil and Water Assessment Tool (SWAT) and Variable Infiltration Capacity (VIC) models for catchment-scale drought assessment and irrigation planning?, Journal of Hydrology, (592): 1-22.

38. Deardorff, J. W. (1978) Efficient prediction of ground surface temperature and moisture with inclusion of a layer of vegetation, Journal of Geophysical Research, (83): 1889-1903. https://doi.org/10.1029/JC083iC04p01889

39. Dickinson, R. E. (1984). Modelling evapotranspiration of three-dimensional global climate models, in Climate Processes and Climate Sensitivity, Geophys. Monogr. (29): 58-72

40. Diwakar S. K., Kaur S. and Patel N. (2014). Hydrologic assessment in a middle Narmada basin, India using SWAT Model. International Journal of Engineering Technology and Computer Research (IJETCR), 2 (6): 10-25.

41. Duband, D., Obled, C. and Rodriguez, J. Y. (1993). Unit-hydrograph revised - an alternate iterative approach to UH and effective precipitation identification, Journal of Hydrology, 150(1): 115-149. doi:10.1016/0022-1694(93)90158-6

42. Ducoudre, N. I., Laval, K. and Perrier, A. (1993). SECHIBA, a new set of parameterizations of the hydrologic exchanges at the land atmosphere interface within the LMD atmospheric general circulation model, J. Clim, (6): 248-273.

43. Dukic, V. and Eric R. (2021). SHETRAN and HEC HMS Model evaluation for runoff and soil moisture simulation in the Jičinka River Catchment (Czech Republic), MDPI Journal of Water, 13 (6): 10.3390/w13060872

44. de Oliveira Serrão, E. A., Silva, M. T., Ferreira, T. R., de Ataide, L. C. P., dos Santos, C. A., de Lima, A. M. M. and Gomes, D. J. C. (2021). Impacts of land use and land cover changes on hydrological processes and sediment yield determined using the SWAT model. International Journal of Sediment Research.

45. El-Rawy, M., Mohammed, G. A., Zijl, W., De Smedt, F. and Batelaan, O. (2011). Inverse modeling combined with Kalman filtering applied to a Groundwater catchment. In MODFLOW and More 2011 425-429.

46. Emami, F., and Koch, M. (2019). Modeling the impact of climate change on water availability in the Zarrine River Basin and inflow to the Boukan Dam, Iran. Climate, 7(4):51.

47. Engel B., D. Storm, M. White, and J. G. Arnold. (2007). A hydrologic/water quality model application protocol. J. American Water Resources Association, Vol 43(5):1223-1236.

48. Eyring, V., Bony, S., Meehl, G. A., Senior, C. A., Stevens, B., Stouffer, R. J., and Taylor, K. E. (2016). Overview of the Coupled Model Intercomparison Project Phase 6 (CMIP6) experimental design and organization, Geosci. Model Dev., (9): 1937–1958, 2016, doi:10.5194/gmd-9-1937-2016.

49. Fard, M. D., and Sarjoughian, H. S. (2021). A RESTful framework design for componentizing the water evaluation and planning (WEAP) system. Simulation Modelling Practice and Theory, (106): 102199.

50. Fleming, M. (2002). Continuous hydrologic modeling with HMS: parameter estimation and model calibration and validation (Doctoral dissertation, MSc Thesis, Tennessee Technological University).

51. Francini, M. and Pacciani, M. (1991). Comparative analysis of several conceptual rainfall-runoff models, J. Hydrol., (122): 161-219.

52. Ghosh, S. and Dutta, S. (2012). Impact of climate change on flood characteristics in Brahmaputra basin using a macro-scale distributed hydrological model. Journal of Earth System Science, 121(3): 637-657.

53. Gobiet, A., Kotlarski, S., Beniston, M., Heinrich, G., Rajczak, J.and Stoffel, M. (2014). 21st century climate change in the European Alps-A review. Science of the Total Environment, (493): 1138-1151.

54. Gupta, H. V., Sorooshian, S. and Yapo, P. O. (1999). Status of automatic calibration for hydrologic models: Comparison with multilevel expert calibration. *J. Hydrologic Eng.* 4(2): 135-143.

55. Guhathakurta, P. and Rajeevan, M. (2008). Trends in the rainfall pattern over India. Int. J. Climatol., 28:1453-1469.

56. Guhathakurta, P., Sreejith, O. P. and Menon, P. A. (2011). Impact of climate change on extreme rainfall events and food risk in India. J. Earth Syst. Sci., 120:359-373. https://doi.org/10.1007/s12040-011-0082-5.

57. Hargreaves, G.H. and Samani, Z. A. (1982). Estimating potential evapotranspiration. Journal of Irrigation and Drainage Engineering, (108): 223-230.

58. Himanshu, S. K., Pandey A. and Shrestha, P. (2016). are published the paper on Application of SWAT in an Indian river basin for modeling runoff, sediment and water balance in Ken River basin, India in Springer. Environmental Earth Sciences 76(1):3. DOI:10.1007/s12665-016-6316-8

59. Himanshu, S. K., Pandey, A. and Shrestha, P. (2017). Application of SWAT in an Indian river basin for modeling runoff, sediment and water balance, Environ. Earth Science 76:3. DOI 10.1007/s12665-016-6316-8.

60. IPCC (2014). Climate change 2014: synthesis report. Contribution of working groups I, II and III to the fifth assessment report of the Intergovernmental Panel on Climate Change (IPCC), Geneva, Switzerland, 151.

61. Ismail, H., Kamal, M. R., Hin, L. S., and Abdullah, A. F. (2020). Performance of HEC-HMS and ArcSWAT Models for Assessing Climate Change Impacts on Streamflow at Bernam River Basin in Malaysia. Pertanika Journal of Science & Technology, 28:3.

62. Jain, S. K. and Kumar, V. (2012). Trend analysis of rainfall and temperature data for India, Current Science, 102 (1): 37-49.

63. Jain, M. and Sharma, S. T. (2014). Hydrological modeling of Vamsadhara River basin, India, using SWAT. International Conference on Emerging

Trends in Computer and Image Processing (ICETCIP 2014), Paltaya, 15-16 December 2014, 82-86.

64. Jha, M., Gassman, P. W., Arnold, J. G., Secchi, S. S., Campbell, T. and King, C. L. (2004). Hydrologic modeling of upper Mississippi river basin using SWAT, The Canadian Society for Engineering in Agricultural, Food and Biological Systems, Paper No. 042069

65. Kanani, H., Yadav, S. M. and Waikhom, S. I. (2017). Evaluation of drinking water supply demand for peri-urban region, International Journal of Advance Research in Engineering, Science & Technology, 4: 2394-2444

66. Kabeja, C., Li, R., Guo, J., Rwatangabo, D. E. R., Manyifika, M., Gao, Z. and Zhang, Y. (2020). The Impact of Reforestation Induced Land Cover Change (1990-2017) on Flood Peak Discharge Using HEC-HMS Hydrological Model and Satellite Observations: A Study in Two Mountain Basins, China. Water, 12(5): 1347.

67. Khadka C., Arya, K. P., Jonasova, M. E., Upadhyaya, A., Dhungana, N., Cudlin, P. and Vacik, H. (2018). Evaluating participatory techniques for adaptation to climate change: Nepal case study, Forest Policy and Economics, 97:73-82. https://doi.org/10.1016/j.forpol.2018.08.017

68. Khaladkar, R. M., Mahajan, P. N. and Kulkarni, J. R. (2009). Alarming rise in the number and intensity of extreme point rainfall events over the indian region under climate change scenario. RR 123, Indian Institute of Tropical Meteorology, ISSN 0252-1075. http://www.imdpune.gov.in/Clim_Pred_LRF_New/Reports. html.

69. Khare, D., Singh, R. and Shukla, R. (2014). Hydrological modelling of Barinallah watershed using ArcSWAT model. International Journal of Geology, Earth and Environment Sciences, 4(1): 224-235.

70. Klemeš, V. (1983). Conceptualization and scale in hydrology. Journal of Hydrology, 65: 1

71. Kothyari, U. C. and Singh, V. P. (1996). Rainfall and temperature trends in India. Hydrol. Process., 10:357-372.

72. Krishnakumar, K. N., Rao, G. S. and Gopakumar, C. S. (2009). Rainfall trends in twentieth century over Kerala, India. Atmos. Environ., 43:1940-1944. https://doi.org/10.1016/j.atmosenv.2008.12.053.

73. Kumar, K. R., Sahai, A. K., Kumar, K. K., Patwardhan, S. K., Mishra, P. K., Revadekar, J. V., Kamala, K. and Pant, G. B. (2006). High-resolution climate change scenarios for India for the 21st century. Curr. Sci., 90(3): 334-345.

74. Kundu, S., Khare, D. and Mondal, A, (2017). Interrelationship of rainfall, temperature and reference evapotranspiration trends and their net response to the climate change in Central India. Theoret. Appl. Climatol., 130:879-900. https://doi.org/10.1007/ s00704-016-1924-5.

75. Lal, M. and Singh, S. K. (2001). Global warming and monsoon climate. Mausam, 52(1): 245-262.

76. Lamichhane, S. and Shakya, N. M. (2020). Shallow aquifer Groundwater dynamics due to land use/cover change in highly urbanized basin: The case of Kathmandu valley. Journal of Hydrology: Regional Studies, 30: 100707.

77. Legates, D. R. and McCabe Jr. G. J. (1999). Evaluating the use of "Goodness-of-Fit" measures in hydrologic and hydroclimatic model validation. Water Resources Research, 35: 233-241. http://dx.doi.org/10.1029/1998WR900018

78. Liang. X., Lettenmaier, D. P., Wood, E. F. and Burges, S. J. (1994). A simple hydrologically based model of land surface water and energy fluxes for general circulation models, Journal of Geophysical Research, 99(7): 14415-14428.

79. Louis, J., A (1979). Parametric model of vertical eddy fluxes in the atmosphere Boundary Layer Meteorel., (17): 187-202.

80. Madsen, H. (2000). Automatic calibration of a conceptual rainfall-runoff model using multiple objectives, Journal of Hydrology 235(3):276-288. DOI:10.1016/S0022-1694(00)00279-1

81. Mahmood, R., Jia, S. and Zhu, W. (2019). Analysis of climate variability, trends, and prediction in the most active parts of the Lake Chad basin, Africa. Sci. Rep., 9: 6317 (2019). https://doi.org/10.1038/s41598-019-42811-9

82. Mansouri, S., Ouerdachi, L., and Remaoun, M. (2017). Inter-region planning and analysis of water resources by using WEAP model Seybouse (Annaba) and Coastal East of Constantine (El-Taref). Journal of Water and Land Development, 33(1): 115-122. Model. Journal of Indian Water Resources Society.

83. Mathenge, M. W. and Gathuru, G. M. (2020). Spatial-temporal variation of groundwater recharge from precipitation in the Stony Athi sub-catchment, Kenya, International Journal of Environmental Sciences 3(1):21. DOI:10.47604/ijes.1079

84. Mengistu, D., Bewket, W., Dosio, A., and Panitz, H. J. (2021). Climate change impacts on water resources in the Upper Blue Nile (Abay) River Basin, Ethiopia. Journal of Hydrology, 592: 125614.

85. Mehrotra, D. and Mehrotra, R. (1995). Climate change and hydrology with emphasis on the Indian subcontinent. Hydrol. Sci., J., 40(2):231-242. https://doi.org/10.1080/02626669509491406

86. Metobwa, O. G. M. Mourad, K. A. and Ribbe, L. (2018). Water Demand Simulation Using WEAP 21: A Case Study of the Mara River Basin, Kenya, International Journal of Natural Resource Ecology and Management, 3(1): 9-18. doi: 10.11648/j.ijnrem.20180301.12

87. Mishra, V., Bhatia, U. and Tiwari, A. D. (2020). Bias-corrected climate projections for South Asia from Coupled Model Intercomparison Project-6(**7**):338 . https://doi.org/10.1038/s41597-020-00681-1

88. Mondal, A., Khare, D. and Kundu, S. (2015). Spatial and temporal analysis of rainfall and temperature trend of India. Theoret. Appl. Climatol.,

(122):143-158. https://doi.org/10.1007/s00704-014-1283-z.

89. Monteith, J. L. (1965). Evaporation and the Environment. 19th Symposia of the Society for Experimental Biology, 19: 205-234.

90. Moriasi, D. N., Arnold, J. G., Van Liew, M. W., Bingner, R. L., Harmel, R. D., and Veith, T. L. (2007). Model evaluation guidelines for systematic quantification of accuracy in watershed simulations. Transactions of the ASABE, 50(3): 885-900.

91. Mujumdar, P. P. and Ghosh, S. (2008). Modeling GCM and scenario uncertainty using a possibilistic approach: Application to the Mahanadi River, India, Water Resources Research, 44: 6

92. Naidu, C. V., Rao, B. R. S. and Rao, D.V. B. (1999). Climatic trends and periodicities of annual rainfall over India. Meteorol. Appl., 6: 395-404.

93. Narendra, H., Eldho, T. I. and Ghosh, S. (2017). Climate change impact assessment of a river basin using CMIP5 climate models and the VIC hydrological model, Hydrological Sciences Journal, 63(4): 596-614. https://doi.org/10.1080/02626667.2018.1441531

94. Nash, J. E. and Sutcliffe, J. V. (1970). River flow forecasting through conceptual model. Part 1-A Discussion of Principles. Journal of Hydrology, 10:282-290.http://dx.doi.org/10.1016/0022-1694(70)90255-6

95. Neitsch, S. L., Arnold, J. G., Kiniry, J. R., Williams, J. R. and King, K. W. (2002). Soil and Water Assessment Tool Theoretical Documentation. Ver. 2000. Temple, Tex.: USDA-ARS Grassland Soil and Water Research Laboratory and Texas A&M University, Blackland Research and Extension Center.

96. Oki, T., and Kanae, S. (2006). Global hydrological cycles and world water resources. science, 313(5790): 1068-1072.

97. Oliveira A. S. E et al., (2021). Impacts of land use and land cover changes on hydrological processes and sediment ~ yield determined using the SWAT model, International Journal of Sediment Research, https://doi.org/10.1016/j.ijsrc.2021.04.002

98. Osoro, G. M., Mourad, K. A. and Ribbe, L. (2018). Water demand simulation using WEAP 21: a case study of the Mara River Basin, Kenya.

99. Oti, J. O., Kabo-Bah, A. T., and Ofosu, E. (2020). Hydrologic response to climate change in the Densu river basin in Ghana. Heliyon, 6(8): 04722.

100. Ouédraogo, W. A. A., Raude, J. M., and Gathenya, J. M. (2018). Continuous modeling of the Mkurumudzi River catchment in Kenya using the HEC-HMS conceptual model: calibration, validation, model performance evaluation and sensitivity analysis. Hydrology, 5(3): 44.

101. Pachauri, R. K., Meyer, L., Plattner, G. K. and Stocker, T. (2015). IPCC, 2014: Climate Change 2014: Synthesis Report. Contribution of Working Groups I, II and III to the Fifth Assessment Report of the Intergovernmental Panel on Climate Change., IPCC.

102. Pal, I. and Al-Tabbaa, A. (2009). Trends in seasonal precipitation extremes-an indicator of climate change in Kerala, India. J. Hydrol.,

367:62-69. https://doi.org/10.1016/j.jhydrol.2008.12.025

103. Pal I, Al-Tabbaa A (2010) Regional changes in extreme monsoon rainfall defcit and excess in India. Dyn Atmos Oceans 49: 206-214. https://doi.org/10.1016/j.dynatmoce.2009.07.

104. Panda, A. and Sahu, N. (2019). Trend analysis of seasonal rainfall and temperature pattern in Kalahandi, Bolangir and Koraput districts of Odisha, India. Atmos. Sci. Lett., https://doi.org/10.1002/asl.932.

105. Pandey, B. K., Khare, D., Kawasaki, A. and Meshesha, T. W. (2021). Integrated approach to simulate hydrological responses to land use dynamics and climate change scenarios employing scoring method in upper Narmada basin, India, J. Hydrol., 598: 123629. https://doi.org/10.1016/j.jhydrol.2021.126429.

106. Patel, D. P., Ramirez, J. A., Srivastava, P. K., Bray, M., and Han, D. (2017). Assessment of flood inundation mapping of Surat city by coupled 1D/2D hydrodynamic modeling: a case application of the new HEC-RAS 5. Natural Hazards, 89(1): 93-130.

107. Patel, D., Ramirez, J., Srivastava, P., Bray, M. and Han, D. (2017). Flood risk assessment through 1D/2D couple HEC-RAS hydrodynamic modeling-A case study of Surat City, Lower Tapi Basin, India. In EGU General Assembly Conference Abstracts :1702.

108. Patil, N. S., Chetan, N. L., Nataraja, M., and Suthar, S. (2020). Climate change scenarios and its effect on Groundwater level in the Hiranyakeshi watershed. Groundwater for Sustainable Development, 10,100323.

109. Patra, J. P., Mishra, A., Singh, R. and Raghuwanshi, N. S. (2012). Detecting rainfall trends in twentieth century (1871–2006) over Orissa State, India. Clim. Change., 111:801-817. https://doi.org/10.1007/ s10584-011-0215-5.

110. Penman, H.L. (1948) Natural evaporation from open water, bare soil and grass, Proceedings of the Royal Society of London, 193: 120-145. https://doi.org/10.1098/rspa.1948.0037

111. Priestley, C. H. B. and Taylor, R. J. (1972). On the Assessment of Surface Heat Flux and Evaporation Using Large Scale Parameters. Monthly Weather Review, 100: 81-92. http://dx.doi.org/10.1175/1520-0493(1972)100<0081:OTAOSH>2.3.CO;2

112. Priyanka and Patil., N. S. (2016). Runoff modelling for Malaprabha Sub basin using SWAT hydrological model, Int. J. Res. Engg. Tech., 5(7): 35-38.

113. Psomas, A., Panagopoulos, Y., Konsta, D., and Mimikou, M. (2016). Designing water efficiency measures in a catchment in Greece using WEAP and SWAT models. Procedia engineering, 162: 269-276.

114. Radhakrishnan, K., Sivaraman, I., Jena, S. K. and Sarkar, S. and Adhikary, S. (2017). A climate trend analysis of temperature and rainfall in India. Clim Chang Environ Sustain 5(2):146-153. https://doi.org/10. 5958/2320-642X.2017.00014.X.

115. Rajeevan, M., Bhate, J., Kale, J. and Lal, B. (2006). A high resolution daily gridded rainfall data for the Indian Region: analysis of break and active monsoon spells, Current Science 91:10.

116. Rangari, V. A., Umamahesh, N. V. and Bhatt, C. M. (2019). Assessment of inundation risk in urban floods using HEC RAS 2D. Modeling Earth Systems and Environment, 5(4): 1839-1851.

117. Rawls, W. J., Brakensiek, D. L. and Saxtonn, K. E. (1982). Estimation of soil water properties. Transactions of the ASABE, 25(5): 1316-1320.

118. Reshmidevi, T. V., Kumar, D. N., Mehrotra, R. and Sharma, A. (2018). Estimation of the climate change impact on a catchment water balance using an ensemble of GCMs. Journal of Hydrology, 556: 1192-1204.

119. Rickards, N., Thomas, T., Kaelin, A., Houghton-Carr, H., Jain, S. K., Mishra, P. K. and Rees, G. (2020). Understanding future water challenges in a highly regulated Indian river basin-modelling the impact of climate change on the hydrology of the Upper Narmada. Water, 12(6): 1762.

120. Roberts, J. (1983). Forest transpiration: a conservative hydrological process ? J. Hydrol. 66: 133-141.

121. Roy, D., Begam, S., Ghosh, S. and Jana, S. (2013). Calibration and validation of HEC-HMS model for a river basin in eastern India, ARPN Journal of Engineering and Applied Sciences, 8:1.

122. Sahu, M., Lahari, S., Gosain, A. K. and Ohri, A. (2016). Hydrological modeling of Mahi basin using SWAT. Journal of Water Resource and Hydraulic Engineering, 5: 68-79.

123. Sahraei, S., Asadzadeh, M., and Unduche, F. (2020). Signature-based multi-modelling and multi-objective calibration of hydrologic models: Application in flood forecasting for Canadian Prairies. Journal of Hydrology, (588): 125095.

124. Sahukhal, R. and Bajracharya, T. R. (2019). Modeling water resources under competing demands for sustainable development: A case study of Kaligandaki Gorge Hydropower Project in Nepal. Water Science and Engineering, 12(1): 19-26.

125. Saleem, M., Ram, S., Mahmood, G., Hasan, M. A. and Waseem, M. (2019). Aquifer modelling in Greater Noida region (UP) using MODFLOW. In Smart Cities-Opportunities and Challenges, 755-766, Springer.

126. Salem, A., Dezso, J. and El-Rawy, M. (2019). Assessment of Groundwater recharge, evaporation, and runoff in the Drava Basin in Hungary with the WetSpass model. Hydrology 2019, 6(23). https://doi: 10.3390/hydrology6010023

127. Scanlon, B. R., Healy, R. W. and Cook, P. G. (2002). Choosing appropriate techniques for quantifying groundwater recharge. Hydrology Journal, 10: 18-39.

128. Schaperow, J. R., Li, D., Margulis, S. A. and Lettenmaier, D. P. (2021). A near-global, high resolution land surface parameter dataset for the

variable infiltration capacity model, Scientific 8(216):1-14. https://doi.org/10.1038/s41597-021-00999-4.

129. Scharffenberg W. and Fleming M. (2016). Hydrologic modelling system HEC-HMS v4.2: User's Manual. USACE, Hydrologic Engineering Center, Davis.

130. Scharffenberg, W. A. and Fleming, M. J. (2006). Hydrologic modelling system HEC-HMS: user's manual. US Army Corps of Engineers, Hydrologic Engineering Center

131. Scharffenberg, (2018). Hydrologic Modelling System HEC-HMS User's Manual version 4.3. Davis, CA: US Army Corps of Engineers Institute for Water Resources Hydrologic Engineering Centre (HEC). Available at: https://www.hec.usace.army.mil/software/hec-hms/documentation/HECHMS_Users_Manual_4.3.pdf

132. Shahraki, A. S., Shahraki, J., and Monfared, S. A. H. (2016). An application of WEAP model in water resources management considering the environmental scenarios and economic assessment case study: Hirmand catchment. Modern Applied Science, 10(5):49-56.

133. Shivhare, V., Goel, M. K., and Singh, C. K. (2014). Simulation of surface runoff for Upper Tapi sub-catchment area (Burhanpur watershed) using SWAT. The International Archives of Photogrammetry, Remote Sensing and Spatial Information Sciences, 40(8):391.

134. Shuttleworth, W. J. (1993). Evaporation. In: D.R. Maidment (Editor), Handbook of Hydrology. McGraw Hill, New York.

135. Singh, M., Shinde, V., Pradhan, S. K., Chalodiya, A. L. and Shukla, K. N. (2014). Hydrologic modelling of Mahanadi River basin in India using rainfall-runoff model. Nature Environment and Pollution Technology, 13(2): 385.

136. Singh, W. R. and Jain, M. K. (2015). Continuous hydrological modelling using soil moisture accounting algorithm in Vamsadhara River basin, India. Journal of Water Resource and Hydraulic Engineering, 4(4): 398-408.

137. Siqueira, V. A., Sorribas, M. V., Bravo, J. M., Collischonn, W., Lisboa, A. M. V. and Trinidad, G. G. V. (2016). Real-time updating of HEC-RAS model for streamflow forecasting using an optimization algorithm. RBRH, 21(4): 855-870.

138. Srivastava, A. K., Rajeevan, M. and Kshirsagar, S. R. (2009). Development of a high resolution daily gridded temperature data set (1969-2005) for the Indian region, Atmos. Sci. Let. (2009), DOI: 10.1002/asl.232.

139. Srivastava, A., Deb, P. and Kumari, N. (2018). Multi-Model approach to assess the dynamics of hydrologic components in a tropical ecosystem, Water Resources Management. https://doi.org/10.1007/s11269-019-02452-z

140. Stephenson, D. B., Douville, H. and Rupakumar, K. (2001). Searching for a fingerprint of global warming in the Asian summer monsoon. Mausam,

52(1): 213-220.

141. Swain, N. R., Christensen, S. D., Snow, A. D., Dolder, H., Espinoza-Dávalos, G., Goharian, E. and Burian, S. J. (2016). A new open-source platform for lowering the barrier for environmental web app development. Environmental Modelling & Software, 85: 11- 26.

142. Swain, S., Taloor, A. K., Dhal, L., Sahoo, S. and Al-Ansari, N. (2022). Impact of climate change on groundwater hydrology: a comprehensive review and current status of the Indian hydrogeology. Appl. Water. Sci., 12:120. https://doi.org/10.1007/s13201-022-01652-0.

143. Tassew, B. G., Belete, M. A. and Miegel, K. (2019). Application of HEC-HMS model for flow simulation in the Lake Tana basin: The case of Gilgel Abay catchment, upper Blue Nile basin, Ethiopia. Hydrology, 6(1): 21.

144. Teklebirhan, A., Dessie, N. and Tesfamichael, (2012). Groundwater recharge, evapotranspiration and surfacer estimation using WetSpass modeling method in Illala catchment, Northern Ethiopia, Momona Ethiopian Journal of Science (MEJS), Volume 4(2):96-110.

145. Thomas, T., Gunthe, S. S., Ghosh, N. C. and Sudheer, K. P. (2015). Analysis of monsoon rainfall variability over Narmada basin in central India: Implication of climate change. J. Water, Clim. Chang., 6(3): 615-627. https://doi.org/10.2166/wcc.2014.041.

146. Uniyal, B., Jha, M. K. and Verma, A. K. (2015). Assessing climate change impact on water balance components of a river basin using SWAT model. Water Resources Management, 29(13): 4767-4785.

147. Van Griensven, A. and Bauwens, W. (2003). Multi-objective autocalibration for semi-distributed water quality models. Water Resources Research, 39 (12).

148. Van Liew, M. W., Arnold, J. G. and Bosch, D. D. (2005). Problems and potential of auto calibrating a hydrologic model. Transactions of the ASAE, 48(3): 1025-1040.

149. Wang, Z. M., Batelaan, O. and De Smedt, F. (1996). A distributed model for water and energy transfer between soil, plants and atmosphere (WetSpa). Physics and Chemistry of the Earth, 21(3): 189-193.

150. Wara, C., Thomas, M., Mwakurya, S. and Katuva, J. (2019). Development of river rating curves for simple to complex hydraulic structure based on calibrated HEC-RAS Hydraulic Model, in Kwale, Coastal Kenya. Journal of Water Resource and Protection, 11(04): 468.

151. Wilk, J. and Hughes, D. A. (2002). Simulating the impacts of land-use and climate change on water resource availability for a large south Indian catchment. Hydrol. Sci. J., 47(1): 19-30. https://doi.org/10.1080/02626660209492904.

152. Willmott, C.J. (1981). On the validation of models. Physical Geography, (2): 184-194.

153. Yilmaz, B. (2015). Assessing climate change impacts on Gediz Basin water balance with WEAP and HEC-HMS model. J. Multidiscip. Eng. Sci.

Technol, (2): 3017-3020.

154. Zema, D. A., Denisi, P., Taguas Ruiz, E. V., Gómez, J. A., Bombino, G., and Fortugno, D. (2016). Evaluation of surface runoff prediction by a NN-AGNPS model in a large mediterranean watershed covered by olive groves. Land degradation & development, 27(3):811-822.

155. Zhao, R. J., Zhang, Y. L., Fang, L. R. Liu, X. R. and Zhang, Q. S. (1980). The Xinanjiang model, hydrological forecasting, proceedings Oxford Symposium, IASH (129): 351-356.

APPENDIX-A Project summary

Table A.1: Summary

Project objectives			
Objectives as per project document		Revised objective	Reasons for revision
i) Application and performance evaluation of select hydrological models for simulation of surface water, and groundwater processes. ii) Assessment of present and future water availability under alternate scenarios of climate change. iii) Integrated water allocation planning and management based on future scenario of water availability. iv) Flood plain mapping. v) Formulation of adaptation measures in the context of climate change.		None	None
***Manpower* deployed (against sanctioned manpower)**			
Sanctioned		Deployed	
Designation	Person months	Designation	Person months
Research Scientist	60	Research Scientist	70
JRF	300	JRF	108
Infrastructure/ equipment			
Planned (as per project proposal)		Developed/ procured	Reasons for deviation
i) Laptop- ZBook Mobile Workstation ii) Desktop & Accessories iii) Camera iv) Software/Portable hard disks /Pen drives/Accessories		Not procured Procured Procured No licensed software was procured; one 4 TB hard disk and pen drive purchased	Administrative delays and no approvals for rest of the listed items
Field work			
Planned (as per project proposal)		Completed	Reasons for deviation
Soil sampling, infiltration and hydraulic conductivity tests		Completed	
Workshop/ Capacity building/ technology transfer			

Planned (as per project proposal)	Organized	Reasons for deviation
Stakeholder Workshops - 4	Organized - 2	Could not be organized due to Covid & non-availability of officials in monsoon season
Study area		
Planned	Extended	
Upper Narmada basin in Central India	None	
New data generated in the project		
Planned (as per project proposal)	Achievement	Reasons for deviation
None		
Envisaged contribution of the project		
Planned (as per project proposal)	Contribution made	Reasons for deviation
1) The results of the study will be helpful in the assessment of the water resources in the present as well as into the future incorporating the impacts of climate change through various hydrological models. 2) The study shall address the issues related to future climate change impacts on water availability, and the likely scenario of extreme events like floods and droughts.	All	None
How research outcome benefited the end user department and society		
Planned (as per project proposal)	Benefit derived	Reasons for deviation
1) The research outcome shall help to understand the various hydrological processes in Narmada basin through use of multiple hydrological models specifically designed to address a particular component of the hydrological cycle based on their advantages and limitations. 2) The research outcome will also benefit the various stakeholders, decision	All The findings of the stud have been communicated to various stakeholders and decision makers through workshops, training and lectures in high level meetings. Publications in international conference and national conferences.	None

makers, and scientific community by helping them to understand the issues of climate change and help in developing water resources management strategies. 3) The recommendations of the study will help the State to harness and develop the water resources in a sustainable manner by having a foresight into the water availability and occurrence of extreme events under the future scenarios of climate and help to adapt to the changing scenario accordingly. 4) The study will also be helpful to the research community and its outcome may be published in International and National peer-reviewed Journals and presented in International and National conferences.	Communication to reputed high impact factor journals to be initiated after the submission of final report. State can plan to harness and utilize the water resources based on the climate change impacts assessments and plan for additional harnessing of the water available in future through construction of more storage facilities in the study area.	
End-of-project deliverables		
Planned (as per project proposal)	Achieved	Reasons for deviation
1) Application of various models pertaining to surface water hydrology, groundwater hydrology, basin planning, optimal water utilization and their inter-comparisons 2) A comprehensive methodology for the integrated assessment of climate change. 3) Evaluation of the impact of climate change on the water resources in Narmada basin. 4) Development of suitable adaptation measures for	All	None

adapting to the future climate change scenario.					
Outsourcing (>1 lakh)/ consultancy (All)					
Consultant (name and qualifications), organization / outsource agency		Work assigned		Estimated cost Rs	Actual cost Rs
None		None			
Financial achievement					
S No	Head	Approved budget	Approved revised budget	Final expenditure	Reasons for deviation
1.	Remuneration/Emoluments for Manpower etc.	13795896	NA	7941974	Manpower not recruited
2.	Travelling Expenditure	5150000	NA	446140	Limited tours
3.	Infrastructure/Equipment	4285000	NA	276499	Equipment purchased under other projects were utilized. High end systems and software viz., ArcGIS/MODLFOW/RIVERWARE etc. were not procured.
4.	Experimental Charges/Field work/Consumables	240000	NA	48814	No printing of hard copies of reports
5.	Capacity building/Technology transfer	750000	NA	0	Stakeholder workshops clubbed along with other PDS
6.	Contingency	375000	NA	12262	
7.	Outsourcing/ consultancy	400000	NA	0	GIS work not outsourced

	Total	**24995896**	**NA**	**8725689**	

Table A.2: Quantitative outcome

i. Research papers published/ submitted		
S No	Research paper (National/ International Journal/ conferences/ symposium/ workshop/ seminar)	Impact factor for Journal

Reports/Monographs/Internal publications brought out	
S. No.	Reports/Monographs/Internal publications
1	Five Interim Reports have been submitted at the end of each completed year. Final Report is being submitted now.

ii. New techniques/models/ software/ knowledge developed, if any

iii. Web site/ application developed				
Name	Web address	Server location	Launch date	Details of information available
None				

iv. Patents filed/awarded, if any

Workshop/ conferences/ seminars/capacity building programmes organised			
S. No.	Topic	Dates, duration, No. of participants	Report published (Y/N)
	None		

v. Stake holders feedback and action taken on constructive feed back		
S No.	Feedback received	Action taken
Stake holder meet (Topic and date)		
1.	Stakeholders Workshop on "Integrated Assessment of the Impacts of Climate Change on the Hydrology of Narmada Basin through Hydrological Modelling Approaches" on 27.03.2019	The stakeholders from various line departments, and field organizations appreciated the work being carried out in the study which was initiated based on the requirement of WRD, M.P. for such study in the region. The member suggested using CMIP6 based GCM projections for climate change impact assessments. The First Interim Report and the progress of the study were showcased.
2.	Stakeholders Workshop on "Integrated Assessment of the Impacts of Climate Change on the Hydrology of Narmada Basin through	The stakeholders were satisfied with the progress of the study and the modelling efforts being applied to model various facets of the hydrology. Climate change impacts on the surface water runoff and extreme events were showcased using few

	Hydrological Modelling Approaches" on 08.01.2021	hydrological models' setup for the study area. The Interim Reports and the progress of the study were showcased and appreciated by the participants. The progress of the study was presented in the various R&D sessions and the suggestions were incorporated. It was suggested to drop the RIVERWARE software due to its high initial costs and regular annual maintenance costs. Similarly, the other licensed software including MIKE FLOOD and RIBASIM were not available due to license related issues. The study has been showcased in other high level meetings and with decisions makers at various forums from time to time.

vi. Field observations obtained, thematic maps generated (water quality and salinity, isotope, soil moisture, stage and discharge, sediment, water level, river cross sections, geophysical/ resistivity survey, hydrogeological investigations etc.)

S No	Parameter, frequency, period, groundwater/ river/ tank/ hand pump/ spring/ sea-water	Number (planned)	Numbers (measured)
	Thematic maps of land use land cover, soil type, DEM have been prepared	NA	NA

vii. Field installations (piezometers, river stage/ discharge, soil moisture etc.)

S. No	Name, make/ model	Unit price, total price, quantity	Date of installation	% utilization	Remarks regarding maintenance/ breakdown
	None				

viii. Equipment/ software purchased

a. Equipment purchased

S. No	Name, make/ model	Unit price, total price, quantity	Date of installation	% utilization	Remarks regarding maintenance/ breakdown
1.	Dell Desktop with monitor	56999/-	15.10.2019	100%	None
2.	D3500 Camera	27500/-	14.11.2019	100%	None
3.	Dell Workstation	129000/-	16.01.2020	100%	None

4.	ACER Desktop	56000/-	19.11.2020	100%	None
5.	ACER Desktop	60000/-	14.06.2022	100%	None

b. Software purchased

S. No	Name, version, license	Unit price, total price, quantity	Date of installation	% utilization	Remarks regarding maintenance/ breakdown
	None				

ix. Plans for utilizing the equipment facilities in future

S. No.	Installation/ equipment	Planned future use
1.	Dell Desktop with monitor, Dell Workstation, ACER Desktop, ACER Desktop	For writing papers to be published in high IF Journals and Conferences

x. Data dissemination policy for data generated in the project

No new data has been generated in the project. The findings obtained from the study shall be disseminated through reports and publications in journals and conferences.

xi. Number of post-graduate/doctoral candidates completed their courses

1. Sh. Sachin Patel, M. Tech Dissertation
2. Sh. Prashant, M. Tech Dissertation
3. Ms. Akanksha Soni, M. Tech Dissertation

xii. Foreign deputation/visit of PI/Co-PIs/students, if any

None

A.3 Activity chart

S. No.	Items of work	Year 1				Year 2				Year 3				Year 4				Year 5			
		Q1	Q2	Q3	Q4	Q1	Q2	Q3	Q4	Q1	Q2	Q3	Q4	Q1	Q2	Q3	Q4	Q1	Q2	Q3	Q4
1	Field visit to the basinareas and interaction withthe decision makers and stakeholders.																				
2	Collection of hydro-meteorological datainclding rainfall and weather datasets from CWC, WRD, SLR, IMD, Agriculture.																				
3	Collection of hydrological data including the gauge, discharge, groundwaterlevels, water quality etc., from Central Water Commission, Narmada Control authority, Narmada Valley Development Corporation, Central Groundwater Board, andWater ResourcesDepartment.																				
4	Collection of literature/reports/manuals pertaining to studiesalready carried out by theline departments mainly onwater availability, floods,climate change, DPR"s of completed/ongoing/proposed projects.																				
5	Collection of demographic data/irrigation statistics/cropped area and sources of irrigation datafrom the District Planning Offices / Revenue Department.																				
6	Procurement of high-resolution satellite digital datasets for identification of land use/land cover and digital elevation models.																				

7	Field experiments for evaluation of hydrologic soil properties including infiltration and hydraulicconductivity of soils and collection of soil samplesfor related laboratory analysis to ascertain other soil properties.																				
8	Detailed soil survey by reputed firms i.e. NBLSSUP/ AISLUP for the dominant soil groups in the study area.																				
9	Land use / land cover classification.																				
10	Preparation of maps on soil type/texture, topography, contour, settlements, geology, hydrogeology in GIS environment.																				
11	Processing and analysis of historical datasets on precipitation, temperature, discharge, groundwater levels etc.																				
12	Assessment of climate change signals in the basin based on the historical datasets of precipitation and temperature during the baseline period.																				
13	First Stakeholders Workshop to showcase the progress of the efforts, gaps in data collection and interaction to understand the major issues in the basin.																				
14	Preparation of First Interim Report at the end of first year.																				
15	SWAT model set-up, calibration and validation to simulate the runoff processes.																				
16	VIC model set-up, calibration and validation to simulate the runoff processes.																				
17	HECHMS model set-up, calibration and validation to simulate the runoff processes.																				
18	NAM model set-up,calibration and validation to simulate the runoff processes.																				
19	Setup of MODFLOW, calibration and validation for groundwater flow modelling.																				
20	WEAP model setup for the present scenario for basin planning (baseline).																				
21	HECRAS setup, calibration and validation for flood modelling.																				
22	*Second Stakeholders Workshop.*																				
23	***Preparation of Second Interim Report.***																				
24	Setup of Model MUSE, calibration and validation for groundwater flowmodelling.																				
25	RIBASIM model setup for the present scenario for basin planning (baseline).																				
26	RIVERWARE setup, calibration and validation for reservoir operation based on historical inflows and demands.																				
27	Climate change impact assessment on future surface water availability using SWAT.																				
28	Climate change impact assessment on future surface water availability using VIC.																				
29	Climate change impact assessment on future surface water availabilityusing NAM.																				
30	Impact assessment of climate change on future groundwater availability using MODFLOW.																				
31	Third Stakeholders Workshop.																				
32	***Preparation of ThirdInterim Report.***																				
33	Climate change impact assessment on future surface water availability using HECHMS.																				

34	Impact assessment of climate change on future groundwater availability using MUSE.																			
35	Water allocation planningbased on future scenario using WEAP.																			
36	Optimal reservoir operation strategies based on future scenario using NIHReSyp.																			
37	Flood modelling and mapping based on future scenario using HECRAS.																			
38	Fourth StakeholdersWorkshop.																			
39	***Preparation of Fourth Interim Report.***																			
40	Water allocation planning based on future scenario using RIBASIM.																			
41	Optimal reservoir operation strategies based on future scenario using RIVERWARE.																			
42	Adaptation measures for expected hydrological changes in the future.																			
43	Final Stakeholders Workshop to disseminate the findings.																			
44	***Preparation of Final Report covering all theaspects.***																			

All the items as planned have been completed except for two Stakeholder Workshops due to the cited reasons. As advised RIVERWARE and RIBASIM based applications were not carried out due to very high licensing costs for the software. A short extension was sought for six months to complete some of the work elements related to flood modelling using HEC-RAS and groundwater modeling using MUSE, which was granted. The reservoir operation could not be completed due to shortage of manpower in the project.

Appendix B Supplementary results

None